NASA SP-267

PHYSICAL STUDIES OF MINOR PLANETS

NATIONAL AERONAUTICS AND SPACE ADMINISTRATION

NASA SP-267

PHYSICAL STUDIES OF MINOR PLANETS

Edited by T. GEHRELS

Scientific and Technical Information Office 1971
NATIONAL AERONAUTICS AND SPACE ADMINISTRATION
Washington, D.C.

For sale by the Superintendent of Documents,
U.S. Government Printing Office, Washington, D.C. 20402
Price $3.00 (paper cover) Stock Number 3300–0428
Library of Congress Catalog Card Number 73–169176

Page intentionally left blank

Page intentionally left blank

FOREWORD

The understanding of the origin and evolution of the solar system is one of the major scientific goals of space research. The important data in this respect are the physical and chemical properties of the solar system at the time of its formation. Bodies of the size of the Moon and planets have necessarily undergone substantial evolution in the last 4.5 billion years and these evolutionary processes have altered much of the initial record of their formation. However, smaller bodies–asteroids, comets, and meteorites–probably contain a less altered record of the early history of the solar system. The rapid advances in space technology have cleared the way for man to consider flights to and rendezvous with the asteroids during this century. The development of the scientific rationale for investigations of the minor planets is a precursor requirement in the planning of specific space missions. The publication of this book is a step to the asteroids.

HOMER E. NEWELL
Associate Administrator
National Aeronautics and
Space Administration

Page intentionally left blank

PREFACE

We are now on the threshold of a new era of asteroid studies. There was a previous period of great activity on minor planets in the nineteenth century when time and effort of astronomers were devoted to discovery and orbit determination, and this work has been pursued by some until the present time. Physical studies, however, have not been popular, at least not among astronomers. The lack of appreciation is coming to an end with the presently growing realization that asteroids, comets, and meteoritic matter are basic building blocks of the original solar nebula. Their exploration gives data for the study of the origin and history of the solar system.

To promote new and increased exploration, including that with spacecraft, five people wished to hold an international conference and, when they became aware of their common idea, a joint Organizing Committee was formed; the members are H. Alfvén, G. Arrhenius, A. Bratenahl, T. Gehrels, and C. J. van Houten. Endorsement and partial support were given by the International Astronomical Union and it became the 12th Colloquium of the IAU entitled "Physical Studies of Minor Planets." The National Science Foundation and the National Aeronautics and Space Administration gave substantial financial support to make the attendance of 34 of the participants possible.

The meeting was held in Tucson, Ariz., March 6-10, 1971. On the first two days there were excursions to the Kitt Peak and Catalina Observatories, and a hike to Seven Falls in the Catalina foothills. The scientific sessions were held in the mornings and evenings of March 8, 9, and 10; the afternoons were open for informal meetings. Luncheon speakers were S. F. Singer on the environmental problems of the supersonic transport (SST), F. L. Whipple describing the Mt. Hopkins Observatory, and A. B. Meinel speaking on synthesized telescopes and also giving a brief description of his new proposal for the usage of solar energy. The scientific meetings were held in Meinel's Optical Sciences Center; they were opened with a welcome address by the Provost of the University of Arizona, A. B. Weaver. The Chairmen were, in order of the sessions, M. Dubin, J. L. Weinberg, G. P. Kuiper, H. C. Urey, C. F. Hall, and W. E. Brunk.

The interest in this colloquium was much greater than we had expected. There were about 140 participants. (See list at the end of this book.) The program was crowded, with closely timed presentations and discussions, as can be seen from the large number of papers in this book. Some otherwise valuable papers were turned down as being outside the scope of this colloquium; for instance, those on orbit improvement.

On the other hand, there are some papers and discussions included in this book even though they were not presented at the meeting. In some respects, therefore, the book is independent of the colloquium. Several papers had been invited long beforehand with the request to publish them as review papers. The lack of a modern textbook on minor planets is keenly felt, and the proceedings of this meeting, with these additions, should provide a good reference book. The book could be especially useful if published promptly, and the request was therefore made to bring manuscripts to the meeting. After the meeting some of the papers and discussions have been improved, and we thank the referees for their help.

The organization of the book is the same as that of the colloquium, which had discussion of observations on the first day, of the origin of asteroids and interrelations with comets, etc., on the second, and of space missions and future work on the third day. The papers are preceded by a general "Introduction," which keeps in mind the interests of people not previously familiar with asteroids; as a partial summary of the book, it may be of interest also to insiders. This "Introduction" was not presented at the meeting. Gill and Haughey had a manuscript "Mission to an Asteroid" written for a program study at NASA Headquarters; I had a first draft of an introduction for this book, and we combined the two manuscripts. Finally, to optimize this as a textbook, Mildred Matthews compiled the index.

Thanks are due to Mildred Matthews and to the editorial group at NASA Headquarters for their careful work in preparing the manuscripts for publication, to Shirley Marinus and several local assistants for the smooth organization of the meetings, and to the agencies and individuals mentioned above that supported the colloquium and set the pattern for an effective and pleasant exchange of ideas and information.

TOM GEHRELS
Lunar and Planetary Laboratory
The University of Arizona

CONTENTS

Part II—ORIGIN OF ASTEROIDS INTERRELATIONS WITH COMETS, METEORITES, AND METEORS

Part III—POSSIBLE SPACE MISSIONS AND FUTURE WORK

INTRODUCTION

TOM GEHRELS
University of Arizona

and

JOCELYN R. GILL AND JOSEPH W. HAUGHEY
NASA, Office of Space Science and Applications

HISTORICAL NOTES

Kepler, in his *Mysterium Cosmographicum,* probably was the first to point out that a planet was missing between the orbits of Mars and Jupiter. The Titius-Bode expression of planetary distances from the Sun ($r = 0.4 + 0.3 \times 2^n$) was formulated in 1772. That expression and the discovery of Uranus in 1781 stimulated plans to search for the missing planet at 2.8 AU, and at a congress in 1796 a group of astronomers undertook to search, each an assigned part of the sky, for the missing planet. Ceres was not found by any of that group, but by Piazzi at Palermo, rather by chance, on January 1, 1801.

In the early literature there occurred some mention that the orbits of Ceres, Pallas, Juno, and Vesta nearly intersect, and the possibility of a common origin was raised. At our request, Herget looked into this matter and table I gives for various pairs of asteroids the closest distance and the eccentric anomalies at which the closest approach occurs. The surmise of intersecting orbits appears without basis.

Asteroids were observed visually in the telescope by checking positions noted on star maps to detect motion among the stars. The asteroid work in the middle of the 19th century stimulated the making of the first stellar atlas, the *Bonner Durchmusterung.* The brightness of the asteroids was determined by comparison with the *Bonner Durchmusterung,* and because it has serious errors in the faint end of the magnitude scale, the asteroids were assigned magnitudes that were systematically off by as much as 1 or 2 mag.

One hundred asteroids had been found by 1868 and that number trebled by 1890. In 1892, Max Wolf of Heidelberg adopted a photographic method. The magnitude error, however, was propagated also to the photographic determinations. The asteroid magnitudes became reliable, to about ±0.1 mag, in 1958 when the IAU adopted a new magnitude system for the asteroids.

The observations of minor planets are still being conducted at several observatories, but mostly for astrometric purposes. Historical notes on

TABLE I.—*Closest Distance Between Asteroids and Eccentric Anomalies of Closest Approach*

[Herget, 1971, personal communication]

Planet pair	Closest distance, AU	$E(1)$	$E(2)$
Ceres-Pallas	0.17	35°	58°
	.06	218	260
Ceres-Juno	.63	0	81
	.85	142	256
Ceres-Vesta	.40	44	310
	.51	222	113
Pallas-Vesta	.08	49	293
	.45	265	114
Juno-Vesta	.38	295	78
	.45	85	267
Pallas-Juno	.50	30	88
	.79	268	327

(disappointments experienced in) the use of asteroids to determine fundamental astronomical constants are found in the paper by Rabe,[1] whereas Vesely[2] discusses the history of pole determinations in photometry. The procedures at the telescope are described by Roemer.[3] Sometimes an additional plate is taken, guided on stars in a known magnitude sequence for calibration of the asteroid magnitude (photometric procedures were described by Gehrels, 1970).

The advent of fast electronic computers has improved and accelerated the process of orbit computation drastically. In the 1971 *Ephemeris* volume there are 1748 numbered asteroids. In addition, there are several thousand that have not been observed in subsequent apparitions, or that have for other reasons only a preliminary designation.

NAMES AND CATALOGS

A preliminary designation, at least after 1925, is made as follows: The year is followed by a letter indicating in which half of the month the finding occurred and the second letter gives the order of the discovery within that half month; for instance, the first asteroid discovered in the second half of March 1971 was 1971 FA. A preliminary orbit is computed from at least three observations within that first apparition. If the object is found during another apparition, a permanent number is assigned and the discoverer may name the planet. An effort is made to give all asteroids a name; originally the custom was to put all asteroid names into feminine form, but that convention is no longer followed.

[1]See p. 13. [2]See p. 133. [3]See p. 3.

The cataloging of asteroids was done at the Rechen Institut in Germany; the yearly ephemerides volumes *Kleine Planeten* were published until 1944 and the ones from the Institute of Theoretical Astronomy in Leningrad started in 1947. From 1949 through 1952, the Minor Planet Center in Cincinnati also published ephemerides, but by international agreement in 1952 this was discontinued. Since then Cincinnati publishes the *Minor Planet Circulars* for observations, new orbits, and ephemerides, while Leningrad issues the yearly *Ephemeris* for numbered planets including their orbital elements. (See Herget.[4]) The *Astronomical Circular,* published by the Kazan or Englehart Observatory, and other scattered observatory publications list asteroid observations and calculations. New findings that are of urgent importance are transmitted to the IAU bureau at the Smithsonian Astrophysical Observatory in Cambridge, Mass., which in turn transmits this information to other observatories. A complication of searches for new objects is that many rockets or rocket parts are in orbit around Earth. (See Aksnes.[5])

The aim of this book and of the colloquium is to concentrate on physical studies, and we will not dwell on the applications of asteroid work in celestial mechanics. The work of precise orbit determination is crucial for determination of individual masses of asteroids, and this is discussed by Schubart.[6]

PHYSICAL CHARACTERISTICS

Hapke[7] opened his paper with these words: "The picture that most of us have in our minds of a typical asteroid is probably of a large, irregularly shaped chunk of iron, unrusted by exposure to oxygen or water, and with a surface kept clean and dust free by the sandblasting effect of repeated micrometeorite impacts." We wonder just how many people would think of asteroid surfaces that way, rather than of a dusty, rubbled regolith as the artist made for Geographos in the frontispiece. Hapke himself and others in this book endorse that artist's concept; in fact, at the colloquium there was some discussion of the possible materials and texture for the dusty surface.

The apparent diameters of Ceres, Pallas, Juno, and Vesta during oppositions when they are favorably near perihelion are about 0".6, 0".6, 0".2, and 0".4, respectively. Only these four and Eros have been measured directly. (See the paper by Dollfus[8] and the ensuing discussion.) Eros' apparent diameter was about 0".18 when van den Bos and Finsen (1931) observed it, and this is considered too small for reliable size determination. The reflectivity is determined from size and brightness measurements; both are needed. New techniques of infrared observations to determine diameters are discussed by Allen,[9] and by Matson[10] who makes an interesting comparison of size and reflectivity.

---

[4]See p. 9.
[5]See p. 649.
[6]See p. 33.
[7]See p. 67.
[8]See p. 25.
[9]See p. 41.
[10]See p. 45.

Spectrophotometry is reviewed by Chapman et al.,[11] who also describe their own discovery of a spectral feature near 0.92 μm for Vesta and a few other asteroids; they give an interpretation in terms of absorption by Fe^{2+}. The integrated colors of asteroids vary but generally resemble the Moon and Mercury in showing a brownish-gray hue.[12] The photometric properties may resemble the Moon's, but this could be a misleading statement as there are considerable differences, as yet poorly determined. The nature of the surface can be studied with detailed photometry[13] and polarimetry.[14] Radar measurements may be used for a few asteroids, but only the largest radio telescopes have enough signal-to-noise ratio.[15]

When a photometric lightcurve has two nearly identical maxima and minima, it is concluded that the lightcurve is caused by effects of shape rather than by reflectivity differences over the surface.[16] The fact that lightcurves of the asteroids repeat over many periods is an indication that they do not wobble in space like spinning tops, but rather rotate about one axis only. Rotation periods are generally found between 3 and 19 hr; they are listed in table I of Taylor.[17] Geographos is known to be highly elongated because of its large amplitude of the light variation.[18] After the colloquium, a new Apollo asteroid was found[19] and its lightcurve was observed; this object also has a steep lightcurve, which is more irregular than that of Geographos, suggesting a more irregular shape for the object. Trojan asteroid Hektor also has a large amplitude of the lightcurve, but this object is so large that it may not be able to sustain itself gravitationally as a single elongated body; it may be a double object as suggested by Cook.[20] However, Hartmann (1972) derives for gravitational crushing and collapse to spherical shape a critical diameter of 680 km for rocks and 120 km for meteoritic material; Hektor is 110 km long and 40 km wide and therefore is a marginal case. The fact that asteroids can have exceptional shapes was noticed early in the 20th century for Eros.[21] The determination of the shapes, orientation of axes, and the analysis of lightcurve observations are discussed by Lacis and Fix,[22] and by three of the six high-school teachers working on a NASA-sponsored photometric program in Tucson: Dunlap,[23] Taylor,[24] and Vesely.[25]

STATISTICS AND GROUPS

Asteroids travel in prograde orbits defined by elements: the semimajor axis *a*, eccentricity *e*, and inclination to the ecliptic plane *i*. There is some preference for the direction of the semimajor axes to occur more frequently in the same direction as that of Jupiter. (This is seen in figure 2 of Lindblad and

---

[11]See p. 51.
[12]See p. 67.
[13]See, however, p. 79.
[14]See pp. 91 and 95.
[15]See p. 165.
[16]See p. 257.
[17]See p. 123.
[18]See p. 153.
[19]See p. 647.
[20]See pp. 155 and 162.
[21]See p. 133.
[22]See p. 141.
[23]See p. 147.
[24]See p. 117.
[25]See p. 133.

Southworth.[26]) Like stars, asteroids may be listed according to their apparent magnitudes, ranging from 7 mag to the faintest seen in a reasonably large telescope, viz., 16 to 17 mag for the 154 cm Catalina reflector and 21 mag, the faintest photographed to date. These apparent magnitudes may be converted to absolute magnitudes, converted to zero phase angle and 1 AU distances to Sun and Earth, in order to give a representation of size.

A systematic photographic survey of the asteroid belt was made in the Yerkes-McDonald survey (MDS) to 16 mag. The Palomar-Leiden survey (PLS) gave a spot check, rather than a systematic survey around the ecliptic, and the corrections to completion are uncertain. The PLS does, however, give statistics to the 20th apparent magnitude for about 2000 asteroids and orbital characteristics for 1800. Valuable additions and clarification of MDS and PLS data occur in the papers—and in the ensuing debates—of van Houten,[27] Kiang,[28] Kresák,[29] Dohnanyi,[30] and Lindblad and Southworth.[31] In summary, it appears to us that there are no systematic errors in the PLS but that, because only a 12° by 18° area was photographed, there are selection effects and the corrections to completion are uncertain.

The total number of asteroids brighter than $B(a, 0) = 21.2$ (1.6 km in diameter), derived from the PLS, is $4.8\ (\pm 0.3) \times 10^5$ (Gehrels, 1971). Collisions continually occur to cause a steep frequency-size relation. The total mass in the asteroid ring is not so easily derived because the mass density and reflectivity of all but a few are unknown, but it appears to be about twice the mass of Ceres, or 2.4×10^{24} g, or 0.4×10^{-3} the mass of Earth. (See Schubart.[32]) The comparison with the masses of planets is qualitatively shown in figure 1 of Arrhenius and Alfvén.[33]

Whereas the asteroids on the inner side of the belt are concentrated toward the plane of the ecliptic, with $\bar{i} \sim 4°$, this concentration gradually diminishes, $\bar{i} \sim 11°$ near $a = 3.2$ AU, and the concentration toward the ecliptic plane is generally less for larger objects. (See van Houten[34] and Kiang.[35]) The outer boundary of the asteroid belt is not well defined but the inner one is rather sharply limited,[36] except for the Mars-crossing asteroids. When they can come close to Earth they are called "Amor-type asteroids"; they are defined to have aphelion distance between 1.00 and 1.38 AU (Gehrels, 1972). When the orbit of Earth is also crossed, the object is called an "Apollo asteroid" after one of these objects. Table II of Marsden[37] and table I of Roemer[38] give characteristics of these groups. Alfvén and Arrhenius[39] select from these a subgroup of asteroids having lower eccentricities as candidates for space missions.

R. B. Hunter (1967) predicted the possibility that asteroids would occur between Jupiter and Saturn. Rabe (personal communication) believes these

---

[26]See p. 351.
[27]See p. 183.
[28]See p. 187.
[29]See p. 197.
[30]See p. 263.
[31]See p. 337.
[32]See p. 33.
[33]See p. 214.
[34]See p. 183.
[35]See p. 187.
[36]See p. 177.
[37]See p. 419.
[38]See p. 644.
[39]See p. 473.

regions to be rather unstable, although perhaps asteroid orbits roughly half-way between Jupiter and Saturn, if they are of small or moderate eccentricity, may be able to avoid approaches to both major planets and thus remain stable. No asteroids between Jupiter and Saturn have been found in the PLS down to 20.5 mag.[40]

The orbital periods of the asteroids are mostly between 2 and 6 yr, which is to be compared with 11.86 yr for Jupiter. Gaps and/or groups occur at certain commensurabilities. Three asteroid distributions are especially noted, separated by gaps called Kirkwood gaps after their discoverer. The principal gaps occur at 5.9, 4.8, and 4.0 yr (i.e., at 2:1, 5:2, and 3:1 ratios to Jupiter's mean motion), but objects are present, in resonance with Jupiter. Groupings[41] and families of asteroids are generally named after representative asteroids. Their mean motion as seen from the Sun is often considered; for instance, at the above 2:1, 5:2, and 3:1 commensurabilities, we have, respectively, Hecuba near 600, Minerva near 750, and Hestia near 900 arcsecs/day. Table II shows characteristics of a few representative asteroids.

The present eccentricities and inclinations of the asteroids have been affected by Jupiter's perturbations, but values of these may be computed such that they are free of most long-range perturbations. The three-dimensional distribution of these unperturbed elements (called "proper" elements) shows groupings of the minor planets against a general background. These groupings are referred to as Hirayama families; Hirayama found 10 of them and Brouwer extended the number to 458 out of 1537, or 30 percent of known asteroids. Presumably the members of each family are fragments of a collisional breakup; the chance of collision is estimated by Hills[42] and

TABLE II.—*Orbital Characteristics of Representative Asteroids*

Asteroid	q, AU	Q, AU	e	i	Mean motion, arcsec/day
1932 HA Apollo	0.65	2.31	0.56	6°	1959
1221 Amor	1.08	2.76	.44	12	1333
434 Hungaria	1.80	2.08	.07	23	1309
46 Hestia	2.09	2.95	.17	2	885
719 Albert	1.19	3.98	.54	11	854
93 Minerva	2.36	3.14	.14	9	776
1 Ceres	2.55	2.99	.08	11	771
108 Hecuba	2.96	3.49	.08	4	614
153 Hilda	3.38	4.58	.15	8	448
279 Thule	4.15	4.41	.03	2	400
624 Hektor	5.02	5.22	.02	18	306
944 Hidalgo	1.98	9.66	.66	43	253

[40]See p. xvii.

[41]See p. 173.

[42]See p. 225.

Burns.[43] Some of these families are rather tightly packed, others are loose and may not even constitute real groups. (See the paper by Lindblad and Southworth.[44]) The consideration of nongravitational forces, in this case the ones by collision, are important. Collisions tend to diminish e and i, but more sharply the collisions may form jetstreams characterized by high space density and low relative velocity of members. Now we have arrived at a rather complex situation where inelastic collisions may cause accretion as well as dissipation; the new theoretical developments are introduced by Alfvén[45] and the degree of elasticity is studied by Trulsen.[46]

TROJAN ASTEROIDS

There are also accumulations at 1:1 and these are referred to as the Trojans. Sixteen members of the Trojans are definitely known and many others are suspected. The large number of Trojans and their asteroidlike size distribution suggests that they have a similar origin; e.g., that they were formed at their present location by condensation from the solar nebula.

The Trojans occur near points of equilateral triangles with the Sun and Jupiter in the plane of Jupiter's orbit. These lagrangian points L_4, preceding Jupiter, and L_5, west of Jupiter, are fairly stable points and permit large librations of the Trojans about these points. Rabe[47] discusses the possible Trojan origin of the Jupiter family of comets.

ORIGIN AND EVOLUTION OF THE ASTEROIDS

Asteroids and comets should be studied intensively because they are made of primeval matter of the solar system and are less affected by later action as is the case on the Moon, Mercury, etc. The comets, certain satellites, Trojans, ordinary asteroids, Mars-orbit crossers, meteorites, and meteors should be studied simultaneously because they are records for various parts of the solar system. A basic separation of cosmic material is generally recognized to be as follows: (1) earthy materials, solid at temperatures up to 2000 K, (2) the ices, vaporizing at about 300 K, and (3) the gases. This separation should be kept in mind for the study of the relative importance of asteroids, comets, and planets.

The three largest asteroids do not fit the normal frequency-size distribution. This has been explained by Hartmann (1968) as due to their having reached a range of sizes where the gravitational cross section was larger than the geometric one. The theory of Hills[48] considers the terrestrial planets similarly to be large asteroids. The number-size distribution[49] of the asteroid ring shows a discontinuity near about 20 km diameter. This may be due to two modes of asteroid formation: the asteroids brighter than about the 12th apparent

---

[43]See p. 257.
[44]See p. 337.
[45]See p. 315.
[46]See p. 327.
[47]See p. 407.
[48]See p. 225.
[49]See pp. 294 and 297.

magnitude may be original condensations whereas the ones fainter than about 16 mag may be fragments of subsequent collisions. Alfvén has suggested that the present rotation rates, which have been observed only for the larger asteroids, are remnants of the original rotations obtained during formation, but this was debated by Whipple.[50] (Also see Burns.[51]) Dohnanyi[52] finds that the number-size distribution for the brighter asteroids $[B(1,0)<11]$ may be compatible with a collision mechanism; this is a surprising conclusion.

Arrhenius and Alfvén[53] make introductory remarks on jetstream theory (also see Alfvén[54]) and on the application of studies of the Moon and meteorites to those of asteroids. Sustained jetstream accretion is discussed by Giuli[55] and the formation of comets by Vanýsek.[56] A mechanism for chondrule accumulation is proposed by Whipple.[57]

INTERRELATIONS WITH COMETS

The distinction between asteroids and comets is made, at the telescope, on the basis of visibility of a coma. Marsden[58] concluded that asteroid 944 Hidalgo may be an extinct cometary nucleus. The same has been surmised for 1566 Icarus. Nongravitational forces, in this case the ones that are presumably caused by the outgassing of the cometary nucleus, and the interrelations of comets and asteroids, are discussed by Marsden and by Sekanina.[59]

Some of the Mars-orbit crossers may be extinct nuclei of short-period comets, Icarus is an example, whereas a more asteroidal group has Geographos as the example. Characteristics of asteroids with $q \leqslant 1.15$ AU are shown in table II of Marsden and their observational status is given in table I of Roemer.[60] The orbits of the Apollo asteroids may not be stable whereas the ones crossing the Mars orbit but not that of Earth appear to be stable in terms of the age of the solar system. (See Williams.[61]) Their dynamical lifetime is limited by collision with and close approach to Earth, Mercury, Venus, and Mars. Their lifetime as live comets, wherein they emit gases to form envelopes and tails, is determined by solar radiation. The rate of evaporation and the dimensions of the nuclei are also factors in this lifetime, which is estimated to be less than 10^4 yr. Dynamically, however, the lifetime may be 10^4 times longer. This could mean that the space inside Jupiter's orbit is filled with the remnants of 10^4 to 10^5 extinct comets for every live comet.

A basic question, debated at the colloquium, is to what extent the meteorites originate from the common asteroids, from Apollo asteroids, or from the comets.[62] Anders[63] argues that only 10 percent of the asteroids can be parent bodies of the meteorites and that these are the ones with high

---

[50]See p. 249.
[51]See p. 257.
[52]See p. 263.
[53]See p. 213.
[54]See p. 315.
[55]See p. 247.
[56]See p. 465.
[57]See p. 251.
[58]See p. 413.
[59]See p. 423.
[60]See p. 644.
[61]See p. 177.
[62]See p. 447.
[63]See p. 429.

eccentricity. In connection with this problem, the origin and properties of meteors were also discussed.[64]

SMALL PARTICLES

The mass range of small particles at distances between 0.1 and 30 AU is estimated to be from 10^{-12} to 10^{2} g. Whipple (1967) has estimated that the total mass of the interplanetary dust is about 2.5×10^{19} g (for comparison, Ceres' mass[65] is 1.2×10^{24} g); the dust cloud is completely replenished on a time scale of about 1.7×10^{5} yr, and this requires that about 2×10^{14} g/yr has to be added. We get into the problem of the origin of the zodiacal cloud where the main question is whether these particles come from the comets or from the asteroids, or both. Previous knowledge of small particles, their occurrence and physical properties, is based primarily on Earth observations of meteoroids, comets, asteroids, and the zodiacal and counterglow light. (The word gegenschein, incidentally, has been replaced by counterglow throughout this book.) The counterglow measures have been taken to derive an upper limit to the debris in the asteroid region. The measures of meteoroid flux (number of particles per unit time) have been made by visual, photographic, and radar observations from the ground and by experiments in sounding rockets, satellites, and space probes. None of these observations measure meteoroid flux as a function of mass directly. Light intensity is the usual parameter observed from the ground. It is interpreted through empirical relations from other data and by theory to determine meteoroid mass and velocity distribution. The best information to date comes from photographic observations. The meteor population so determined is subject to error because of several limitations in the data: Only Earth-crossing meteoroids are observed, a restricted range of masses is covered, conversion of luminosity to mass is uncertain, and the meteoroid composition is not well defined. The estimated mass range of the photographic meteors is 10^{-3} g or larger. The velocity of meteoroids can be obtained by reflecting a radar beam from ionized meteor trails. Interpretation of these data requires a theoretical relation between meteor ionization and mass. Because of selection effects, however, radar observations are considered less reliable than photographic measures. The estimated mass range for the radar measures is 10^{-6} to 10^{-2} g.

Acoustic impact and penetration sensors[66] on space-borne missions measure some product of mass and velocity. Penetration sensors probably give a more accurate description of meteoroid flux than either photography or radar. But the interpretation of physical damage to the sensors is subject to errors in the conversion from sensor thickness to meteoroid mass. There remain unresolved problems in the interpretation of the acoustic impacts also.

Surface brightness of the zodiacal light[67] is measured as a function of the angular distance from the Sun. The size distribution deduced from these data is

---

[64]See p. 395.
[65]See p. 33.
[66]See pp. 366 and 607.
[67]See pp. 377 and 363.

usually in vast disagreement with distributions determined by other techniques because different assumptions have been made. Nevertheless, recent spatial densities from penetration satellites, when extrapolated, are consistent with the zodiacal light results.

The large meteoroids ranging in mass from a few kilograms to 10^6 kg may be of asteroidal origin. It is difficult to derive the meteoroid flux from "falls." The flux value depends on the probability of seeing the "fall" and establishing the relation between the mass found and the original mass. Both cometary and asteroidal meteoroid orbits contain selection effects. The photographic measures show two peaks in a typical distribution relative to Earth. The second peak is attributed to meteoroids in retrograde orbits because their higher rate of entry is more easily detected than the slower moving, direct orbits. This selection effect distorts meteor numbers in both distance and velocity and is inherent in the photographic technique. Among the average velocities so determined are 20 km/s by Dohnanyi (1966), 17 km/s by Kessler (1969) for a gravitational Earth and 15 km/s for a nongravitational one, 19 km/s by Dalton (1965), 22 km/s by Whipple (1963), and 30 km/s by Burbank et al. (1965). Radar measurements do not exhibit the bimodal shape of the velocity distribution of the photographic measures. The high-velocity peak is not attained because the more numerous small meteors have a diffuse, ionized wake. Before removing selection effects, the investigators at the Smithsonian Astrophysical Observatory get a higher average velocity from radar measurements.

Kessler computes the probability of finding an asteroid at a given distance from the Sun. He has also flux levels for calculating the hazard to interplanetary flight; he gives the flux for interplanetary missions as 10^{-16} g/cm^2/s. Near Earth, protection from 0.02 g particles is required, although encounters with particles as large as 200 g are possible. Kessler has used the counterglow to place an upper limit on the spatial density of the asteroidal debris and he gives the flux measured by Pegasus and Explorer satellite penetration experiments as reported by Naumann as the best estimate. The density of debris may be enhanced in the asteroid belt, but at 2.5 AU the lower velocity causes the penetration flux to be comparable to that at Earth. (See also the paper by Whipple.[68])

According to Öpik (1968), the origin of those centimeter- to meter-size stony and nickel-iron fragments of interplanetary stray bodies, which have survived the passage through Earth's atmosphere and are now preserved in museums, is at present most commonly ascribed to the asteroid belt. The Lost City meteorite (McCrosky, 1970), whose orbit was calculated from photographic observations to have an aphelion of 2.35 AU, supports this assumption. If indeed the collision probability in the asteroid belt is high enough, a large number of fragments of all sizes result. With an orbital change, presumably obtained in the collision, these might be diverted to Earth's space.

[68]See p. 389; Kessler's paper is on p. 595.

Öpik (1968) discussed the statistics of inclination and eccentricity for several classes of small bodies. The statistics of true meteorite orbits are very incomplete because of the difficulty of obtaining satisfactory observations. The existing evidence shows that when the meteorite orbits are compared to belt asteroids and the ones that cross Mars' orbit, they have inclinations too small for their high eccentricities. The Mars and belt asteroids, on the other hand, have average eccentricities that are too small for their corresponding inclinations. Absence of dilution (equipartition) among the Mars-orbit-crossing asteroids implies insignificant perturbations during the age of the solar system.

The periodic comets set a lower limit to meteorite debris input. Their orbital elements have remarkable similarity and their repeated revolutions in a short period must make a considerable contribution to the debris in the solar system. This may even exceed that from the "almost parabolic" members of the cometary cloud that are not periodic; these surround the solar system. For meteoroids it is worth noting that because of their ablation and breakup in the atmosphere, the low-velocity objects are strongly favored by the selection process. But, for the fireballs this selection effect does not work and their low relative velocities cannot be explained solely by this means; they may form a real, physically unique population.[69]

LAUNCH VEHICLE AND PROPULSION REQUIREMENTS FOR ASTEROID MISSIONS

A program for exploration of an asteroid may be as important as exploration of the planets in order to study a primitive stage in the development of the solar system. As an aside, the satellites of Mars, Phobos and Deimos, comparable in size to asteroids, also are interesting objects in their own right;[70] Hills[71] made the prediction that few impact craters will be found on the satellites of Jupiter. A great debate[72] ensued over the timing of asteroid missions as there are so many preparatory ground-based studies still to be performed.

A flight to a near asteroid might be a flyby,[73] a rendezvous,[74] an orbiter, or a sample-return[75] mission. The mission might involve a man[76] or it might be completely automated. The precise launch vehicle and propulsion requirements will vary as a function of the mission objectives and the weight of the scientific package required to obtain the objectives. Some of the planning aspects for an asteroid mission are reviewed[77] and a specific mission is described.[78] A few examples of scientific experiments in the Pioneer program are reviewed[79] and a beginning with specific suggestions was made.[80]

The difficulty with all ground-based observations of the asteroids is the lack of resolution on the surface so that the need is obvious for flyby missions to

[69]See p. 447.
[70]See p. 399.
[71]See p. 225.
[72]See pp. 473 and 479.
[73]See p. 527.
[74]See p. 503.
[75]See p. 513.
[76]See p. 539.
[77]See pp. 489 and 561.
[78]See p. 543.
[79]See pp. 607, 617, and 633.
[80]See p. 561.

take detailed pictures and to make photometric and polarimetric measurements over a wide spectral range. The range of phase angle attained during a flyby is much greater than that from Earth. A space-probe landing should be instrumented to study the surface in detail and collect samples that give precise information on the structure and composition of the asteroid.

An unmanned flyby of a near asteroid would be the least demanding of the various asteroid missions and could be accomplished with presently available launch vehicles (e.g., Atlas/Centaur) and a Pioneer-type spacecraft[81] weighing approximately 200 kg. The flight time for this mission would be approximately 100 days and the communication distance at encounter would be about 0.5 AU. This flyby mission would have a 40 day launch window and would be a relatively inexpensive space mission.

The unmanned rendezvous and/or orbiter mission[82] would require additional propulsion capability beyond that indicated for a flyby. This increased propulsion capability could be supplied by either a high-performance chemical-propulsion stage or a solar electric-propulsion[83] system utilized as the final stage for the Atlas/Centaur, Titan IIIC, or Titan IIID/Centaur launch vehicle. An asteroid rendezvous mission to Icarus or Geographos could be accomplished using a solar electric-propulsion system optimized for use with a Titan IIID/Centaur launch vehicle. The net spacecraft mass for a rendezvous with Geographos would be 1800 kg. The departure date for this Geographos rendezvous could be in August 1977 and the related flight time would be about 650 days. The reference power for the solar electric-propulsion system would be 40 kW and rendezvous would take place at about 1.1 AU. The departure date for an Icarus rendezvous could be in September 1978 with a flight time of some 670 days.

An asteroid rendezvous mission[84] is a relatively high-energy mission and would cost an order of magnitude more than a simple flyby of either Icarus or Geographos. An unmanned sample-return mission[85] would require a launch vehicle of even higher performance than for the rendezvous mission (e.g., Saturn V with appropriate upper stage). The amount of scientific information that could be collected from such a mission would, of course, be considerably greater in kind and quantity of data obtained.

A manned expedition[86] to a near asteroid would undoubtedly benefit from the availability of a space nuclear-power capability. A nuclear electric capability could be used to provide the power needed to propel an electric-propulsion spacecraft and/or to meet the onboard power requirements for the astronauts and their scientific instruments. Thermal nuclear rocket propulsion, when available, should provide an increase in performance over that presently obtainable from a comparable chemical stage. This increased performance would be most useful in accomplishing a manned exploration mission to an asteroid.

---

[81]See p. 612.
[82]See p. 503.
[83]See p. 489.
[84]See p. 503.
[85]See p. 513.
[86]See p. 539.

Any mission to an asteroid in this decade will probably use the current U.S. space transportation system. (See fig. 1.) At the end of this decade, however, if an operational space shuttle is available, missions to selected asteroids could be accomplished in part using this potentially cost-effective mode of transportation. When the space shuttle mode of transportation is used, appropriate upper stages will be required to operate in conjunction with the shuttle to accomplish an asteroid mission. These upper stages might be presently available ones (e.g., Centaur, Agena, Transtage, etc.), or entirely new stages designed to be used with the space shuttle (e.g., space tug, versatile upper stage, etc.). Mission requirements and the availability of an operational shuttle will dictate the appropriate transportation system to be used in accomplishing a mission to an asteroid.

In summary, it is seen that the initial mission to an asteroid might be a flyby of Eros or Geographos. This flyby could be followed by an automated orbiter or rendezvous mission making television or spin-scan imaging and photo-polarimetric reconnaissance of the asteroidal surface. The orbiter could be appropriately followed by an automated sampling and return to Earth of selected asteroidal rocks. This automated mission could be followed by a manned mission to a suitable asteroid. Such a mission approach would represent a logical step-by-step sequence of exploration.

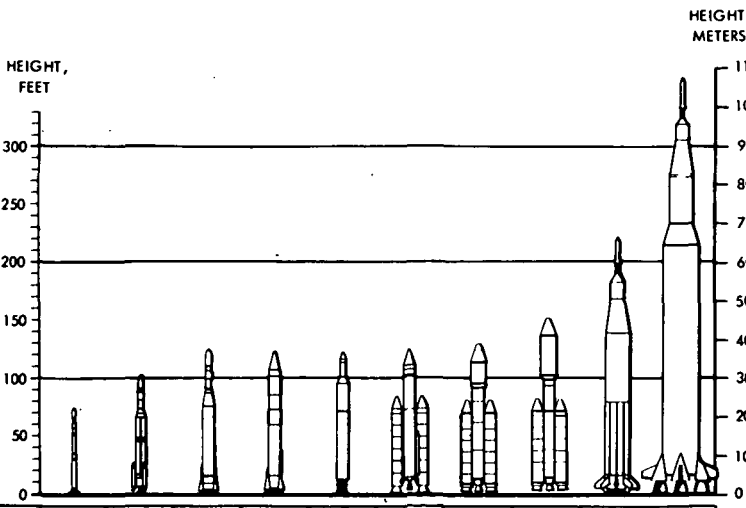

VEHICLE	SCOUT	LONG TANK THAT DELTA	ATLAS-AGENA D	ATLAS-CENTAUR	TITAN IIIB* AGENA	TITAN IIIC	TITAN IIID	TITAN IIID CENTAUR	SATURN IB	SATURN V
PAYLOAD-KG (185 KILOMETERS)	180	1130	3810	5100	4100	12 200	13 600	15 900**	18 600	118 000
PAYLOAD-KG (MARS-VENUS)	-	230	320	730	410	1270	-	3860	-	36 300

PAYLOAD VALUES ARE FOR EAST LAUNCH FROM ETR EXCEPT FOR SCOUT WHICH IS FROM WALLOPS
*NO LAUNCH FACILITIES AVAILABLE FOR TITAN IIIB AT ETR
**CENTAUR STAGE REQUIRES STRUCTURAL MODIFICATION FOR 15 900 KG PAYLOAD PRESENT CAPABILITY DUE TO STRUCTURAL LIMIT IS 6360 KG

Figure 1.–Current U.S. space transportation system.

Toward the end of the book, the topics return to the ones with which it started–ephemerides[87] and telescopic observation[88]–but this time more specifically having the future needs of the space program in mind. Finally there is a summary of the colloquium in terms of what appears urgent and interesting to do in the future.[89]

SOURCE BOOKS ON ASTEROIDS

Astronomical textbooks generally have only a few pages on minor planets; the asteroids are treated somewhat as "vermin of the sky." To a stellar astronomer who gets trails made by moving asteroids on his long-exposure plate they, indeed, must be a nuisance. Incidentally, space junk is also becoming an increasing problem;[90] an extension of the *National Geographic-Palomar Atlas* to the Southern Hemisphere, for instance, will be seriously hampered by long trails.

The new book by Hartmann (1972) has a good review chapter on asteroids. Krinov (1956), Watson (1962), and Roth (1962) have written brief semipopular reviews; Roth's historical section is a delight. There are articles written by Harwood (1924) and Arend (1945), but they are out of date. As inaccessible to readers in the United States as Arend's writing is the book by Putilin (1953), which is not too serious because it is mostly a review of certain procedures in positional work.

A semipopular introduction to the Trojan planets has been made by Wyse (1938) and Nicholson (1961). Short articles on asteroids have been written by Nicholson (1941), Porter (1950), Struve (1952), Miller (1956), and Ashbrook (1957). A splendid article on asteroids was written by Richardson (1965). The literature on asteroids and comets was reviewed recently (Gehrels, 1971). Summary reports of this colloquium have been made by Matthews (1971) and Hartmann (1971).

REFERENCES

Arend, S. 1945, Quelques Aspects du Problème des Astéroïdes. Editions l'Avenir. Brussels. Also, Ciel Terre 9-12, 1945.

Ashbrook, J. 1957, Naming the Minor Planets. Sky Telescope 17, 74-75.

Bos, W. H. van den, and Finsen, W. S. 1931, Physical Observations of Eros. Astron. Nachr. 241, 329-334.

Burbank, P. B., Cour-Palais, B. G., and McAllum, W. E. 1965, A Meteoroid Environment for Near Earth, Cislunar and Near-Lunar Operations. NASA TN D-2747.

Dalton, C. C. 1965, Statistical Analysis of Photographic Meteor Data, Part II: Verniani's Luminous Efficiency and Supplemented Whipple Weighting. NASA TN-X-53360.

Dohnanyi, J. S. 1966, Model Distribution of Photographic Meteors, pp. 340-341. Bellcomm, Inc.

Gehrels, T. 1970, Photometry of Asteroids. Surfaces and Interiors of Planets and Satellites (ed., A. Dollfus), ch. 6. Academic Press, Inc. London and New York.

---

[87]See p. 639.
[88]See p. 643.
[89]See p. 653.
[90]See p. 649.

Gehrels, T. 1971, Asteroids and Comets. Int. Union Geodesy Geophys. Rept. Trans. Amer. Geophys. Union **52**, 453-459.

Gehrels, T. 1972, Physical Parameters of Asteroids. From Plasma to Planet. Proc. Nobel Symp. no. 21. Nobel Foundation. Stockholm.

Hartmann, W. K. 1968, Growth of Asteroids and Planetesimals by Accretion. Astrophys. J. **152**, 337-342.

Hartmann, W. K. 1971, Asteroids and Planetesimals. Icarus **15**, in press.

Hartmann, W. K. 1972, Planetary Science. Bogden & Quigley, Inc., Pub. Tarrytown-on-Hudson, in press.

Harwood, M. 1924, Variations in the Light of Asteroids, Harvard Col. Observ. Circ. 269.

Hunter, R. B. 1967, Motions of Satellites and Asteroids Under the Influence of Jupiter and the Sun. II. Asteroid Orbits Close to Jupiter. Mon. Notic. Roy. Astron. Soc. **136**, 267-277.

Kessler, D. J. 1969, Average Relative Velocity of Sporadic Meteors in Interplanetary Space. AIAA J. 7(12), 2337-2338.

Krinov, E. L. 1956, Dwarf Planets. State Publication of Technical-Theoretical Literature. Moscow.

McCrosky, R. E. 1970, The Lost City Meteorite Fall. Sky Telescope **39**, 154-158.

Matthews, M. S. 1971, The Asteroid Conference in Tucson. Sky Telescope **42**, 22-24.

Miller, T. W. 1956, The Classification of the Minor Planets by the Elements. J. Brit. Astron. Ass. **66**, 97-102.

Nicholson, S. B. 1941, The Countless Asteroids. Leaflet no. 147. Publ. Astron. Soc. Pac.

Nicholson, S. B. 1961, The Trojan Asteroids. Leaflet no. 381. Publ. Astron. Soc. Pac.

Öpik, E. J. 1968, The Cometary Origin of Meteorites. Ir. Astron. J. **8**, 197.

Porter, J. G. 1950, The Minor Planets. J. Brit. Astron. Ass. **61**, 4-15.

Putilin, I. I. 1953, Minor Planets. State Publication of Technical-Theoretical Literature. Moscow.

Richardson, R. S. 1965, The Discovery of Icarus. Sci. Amer. **212**(4)

Roth, G. D. 1962, The System of Minor Planets. Faber & Faber, Ltd. London.

Struve, O. 1952, The Minor Planets. Sky Telescope **11**, 163-166.

Watson, F. G. 1962, Between the Planets, revised edition. Doubleday & Co., Inc. Garden City, N.Y.

Whipple, F. L. 1963, On Meteoroids and Penetration. J. Geophys. Res. **68**(17), 4929-4939.

Whipple, F. L. 1967, On Maintaining the Meteoritic Complex. The Zodiacal Light and the Interplanetary Medium (ed., J. L. Weinberg), pp. 409-426. NASA SP-150.

Wyse, A. B. 1938, The Trojan Group. Leaflet no. 114. Publ. Astron. Soc. Pac.

PART I

OBSERVATIONS

Page intentionally left blank

ASTROMETRIC OBSERVATIONS

ELIZABETH ROEMER
University of Arizona

If one wants to study the physical characteristics of individual asteroids, he must first find them and be prepared to track them accurately during observation. To make the necessary predictions, the positions of asteroids are measured in reference frames defined by stars of known coordinates as the input information for calculation of orbits and ephemerides. Continuation of positional observations over lengthening arcs provides the basis for improvements of orbits and increased accuracy of ephemerides.

Direct photographs, from which positions relative to background stars are measured, may be made with relatively short-focus instruments of wide field. Astrographs with multicomponent lenses of various designs or catadioptric systems of the Schmidt or Maksutov type are in common use. Typical instruments have fields of several degrees diameter and reach to 16 to 17 mag on plates of scale 1 to 3 arcmin/mm. The overwhelming majority of astrometric observations of minor planets are obtained with such instruments. On a wide-field plate, images of a number of minor planets are usually found in all ecliptic fields; with powerful instruments the number may be very large.

A limited number of faint objects of compelling interest may be observed with powerful long-focus instruments such as the 154 cm *f*/13.5 NASA reflector of the Catalina Station of the Lunar and Planetary Laboratory. Observations of objects as faint as 20 to 21 mag can be obtained with this instrument, but the limited field (30′ at scale 10 arcsec/mm in the focal plane) restricts its practical use to special objects for which a fairly reliable prediction of position (within 5′ to 10′) can be made.

Particularly for faint objects observed at long focal length, it is nearly essential that the motion of the asteroid be compensated during the exposure. On plates taken by this "Metcalf method," star images appear as trails whose length corresponds to the amount of the differential motion during the exposure. The asteroid of perfectly matched motion appears as a small round dot. If asteroids are relatively bright, or the optical system very fast, exposures may be guided carefully on a star, in the same way as for conventional astronomical photography. The moving object will almost invariably appear elongated to some degree on plates taken by this "Wolf method."

Identification of moving objects on long-focus plates is usually a trivial matter, for normal exposure durations and scale in the focal plane lead to conspicuous displacements. For observations made with wide-field instruments of short focal ratio, it may be necessary to examine pairs of plates rather carefully with a blink comparator to locate all objects of interest. This process may be very tedious, often taking many times longer than acquisition of the plates at the telescope. Even when they are not needed for blink examination, there are many advantages of taking plates in pairs. Photographic defects can be recognized immediately, the reality of near-threshold images is easily tested, and a check on identification of the asteroid as well as on reduction calculations is obtained through comparison of the observed and calculated motions.

Although automatic measuring engines are being used to an increasing degree in measurement of astronomical plates, most such machines are limited in the dimensions of images with which they can deal. This limit is typically of the order of 250 μm. Thus images of moving objects, or of stars on plates taken by the Metcalf method, presently require hand measurement. In our normal procedure, whenever images are sufficiently elongated to degrade the accuracy of direct bisection, the ends of the trails are measured instead. The mean is then taken as representing adequately the position of the star (or of the moving object) at the midexposure time. In exceptional cases of very rapid motion, we have interrupted the exposure for some seconds at the midtime to produce an astrometric reference point. This procedure was followed, for example, on the recovery plates of 1566 Icarus in June 1968. On those plates the motion during the 8 min of exposure needed at the Catalina 154 cm telescope to produce recognizable images of the minor planet, then of 16 to 17 mag, led to star trails 16 mm long.

For hand measurement of plates of ordinary good quality, projection-type measuring engine viewing systems are generally quite satisfactory. But for plates of inferior image quality—heavily fogged in moonlight, weakly exposed, or distorted images—machines arranged for direct viewing by a monocular or binocular microscope provide far better control over contrast and image visibility.

Although it may be unnecessary to mention it, it has occasionally been forgotten that the *time* of the observation is as essential to an astrometric observation of a solar system object as are the coordinates of right ascension and declination. The *mean* of the beginning and end times of the exposure is the appropriate parameter. The accuracy needed in the time will depend upon the rate of motion, but it is conventional to give an accuracy of 1 s unless the rate of motion is such as to make that insufficient.

Reductions of position are made with respect to background stars for which coordinates are available from an appropriate catalog. On wide-field plates, sufficient stars for reduction can almost invariably be found in such a source as the very convenient Smithsonian Astrophysical Observatory (SAO) *Star*

Catalog (1966). This catalog contains the positions and proper motions of 258 997 stars (an average of 6 deg^{-2} over the sky) for the epoch and equinox 1950.0, compiled from a considerable number of fundamental and zone catalogs and reduced, insofar as possible, to a homogeneous system, that of the FK4. Charts are available (SAO, 1969) that greatly facilitate identification of reference stars.

A catalog such as the SAO *Star Catalog* does not contain enough stars to give an adequate reference frame within the very limited field of long-focus reflectors. Further, zone stars will usually be too bright to measure on plates taken for objects of 17 to 21 mag. The many volumes of the *Astrographic Catalogue* (see the brief description by Van Biesbroeck, 1963), the joint enterprise of a number of observatories, may provide a satisfactory reference star system for such plates. As an alternative, it may be necessary to determine coordinates of a suitable set of reference stars by measurement with respect to zone stars on a wide-field plate.

Appropriate procedures to make the transformation from rectangular coordinates measured on the plates to the astronomical coordinates of right ascension and declination depend on the geometry of the projection of the sky onto the photographic plate or film, and thus on the nature of the telescope optical system. Many detailed treatments of this problem have been published; a general review of the standard procedures has been given by König (1962). Over limited fields, even with Schmidt cameras, the linear transformation between measured and tangential coordinates may give satisfactory results. If reductions to high accuracy are required over large fields, more sophisticated procedures may be required. It may be necessary to represent more accurately both the projection geometry and the correction terms that stem from imperfect adjustment of the optical system, variations of refraction and stellar aberration across the field, scale differences arising from color variations among stars, optical aberrations of the telescope, and the like. The field correctors often used with long-focus Cassegrain telescopes, and the field flatteners used with Ritchey-Chrétien telescopes, characteristically introduce a radial scale term that can be fairly large. For examples of recent discussions of these more complex astrometric problems, see Dixon (1962, 1963), Eichhorn et al. (1970), and Kristian and Sandage (1970).

No matter what the source of reference stars and the reduction procedure, it is highly desirable to introduce redundancy into the solution for checking purposes. Even such gross mistakes as misidentification of reference stars do sometimes occur. In the vast work of the *Astrographic Catalogues* (AC or sometimes, somewhat incorrectly, CdC), misprints in both star coordinates and plate constants can be found. Because some plate epochs are as remote as the 1890's, accumulated proper motions are a principal source of error, often leading to residuals of individual stars of 1″ to 2″ from a "best" solution. The epochs of observation of the reference stars from which the *Catalogue* preliminary plate constants were determined, usually without correction for

proper motion to the epoch of the AC plates, were even more remote. This situation is being remedied for the northern sky as good proper motions for the reference stars become available with completion of the AGK3. New plate constants for the *Astrographic Catalogue* zones north of +40° have been published by Günther and Kox (1970*a*,*b*), and for the zone from +35° to +40° by Eichhorn and Gatewood (1967). Work on zones south of +36° (to -2°), under the direction of P. Lacroute, is progressing as results from the AGK3 become available. Improvement in the southern hemisphere will have to await improvement of the observational histories of stars defining the fundamental coordinate system.

The use of field plates for determination of coordinates of intermediate reference stars in a good modern catalog system would give a higher accuracy than direct use of the *Astrographic Catalogue* for reduction of long-focus plates. The labor involved in the measurement and reduction is significantly greater, however; and because it would be necessary to acquire the additional plate material with a different instrument, immediate measurement and reduction might be precluded in some circumstances. By such methods one could, in principle, aim for positions good to something like ±0".5 in special cases in which improvement in accuracy might be critical for success of space missions. It would be useful to have available a list (hopefully short) of potential targets for which high accuracy might be required.

REFERENCES

Dixon, M. E. 1962, 1963, Astrometry With a Schmidt Camera. Mon. Notic. Roy. Astron. Soc. (S. Africa) **21**, 180-186 and **22**, 6-10, 32-36.

Eichhorn, H., and Gatewood, G. D. 1967, New Plate Constants for the Northern Hyderabad Zone (+35° to +40°) of the Astrographic Catalogue, in Part Computed by the Plate Overlap Method. Astron. J. **72**, 1191.

Eichhorn, H., Googe, W. D., Lukac, C. F., and Murphy, J. K. 1970, Accurate Position of 502 Stars in the Region of the Pleiades. Mem. Roy. Astron. Soc. **73**, 125-152.

Günther, A., and Kox, H. 1970*a*, Tables of Definitive Plate Constants for the Zones Greenwich, Rome-Vatican, Catania, Helsingfors of the Astrographic Catalogue [Carte du Ciel]. Astron. Astrophys. Suppl. Ser. 3(2), 85-180.

Günther, A., and Kox, H. 1970*b*, Definitive Plate Constants for the Astrographic Catalogue North of +40° Declination. Astron. Astrophys. **4**, 156-158.

König, A. 1962, Astrometry With Astrographs. Astronomical Techniques (ed., W. A. Hiltner). Stars and Stellar Systems (eds., G. P. Kuiper and B. M. Middlehurst), vol. II, ch. 20. Univ. of Chicago Press. Chicago.

Kristian, J., and Sandage, Allan. 1970, Precise Position of Radio Sources, II. Optical Measurements. Astrophys. J. **162**, 391-398.

Smithsonian Astrophysical Observatory. 1966, Star Catalog, vols. 1-4, Publ. 4652. Smithsonian Institution. Washington, D.C.

Smithsonian Astrophysical Observatory. 1969, Star Atlas of Reference Stars and Nonstellar Objects. MIT Press. Cambridge.

Van Biesbroeck, G. 1963, Basic Astronomical Data (ed., K. Aa. Strand). Stars and Stellar Systems (eds., G. P. Kuiper and B. M. Middlehurst), vol. III, app. I, p. 471. Univ. of Chicago Press. Chicago.

DISCUSSION

BRATENAHL: How precisely could the positions of an asteroid—Eros, for instance—be measured?

ROEMER: It would be reasonable to go to 0".5, or possibly even to 0".2, if circumstances justified the special effort that would be necessary.

Page intentionally left blank

THE WORK AT THE MINOR PLANET CENTER

PAUL HERGET
Cincinnati Observatory

The Minor Planet Center at the Cincinnati Observatory is engaged in three kinds of activities: (1) the publication and distribution of the Minor Planet Circulars (MPC's), (2) the collection and maintenance of a complete file of minor planet observations, and (3) the computation of orbital elements and ephemerides.

The MPC's are single, looseleaf sheets, printed on both sides, containing (1) all observations of minor planets as reported to us by the various observatories, (2) orbital elements and residuals of differential corrections, and (3) ephemerides of minor planets not included in the annual ephemeris volume published by the Institute of Theoretical Astronomy in Leningrad. The MPC's were started in 1947; their number reached 1000 by November 20, 1953; 2000 by May 9, 1960; and 3000 by October 1, 1969. The mailing distribution list contains about 125 foreign and 65 domestic addresses, mostly astronomical observatories and libraries. A small supply is preserved for future uses. At present the material is prepared on punched cards and proofread in advance. Multilith master sheets are then printed directly from a magnetic tape on the IBM 1401.

The minor planet observation file is now maintained on magnetic tape, and there is also a complete file of punched cards in storage. It is intended to be complete since 1939, and it also contains all previous observations that we have had occasion to keypunch and use, mostly in carrying out well-determined differential corrections over an arc of many years. Each observation contains the planet's number or provisional designation; the time of observation in U.T.; $\alpha(1950.0)$; $\delta(1950.0)$; a three-digit observatory code; and provision for magnitude, residuals, 10-day motion, and a reference. On the magnetic tape these data are sorted in order of planet number and date. The total now exceeds 130 000. We have standard programs that permit us to print and/or punch all the observations between any given pair of limits, to print and/or delete any specific observation, and to add new or corrected observations. Because the more than 12 000 observations of the *Palomar-Leiden Survey of Faint Minor Planets* (van Houten et al., 1970) consist mostly of faint objects that may never be observed again, they have not been included in this file unless they have been identified with some otherwise known object. We then

use the provisional designation, NNNN P-L, where NNNN is the four-digit number (greater than 2000) that has been assigned in the Palomar-Leiden survey. All the observations of the survey are in storage and available on punched cards.

Preliminary orbits of newly discovered objects, extending over a heliocentric arc of not more than 90°, are computed by the variation of geocentric distances (Herget, 1965). This method has the advantage of incorporating all the available observations simultaneously; and if there is a sufficient number of observations, it is not subject to any critical cases. In the event that the observations as given are dynamically inconsistent for any reason, the solution quickly iterates to zero.

The differential correction of an orbit based on observations extending over a long arc requires the computation of a trajectory that includes accurate perturbations by all the major planets. During the years 1955 to 1967 these computations were performed on the calculator at the Naval Ordnance Research Center, Dahlgren, Va., by the method of variation of arbitrary vectorial constants (Musen, 1954). The resulting orbit for each completed planet was then carried forward so as to produce on microfilm all the ephemerides until A.D. 2000. These ephemerides have an interval of 10 days; they include the heliocentric and geocentric distances and the phase angle; and they extend to 8 hr elongation on either side of the Sun. This work was completed for 465 minor planets, and we have approximately 12 000 future ephemerides on file. For a few years we also had the computations organized for the IBM 1410, using the method described in Herget (1962). This proved to be more effective, because the program had no singularity for very small eccentricities. At present we compute on the IBM 360 by means of Cowell's method, using J. Schubart's N-body program, and the latter has been augmented to include the integration of the variational equation for the six usual starting values and two optional variable planetary masses. The output of this program is coordinated directly with the differential correction program.

We continue to examine all observations for possible identifications, as witness Bardwell's recent success in identifying 155 Scylla. Currently we are engaged in providing various special ephemerides for the physical observation of selected minor planets and for using some minor planets in lieu of standard stars in stellar spectroscopic observations.

For the past 10 yr we have provided a plate reduction service for all who may wish to use it. We have 300 000 comparison stars on magnetic tape, taken from the Yale Zones, the AGK2, Cape Photographic Durchmusterung, etc., as provided in machine-readable form by the U.S. Naval Observatory. We have reduced hundreds of plates taken and measured at Indiana, Tokyo, and Nice, and lesser numbers at other observatories. This program includes various checks, it exhibits the root-mean-square error of the comparison stars and thereby affords an estimate of the accuracy of the position of the minor planet.

The orbits of nearly all of the ordinary, numbered minor planets are now of good quality. At the Cincinnati Observatory we have an operational capability to handle all the classical situations that might arise, and we propose to continue this posture in the future.

In the following appendix, the work at the Institute of Theoretical Astronomy at Leningrad and the cooperative program with the Cincinnati Observatory is described.

APPENDIX–THE WORK AT THE INSTITUTE OF THEORETICAL ASTRONOMY AT LENINGRAD

In the absence of Dr. Chebotarev who was unable to attend this meeting, I shall attempt to present a summary based upon our long and fruitful collaboration over the last quarter century, beginning with Professor Subbotin and continuing with N. S. Yakhontova, Dr. Makover, and now Dr. Chebotarev. Shortly after the end of World War II, the Institute of Theoretical Astronomy (ITA) undertook the publication of an annual ephemerls volume of all numbered minor planets to provide for the function formerly served by G. Stracke's (1942) *Kleine Planeten.* To avoid duplication of effort, Dr. Dirk Brouwer arranged an agreement in 1952 whereby ITA undertook to accept and incorporate all ephemerides transmitted by the Cincinnati Observatory and to provide for the computation of all the remaining ephemerides. In return, the Cincinnati Observatory receives 150 copies of the ephemeris volume annually. This has proved to be the beginning of an excellent cooperative program.

About 1961 Yakhontova provided a list arranged into four groups of all the numbered minor planets: (1) those for which ITA could provide reliable, accurate ephemerides; (2) those for which the ephemerides were based upon approximate perturbations by Jupiter only; (3) those for which the ephemerides were based only upon elliptic elements without perturbations; and (4) those for which no ephemerides were being computed. The computations that were undertaken at the Cincinnati Observatory were therefore selected from the last two groups. This division of labor has resulted in the computation of orbits and ephemerides for somewhat more than two-thirds of all the numbered minor planets being undertaken by the ITA.

As better electronic computing machines were developed over the last decade, more and more differential corrections were performed, first including only approximate perturbations by Jupiter, and more recently including accurate perturbations by all the major planets. These improved elements provide more reliable ephemeris predictions. Also, in recent years extended ephemerides have been published for a selected list of the brighter minor planets. Beginning last year, the interval covered by each regular ephemeris has been extended from 50 to 70 days in length.

In August 1970, ITA celebrated the dedication of its own BESM 4 electronic computer by being host to the IAU Colloquium on the Origin and Nature of Comets. More than 30 international guests were in attendance. In

recent years, ITA has directed a minor planet observing program on the 40 cm astrograph at the Crimean Astrophysical Observatory. All the computations of the plate reductions are performed at ITA. More than 1000 observations per year are provided by this program. The theoretical studies on general perturbation methods, improved orbit computing methods, investigations of cometary orbits, etc., are referenced in the triennial report of Commission 20 in the *Transactions of the IAU.*

REFERENCES

Herget, P. 1962, On the Variation of Arbitrary Vectorial Constants. Astron. J. 67, 16-18.
Herget, P. 1965, Computation of Preliminary Orbits. Astron. J. 70, 1-3.
Houten, C. J. van, Houten-Groeneveld, I. van, Herget, P., and Gehrels, T. 1970, Palomar-Leiden Survey of Faint Minor Planets. Astron. Astrophys. Suppl. 2, 339-448.
Musen, P. 1954, Special Perturbations of the Vectorial Elements. Astron. J. 59, 262-267.
Stracke, G. 1942, Über die geometrischen Grössen und die Masse der Kleinen Planeten. Astron. Nachr. 273, 24-28.

DISCUSSION

BANDERMANN: The observed magnitude of the asteroid at discovery may be different at a time of later search for that asteroid due to rotation, etc. Is that considered?

HERGET: The magnitude is used only as an approximate identification criterion.

DUBIN: How well do we know the asteroids for which there are orbital elements?

HERGET: Of those that are numbered, none of them are going to be lost any more; but there are some old numbered ones that cannot be recovered.

THE USE OF ASTEROIDS FOR DETERMINATIONS OF MASSES AND OTHER FUNDAMENTAL CONSTANTS

EUGENE RABE
Cincinnati Observatory

This report does not attempt to review all past and present work using asteroids for determinations of planetary masses and other fundamental constants. This would be a very large undertaking, and too extensively outside of the scope of a colloquium devoted to physical studies of minor planets. It seems preferable to concentrate more on principles involved, while mentioning only some of the various results obtained. At the same time, it will be appropriate to take note of the changed situation resulting from the recent development of certain modern methods and facilities that make it possible to determine some of the constants more accurately in other ways, thus partly eliminating the once dominant role of the minor planets.

DETERMINATION OF PLANETARY MASSES

Because the orbital motion of any planet or other body in the central gravitational field of the Sun is influenced also by the perturbing gravitational forces of the major planets, it is evident at once that in principle it is possible to determine the masses of these disturbing planets from a careful comparison of the computed and observed motion of the selected object. In most cases, provisional but already fairly good values of the masses, orbital elements, and other unknowns involved can be used as the basis of such a comparison, and thus the quantities to be determined will be corrections to the provisional values. Generally, therefore, it will be sufficient to establish linear observation equations relating the sought-for corrections with the residuals, observation minus calculation, or $O - C$. None of the actual equations relating the various unknowns and the computed positions will be given or derived in this descriptive report, which emphasizes general principles and aspects rather than the too numerous procedural details involved.

The accuracy or even feasibility of any mass determination will depend, of course, aside from the computational or analytical precision of the orbits involved, first, on the magnitude of the perturbations produced by the mass that one wants to improve and, second, on the accuracy as well as the adequate number and distribution of the observed positions. The orbits of the major

planets themselves, and extended series of observations of the Sun and the principal planets, have been available for a long time and have indeed been used for the determination of improved masses on the basis of their *mutual* attractions. The attainable accuracy has been rather limited, however, because until recently the degree of precision of the orbital theories of some of the major planets was not very high, and the comparative smallness of the perturbations involved magnified the relative seriousness of orbital theory defects in the resulting mass corrections. Also, on the observational side, the attainable accuracy of positions of the Sun and major planets is severely hampered by the difficulties inherent in ascertaining the observed coordinates of the centers of such disk-shaped and more or less diffuse objects. Asteroids, on the other hand, can be observed accurately and easily because of their lightpoint images, at least if they are relatively bright. As to their orbits, it is frequently possible to select minor planets that are strongly perturbed by one or several of the major planets, so that optimum conditions exist for the desired mass determinations, provided that well-distributed observations can be obtained. This proviso is important because corrections to the orbital elements of the asteroid in question must be determined simultaneously with the sought-for mass corrections. If the asteroid's heliocentric orbit remains poorly determined, for instance, because it can be observed only near perihelion, then the uncertainties of the orbital elements will unavoidably affect also those of the intimately related mass corrections.

An additional and rather important advantage of the use of asteroids arises from the fact that their own masses are completely negligible, compared to those of the major planets. When dealing with the variations produced in the orbit of an asteroid by the sought-for correction to the mass of a given major planet, one does not have to consider any second-order effects of these orbital changes on the motion of the disturbing or any other major planet, nor does one have to determine or correct the mass of the asteroid. Furthermore, one needs to analyze only the observations of the asteroid, regardless of the number of major planets whose mass corrections are introduced into the observation equations. In contrast to these simplifications, the $O - C$ of any major planet cannot normally be treated separately and independently from those of all the others whose orbits may be affected by the mass corrections involved in the solution. At least when considering substantial mass corrections, one also has to investigate the magnitude of any possibly noticeable second-order effects produced by the first-order orbital variations. It is true that for an asteroid with very large perturbations, a second iteration to the solution may be necessary if the orbital changes produced by the initial correction of the disturbing mass are also substantial, but this additional procedure is still limited to the same set of observations of just one object, even if several planetary masses are being corrected simultaneously.

For the reasons mentioned in the preceding two paragraphs, mass determinations using asteroid observations have long been considered to be more accurate and also more convenient than those using observations of major

planets and of the Sun. Recently, though, the availability of radar observations of Venus and Mercury has made it possible to increase greatly the accuracy with which the motions and masses of these planets and of Earth can be determined from solutions based on a combination of radar and optical observations of these inner planets and on rigorous numerical integrations of their motions. An even more striking increase in accuracy became apparent when the radio tracking data of the Mariner 2 and 4 space probes were analyzed to determine improved mass values for Venus and Mars, respectively. Obviously the high accuracy with which the very large perturbations produced by the close approaches can be observed by means of Doppler tracking data is superior to the accuracy obtainable from optical observations of even the most favorable asteroid orbits. In passing, it should be noted that the observed orbits of natural satellites can also be used, together with Kepler's third law, to determine the mass of the primary, but that in practice the observational difficulties have tended to limit the attainable accuracy rather severely.

CONSTANTS RELATED TO THE MOTION OF EARTH

So far only mass variations have been mentioned as affecting the observable motion of an asteroid, aside from any necessary corrections to its orbital elements. Because all observations are made from the moving Earth, any thorough analysis of the $O - C$ of asteroids approaching relatively close to Earth has to consider also the possible need for correcting some of the elements of Earth's orbit. In this connection, it should be noted again that corrections to the masses of disturbing planets will affect not only the motion of the asteroid under consideration but also the motion of the Earth-Moon barycenter. Consequently, the observation equation coefficients providing for such effects on the $O - C$ may have to be augmented by the relevant (normally much smaller) effects due to the adjusted *perturbations* of the Earth+Moon orbit. The basic elements for which corrections may be necessary are the mean longitude or mean anomaly at some zero epoch, the longitude of perihelion, the orbital eccentricity, and the obliquity (inclination) of the ecliptic relative to the equator. The mean motion or the semimajor axis, on the other hand, is known much more accurately from long series of observations of the Sun, while the longitude of the node on the equator is intimately connected with the basic definition of the fundamental reference system and thus with the effects of precession. The constants related to the reference frame will be considered in another section. Obviously, the four element corrections to be considered for the orbit of the Earth-Moon barycenter are easily introduced into the observation equations by the same principles as those to the elements of the asteroid orbit. It is evident that especially asteroids of the Eros type will be well suited for actual determinations of such corrections because of the magnification of their effects on the computed positions during all close approaches to Earth.

The orbital elements just considered are those of the Earth-Moon barycenter, while Earth itself moves about this barycenter in accordance with the Moon's orbital revolutions around Earth. Consequently, the geocentric position of any asteroid is also a function of the so-called constant of the lunar equation, which is the coefficient of the periodic displacement of an object at a distance of 1 AU in the plane of the Moon's orbit, caused by the motion of Earth's center about the barycenter (with the Earth-Moon distance equal to its mean value). This constant L can therefore also be determined from asteroid observations, in particular from $O - C$ of asteroids like Eros or Amor during close approaches. L in turn is related to the Moon/Earth mass ratio μ through an equation involving also the parallaxes of Sun and Moon. Because these parallaxes were supposed to be known more accurately than μ, many determinations of μ have been made by deriving L from close-approach residuals of minor planets and then calculating μ from this equation. Today, however, μ is one of the primary constants in the newly adopted IAU system of fundamental constants, essentially because of its more accurate and more direct determination from radar observations and space probes, whereas L is now a derived constant. It still enters the computation of geocentric ephemeris positions of planets and asteroids, but it is pointless to try to improve it from observed asteroid residuals in right ascension and declination.

SOLAR PARALLAX AND ASTRONOMICAL UNIT

A similarly reversed situation exists today with regard to the solar parallax $\pi_\odot$ and the astronomical unit, which are related through the definition of $\pi_\odot$ as the angle subtended by Earth's equatorial radius R_e at a distance of 1 AU. (The mean distance of the Earth-Moon barycenter from the Sun does not equal 1 AU, but differs from it by a very small and well-defined amount.) Because asteroids are observed from locations on the surface of Earth, and not from its center, the resulting parallactic displacements on the sky are inversely proportional to the geocentric distance, and thus they increase again with the object's approach to Earth. Consequently, asteroids like Eros could be and have been used to determine $\pi_\odot$ in this fashion, by the "trigonometric method." The astronomical unit, expressed in meters, could then be calculated from $\pi_\odot$ and the known value of R_e. Today, however, radar observations of Venus are used, for instance, to determine its varying distance from Earth in meters (actually in light-seconds, converted into meters by means of the rather accurately known velocity of light). Because the interplanetary distances are well known in astronomical units, the comparison yields a relatively direct determination of the astronomical unit, and $\pi_\odot$ becomes a derived constant.

A very important relation between the mass $m_{\oplus+\mathbb{C}}$ of the Earth-Moon barycenter, the solar parallax $\pi_\odot$, and the Moon/Earth mass ratio μ results from the combination of two equations: the first one governing the acceleration of gravity at the distance R_e from Earth's center and the second one representing Kepler's third law for a particle moving around the Sun in

circular orbit at a distance of 1 AU. This relation can be used to compute $\pi_\odot$ and thus the astronomical unit from an improved mass $m_{\oplus+\mathbb{C}}$ of Earth and Moon, as obtained from the observed motion of an asteroid such as Eros or Amor. This approach is known as the "dynamical method" for determining $\pi_\odot$ and the astronomical unit from asteroid observations because it is actually a determination of $m_{\oplus+\mathbb{C}}$. Because μ enters the relation between $m_{\oplus+\mathbb{C}}$ and $\pi_\odot$ only in the form of a factor $1 + \mu$, the uncertainty of the adopted value of μ was not very significant in these earlier determinations of $\pi_\odot$ and the astronomical unit through $m_{\oplus+\mathbb{C}}$. In today's IAU system of astronomical constants, however, the astronomical unit as directly determined from radar observations of major planets is a primary constant. Because not only $\pi_\odot$ but also $m_{\oplus+\mathbb{C}}$ is a function of the astronomical unit, the $m_{\oplus+\mathbb{C}}$ value consistent with the adopted value of the astronomical unit will eventually be used as a derived constant. Presently the IAU system still lists conventional but clearly outdated values for the planetary masses, essentially for practical reasons related to the preparation and publication of ephemerides.

CONSTANTS RELATED TO THE COORDINATE SYSTEM

Because the comparison of calculated and observed asteroid positions involves the use of a given system of celestial coordinates, so that any changes in the positions of the equator and equinox relative to the stars, as well as in the precessional rates of change, would affect the resulting $O - C$, it is clear that the constants defining orientation and motion of the reference frame can also be determined or corrected by means of asteroids. Moreover, because there may be local distortions and systematic errors even in the best available fundamental star catalogs, which in practice define and represent the adopted reference system in the various areas of the sky, it is possible to determine such errors of a local nature also from the observed positions of asteroids (referred to the catalog stars) as they move across sufficiently large parts of the celestial sphere. If the *computed* positions are based on excellent and dynamically definitive orbits, their comparison with a sufficient number of *observed* positions of high accuracy will reveal any local distortions in the right ascensions and declinations of the adopted fundamental system of reference.

Most of the asteroid observations, whether photographic or visual, are *relative* ones, referred to nearby catalog stars. There is considerable merit, therefore, in making and using *absolute* meridian circle observations of the first four minor planets, Ceres, Pallas, Vesta, and Juno, for which ephemerides of high internal accuracy are published in the *American Ephemeris and Nautical Almanac* for each year since 1952. Determinations of the equator, equinox, and the annual precession in longitude from such observations have the advantage of being independent of star catalogs. Compared to similar determinations from observations of the Sun, Mercury, and Venus, the starlike appearance of the asteroids again holds the promise of higher accuracy. Finally, such observations can easily be connected to similar fundamental observations

of neighboring stars, so that catalogs can be improved at the same time. In any such projects aiming for perfect rigor, corrections to the orbital elements of the asteroids and of the Earth-Moon barycenter will have to be determined with the desired corrections to the constants defining the reference system and its precessional motion.

SOME HISTORICAL NOTES, REMARKS ON FUTURE PROSPECTS

References to the older determinations of masses and other fundamental constants can be found in a paper by Harkness (1891). Here it may suffice to mention the determination (probably the first) of a planetary mass by means of an asteroid, namely that by Gauss of Jupiter from the motion of Pallas, leading to a result of 1/1042.86 for Jupiter's mass in units of the solar mass. Many astronomical constant determinations made subsequent to Harkness' compilation are listed and discussed in an encyclopedia article by Bauschinger (1920), whereas a number of more recent results, up to the year 1963, are considered by Böhme and Fricke (1965).

Soon after the discovery of 433 Eros in 1898 it became clear that this minor planet was exceptionally well suited for the determination of the solar parallax $\pi_\odot$ by the trigonometric method, as well as for the derivation of $m_{\oplus+\leftmoon}$, because of its rather close approaches to Earth *and* its observability in all parts of its heliocentric orbit. It was also pointed out by Russell (1900) that because of its substantial perturbations by Mars, this asteroid should be able to yield an accurate determination of the mass of Mars. Because for quite some time Eros has actually been used as the principal tool for determinations of the solar parallax and of $m_{\oplus+\leftmoon}$, the history of these results may be outlined here in some detail. As to the direct, trigonometric determinations of $\pi_\odot$ from Eros, Hinks found $\pi_\odot = 8''.807 \pm 0''.003$ (*probable* error) from the photographic right ascensions of the 1900-01 close approach (Hinks, 1909) and $8''.806 \pm 0''.004$ from the micrometric ones (Hinks, 1910), whereas Spencer Jones (1941) obtained the total result $8''.790 \pm 0''.001$ from the well-prepared 1930-31 approach. The first dynamical determinations of $\pi_\odot$, through $m_{\oplus+\leftmoon}$, were based on relatively short orbital arcs, but from observations from 1893 (prediscovery positions) through 1914 Noteboom (1921) derived $1/m_{\oplus+\leftmoon} = 328\,370 \pm 68$. This value for the reciprocal of the mass of Earth and Moon was changed only slightly when Witt (1933) found 328 390±69 from the much longer time interval 1893-1931. The related value of the solar parallax is $8''.7988 \pm 0''.0006$. The subsequent determination by Rabe (1950) from the more recent time interval 1926-45, with the results $1/m_{\oplus+\leftmoon} = 328\,452 \pm 43$ and $\pi_\odot = 8''.7984 \pm 0''.0004$, essentially seemed to confirm the preceding dynamical results, and thus to maintain the inexplicably large discrepancy with the formally also very accurate trigonometric determination by Spencer Jones. This disagreement became even more puzzling when the first reliable radar measurements of the Earth-Venus distance were all found to point to a solar parallax of very nearly $8''.7940$, about halfway between the presumably best

results from the other two methods. Because of this situation, Rabe and Francis in 1966 undertook a reinvestigation of the Eros motion by means of IBM 7094 integrations using the value $1/m_{\oplus+\mathbb{C}} = 328\,912$, which is consistent with the astronomical unit adopted by the IAU in 1964, extending the comparison with observations through the period 1926-65. It became evident then that the true value of $m_{\oplus+\mathbb{C}}$ was indeed close to 1/328 912 (Rabe and Francis, 1967*a*), and it was found that a conceptual error had led to erroneous mass coefficients in the original 1926-45 observation equations. The erroneous nature of these coefficients was discovered independently also by Schubart and Zech (1967) when they tried to reconcile the dynamical value of the astronomical unit with the radar measures, after Schubart had first found that the observations of 1221 Amor seemed to call for an Earth+Moon mass fairly consistent with the radar results for the astronomical unit. Rabe's corrected 1926-45 determination (Rabe, 1967) produced for $1/m_{\oplus+\mathbb{C}}$ the result 328 863±29 (*mean* errors are quoted from here on) from a 13-unknowns solution, whereas from the extended 1926-65 arc Rabe and Francis (1967*b*) obtained the comparable result 328 890±16. The gain in accuracy corresponds roughly to the longer arc involved. The most disappointing finding was that the masses of Mars, Venus, and Mercury are very poorly determined from the Eros solutions, contrary to earlier predictions and expectations. This fact has been confirmed even by the as yet most comprehensive and rigorous study of the Eros motion, namely that by Lieske (1968), for which all the 1893-1966 observations have been reduced to the uniform reference system of the FK4. Lieske's result $1/m_{\oplus+\mathbb{C}} = 328\,915\pm4$ almost approaches in its small formal error those from radar determinations and space probes, which now point to a true value near 328 900±1. While the dynamical and radar determinations of the astronomical unit have thus been reconciled, in close agreement with the IAU value 8".794 05 for the solar parallax, a full explanation of the still discordant trigonometric result 8".790±0".001 has not been given as yet.

It appears that the motion of Eros will remain of some value for determinations of $m_{\oplus+\mathbb{C}}$ even in the future, especially if it should be possible to secure precise radar observations of its distance during close approaches. As to Amor, Schubart (1969) has noted the fact that the lack of observations outside of the perihelion approaches significantly reduces the accuracy of the results for $m_{\oplus+\mathbb{C}}$. The motion of 1566 Icarus, on the other hand, from which Lieske and Null (1969) obtained a good determination of the mass of Mercury, will probably remain important for this purpose, at least until space probes make close approaches to this planet. In general, though, it looks as if the future use of asteroids for determinations of the masses of the *inner* planets will have a strong competition from space probes, as well as from comprehensive adjustments of the (rigorously integrated) orbits and masses of these planets on the basis of combined radar and optical observations of their own motions. As to the latter approach, the relevant investigation by Ash, Shapiro, and Smith (1967), based on a still relatively short time interval, already reveals

the high accuracy obtainable in this way not only for the planetary masses involved, but even for the Moon/Earth mass ratio μ. As to space probes, the even greater accuracy with which they seem to be able to determine planetary masses is apparent in the result from Mariner 2 for Venus, as quoted by Clemence (1966), and in the one from Mariner 4 for Mars, as obtained by Null (1967).

For most of the asteroids, though, Jupiter is the principal disturbing planet, and many investigators have recently taken up the proposal made in 1873 by Hill (1907) to improve Jupiter's mass on the basis of the particularly large perturbations experienced by certain minor planets in consequence of their closeness to the 2/1 commensurability with respect to Jupiter's mean motion. A recent determination by Klepczynski (1969), for instance, combines the four separate mass corrections obtained from the motions of 10 Hygiea, 24 Themis, 31 Euphrosyne, and 52 Europa into the result $1/m_{\odot} = 1047.360 \pm 0.004$, with a mean error much smaller than the one appearing in Bec's (1969) determination from Jupiter's ninth satellite: $1/m_{\odot} = 1047.386 \pm 0.041$. On the other hand, an even more recent determination from the disturbed motion of the Hilda group planet 334 Chicago (which approaches Jupiter to within 1.1 AU) by Scholl (1971) gave the result $1/m_{\odot} = 1047.325 \pm 0.010$. The minor planet results by Klepczynski and Scholl differ by 3.5 times the larger mean error, and there are other relevant determinations from individual asteroids with formal errors much smaller than the actual differences between some of the results. Nevertheless, it appears that the combination of numerous results from asteroids should eventually give us a Jupiter mass more precise than one can get from satellites.

Because space missions may soon be used also for more accurate determinations of the mass of Jupiter, the major planet whose mass can now be most usefully determined by means of minor planet observations is Saturn. Such a determination, using 944 Hidalgo, has been made by Marsden (1970), who suggests that it would be worthwhile to verify his result (1/3498.5) by means of several minor planets with aphelion distances greater than 4 AU.

Corrections to the orbital elements of the Earth-Moon barycenter and to the constants defining the equatorial reference system have been included in some comprehensive solutions, especially in those using Eros, sometimes simply to prevent other unknowns from unduly absorbing some of their effects. In this connection, Lieske (1970) found that corrections to the adopted precession in longitude and to Newcomb's rate of change of the obliquity of the ecliptic are not well determined from the Eros data. As to systematic programs using asteroids, the papers by Brouwer (1935), Clemence (1948), Schmeidler (1958), and Petri (1958) may be consulted. First results from meridian observations of the first four numbered planets have been obtained and discussed by Jackson (1968). He finds that the results are considerably less accurate than predicted by Clemence (1948). This is because of the clustering of the observations around opposition and also the less-than-anticipated precision of the individual measures. It is still concluded, however, that meaningful corrections to the

coordinate system can indeed be obtained from the observations of all four planets during a planned program, if an effort is made to secure observations as close to quadrature as possible. This last requirement is necessary for a satisfactory separation of the corrections to the minor planet orbit from those to the orbit of the Earth. For photographic asteroid observations, the program initiated by Brouwer (1935) has, to a limited extent, been completed by Pierce (1971). Aside from orbital corrections for the 15 minor planets involved, Pierce determines *local* corrections, $\Delta\alpha$ and $\Delta\delta$, for 54 small areas of the *Yale Catalogue* zones, and for 60 such areas in the *Boss General Catalogue.* These catalog corrections are the principal objective of this paper; only rough estimates of the equinox and equator corrections are given, as arithmetic means of all the individual area corrections, and no attempt is made to obtain corrections to Earth's orbit based on volume XIV of the *Astronomical Papers of the American Ephemeris.* Considering the relatively large and somewhat erratic area corrections obtained, it appears that supplementary results from absolute determinations of equinox and equator, using meridian observations of Ceres, Pallas, Juno, and Vesta, would be of great value in future attempts to disentangle the basic coordinate corrections from the local distortions of star catalogs. In conclusion, it seems fair to say that the further use of asteroids will be of considerable value for future improvements of the fundamental reference frame and for future determinations of the elements of any improved Earth orbit or theory.

REFERENCES

Ash, M. E., Shapiro, I. I., and Smith, W. B. 1967, Astronomical Constants and Planetary Ephemerides Deduced From Radar and Optical Observations. Astron. J. 72, 338-350.

Bauschinger, J. 1920, Bestimmung und Zusammenhang der Astronomischen Konstanten. Encyklopädie der Mathematischen Wissenschaften, vol. VI, pt. 2, pp. 844-895.

Bec, A. 1969, Détermination de la Masse de Jupiter par l'Étude du Mouvement de son Neuvième Satellite. Astron. Astrophys. 2, 381-387.

Böhme, S., and Fricke, W. 1965, Astronomical Constants. A Survey of Determined Values. Proc. IAU Symp. no. 21, The System of Astronomical Constants, pp. 269-293.

Brouwer, D. 1935, On the Determination of Systematic Corrections to Star Positions From Observations of Minor Planets. Astron. J. 44, 57-63.

Clemence, G. M. 1948, The Value of Minor Planets in Meridian Astronomy. Astron. J. 54, 10-11.

Clemence, G. M. 1966, Masses of the Principal Planets. IAU Trans. XIIB, 609-614.

Harkness, W. 1891, The Solar Parallax and Its Related Constants, Including the Figure and Density of the Earth. Washington Observations for 1885, app. III. Washington.

Hill, G. W. 1907, On the Derivation of the Mass of Jupiter From the Motion of Certain Asteroids. Collected Mathematical Works, vol. 1, pp. 105-108. (Johnson Reprint Corp., New York, 1965.)

Hinks, A. R. 1909, Solar Parallax Papers no. 7: The General Solution From the Photographic Right Ascensions of Eros, at the Opposition of 1900. Mon. Notic. Roy. Astron. Soc. 69, 544-567.

Hinks, A. R. 1910, Solar Parallax Papers no. 9: The General Solution From the Micrometric Right Ascensions of Eros, at the Opposition of 1900. Mon. Notic. Roy. Astron. Soc. 70, 588-603.

Jackson, E. S. 1968, Determination of the Equinox and Equator From Meridian Observation of the Minor Planets. Astronomical Papers of the American Ephemeris, vol. XX, pt. 1, pp. 1-131.

Klepczynski, W. J. 1969, The Mass of Jupiter and the Motion of Four Minor Planets. Astron. J. **74**, 774-775.

Lieske, J. H. 1968, Mass of the Earth-Moon System From Observations of Eros, 1893-1966. Astron. J. **73**, 628-643.

Lieske, J. 1970, On the Secular Change of the Obliquity of the Ecliptic. Astron. Astrophys. **5**, 90-101.

Lieske, J. H., and Null, G. W. 1969, Icarus and the Determination of Astronomical Constants. Astron. J. **74**, 297-307.

Marsden, B. G. 1970, On the Relationship Between Comets and Minor Planets. Astron. J. **75**, 206-217.

Noteboom, E. 1921, Beiträge zur Theorie der Bewegung des Planeten 433 Eros. Astron. Nachr. **214**, 153-170.

Null, G. W. 1967, A Solution for the Sun-Mars Mass Ratio Using Mariner IV Doppler Tracking Data. Astron. J. **72**, 1292-1298.

Petri, W. 1958, Praktische Auswertung von Meridianbeobachtungen kleiner Planeten. Astron. Nachr. **284**, 219-226.

Pierce, D. A. 1971, Star Catalog Corrections Determined From Photographic Observations of Selected Minor Planets. Astron. J. **76**, 177-181.

Rabe, E. 1950, Derivation of Fundamental Astronomical Constants From the Observations of Eros During 1926-1945. Astron. J. **55**, 112-126.

Rabe, E. 1967, Corrected Derivation of Astronomical Constants From the Observations of Eros 1926-1945. Astron. J. **72**, 852-855.

Rabe, E., and Francis, M. P. 1967*a*, Motion of Eros and the Astronomical Unit. Astron. J. **72**, 316-317.

Rabe, E., and Francis, M. P. 1967*b*, The Earth+Moon Mass and Other Astronomical Constants From the Eros Motion 1926-1965. Astron. J. **72**, 856-864.

Russell, H. N. 1900, The General Perturbations of the Major Axis of Eros by the Action of Mars. Astron. J. **21**, 25-28.

Schmeidler, F. 1958, Über die Bestimmung absoluter Koordinaten-systeme mit Hilfe von Planetenbeobachtungen. Astron. Nachr. **284**, 205-218.

Scholl, H. 1971, Correction to the Mass of Jupiter Derived From the Motion of 153 Hilda, 279 Thule, and 334 Chicago. Proc. IAU Colloq. no. 9, The I.A.U.-System of Astronomical Constants (Heidelberg, 1970). *Celest. Mech.*, in press.

Schubart, J., and Zech, G. 1967, Determination of the Astronomical Unit by the Dynamical Method. Nature **214**, 900-901.

Schubart, J. 1969, The Minor Planet 1221 Amor. Astron. Astrophys. **2**, 173-181.

Spencer Jones, H. 1941, The Solar Parallax and the Mass of the Moon From Observations of Eros at the Opposition of 1931. Mem. Roy. Astron. Soc. **66**, pt. 2, 1-66.

Witt, G. 1933, Baryzentrische Ephemeride des Planeten 433 Eros für die Perihelopposition 1930-1931. Astron. Abhand. Ergänzungsh. Astron. Nachr. 9(1), 1-30.

DISCUSSION

MARSDEN (in reply to a question by Kiang about 1362 Griqua): Because of its libration about the 2:1 resonance, 1362 Griqua does not seem to be as suitable an object for determining the mass of Jupiter as it was thought to be. We attempted to make a determination from the observations of 1935 to 1965 but were unable to obtain a significant correction to the adopted value. The Hill planets, which do not librate and which have longer observational histories, seem to be rather more suitable.

ALFVEN: Have effects of nongravitational forces been detected in the motion of minor planets?

MARSDEN: No. There are a few cases where it seemed that small systematic trends remained in the residuals after accurate orbit solutions had been made, but I am confident that these are due to errors in the adopted masses of the perturbing planets. I had initially suspected that the motion of 887 Alinda and 944 Hidalgo were affected by nongravitational forces and that these objects were dying cometary nuclei, but it is clear that the residuals may be removed if one makes reasonable changes in the masses of Earth and Saturn. I hasten to add that this is not true in the case of comets, where the residuals are usually very much larger.

Page intentionally left blank

DIAMETER MEASUREMENTS OF ASTEROIDS

AUDOUIN DOLLFUS
Observatoire de Paris

Direct optical measurements of asteroid diameters obtained by telescopic observations are scarce. Although several adequate instrumentations and techniques are available for the purpose, they have not been used. The importance of these determinations should be stressed for the attention of observers.

The *filar micrometer* was used only by one observer during the last century, and no additional measures have been made since. This was in 1894 and 1895 when E. Barnard (1902) used the 90 cm refractor of Lick Observatory, and the 100 cm refractor of Yerkes Observatory. The results are as follows:

Ceres: apparent diameter at 1 AU: 1".060, or 770 km (28 nights)
Pallas: apparent diameter at 1 AU: 0".675, or 490 km (5 nights)
Juno: apparent diameter at 1 AU: 0".266, or 195 km (5 nights)
Vesta: apparent diameter at 1 AU: 0".531, or 390 km (21 nights)

These filar micrometer measurements are difficult to make when the disks are only slightly larger than the image of the diffraction pattern blurred by atmospheric seeing; the accuracy is necessarily poor, especially for Juno; the last decimals given are not significant.

The *interferometer* with a double slit in the wavefront was used by M. Hamy (1899) with the 60 cm coudé refractor of the Paris Observatory, but only on Vesta: apparent diameter at 1 AU: 0".54, or 400 km (8 nights).

Once again, this technique was not used again, despite the improvements in interferometric techniques and the larger telescopes now available.

The *double-image micrometer* has been used more recently in France by several collaborating observers. For descriptions of the double-image micrometer, see papers by P. Muller (1949) and A. Dollfus (1954). Although the survey is not yet complete, some of the as yet unpublished preliminary results are summarized in table I.

For small apparent diameters of only two to three times the effective resolving power of the telescope, large uncertainties remain in the measurements, and systematic errors occur. Some of them were computed or simulated at the laboratory by H. Camichel (1958), A. Dollfus (1963), and M. Hugon et al. (Camichel et al., 1964).

TABLE I.–*Double-Image Diameter Measurements of Asteroids (Preliminary Results)*

Date	Observers	Telescope	Apparent stellar diameter (measured)	Asteroid apparent diameter (measured)	Distance, AU	Diameter at 1 AU	Average at 1 AU
Vesta:							
June 5, 1967	A. Dollfus and	83 cm Meudon	–	0".48	1.196	0".57	
	J. Focas	83 cm Meudon	–	.48	1.196	.57	0".60
July 11, 1967	P. Muller	83 cm Meudon	–	.42	1.454	.61	±0".10
July 21, 1967	P. Muller	83 cm Meudon	–	.43	1.553	.67	
Pallas:							
June 7, 1969	A. Dollfus and	107 cm Pic-du-Midi	0".29	.53	2.513	1.34	
	J. Lecacheux	107 cm Pic-du-Midi	.23	.50	2.513	1.25	1".27
June 8, 1969	A. Dollfus and	107 cm Pic-du-Midi	.31	.49	2.510	1.24	±0".35
	H. Camichel	107 cm Pic-du-Midi	.34	.50	2.510	1.25	

The error limits given in the table, ±0".10 for Vesta and ±0".35 for Pallas, are only estimates based on the practice of the laboratory simulations, taking into account the seeing conditions at the telescope when measurements were made.

The measurement of Vesta agrees with the values of Barnard (1902) and Hamy (1899); but the diameter of Pallas is larger than the Barnard value by a factor on the order of 2. This very large discrepancy casts a doubt on the overall accuracy of the presently available determinations of asteroid diameters.

The *diskmeter,* designed by H. Camichel (1953), is a device producing a small artificial bright disk in the field of the telescope, with adjustable brightness, color, blurring, and diameter. Looking first at a nearby star, the observer adapts the brightness, color, and instrumental blurring for an artificial image of negligible apparent diameter, to reproduce as closely as possible the brightness configuration of the stellar image. Then, looking at the asteroid (or a small satellite), the observer readapts brightness and color, and without changing the blurring adjustment, increases the diameter of the artificial image until reproducing the behavior of the object in the field.

This kind of instrument was successfully used by H. Camichel with the French Pic-du-Midi 60 cm refractor and by G. P. Kuiper with the Palomar 500 cm reflector on Neptune, Pluto, and planetary satellites. Kuiper used a diskmeter to measure some asteroids, but the details of this work have not been published.[1]

This technique seems to be particularly well adapted for asteroid diameter determinations and should be used.

The *occultation* of asteroids by the edge of the Moon provides curves of brightness variations with time, from which the apparent disk diameter can be derived with an excellent accuracy. For stellar objects of negligible apparent diameter, the photoelectric lightcurves recorded with a time resolution of a millisecond display a drop of brightness lasting some tenths of milliseconds, associated with at least one maximum and one minimum due to the diffraction pattern (see fig. 1); the higher order diffraction variations vanish into the noise

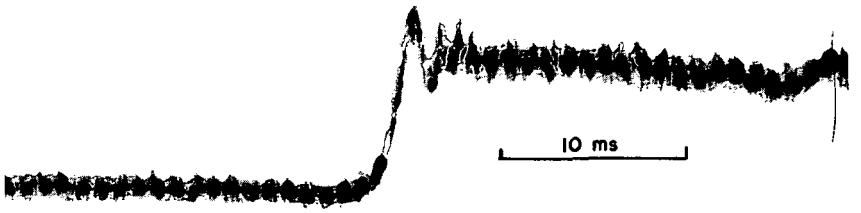

Figure 1.—Lightcurve of the lunar occultation of ϵ-Capricorni, 4.7 mag, B5p. December 9, 1964, at $19^h31^m48^s$; green filter. (60 cm telescope of Meudon Observatory, France; photoelectric observation by G. Spaak.)

[1]*Note added in proof, by T. Gehrels:* A summary paragraph occurs on p. 352 of *Surfaces and Interiors of Planets and Satellites* (ed., A. Dollfus; Academic Press, Inc.; London; 1970); the wording of that paragraph was checked with G. P. Kuiper.

TABLE II.–*Asteroidal Diameter Determinations Available in 1970*

Asteroid	Technique	Number of independent measures	Apparent diameter at 1 AU	Average apparent diameter at 1 AU	Diameter, km	Normal reflectivity, n_v
Vesta	Filar	21	0".53			
	Interference	8	.54	0".56	410	0.40
	Double image	4	.60			
Ceres	Filar	28	1.06	1.06	770	0.13
Juno	Filar	5	.27	.27	195	0.27
Pallas	Filar	5	.68			
	Double image	4	1.27	(.97)	(700)	(0.055)

level. For some bright stars, small apparent diameters of the order of 0".005 are large enough to smear out the first minimum of light. Larger apparent diameters will change the slope of the lightcurve.

Figure 1 shows one of our curves obtained at Meudon Observatory on the star ϵ-Capricorni, 4.7 mag, with a telescope of 60 cm diameter. A telescope of 200 cm produces the same noise level with a star of 7.3 mag. The brightest asteroids are expected to have apparent diameters larger than 0".05, thus permitting a relaxation of the time resolution on the order of 30 times; the same noise level is obtained with a gain of brightness of 3.8 mag, and the technique reaches a magnitude of about 11, provided by at least 15 asteroids. Further decrease of time resolution could be tried and larger telescopes used.

This interesting technique has not yet been used for asteroids.

CONCLUSION

The asteroidal diameter determinations currently available are summarized in table II.

The double-image micrometer, the interferometer, the diskmeter, and the lunar occultation photometry are suitable techniques available for refinement of these determinations and for their extension to a larger number of objects.

REFERENCES

Barnard, E. 1902, On the Dimensions of the Planets and Satellites. Astron. Nachr. 157, 260-268.

Camichel, H. 1953, Nouvelle Méthode de Mesure des Diamètres des Petits Astres et ses Résultats. Ann. Astrophys. 16, 41.

Camichel, H. 1958, Erreur Systématique sur la Mesure des Diamètres des Petits Astres Avec le Micromètre a Double Image. Ann. Astrophys. 21, 217-228.

Camichel, H., Hugon, M., and Rösch, J. 1964, Mesure du Diamètre de Mercure par la Méthode de Hertzsprung le 7 Novembre 1960. Icarus 3, 410-422.

Dollfus, A. 1954, L'Observation à la Tour Eiffel du Passage de Mercure Devant le Soleil Pour la Mesure de son Diamètre. L'Astronomie 68, 337-345.

Dollfus, A. 1963, Mesure du Diamètre de Mercure lors de son Passage Devant le Soleil le 7 Novembre 1960. Icarus 2, 219-225.

Hamy, M. 1899, Sur la Mesure Interférentielle des Petits Diamètres. Application aux Satellites de Jupiter et à Vesta. Bull. Astron. 16, 257-274.

Muller, P. 1949, Sur un Nouveau Micromètre à Double Image, ses Possibilités et Quelques Questions Connexes. Bull. Astron. 14, 177-313.

DISCUSSION

VEVERKA: You quoted the diameter measurements of the first four asteroids made by Barnard with a filar micrometer. The apparent diameter of Juno was given as 0".3. How meaningful, in your opinion, are such measurements when even at best "seeing" causes a smearing of 0".2 to 0".3? I realize that Barnard's measurements are internally quite consistent, but I would like to have an estimate of the absolute uncertainty involved, including systematic errors.

DOLLFUS: One of the purposes of my presentation was precisely to warn about the difficulty of the method. Barnard was a very experienced observer for filar micrometry,

and was well aware of all the difficulties of the problem. However, we should not overestimate the accuracy of his measurements, and systematic error of 0".10 could be considered as highly probable. This is why the Barnard results, despite the high training and reputation of the author, should be checked when possible by other techniques.

GEHRELS: This does raise a problem. People like Barnard who did this type of work must have had a feeling of their precision and if I take it strictly from what you are saying then it would also concern Barnard's measurements of Ceres and Vesta. Should we not be allowed some confidence in these measures?

DOLLFUS: He did observations during several long periods of time but the gist lies in the systematic errors and against them accumulation of data does not really improve the result. The point is that the measures are distorted; one can in some respects simulate the conditions at the laboratory and study the systematic errors.

GEHRELS: In these measurements can you make a comment on which way the error might go? Should we expect measurements that are too large or too small?

DOLLFUS: Uncorrected filar measurements are too large; at the limit, a point source gives the apparent diameter of the diffraction pattern blurred by atmospheric turbulence.

KUIPER: Certainly Barnard should be considered a very keen observer. He was aware of what the atmosphere did to spoil the image and he would not use a night if it was not good. I have confidence in his diameters; the absolute errors would be somewhat similar to the case of close binaries, and guessed to be 10 percent or perhaps from 20 to 25 percent, but they are real measures.

DOLLFUS: I was not clear in my statement. For disks with diameters of the order of the size of the diffraction pattern, a correction is to be applied. This is precisely the case of the asteroids; but it is difficult to judge what is the contribution of the diffraction if one includes the blurring due to atmospheric turbulence.

KUIPER: The diffraction was 0".12 and the overall blurring not more than 0".2. What counts is the square root of the sum of the squares, and therefore the diffraction is the least important in the final value. Certainly it has all the uncertainties that we are all aware of and Barnard was aware of. Values of the order of 0".5 would be essentially correct. Values smaller than 0".3 I would consider dubious.

CHAPMAN: There has been one recent test of the methods that have been used and described by Dollfus and Kuiper for determining asteroid diameters. Dollfus has summarized the modern attempts that have been made to determine the diameter of Neptune using these same methods. (See Dollfus, 1970.) All attempts to measure the diameter during the last half century *prior* to the recent stellar occultation by Neptune agreed with each other but differed from the correct value by more than 10 percent. The 2".5 diameter of Neptune is an order of magnitude larger than the largest asteroid diameters. Considering, in addition, that smearing by diffraction and seeing is of the same order as asteroid diameters, the failure of these methods to reach higher accuracy than 10 percent on Neptune (even taking account of the problems of limb darkening) casts doubt on any direct diameter measurements of asteroids.

DOLLFUS: The problem of the diameter determinations of Neptune is of a different nature: The limitations in Neptune measurements are altogether the lack of brightness and the limb darkening. Most of the earlier diameter measurements of Neptune concluded too small diameters because of the limb-darkening effect on a disk of very low brightness. However, our last telescopic measurements were obtained with the new Pic-du-Midi telescope, which gives three times more brightness than the previous one; a value of 2".23 was obtained, almost 10 percent larger than the previous measurements. This last value was considered by the observers as far better than the older. The value was later compared with the star occultation result; the agreement is within 3 percent and unexpectedly accurate in view of the difficulty of measuring so dark an object.

The case of minor planets is not the same. Observations are no longer limited by the lack of brightness; the average surface brightness is at least *30 times* larger, with no limb

darkening; the measurements, in this respect, are far easier. However, the diameters being smaller, careful laboratory analysis of the systematic errors introduced by the spreading of the images should be carried out for final evaluation.

DISCUSSION REFERENCE

Dollfus, A. 1970, Diamètres des Planètes et Satellites. Surfaces and Interiors of Planets and Satellites, ch. 2, pp. 45-139. Academic Press, Inc. London and New York.

Page intentionally left blank

ASTEROID MASSES AND DENSITIES

JOACHIM SCHUBART
Astronomisches Rechen-Institut
Heidelberg

Before 1966, when Hertz (1966) published his first direct determination of the mass of Vesta, all our knowledge on asteroid masses was based on estimates. The masses of the first four minor planets resulted from the measured diameters by Barnard (1900) (see the paper by Dollfus in this volume[1]) and from estimated mean densities. The diameters of the smaller objects were derived from their brightness and an estimate of their reflectivity (usually the reflectivity of the Moon was adopted). In 1901, Bauschinger and Neugebauer (1901) derived a value for the total mass of the first 458 asteroids. All the diameters were computed from the brightness with an assumed value for the reflectivity. The diameter of Ceres found in this way is very close to Barnard's (1900) value. The mean density of the 458 asteroids was put equal to that of Earth, and their total mass resulted as 3×10^{-9} solar mass. Stracke (1942) used the same method with an increased material, but the addition of more than 1000 faint asteroids did not bring a significant change in the estimate of the total mass. The report on the McDonald asteroid survey (Kuiper et al., 1958) does not contain another estimate of the total mass of the asteroid ring, but it points to the possibility of a very rapid increase in the number of asteroids with decreasing absolute brightness. If this increase is strong enough, each interval of 1 mag in absolute magnitude can contribute the same amount to the total mass. In the range of magnitudes covered by the Palomar-Leiden survey (PLS) (van Houten et al., 1970), there are no indications for such a strong increase.

The attempts to find gravitational evidence on asteroid masses started with the total mass, but von Brunn (1910) demonstrated that at his time it was not possible to detect gravitational effects caused by the total mass of the asteroids. In the paper mentioned above, Stracke (1942) expressed the hope that accurate orbital theories of the first four minor planets and of Eros can answer the question of the gravitational effects of the total mass, if these theories are compared with the observations of a sufficiently long interval of time.

---

[1]See p. 25.

Actually, it was an orbital theory of 197 Arete that permitted the first gravitational determination for the mass of a single minor planet. Hertz discovered that Arete approaches Vesta within 0.04 AU once every 18 yr. Five such approaches have occurred since the discovery of Arete in 1879. A close commensurability corresponding to the ratio 4:5 of the mean motions of Arete and Vesta allows the repetition of the approaches, which cause the perturbations by Vesta in the mean longitude of Arete to accumulate. Although the total effect of the attraction of Vesta is small and the observations have various qualities, Hertz (1968) succeeded in determining the mass of Vesta from an orbital theory of Arete, which included numerical integrations and differential corrections. Using 72 observations from 28 oppositions of Arete, the mass of Vesta resulted as 1.20×10^{-10} solar mass, the formal mean error being 10 percent of the result. An earlier value based on only 59 observations of Arete was close to this result (Hertz, 1966).

I came in touch with the problems of asteroid masses when I studied the effects caused in the orbits of the first four minor planets by possible errors in the system of planetary masses (Schubart, 1970*b*). With the aid of numerical tests, I found that the members of the pairs Ceres-Pallas and Ceres-Vesta cause observable gravitational effects in the mean longitude of the respective other member if the whole span covered with observations is considered. Especially the mass of the largest body, Ceres, may not be neglected in an accurate theory of all the observations of Pallas or Vesta. The mass of Ceres can result from such a theory if it is introduced as an additional unknown in a differential correction. The tests showed that a theory of Pallas gives the best chance to determine the mass of Ceres. The reason for the observable interaction between Ceres and Pallas is given by the ratio of their mean motions, which is close to 1:1. As in the case of Vesta and Arete, the repetition of equal configurations causes an accumulation of the perturbations. Gauss realized this when he had obtained the first reliable orbital elements of Ceres and Pallas in 1802, and he thought of the possibility to determine the masses of the two planets from the accumulated effects after a sufficiently long interval of time (von Zach, 1874).

In 1970, I started with a first attempt to derive the mass of Ceres from observations of Pallas (Schubart, 1970*a*). I used an *N*-body program (Schubart and Stumpff, 1966) for the numerical integration of the orbit of Pallas. The computations started with Duncombe's (1969) elements of Ceres and Pallas. G. Struve (1911) published a list of 63 normal positions of Pallas, obtained from the same number of oppositions in the interval from 1803 to 1910. I selected 47 of these positions for my work, but I have to mention that this material is very inhomogeneous because Struve took a part of the places from much older sources without change. Combining the 47 positions with 27 positions of Pallas from 13 oppositions, 1927-68, I obtained the value 6.7×10^{-10} solar mass for the mass of Ceres in a differential correction (Schubart, 1970*a, b*). The formal mean error was less than 10 percent of the result, but this does not account for possible systematic effects. Tests showed

that the uncertainties in the masses of Mars and Jupiter will not affect the result, and I do not believe that impacts have caused an observable effect in the motion of the planets under consideration. A real source of error is given by the systematic errors in the right ascensions of the reference stars used during various periods. Fortunately, the effects caused by Ceres in the observations of Pallas are much larger than these errors, but corrections are necessary in a more accurate theory.

To find an indication for the sign of a possible correction to my first value for the mass of Ceres, I started to explore the independent way of determining the mass from the observations of Vesta. Leveau (1896, 1910) derived a reliable and homogeneous set of 252 normal positions from 68 oppositions of Vesta for the interval from 1807 to 1904. He applied systematic corrections to the observations as far as he knew them. The positions appeared in two parts together with his theory of Vesta. From this material, I took a comparatively small selection of 70 places from 17 oppositions, 1807-1903/04. Combining this with 48 places of Vesta from 13 oppositions, 1923-68, I used the same method as before and obtained the smaller value of 5.1×10^{-10} solar mass for the mass of Ceres. A small mean error resulted again, but this is due to the large number of observations and to their small scatter. Because Vesta is less sensitive to changes in the mass of Ceres (Schubart, 1970*b*), the result derived from it should have a lower weight in comparison with that from Pallas. Systematic errors can affect the result from Vesta in a stronger way.

Quite recently, I examined the first observations of Pallas in Struve's (1911) list more closely. They are taken from a paper by Gauss that was unpublished at the time of his death, but a more original and accurate form of these positions is given elsewhere in his publications. Making use of these original positions and dropping one with a large residual, I obtained a decrease in my former result for the mass of Ceres by about 4 percent. Because the result from Vesta indicates that even this new value may be too large, I propose to adopt

$$(6.0 \pm 0.7) \times 10^{-10} \text{ solar mass}$$

as the result for the mass of Ceres, until a more reliable value becomes available. The mean error proposed here is an estimate.

The next important problem is the direct determination of a value for the mass of Pallas. This mass is probably much smaller than that of Ceres because the volumes of Pallas and Ceres are approximately in a ratio of 1:4 according to the measured diameters (Barnard, 1900). On principle, a treatment of the observations of Ceres should give a result for the mass of Pallas, but this will be subject to a large uncertainty and also will depend on the adoption of a value for the mass of Vesta (Schubart, 1970*b*). At the moment, I adopt 1/4 of the mass of Ceres as an estimate for the mass of Pallas.

In the case of Juno and all the asteroids discovered after Vesta, the method of estimating reflectivity and mean density is still the best one for a mass

determination. According to their absolute magnitude g these bodies are all comparatively small (Kuiper et al., 1958). An estimation of the total mass of these bodies is especially interesting. To demonstrate a simple method for this, I assume that all these minor planets have the same reflectivity and mean density as Ceres. It is easy to correct the result for other mean values of reflectivity and density. In table I, N is the number of objects in half-magnitude intervals of g. Each interval is characterized by the mean value of g. The values of N are taken from Kuiper et al. (1958, table 15), but additions were made to account for the members of the Hilda and Trojan groups. N_1 is the number of objects with absolute magnitude g that would have a total mass equal to that of Ceres. N_1 results from

$$\log N_1 = 0.6(g - 4)$$

Therefore, N/N_1 is the mass contribution of each half-magnitude interval in units of the mass of Ceres. In this unit, the total mass of the asteroids with $6.0 < g < 10.5$ results as 0.74 from table I. The PLS (van Houten et al., 1970, fig. 6) allows an extension of table I to fainter asteroids, but their mass contribution is small. The intervals $10.5 < g < 13.5$ and $13.5 < g < 16.5$ contribute only 0.06 and 0.01, respectively, in the above unit. This gives the estimate of 0.8 mass of Ceres for the total mass of the objects considered. A lower value results if the average reflectivity is higher or if the mean density is lower than that of Ceres. If the sum of the masses of Pallas and Vesta is put equal to 0.45 mass of Ceres, the mass of Ceres results as nearly equal, or possibly even equal to the mass of the remaining minor planets with $g < 16.5$. According to my result, two masses of Ceres correspond to 1.2×10^{-9} solar mass, or to 2.4×10^{24} g. This value is lower than the early estimates of the total mass mentioned above. It is not very far from some of the more recent estimates (Allen, 1963; Anders, 1964, pp. 693-694; Dohnanyi, 1968, 1969).

The directly determined masses of Ceres and Vesta in combination with the measured diameters allow an attempt to derive the mean densities. Barnard's

TABLE I.–*Mass Contribution of Half-Magnitude Intervals in Absolute Magnitude* g

g	N	$\log N_1$	Mass (Ceres = 1)
6.25	3	1.35	0.134
6.75	3	1.65	.067
7.25	11	1.95	.124
7.75	14	2.25	.079
8.25	32	2.55	.090
8.75	61	2.85	.086
9.25	90	3.15	.063
9.75	150	3.45	.053
10.25	240	3.75	.043

(1900) diameter of Ceres is 768 km, so that a mass of 1.2×10^{24} g leads to a mean density of 5 g-cm^{-3} for Ceres. Dollfus (1970) estimates the error of the diameter as about ±6 percent, so that the value of the density is uncertain by about 20 percent according to this. The uncertainty coming from the mass is only about 10 percent. The mean density of Vesta came out much larger at first (Hertz, 1968), but the value was based on Barnard's diameter, which is probably too small. A recent measurement published by Dollfus (1970) makes the volume of Vesta equal to 1/5 the volume of Ceres. Because the masses are in the same ratio, this measurement points to the same densities for Vesta and Ceres. However, the relative uncertainty in the measured diameter of Vesta is comparatively large.

T. Gehrels directed my attention to the way of getting a lower limit for the mean density of a rotating asteroid (Gehrels et al., 1970; Gehrels, 1970). If the period of rotation is less than a critical value depending on the density, the planet will be rotationally unstable and tend to break up. This was, for instance, mentioned by Kuiper (1950). Asteroid 1566 Icarus has the shortest known period of rotation (Gehrels, 1970), and this might require a density greater than 3 g-cm^{-3}, but further considerations are necessary because cohesive forces can probably not be neglected.

ACKNOWLEDGMENTS

I thank T. Gehrels for valuable comments and the Deutsche Forschungsgemeinschaft for financial support. I used the computers at the Deutsches Rechenzentrum in Darmstadt and at our institute for the mass determinations of Ceres.

REFERENCES

Allen, C. W. 1963, Astrophysical Quantities, pp. 152-153. Second ed. Athlone Press. London.

Anders, E. 1964, Origin, Age, and Composition of Meteorites. Space Sci. Rev. 3, 583-714.

Barnard, E. E. 1900, The Diameter of the Asteroid Juno (3), Determined With the Micrometer of the 40-Inch Refractor of the Yerkes Observatory, With Remarks on Some of the Other Asteroids. Mon. Notic. Roy. Astron. Soc. 61(2), 68-69.

Bauschinger, J., and Neugebauer, P. V. 1901, Tabellen zur Geschichte und Statistik der kleinen Planeten. Königl. Astron. Rechen-Inst. Berlin, Veröffentlichungen 16, 1-77.

Brunn, A. von. 1910, Über die Masse des Planetoidenringes. Schr. Naturforschenden Gesellschaft Danzig, Neue Folge 12(4), 101-148.

Dohnanyi, J. S. 1968, Collisional Model of Asteroids and Their Debris. Physics and Dynamics of Meteors, IAU Symp. 33, pp. 486-503. D. Reidel. Dordrecht.

Dohnanyi, J. S. 1969, Collisional Model of Asteroids and Their Debris. J. Geophys. Res. 74(10), 2531-2554.

Dollfus, A. 1970, Diamètres des Planètes et Satellites. Surfaces and Interiors of Planets and Satellites (ed., A. Dollfus), pp. 45-139. Academic Press, Inc. London and New York.

Duncombe, R. L. 1969, Heliocentric Coordinates of Ceres, Pallas, Juno, Vesta 1928-2000. Nautical Almanac Office, U.S. Naval Observatory, Washington, D.C., Astron. Papers 20(2), 133-309.

Gehrels, T. 1970, Photometry of Asteroids. Surfaces and Interiors of Planets and Satellites (ed., A. Dollfus), pp. 317-375. Academic Press, Inc. London and New York.

Gehrels, T., Roemer, E., Taylor, R. C., and Zellner, B. H. 1970, Minor Planets and Related Objects. IV. Asteroid (1566) Icarus. Astron. J. 75, 186-195.

Hertz, H. G. 1966, The Mass of Vesta. IAU Central Bureau for Astron. Telegrams, Circ. 1983.

Hertz, H. G. 1968, Mass of Vesta. Science 160, 299-300.

Houten, C. J. van, Houten-Groeneveld, I. van, Herget, P., and Gehrels, T. 1970, The Palomar-Leiden Survey of Faint Minor Planets. Astron. Astrophys. Suppl. 2, 339-448.

Kuiper, G. P. 1950, On the Origin of Asteroids. Astron. J. 55, 164.

Kuiper, G. P., Fujita, Y., Gehrels, T., Groeneveld, I., Kent, J., Van Biesbroeck, G., and Houten, C. J. van. 1958, Survey of Asteroids. Astrophys. J. Suppl. 3, 289-428.

Leveau, G. 1896, Positions Normales de Vesta Employées dans la Comparaison de la Théorie Avec les Observations (Appendix). Ann. Observ. Paris Mem. 22, A315-A317.

Leveau, G. 1910, Observations Méridiennes de Vesta Faites de 1890 à 1904 et Comparaison Avec les Tables (Appendix). Ann. Observ. Paris Mem. 27, B41-B43.

Schubart, J. 1970*a*, The Mass of Ceres. IAU Central Bureau for Astron. Telegrams, Circ. 2268.

Schubart, J. 1970*b*, The Planetary Masses and the Orbits of the First Four Minor Planets. Paper presented at IAU Colloquium no. 9. (1971, Celest. Mech., to be published.)

Schubart, J., and Stumpff, P. 1966, On an N-Body Program of High Accuracy for the Computation of Ephemerides of Minor Planets and Comets. Astron. Rechen-Inst. Heidelberg, Veröff. 18, 1-31.

Stracke, G. 1942, Über die geometrischen Grössen und die Masse der kleinen Planeten. Astron. Nachr. 273, 24-28.

Struve, G. 1911, Die Darstellung der Pallasbahn durch die Gauss'sche Theorie für den Zeitraum 1803 bis 1910. Doctoral Dissertation. Friedrich-Wilhelms-Universität zu Berlin.

Zach, F. X. von. 1874, Carl Friedrich Gauss Werke, vol. 6, pp. 215-216. Königl. Gesellschaft der Wissenschaften zu Göttingen.

DISCUSSION

VEVERKA: You referred to the mean density of Icarus as being 3.0 g/cm^3. I believe this number is taken from a paper by Gehrels, Roemer, Taylor, and Zellner (1970) and is only a plausible guess to which undue physical importance should not be attached.

BRATENAHL: Is there a search for other close encounters besides 197 Arete and Vesta?

SCHUBART: I do not know. It is possible that Hertz made such a search when he discovered the case of Arete and Vesta.

HERGET: Yes. One must find a close approach to one of the more massive minor planets, and there just is none such, less than several million miles, amongst the known objects.

RABE: How large (approximately) are the longitude perturbations produced by the mutual actions of Ceres and Pallas?

SCHUBART: I found residuals of 40 arcsec between some of the early observations of Pallas and a computation based on modern orbital elements when I neglected the mass of Ceres. (See my earlier paper, Schubart, 1970.) I expect the effects in the longitude of Ceres to be comparatively small; but Dollfus mentioned in his paper given here[2] that the diameter of Pallas measured by Barnard may be too small. Therefore, my estimate of the mass of Pallas can be too low. If this is so, it will not be so difficult to determine the mass of Pallas from the observations of Ceres.

---

[2]See p. 25.

SCHUBART (in reply to a question by Roosen): My estimate of the total mass of the asteroids refers to the observable objects. The mass contribution of the unobservable small asteroids with a diameter of less than 1 km is unknown.

KIANG: I may point out, that many decades ago attempts were made by Harzer to determine the total mass of the asteroid ring from gravitational effects using the perturbations on the orbit of Mars. A rather large, but extremely uncertain value of about one-tenth the mass of Earth was obtained.

SCHUBART: Harzer made his determination before the effects of relativity became known. It is, therefore, not based on real effects due to the asteroids; compare also von Brunn's (1910) work. We should not use gravitational determinations of the total mass, unless they are confirmed with modern computing techniques.

DISCUSSION REFERENCES

Brunn, A. von. 1910, Über die Masse des Planetoidenringes. Schr. Naturforschenden Gesellschaft Danzig, Neue Folge 12(4), 101-148.

Gehrels, T., Roemer, E., Taylor, R. C., and Zellner, B. H. 1970, Minor Planets and Related Objects. IV. Asteroid (1566) Icarus. Astron. J. 75, 186-195.

Schubart, J. 1970. The Planetary Masses and the Orbits of the First Four Minor Planets. Paper presented at IAU Colloquium no. 9. (1971, Celest. Mech., to be published.)

Page intentionally left blank

THE METHOD OF DETERMINING INFRARED DIAMETERS

DAVID A. ALLEN
Hale Observatories

Over the past decade, largely because of the pioneer work of F. J. Low in Tucson, it has become possible to make accurate and reliable astronomical measurements at infrared wavelengths as long as 20 μm. At such wavelengths we see solar system bodies not by reflected sunlight but by their own thermal emission. The larger asteroids, though subtending small angles, give signals at 10 μm comparable in intensity with those from the brightest stars. It is now possible to determine the absolute flux from such asteroids to an accuracy of about 10 percent. Because an asteroid might reasonably be expected to have no atmosphere and no internal source of heat, the thermal radiation it emits must just balance the solar radiation it absorbs, and the measured flux will depend only upon its size. Infrared measurements therefore provide an opportunity to determine the diameters of the brighter asteroids.

ASSUMPTIONS

Certain assumptions must be made before the infrared flux can be converted into a diameter. The ideal asteroid must not rotate (when viewed from the Sun) and must be a smooth spherical blackbody at the observing wavelength ($\sim 10\,\mu$m). In addition, the proportion of solar energy scattered by each element of surface must be represented by a single albedo, A (the Bond albedo). Then a measurement of the optical flux from the asteroid gives us the product $d^2A \equiv p$, where d is the diameter. The absorbed solar energy is proportional to $1 - A = 1 - p/d^2$, and the infrared flux is a complex function of d^2 that has previously been derived (Allen, 1970). Each infrared measurement can be converted directly to a diameter. In view of the assumptions made in defining this dimension, it will be called the infrared diameter. The relationship between infrared and true diameter is discussed below.

RESULTS

The infrared facility at the University of Minnesota (Ney and Stein, 1968) has been used to determine the infrared diameters of Ceres and Juno (Murdock, unpublished) and Vesta (Allen, 1970). The results are given in table I. It will be seen that in each case the infrared diameter exceeds Barnard's

TABLE I.–*Infrared Diameters of Three Asteroids*

Asteroid	Number of determinations	Infrared diameter, km	Barnard's diameter, km	Density, g-cm^{-3}	Reference to mass
Ceres	6	1160 ± 80	770	1.6 ± 0.7	Schubart (1970)
Juno	4	290 ± 20	220	–	–
Vesta	11	570 ± 10	380	2.5 ± 0.7	Hertz (1968)

micrometer measures by about 50 percent, but that the corresponding densities seem more reasonable than those obtained by using Barnard's values (5.5 for Ceres and 8.5 for Vesta).

DISCUSSION OF RESULTS

An asteroid will not, in general, be ideal, and the infrared diameter may bear little relationship to the linear dimension. For the larger bodies, at least, the figures will be similar. Table II shows the effect on the infrared diameter caused by a breakdown of the various assumptions.

TABLE II.–*Breakdown of Assumptions*

Assumption	Effect on diameter, percent	Sense[a]
Blackbody	< 5	+
Shape, roughness	15 to 35	–
Rotation:		
Dust	15	+
Rock	50	+
Albedo	8	±
Absolute calibration	5	±

[a]+: linear diameter is greater than infrared diameter;
–: linear diameter is less than infrared diameter.

Blackness

Observations at two or three wavelengths in the 8 to 14 μm atmospheric window and around 20 μm have shown that Ceres, Juno, and Vesta are graybodies to within experimental uncertainty. Observations of the Moon and Mercury show these bodies to be close to black. It seems unlikely that asteroids have emissivities below 0.95.

Roughness

The Moon and Mercury at full phase emit 30 percent more flux than would a smooth sphere because mountain slopes predominantly seen near the limb are

warmer than level terrain. In the extreme an asteroid might emit as a flat disk; the infrared diameter would then be 35 percent too large.

Rotation

If an asteroid rotates, it emits some of its thermal radiation on the night side and the signal received at Earth is reduced. The exact reduction depends on the period and on the nature of the surface. The table shows the magnitude of the effect for a rotation period equal to that of Vesta and for two types of surface—solid rock and porous dust. We expect the largest asteroids to retain a cover of dust, as does the Moon, but smaller bodies with weaker surface gravities will probably behave as solid rock, and the infrared diameter will be much too low.

Albedo

Even if the reflected sunlight is not well represented by the Bond albedo, the effect on an asteroid's diameter is slight. The figure in the table refers to a factor 2 error in albedo.

Variability

There is no evidence for variation of the infrared flux from the three asteroids discussed above. Matson[1] has, however, found some to vary considerably. In such cases, simultaneous optical and infrared measurements are needed to determine whether the variations are caused by changing albedo or shape or both.

CONCLUSIONS

With current detectors it is possible to measure reliable infrared diameters for several dozen asteroids. Notwithstanding the errors and uncertainties, these may be the most reliable dimensions currently available. When more accurate diameters are measured (Dollfus[2]), the infrared data will give us information on the roughness and thermal properties of the asteroids.

REFERENCES

Allen, D. A. 1970, Infrared Diameter of Vesta. Nature **227**, 158.
Hertz, H. G. 1968, Mass of Vesta. Science **160**, 299.
Ney, E. P., and Stein, W. A. 1968, Observations of the Crab Nebula. Astrophys. J. **152**, L21.
Schubart, J. 1970, The Mass of Ceres, IAU Circ. 2268.

---

[1]See p. 45.
[2]See p. 25.

DISCUSSION

ALLEN (in reply to a question by KenKnight): In the rotation calculation, I assumed Earth to be on the asteroid's equator. If we look pole-on, rotation has no effect. The corrections to infrared diameters are reduced if we do not face their equators.

BRECHER: F. C. Gillett of UCSD has communicated to me the results of his independent observations of the three largest asteroids in the infrared, namely that high surface temperatures of 245 to 270 K were obtained. The blackbody temperature in that region of the belt should be ~170 K. What sort of assumptions about albedos, etc., does one have to make to account for such a large discrepancy between expected and observed surface temperature of asteroids?

ALLEN: There are two points . . . first, I do not agree with your calculated temperature and find values around 240 K more appropriate. Secondly, the apparent temperature for a spread of temperatures from subsolar point to limb varies with observing wavelengths, and this effect must be taken into account.

ALLEN (in reply to a question by Bender): I use as the basic temperature the subsolar point temperature equivalent to a flat body facing the Sun; the temperature varies across the disk. If an asteroid rotates, the temperature is reduced.

ANONYMOUS: I am worried by the low densities implied by the diameter for Ceres. To get densities down to 1.6 g-cm^{-3} or so you must assume a proportion of ice, and this has important consequences for the stability of Ceres or any body of that size.

ALLEN: Do not overinterpret the densities I give; I was a bit hesitant about including them in the slide at all. The figure for Ceres was 1.6, but this varies as the third power of the diameter; when you take into account the uncertainties, it could be anywhere from 0 to 4.

SCHUBART (in reply to a request by Chairman Dubin to comment on this paper): The infrared diameters are very valuable because they indicate the sign of possible errors in the diameters measured earlier.

GEHRELS (editorial comment added after the conference): Barnard's value for Vesta may need some revision: Using the diameters of Dollfus[3] and the masses of Schubart[4] one obtains 5 g-cm^{-3} for both Ceres and Vesta. Also see the discussion after the diameter paper of Dollfus.[3]

As for the smaller bodies behaving as solid rocks, this may be an incorrect concept. (See the paper by Hapke,[5] the polarization paper of Dollfus,[6] and discussion remarks by Anders.[7]) Of course, one needs a much thicker layer of dust against infrared penetration than for visual light.

---

[3]See pp. 25 and 29.
[4]See p. 33.
[5]See p. 67.
[6]See p. 95.
[7]See p. 115.

INFRARED OBSERVATIONS OF ASTEROIDS*

DENNIS L. MATSON
California Institute of Technology

This paper is a brief preliminary report about a program of reconnaissance photometry designed to study the thermal radiation emitted from asteroids. Observations of thermal radiation, and their subsequent interpretation, can provide new knowledge that presently cannot be gained by any other method. The emitted thermal power is by and large that portion of the insolation which is absorbed. Part of the asteroid's emission spectrum can be observed through windows in Earth's atmosphere. With the aid of models for the details of energy transfer at the asteroid's surface, and accurate visual photometry, reliable estimates can be made for some of the important parameters in the models. Of particular interest are Bond albedo, size, emissivity, and thermal inertia.

Infrared observations were made through bandpasses centered at 8.5, 10.5, and 11.6 μm ($\Delta\lambda$ = 0.5, 0.5, and 1.0 μm, respectively). The observations were made from July 21, 1969, to July 27, 1970, using the Hale Observatories' 1.52 m telescope at Mt. Wilson. A total of 26 objects was observed: 1 Ceres, 2 Pallas, 3 Juno, 4 Vesta, 5 Astraea, 6 Hebe, 7 Iris, 8 Flora, 9 Metis, 15 Eunomia, 16 Psyche, 18 Melpomene, 19 Fortuna, 20 Massalia, 25 Phocaea, 27 Euterpe, 39 Laetitia, 44 Nysa, 68 Leto, 80 Sappho, 145 Adeona, 163 Erigone, 192 Nausikaa, 313 Chaldaea, 324 Bamberga, and 674 Rachele. Most of the program asteroids were observed through the 11.6 μm bandpass, and bright objects were measured at all three wavelengths. The observational coverage varies from good for the bright objects, which were observed at a number of phase angles, to poor for those asteroids observed only once.

Phase data for 4 Vesta and 7 Iris are shown in figures 1 and 2. Each point represents the weighted nightly mean. The curve in each of these figures is the average using both the 4 Vesta and 7 Iris data. This curve is used to correct all the 11.6 μm thermal emission observations to zero phase angle. For any given angle, the phase variation is a function of the temperature distribution, which in turn is a function of the thermal properties of the asteroidal surface, the orbit, the rotational period, and the aspect geometry. The regions on each side of opposition where the phase angle is large are the two most important critical regions for testing thermal models. Under the proper circumstances, additional

*This paper is contribution no. 2039 of the Division of Geological and Planetary Sciences.

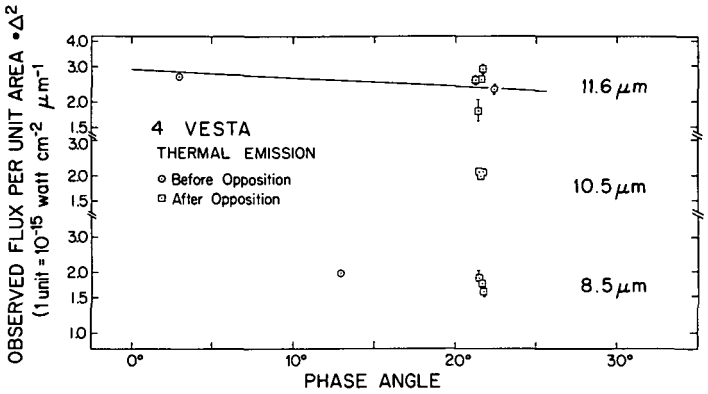

Figure 1.–Phase data for 4 Vesta. The curve through the 11.6 μm data is the phase function used for the reduction of the data presented in figure 3. Errors for some of the data are less than the size of the plotted symbol. Allen's (1970) data for the same opposition have not yet been reduced to the present photometry systems.

critical regions can be provided by aspect differences from one opposition to another.

The ordinate on the phase plots is calibrated by the assumption that α-Bootis has a flux per unit area at Earth of 4.1, 1.8, and 1.2×10^{-15} W-cm^{-2} per micrometer for 8.5, 10.5, and 11.6 μm, respectively. The accuracy of this calibration is not known. The calibrations currently for use in the 8 to 14 μm region have a range of about 20 percent.

All measurements reported here were made with respect to three new stellar photometry systems that were established from observations obtained concurrently with the asteroid program and using the same equipment (Matson, 1971).

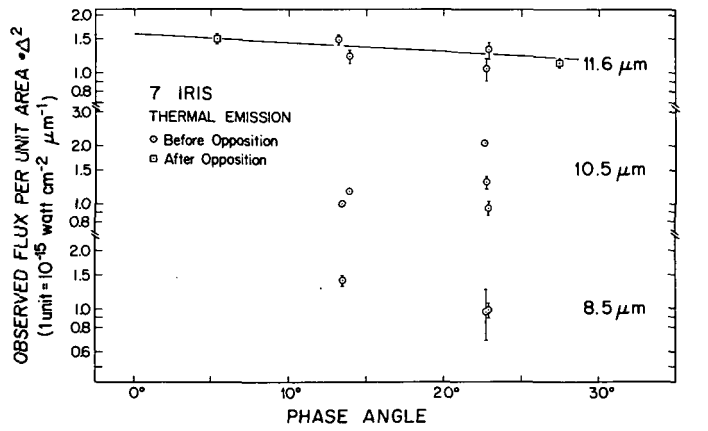

Figure 2.–Phase data for 7 Iris. Some of the scatter is due to the lightcurve.

The scatter shown by the 7 Iris data is due to the lightcurve variation of that asteroid. In fact, enough data are available to construct a composite lightcurve of the thermal emission at 10.5 μm. Correlation of these data with the phase of the visible lightcurve will enable one to differentiate between a spotted asteroid and an irregularly shaped object. This can also be accomplished with the infrared data alone by using observations from two bandpasses to obtain the color temperature as a function of the rotational phase angle. For this method the propagation of observational errors is not as favorable as when using the visible and infrared data.

The error bars on the two phase variation plots represent the propagation of all random and nominal errors incurred in transferring the asteroid observation to α-Bootis. The bounds are intended to delimit the region where the probability of the "true value" is two-thirds or greater.

Table I tabulates some simple models that have been used to analyze the same 4 Vesta data. The parameters, as it can be seen, vary as the model is changed. The common assumption of the three models in table I is that each elemental area on the surface radiates like a blackbody. Phase effects, other than for the corrections applied to the observational data, have been ignored. The albedo parameter has been assumed to be independent of wavelength. This parameter is a weighted average over the solar spectrum. The weight is the amount of energy absorbed at each wavelength.

TABLE I.—*Simple Models for 4 Vesta*

Description	Method of handling temperature T distribution	Model albedo	Model radius, km
Flat disk	T = constant	0.13	264
Smooth, nonrotating sphere	$T=\left[\frac{(1-a)S\cos\phi}{\sigma}\right]^{1/4}$	.085	328
"Rough," nonrotating sphere	$T=\left[\frac{(1-a)S}{\sigma}\right]^{1/4}(\cos\phi)^{1/6}$	.098	306

σ = Stefan-Boltzmann constant; ϕ = angle between heliocentric radius vector and local surface normal; and S = solar constant at the asteroid.

The albedos provided by the models are surprisingly low and the corresponding sizes are large compared to disk measurements. The models and the absolute calibration of the photometry have a systematic error of unknown size and it is premature to assume that the albedo anomaly is due to some unexpected property of asteroidal surfaces. Currently, detailed thermal models that take rotation and the direction of the pole into account are being examined. The simple models (table I) err chiefly in their treatment of the

infrared phase integral and are used only for a differential comparison of the data.

Table I shows that the changes in parameters from model to model are small enough that it is safe to draw some conclusions at this time. For this purpose, the "rough," nonrotating sphere model is employed because it represents the Moon better than the other two. Normalization to 4 Vesta enables a differential comparison to be made between asteroids. The arbitrary normalization is set at 210 km radius and 0.3 albedo. In this way systematic errors from many diverse sources are mitigated, but other errors are introduced. For example, error from the visible phase integral q for 4 Vesta is introduced if the result is interpreted as the Bond albedo. The 11.6 μm infrared data are corrected to zero phase angle and the visible data, $B(1, 0)$, are taken from Gehrels (1970). The resulting model radius and model albedo are plotted in figure 3.

The first things to note are the infrared points for 1 Ceres and 2 Pallas. Already they are in reasonable agreement with published data. Part of the difference is the result of the adopted normalization and the model.

The asteroids vary in the albedo parameter from about 0.03 for 324 Bamberga to about 0.3 for several objects. 324 Bamberga is extremely dark. Presently it is the darkest member of a group of large, dark asteroids. By contrast, 4 Vesta appears to be unique—the only known large, light-colored asteroid. Objects of comparable albedo are not encountered until the 50 to 90 km radius interval is reached. Type I bias is the discrimination against small,

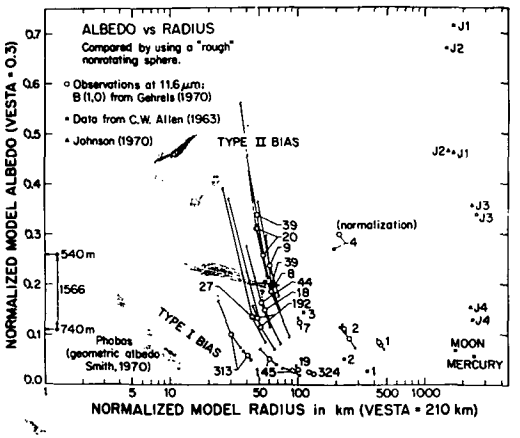

Figure 3.—Differential comparison of the model parameters for selected asteroids. The error bars are for the infrared photometry only. The errors in albedo and radius are correlated and lie along trajectories defined by $B(1, 0)$ = constant. Errors in $B(1, 0)$ and the phase correction are not plotted. The lightcurves appear to be responsible for much of the scatter of values for the smaller asteroids. The ordinate for the data from the literature is the Bond albedo, which is approximately equivalent to the normalized model albedo. Data for Icarus is from Gehrels et al. (1970) and Veverka and Liller (1969).

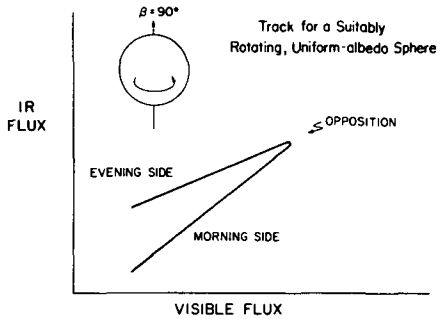

Figure 4.–Infrared flux as a qualitative function of visible flux for a rotating, spherical minor planet with uniform albedo and zero obliquity.

dark asteroids. 313 Chaldaea was obtained near the end of the program when a small number of objects that were thought to be too faint for detection were observed. Considering this bias, it seems likely that there exist small, dark asteroids comparable in size and albedo to Phobos. Infrared observations of Phobos are extremely important. This control point will help to remove distortion in the radius and albedo scales due to differences in surface morphology between large and small asteroids.

At the other extreme of the albedo range is type II bias. Here objects are unduly favored by observational selection. It is surprising that more of them were not discovered. This implies that they are not particularly abundant in the time and space regions sampled.

At this time 20 Massalia and 39 Laetitia are the asteroids with the highest albedo. Their data are dispersed because of their lightcurves. In this reduction, their albedo is in the same class as 4 Vesta and perhaps J3, using Johnson's (1970) lunar-model values for the Bond albedo.

For the large bodies without atmospheres, the trend in the inner part of the solar system is one of low albedo. The Moon, Mercury, and perhaps J4 can be thought of as part of a branch of large, dark objects. The light objects appear to be singular with no trend except for the sheer size of the Galilean satellites of Jupiter. At a radius of about 100 km the dark asteroids continue but they are now joined by objects with higher albedos.

Considering the errors in the model and in the data, it would be risky to draw conclusions about any of the smaller features of figure 3.

Infrared observations also have other applications that are not related to the main thrust of this project. For example, they can aid in the study of rotating asteroids. Consider a rotating, spherical asteroid with an absolutely uniform albedo. Figure 4 shows how the visible and infrared fluxes will be related. Before opposition, warm material is still seen after it crosses the evening terminator. After opposition, the morning terminator of the asteroid is viewed and cool material on the night side contributes only a small amount to the infrared radiation.

ACKNOWLEDGMENTS

The author thanks Bruce C. Murray for suggestions, encouragement, and discussions throughout the course of this project. Gordon Hoover assisted with all of the observations and was indispensable to the program. A special thanks goes to the staff of the Hale Observatories for the many courtesies that they rendered. This work was supported by the National Aeronautics and Space Administration Grant NGL 05-002-003.

REFERENCES

Allen, C. W. 1963, Astrophysical Quantities. Athlone Press. London.

Allen, David A. 1970, Infrared Diameter of Vesta. Nature **227**, 158-159.

Gehrels, T. 1970, Photometry of Asteroids. Surfaces and Interiors of Planets and Satellites (ed., Dollfus), ch. 6, pp. 317-375. Academic Press, Inc. New York.

Gehrels, T., Roemer, E., Taylor, R. C., and Zellner, B. H. 1970, Minor Planets and Related Objects. IV. Asteroid (1566) Icarus. Astron. J. **75**, 186-195.

Johnson, Torrence Vano. 1970, Albedo and Spectral Reflectivity of the Galilean Satellites of Jupiter, p. 58. Ph. D. Thesis, Calif. Inst. of Tech.

Matson, D. L. 1971, Ph. D. Thesis, in preparation.

Smith, Bradford A. 1970, Phobos: Preliminary Results From Mariner 7. Science **168**, 828-830.

Veverka, J., and Liller, W. 1969, Observations of Icarus: 1968. Icarus **10**, 441-444.

DISCUSSION

ANONYMOUS: What happens to the albedo as the size decreases?

MATSON: As the slide showed, we continue to get dark objects but we also seem to be seeing lighter objects at a model radius of about 60 km. Although we say there are some lighter objects, I could not really say which ones because I am worried about the extent of the lightcurve variation of these small objects.

ANONYMOUS: *It would seem to me that the type of model that you consider should* take into account the scattering properties of the surface material. Is this being done?

ALLEN: This is fairly ineffective. I think one cannot as yet try to arrive at any conclusions. Roughness and shape are the most important things and if we ultimately get accurate diameters, from some other method, and we only have two unknowns left, then eventually it can be solved–but not yet.

ANONYMOUS: What if the emissivities are not unity?

MATSON: For the brighter objects there are things that can be done (using observations at three wavelengths), and I am running models for Vesta that are fairly sophisticated in order to check. But for those asteroids with radii of less than 100 km I do not have much hope for improving the situation with the present data. For the smaller objects there is currently data at only 11.6 μm. With future observations we may be able to work out some of the difficulties.

A REVIEW OF SPECTROPHOTOMETRIC STUDIES OF ASTEROIDS*

CLARK R. CHAPMAN, TORRENCE V. JOHNSON, AND THOMAS B. McCORD
Massachusetts Institute of Technology

It has long been realized that studies of the colors of asteroids provide useful clues to their composition. However, only since the development of photoelectric photometry have measurements of asteroid colors proven to be reliable. Recently, with advances in sensors and data systems, it has become possible to measure precisely the spectral reflectivity curves of asteroids from 0.3 to 1.1 μm with higher spectral resolution than that of the *UBV* system.

Until recently, attempts to determine asteroid composition by comparing color indices for asteroids with spectral reflectivities or color indices for meteorites and terrestrial rocks have not been fruitful (Kitamura, 1959; Watson, 1938). It has been noted that the mean color indices for asteroids fall within the range for rocks and meteorites. However, there are far too many minerals for a one-dimensional characterization of asteroid color (color index) to suggest even a compositional class, let alone a specific composition. But when the full spectral reflectivity curve is well defined, for instance in the 24 narrowband interference filters we have been using, the measurements are considerably more diagnostic. Especially diagnostic are well-defined absorption bands as have been found for Vesta (McCord et al., 1970) and a few other asteroids. For instance, the position of the center of the prominent band near 0.9 μm due to Fe^{2+} is dependent on mineralogy. Spectral reflectivity measurements of rocks and meteorites that have been published show a variety of spectral features ranging in strength from a percent to a few dozen percent that are repeatable for different rocks of identical mineralogy. An understanding of the basic physics of the production of absorption bands in solids is well developed, and it is possible to infer mineralogy from spectra containing such bands with considerable confidence. On the other hand, some solids show relatively featureless spectra, characterized only by their sloping trend and perhaps a few inflection points. Obviously such spectra cannot be uniquely

*Contribution No. 30 of the Planetary Astronomy Laboratory, Dept. of Earth and Planetary Sciences, MIT. A more complete treatment of this subject is found in Chapman (1971).

diagnostic, but they can certainly rule out many possible compositional classes. A complete catalog of spectral reflectivities for all common rocks and meteorites has not yet been assembled, though many measurements have been made (Adams, unpublished; Adams and Filice, 1967; Hunt and Salisbury, 1970; Hunt and Salisbury, 1971). Once such a catalog is constructed it should be possible to determine much about the mineralogical composition of measured asteroids, particularly those with absorption bands in their spectra.

Of great interest is the possibility of relating the many distinct classes of meteorites to specific asteroids, asteroid families, or portions of the asteroid belt, and of extending the many results of meteoritics to the asteroids. It is significant that the first conclusive identification of asteroid composition (McCord et al., 1970) shows that Vesta has a composition very similar to the Nuevo Laredo basaltic achondrite. It should soon be possible to relate the common classes of meteorites to specific asteroid families or parts of the belt, which will be a test of our understanding of the processes that transport asteroidal fragments into Earth-crossing orbits. Because the gross characteristics of most asteroid orbits probably have not changed substantially during the age of the solar system, what understanding has been achieved of the thermal and chemical environments where meteorites were formed (Anders, 1971) can then be tied to a specific location in the early solar system.

Even when unique compositional identifications are not possible, spectral reflectivity measurements permit a sorting of asteroids into classes of similar composition. Asteroids with similar reflectivities may well be genetically related, especially when the asteroid population is examined statistically. Thus we will attempt to correlate asteroid colors with orbital characteristics, size, and lightcurves. We now describe some kinds of correlations that should be searched for and some implications such correlations might have if found.

Correlation between color and semimajor axis a or the Jacobi constant (Tisserand invariant) may well be indicative of differences in the condensation of the solar nebula as a function of distance from the Sun. To the extent that it may be possible that ices could be stable over long durations in the outer parts of the asteroid belt (Watson, Murray, and Brown, 1963), some correlations with a could reflect on-going processes or conditions in the asteroid belt integrated over the age of the solar system.

Asteroids with unusual inclinations or eccentricities have orbited the Sun in a different space environment than have most asteroids. In particular, the spatial density of small asteroids, meteoroids, micrometeoroids, and interplanetary dust is probably substantially lower away from the main part of the asteroid belt. On the other hand, the relative impact velocities against such space debris will be higher for asteroids in inclined or eccentric orbits. The glasses produced by hypervelocity micrometeoroid bombardment of the lunar regolith modifies spectral reflectivity curves for the Moon, primarily by lowering albedo and diminishing absorption band intensity (Adams and McCord, 1971). Also, it seems possible that there could be a greater meteoritic

component (i.e., a contamination of the original asteroidal composition by material not originating on that asteroid) in asteroidal regoliths than the few percent determined for the lunar mare regolith. In fact, depending upon the mass-frequency relation for the population of impacting particles to which an asteroid is subject, a substantial regolith may never form on some asteroids. Any correlation of asteroid spectral reflectivity with variables correlated with an asteroid's impact environment may shed light on these processes.

Several dozen Hirayama families, possible families, or jetstreams of asteroids with similar orbital elements have been recognized (e.g., see Arnold, 1969). It is particularly interesting to examine the colors of asteroids as a function of family. Though it is widely believed that members of a family are products of a collision or collisions, alternative hypotheses have been proposed. Fragmental family members might generally be expected to have identical colors, but differences within a certain family could be interpreted in terms of a highly differentiated asteroid being broken up or of the collisional fragmentation of two asteroids of similar size. Some asteroids have unusual rotation periods that may result from collisions. Other asteroids have large-amplitude lightcurves, suggesting either a markedly nonspherical shape or great differences in surface albedo on different sides of the asteroid. Either might result from initial conditions or from a major collision. Correlations between such characteristics and color might prove valuable, especially if these asteroids can also be related to particular meteorite groups.

It is clear that studies of asteroid spectral reflectivities have great promise for shedding light on the origin, history, and current processes and state of the region of the solar system between 2 and 4 AU. But it is also clear that there are many variables to consider and hence much data are required for definitive conclusions. Future programs should take into account the following requirements:

(1) It is imperative that the largest possible number and variety of asteroids be observed. This means that very faint (hence small) asteroids must be observed as well as the major ones. Several members of each asteroid family should be observed and of unusual classes of asteroids such as Apollo asteroids, Trojans, and dead comets.

(2) Asteroids should be observed at as many wavelengths throughout the visible and as far into the infrared (where most absorption bands occur) as possible. Ability to recognize reflectivity features at the 1 percent level would be desirable, and ability to measure band positions to 0.01 μm would be valuable.

(3) Individual asteroids should be observed over a complete rotation and at a variety of solar phase angles. Reflectivity curves undoubtedly vary with phase angle and probably differently for different asteroids. Some small variation of color with rotation has been detected for at least one asteroid.

EARLY STUDIES OF ASTEROID COLORS

Photographic

It had long been assumed that asteroids were gray reflectors of the solar spectrum and they have been used from time to time as comparison stars. Bobrovnikoff (1929) first questioned this premise and attempted to measure the characteristics of asteroid spectra. He compared microphotometric tracings of photographic spectra with *G*-type stars; he concluded that (1) he was observing reflection spectra with no emission features, (2) that Ceres and Vesta lacked any major absorptions in the visible like those of Jupiter, (3) that asteroids have relatively low reflectivity in the violet and ultraviolet, and (4) that there were differences between asteroids. Bobrovnikoff's tracings seem to show definitely that Pallas is relatively more reflective near 0.4 μm than other asteroids studied. But Watson (1938) regards many of Bobrovnikoff's conclusions as uncertain because of a lack of standardization of the spectra. Certainly there are some discrepancies with recent photoelectric data for some asteroids discussed by Bobrovnikoff.

Microphotometric tracings of spectra of three asteroids by Johnson (1939) yielded the incorrect result that these asteroids were substantially bluer than the Sun. Recht (1934) reached a similar erroneous conclusion from a more extensive study of the color indices of 34 asteroids obtained from magnitude measurements on normal photographic and panchromatic plates. Recht's measurements have been criticized by several subsequent writers. They show a large scatter because, among other reasons, the measurements of the two colors were often made from plates taken on different nights, and there is a strong correlation between the color index derived by Recht and the apparent magnitude of the asteroid—such a correlation being indicative of a spurious systematic error in the photographic measurements. There is little if any agreement between Recht's color indices and recent *UBV* photoelectric photometry. Watson (1940) obtained more realistic color indices for seven asteroids, but their reliability is difficult to gage.

Perhaps the most ambitious and reliable of the early photographic colorimetry is that of Fischer (1941). Though Fischer's data show less scatter than Recht's, the random errors are nevertheless uncomfortably large. Of the 30 asteroids for which Fischer obtained color indices, a fair number have photoelectric $B - V$ colors that correlate reasonably well in a relative sense with Fischer's values. In figure 1, Fischer's color indices have been rescaled and plotted so that their mean and range match the photoelectric values, but no absolute calibration is intended. It is probably true that most of Fischer's bluer asteroids are in fact bluer than his redder ones, but finer distinctions probably have no meaning. Fischer reported statistically significant correlations between color index and two related orbital characteristics: semimajor axis and Jacobi constant. The correlation is in the same sense as evident in subsequent photoelectric work (see later section), but one should be aware of the potential

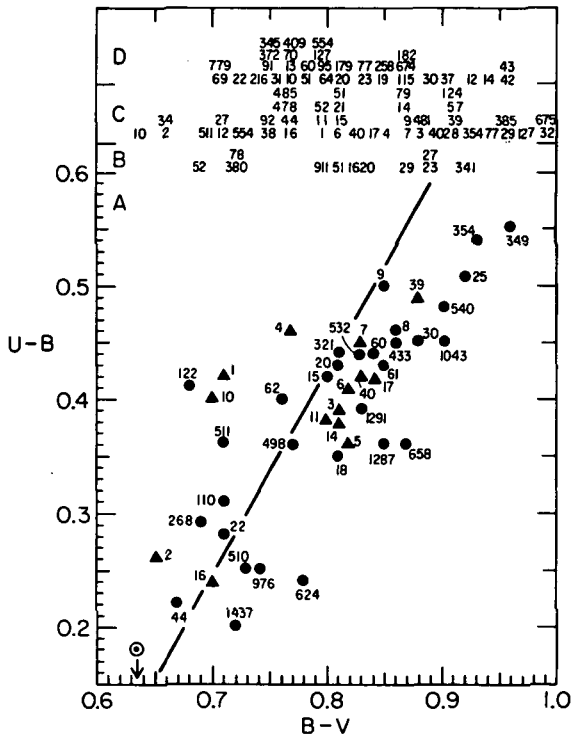

Figure 1.–Asteroid colors from photoelectric and photographic photometry. (A) $B - V$, $U - B$ colors for asteroids summarized in Gehrels (1970). Triangles indicate those asteroids that have also been observed in the present authors' spectral reflectivity program. The line is the stellar main sequence and its intersection with the arrow in the lower left is the *UBV* color of the Sun. (B) $B - V$ colors for asteroids for which no U color has been measured (Gehrels, 1970). (C) Approximate scaling of photoelectric color indices of Kitamura (1959). (D) Approximately rescaled photographic color indices of Fischer (1941); probably only the gross distinction between asteroids on the left and to the right is meaningful for Fischer's colors. Also see figure 1 of the paper by Hapke.[1]

in this early photographic work for systematic apparent-magnitude-dependent errors that themselves would be weakly correlated with semimajor axis.

The largest sample of asteroids for which photographic color indices have been determined is contained in the work summarized by Sandakova (1962). At the time of writing, we have not been able to obtain the original published description of these data and their reduction. It is worth noting that seven asteroids with color indices reported in Sandakova (1962) show poor agreement with recent *UBV* work and that very large scatter is evident in the data for the 10 asteroids reported. Sandakova reports no correlation of colors

[1]See p. 69.

in the complete sample with a, but a large difference in color between asteroids with unusually small and unusually large orbital Jacobi constants.

Photoelectric

An early photoelectric program to study asteroid colors was carried out by Kitamura (1959) in the mid-1950's. Forty-two asteroids were measured with a 1P21 photomultiplier in two colors with effective wavelengths somewhat longward of the standard B and V colors. From a graph presented by Kitamura of the color indices of six stars with known $B - V$ colors, it is possible to make an approximate conversion of his color index to $B - V$. The resulting values have a slightly redder mean and greater range than $B - V$ colors obtained by Gehrels, Kuiper, and their associates, so we have applied some corrections to Kitamura's colors for plotting in figure 1. The several cases of multiple measurements of the same asteroid show small scatter in Kitamura's data and the agreement for those asteroids for which $B - V$ colors are known is good. Kitamura reports negative attempts to correlate his color indices with the proper orbital elements, magnitude $B(1, 0)$, and rotation period. Though his figures show no correlation with $B(1, 0)$ or mean motion, there appears to be a definite correlation with proper eccentricity e'. The sign of the correlation is such as to amplify the expected correlation of the Jacobi constant with respect to a correlation with a. His table also shows a possible correlation of color index with extreme a, such that asteroids with $a > 3$ AU are bluer than those with $a < 2.3$ AU (but the statistics are poor).

UBV PHOTOELECTRIC PHOTOMETRY

Since the mid-1950's Gehrels, Kuiper, and their associates have published a series of papers on photoelectric photometry of asteroids in the standard *UBV* system. Gehrels has published a table summarizing these results (Gehrels, 1970) and we have plotted them in parts A and B of figure 1. The plotted colors include the small corrections made by Gehrels for reddening with phase; he used lunarlike phase relations, the applicability of which to asteroids has been largely untested. The consistency of most of the *UBV* data is quite good, and most of the plotted asteroids are probably known to at least 0.05 mag in both colors. Of course, there are rarely sufficient data to determine the ranges of variation in color with rotation and phase for the individual asteroids, and such variations would contribute to the scatter. One asteroid, 1566 Icarus, has a typical $B - V$ color but its $U - B$ value is so large that the point is off the scale of the figure.

There is a fair spread of asteroid colors evident in the figure with a trend somewhat redder than the stellar main sequence. There is a major clumping around $(B - V, U - B) = (0.83, 0.4)$ and a lesser one near $(0.7, 0.25)$. There is some spread of the main clump both to the upper right and to the left. The numbers of several asteroids for which only $B - V$ colors exist are plotted in part B of the figure. In sum, there is a general dearth of asteroids with $B - V$

colors near 0.75. For purposes of comparison, Kitamura's rescaled colors are plotted in part C of the figure and Fischer's rescaled colors in part D. In general, these three sets of data show fair agreement, but there are discrepancies.

Parts A and B of figure 1 are replotted in figure 2 showing the distribution in color of five groupings by asteroid semimajor axis. A correlation is evident, though it is due almost entirely to the extreme values of a. Ten of the 13 asteroids with $a > 3.0$ have $B - V \leqslant 0.8$ whereas none of the five asteroids with $a < 2.3$ is so blue. Asteroids with $2.75 < a < 3.0$ show the greatest range of colors. If several times as many asteroids could be plotted, we might begin to see statistically significant clusterings of a values in the plane of figure 2, but it is premature to draw strong conclusions from the present sample.

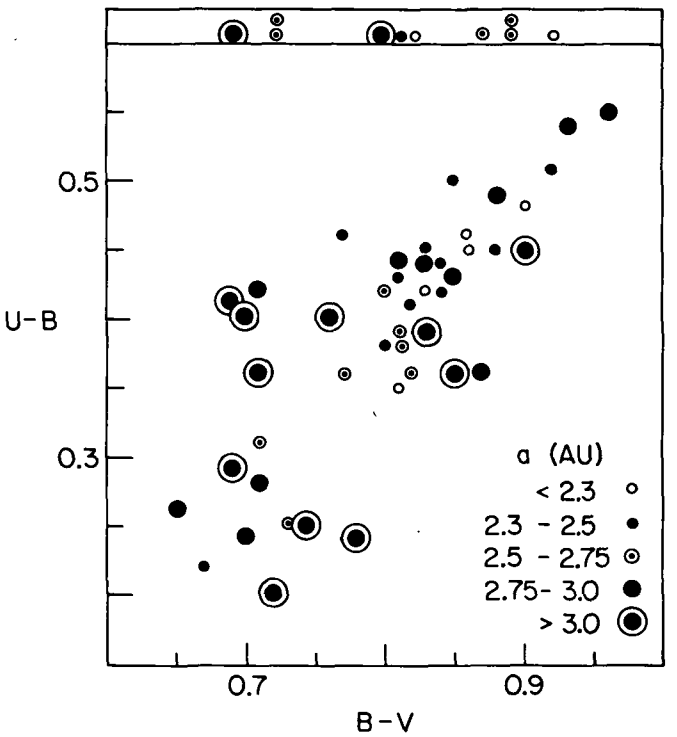

Figure 2.–Color of asteroids from parts (A) and (B) of figure 1 plotted in five groups according to size of semimajor axis.

We have noted that the correlation of *UBV* asteroid colors is somewhat stronger with the Tisserand invariant against perturbation by Jupiter (Jacobi constant) than with a alone. Nevertheless, the correlation is far from perfect and there are several extreme exceptions.

SPECTRAL REFLECTIVITY FROM NARROWBAND FILTER PHOTOMETRY

McCord and his associates have been undertaking a program of measuring the spectral reflectivities of all major solar system objects from 0.3 to 1.1 μm, and out to 2.5 μm when possible. After enticing results were obtained for Vesta, a program was begun to look at as many other asteroids as possible. This program constitutes the major portion of Chapman's doctoral dissertation, now in preparation. Although a program of strictly asteroid photometry has not yet been funded, telescope time has been available for asteroid observations during hours when other objects of high priority were below the horizon. To date we have observations of some sort of 32 asteroids, of which 12 have been partly reduced and will be discussed later.

McCord's (1968) double-beam photometer has been used in making observations of asteroids in a variety of modes on several telescopes at Mt. Wilson, Mt. Palomar, and Kitt Peak. A set of 24 narrowband interference filters from 0.3 to 1.1 μm are used concurrently, sometimes in a spinning-filter-wheel mode (3 rpm), and sometimes incrementally over a period of about 1 hr. The sky is observed in the second beam of the photometer with a 10 Hz chopping system and is subtracted from the signal. For some runs an S-1 phototube is used over the entire range 0.3 to 1.1 μm, whereas for others the S-20 is substituted for the wavelengths to which it is sensitive. Most of the data reported in this paper were taken with the S-1 tube alone. A pulse-counting data system is used. Air-mass corrections are determined from observations in each filter of the standard stars of Oke (1964) by taking values at equal air mass and correcting for time-dependent changes. The data are reduced to spectral reflectivity using the stellar standardizations and the solar spectrum of Labs and Neckel (1968). However, integration over solar spectral lines and bands with square-wave filter response produces error, especially near large solar lines in the ultraviolet. All standard stars are ultimately tied to α-Lyrae by Oke and Schild (1970) and, therefore, systematic errors in α-Lyrae's flux distribution will affect our results. However, theoretical models for α-Lyrae and observations presently agree to within a few percent over our spectral range. Deviations of a few percent of particular filters from the general trends that are observed for all solar system objects are smoothed out. All sources of error are very small, however, so the accuracy of our standardizations is a few percent, except for one or two ultraviolet filters. The relative comparisons between solar system objects are even more precise. The reflectivity curves are scaled to unity at 0.56 μm for purposes of comparison.

Reflectivity curves obtained in this manner bear some relation to *UBV* colors but provide much more information. Asteroids with identical *UBV* colors may differ greatly in the red and near infrared regions where important absorption bands are common. In fact, the details of spectral reflectivity curves in the 0.3 to 0.6 μm region can differ somewhat for asteroids with identical *UBV* colors, although the overall trends must correlate. Thus, far more

information is contained in the complete reflectivity curve than in *UBV* measurements, but they can still be related to each other. It would, of course, be desirable to extend the range of reflectivity measurements, particularly into the infrared where there are a variety of highly diagnostic solid absorption bands, but nearly all asteroids are so faint that they are difficult to observe with available systems beyond 1.1 μm.

EARLY SPECTRAL REFLECTIVITY MEASUREMENTS OF THE FOUR MAJOR ASTEROIDS

The first spectral reflectivity study of an asteroid by McCord and his associates (1970) turned out to be particularly exciting. Measurements of Vesta made at Cerro Tololo in December 1969 and with a different filter set at Mt. Wilson in October 1968 showed a very deep absorption band centered near 0.915 μm. The band is the most prominent absorption band yet found on any solid solar system body. McCord, Adams, and Johnson have interpreted the composition indicated by the spectral reflectivity curve of Vesta to be that of certain basaltic achondrite meteorites (Mg-rich orthopyroxene or pigeonite). This identification, of course, refers to the composition of the Vesta *surface* minerals that, because of their abundance and albedo, contribute the bulk of Vesta's reflected light.

A subsequent study of Vesta (Johnson and Kunin, 1971) has shown that the primary characteristics of the spectral reflectivity curve do not change as Vesta rotates. The asteroid was observed continuously for a few hours with the Mt. Wilson 152 cm reflector and no changes were detected except for statistically marginal evidence for the dark side being somewhat more reflective (relatively) than the light side in the violet. This change is in the same direction as a correlation of *UBV* color with lightcurve reported by Gehrels (1967). Two runs showing approximately opposite sides of the asteroid are presented in figure 3. It is particularly noteworthy that the 0.9 μm absorption band remains unchanged in position on opposite sides of the asteroid because band position is a sensitive indicator of mineralogical composition. Evidently the gross surface composition of Vesta is quite homogeneous on a large scale.

We observed the three other bright asteroids (Ceres, Pallas, and Juno) in June 1970, using twilight time on the 508 cm reflector. Good signals were obtained during the short intervals available to us for observing, but standardization was difficult because of lack of time. Certain fluctuations for individual filters in the reduced data for two of the asteroids can be ascribed to the poor calibration of the particular standard star against which they were observed. These have been smoothed out, but the smoothings do not change the major characteristics of the spectral reflectivity curves. The spectral reflectivities of the three asteroids are plotted with Vesta as a reference in figure 4.

Pallas is much brighter than the other asteroids in the violet, confirming Bobrovnikoff's early conclusion and *UBV* data. Juno shows a reflectivity

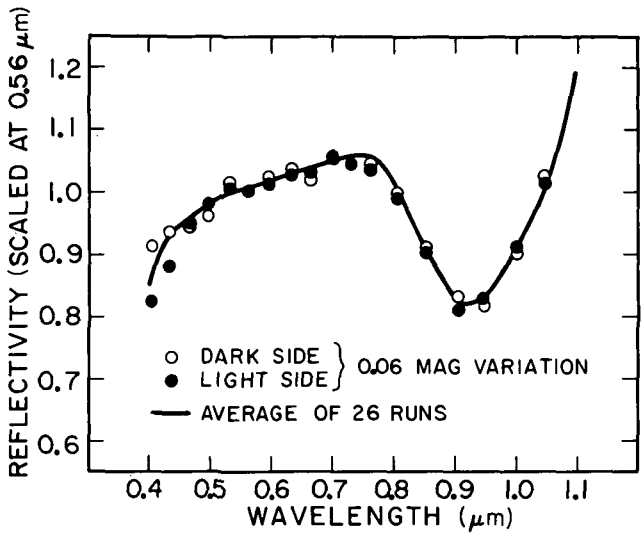

Figure 3.–Spectral reflectivity of 4 Vesta. Individual runs on approximately opposite sides of the asteroid are plotted on the mean curve of 26 runs. Mt. Wilson 152 cm reflector, February 16, 1970.

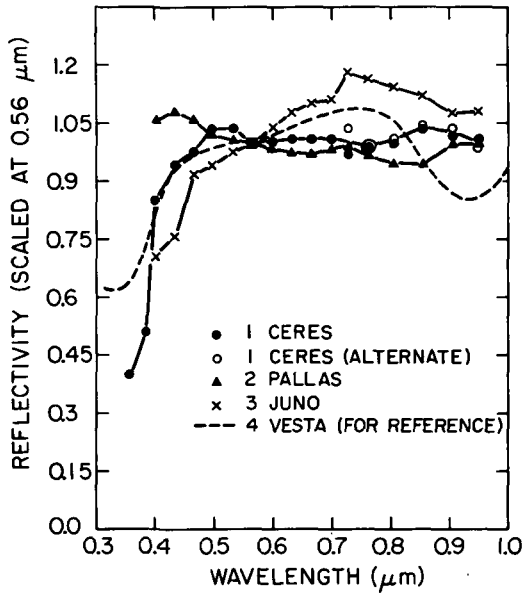

Figure 4.–Spectral reflectivity curves for Ceres, Pallas, and Juno (with Vesta for comparison); Mt. Palomar 508 cm reflector, June 24 to 29, 1970. Square indicates scaling to unity at 0.56 μm. Alternative methods of reducing Ceres data against ξ^2-Ceti shown for $\lambda > 0.7$ μm. Some smoothing applied to Pallas and Juno to correct for deviations due to the standard star η-Piscium.

peak near 0.7 μm and has a much redder slope in the visible than the other three major asteroids. None of the first three asteroids shows a noticeable absorption band to compare with that of Vesta, although Juno does diminish in reflectivity near 1.0 μm. Ceres is quite bright in the blue but falls off sharply in the ultraviolet, which confirms its unusual *UBV* color shown in figure 1. All four major asteroids are different in color, but we do not feel confident of making a unique identification on the basis of these preliminary data. The flat, even bluish, trend of the reflectivity curve for Pallas is suggestive of ices, but the low albedos that have been inferred for Pallas (Matson;[2] Veverka, 1970) are inconsistent with ices. John Adams has told us that metallic meteorites show similar flat spectral reflectivities, but no definitive identification is possible until a wide variety of meteorites (such as carbonaceous chondrites) have been studied and their reflectivities cataloged.

SPECTRAL REFLECTIVITIES OF 11 ASTEROIDS

We used the Mt. Wilson 152 cm reflector in October 1970 to measure the spectral reflectivities of 11 asteroids. An example of the data for one of these asteroids (192 Nausikaa) is shown in figure 5. The error bars are standard deviations of the means of nine runs. A fairly prominent absorption band is

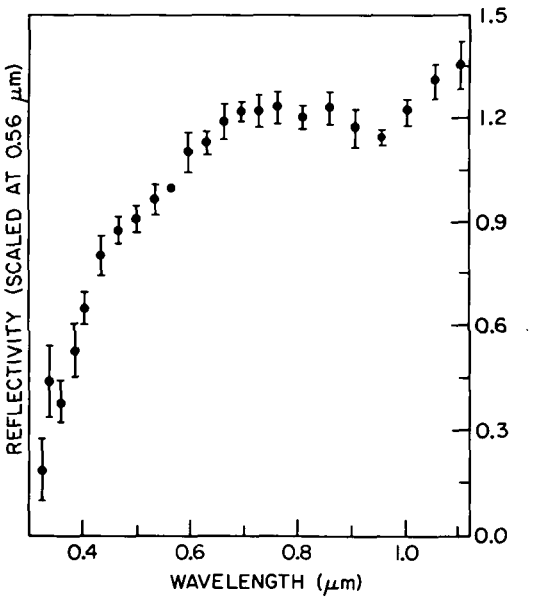

Figure 5.–Spectral reflectivity for 192 Nausikaa, mean of 9 runs; Mt. Wilson 152 cm reflector, October 10, 1970. ξ^2-Ceti was used as the standard star. Error bars are standard deviations of the mean. Preliminary reduction.

[2]See p. 48.

apparent, though less deep than that of Vesta. We wish to postpone attempting a conclusive mineralogical identification until further observations of 192 have been reduced. Chapman (1971) will discuss the final reduction for these 11 asteroids and others observed after October 1970.

The spectral reflectivity curves for the 11 asteroids, including 192, are shown in figure 6. An approximate indication of the standard deviations of the points in the middle portions of the reflectivity curves is indicated in the figure. The smooth curves were drawn through the error bars. Most of the indicated features are probably real, but some of the smaller bumps and dips should await confirmation and improvements in our standardization.

The reflectivity curves have been plotted in three groups in figure 6. The Vesta curve is also shown for comparison with each group. The top curves are those with the bluest trend and the bottom group contains the reddest, but we do not intend to suggest three distinct groupings from what may be a more or less continuous spectrum of color trends.

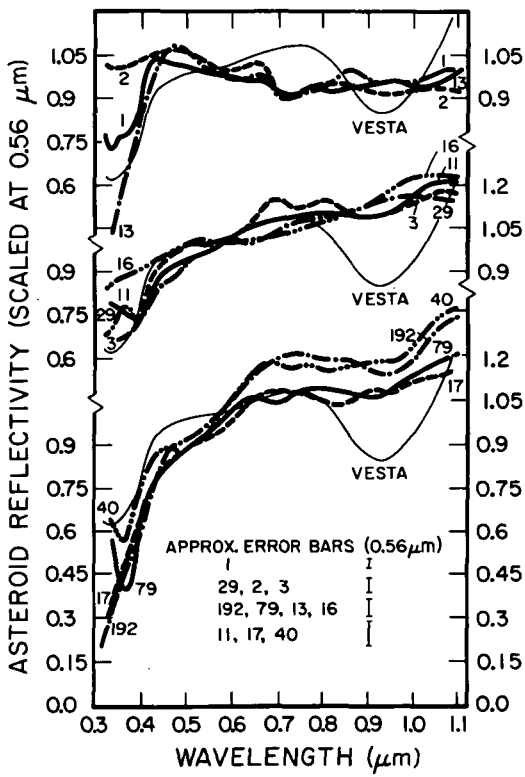

Figure 6.–Spectral reflectivity curves for asteroids 1, 2, 3, 11, 13, 16, 17, 29, 40, 79, and 192 (with Vesta for comparison). Mt. Wilson 152 cm reflector, October 9 to 12, 1970. Observations reduced against ξ^2-Ceti and smooth curves scaled approximately to unity at 0.56 μm; typical error bars are indicated.

Although the reflectivities shown here have not been corrected for any reddening with phase and the observations cover a range of phases among the various asteroids shown, there is no correlation between the phase angle at time of observation and the apparent color trend. The differences between most of these asteroid spectral curves far exceed effects due to phase angle, particle size, and similar variables. These differences are almost certainly due to compositional variations among the asteroids. The wide range of compositions implied is most significant. An imperfect correlation between color trend and semimajor axis is evident for these 12 asteroids, but of course the statistics are poor.

The members of the reddish group are very dark in the ultraviolet and show prominent inflection points near 0.4 and 0.7 μm. (The upturns in the far ultraviolet for 40 Harmonia and 79 Eurynome may not be real.) A possible cause for the broad relative absorption near 0.5 μm for the reddish asteroids is a band due to Ti^{3+}. Asteroids 1 Ceres, 2 Pallas, and 13 Egeria show a bluish trend, except that Ceres and Egeria have sharp turndowns toward the ultraviolet. Except for 3 Juno, the intermediate asteroids (11 Parthenope, 16 Psyche, and 29 Amphitrite) lack the rise near 0.7 μm characteristic of the redder asteroids. All the intermediate asteroids are moderately reflective in the ultraviolet, except 16, which is very reflective by comparison. Some of the asteroids other than 4 and 192 show hints of the 0.9 μm absorption band, but we must await reduction of additional observations of these objects to be sure. It is certainly a fair generalization that absorption bands as prominent as that of Vesta are unusual.

Two of the 12 asteroids studied are members of the same Hirayama family (Brouwer's 25th family). These two asteroids (17 Thetis and 79 Eurynome) have reflectivity curves that are identical to each other to within observational errors. This observation is consistent with the hypothesis that the family is composed of fragments from a single asteroid. We are attempting to observe other pairs of family members to see if this is a general rule.

SUMMARY AND CONCLUSIONS

The results of the MIT program that have been presented here are preliminary. Altogether we have obtained fairly comprehensive spectral reflectivity observations for 23 asteroids, and some data on 9 others. Of these, 12 have been partially reduced and described in this paper; the remainder will be reduced very soon. Through cooperation with Dennis Matson, we have obtained data on 12 asteroids that were included in his thermal infrared program.[3] These preliminary results are most promising because they demonstrate that the asteroids have a wide variety of surface compositions and that many of the spectral reflectivities do contain diagnostic bands and inflections that may lead to precise mineralogical identifications. Even when explicit

[3]See p. 45.

identification is not possible, these data at 24 wavelengths permit the separation of asteroids with far greater discrimination than is possible in the three-color *UBV* work.

The full value of spectral reflectivity studies will only be achieved, however, once spectral reflectivities of many dozens or several hundred asteroids have been studied and once a comprehensive catalog of meteorite and rock spectral reflectivities has been assembled. Both of these goals can be achieved within a couple years, and we hope to make progress in these directions.

REFERENCES

Adams, J. B., and Filice, A. L. 1967, Spectral Reflectance 0.4 to 2.0 Microns of Silicate Powders. J. Geophys. Res. **72**, 5705-5715.

Adams, J. B., and McCord, T. B. 1971, Alteration of Lunar Optical Properties: Age and Composition Effects. Science **171**, 567-571.

Anders, E. 1971, Meteorites and the Early Solar System. Annu. Rev. Astron. Astrophys. **9**, in press.

Arnold, J. R. 1969, Asteroid Families and "Jet Streams." Astron. J. **74**, 1235-1242.

Bobrovnikoff, N. T. 1929, The Spectra of Minor Planets. Lick Observ. Bull. 407, pp. 18-27.

Chapman, C. R. 1971, Surface Properties of Asteroids. Doctoral Dissertation. MIT. In preparation.

Fischer, H. 1941, Farbmessungen an kleinen Planeten. Astron. Nachr. **272**, 127-147.

Gehrels, T. 1967, Minor Planets. I. The Rotation of Vesta. Astron. J. **72**, 929-938.

Gehrels, T. 1970, Photometry of Asteroids. Surfaces and Interiors of Planets and Satellites (ed., A. Dollfus), pp. 317-375. Academic Press, Inc. London.

Hunt, G. R., and Salisbury, J. W. 1970, Visible and Near-Infrared Spectra of Minerals and Rocks (pt. I). Mod. Geol. **1**, 283-300.

Hunt, G. R., and Salisbury, J. W. 1971, Visible and Near-Infrared Spectra of Minerals and Rocks (pt. II). Mod. Geol. **2**, 23-30. (Pts. III-IV, in press.)

Johnson, W. A. 1939, Spectrophotometric Study of Three Asteroids. Harvard Col. Observ. Bull. 911, pp. 13-16.

Johnson, T. V., and Kunin, J. 1971, Vesta: Variation of Color With Rotation. In preparation, 1971.

Kitamura, M. 1959, A Photoelectric Study of Colors of Asteroids and Meteorites. Publ. Astron. Soc. Jap. **11**, 79-89.

Labs, D., and Neckel, H. 1968, The Radiation of the Solar Photosphere from 2000Å to 100μ. Z. Astrophys. **69**, 1-73.

McCord, T. B. 1968, A Double Beam Astronomical Photometer. Appl. Opt. **7**, 475-478.

McCord, T. B., Adams, J. B., and Johnson, T. V. 1970, Asteroid Vesta: Spectral Reflectivity and Compositional Implications. Science **168**, 1445-1447.

Oke, J. B. 1964, Photoelectric Spectrophotometry of Stars Suitable for Standards. Astrophys. J. **140**, 689-693.

Oke, J. B., and Schild, R. E. 1970, The Absolute Spectral Energy Distribution of Alpha Lyrae. Astrophys. J. **161**, 1015-1023.

Recht, A. W. 1934, Magnitudes and Color Indices of Asteroids. Astron. J. **44**, 25-32.

Sandakova, E. V. 1962, O Pokazatelyakh Tsveta Malykh Planet. Publ. Astron. Observ. Kiev, no. 10, pp. 3-15.

Veverka, J. 1970, Photometric and Polarimetric Studies of Minor Planets and Satellites. Doctoral Dissertation, Harvard Univ.

Watson, F. G. 1938, Small Bodies and the Origin of the Solar System. Doctoral Dissertation, Harvard Univ.

Watson, F. G. 1940, Colors and Magnitudes of Asteroids. Harvard Col. Observ. Bull. 913, pp. 3-4.

Watson, K., Murray, B. C., and Brown, H. 1963, Stability of Volatiles in the Solar System. Icarus **1**, 317-327.

DISCUSSION

BRATENAHL: What is the limit in apparent magnitude your technique can be pushed to?

CHAPMAN: We have had no difficulty measuring several asteroids per night brighter than 12 mag. The problem is with the interesting wavelength interval beyond the response limit of S-20 photomultipliers (~750 nm). With sufficient time on a large telescope it should be possible to measure 15 and 16 mag objects to some precision out to 1050 nm, using an S-1 tube. Still fainter asteroids could be measured shortward of 750 nm provided they could be accurately located with respect to a guide star.

GEHRELS: Lightcurves have been obtained by direct visual setting on a moving asteroid–with the B or V filter, 1P21 tube, and an integration time of a minute–down to $V \sim 16.5$ with a 154 cm telescope; the precision is about ±0.004 mag.

JOHNSON: In comparing spectral reflectivity measurements with standard *UBV* photometry, several things should be kept in mind: (1) our filters have considerably narrower bandpasses; (2) we must observe sequentially in 24 of them instead of one, two, or three; (3) the S-1 surface has a low quantum efficiency (about 0.1 percent compared to ~10 percent for an S-20); and (4) our program requires frequent measurements of standard stars at all 24 wavelengths.

Page intentionally left blank

INFERENCES FROM OPTICAL PROPERTIES CONCERNING THE SURFACE TEXTURE AND COMPOSITION OF ASTEROIDS

BRUCE HAPKE
University of Pittsburgh

The optical properties of the asteroids are compared with those of the Moon and various terrestrial, lunar, and meteoritic materials. It is concluded that the surfaces of most of the asteroids are covered with at least a thin layer of unconsolidated, fine-grained powder similar to lunar soil. None of the asteroids appear to have compositions corresponding to pure nickel/iron meteorites.

The picture that most of us have in our minds of a typical asteroid is probably of a large, irregularly shaped chunk of iron, unrusted by exposure to oxygen or water, and with a surface kept clean and dust free by the sandblasting effect of repeated micrometeorite impacts. However, consideration of the known optical properties of asteroids suggests a rather different model. It is the purpose of this paper to review briefly the optical characteristics of asteroids and to compare them with other extraterrestrial and terrestrial materials to obtain information concerning the nature of the outer surfaces of the minor planets.

OPTICAL PROPERTIES OF ASTEROIDS

The optical characteristics of the asteroids that this paper will be concerned with include the visual albedo, *UBV* color indexes, brightness-phase curve, and polarization-phase curve. These properties are summarized in table I and figure 1. In the tables and figures, the following were used: the visual geometric albedo; $U - B$ and $B - V$, differences between *UBV* color indexes relative to the Sun; $\partial m_v/\partial\alpha$, the slope of the apparent visual magnitude m_v versus phase angle α for $5^\circ < \alpha < 25^\circ$; the opposition effect defined as the ratio of brightness at $\alpha = 1^\circ$ to that at $\alpha = 5^\circ$; the value of polarization at the minimum of the polarization-phase curve; α^-, phase angle at which the minimum occurs; α_0, phase angle (other than 0° and 180°) at which the polarization is zero. The data for table I and figure 1 are taken primarily from the review paper by Gehrels (1970) and from these additional sources: Dollfus (1961), Harris (1961), Miner and Young (1969), Gehrels (1956), Allen (1963),

TABLE I.—*Optical Properties of Asteroids and the Moon*

Body	Diameter, km	Geometric albedo, percent	$U-B$, mag	$B-V$, mag	$\frac{\partial m_v}{\partial \alpha}$	Opposition effect	Polarization minimum, percent	α^-	α_0
1 Ceres	770	13	0.31	0.08	0.05	–	−1.8	8°	17°
2 Pallas	490	11	.16	.02	.04	–	−1.3	10	18
3 Juno	190	27	.29	.18	.03	–	–	–	–
4 Vesta	390	45	.36	.14	.03	1.26	−0.6	10	22
20 Massalia	–	–	.33	.18	.03	1.32	–	–	–
1566 Icarus	0.5	30	.56	.17	.03	–	–	–	–
Moon	3470	12	.32	.29	.03	1.29	−1.0	10	23

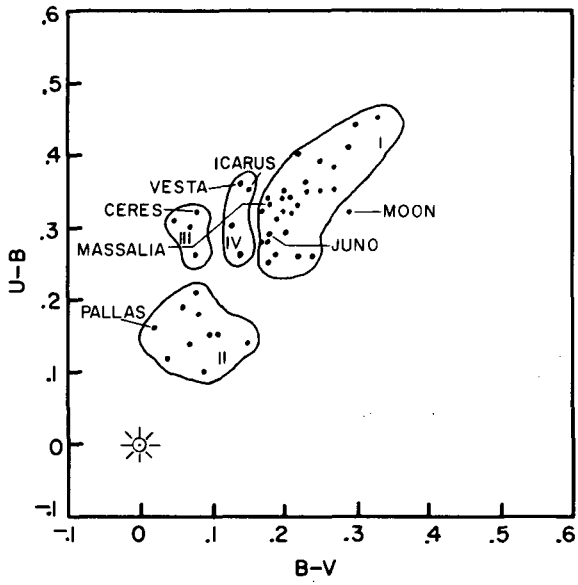

Figure 1.—Differences between *UBV* indexes of asteroids and the Moon relative to the Sun. Also see figure 1 of the paper by Chapman, Johnson, and McCord.[1]

Goldstein (1968), and Veverka (in this volume[2]). Included in table I and figure 1 are data for the Moon for comparison.

Because of the faintness of the asteroids, detailed optical data exist only for relatively few bodies. To calculate the geometric albedo from the absolute magnitude, the diameter must be known; but only a few of the largest of the minor planets show disks. (See the paper by Dollfus.[3]) Detailed reflectivity curves have been published for only one asteroid, Vesta (McCord, Adams, and Johnson, 1970); for the rest, only the *UBV* indexes are known.[4] The degree to which the optical properties of the larger bodies are representative of all asteroids is not clear. Also, among the fainter asteroids, high-albedo objects, such as Vesta, will be preferentially discovered and observed over low-albedo bodies, such as Pallas.

OPTICAL PROPERTIES OF GEOLOGICAL MATERIALS

Because the only optical information available for most of the asteroids are their *UBV* indexes, the greatest attention will be given to the interpretation of these spectral data. To facilitate comparison with the various laboratory

[1]See p. 55.

[2]See pp. 79 and 91.

[3]See pp. 25, 30, and xv.

[4]*Editorial note:* Additional data now are available in the paper by Chapman, Johnson, and McCord, p. 51.

materials, it is necessary to discuss the processes that influence the reflection of light from complex surfaces in the near-UV, visible, and near-IR wavelength region.

Absorption Processes

Materials of geological interest absorb light by a variety of processes, which will be described briefly. For further information, references such as Garbuny (1965) and Burns (1970) should be consulted.

Metallic Conductivity.—Metals contain electrons that are not bound to any particular atom but are free to move about the lattice. The electrons are able to respond rapidly to varying electromagnetic fields and rearrange themselves to prevent the penetration of fields into the interior of the metal. The coefficient for the absorption of electromagnetic waves is thus extremely high in the UV-IR range.

Charge Exchange.—A number of nonmetals contain cations that can exist in more than one valence state. If these cations are not separated by too great a distance in the solid-state lattice, then certain electrons, although momentarily bound to a given ion, may nevertheless be able to move about the lattice from one atom to another by a series of oxidation-reduction reactions. The absorption coefficients of these materials are also very high. Important examples are magnetite Fe_3O_4 and ilmenite $FeTiO_3$.

Electronic Transitions.—Several transition elements have *d* electron shells that are degenerate in the free ion. However, when the ion is in a solid-state lattice, the anisotropy of the electric fields from the surrounding anions removes the degeneracy and may produce states separated by energies corresponding to UV-IR wavelengths. The most important element involved in this type of absorption is iron because of its cosmological abundance. Other elements that also may be significant in determining the colors of certain minerals and glasses are Ti, Cr, and Mn. The ferrous ion Fe^{2+} has a weak electron-transition band near 1000 nm. This band has been effectively exploited by McCord and his coworkers (McCord and Johnson, 1970; McCord, Adams, and Johnson, 1970; see the paper by Chapman in this volume[5]) for the remote identification of lunar and asteroidal materials. The ferrous band is especially useful because its exact position depends on the detailed mineralogy of the crystals in which the ion is located and thus often allows identification of the type of rock present on the surface of a body. The ferric ion Fe^{3+} has an extremely strong absorption band near 235 nm; this band has not yet been exploited astrophysically because of the ozone cutoff in Earth's atmosphere. Paradoxically, the presence of iron ions can cause a mineral to be red, green, or blue, depending on the valence states of the iron.

Other.—Other processes, such as band-gap conductivity and color centers, are not discussed here either because they are not important for materials of

[5]See p. 51.

interest to this paper or because their region of light absorption lies outside the range of UV-IR wavelengths.

Scattering Processes

Light diffusely reflected from a complex surface consists of rays that have been scattered by two processes: (1) rays that have been reflected from the outer surfaces of grains and (2) rays that have penetrated several wavelengths into the interior of grains and subsequently have been scattered out of the surface by some irregularity. The reflection coefficient for surface-scattered rays is determined, according to the well-known Fresnel laws, by the index of refraction and absorption coefficient of a grain of surface material. The intensity of the volume-scattered ray is determined primarily by the absorption coefficient. For a weakly absorbing material, such as MgO or pure enstatite $MgSiO_3$, the reflection is dominated by volume scattering and the albedo of the substance is high. For a strongly absorbing material, such as a metal, the reflection is almost entirely by surface scattering; the albedo is low because each reflection is a rather inefficient process. A high albedo almost invariably implies a small volume-absorption coefficient.

UBV Colors

The *UBV* properties of a number of terrestrial, lunar, and meteoritic materials are shown in figures 2, 3, and 4, respectively. The enclosed portions of the diagrams are those regions in which asteroids are found. The spectral data were obtained from freshly prepared materials using a Carey 14 spectrophotometer with an attachment to measure nonspecular radiation diffusely scattered at a phase angle of about 60°. The $U - B$ and $B - V$ indexes were calculated from the ratios of reflectivities relative to MgO smoke at wavelengths of 360, 440, and 550 nm and thus they correspond to data taken through narrowband filters.

Metallic iron, the Ni/Fe meteorites, magnetite, and ilmenite are highly absorbing at all wavelengths and thus have *UBV* difference indexes that are very close to zero and that may even be slightly negative. Magnetite is the major opaque mineral in terrestrial igneous rocks and ilmenite in lunar materials.

Several nonopaque, rock-forming minerals, such as pyroxene and olivine, have an absorption edge in the near-UV or visible region; and it is this edge that is partly characterized by the *UBV* indexes. The nature of this edge is uncertain, but it is known to be strongly affected by the presence of Fe (Shankland, 1968). The edge may involve charge transfer, the tail of the Fe^{3+} UV band, or both.

An extremely important property of this edge is that for most substances it causes the slope of the spectral reflectivity to depend strongly on the size of the particles that make up the reflecting surface. The smaller the size, the

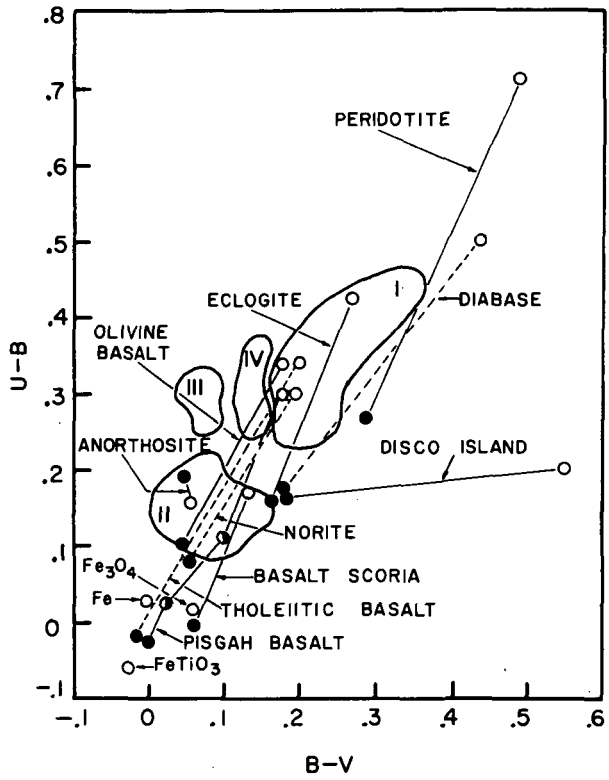

Figure 2.–Color difference diagram for terrestrial rocks. Filled circles indicate solid surfaces; open circles, powder finer than 37 μm in grain size; half-filled circles, powders coarser than 37 μm.

greater the slope and the larger the *UBV* difference indexes. The reason for this behavior is that a change of particle size has the opposite effect on the reflectivities of opaque and nonopaque materials. As the particle size of an opaque substance is reduced, the surface becomes more complex and a ray requires more reflections, on the average, to escape from the surface. For a weakly absorbing material, as the particle size is decreased, the density of boundary surfaces, which are primarily responsible for scattering the rays out of the medium, increases; thus the average pathlength through the material is decreased, causing reduced absorption.

Hence, the effect of decreasing particle size is to reduce the reflectivity on the short-wavelength side of the edge, where surface scattering dominates, and to increase reflectivity longwards of the edge, where most rays are volume scattered, resulting in an increased slope at the edge. This effect is shown by all the materials in figures 2 to 4, where filled symbols represent solid, but unpolished, surfaces and open symbols represent powders. The sole exception is anorthosite, in which the edge is well below 360 nm.

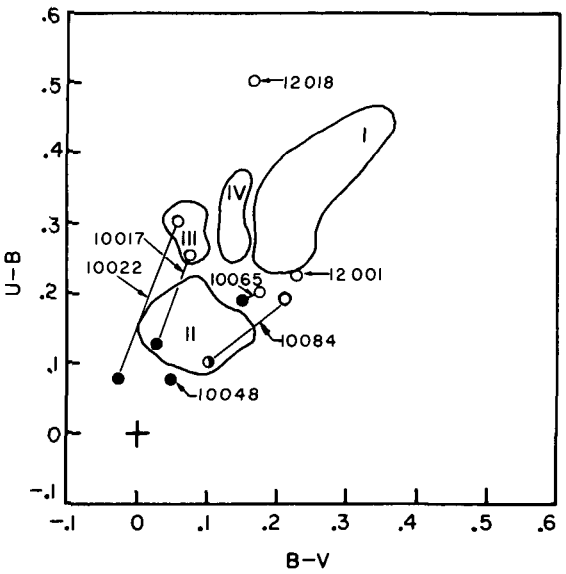

Figure 3.–Color difference diagram for lunar materials. Numbers are NASA designations. Filled circles indicate solid surfaces; open circles, powders finer than 37 μm in grain size; half-filled circles, powders coarser than 37 μm. Nos. 10017, 10022, and 12018 are crystalline rocks; 10048 and 10065 are breccia; 10084 and 12001 are soil.

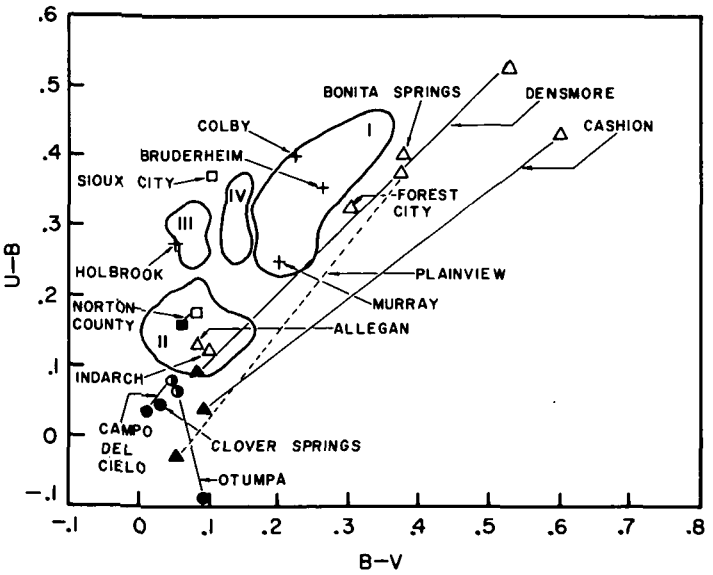

Figure 4.–Color difference diagram for meteorites. Filled symbols indicate solid surfaces; open symbols, powders finer than 37 μm in grain size; half-filled symbols, powders coarser than 37 μm. Plus signs indicate low-iron chondrite powder finer than 37 μm; circles, irons; triangles, high-iron chondrites; squares, achondrites.

DISCUSSION OF RESULTS

UBV Comparisons

In comparing the data for the asteroids (fig. 1) with those for laboratory materials (figs. 2 to 4), several points should be kept in mind.

(1) The colors of the asteroids were obtained with comparatively wide band filters, whereas the laboratory data were taken with the equivalent of narrowband filters.

(2) The laboratory spectra were taken at a phase angle of approximately 60°. Most substances, however, exhibit some reddening with phase. Thus, to be directly compared with the asteroid colors, which have generally been observed at small phase angle, the points of figures 2 to 4 should be moved somewhat inward toward the origin.

(3) The meteorite and asteroidal materials may have undergone unknown degrees of modification. Asteroidal surfaces will be affected by impact melting and vaporization, solar-wind spluttering, and other radiation damage. Meteoritic materials, particularly the finds and old falls in figure 4, will be affected by oxygen and water in the terrestrial atmosphere. The effect of such chemical alteration is to increase the color differences of meteorites over their values in space. However, all of these corrections will only serve to enhance the conclusions that will be made here from the *UBV* data.

The asteroids all have positive $U - B$ and $B - V$ indexes; that is, they are considerably redder than the Sun. They appear to be arranged into at least three and probably four groups, which are arbitrarily labeled in figure 1. The Moon appears to belong to color group I. Comparison of figures 1 to 4 discloses several additional interesting features.

(1) None of the asteroids lie in the low color-index region occupied by the iron meteorites and other highly absorbing materials, either in solid or powder forms. Thus, none of the asteroids appear to be pure Ni/Fe. To increase the *UBV* indexes, some silicate materials must be added to the iron, which would produce a material resembling stony iron meteorites.

(2) Many other solid surfaces have *UBV* difference indexes that are smaller than for any asteroid group. Several solid surfaces, as well as powders, lie near the group II position, but no solid surface corresponds to group I, III, or IV. (The only terrestrial rock that was found to have a large color was peridotite. This rock consists almost entirely of olivine, a transparent, iron-rich mineral. However, no meteorite with a composition similar to pure peridotite is known.) Thus, depending on composition, group II asteroids could have solid or powdered surfaces or mixtures, whereas asteroids of the other

groups appear to have surfaces that are morphologically similar to powdered silicate rocks and stony meteorites.

(3) The direction of change of the color difference indexes upon pulverization lies parallel to the displacements of groups I, III, and IV from group II, and also depends on content of metallic iron. Powders of high-iron chondritic meteorites and Disco Island basalt, which contain metallic iron, tend to lie toward the upper right part of the diagrams. Powders of most of the terrestrial and lunar basalts, achondrites, and low-iron chondrites tend to be displaced farther toward the upper left. Many of the high-iron chondrites lie outside the asteroid fields, possibly because of oxidation by the terrestrial environment.

(4) Lunar soil has different *UBV* values than pulverized lunar crystalline rocks, even though the two materials have similar compositions. Hapke, Cassidy, and Wells (1971) have suggested that this difference is due to a component in the lunar soil that has been deposited directly from a vapor. The vapor is probably generated by meteorite impacts and by solar-wind sputtering. These processes, however, may be expected to be less important in the asteroid belt than on the Moon because of the lower relative velocity of meteorite collisions and the reduced flux of solar wind.

(5) The correlations of *UBV* position with metallic iron content suggests that it eventually may be possible to associate the parents of various types of meteorites with different asteroid groups, although to attempt specific identifications before the effects of the space and terrestrial environments are understood would be premature. The various asteroid groups also may represent different conditions of surface pulverization.

OTHER OPTICAL COMPARISONS

Other optical properties of asteroids and the Moon are summarized in table I. The albedos of most of the asteroids are sufficiently low that their surfaces could consist of either solids or powders of iron-rich material. However, Vesta has such a high albedo that its surface can only be a pulverized, iron-poor substance, such as low-iron achondrite. It is well known that the strongly backscattering nature of the lunar photometric function, represented in table I by $\partial m_v/\partial\alpha$, is due to blocking and shadowing of sunlight in the fine-grained, dark particles of lunar soil (Hapke and Van Horn, 1963). The asteroids of table I have phase function slopes that are as large or larger than the Moon's, implying surfaces of equal or greater complexity, which could be readily produced by powder.

The opposition effect is not as well understood as the backscatter effect, but it is known to be much more pronounced for fine powders than for coarse surfaces. Table II gives the opposition effect for some olivine basalt powders as

TABLE II.—*Opposition Effect of Basalt Powders*

Size, μm	Opposition effect		Geometric albedo, percent	
	N	I	N	I
10	1.20	1.28	45	11
50	1.04	1.11	14	10
Solid	–	1.12	8	11

I = irradiated by a simulated solar wind; N = not irradiated.

a function of particle size. Only particles smaller than about 50 μm seem to have an opposition effect as large as that of the asteroids.

The negative branches of the polarization-phase curves of asteroids seem to be generally similar to the Moon's, although the details vary from body to body. As shown by Lyot (1929), a lunar-type negative branch requires a fine-grained, dark powder. The negative branch can be altered by changing either the grain size or the opacity of the particles. The polarization curve for Ceres seems to correspond better to coarse-grained material than to fine powder, although Ceres exhibits strong backscatter.

In conclusion, the optical properties of asteroids are generally consistent with a surface coating of fine, loose powder, similar to the dust that covers the surface of the Moon. Similar conclusions were reached earlier by Gehrels, Coffeen, and Owings (1964). It is possible, of course, to imagine other materials with a morphology that is fine scaled and complex, such as some sort of volcanic or impact-generated foam or scoria. However, dust appears to be a ubiquitous material in the solar system, and there appear to be no strong arguments against the presence of dust on the surfaces of most of the asteroids. The dust is generated readily by collisions between asteroids of all sizes. It will cling readily to surfaces of asteroids, in spite of their low gravity, by the same electrostatic and intermolecular van der Waals and covalent adhesive forces that cause grains of lunar soil to clump together. This pulverized layer needs to be only a few layers thick to account for the observed optical properties; however, there is no reason to suppose that it is not much thicker in places, particularly in concavities where it is protected from disturbance.

ACKNOWLEDGMENT

I thank E. Skopinski for his valuable assistance in the preparation of this paper. This research was supported by NASA grant NGR 39-011-085.

REFERENCES

Allen, C. 1963, Astrophysical Quantities. Athlone Press. London.

Burns, R. 1970, Mineralogical Applications of Crystal Field Theory. Cambridge Univ. Press. London.

Dollfus, A. 1961, Polarization Studies of Planets. Planets and Satellites (eds., G. Kuiper and B. Middlehurst), p. 343. Univ. of Chicago Press, Chicago.

Garbuny, M. 1965, Optical Physics. Academic Press, Inc. New York.
Gehrels, T. 1956, Photometric Studies of Asteroids. V. The Lightcurve and Phase Function of 20 Massalia. Astrophys. J. **123**, 331.
Gehrels, T. 1970, Photometry of Asteroids. Surfaces and Interiors of Planets and Satellites (ed., A. Dollfus), p. 319. Academic Press, Inc. New York.
Gehrels, T., Coffeen, D., and Owings, D. 1964, Wavelength Dependence of Polarization. III. The Lunar Surface. Astron. J. **69**, 826.
Goldstein, R. 1968, Radar Observations of Icarus. Science **162**, 903.
Hapke, B., Cassidy, W., and Wells, E. 1971, The Albedo of the Moon: Evidence for Vapor-Phase Deposition Processes on the Lunar Surface. Proc. Apollo 12 Lunar Sci. Conf. Geochim. Cosmochim. Acta, to be published.
Hapke, B., and Van Horn, H. 1963, Photometric Studies of Complex Surfaces, With Applications to the Moon. J. Geophys. Res. **68**, 4545.
Harris, D. 1961, Photometry and Colorimetry of Planets and Satellites. Planets and Satellites (eds., G. Kuiper and B. Middlehurst), p. 272. Univ. of Chicago Press. Chicago.
Lyot, B. 1929, Recherches sur la Polarisation de la Lumière des Planètes et de Quelques Substances Terrestres. Ann. Observ. Paris Meudon 8(1).
McCord, T., Adams, J., and Johnson, T. 1970, Asteroid Vesta: Spectral Reflectivity and Compositional Implications. Science **168**, 1445.
McCord, T., and Johnson, T. 1970, Lunar Spectral Reflectivity (0.30 to 2.50 Microns) and Implications for Remote Mineralogical Analysis. Science **169**, 855.
Miner, E., and Young, J. 1969, Photometric Determination of the Rotation Period of 1566 Icarus. Icarus **10**, 436.
Shankland, T. 1968, Band Gap of Forsterite. Science **161**, 51.

DISCUSSION

BRECHER: The spectral reflectivity data of McCord, Adams, and Johnson (1970) indicated the presence on Vesta's surface of material similar to basaltic achondrites. But these are known to be similar to the silicate part of the mesosiderites while a large ($\leq$50 percent by volume) Ni/Fe content would be more consistent with Schubart's density for Vesta. Could your data rule out the presence of Ni/Fe in Vesta's surface material?

HAPKE: No. The spectrum of metallic Ni/Fe is essentially flat; therefore, its presence will reduce the contrast of silicate spectral bands but will not completely obscure them.

CHAPMAN: It is true that the mineralogical composition of the silicate portion of some mesosiderites should yield a spectral reflectivity similar to that our group has observed for Vesta. Because the albedo of the metallic portion of such meteorites is so much lower than the albedo of the silicate portion, it would make little change in the shape of the reflectivity curve (except possibly in the UV), even if present in equal proportions. The presence of such a dark component, with a relatively featureless spectral reflectivity, might help to explain why the albedo of Vesta, implied by some recent diameter estimates, is lower than might be expected for the identified silicates.

DISCUSSION REFERENCE

McCord, T., Adams, J., and Johnson, T. 1970, Asteroid Vesta: Spectral Reflectivity and Compositional Implications. Science **168**, 1445.

Page intentionally left blank

THE PHYSICAL MEANING OF PHASE COEFFICIENTS

J. VEVERKA
Cornell University

The question of what information about an asteroid's surface is contained in a measurement of the phase coefficient between phase angles of 10° and 30° is examined in detail. Contrary to some past claims it is shown that absolute reflectivities cannot be derived from phase coefficients. Furthermore, typical asteroid phase coefficients cannot be interpreted unambiguously. This is because the observed phase coefficient may depend as much on the photometric properties of an individual surface element as on the degree of large-scale surface roughness, and these two effects are impossible to separate if only disk integrated measurements are available. The wavelength dependence of asteroid phase coefficients should be small and should contain little information about the surface. In the case of irregular asteroids with macroscopically rough surfaces, the importance of large-scale shadowing, and hence the observed phase coefficient, will depend on the aspect of the asteroid. In such cases, therefore, phase coefficients must be carefully defined to be meaningful. It should be possible, in some cases, to estimate the relative surface roughness of two quasi-spherical asteroids by combining photometric and polarimetric observations. For example, if the two asteroids have almost identical polarization curves but quite different phase coefficients, it is likely that the asteroid with the larger phase coefficient has a macroscopically rougher surface.

One of the aims of asteroid photometry is to obtain information about the physical characteristics, such as texture, composition, and large-scale roughness, of asteroid surfaces. In this paper I wish to concentrate on a single aspect of asteroid photometry and consider in detail what information can be derived from observed phase coefficients. For instance, is it possible, as Bell (1917), Stumpff (1948), Widorn (1964), and recently Gehrels et al. (1970) have tried to do, to determine the absolute reflectivities of asteroids in this way?

I will use the term "phase coefficient" in a restricted sense. From Earth, few asteroids can be observed at phase angles larger than 30°. Also, at very small phase angles an additional surge in brightness (the "opposition effect") is usually present (Gehrels, 1956, 1967). The details of this opposition surge contain important information about the surface texture (Hapke, 1963; Irvine, 1966), but few asteroids have been observed at sufficiently small phase angles to determine accurately this part of their phase curves. I will therefore use the term "phase coefficient" to mean the slope (in magnitudes per degree of phase) of the observed phase curve between 10° and 30°. The problem of

understanding the physical implications of this quantity (which I will denote by β) can be divided into two parts:

(1) To adequately describe the scattering properties of an individual small element of the surface of a typical asteroid
(2) To determine what additional effects are introduced by shadowing due to large-scale roughness

These two questions are dealt with in turn in the next two sections.

THE SCATTERING PROPERTIES OF A SMALL SURFACE ELEMENT

Observational evidence suggests that the surface of a typical asteroid is similar to that of the Moon; that is, microscopically rough and intricate, and made up largely of a dark material in which multiple scattering is not dominant. The scattering properties of such surfaces have been considered by Irvine (1966); his model gives an exact treatment of the scattering properties of a dark, particulate layer under the following assumptions:

(1) All particles are spherical and of uniform radius.
(2) The particles are large enough that shadowing can be dealt with in terms of geometric optics.
(3) The particles are dark enough for multiple scattering to be negligible.

When a parallel beam of light is incident on an element of such a surface, at an angle i, the specific intensity I of the light scattered at an angle ϵ (making a phase angle α with the incident direction) is given by

$$I(i, \epsilon, \alpha) \propto \left[\bar{\omega}_0 \Phi(\alpha)\right] \frac{\cos i}{\cos i + \cos \epsilon} S(i, \epsilon, \alpha; D) \qquad (1)$$

where

$\bar{\omega}_0$ = scattering albedo of a single particle
$\Phi(\alpha)$ = phase function of a single particle
$S(i, \epsilon, \alpha; D)$ = Irvine shadowing function for the surface

The parameter D is related to the compaction of the surface as follows. If ρ is the mean density of a macroscopic volume element of the surface, and ρ_0 is the mean density of a single particle, then

$$D \equiv \frac{3}{4\pi} \frac{\rho}{\rho_0}$$

For uniform, equally hard spheres, D cannot exceed 0.176 (Beresford, 1969). For the Moon's top surface, Hapke (1963) estimates $\rho/\rho_0 \cong 0.1$, which corresponds to $D = 0.024$.

Using the equations given by Irvine, it is easy to show that $S(i, \epsilon, \alpha; D)$ does not depend strongly on either i or ϵ individually, so that

$$S(i, \epsilon, \alpha; D) \simeq S(\alpha, D)$$

Therefore equation (1) may be rewritten as

$$I(i, \epsilon, \alpha) \sim \tilde{\omega}_0 \frac{\cos i}{\cos i + \cos \epsilon} f(\alpha, D) \tag{2}$$

where $f(\alpha, D) \equiv S(\alpha, D)\, \Phi(\alpha)$.

Although this equation is based on simplifying assumptions, it does adequately represent laboratory measurements on dark, microscopically rough surfaces. Furthermore, it holds even for surfaces in which the individual particles are not physically separate but are fused together as, for example, in furnace slag.

The validity of equation (2) can be easily tested for any surface in the laboratory by making measurements of $I(i, \epsilon, \alpha)$ as a function of α at a series of fixed values of ϵ; say at $\epsilon = 0°$, $30°$, and $60°$. From each set of measurements corresponding to a given ϵ, an empirical $f(\alpha, D)$ can be determined using equation (2). If this equation is applicable to the surface, all the $f(\alpha, D)$ values so obtained will be identical.

Such a test is carried out, using measurements on a sample of dark furnace slag (Halajian, 1965), in figure 1 where all the $f(\alpha, D)$ values have been normalized to unity at $\alpha = 10°$. Because a single $f(\alpha, D)$ is indicated, equation (2) appears to be valid for this surface, even though this surface is not "particulate" in the usual sense. This test can be carried out with equal success for dark surfaces which *are* particulate in the normal sense. In fact, Halajian

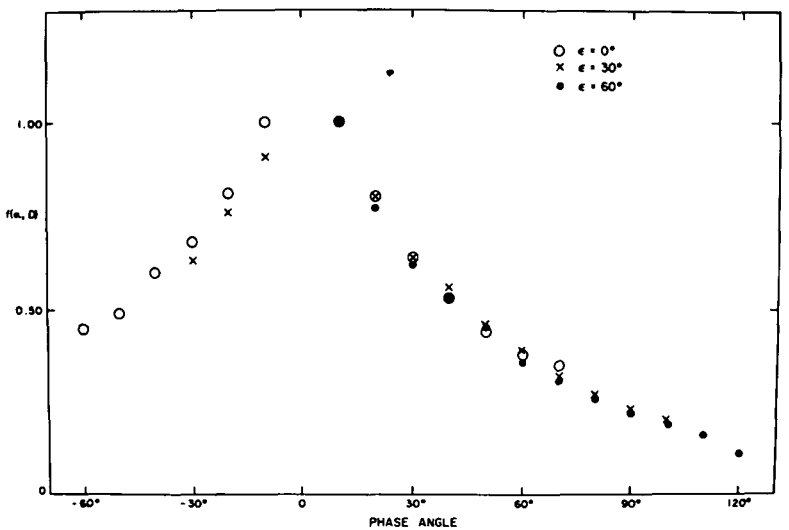

Figure 1.–The f function for a layer of dark furnace slag, from measurements in V by Halajian (1965). This sample has a normal reflectivity of 0.09 and photometric properties very similar to those of the lunar surface. The function is normalized to unity at $\alpha = 10°$.

(1965) found that many particulate surfaces (volcanic cinders, for example) have values of $f(\alpha, D)$ almost identical to that shown in figure 1, which incidentally, is very similar to that of the lunar surface.

I will now show that the $f(\alpha, D)$ shown in figure 1 can be adequately reproduced using the Irvine model. In doing this, it is convenient to choose for $\Phi(\alpha)$, the one parameter family of single particle phase functions introduced by Henyey and Greenstein (1941),

$$\Phi_{HG}(\alpha, G) = \frac{1 - G^2}{(1 + G^2 - 2G \cos \alpha)^{3/2}} \tag{3}$$

The parameter $G \equiv <\cos \alpha>$ describes the nature of the scattering. For $G = +1$, there is complete backscattering; for $G = -1$, complete forward-scattering; and for $G = 0$ the scattering is isotropic.

The measured $f(\alpha, D)$ shown in figure 1 can only be matched for a very small range of G (0.30 to 0.35) (fig. 2). This indicates that effectively the individual particles are slightly backscattering, a result to be expected for large, opaque particles with rough surfaces. In figure 2, a reasonable choice of $D = 0.03$ is used, but the conclusions do not depend strongly on the value of D.

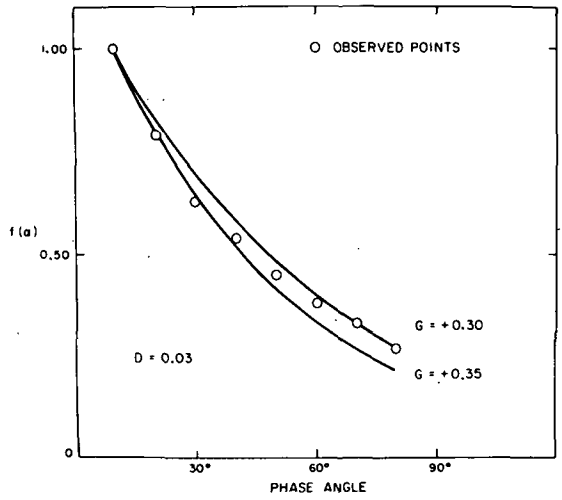

Figure 2.–Comparison of the f function of figure 1 with two theoretical predictions using the Irvine model and a Henyey-Greenstein phase function. The points represent the mean values of f at each phase angle, taken from figure 1.

I conclude that the Irvine model is adequate for describing the scattering properties of dark, microscopically intricate surfaces. Furthermore, it seems immaterial whether the particles of the surface are physically free or fused together.

THE EFFECTS OF LARGE-SCALE ROUGHNESS: MACROSCOPIC SHADOWING

Unfortunately, the general problem of shadowing on a randomly rough two-dimensional surface is extremely complicated. Ideally, one wishes to know for each angle of illumination and each angle of observation what parts of the surface are both illuminated and seen. The surface can be specified statistically in terms of the height deviations from an arbitrary mean level or in terms of the distribution of surface slopes. So far, solutions exist only for one-dimensional surfaces (for example Beckmann, 1965, and Saunders, 1967), and I will therefore use a contrived, but convenient model, first introduced by Hämeen-Anttila et al. (1965). In this model the surface is assumed to be bounded on top by a plane that is punctured by countless paraboloidal craters, whose axes of revolution are perpendicular to the plane. The shape of a crater is determined by the parameter $Q \equiv H/R$, where H is the crater depth and R is its radius at the top level.

To study the effects of large-scale shadowing on the photometric properties of asteroids, it is convenient to first consider a model planet that is spherical and completely covered with paraboloidal craters of shape Q. (It is assumed that the craters do not overlap.) As Q increases from zero, so does the roughness of the model planet. The rms slope of such a surface is given by

$$\theta_{\mathrm{rms}} = \arctan \frac{2Q}{3} \tag{4}$$

and Q is related to the maximum surface slope by the relation

$$Q = \frac{\tan \theta_{\max}}{2} \tag{5}$$

For $\theta_{\max} \leqslant 35°$, for example, $Q \leqslant 0.35$.

It is implicitly assumed in the model that, on the one hand, the number of craters per resolution element is very large, whereas on the other hand, each crater is large enough to contain a large number of individual scattering elements. Also, the surface reflectivity is assumed to be low enough that shadows are not affected by multiple scattering.

To determine the total amount of light $j(\alpha)$ scattered by the model planet toward Earth at a phase angle α, an integration over the illuminated part of the disk must be performed:

$$j(\alpha) \propto \iint \bar{I} \cos \epsilon \, d\sigma \tag{6}$$

where $\cos \epsilon \, d\sigma$ is the projected area of the surface element $d\sigma$, and $\bar{I}$ is the effective specific intensity of the light scattered by that element toward Earth. Numerically, this process is conveniently carried out by the method of Horak (1950) in which the integration is replaced by a weighted sum over a grid of points covering the illuminated part of the disk. At each point of this grid, $\bar{I}$ is

found by calculating the mean specific intensity of the light scattered from a paraboloidal crater (see Hämeen-Anttila et al., 1965, for details), each element of which scatters according to Irvine's law.

Clearly, the $j(\alpha)$ calculated in this way for a surface with $Q > 0$ will be less than that found when $Q = 0$ at all phase angles $\alpha > 0$. We will, in fact, have the following relationship:

$$j(\alpha, Q) = j(\alpha, 0)\, \Sigma(\alpha, Q) \tag{7}$$

where $\Sigma(\alpha, Q)$ is *a macroscopic shadowing function* that depends only on α and Q (and, of course, on the model of surface roughness) but not on $f(\alpha, D)$. Thus, the effective scattering law for the rough model planet may be considered to be

$$I_R(i, \epsilon, \alpha) = I(i, \epsilon, \alpha)\, \Sigma(\alpha, Q) \tag{8}$$

where $I(i, \epsilon, \alpha)$ is given by equation (1) and $\Sigma(\alpha, Q)$ can be determined by the calculation described above. For a macroscopically smooth planet ($Q = 0$), $\Sigma(\alpha, 0) = 1$ for all α and

$$I_R\,(i, \epsilon, \alpha) = I(i, \epsilon, \alpha)$$

The values of $\Sigma(\alpha, Q)$ for this model, found using either a 36 or 100 point grid over the illuminated part of the planet and a 2500 point grid over each crater, are shown in figure 3. The numerical accuracy of these values is better than 1 percent. The results of figure 3 can now be used to study the effects of large-scale surface roughness on the photometric parameters of the model planet once $f(\alpha, D)$ is specified. Because the $f(\alpha, D)$ shown in figure 1 is very

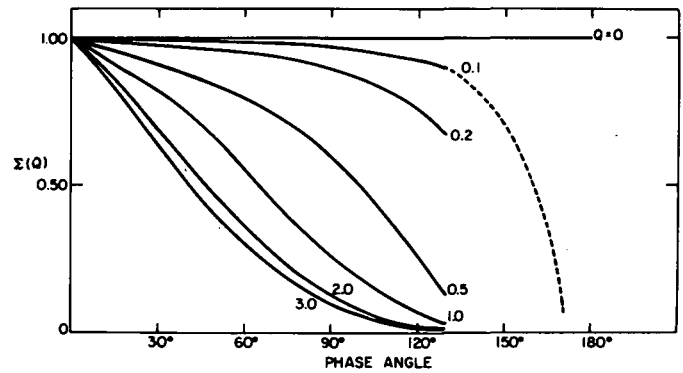

Figure 3.–The macroscopic shadowing function $\Sigma(Q)$ versus phase angle α for various values of Q. The nature of Σ depends on the specific model of large-scale surface roughness used (in this case the surface is assumed to be covered with paraboloidal craters), but is independent of $f(\alpha, D)$. Note that beyond $Q = 2$, increasing the surface roughness produces little change in Σ. Values of $\Sigma(Q)$ were calculated for $\alpha = 0°$, $10°$, $20°$, $50°$, $90°$, $130°$, and $170°$; for all $Q > 0$, $\Sigma(170°, Q)$ was found to be less than 0.001.

similar to that of the Moon, it is of interest to use it in these calculations. For this purpose, it may be extended linearly (on a magnitude scale) from $\alpha = 10°$ to $\alpha = 0°$; that is, at 0.026 mag/deg, thus in effect neglecting any opposition effect. Values of the phase coefficient β (between $\alpha = 10°$ and $\alpha = 30°$) and of the phase integral

$$q \equiv 2\int_0^{\pi} \frac{j(\alpha, Q)}{j(0, Q)} \sin\alpha \, d\alpha \tag{9}$$

for this model planet are shown in figure 4 as functions of the roughness parameter Q. The phase coefficient is seen to increase significantly as the surface gets rougher until about $Q = 2$; for larger values of Q the additional increase in β is slight. The phase integral, on the other hand, decreases appreciably as Q increases, but again a leveling off occurs beyond $Q \cong 2$. Note that the phase coefficient β of the disk integrated light is related to *the laboratory phase coefficient* β_{lab}, the slope of $f(\alpha, D)$ (on a magnitude scale), by the relation

$$\beta = \beta_{lab} + \beta_{ls} \tag{10}$$

where β_{ls} is the phase coefficient of a Lommel-Seeliger planet (that is, a planet with $Q = 0$ and $f(\alpha, D) = 1$). Between $\alpha = 10°$ and $\alpha = 30°$, $\beta_{ls} \cong 0.006$

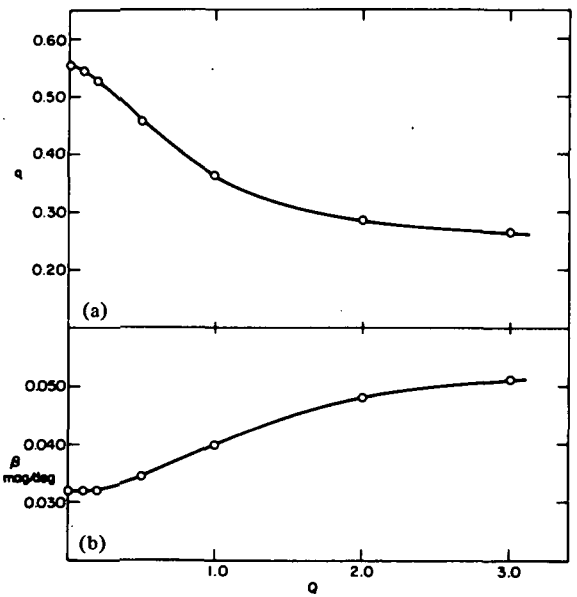

Figure 4.–(*a*) The phase integral q of the model planet versus the surface roughness (represented by the parameter Q). The f function shown in figure 1 extrapolated to $\alpha = 0°$ as described in the text was used in this calculation. (*b*) The corresponding variation of the phase coefficient β measured between $\alpha = 10°$ and $\alpha = 30°$.

mag/deg. Hence, because over the same interval of phase angles, $\beta_{lab} = 0.026$ mag/deg for the surface of figure 1, $\beta = 0.032$ mag/deg for $Q = 0$ in figure 3.

For a scattering law of type (1), the geometric albedo p of the model planet is independent of Q.

Thus, for the above model, it can be concluded that–

(1) Large-scale surface roughness has a strong effect on both the phase integral and the phase coefficient, but none on the geometric albedo.
(2) From equation (1) it follows that the phase coefficient is independent of the single particle albedo $\bar{\omega}_0$, but the geometric albedo is not.
(3) Therefore, in view of conclusions (1) and (2), there can be, in general, no correlation between β and p.
(4) Within the framework of this model, β and q are independent of wavelength, unless $\Phi(\alpha)$ has a wavelength dependence. But because it is assumed that the particles of the model surface are opaque and large compared to the wavelength, the wavelength dependence of $\Phi(\alpha)$ will be small.

SOME RELEVANT LABORATORY RESULTS

Laboratory work with dark, microscopically complex surfaces (Halajian, 1965; Halajian and Spagnolo, 1966) is in accord with these conclusions. Even in the laboratory, when macroscopic shadowing is not important, no general correlation between β_{lab} and the surface reflectivity is found. Also, the observed wavelength dependence of β_{lab} is very small, but there is an interesting trend for β_{lab} to decrease slightly with increasing wavelength. Because the reflectivity of the samples used in this work tends to increase slightly with increasing wavelength, this suggests that the breakdown of the Irvine model is at least in part due to the increased importance of multiple scattering at longer wavelengths. Multiple scattering makes it easier for light to escape from the surface; this effect is relatively more important at large phase angles because it is then more difficult for singly scattered photons to escape from within the surface. Thus multiple scattering helps to get relatively more light out of the surface at large phase angles than near opposition. This tends to make phase coefficients smallest at those wavelengths at which multiple scattering is most important; that is, usually in the red portion of the spectrum. But for dark surfaces this effect is very small.

Laboratory work such as that referred to above (Halajian, 1965; Halajian and Spagnolo, 1966) shows conclusively that no mineralogical information is contained in phase coefficients; at best one can distinguish materials in which multiple scattering is dominant from those in which it is negligible. In addition, this work shows that away from opposition ($\alpha > 10°$) phase coefficients contain no information about whether a surface is particulate. For example, as already noted, both particulate samples of volcanic cinders and solid samples of

furnace slag reproduce the lunar photometric function in V equally well as phase angles larger than a few degrees.

A SERIOUS COMPLICATION: NONSPHERICAL ASTEROIDS

A serious complication in interpreting phase coefficients is that many asteroids are not even approximately spherical. What can be said about the brightness variations *with phase* of an irregular asteroid whose aspect changes with time? Clearly, as the aspect changes, so will the importance of large-scale shadowing.

Consider the following idealized example of an ellipsoidal asteroid. Two of the semiaxes are equal to A, and the third is equal to $B \gg A$. The asteroid rotates about one of the short axes. Two extreme cases may occur: (1) the asteroid is viewed pole-on and the light fluctuations are minimum and (2) the rotation axis of the asteroid is perpendicular to the line of sight and the light variations are maximum. Also, suppose that a spherical planet of the same material and surface macrostructure has a phase coefficient β_{sphere}.

In case (2), at maximum light, the situation is identical to case (1) and

$$\beta_{\max} = \beta_{(1)} < \beta_{\text{sphere}} \tag{11}$$

The inequality follows from the fact that on the ellipsoid, at maximum light, the average i and ϵ are effectively smaller than on the sphere, and the effects of shadowing are therefore less important. However, at minimum light, the average i and ϵ are effectively larger than in the case of a sphere and therefore shadowing is more important. Hence

$$\beta_{\min} > \beta_{\text{sphere}} > \beta_{(1)} \tag{12}$$

Usually, in case (2), β would be determined by using the mean magnitude of the lightcurve, so that

$$\beta_{(2)} \equiv \frac{\beta_{\max} + \beta_{\min}}{2} > \beta_{(1)} \tag{13}$$

Therefore, it is possible to predict that for an irregular asteroid whose aspect changes with time and whose surface is macroscopically rough:

(1) The apparent β is largest when the amplitude of the lightcurve is maximum.

(2) If the aspect of an asteroid stays approximately constant during an opposition, then the phase coefficient determined from the minima of the lightcurve should be larger than that determined from the maxima; that is

$$\beta_{\min} > \beta_{\max}$$

Thus, to even meaningfully define a phase coefficient for a very irregular asteroid whose aspect changes significantly with time may require a long series of accurate observations.

CONCLUSIONS

In summary, the situation appears bleak. One cannot expect to derive the geometric albedos of asteroids from their phase coefficients. The contrary claim by Widorn (1964) and others is largely based on a fortuitous empirical relationship obtained by plotting β against p for the Moon and some of the large planets. Jupiter and Venus are intrinsically bright (large p) and have cloud decks in which multiple scattering is important (low β). Mercury and the Moon are intrinsically dark (low p) and have rough dark surfaces (high β). Thus one can arrive at the unfounded conclusion that β must always be inversely correlated with p, which in the case of dark surfaces certainly need not be true.

Because the degree of surface roughness (Q in the above model) of any particular asteroid is not known, one cannot convert an observed phase coefficient β in its laboratory counterpart β_{lab}. Furthermore, even if this were possible, little diagnostic information could be obtained from β_{lab}. (See the previous discussion of β_{lab}.)

In addition, for very irregular asteroids with rough surfaces it may be difficult to even define a meaningful phase coefficient (as discussed in the preceding section). Fortunately, there are some asteroids, Ceres and Flora, for example, that are almost spherical, so that at least this complication does not arise. Flora has a phase coefficient similar to that of the Moon: 0.028 mag/deg in V (Veverka, 1971). If it is composed of photometrically similar material, its surface roughness must also be similar. If it is rougher than the Moon, its surface material must be less backscattering, and vice versa. The phase coefficient of Ceres, 0.050 mag/deg in V (Ahmad, 1954), is considerably larger than that of the Moon. This is probably not entirely due to surface roughness because, as figure 4(*b*) shows, for lunarlike materials it is difficult to increase β beyond 0.05 mag/deg by increasing surface roughness. This suggests that the surface material of Ceres is intrinsically more backscattering than that of the Moon.

According to the above model the color dependence of asteroid phase coefficients should be small. This does seem to be the case. For Vesta, for example, $\beta_V = 0.0253$ mag/deg, $\beta_B = 0.0264$ mag/deg, and $\beta_U = 0.0291$ mag/deg (Gehrels, 1967). Because the reflectivity of Vesta increases with increasing wavelength in the *UBV* region of the spectrum, this slight decrease in β with increasing wavelength may perhaps be attributed to the increased importance of the small, multiply scattered component at long wavelengths, as suggested above. If this is true, then the wavelength dependence of asteroid phase coefficients mostly contains information about the wavelength dependence of the surface reflectivity, information that can be obtained more easily from a single spectral reflectivity measurement.

Finally, I would like to stress again that typical asteroid phase coefficients (0.025 to 0.035 mag/deg) cannot be interpreted unambiguously. This is because the observed phase coefficient may depend as much on the photometric properties of an individual surface element $f(\alpha, D)$ as on the degree of large-scale roughness $\Sigma(\alpha, Q)$. (See preceding discussions of these functions.) If only disk integrated measurements of the scattered light are available, these two effects cannot be separated. In spite of this, there does seem to be some point in looking for objects with unusual phase coefficients, such as Ceres.

In some cases, it should be possible to estimate the relative surface roughness of two quasi-spherical asteroids by combining photometric and polarimetric observations. For example, if the two asteroids have almost identical polarization curves, but quite different phase coefficients, it is likely that the asteroid with the larger phase coefficient has a macroscopically rougher surface.

ACKNOWLEDGMENTS

I wish to thank C. Sagan and F. L. Whipple for their advice and generous assistance. The numerical calculations described in this paper were carried out at the Smithsonian Astrophysical Observatory, and I am grateful to the Smithsonian Foundation for support during this phase of the project. This work was also supported in part by NASA NGR 33-010-082.

REFERENCES

Ahmad, I. I. 1954, Photometric Studies of Asteroids. IV. The Light Curves of Ceres, Hebe, Flora, Kalliope. Astrophys. J. **120**, 551.

Beckmann, P. 1965, Shadowing of Random Rough Surfaces. IEEE Trans. Antennas Propagat. **Ap-13**, 384.

Bell, L. 1917, The Physical Interpretation of Albedo. Astrophys. J. **45**, 1.

Beresford, R. H. 1969, Statistical Geometry of Random Heaps of Equal Hard Spheres. Nature **224**, 550.

Gehrels, T. 1956, Photometric Studies of Asteroids. V. The Light Curve and Phase Function of 20 Massalia. Astrophys. J. **123**, 331.

Gehrels, T. 1967, Minor Planets. I. The Rotation of Vesta. Astron. J. **72**, 929.

Gehrels, T., Roemer, E., Taylor, R. C., and Zellner, B. H. 1970, Minor Planets and Related Objects. IV. Asteroid (1566) Icarus. Astron. J. **75**, 186.

Halajian, J. D. 1965, Photometric Measurements of Simulated Lunar Surfaces. Grumman Res. Dept. Rept. RE-219.

Halajian, J. D., and Spagnolo, F. J. 1966, Photometric Measurements of Simulated Lunar Surfaces. Grumman Res. Dept. Rept. RE-245.

Hämeen-Anttila, K. A., Laakso, P., and Lumme, K. 1965, The Shadow Effect in the Phase Curves of Lunar Type Surfaces. Ann. Acad. Sci. Fenn. Ser. A. **172**.

Hapke, B. W. 1963, A Theoretical Photometric Function for the Lunar Surface. J. Geophys. Res. **68**, 4571.

Henyey, L. G., and Greenstein, J. L. 1941, Diffuse Reflection in the Galaxy. Astrophys. J. **93**, 70.

Horak, H. G. 1950, Diffuse Reflection by Planetary Atmospheres. Astrophys. J. **112**, 445.

Irvine, W. M. 1966, The Shadow Effect in Diffuse Reflection. J. Geophys. Res. 71, 2931.
Saunders, P. M. 1967, Shadowing on the Ocean and the Existence of the Horizon. J. Geophys. Res. 72, 4643.
Stumpff, K. 1948, Concerning the Albedos of Planets and the Photometric Determination of Diameters of Asteroids. Astron. Nachr. 276, 118.
Veverka, J. 1971, Photopolarimetric Observations of the Minor Planet Flora. Icarus 15, 11.
Widorn, T. 1964, Phase Coefficients and Phase Integrals. Mitt. Wien Sternw. 12, 17.

DISCUSSION

HAPKE: It is very likely true, as Veverka has stated, that one could not make a phase function as steep as Ceres' with lunar soil roughened in some fashion. However, the following conceptual model shows that it is possible to construct a surface with a phase function as steep as one wishes. Imagine a body with a relatively smooth surface; such a body would have a phase function something like that corresponding to Lambert's law. Now replace the smooth surface by large dark particles. Since the phase function of the body is given by the product of the phase function of the particles and their shadowing function, the body phase function will be steepened. Next, replace the particles by clumps of smaller particles. Now the phase function of the body involves a product: the phase function of the smaller particles times that of the clumps times the shadowing function. The body phase function is even steeper. This procedure can be followed until the diffraction limit for casting sharp shadows is reached. Such a hierarchy of clumps of material similar to lunar soil may not be a completely unreasonable model in view of the very low surface gravity on asteroids.

ASTEROID POLARIMETRY: A PROGRESS REPORT

J. VEVERKA
Cornell University

This is a brief report on the present status of asteroid polarimetry. A detailed paper is in preparation jointly with T. Gehrels.

The first polarization measurements of asteroids were made by Lyot (1934), who photographically determined the polarization curves of Ceres and Vesta. These curves are reproduced by Dollfus[1] (1961). Unfortunately, because of the low sensitivity of the photographic method, they do not agree very well with recent photoelectric measurements.

The first photoelectric polarization measurements of asteroids were made by Provin (1955) (details of this work are given by Dollfus,[1] 1961), and in recent years this work has been extended by Gehrels (unpublished) and by Veverka (1970). To date, fairly complete polarization curves for about a dozen asteroids have been obtained, and at least partial data are available for twice that number. Invariably, all asteroids for which sufficient data have been accumulated show lunarlike polarization curves with well-developed negative branches. This suggests that asteroid surfaces generally consist of a microscopically intricate, porous material in which multiple scattering is not dominant (Lyot, 1929). But, although these curves have similar shapes, they can differ considerably in detail (fig. 1). It is clear from figure 1 that, for example, the polarization curves of Ceres and Vesta are significantly different from each other, and from that of the Moon. It is therefore reasonable to suppose that some information about the composition and texture of asteroid surfaces can be obtained by matching these curves in the laboratory. Such work is now in progress using powdered meteorite surfaces.

Asteroid polarization curves are also phenomenologically useful because from them one can estimate the absolute reflectivities of the surfaces. For dark, texturally complex surfaces, h, the slope of the linear part of the polarization curve beyond the inversion angle, seems to be inversely correlated with surface reflectivity. This relationship has been exploited by KenKnight et al. (1967), Widorn (1967), Gehrels et al. (1970), and others. Veverka (1971*a*) gives a short discussion of this method. Presently, the drawback is that this relationship has been calibrated adequately only for lunar regions and for

[1]See p. 96.

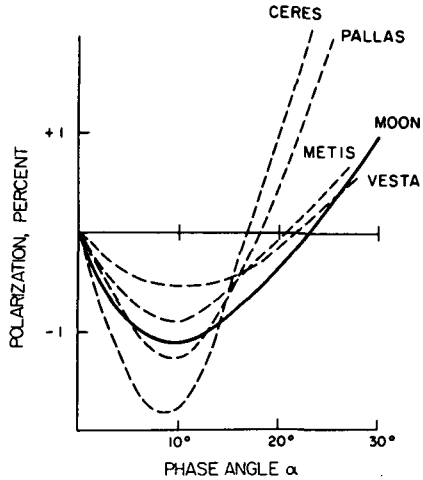

Figure 1.—A comparison of the polarization curves of the Moon and four asteroids. The lunar curve is from Lyot (1929). The asteroid curves are based on previous measurements as follows: Ceres and Pallas from Provin (1955; details given in Dollfus, 1961), Gehrels (unpublished), and Veverka (1970); Vesta from Gehrels (unpublished) and Veverka (1970); and Metis from Veverka (1970). The measurements by Gehrels were made either at 0.52 or 0.56 μm; all others were made in integrated light. Note that from Earth few asteroids can be observed at phase angles larger than 30°.

possible lunar materials. But in view of the results of McCord, Adams, and Johnson[2] (1970) it may be more appropriate to calibrate the relationship by using pulverized meteorite surfaces. Nevertheless, the calibration now available is probably adequate to yield reasonable estimates of asteroid reflectivities. For example, one finds in this way 0.25 ± 0.07 for the reflectivity of Vesta (Veverka, 1971*a*) and 0.16 ± 0.03 for that of Flora (Veverka, 1971*b*), both in visible light.

An interesting possibility being investigated in the laboratory is that for dark, microscopically intricate surfaces, the minimum of the negative branch of the polarization curve P_{min} may be a crude indicator of surface reflectivity. Data for volcanic cinders and ashes by Lyot (1929) suggest that this may be the case (the deeper the negative branch, the lower the reflectivity). If such a relationship could be established, even approximately, it would provide a means of estimating the absolute reflectivity of an asteroid from a single measurement at a phase angle near 10°. This would be of special importance in the case of Trojan asteroids because they cannot be observed at sufficiently large phase angles to determine h, and there is at present no reliable way of estimating their reflectivities. (See, for example, Dunlap and Gehrels, 1969.) Furthermore, Trojans are faint and difficult to locate, making the determination of a complete polarization-phase curve a formidable task.

[2]See p. 51.

It has been suggested (Gehrels and Teska, 1963) that simultaneous polarization and brightness measurements can be used to decide conclusively to what extent the short-period brightness fluctuations of asteroids are due to changes in surface reflectivity, rather than to changes in the projected surface area. The idea is to observe at large phase angles where the polarization should be positive and inversely correlated to surface reflectivity (Gehrels, 1970). Such observations are difficult because at large phase angles asteroids are not well placed in the sky, and can be observed for only a few hours, making it impossible, in general, to follow a complete rotation during any one night. So far, no polarization-brightness variations related to rotation have been established, but only two asteroids have been observed simultaneously in brightness and in polarization: Pallas (Gehrels, unpublished) and Eunomia (Veverka, 1970).

ACKNOWLEDGMENTS

I wish to thank T. Gehrels, W. Liller, C. Sagan, and F. L. Whipple for helpful discussions. Some of the observations reported in this paper were made at Harvard. The Harvard polarimeter project is supported by AFOAR contract no. F19-628-68-C-0228. This work was supported in part by NASA NGR 33-010-082.

REFERENCES

Dollfus, A. 1961, Polarization Studies of Planets. Planets and Satellites (eds., G. P. Kuiper and B. M. Middlehurst), ch. 9. Univ. of Chicago Press. Chicago.

Dunlap, J. L., and Gehrels, T. 1969, Minor Planets. III. Lightcurves of a Trojan Asteroid. Astron. J. 74, 796.

Gehrels, T. 1970, Photometry of Asteroids. Surfaces and Interiors of Planets and Satellites (ed., Dollfus), ch. 6. Academic Press, Inc. New York.

Gehrels, T., Roemer, E., Taylor, R. C., and Zellner, B. H. 1970, Minor Planets and Related Objects. IV. Asteroid (1566) Icarus. Astron. J. 75, 186.

Gehrels, T., and Teska, T. M. 1963, The Wavelength Dependence of Polarization. Appl. Opt. 2, 67.

KenKnight, C. E., Rosenberg, D. L., and Wehner, G. K. 1967, Parameters of the Optical Properties of the Lunar Surface Powder in Relation to Solar Wind Bombardment. J. Geophys. Res. 72, 3105.

Lyot, B. 1929, Studies of the Polarization of Planets. NASA TT F-187.

Lyot, B. 1934, Polarisation des Petites Planètes. Bull. Astron. 67, 3.

McCord, T. B., Adams, J. B., and Johnson, T. V. 1970, Asteroid Vesta: Spectral Reflectivity and Compositional Implications. Science 168, 1445.

Provin, S. 1955, Preliminary Observations of the Polarization of Asteroids (abstract). Publ. Astron. Soc. Pac. 67, 115.

Veverka, J. 1970, Photometric and Polarimetric Studies of Minor Planets and Satellites. Ph. D. Thesis. Harvard Univ.

Veverka, J. 1971*a*, The Polarization Curve and the Absolute Diameter of Vesta. Icarus 15, 11.

Veverka, J. 1971*b*, Photopolarimetric Observations of the Minor Planet Flora. Icarus 15(3), in press.

Widorn, T. 1967, A Photometric Method of Estimating the Diameters of Minor Planets. Ann. Univ. Sternwarte Wien 27, 112.

DISCUSSION

GEHRELS (added after the conference): I think it dangerous in principle to calibrate with meteoritic material; one is then likely to derive meteoritic characteristics. The calibration should, instead, be done with asteroids and perhaps satellites. We must obtain good diameter measurements, possibly from space missions.

PHYSICAL STUDIES OF ASTEROIDS BY POLARIZATION OF THE LIGHT

AUDOUIN DOLLFUS
Observatoire de Paris

Curves of polarization are available at present for asteroids Vesta, Ceres, Pallas, Iris, Flora, and Icarus. These curves are compared with those of the satellites of Jupiter and Mercury, the Moon, and Mars. Laboratory simulations had already proved that the Moon's surface behaves like a powder of pulverized basalts; the recent confirmation by direct exploration is proving the significance of the method for remote determination of the surface properties of celestial bodies. The simulation of the Martian surface is found on small grained powders oxidized by ferreous limonite or goethite. New laboratory measurements were conducted to prepare the simulation of the asteroidal surfaces. Samples of the lunar surface returned to Earth provide impact-generated regolith and bare rocks superficially pitted and etched by impacts of the types suggested to be found on asteroidal surfaces; they were analyzed polarimetrically.

Preliminary interpretations show that Vesta departs significantly from the other asteroids and cannot be covered by frost deposits or by aggregate cosmic dusts; a regolith-type surface generated by impacts or a coating of cohesive grains is indicated.

Ceres, Pallas, and Iris are darker, and their polarizations do not suggest a pure regolithic surface, but cohesive grains or aggregates of dust are indicated.

Icarus is 10^8 times smaller in mass; its polarization authorizes a fluffy, loosely aggregated dust deposit; however, a cometary model with stones embedded in ice is perhaps not ruled out on the basis of the present data.

The way in which deep-space missions near the asteroidal belt can improve these results is discussed.

ANALYSIS OF THE REMOTE SURFACE CHARACTERISTICS OF THE ASTEROIDS BY POLARIZATION

Telescopic observations permit determination of the amount of polarization P of the light received from asteroids. The plot of these measurements as a function of the phase angle α defines the "curve of polarization" of an asteroid. This curve characterizes the mineralogic properties and structural texture of the asteroidal surface. These curves can be compared from asteroid to asteroid and with other celestial bodies, and simulated by laboratory measurements on different kinds of mineralogic samples.

POLARIZATION MEASUREMENTS AVAILABLE ON ASTEROIDS

The first curves of polarization on asteroids were derived in France by B. Lyot (1934). He used a photographic polarimeter attached to the 100 cm reflector of Meudon Observatory.[1] A curve of polarization was obtained for Vesta in 1934 and Ceres in 1935. These curves were published later by A. Dollfus (1961) and are reproduced again in figures 1 and 2. The curve for Vesta (fig. 1) starts with a negative branch (electric vector maximum in the plane through the Sun, asteroid, and Earth) having a minimum of about $P_{min} = -1.0$ percent near $\alpha = 12°$ and then rises to cross the $P = 0$ value at $\alpha = 26°$. Ceres (fig. 2) displays a more pronounced negative branch with P_{min} near -1.3 percent and $\alpha_0 = 17°$. Then, the polarization is positive (major electric vector perpendicular to the plane of vision) and rises steeply.

Later, S. Provin (1955), with the assistance of J. S. Hall and A. A. Hoag at the U.S. Naval Observatory, Washington, D.C., used a photoelectric polarimeter on Ceres, Pallas, and Iris. His curves were republished with additional information by A. Dollfus (1961). Figure 3 reproduces the curves for Ceres; the agreement with Lyot's curves (fig. 2) is not perfect, the negative branch being more pronounced and the slope, near the inversion point, being steeper. Pallas (fig. 4) is similar to Ceres. For Iris (fig. 5), Provin followed the variation of polarization as a function of time during more than a complete photometric light period (fig. 6); the phase angle was 27° and provided an average polarization of +1.2 percent; no significant variations were detected, proving

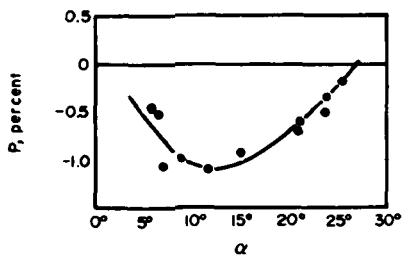

Figure 1.–Curve of polarization of Vesta. (1934 observations of B. Lyot; 100 cm refractor of Meudon Observatory; photographic polarimeter.)

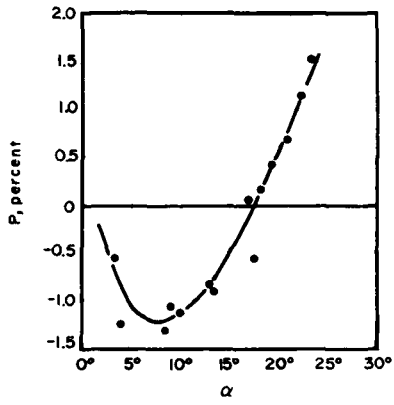

Figure 2.–Curve of polarization of Ceres. (1935 observations of B. Lyot; 100 cm reflector of Meudon Observatory; photographic polarimeter.)

[1]See p. 91.

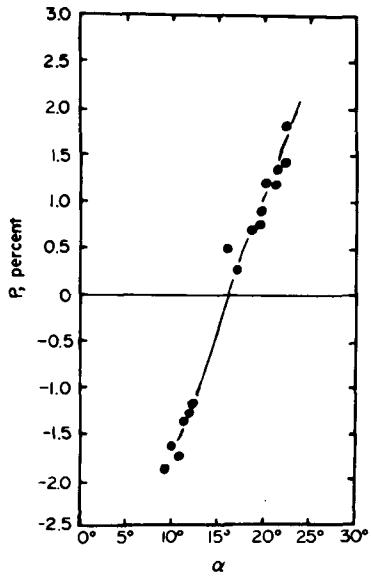

Figure 3.–Curve of polarization of Ceres. (1954 observations of D. C. Provin, U.S. Naval Observatory; photoelectric polarimeter.)

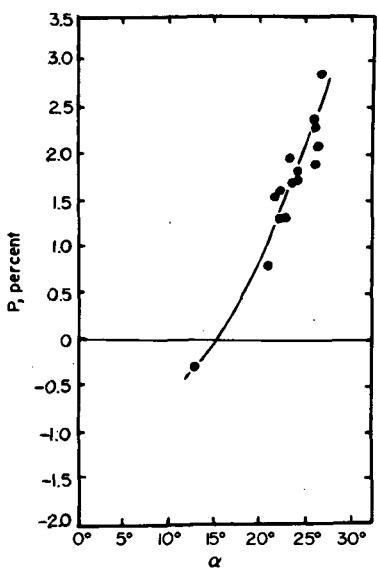

Figure 4.–Curve of polarization of Pallas. (Observations of D. C. Provin, U.S. Naval Observatory; photoelectric polarimeter.)

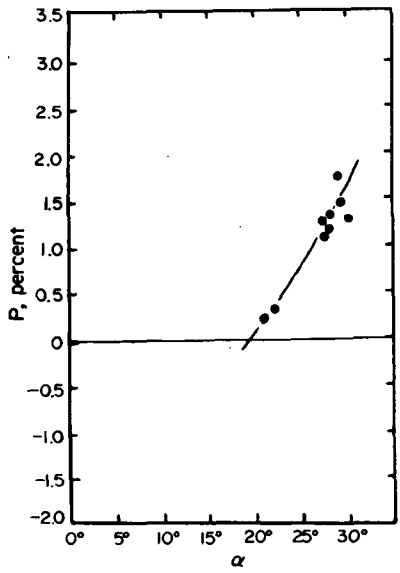

Figure 5.–Curve of polarization of Iris. (Observations of D. C. Provin, U.S. Naval Observatory; photoelectric polarimeter.)

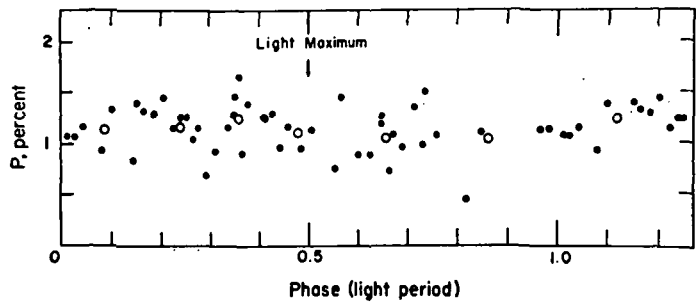

Figure 6.–Sixty-seven measurements of the amount of polarization of Iris, near $\alpha = 27°$, plotted as a function of the phase of the lightcurve. Open circles give normal points. (Observations of D. C. Provin.)

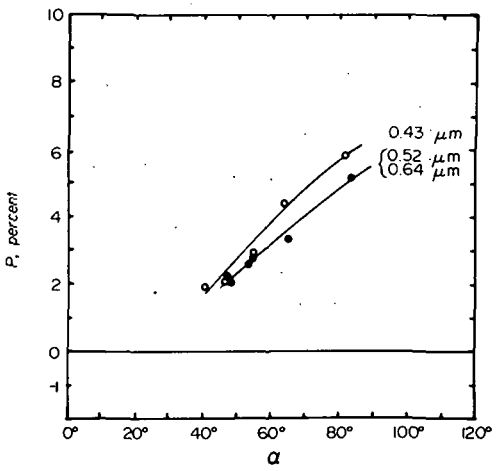

Figure 7.–Curves of polarization of Icarus obtained on the occasion of close encounter with Earth in 1968 by T. Gehrels. The values for 0.64 and 0.52 μm are grouped in the same curve; the other curve and open circles are for 0.43 μm.

that the physical properties of the surface were the same on the different parts of the asteroid successively seen from Earth as a result of its rotation.[2]

The next polarization curve for an asteroid was obtained by T. Gehrels et al. (1970) on Icarus. Making use of its flyby in the vicinity of Earth in 1968, the authors collected photoelectric polarization measurements in seven colors at the Catalina Station, Arizona. Figure 7 shows the polarization curves in red and blue light derived from the published measurements. Figure 8, taken from the Gehrels publication, compares the polarization (normalized) of Icarus, as a

[2]See, however, p. 72 of *Applied Optics* **2**, 1963; Provin may have been observing Iris near pole-on aspect.

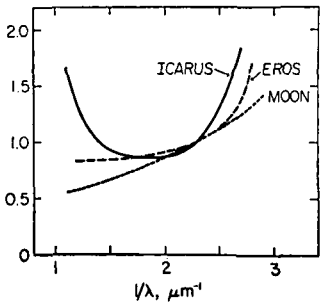

Figure 8.—Normalized polarizations of Icarus, Eros, and the Moon as functions of the inverse of wavelength. (Measurements for Eros are unpublished; observations of B. H. Zellner.)

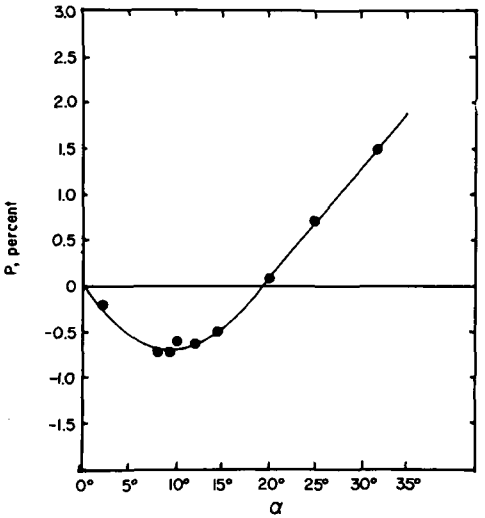

Figure 9.—Curve of polarization of Flora obtained in 1968-69 by J. Veverka at Harvard Observatory. (Photoelectric polarimeter.)

function of the inverse of the wavelength, with Mare Crisium of the Moon and unpublished results on Eros.

In 1968-69, J. Veverka (1971), using a photoelectric polarimeter with the Harvard 155 cm telescope, derived the polarization curve for Flora reproduced in figure 9.

COMPARISON WITH OTHER CELESTIAL OBJECTS

It is relevant to compare these polarization curves of Ceres, Pallas, Vesta, Iris, Icarus, and Flora with those of other celestial bodies practically devoid of atmospheres.

Figure 10 shows the polarization curves of the four major satellites of Jupiter obtained by A. Dollfus (unpublished) with a photoelectric polarimeter attached to the 60 cm Meudon reflector and the 107 cm Pic-du-Midi reflector. The negative branches are systematically less pronounced, and the inversion angle smaller, than for asteroids.

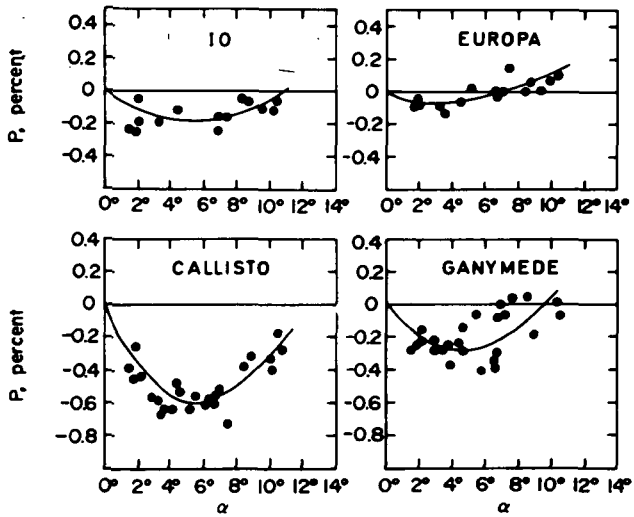

Figure 10.—Curves of polarization of the four Galilean satellites of Jupiter obtained by A. Dollfus with the 60 cm reflector of Meudon Observatory and the 107 cm reflector of Pic-du-Midi Observatory. (Photoelectric polarimeter; previously unpublished results.)

Figure 11 shows the complete polarization curve in orange light (580 nm) for Mercury based on observations by B. Lyot (1929) and A. Dollfus (unpublished). The inversion angle occurred at 24° and the negative branch is well pronounced.

Figure 12 shows in great detail the negative branch for the polarization curve of the Moon. This curve is almost identical to the case of Mercury; the minimum of polarization occurs near $\alpha = 12^\circ$ with the value $P_{min} = -1.2$ percent. The inversion angle occurs at $\alpha_0 = 24^\circ$ and is almost independent of the albedo and the area on the Moon. Then, the polarization is positive and the steepness of the curve increases as albedo and wavelength decrease.

Figure 13 illustrates the polarization curves of planet Mars at three wavelengths. The observations, collected by A. Dollfus and J. Focas (1969), only include measurements selected when the atmosphere of Mars was apparently free of aerosols. The negative branch for $\lambda = 0.61$ μm is almost identical to the case of the Moon and Mercury.

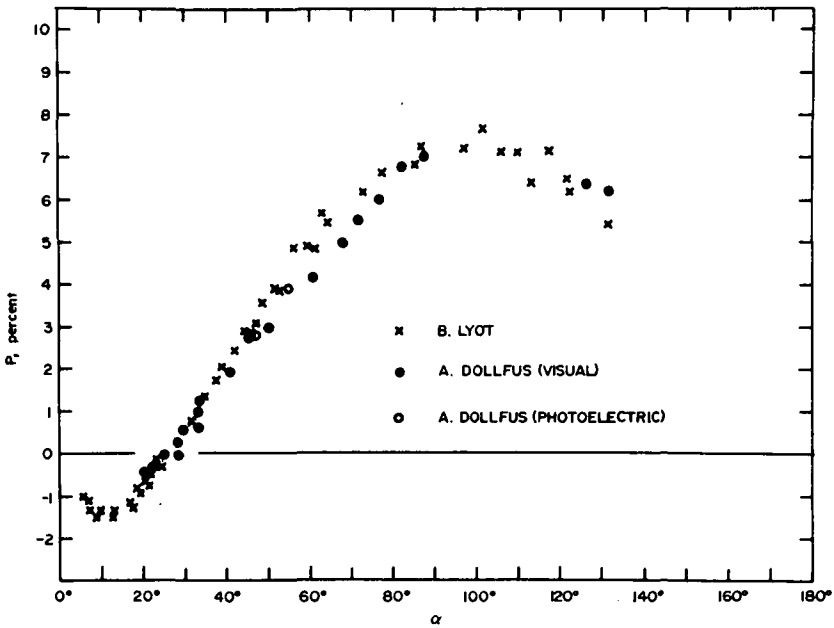

Figure 11.–Curve of polarization of planet Mercury in orange light (580 nm). Measurements by B. Lyot and A. Dollfus of Meudon and Pic-du-Midi Observatories. (Visual and photoelectric polarimeters.)

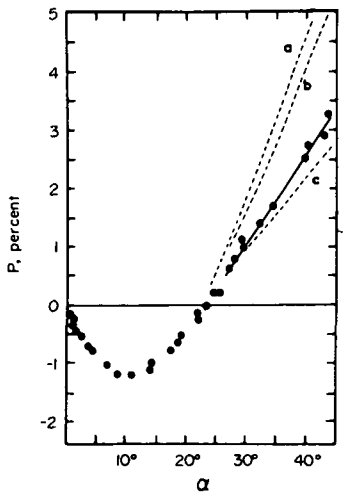

Figure 12.–Detailed observations of the negative branch of the polarization curve for the Moon (orange light). The negative branch is independent of wavelength and area on the Moon. The dashed curves *a*, *b*, and *c* are from Oceanus Procellarum, Mare Serenitatis, and Hipparchus, respectively.

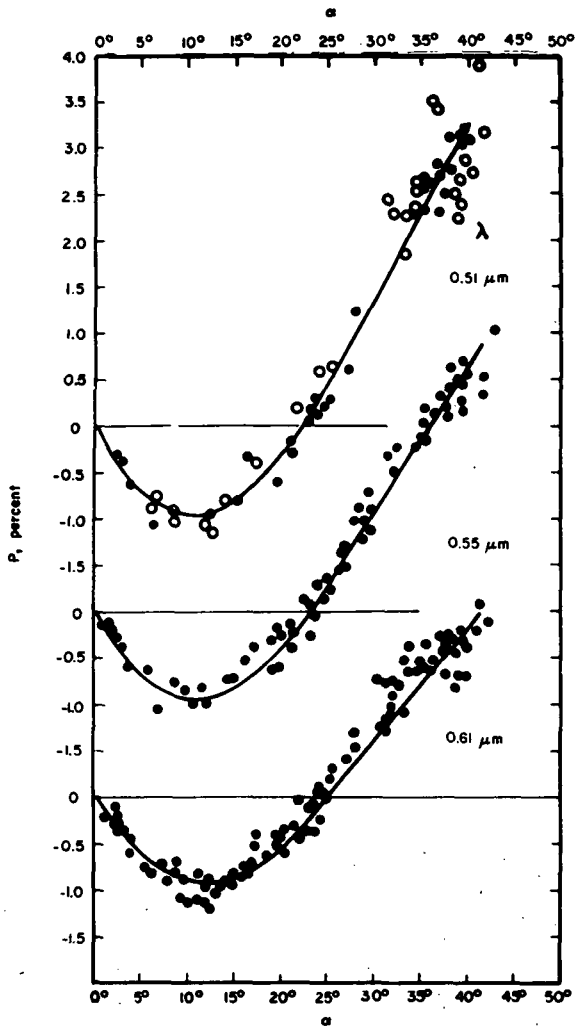

Figure 13.–Curves of polarization of the light area at the center of Mars' disk for wavelengths of 0.61, 0.55, and 0.51 μm. Observations by J. Focas and A. Dollfus at Meudon and Pic-du-Midi Observatories. The measurements are selected for absence of detectable aerosols in the Martian atmosphere. •: visual polarimetry (clear regions); o: photoelectric polarimetry.

INTERPRETATION OF THE POLARIZATION CURVES OF THE MOON, MARS, AND MERCURY

The negative branches of the polarization curves on the Moon, Mercury, and Mars are strikingly identical, when compared to those of other celestial bodies; they are very well developed with a minimum near −1.2 percent and an

inversion angle of about 24°. These properties correspond to an extreme case reached only by very specific types of materials; these criteria fortunately provide a discriminative identification of the nature and structure of these planetary surfaces.

The behavior of these negative branches was found by B. Lyot (1929) to be reproduced on volcanic ashes. Since this pioneering work, extensive studies were developed by A. Dollfus (1955, 1956, 1962), who found this characteristic shape of the curve to be typical of fine powders mixed together and made of very absorbing material of different grain sizes as small as a few micrometers. Laboratory measurements (Dollfus, 1956) proved that multiple scattering between the absorbing grains is responsible for the negative branch.

Other optical criteria, like the spectral variation of the albedo (for Mars), or the spectral variation of the polarization maximum (for the Moon), enable one to discriminate the nature of the absorbing material from which the powder originates. For the Moon, the best optical laboratory simulation was found in finely pulverized basalts (Dollfus et al., 1971*a*). For the planet Mars, the small grains should be ferreous oxides, like goethite or limonite, or coatings by these oxides (Dollfus, 1956; Dollfus et al., 1969).

The remote identification was recently successfully confirmed, in the case of the Moon, by the lunar samples returned to Earth by the Apollo missions. Figure 14(*a*) displays a microphotograph of a pulverized basalt selected in 1954 as being the best simulation of the lunar surface for the optical properties concerned. This picture was published 16 yr ago and again in 1962 by A. Dollfus (1955, 1962). Figure 14(*b*) is a microphotograph of a sample of lunar

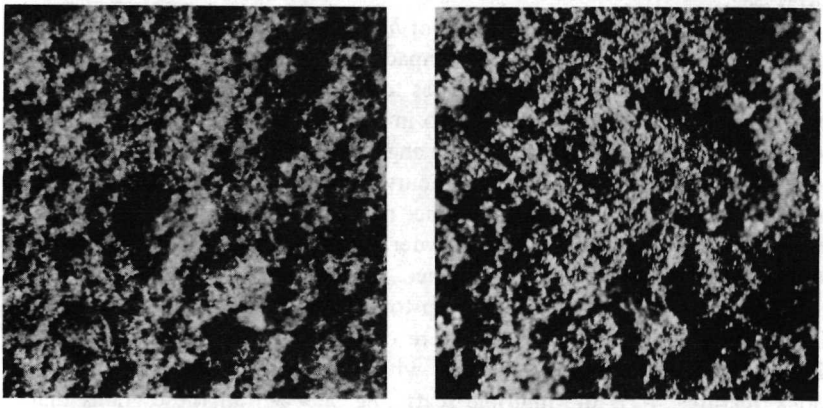

(a) (b)

Figure 14.—(*a*) Microphotograph of a pulverized basalt from lava flow simulating the optical properties of the lunar surface. Original size: 3 by 3 mm. This picture was obtained in 1954 and published in 1955 (Dollfus, 1955). (*b*) Microphotograph of an Apollo lunar fines sample obtained in 1970 in the same conditions as (*a*).

fines returned to Earth by the Apollo 11 mission and photographed under the same conditions as figure 14(*a*). The striking similarity is convincing as regards the validity of the polarimetric criteria from remote identifications. (See also Geake et al., 1970.)

LABORATORY POLARIZATION STUDIES RELEVANT TO ASTEROID PROBLEMS

For the purpose of interpreting the asteroid's polarization curves, we are developing, at Meudon Observatory, a program of laboratory measurements on samples expected to simulate the asteroidal conditions. This survey is still in progress.

Among the likely candidates for the simulations of the superficial properties of asteroids are frost deposits, aggregated cosmic dust, impact-generated regolith from lunar or meteoritic material, and bare rocks superficially pitted and etched by impacts and possibly coated by adhesive grains.

Laboratory measurements on the polarization of frost deposits were obtained by A. Dollfus (1955); the amount of polarization is very low for all phase angles.

Optical measurements on deposited cosmic dust are difficult, although some preliminary indications are obtained (see below).

Particularly relevant to the asteroidal problems are the lunar surface samples returned to Earth by the Apollo missions. These minerals were exposed to the etching, weathering, or disaggregation by long space exposure and meteoritic impacts; these processes should reproduce those operating on asteroidal surfaces.

Of special interest are the samples of *lunar fines* collected at the surface of the regolith layer and generated by impact pulverization of the lunar surface. Figure 15 shows the polarization curves for Apollo lunar fines sample 10084,6 from Mare Tranquillitatis. The albedo in orange light is 0.075. The curves of polarization for the full range of phase angles are given in five wavelengths. The negative branches of the polarization curves, given in figure 15, bottom right, are identical to those of the lunar surface measured through telescopes, proving that the physical structure of the powder in the laboratory retains the original configuration it had on the lunar surface. Electron microscope scanning images of the grains are given in figure 16, up to a scale releasing details smaller than the wavelength. These documents were obtained at Manchester by Dr. J. E. Geake. The texture is very complex with grains of all sizes, showing many shock features. It is the multiple scattering between all these grains that is responsible for the deep negative branch of polarization with inversion angle as high as 24°.

The *lunar rocks* should also be compared to asteroids because, as a result of the low value of their escape velocities, the small asteroids hardly retain the powder ejected by impacts (although cohesion and adherence due to vacuum

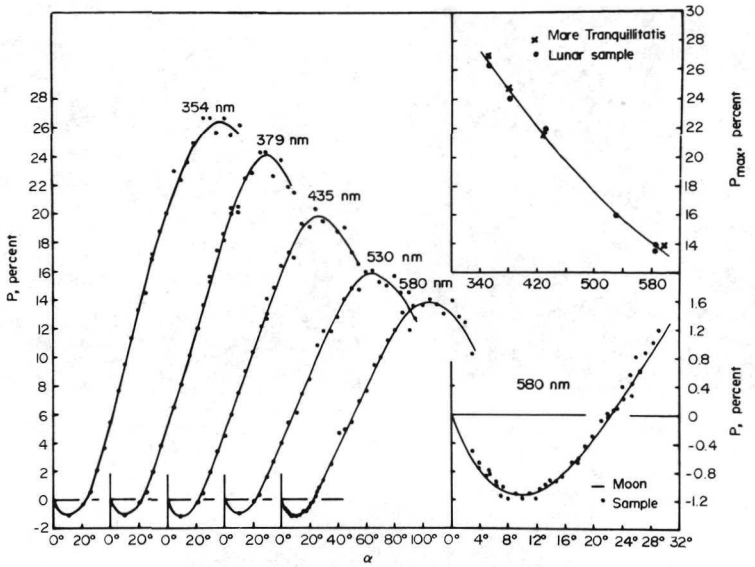

Figure 15.–Curves of polarization of the Apollo 11 lunar fines sample 10084,6 from the regolith surface of Mare Tranquillitatis. Photoelectric measurements are given in five wavelengths. (Meudon Observatory.)

may replace the gravitational retention); this is precisely the case for the rocks collected at the surface of the lunar regolith.

Figures 17 and 18 correspond to a *lunar crystalline rock,* Apollo sample 12051,51. The albedo in orange light is 0.24 and the color is reddish; further information is found in Dollfus et al. (1971*a*). The maximum of polarization (fig. 17) is higher than on the fines (fig. 15) and occurs for larger phase angles. The negative branch, reproduced on a larger scale in figure 18, is definitely less pronounced than for the lunar fines (fig. 16), with a minimum of −0.4 percent only (against −1.2 percent for the fines) and an inversion angle of 16° (against 24° for the fines). The explanation is given by the electron scanning microscope images obtained for the purpose by Dr. J. E. Geake and reproduced in figure 18; the texture is definitely smoother than the samples of fines. The picture at top right, with the highest magnification, characterizes the average texture and can be compared with the picture of the lunar fines taken with the same magnification; the multiple scattering is less efficient in these structures; furthermore, an appreciable fraction of the surface releases glassy aspects due to splashes of melted silicates reproduced in the picture at center; these areas are almost devoid of appreciable multiple scattering. Finally, because of the smaller effect of the multiple scattering, this typical lunar crystalline rock gives a small negative branch of polarization.

Figure 19 characterizes a particularly *glassy lunar rock,* Apollo sample 12002,102. The albedo is 0.13 in orange light. The largest fraction of the

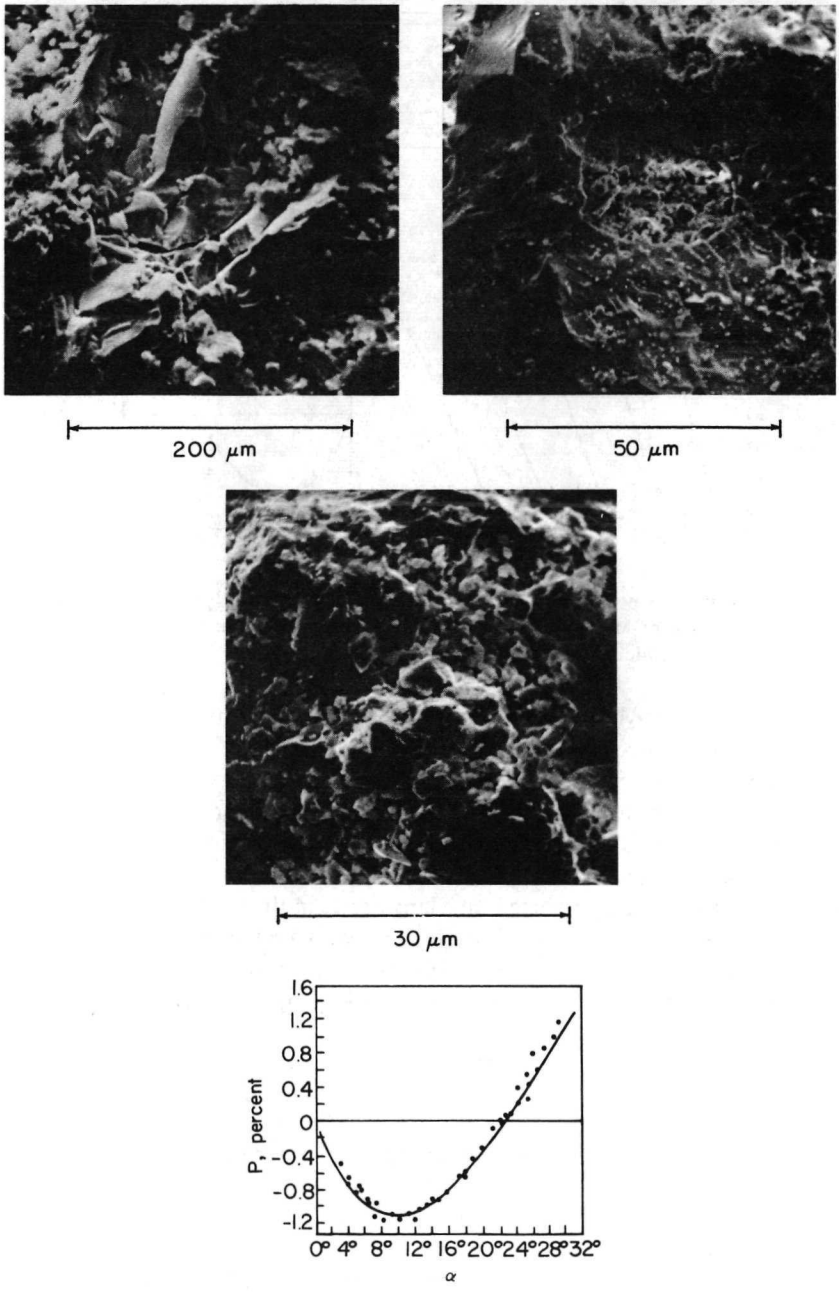

Figure 16.–Electron scanning microscope pictures of Apollo lunar fines sample 10084,6 and its negative branch of polarization. (The pictures were obtained by J. E. Geake at Manchester.)

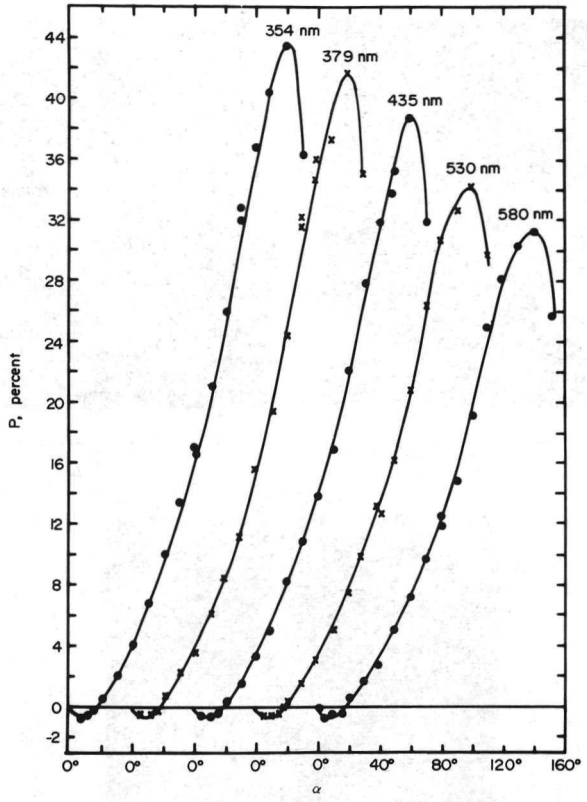

Figure 17.–Curves of polarization of Apollo lunar crystalline rock 12051,51. The photoelectric measurements were made in five wavelengths. (Meudon Observatory.)

surface appears to be almost smooth, as strikingly seen in the image on top right. A still greater enlargement is shown in the picture at center. The multiple scattering should be limited and the negative branch of polarization very small; the curve, reproduced at bottom, has a minimum of -0.2 percent only and an inversion angle of 10°.

Figure 20 belongs to a *lunar breccia,* Apollo sample 10059,36, with albedo 0.095 and an almost gray color. Each of the three images is centered on the same area, with increased enlargement, by factors of about 3. This is a cohesive mixture of grains, exceptionally rough in all scales; some glassy grains are incorporated; the picture at center shows a glassy fragment cemented (in the upper half) with a clump of very small cohesive grains (lower half). But the multiple scattering is dominant, and the negative branch of polarization is almost as pronounced as in the case of the lunar fines.

Additional results on polarization properties of lunar rocks and fines are found in the two papers by Geake et al. (1970) and Dollfus et al. (1971*b*).

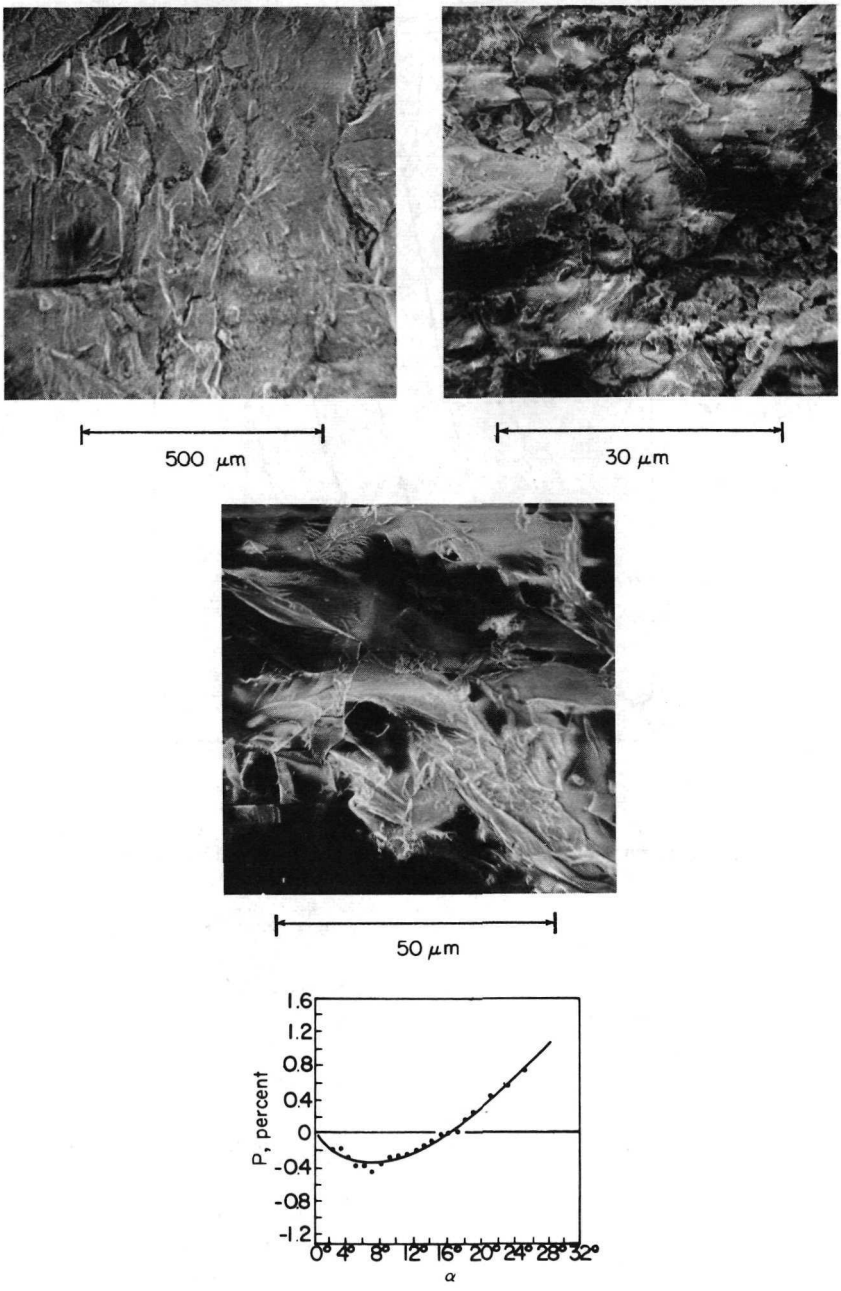

Figure 18.–Electron scanning microscope pictures of Apollo lunar crystalline rock 12051,51 and the negative branch of its polarization curve. (The pictures were obtained by J. E. Geake at Manchester.)

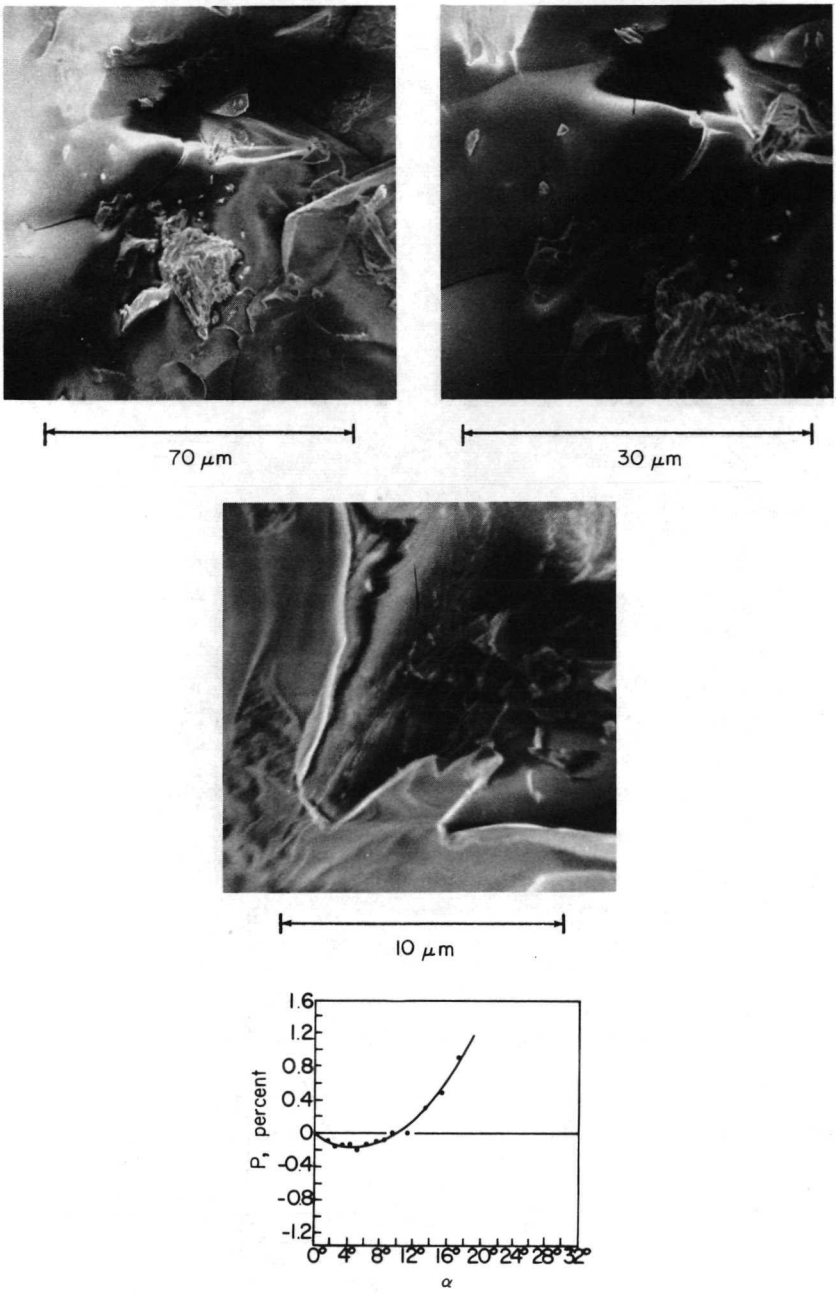

Figure 19.—Electron scanning microscope pictures of glassy Apollo lunar rock 12002,102 and the negative branch of its polarization curve. (The pictures were obtained by J. E. Geake at Manchester.)

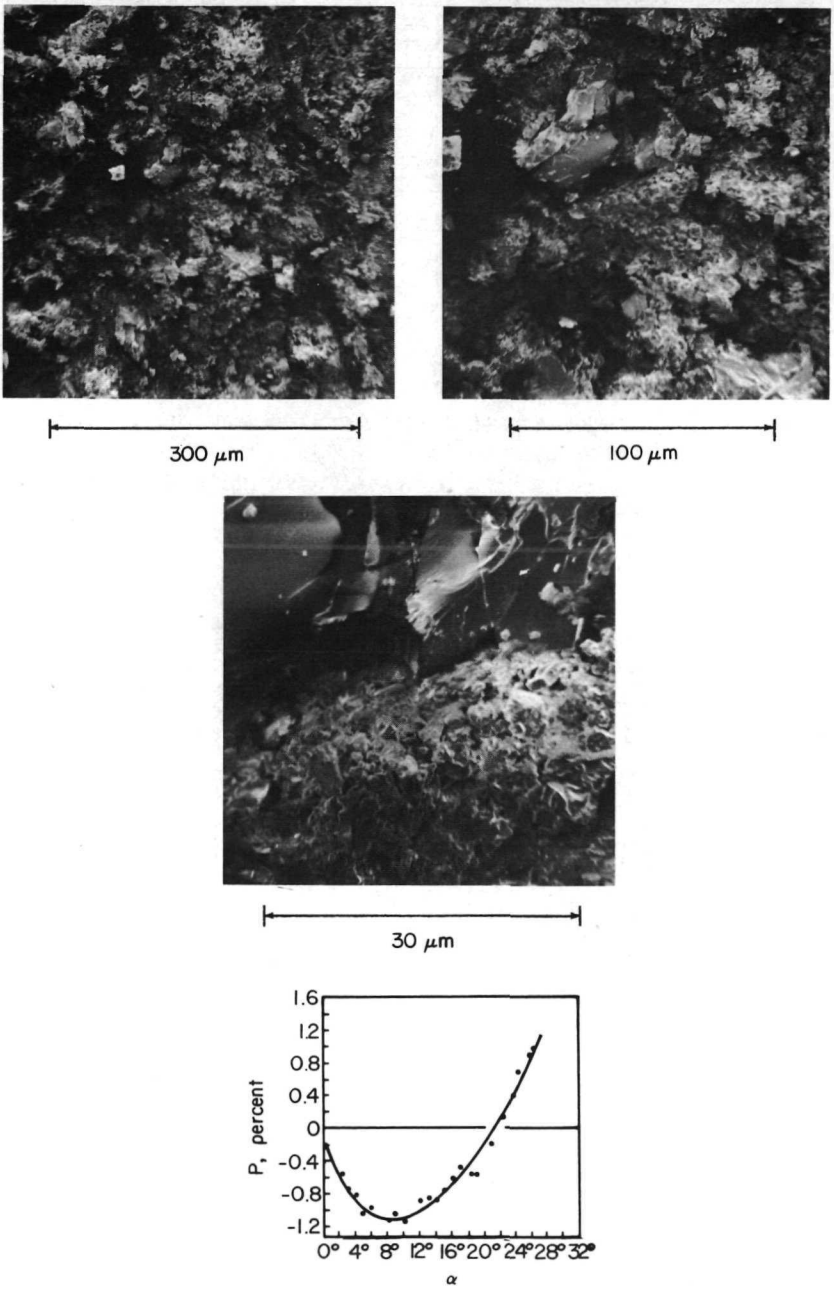

Figure 20.–Electron scanning microscope pictures of Apollo lunar breccia 10059,36 and the negative branch of its polarization curve. (The pictures were obtained by J. E. Geake at Manchester.)

INTERPRETATION OF THE POLARIZATION CURVES OF ASTEROIDS

From the previous polarimetric results, combined with other optical or physical data available, models of the nature of the asteroidal surfaces can be derived, or at least indicated.

For Vesta the diameter is known to be of the order of 410 km (see A. Dollfus[3]) and the corresponding albedo is 0.40. This high value is compatible with frost deposits but excludes aggregated cosmic-dust coatings. The presence of polarization, in turn, excludes frost deposits, but agrees with solid surfaces.

The spectral reflectivity curves between 0.35 and 1.1 μm observed by McCord et al. (1970)[4] show a pronounced dip at 0.9 μm found on Mg-rich orthopyroxene and recognized on samples of basaltic achondrites. On account of its deeper negative branch, the shape of the polarization curve excludes a glassy surface of the type displayed in figure 19, and also the average lunar rock structures shown in figure 18; more multiple scattering is needed and involves more rugged surfaces.

The negative branch of polarization is not incompatible with a regolith layer resulting from fragments generated by impacts on a light basaltic achondrite mineral. For an assumed density of 3.3 g/cm^3, the escape velocity is 140 m/s and a large fraction of the ejecta produced by impacts should be lost in space; however, the cohesion of grains in vacuum may help to retain sticky grains.

For Ceres, the diameter of about 770 km is definitely larger than that for Vesta, and the darker albedo of 0.13 is similar to the case for the Moon and Mercury. For Pallas, some inconsistencies remain between diameter measurements (see A. Dollfus[5]), but the size is intermediate between that of Ceres and Vesta, with an albedo not higher than that of Ceres. The diameter of Iris has not yet been measured but belongs to the Ceres' or Pallas' range of sizes. Although polarimetric measurements should be continued, all three of these asteroids apparently display the same type of polarization curves, with an inversion angle near 18° and a negative minimum as high as 1.7 percent.

The low albedo and high negative branch of polarization exclude frost deposits on these three objects but characterize surface structures and composition definitely different from that for Vesta. The reflection spectrum from Pallas, and probably Ceres, obtained by McCord et al. (1970) does not show the 0.9 μm band seen on Vesta. With escape velocities of the order of 250 m/s, these bodies should retain more easily ejected fragments from impacts, as Vesta does, but nevertheless the polarization curves depart from the characteristics of the lunar fines and, despite the similarity in albedo, exclude a pure lunar type regolithic powdered layer.

The polarimetric properties may indicate cohesive grains but do not rule out, with the present data, a loose aggregate of gently deposited cosmic dust; more observational and laboratory work is to be performed.

---

[3]See p. 28.
[4]See also p. 60.
[5]See p. 25.

For Icarus, the measurements of figure 7 refer to a body belonging to a completely different range of sizes. The diameter of nearly 1 km (Gehrels et al., 1970) gives a mass on the order of 10^8 times smaller than for the other asteroids polarimetrically analyzed. The escape velocity of 0.35 m/s rules out the retention of any kind of ejecta resulting from impacts. The maximum of polarization of 7 percent almost excludes bare rock with an albedo of 0.26 assumed by Gehrels et al. (1970), but authorizes a fluffy, loosely aggregated deposit of (cosmic) dust. However, a cometary model with stones embedded on ice is perhaps not ruled out on the basis of the current polarimetric data available.

POSSIBILITIES FOR FUTURE WORK

In addition to the refinement and extension of the ground-based telescopic techniques currently used, major results could be expected from space missions near the asteroidal belt.

For the minor planets of the main belt, the phase angle observable from Earth is limited to the range between 0° and about 30°. Space missions will reveal the shape of the curves near their maxima, occurring between 90° and 120°, and determine the highest value of the polarization P_{max}. Together with the albedo A, deduced from the direct measurements of the diameters, these values of P_{max} are basic for the telescopic determinations of the composition of these celestial bodies.

For instance, in the case of the Moon, the determinations of P_{max} for areas of different albedo plotted on a logarithmic scale as a function of A display a linear relation between log A and log P_{max}, as seen in figure 21 (Dollfus and

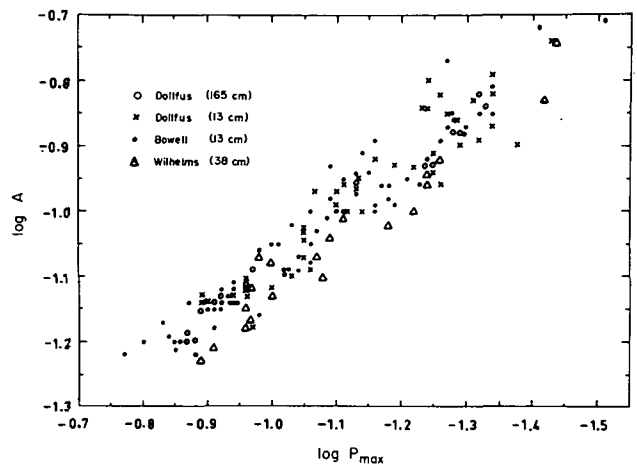

Figure 21.–Albedo of 146 areas of the lunar surface plotted as a function of their maximum of polarization P_{max} in logarithmic scale. Measurements in orange light.

Bowell, 1971). Comparisons with mineralogic samples, summarized in figure 22, demonstrate that several compositions have to be ruled out as candidates for simulation of the optical properties of the Moon, namely, sands, clays, chalks, crushed rocks, pulverized meteorites, ignimbrites, vitric basalts, and most of the volcanic ashes. On the contrary, the pulverized basalts from lava flows fit the optical properties of the lunar regolith very well (Dollfus et al., 1971*a*; Dollfus and Titulaer, 1971). The subsequent confirmation of this result by the direct exploration of the Moon again accredits the significance of the polarimetric technique for remote analysis of the composition of planetary surfaces.

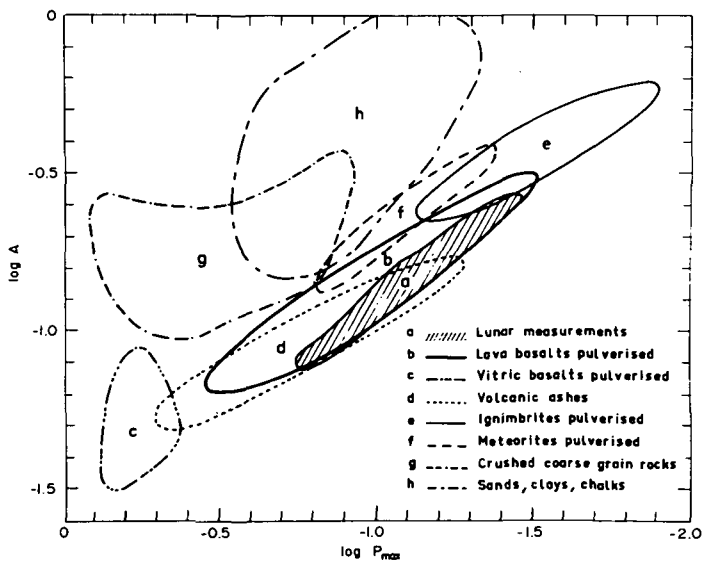

Figure 22.—Domains occupied by different kinds of terrestrial and meteoritic samples in a log A versus log P_{max} plot similar to figure 21. The domain for lunar measurements is derived from figure 21 after normalization of the albedo scale with the Apollo lunar samples returned to Earth.

Figure 23 further refines the determination by taking into account the spectral variation of P_{max} and A. Measurements at five wavelengths for each sample gave five dots in the log A - log P_{max} plot, alined along a segment represented in figure 23; location, length, and slope of these segments characterize still more precisely the surface and again strengthen the optical similarities between the lunar regolith and terrestrial pulverized basalts.

Spaceborne measurements on minor planets will characterize the asteroidal surfaces by dots in figure 22 and segments in figure 23 and will provide specific data for compositional comparison and simulation.

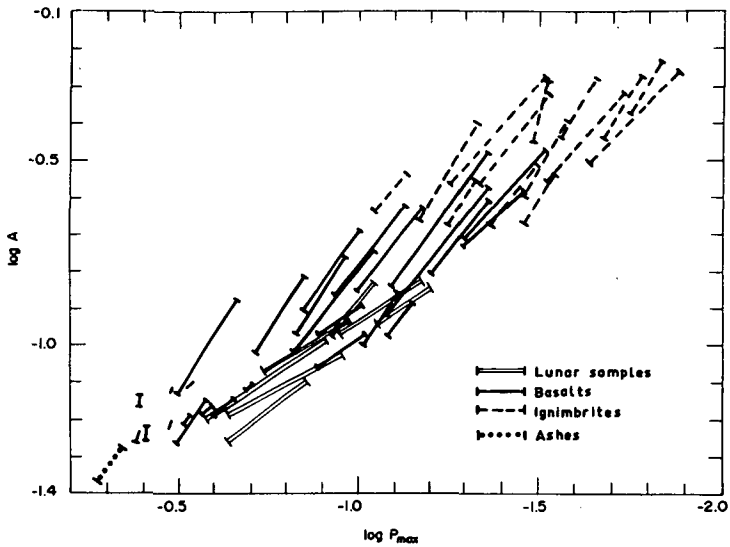

Figure 23.—Log A versus log P_{max} plot for 38 volcanic samples of pulverized basalts, ignimbrites, and ashes, and five Apollo lunar fines samples, measured at five wavelengths. The left and right ends of each segment correspond respectively to the wavelengths 354 and 580 nm.

REFERENCES

Dollfus, A. 1955, Étude des Planètes par la Polarisation de la Lumière. Doctoral Thesis, Univ. of Paris. (1964, NASA TT F-188.)

Dollfus, A. 1956, Polarisation de la Lumière Renvoyée par les Corps Solides et les Nuages Naturels. Ann. Astrophys. **19**, 83.

Dollfus, A. 1961, Polarization Studies of Planets. Planets and Satellites (ed., G. P. Kuiper), pp. 389-390. Univ. of Chicago Press. Chicago.

Dollfus, A. 1962, The Polarization of Moonlight. Physics and Astronomy of the Moon (ed., Z. Kopal), ch. 5. Academic Press, Inc. London.

Dollfus, A., and Bowell, E. 1971, Polarimetric Properties of the Lunar Surface and Its Interpretations, Part I. Telescopic Observations. Astron. Astrophys. **10**, 29-53.

Dollfus, A., Bowell, E., and Titulaer, C. 1971*a*, Polarimetric Properties of the Lunar Surface and Its Interpretations, Part II. Terrestrial Samples in Orange Light. Astron. Astrophys. **10**, 450-466.

Dollfus, A., and Focas, J. 1969, La Planète Mars: La Nature de sa Surface et les Propriétés de son Atmosphere, d'Après la Polarisation de sa Lumière. I. Observations. Astron. Astrophys. **2**, 63-74.

Dollfus, A., Focas, J., and Bowell, E. 1969, La Planète Mars: La Nature de sa Surface et les Propriétés de son Atmosphere, d'Après la Polarisation de sa Lumière. II. La Nature du Sol de la Planète Mars. Astron. Astrophys. **2**, 105-121.

Dollfus, A., Geake, J., and Titulaer, C. 1971*b*, J. Geophys. Res., in press.

Dollfus, A., and Titulaer, C. 1971, Polarimetric Properties of the Lunar Surface and Its Interpretation. Part III. Astron. Astrophys., in press.

Geake, J., Dollfus, A., Garlick, G., Lamb, W., Walker, G., Steigmann, G., and Titulaer, C. 1970, Luminescence, Electron Paramagnetic Resonance and Optical Properties of

Lunar Material From Apollo 11. Proc. Apollo 11 Lunar Sci. Conf. Geochim. Cosmochim. Acta 34, suppl. 1, vol. 3, 2127-2147.

Gehrels, T., Roemer, E., Taylor, R., and Zellner, B. 1970, Minor Planets and Related Objects. IV. Asteroid (1566) Icarus. Astron. J. 75, 186-195.

Lyot, B. 1929, Recherches sur la Polarisation de la Lumière des Planètes et de Quelques Substances Terrestres. Doctoral Thesis, Univ. of Paris. (1964, NASA TT F-187.)

Lyot, B. 1934, Polarisation des Petites Planètes. C.R. Acad. Sci. 199, 774.

McCord, B., Adams, J. B., and Johnson, T. V. 1970, Asteroid Vesta: Spectral Reflectivity and Compositional Implications. Science 168, 1445-1447.

Provin, S. 1955, Preliminary Observations of the Polarization of Asteroids. Publ. Astron. Soc. Pac. 67, 115.

Veverka, J. 1971, Photopolarimetric Observations of the Minor Planet Flora. Icarus 15(3), in press.

DISCUSSION

ARRHENIUS: For the case of Vesta, on the basis of the high albedo you rule out lunar dust and powder; probably you have in mind Apollo 11 or 12 dust because the new data on Apollo 14 indicate a much higher albedo.

DOLLFUS: We measured lunar fines on Apollo 12 on the lightest area available and none of them were higher than 0.25.

ARRHENIUS: How about pure feldspar?

DOLLFUS: Pure feldspar is too transparent to produce the curve of polarization observed. It cannot be basalt because basalts are too absorbent.

ANDERS: I do not think we should dismiss the possibility of a regolith on asteroids. True, the escape velocity is low, but impact ejecta have a velocity distribution starting at zero, and so some fraction of the dust and debris will remain on the body. It does not matter that more material is lost than is gained in such an impact, because the loss is all in one place, the crater. The remainder of the body gets showered with low-velocity debris.

Moreover, a few percent of the stony meteorites in each class contain a noble-gas component that seems to represent trapped solar wind. Wänke suggested some years ago that implantation of solar-wind ions might happen in the regoliths of bodies without atmospheres, and this has been beautifully confirmed by Apollo 11 and 12 lunar soils and breccias. Now, meteorites apparently do not come from the Moon, and if the asteroids are too small to have a regolith, we will be hard pressed to find larger bodies without atmospheres where these gas-rich meteorites might form. Comets are too small and too far away and in a region where the solar-wind flux is very low. The moons of Jupiter are too large to permit escape of ejecta and cannot send material into terrestrial space with any efficiency. Thus we are left with the asteroids.

CHAPMAN: Anders has correctly noted that low escape velocity for asteroids need not imply that asteroids are not covered with a regolith or dust layer. The cratering and steady-state loss and accretion processes that govern the development of asteroidal regoliths are complex and depend on many factors. For example, in the case of a large population index for the impacting debris, a "sandblasting" effect may continually remove most or all of the regolith that otherwise would develop in the manner Anders mentioned.

Dr. Dollfus, in the final part of his presentation, has described how measurements of the maxima of asteroid polarization curves have some compositional implications. He argued that such measurements would be an important goal for a space mission. Ground-based spectral reflectivity studies are much cheaper, and they are far more diagnostic of mineralogical composition.

HAPKE: The relation between surface texture and the negative branch of polarization that Dr. Dollfus has described is certainly true. However, another property of materials that also affects the negative branch should be mentioned, and that is albedo. For a powder with a high albedo, such as pure feldspar or enstatite, the negative branch will be

less pronounced than for a dark powder, such as Moon soil, so that there is some ambiguity in the interpretation of the negative polarization branch if the albedo is not known.

VEVERKA: I just want to note that the Lyot polarization curves for Ceres and Vesta were obtained by a rather insensitive photographic method and do not agree too well with more recent photoelectric measurements. One therefore should not base any inferences on them.

PHOTOMETRIC OBSERVATIONS AND REDUCTIONS OF LIGHTCURVES OF ASTEROIDS

RONALD C. TAYLOR
University of Arizona

The brightness-time variation (the lightcurve) of an asteroid is observed to obtain the rate of rotation, some indication of the shape, and the orientation of the rotation axis in space. The brightness-phase relations are observed for the study of surface texture.

This paper deals specifically with observing routines and reductions, including discussions of lightcurves, rotation periods, absolute magnitudes, phase coefficients, opposition effects, and pole determinations. This paper supplements the review chapter by Gehrels (1970). Only photoelectric techniques are considered because the visual and photographic ones are, nearly without exception, not precise enough.

OBSERVING ROUTINE

Photoelectric observations of asteroids were made as early as 1935 by Calder (1935). Calder already observed comparison stars, chosen for their proximity to the asteroid and for similarity in color and magnitude. The comparison star observations allow correction for photometric changes in the quality of the night and to remove extinction effects from the lightcurve. (This, of course, assumes that the comparison star does not vary during the night.) A value for scatter of the comparison readings can be computed as an indication of the quality of the night. Because it is impossible—with a single detector—to observe the comparison star and the asteroid at the same time, interpolation of comparison star readings is necessary. The deviation of the comparison star readings from a smooth secant Z curve is, at good sites as the McDonald and Kitt Peak Observatories, on the order of 0.01 mag; such effects remain uncorrected if no comparison star is observed (for instance, by Miner and Young, 1969, 1971). With careful comparison star corrections, the precision of the lightcurves generally is ±0.003 mag (for the mean of three measurements). With a two-detector photometer this may be improved to ±0.001 mag. (See Gehrels, 1970, fig. 4.)

With slight variations, the generally adopted observing routine is as follows: At the beginning and end of each run a red and a blue standard star

are observed for *B*, *V*, and *U*. The order of the lightcurve observations is *AASAA*; *CC*, *AASAA*, *CC*, etc., where *A* represents the asteroid, *C* the comparison star, and *S* the sky readings. Automatic lightcurve reductions during the night of observing have not as yet been made. As a step toward that goal we have a preliminary automated lightcurve reduction program.

Standard stars (not to be confused with the comparison star) are observed to determine the magnitude of the asteroid; generally the *UBV* system of Johnson and Morgan (Johnson, 1963) is used. If one has a fast-moving telescope, the transfers can be performed during the lightcurve run rather than at the beginning and end of the night. Figure 1 illustrates the transfer routine.

In certain circumstances, one may find it desirable to forsake standard star observations during an asteroid run. In those cases, the comparison stars—and more than one should be observed because of possible variations—can be tied in to standard stars on subsequent evenings.

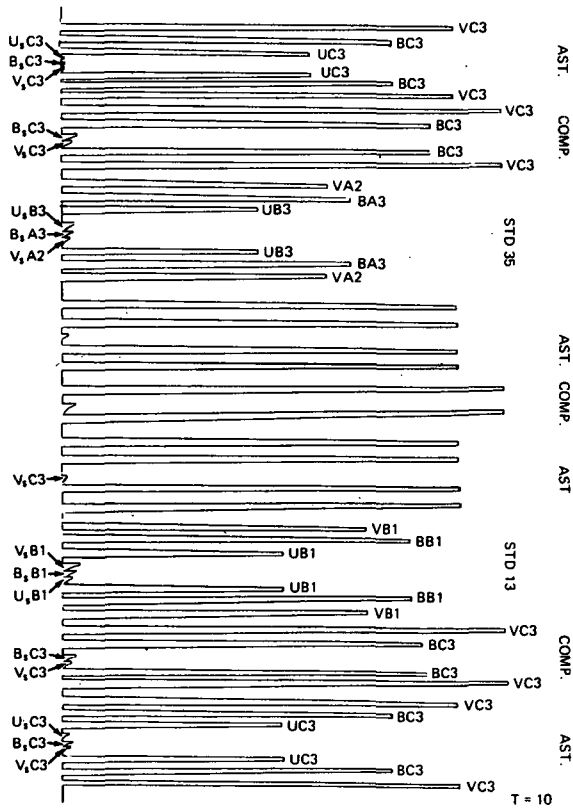

Figure 1.—A reproduction of *UBV* transfer. *V*, *B*, and *U* refer to the filters; the symbols *A*1 to *C*3 indicate gain setting; the subscript *s* shows sky readings; and *T* is the integration time.

As for color variations, Groeneveld and Kuiper (1954*a*) observed in *V* and *B*, but the color variations were only about 0.004 mag; therefore, they discontinued the procedure. Thirty color observations near maxima and minima were done in one evening on 624 Hektor. Little color differences were found, which supports the contention that the large amplitudes (as high as 1.1 mag) of the lightcurves were caused mostly by shape, rather than by a spotty surface (Dunlap and Gehrels, 1969). For Vesta, a slight variation of the $U-V$ color over the surface has been found (Gehrels, 1967*a*). To make a thorough study of color differences over the surface of an asteroid, a multichannel photometer may be an ideal instrument for the observations.

LIGHTCURVE REDUCTIONS AND SYNODIC PERIODS

Most authors have adapted the procedure of plotting each point on the lightcurve as the average of a set of values of the asteroid reading minus the comparison star reading with skies subtracted out, and an extinction correction applied. Generally, open circles have been used to represent uncertain values and, at times, authors have reproduced points to complete a lightcurve. Investigators have varied in taking the mean of from two to four asteroid readings per lightcurve point. In 1967, Gehrels (1967*a*) suggested that for bright objects "... it will be better always to plot the mean of two integrations rather than four, in order to show fine details of the shape of the lightcurve."

It appears that most lightcurves have been plotted using, as an ordinate scale, an arbitrary delta magnitude system between the comparison star and the asteroid. Occasionally authors have used a scale based on the *V* magnitude of the asteroid. Generally lightcurves appear as a plot of points as indicated in figure 2. For clarity, some authors have joined mean lightcurve points with a curve, especially if the lightcurve is not well defined.

Because of the rapid motion of Icarus, corrections for phase and distance, as well as differential extinction, were needed to adjust each lightcurve. I reduced the raw data supplied by Miner and Young (Gehrels et al., 1970) for June 19 and 20, 1968, by the general methods described above. Miner and Young (1969) averaged 3 to 12 data points within a 2.7 min segment, determined a

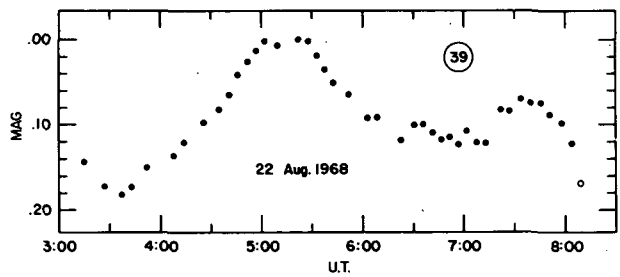

Figure 2.–A typical lightcurve.

mean lightcurve with error bars averaging ±0.015 mag, and smoothed the curve by successively fitting 5 consecutive points to a third-order polynomial. It is of interest to see how the two techniques create different lightcurves. (See figs. 3 and 4.)

Several authors have created mean lightcurves from various observations of the same asteroid. Generally, corrections of some fashion have been applied. Three such techniques are based on phase distance, rotation period, or comparison star magnitude differences (Chang and Chang, 1962; Groeneveld and Kuiper, 1954*a*; van Houten-Groeneveld and van Houten, 1958). With 20 Massalia phase changes caused amplitude variations, therefore a mean lightcurve was constructed from only two intermediate evenings (Gehrels, 1956). In analyzing 18 lightcurves of 6 Hebe over 3 oppositions, I have concluded that mean lightcurves can be made only when the observations are grouped by opposition and similar phase angles (Taylor and Gehrels, 1972). Figure 5 illustrates three mean lightcurves of Hebe. The various causes for the mean lightcurves to look different at various oppositions are discussed by Dunlap.[1]

Synodic periods have generally been determined by an inspection of the lightcurves. On occasion one must inspect the mean lightcurve, especially if the period is long and each lightcurve is short (Chang and Chang, 1962). The mean lightcurve was used with Massalia. The period was determined by dividing the number of cycles into the time intervals between maxima of consecutive lightcurves and of each lightcurve with the mean lightcurve (Gehrels, 1956).

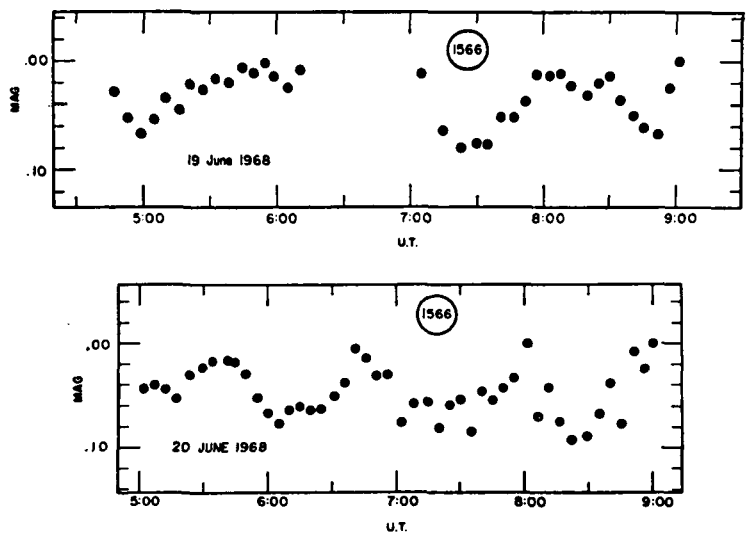

Figure 3.–Icarus data of Miner and Young reduced by standard method.

[1]See p. 147.

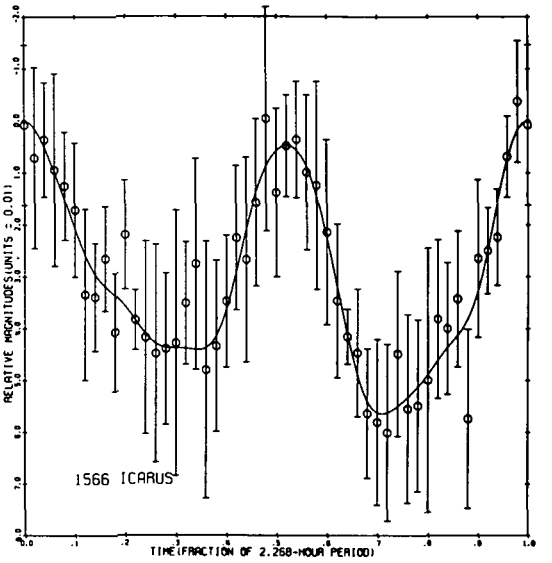

Figure 4.–Icarus data of Miner and Young reduced with their polynomial method.

The period can also be determined with the method of Hertzsprung (1928, 1941), which requires a least-squares routine on the ordered pair (N, T), where N is the number of cycles since the first epoch and T is the time of each epoch in Julian days corrected for light time.

In fitting lightcurves of Vesta for a synodic period determination, it was assumed that the horizontal time axes are parallel. Because of phase changes, only time intervals from adjacent lightcurve epochs were used (Gehrels, 1967*a*). With Hebe, I found that in matching lightcurves one should not necessarily attempt to fit epochs of maximum or minimum light. Comparing these epochs can be misleading because there is evidence that maxima may

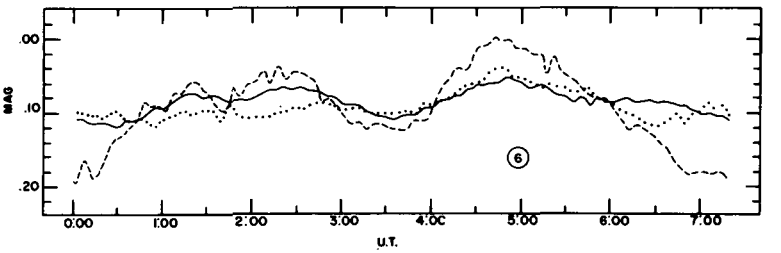

Figure 5.–Mean lightcurves of Hebe. Solid line, seven lightcurves of January and February 1959 at about 5° phase; dotted line, four lightcurves of November and December 1958 and May 1959 at about 22° phase; dashed line, three lightcurves of August 1968 at about 20° phase.

shift with reference to time; in fact, maxima or minima sometimes actually disappear (Taylor and Gehrels, 1972).

ABSOLUTE MAGNITUDE, PHASE COEFFICIENT, AND OPPOSITION EFFECT

Absolute magnitude $V(1, 0)$ is defined as the V magnitude at unit distance from the Sun and Earth at zero-degree phase angle. The phase coefficient refers to the magnitude change per degree of phase. The two values are directly related. Initially, phase coefficients can be determined from just two observations at different phase angles. For example, Groeneveld and Kuiper, with two observations of Eunomia, noted that after allowing for magnitude differences due to distance, there was still a discrepancy of 0.068 mag, which they deduced was due to a phase angle change of 1°.6. They therefore concluded that the phase coefficient was 0.042 mag/deg (Groeneveld and Kuiper, 1954*a*). The same technique has been used by others. Once phase coefficients have been adapted, a preliminary $V(1, 0)$ can be determined as was done using Müller's (1897) average phase coefficients, with known distances and phase for 2 Pallas and 14 Irene (Groeneveld and Kuiper, 1954*b*). There are limitations: With 511 Davida it was found that for two lightcurves the phase angle changed 3°, the aspect about 90°, but the $V(1, 0)$ values varied by 0.25 mag. Groeneveld and Kuiper (1954*a*) concluded that it was not entirely phase variation, and they warned that ". . . the determination of the phase coefficient may contain an effect of *area change,* resulting from a change in aspect."

Hektor had similar type lightcurves; i.e., not sinusoidal and with large amplitude variations; and more consistent values of $V(1, 0)$ were computed by using V_0 rather than mean V (Dunlap and Gehrels, 1969). V_0 is the magnitude of the primary maximum of the lightcurve, whereas mean V is the magnitude at a line on the lightcurve such that the areas enclosed above and below are equal. For Massalia, mean V was used with the additional technique of analyzing the comparison stars in relation to the mean lightcurve to determine the magnitude of the asteroid V_{ast} (Gehrels, 1956).

If several observations exist over a wide range of phase, V_{ast}, corrected for distance, can be plotted as a function of phase. Gehrels (1967*b*) made a plea to define $V(1, 0)$ as the extrapolated V value at zero-degree phase. If one assumes a linear plot, then the slope is the phase coefficient. Twenty-two asteroids were observed and the conclusion drawn that for phase angles between 10° and 20° the average phase coefficient of the asteroids is 0.023 mag/deg (Gehrels, 1957).

Average $B - V$ and $U - B$ values have been plotted versus phase. Giclas (1951) and Haupt (1958) discovered a reddening with phase for various asteroids. No evidence of this phenomenon was found with Icarus (Gehrels et al., 1970). A reddening with phase was found for 110 Lydia (Taylor, Gehrels, and Silvester, 1971) and for 4 Vesta (Gehrels, 1967*a*).

Table I is an updated version of table III of Gehrels (1970); the absolute magnitude $B(1, 0)$ and the mean opposition magnitude $B(a, 0)$ are taken from

TABLE I.–*Asteroid Characteristics*

Asteroid	$B(1, 0)$	$B(a, 0)$	$B - V$, mag	$U - B$, mag	Rotation period, hr	Amplitude range, mag	Number of oppositions	Lightcurve hours	References[a]
1[b]	4.11	7.56	0.71	0.42	9.078	0.04	2	29	[c]1,9,13
2	5.18	8.64	.65	.26	9-12?	0.12 to 0.15	4	39	4,13,16,17,29
3	6.43	9.67	.81	.39	7.213	0.15	3	41	3,9,13,17
4	4.31	6.85	.77	.46	5.342129	0.10 to 0.13	6	119	3,8,12,14,22
5	8.00	11.05	.82	.36	16.806	0.21 to 0.27	3	46	3,9,26
6	6.70	9.40	.82	.41	7.74	0.06 to 0.20	4	97	1,16,23
7	6.84	9.44	.83	.45	7.135	0.04 to 0.29	5	52	4,9,12,15
8	7.48	9.59	.86	.45	13.6	0.01 to 0.04	2	31	1,15,27
9	7.27	9.87	.85	.50	5.064	0.06 to 0.26	4	39	3,9,12,13
10	6.57	10.73	.70	.40	18?	0.20	2	29	13,17,26
11	7.78	10.54	.80	.38	10.67	0.07 to 0.12	3	22	15,16,29
12	8.81	11.27	.....	.....	.....	0.2	1	32	25,26
13	7.97	11.01	.....	.....	7.045	0.12	1	18	4
14	7.41	10.48	.81	.38	11?	0.04	2	10	13
15	6.29	9.48	.80	.42	6.083	0.42 to 0.53	5	38	12,15,26
16	6.89	10.64	.70	.24	4.303	0.11	1	11	15
17	8.69	11.49	.84	.42	12.275	0.12 to 0.36	2	32	12,15
18	7.79	10.16	.81	.35	14	0.35	1	8	9,17
19	8.35	11.08	.....	.....	7.46	0.25	1	15	16
20	7.48	10.13	.81	.43	8.0980	0.17 to 0.24	3	55	3,7,9
21	8.68	11.40	.....	.....	6.133	0.15	1	13	4
22	7.48	11.20	.71	.28	4.147	0.14 to 0.30	3	18	1,9,16
23	8.34	11.49	.89	.....	6.15	0.19	2	17	16,17
24	8.18	12.31	.....	.....	8.5	0.14	1	22	16
25	9.07	11.70	.92	.51	10?	0.18	2	18	12,15

Footnotes at end of table.

TABLE I.–*Asteroid Characteristics*–Concluded

Asteroid	$B(1, 0)$	$B(a, 0)$	$B - V$, mag	$U - B$, mag	Rotation period, hr	Amplitude range, mag	Number of oppositions	Lightcurve hours	References[a]
27	8.56	11.06	.....	.....	8.500	0.15	1	15	3
28	8.15	11.62	.....	.....	15.7	0.22	1	16	16
29	7.26	10.25	.87	.....	5.389	0.13	3	38	4,16,17,26
30	8.78	11.32	.88	.45	13.668	0.14	1	10	9,17
37	8.49	11.68	.89	.....	.....	.....	1	.....	17
39	7.41	10.86	.87	.49	5.138243	0.18 to 0.54	7	53	9,12,13,15,16,20
40	8.45	10.74	.83	.42	9.1358	0.22	1	12	9,13
42	8.84	11.57	.....	.....	.....	0.26	1	6	26
43	9.18	11.30	.....	.....	5.75	0.13	1	16	16
44	8.02	10.71	.67	.22	6.418	0.22 to 0.48	4	42	3,9,13,21
45	8.52	11.87	.....	.....	.....	0.5	1	7	26
51	8.66	11.21	.81	.....	7.785	0.14	2	38	4,16,17
52	7.63	11.69	.69	.....	.....	.....	.....	.....	17
54	8.82	12.15	.....	.....	7.05	0.12	1	13	16
60	10.05	12.67	.84	.44	Long	0.1	2	11	9,26
61	8.77	12.64	.85	.43	11.45	0.30	1	15	29
62	9.83	13.96	.76	.40	.....	.....	.....	.....	17
78	9.13	12.27	.....	.....	8?	0.15	1	6	26
89	8.19	11.18	.....	.....	8?	0.2	1	14	26
110	8.80	11.94	.71	.30	10.92673	0.11 to 0.20	2	52	24
122	9.08	13.34	.68	.41	.....	.....	1	.....	17
162	10.08	14.02	.....	.....	14?	0.3	1	15	26
268	9.55	13.61	.69	.29	.....	.....	.....	.....	17
321	11.38	15.06	.81	.44	2.870	0.38	1	8	15
324	8.14	11.41	.....	.....	8?	0.07	1	5	9
341	12.64	14.75	.92	.....	.....	.....	.....	.....	17

349	7.29	11.04	.96	.55	4.701	0.3 to 0.4	2	54	4,16,17
354	7.56	11.06	.93	.54	4.277	0.14 to 0.30	3	52	4,13,16
380	10.61	13.87	.72	.....	.....	.....	.....	.....	17
433	12.40	11.52	.86	.46	5.270254	0.0 to 1.5	.....	6	2,13,26
451	8.26	12.26	.....	.....	.....	0.10	1	13	26
498	9.99	13.20	.77	.36	.....	.....	.....	.....	17
510	11.04	14.15	.73	.25	.....	.....	.....	.....	17
511	7.13	11.35	.71	.36	5.17	0.06 to 0.25	4	26	4,9,12
532	7.98	11.44	.83	.44	18.813	0.08 to 0.18	2	30	4,13
540	12.22	14.38	.90	.48	.....	.....	.....	.....	29
624	8.67	15.29	.78	.24	6.922533	0.1 to 1.1	4	47	5
658	11.72	15.34	.87	.36	.....	.....	.....	.....	17
911	8.92	15.55	.80	.....	7?	0.3	2	13	5
976	10.55	14.76	.74	.25	.....	.....	.....	.....	17
1043	11.02	15.08	.90	.45	.....	.....	.....	.....	17
1287	12.13	16.04	.85	.36	.....	.....	.....	.....	17
1291	11.46	15.38	.83	.39	.....	.....	.....	.....	17
1437	9.23	15.87	.72	.20	16-20	0.35 to 0.42	3	19	26
1566	17.55	12.24	.80	.66	2.273	0.05 to 0.22	1	24	10,18,28
1620	15.97	13.38	.82	.....	5.2230	1.2 to 2.0	1	47	6,19

[a]The numbers are in brackets in the References.

[b]Fichera (1958) data are not included for reasons expressed by Gehrels and Owings (1962, p. 912).

[c]The timing given in this reference may not be reliable for photometric astrometry (Gehrels, personal communication).

his table II. The $B - V$ and $U - B$ columns are the colors at 5° phase; the period is synodic unless the sidereal period is known. Amplitude ranges and the number of oppositions observed are indicated. The hours column refers to the number of hours of good lightcurves obtained.

Massalia was observed for the expressed purpose of determining magnitude-phase relations at small phase angles, and the opposition effect was discovered: a sharp increase in brightness from 7° phase on toward 0° phase (Gehrels, 1956). Figure 6 illustrates the phase relations along with the opposition effect as they appeared with Lydia (Taylor, Gehrels, and Silvester, 1971). With Lydia, when B and U were plotted as a function of phase, it appeared that the opposition effect was independent of wavelength. Also, the opposition effect for Massalia, Vesta, and Lydia appeared the same, as is illustrated in figure 7 (Taylor, Gehrels, and Silvester, 1971).

Certain asteroids should perhaps be reevaluated in view of our present knowledge of the opposition effect. Three examples are as follows:

(1) The absolute magnitude and phase coefficient of 9 Metis was determined using five observations, four of which were under 6° phase (Groeneveld and Kuiper, 1954*b*).

(2) Observations of Iris near 23° phase yielded consistent $V(1, 0)$ values but a later run at 4° phase was 0.2 mag brighter than expected (van Houten-Groeneveld and van Houten, 1958).

(3) $V(1, 0)$ was found to be different by 0.01 mag for 12 Victoria before and after opposition. For Victoria it was assumed that the opposition effect started at phase angles less than 5°. In the linear plot after opposition, three of four data points lie in the region of 5°

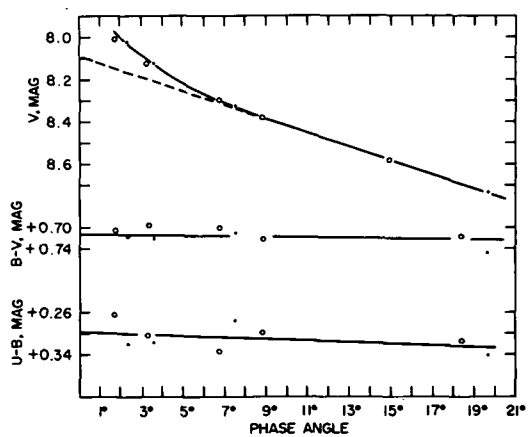

Figure 6.–Phase functions of Lydia. Ordinates: top curve, the observed magnitudes (V on the UBV system) reduced to unit distances from the Sun and Earth; middle curve, the $B - V$ colors; bottom curve, the $U - B$ colors. Open circles are before opposition and filled circles are after opposition.

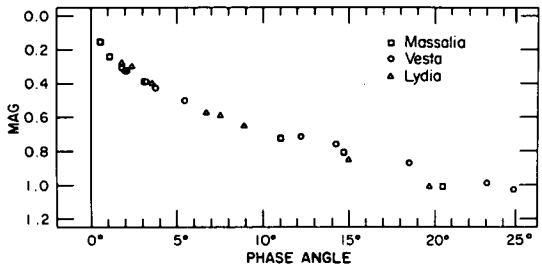

Figure 7.–Magnitude-phase relations of three asteroids.

to 6° phase (Tempesti and Burchi, 1969). If the assumption is made that the opposition effect starts at 7° to 8° phase, I feel there may be a unique $V(1, 0)$.

SENSE OF ROTATION AND POLE DETERMINATIONS

To determine the sense of rotation of Eunomia, Groeneveld and Kuiper (1954*a*) assumed the ecliptic latitude of the pole to be at 90° and used the relation

$$NP = \Delta t_c \pm \frac{\Delta L}{360} P$$

where N is the number of cycles, P is the period, Δt_c is time interval corrected for light time, ΔL is the difference in ecliptic longitudes, the plus sign is used for retrograde rotation, and the minus sign for direct rotation.

A retrograde solution gave smaller residuals in P for the two intervals attempted. "Clearly . . . some uncertainty may be introduced . . . by the assumptions made concerning the position of the rotational axis" (Groeneveld and Kuiper, 1954*a*). The van Houtens with additional data and using the same method confirmed retrograde rotation; they present a concise and informative discussion of limitations in their "Concluding Remarks" (van Houten-Groeneveld and van Houten, 1958).

The sense of rotation of Vesta was determined by using many intervals of both increasing and decreasing longitudes, and by assuming that the latitude of the pole was high (Gehrels, 1967*a*).

Groeneveld and Kuiper (1954*a*) presented a pole determination method and claim 10 percent precision if optimum conditions are met: axis fixed in space and an observation at each of the stationary points of two successive oppositions.

With 39 Laetitia, a formula was developed to adjust the period because of the relative motions of Earth and the asteroid. The formula depends on

knowing the pole orientation. An amplitude-aspect relation derived by Stobbe (1940) and Beyer (1953) for Eros, scaled down, was applied to determine an estimate of the pole. The investigators admittedly had limited precision (van Houten-Groeneveld and van Houten, 1958).

The poles of eight asteroids were calculated by combining two techniques: a sine relation between aspect and amplitudes, and a cosine relation between absolute magnitude changes with respect to aspect (Gehrels and Owings, 1962). It is not clearly established whether a sine relation is proper for those asteroids studied.

With his work on Vesta, Gehrels developed what is now known as "photometric astrometry." The method is basically the same as that used by Groeneveld and Kuiper for finding the sense of rotation of Eunomia. The main difference is that Gehrels did not restrict his analysis to a 90° orientation of the pole. He considered the asteroid-centric longitude changes between observations for various pole possibilities. Those differences were applied as corrections to the number of cycles for each interval. By attempting different orientations, he sought minimum residuals from the mean sidereal period of each trial. His method is " . . . independent of any assumptions regarding the shape of the asteroid and the relationship between amplitude and the aspect." He also introduced a phase shift to correct for the displacement of the center of light on the apparent disk due to the effects of phase. Gehrels compared his data with earlier observations, over 20 000 cycles, to improve the precision (Gehrels, 1967*a*); that part of the analysis will, however, have to be redone, as is planned for a future paper, because the additional cycle correction for each orbital revolution was omitted.

In the Hektor analysis (Dunlap and Gehrels, 1969), photometric astrometry was used, but it was difficult to determine the number of cycles. There were only a few observations over long intervals. As an aid, the relation $\Delta N = \pm N(P_{syn} - P_{sid})/P_{sid}$ was used, where P_{syn} is the synodic period and P_{sid} is the sidereal period. Figure 8 shows how the apparent number of cycles ΔN is changed as a function of longitude for four different pole orientations. That figure assumes the asteroid is on the ecliptic, as was the case with Hektor.

Figure 8 could not be used for Icarus because the asteroid was not on the ecliptic. Figure 9 shows how the apparent number of cycles are affected if the asteroid is 20° above the ecliptic. The entire photometric astrometry routine, including the problems of cycles, was computerized before the Icarus analysis. The concept of light centers was also introduced: the center of the projection of the illuminated part of the disk, as seen from Earth, assuming uniform reflectivity and a spherical shape. The light center is on the great circle through the subsolar and sub-Earth points. The purpose for light centers is basically the same as for Gehrels' phase shift (Gehrels et al., 1970).

In conclusion, it is clearly seen that additional work is needed to improve the quality and the extent of the sample in table I. I feel that high priority should be given to improving pole determinations. For this purpose, high

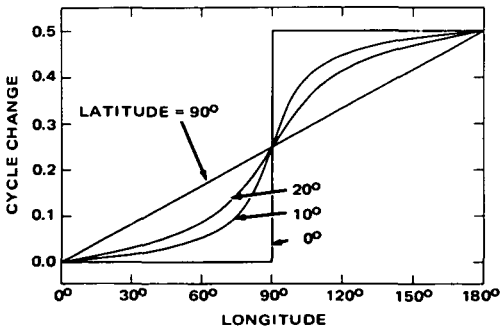

Figure 8.—The apparent change in cycle of asteroid rotation at various longitudes, plotted for four values of the latitude of the pole, 90° longitude of pole; asteroid is on the ecliptic.

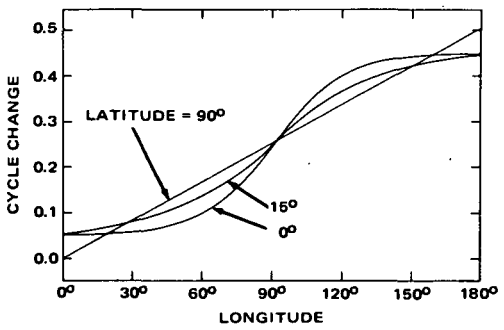

Figure 9.–Same as figure 8 except asteroid is 20° above the ecliptic.

precision is needed in the timing of lightcurves to establish precise epochs of maximum or minimum light. Without precise timing, it is impossible to have high precision when comparing epochs from different oppositions.

ACKNOWLEDGMENT

The asteroid program at the University of Arizona is supported by the National Aeronautics and Space Administration.

REFERENCES[2]

Ahmad, I. I. 1954, Photometric Studies of Asteroids. IV. The Light-Curves of Ceres, Hebe, Flora, and Kalliope. Astrophys. J. 120, 551-559. [1]

Beyer, M. 1953, Der Lichtwechsel und Die Lage der Rotationsachse der Planeten 433 Eros während der Opposition 1951-52. Astron. Nachr. 281, 121-130. [2]

[2]The numbers in brackets are as used in table I.

Calder, W. A. 1935, Photoelectric Photometry of Asteroids. Harvard Bull., no. 904, pp. 11-18.

Chang, Y. C., and Chang, C. S. 1962, Photometric Investigations of Seven Variable Asteroids. Acta Astron. Sinica **10**, 101-110. [3]

Chang, Y. C., and Chang, C. S. 1963, Photometric Investigations of Variable Asteroids. II. Acta Astron. Sinica **11**, 139-148. [4]

Dunlap, J. L., and Gehrels, T. 1969, Minor Planets. III. Lightcurves of a Trojan Asteroid. Astron. J. **74**, 796-803. [5]

Dunlap, J. L., and Gehrels, T. 1971, Minor Planets and Related Objects. VIII. Astron. J. **76**, in press. [6]

Fichera, E. 1958, Astron. Nachr. **284**, 65-70.

Gehrels, T. 1956, Photometric Studies of Asteroids. V. The Light-Curve and Phase Function of 20 Massalia. Astrophys. J. **123**, 331-338. [7]

Gehrels, T. 1957, Photometric Studies of Asteroids. VI. Astrophys. J. **125**, 550-570.

Gehrels, T. 1967*a*, Minor Planets. I. The Rotation of Vesta. Astron. J. **72**, 929-938. [8]

Gehrels, T. 1967*b*, Minor Planets. II. Photographic Magnitudes. Astron. J. **72**, 1288-1291.

Gehrels, T. 1970, Photometry of Asteroids. Surfaces and Interiors of Planets and Satellites (ed., Dollfus), pp. 317-375. Academic Press, Inc. London.

Gehrels, T., and Owings, D. 1962, Photometric Studies of Asteroids. IX. Additional Light-Curves. Astrophys. J. **135**, 906-924. [9]

Gehrels, T., Roemer, E., Taylor, R. C., and Zellner, B. H. 1970, Minor Planets and Related Objects. IV. Asteroid (1566) Icarus. Astron. J. **75**, 186-195. [10]

Giclas, H. L. 1951, Direct Photoelectric Photometry. The Project for the Study of Planetary Atmospheres. Lowell Observ. Rept. 9, pp. 33-72. [11]

Groeneveld, I., and Kuiper, G. P. 1954*a*, Photometric Studies of Asteroids. I. Astrophys. J. **120**, 200-220. [12]

Groeneveld, I., and Kuiper, G. P. 1954*b*, Photometric Studies of Asteroids. II. Astrophys. J. **120**, 529-546. [13]

Haupt, H. 1958, Photoelektrisch-photometrische Studie an Vesta. Mitt. Sonnobs. Kanzelhöhe **14**, 172-173. [14]

Hertzsprung, E. 1928, On the Character of the Variation of SX Aurigae. Bull. Astron. Inst. Neth. **4**, 178-180.

Hertzsprung, E. 1941, Photographic Estimates of 25 Southern Variable Stars. Bull. Astron. Inst. Neth. **9**, 203-215.

Houten-Groeneveld, I. van, and Houten, C. J. van. 1958, Photometric Studies of Asteroids. VII. Astrophys. J. **127**, 253-273. [15]

Houten-Groeneveld, I. van, and Houten, C. J. van. 1972, in preparation. [16]

Johnson, H. L. 1963, Photometric Systems. Basic Astronomical Data (ed., A. K. Strand), vol. 3, pp. 204-224. Univ. of Chicago Press. Chicago.

Kuiper, G. P., Fujita, Y., Gehrels, T., Groeneveld, I., Kent, J., Van Biesbroeck, G., and Houten, C. J. van. 1958, Survey of Asteroids. Astrophys. J. Suppl. Ser. **3**, 289-427. [17]

Miner, E., and Young, J. 1969, Photometric Determination of the Rotation Period of 1566 Icarus. Icarus **10**, 436-440. [18]

Miner, E., and Young, J. 1971, Photometric Observations of 1620 Geographos. Icarus, in press. [19]

Müller, G. 1897, Die Photometrie der Gestirne. Engelman. Leipzig.

Sather, R. E., and Taylor, R. C. 1972, Minor Planets and Related Objects. IX. Astron J. **77**, in preparation. [20]

Shatzel, A. V. 1954, Photometric Studies of Asteroids. III. The Light-Curve of 44 Nysa. Astrophys. J. **120**, 547-550. [21]

Stephenson, C. B. 1951, The Light-Curve and the Color of Vesta. Astrophys. J. **114**, 500-504. [22]

Stobbe, J. 1940, Der Lichtwechsel des Eros. Astron. Nachr. **270**, 1-24.
Taylor, R. C., and Gehrels, T. 1972, Minor Planets and Related Objects. IX. Astron. J. **77**, in preparation. [23]
Taylor, R. C., Gehrels, T., and Silvester, A. B. 1971, Minor Planets and Related Objects. VI. Asteroid (110) Lydia. Astron. J. **76**, 141-146. [24]
Tempesti, P., and Burchi, R. 1969, A Photometric Research on the Minor Planet 12 Victoria. Mem. Soc. Astron. Ital. Nuova Ser. **40**, 415-432. [25]
Univ. of Arizona. 1972, Data to be published by group working with T. Gehrels. [26]
Veverka, J. 1971, Photopolarimetric Observations of the Minor Planet Flora. Icarus, in press. [27]
Veverka, J., and Liller, W. 1969, Observations of Icarus: 1968. Icarus **10**, 441-444. [28]
Wood, H. J., and Kuiper, G. P. 1963, Photometric Studies of Asteroids. X. Astrophys. J. **137**, 1279-1285. [29]

Page intentionally left blank

SUMMARY ON ORIENTATIONS OF ROTATION AXES

CARL D. VESELY
University of Arizona

To evaluate the precision of the previously determined coordinates of the rotation axes (table I) we should review the methods (originally developed for 433 Eros) and logic of the various authors. Table II contains pole coordinates of Eros and the sources of these data. A critical summary of the work will enable us to make some conclusions concerning the poles presented.

EARLY RESEARCH ON THE POLE OF EROS

There is general agreement that greatest rotational amplitude is observed when an asteroid is viewed equatorially, and we can detect three approaches to the determination of the Eros pole: the micrometer position angles observed by van den Bos and Finsen (1931); the graphic presentations used by Watson (1937), Stobbe (1940), and Rosenhagen (1932); and the mathematical model developed by Krug and Schrutka-Rechtenstamm (1936). These initial attempts yielded only approximate values, but the approximations were sometimes refined by analytical methods.

Micrometer Measurements of Position Angles

Eros is the only asteroid to have directly observed micrometer measurements of the position angles of the projection of its long axis. Van den Bos and Finsen (1931) found the position angle rotating over 360° in 5^h17^m and a separation of "about 0".18." The precision of the measurements of the position angle may be ±5° (Van Biesbroeck, personal communication).

In 1931, W. Zessewitsche (1932, 1937) graphically determined the equator of Eros from the observations of van den Bos and Finsen (1931). He determined an average position angle of the line of intersection of the projection of the long axis of Eros with the projection plane perpendicular to the line of sight at a given time and assumed the pole to be this position angle plus 90°. Zessewitsche calculated a value for the inclination of the equator of Eros to the projection plane at that time and determined the pole coordinates. The pole determination enabled him to calculate the Erocentric right ascension

TABLE I.–*Coordinates of the Rotation Axes for Selected Asteroids*

Asteroid no.	Ecliptic longitude, λ_0	Ecliptic latitude, β_0	Right ascension, α_0	Declination, δ_0	Obliquity	Reference
3	71°	49°	52°	70°	28°	Chang and Chang (1962)
4	57	74	310	77	12	Chang and Chang (1962)
	14	80	296	67	3	Cailliatte (1956)
6	145	15	153	27	77	Gehrels and Owings (1962)
7	193±3	15	198	9	70	Gehrels and Owings (1962)
	184	55	212	47	30	Cailliatte (1956)
8	157	10	163	18	84	Gehrels and Owings (1962)
9	186	15±15	192	11	80	Gehrels and Owings (1962)
	348	76	299	60	9	Chang and Chang (1962)
12	242	17	63	3	74	Tempesti and Burchi (1969)
15	250	74	261	51	12	Cailliatte (1960)
20	10	78	299	66	12	Chang and Chang (1962)
39	130	10	135	27	75	Gehrels and Owings (1962)
	115±10	19±5	121	40	64	Sather and Taylor (1972)[a]
	103	61	141	82	21	Cailliatte (1960)
44	358	84	286	66	4	Cailliatte (1956)
	105	30	112	52	58	Gehrels and Owings (1962)
433	13±3	28±1	0	31	72	Vesely (this paper)[a]
511	306	34	300	14	53	Chang and Chang (1963)
	122	10	127	29	84	Gehrels and Owings (1967)
624	324±3	10±2	323	−4	75	Dunlap and Gehrels (1969)[a]
1566	235±30	28±10	239	8	76	Gehrels et al. (1970)[a]
1620	113±8	85±2	262	72	18	Dunlap and Gehrels (1971)[a]

[a]Denotes poles determined by photometric astrometry.

TABLE II.–*Pole Coordinates of Asteroid 433 Eros*

Reference	λ_0	β_0	α_0	δ_0
Zessewitsche (1937)	29°	22°	18°	31°
Rosenhagen (1932)	4	45	342	42
Watson (1937)	349	62	316	51
Krug and Schrutka-Rechtenstamm (1936)	2	53	333	48
Stobbe (1940)	9	38	350	38
Beyer (1953)	353	13	349	9
Cailliatte (1956)	10	46	345	45
Vesely (this paper)	13	28	0	31

and declination d of the Earth. Plotting the observed amplitude A against d, Zessewitsche derived the following empirical relationship:

$$A = 1^{m}.50 - 0^{m}.0275\ |d|$$

where 1.50 mag is the maximum observed amplitude. We refer to this as an amplitude-aspect relationship.

Zessewitsche's method relies on a large number of transformation equations. The value for the inclination of the equator is an important parameter in several of them. Zessewitsche admitted a lack of precision in its calculation.

M. Huruhata (1940) misinterpreted Zessewitsche's pole value and his work must be viewed with suspicion.

Graphic Pole Determinations

F. Watson (1937) plotted the observed amplitude as a function of the ecliptic coordinates of Eros during an opposition. Assuming that the greatest amplitude was observed when Earth was in the equatorial plane of Eros, Watson used a composite of the curves of oppositions from 1893 to 1935 to secure the coordinates of the nodes of the equatorial plane of Eros and its inclination, from which he determined the pole.

Watson used published amplitudes from various oppositions, combining photometric and photographic data without indicating the probable error of the observed magnitudes and included data regarded as imprecise by Stobbe (1940). Checking the original published lightcurves, I found variations between different observers on the same night to be as high as ±0.3 mag, and I completely reject his pole.

J. Rosenhagen obtained an approximate pole from a plot of the amplitude against the Earth's ecliptic coordinates. The refinement will be discussed under "Mathematical Models for Pole Determinations."

J. Stobbe (1940) used Zessewitsche's amplitude-aspect relationship to determine d_B, the Erocentric latitude of Earth from the observed amplitude.

With various assumed pole positions, he calculated a series of d_R values (B = beobachtet; R = rechnet). Using the d_B values as normal points, curves of the d_R values for the various assumed pole values were plotted for the dates of observation. The results were indeterminate, so he used another relationship as follows.

By using a period calculated from the previously approximated pole, Stobbe found $(a_{min} \cdot f)_B$, the observed variation in the time of arrival of the minimum due to change in phase. Using the assumed pole positions, he determined $(a_{min} \cdot f)_R$, the calculated variation. The resulting $B - R$ plot, along with the d_R plot, enabled Stobbe to elect the best assumed pole from pole curves. To determine possible agreement between his possible poles for the 1930-31 opposition and van den Bos and Finsen's (1931) position angles, Stobbe plotted his pole coordinates as points and drew the great circle corresponding to the position angle of the pole. He presumed the intersection of the points and the great circle to be the pole of Eros. The result agreed with one of his values, but not the one he felt best represented the pole of Eros for the opposition 1930-31. Stobbe indicated the disagreement was possibly due to irregularity of the figure or flexure along the long axis and claimed his findings vindicated the often skeptically received (Stobbe, 1940) observations of van den Bos and Finsen (1931).

Although Stobbe selected one pole as most satisfying, we see he has as many poles as he has oppositions. He claimed the pole is not fixed. On the contrary, I believe the slope of an amplitude-aspect plot determined for observations at a certain phase angle and obliquity will be valid for that opposition only and will yield a different pole for another opposition unless the conditions are the same. Stobbe rejected obviously unsure observational data, but the ones he accepted may not be accurate. The inability to secure a single pole may indicate systematic error of the method.

Mathematical Models for Pole Determinations

J. Rosenhagen (1932) showed that his graphically approximated pole (see above) must be refined in terms of Eros' shape. He assumed an elongated body rotating about the short axis, similar to a Poincaré body or symmetrical egg figure, with a brightness proportional to the projected area when viewed equatorially. To yield an Eros maximum amplitude of 1.50 mag required an axial ratio of $a:b = 4.00$ and an eccentricity of $e = 0.97$. Rosenhagen devised an amplitude-aspect relationship based on this model. Starting with the approximate pole, he made differential corrections until he determined the pole yielding the aspect that best conformed to the requirements of the model.

Rosenhagen found that his pole gave the right amplitude for the observations of 1930-31, but would give a maximum amplitude of only 1.14 mag for the earlier oppositions (1901-1903). He blamed systematic deviations of the data due to precession, deformation, and spotting of the asteroid.

Rosenhagen's pole may be challenged for more obvious reasons. He tried to intercompare amplitudes among oppositions whose observational data produced a range of phase coefficients from 0.011 to 0.039 mag/deg and included data that Watson (1937) said was not comparable because of uncertainties in the magnitudes of the comparison stars. Rosenhagen's pole generates little confidence.

W. Krug and G. Schrutka-Rechtenstamm (1936) proposed to determine the brightness of a three-axis ellipsoid model of Eros at full phase while obeying Lambert's law, using only photometric observational data having both amplitude and absolute magnitude reduced to an average opposition. They related absolute brightness to the aspect angle, which was determined from Rosenhagen's pole. A least-squares solution gave a corrected pole. Krug's new pole met the brightness conditions required by the model, but did not permit sufficient maximum amplitude.

Because Krug and Schrutka-Rechtenstamm's pole would not permit maximum amplitude, and they used data from observers common to Rosenhagen, criticized previously, this pole, too, must be considered very doubtful.

F. E. Roach and L. G. Stoddard (1938) revised the work of Krug and Schrutka-Rechtenstamm. They assumed Krug's pole, but related the brightness ratio to the maximum amplitude, omitted observations with no variation, and gave no weight to absolute magnitude. Their least-squares solution allowed for a maximum amplitude of 1.50 mag for Eros. Thus, using old, imprecise photometric data and their own, single photoelectric lightcurve, Stoddard and Roach perhaps improved a model, but shed no further light on Eros' pole.

MORE RECENT POLE DETERMINATIONS

M. Beyer (1953) used Stobbe's (1940) method for his determination of the pole of Eros. Although his observational data are more precise, the pole seems to be unreasonably low.

Cailliatte (1956) used the geocentric coordinates of an asteroid for two observations of the maximum amplitude to determine the longitude of the node and the inclination of the equator of the asteroid. The pole thus determined was used to calculate D, the asterocentric declination of Earth. Cailliatte then plotted an amplitude-aspect relation that he refined using various models. He used the refined amplitude-aspect relationship to correct the original pole. In a later publication (1960) he corrected two earlier poles. Cailliatte's amplitude-dependent method required larger than observed maximum amplitudes for some asteroids (e.g., for 39 Laetitia: 0.68 mag calculated, 0.54 mag observed) and yields generally small obliquities.

Y. C. Chang and C. S. Chang (1962, 1963) determined a number of poles using an amplitude-aspect relationship. They used a single reduced observation and the asteroid's phase coefficient as the factor by which the amplitude varies

with D, citing Cailliatte (1956) as the source. Actually, Cailliatte indicated this was a "restrictive hypothesis," somewhat better than no method at all. The Chang poles have no value.

P. Tempesti and R. Burchi (1969) also made use of an amplitude-aspect relationship:

$$A_i = A_0 - C|d|$$

where A_i is one of 12 observed amplitudes, A_0 is an assumed maximum (unknown), C is a constant (unknown), and d is the asterocentric declination of Earth. They used each A_i and increasing values of C with each assumed A_0. A least-squares solution analyzing the relative minima of residuals indicated $A_0 = 1.50$ mag and $C = 0.0146$ mag-deg^{-1} yielded minimal standard error. They transformed the value received for d into pole coordinates. Tempesti and Burchi stated the error may be large because of the small range of amplitudes. Greater faults appear evident. There is no observational justification of a maximum amplitude of 1.50 mag. Also, a partial lightcurve (4½ hr) of April 6, 1970, gives an amplitude of 0.07 mag at a time when, according to Tempesti, a nearly equatorial view was anticipated.

The early poles of T. Gehrels and D. Owings (1962) were determined using an amplitude-aspect relationship:

$$a = A\ |\sin\gamma|$$

where a is the observed amplitude, A the greatest possible amplitude, and γ the angle between the direction of observation and the axis of rotation. $A \sin\gamma$ master curves were made for different values of A and β_0 plotted as a function of $(\lambda - \lambda_0)$. $\beta = 0$ was assumed; and when only two observations were available, it was assumed $\beta_0 = 8°$. The master curves were superposed on longitude plots of a_1, a_2, and the visual absolute magnitude. A weighted average was given for the determined longitude λ_0, giving half-weight to the absolute magnitude and to poor determinations. The latitude of the pole was determined from the quality of fit to the observations by the different sets of master curves. Gehrels claims little precision for the latitudes and no determination of a sign. The observational data are good and the phase angles were usually small. The pole longitudes are more precise, as they do not depend strongly on the assumed amplitude-aspect function.

Recognizing the unreliability of the amplitude-aspect relationship, Gehrels (1967) developed the photometric astrometry method described by R. Taylor[1] and determined the pole of 4 Vesta in 1967. An error in cycle correction discovered later causes us to lack confidence in this determination. We believe the pole is within ±10° of the published coordinates.

---

[1]See p. 128.

The poles of asteroids 39 (Sather and Taylor, 1972), 624 (Dunlap and Gehrels, 1969), 1566 (Gehrels et al., 1970), and 1620 (Dunlap and Gehrels, 1971) are determined from photometric astrometry. My present photometric astrometry determination of the pole of Eros was done utilizing the observational data of Beyer (1953) for the opposition of 1951-52. This is a preliminary value from the one opposition only.

CRITICAL SUMMARY AND CONCLUSIONS

The precision of Zessewitsche's pole is dependent on the accuracy of the micrometer measurements of the position angle and the value for the inclination of the equator. Zessewitsche recognized the lack of precision in the latter. The poles of Watson, Rosenhagen, and Krug depend on the precision of values determined for the absolute brightness and amplitude obtained in many oppositions. This precision is poor. Stobbe and Beyer used more precise data within oppositions, but had to choose a "best" pole from among several possible poles.

With increased observational precision in recent years, we might expect more reliable pole determinations. We see from table I, however, that little agreement exists. Discounting the apparently incorrect poles of Chang and Tempesti, we still see great disagreement between the poles of Cailliatte and Gehrels.

It may be concluded, then, that we must challenge the fundamental validity of the amplitude-aspect relationship upon which great doubt has already been cast by J. L. Dunlap[2] and seek a more reliable way to determine a precise pole position. Photometric astrometry shows great promise, and we are currently engaged in a program using and further improving that method.

ACKNOWLEDGMENTS

This program is supported by the National Aeronautics and Space Administration.

REFERENCES

Beyer, M. 1953, Der Lichtwechsel und die Lage der Rotationsachse des Planeten 433 Eros während der Opposition 1951-52. Astron. Nachr. **281**, 121-130.

Bos, W. H. van den, and Finsen, W. S. 1931, Physical Observations of Eros. Astron. Nachr. **241**, 329-334.

Cailliatte, C. 1956, Contribution à l'Étude des Astéroïdes Variables. Bull. Astron. Paris **20**, 283-341.

Cailliatte, C. 1960, Contribution à l'Étude des Astéroïdes Variables (Suite). Publ. Observ. Lyon **6**(1), pp. 259-272.

Chang, Y. C., and Chang, C. S. 1962, Photometric Investigations of Seven Variable Asteroids. Acta Astron. Sinica **10**, 101-111.

---

[2]See p. 151.

Chang, Y. C., and Chang, C. S. 1963, Photometric Observations of Variable Asteroids, II. Acta Astron. Sinica **11**, 139-149.

Dunlap, J. L., and Gehrels, T. 1969, *Lightcurves of a Trojan Asteroid*. Astron. J. **74**, 796-803.

Dunlap, J. L., and Gehrels, T. 1971, Minor Planets and Related Objects. VIII. Astron. J. **76**, in press.

Gehrels, T. 1967, The Rotation of Vesta. Astron. J. **72**, 929-938.

Gehrels, T., and Owings, D. 1962, Photometric Studies of Asteroids. IX. Additional Light-Curves. Astrophys. J. **135**, 906-924.

Gehrels, T., Roemer, E., Taylor, R. C., and Zellner, B. H. 1970, Asteroid (1566) Icarus. Astron. J. **75**, 186-195.

Huruhata, M. 1940, The Rotation Period of Eros. Harvard Col. Observ. Circ. 442, pp. 1-6.

Krug, W., and Schrutka-Rechtenstamm, G. 1936, Untersuchungen über Gestalt und Grösse des Planetoiden Eros. Z. Astrophys. **13**, 1-12.

Roach, F. E., and Stoddard, L. G. 1938, A Photoelectric Light-Curve of Eros. Astrophys. J. **88**, 305-312.

Rosenhagen, J. 1932, Einige Bemerkungen zur Helligkeit und zum Lichtwechsel des Planeten Eros. Mitt. Wien. Sternw. **1**(2), 45-52.

Sather, R. E., and Taylor, R. C. 1972, Minor Planets and Related Objects. IX. Astron. J., in preparation.

Stobbe, J. 1940, Der Lichtwechsel des Eros. Astron. Nachr. **270**, 1-24.

Tempesti, P., and Burchi, R. 1969, A Photometric Research on the Minor Planet 12 Victoria. Mem. Soc. Astron. Ital. **40**, 415-432.

Watson, F. 1937, The Physical Nature of Eros. Harvard Col. Observ. Circ. 419, pp. 1-14.

Zessewitsche, W. 1932, Die Bestimmung der Winkelelemente der inneren Bewegung von Eros. Astron. Nachr. **246**, 441-450.

Zessewitsche, W. 1937, On the Rotation of Eros. Observatory **60**, 289-292.

LIGHTCURVE INVERSION AND SURFACE REFLECTIVITY

A. A. LACIS AND J. D. FIX
The University of Iowa

A simplified lightcurve inversion method is applied for the special case where observations are taken in the equatorial plane of the asteroid. The solution is obtained in terms of a spotted two-surface model using Lambert's law and geometrical reflectivities.

The general problem of interpreting the lightcurve of a rotating body in terms of its shape and surface spottiness has been discussed in detail by Russell (1906). However, in the special case where the rotational axis is perpendicular to the line of sight, the analysis may be greatly simplified. Although the ambiguity between the shape and spot contributions to the light variation remains unresolved, it is possible to examine the type of surface reflectivity law and to set some limits on the range of albedo variation that will be consistent with the observed lightcurve.

Without loss of generality (insofar as being able to reproduce the observed lightcurve is concerned) we can assume the asteroid to be spherical in shape. The surface is taken to consist of bright and dark areas that reflect either geometrically ($\propto \cos\gamma$) or diffusely according to Lambert's law ($\propto \cos^2\gamma$) where γ, defined by

$$\cos\gamma = \cos\theta\cos\theta_0 + \sin\theta\sin\theta_0\cos(\phi - \phi_0)$$

is the angle between the outward normal of a surface element and the line of sight in the polar coordinates centered on the asteroid. The polar angle and longitude of the sub-Earth point are designated by θ_0 and ϕ_0, respectively.

In the special case when the observer is in the equatorial plane of the asteroid, the integration over the visible hemisphere is greatly simplified, and we can write the brightness variation of the asteroid as

$$g(\phi_0) = B + \frac{1}{\pi}\int_0^{\pi}\int_{\phi_0-\pi/2}^{\phi_0+\pi/2}[A\sin^2\theta\cos^2(\phi-\phi_0) - B\sin\theta\cos(\phi-\phi_0)]\,h(\phi)\sin\theta\,d\theta d\phi \quad (1)$$

where $g(\phi_0)$ is the ratio of reflected to incident light; B is the normal albedo of the geometrically reflecting surface area; A is the normal albedo of the diffusely reflecting area; and $h(\phi)$ is the spot distribution function that gives, as a function of longitude, the fractional area that reflects diffusely according to the Lambert law. Because no information regarding the latitude distribution of bright and dark areas appears in the lightcurve when the asteroid is viewed from within its equatorial plane, $h(\phi)$ is taken to be constant with latitude. Assuming that $h(\phi)$ can be expressed in the form

$$h(\phi) = \sum_{n=0}^{\infty} (a_n \cos n\phi + b_n \sin n\phi) \tag{2}$$

equation (1) can be integrated to obtain a Fourier series in ϕ_0. By comparing the resulting Fourier coefficients with the corresponding terms obtained from a Fourier analysis of the observed lightcurve, we find that the coefficients for the $\cos n\phi_0$ terms are related by

$$C_0 = B + \left(\frac{2}{3}A - B\right) a_0 \tag{3}$$

$$C_1 = \left(\frac{16}{9\pi}A - \frac{\pi}{4}B\right) a_1 \tag{4}$$

$$C_2 = \frac{1}{3}(A - B)\, a_2 \tag{5}$$

$$C_n = (-1)^{(n+1)/2} \frac{16A}{3\pi n(n^2 - 4)} a_n \qquad (n = 3, 5, \ldots) \tag{6}$$

$$C_n = (-1)^{n/2} \frac{B}{n^2 - 1} a_n \qquad (n = 4, 6, \ldots) \tag{7}$$

where the C_n are the Fourier coefficients obtained from the observed lightcurve and the a_n are the coefficients defined in equation (2). The same relationships apply for the $\sin n\phi_0$ terms.

The above set of relations contains the available information regarding the relative proportion and longitude distribution of geometrically and diffusely reflecting surface areas and the range of albedo combinations that are compatible with the observed lightcurve. The limits for the allowed albedo range are imposed by the physical requirement that the spot distribution function $h(\phi)$ must not become negative or exceed unity.

Because of the infinity of possible solutions, it appears best to consider families of solutions for constant A/B ratios. By specifying a ratio for A/B and by setting $a_0 = 0.5$, we define a model for which the surface is evenly divided between geometrically and diffusely reflecting areas. (See fig. 1.) This allows for the greatest amplitude fluctuation for $h(\phi)$ and marks the approximate center of the allowed albedo range for the specified A/B ratio. The locus of these points falls along the broken line shown in figure 2. Then, keeping the A/B ratio fixed, increasing (or decreasing) A and B simultaneously until $h(\phi)$ becomes negative (or greater than unity), establishes the range of albedo combinations that are compatible with the physical restriction imposed on $h(\phi)$.

This procedure defines two separate albedo regions—one corresponding to bright spots, the other to dark spots. Because all albedo combinations in a given enclosure are equally capable of reproducing the observed lightcurve to the same degree of accuracy, it is clearly impossible to differentiate between bright spot and dark spot models on the basis of the observed lightcurve alone.

The size and location of the limiting enclosures depends both on the size of the lightcurve coefficients and on the proportionality factors appearing in relations (3) through (7). Generally speaking, each additional Fourier term that is included to approximate the observed lightcurve tends to diminish the size of the allowed albedo region. However, because of observational scatter, the higher order Fourier terms become increasingly unreliable. This is an important factor because the $n = 1$ and $n = 2$ terms contain contributions from both geometrically and diffusely reflecting areas. It is only on the basis of terms

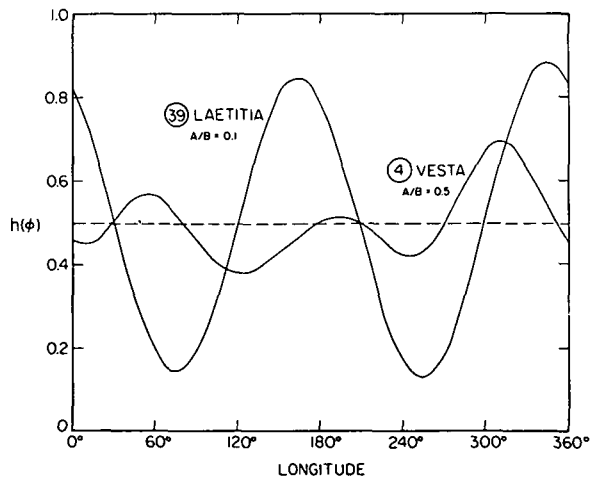

Figure 1.—The fractional area that reflects diffusely according to Lambert's law. For 4 Vesta, $h(\phi)$ includes Fourier terms up to $n = 4$. For 39 Laetitia, terms up to $n = 2$ are included. In both cases $a_0 = 0.5$.

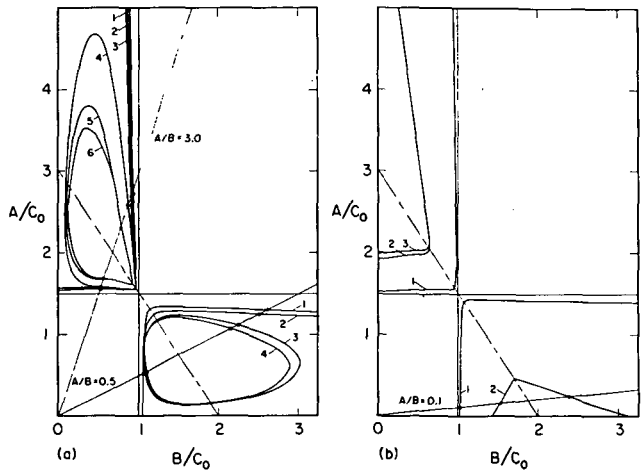

Figure 2.–The most probable albedo combinations for diffuse A and geometrical B reflectivities. Both scales have been normalized in terms of the average normal albedo of the asteroid. The broken line is the locus of points for $a_0 = 0.5$. The numbered curves enclose the allowed albedo combinations as defined by the number of Fourier terms used to approximate the observed lightcurve. (*a*) 4 Vesta, April 10, 1967. (*b*) 39 Laetitia, December 1955.

$n = 3$ and greater that we can verify the presence of diffusely or geometrically reflecting areas.

The lightcurves used in the present analysis are those taken by Gehrels (1967) for 4 Vesta and by van Houten-Groeneveld and van Houten (1958) for 39 Laetitia. These are typical examples of single maximum and double maximum lightcurves that also satisfy the requirement of being observed within the equatorial plane of the asteroid. This is indeed true for 4 Vesta, which is observed in the equatorial plane, although for 39 Laetitia the inclination may be as large as 20°. Also, it should be noted that the phase angle for 4 Vesta was -18° and that of 39 Laetitia was about the same. Although the present calculations are specifically applicable for a zero phase angle, the derived albedo limits should not be significantly affected unless the form of the assumed reflectivity laws changes significantly with phase.

The results of Fourier analyzing the 4 Vesta and 39 Laetitia lightcurves are summarized in table I. For convenience of comparison, the Fourier coefficients of the $\sin n\phi_0$ and $\cos n\phi_0$ terms have been combined and are normalized with respect to C_0, the mean normal albedo of the asteroid. Also included is the root-mean-square difference between the observed points of the lightcurve and the nth Fourier representation.

The difference between the single maximum and double maximum lightcurves is illustrated by the prominence of the even-order terms in the 39 Laetitia lightcurve and the odd-order terms in the 4 Vesta lightcurve.

TABLE I.–*Fourier Analysis of Lightcurves*

n	4 Vesta		39 Laetitia	
	$(C_n^2 + D_n^2)^{1/2}/C_0$	rms/C_0	$(C_n^2 + D_n^2)^{1/2}/C_0$	rms/C_0
0	1.000	0.042	1.000	0.139
1	.056	.011	.025	.137
2	.005	.011	.203	.022
3	.007	.009	.009	.020
4	.002	.009	.022	.016
5	.005	.008	.012	.015
6	.000	.008	.018	.010

Clearly, the even-order terms for 39 Laetitia may be interpreted as being due to the projected area of an irregular object. This leaves a 5 to 10 percent light variation due to the odd-order terms, which may be associated with either a spotted surface or Lambert law reflectivity. However, it appears likely that if 39 Laetitia is observed closer to its equatorial plane, the size of these terms will be somewhat reduced.

For 4 Vesta, interpreting the 1.4 and 1.0 percent light variation contributed by the $n = 3$ and $n = 5$ terms as significant would indicate the definite presence of a Lambert law contribution to the surface reflectivity. The $n = 5$ term seems to suggest bright diffusely reflecting spots on a darker geometrically reflecting surface. However, the limited accuracy of such high-order terms does not necessarily preclude a model with dark spots on a bright geometrically reflecting surface.

REFERENCES

Gehrels, T. 1967, Minor Planets. I. The Rotation of Vesta. Astron. J. 72, 929-938.

Houten-Groeneveld, I. van, and Houten, C. J. van. 1958, Photometric Studies of Asteroids. VII. Astrophys. J. 127, 253-273.

Russell, H. N. 1906, On the Light Variations of Asteroids and Satellites. Astrophys. J. 24, 1-18.

DISCUSSION

VEVERKA: In your analysis you assume a surface composed of areas which scatter either "geometrically" ($\propto \cos\gamma$) or "diffusely" ($\propto \cos^2\gamma$) according to Lambert's law. For asteroids, this is an invalid assumption. For intricate surfaces, in which multiple scattering is not dominant, the first part of the assumption is not too bad at small phase angles, but still, strictly speaking, you can only have "geometric" scattering at opposition and nowhere else. (See, for example, Irvine, 1966.)

However, you can never have Lambert scattering on such a surface at visible wavelengths. At visible wavelengths, even quasi-Lambert scatterers are rare and usually consist of extremely bright patches in which multiple scattering is dominant (for example, snow or MgO). There is no evidence that such areas occur in asteroids, and much evidence that they do not occur (for example, deep negative branches in the polarization curves).

You are therefore trying to force a fit using two generally inappropriate scattering laws, and a probably incorrect shape (a spherical asteroid). Thus the calculation, although interesting, cannot have much application to asteroids.

JOHNSON: The lack of color variation seems to indicate that in many cases the asteroid variation is due to shape rather than spots. Is it possible to make the model yield shape information as well as spot distribution?

LACIS: The even terms of the spot distribution function $h(\phi)$ can be directly associated with the shape of the object. By assuming a constant albedo over the surface, a rough estimate for the shape is given by $R(\phi) = 1 - h(\phi)$. For 39 Laetitia, this relation indicates an oblong object with a length-to-width ratio of approximately 3:2.

KUIPER: When we started our precision photometry of asteroids at McDonald about 1949, we found that the rule was to have two maxima and two minima in the lightcurve. It was concluded that the light variation was primarily due to shape. Variation in surface reflectivity could contribute something, but when the variation is 0.3 mag or more, the main effect must be due to shape.

LACIS: Inverting the lightcurve in terms of a spotted sphere gives us little more than a geometrical model that is capable of reproducing the observed light variation. However, in the case where the observations are made in the equatorial plane of the asteroid, we can infer the type of reflectivity law from the strength of the different Fourier terms present in the observed lightcurve. At opposition, the geometrical reflectivity is a special case of the Lommel-Seeliger law. The assumed Lambert law reflectivity could conceivably refer to a more specular type of reflection law. It is just that the presence of odd Fourier terms ($n = 3, 5, \ldots$) cannot be accounted for in terms of geometrical reflectivity alone.

Also, it may be of interest to note that there is a systematic increase in the odd Fourier terms and a decrease in the even-order terms as the observing point moves away from the equatorial plane of the asteroid. This may be helpful in locating the orientation of the rotational axis.

DISCUSSION REFERENCE

Irvine, W. M. 1966, The Shadow Effect in Diffuse Radiation. J. Geophys. Res. 71, 2931.

LABORATORY WORK ON THE SHAPES OF ASTEROIDS

J. L. DUNLAP
University of Arizona

Photometric lightcurves of about 50 asteroids have been obtained over the past 20 yr, yet very little is known about the shape of these objects. Perhaps 100 lightcurves (including photographic ones) of 433 Eros have been obtained with amplitudes up to 1.5 mag. Some authors[1] have attempted to calculate the dimensions of Eros assuming it to be a three-axis ellipsoid. The most recent determination (35 km, 16 km, 7 km) was given by Roach and Stoddard in 1938. In the case of 624 Hektor, amplitudes up to 1.1 mag were observed on lightcurves in which the primary and secondary maxima differed by less than 0.04 mag. Van Houten (1963) noted that for lightcurve amplitudes greater than 0.2 mag, the two maxima were about the same level and differed by 0.04 mag on the average. This is an indication of the small effect of reflectivity differences between the opposite sides. Assuming then that the light variation of Hektor is due almost entirely to shape, Dunlap and Gehrels (1969) used a cylindrical model with rounded ends to calculate a length of 110 km and a diameter of 40 km. The nearly constant (±0.02 mag) absolute magnitude of the maxima ruled out a third axis being significantly different from the second. More recent lightcurves of 1620 Geographos have been obtained with amplitudes up to 2.0 mag (Dunlap and Gehrels, 1971). If all of this variation is caused by shape, Geographos might be nearly six times longer than wide! However, the 0.1 mag difference between maxima (and an even larger difference in the minima) suggests a possible reflectivity effect that appears to reduce the length-to-width ratio to about 4. It was decided to make a laboratory investigation of the lightcurves of models to clarify our understanding of light variations caused by shape and perhaps enable us to find a particular shape that would reproduce the observations of Geographos. The work is still in progress, but we already have obtained some interesting results.

PRODUCTION OF MODEL LIGHTCURVES

Figure 1 illustrates some of the first of 12 models that have been observed. Each model was made with a Styrofoam center covered with a thin layer of Plasticene and finally dusted with powdered rock. The model was turned about

[1]See p. 133.

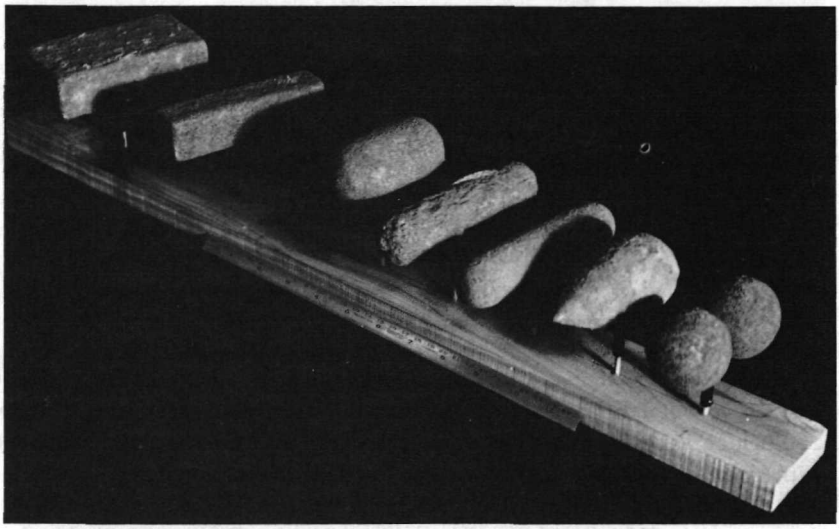

Figure 1.–A sample of some early models.

its shortest body axis by a stepping motor, and integrations were usually made every 3° (or 5°) over 240° (or 360°) of rotation using a photometer as used at the telescopes (Coyne and Gehrels, 1967).

Figure 2 defines the geometry of the observations. The model's rotation axis can be oriented in space around two perpendicular directions. One is the line of sight, a rotation about which causes a change in *asterocentric obliquity*.[2] The

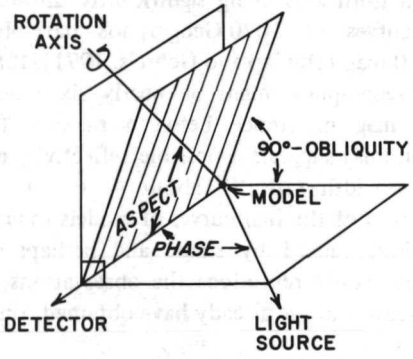

Figure 2.–The geometry of the laboratory observations. (Note that obliquity as defined here is not the same as the obliquity defined in the glossary.)

[2]Throughout this paper, obliquity refers to the dihedral angle between the plane determined by the line of sight and the axis of rotation, and by the plane perpendicular to the scattering plane and containing the line of sight. (See fig. 2.)

other direction is perpendicular to the line of sight at the model's center, about which a rotation causes a change in *aspect* (the angle between the rotation axis and the line of sight). The light source can be moved horizontally to change the *phase*. For each of the models, up to 27 lightcurves were produced by varying the aspect (90°, 60°, 35°), the obliquity (90°, 50°, 15°) and the phase (20°, 40°, 60°). The average probable error estimate of all angle measurements is ±1°.

Figure 3 illustrates all the lightcurves obtained from a smooth-surfaced, long, cylindrical model with rounded ends. One end and part of one side were artificially darkened with graphite powder to produce the apparent reflectivity differences between primary and secondary features seen in the Geographos lightcurves (Dunlap and Gehrels, 1971). Ignoring these differences, the lightcurves illustrate in general the effects of changing the aspect, phase, and obliquity. Several characteristics of the lightcurves can be identified that are used later in making comparisons of models:

(1) Amplitude: the height of the curve from minimum to maximum (The estimated probable error of the amplitudes is ±0.01 mag.)
(2) Shape of minima: sharp, flat, and/or asymmetric
(3) Width of minima at half amplitude

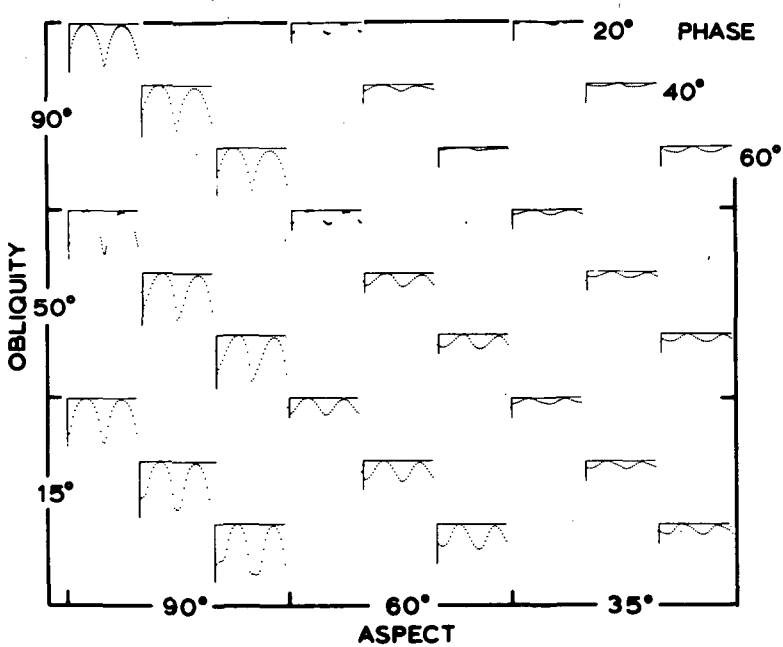

Figure 3.–Model lightcurves in a 3 by 3 by 3 matrix. The model was a cylinder with hemispherical ends having one end darkened and an overall length-to-width ratio of about 4. The lightcurve at 90° obliquity, 90° aspect, and 20° phase (*top left*) has an amplitude of 2.12 mag.

(4) Time shifts of maxima or minima relative to the observation at 90° aspect, 90° obliquity, 20° phase
(5) Lightcurve inversions: maxima become minima and vice versa (time shift is 90°)
(6) Primary and secondary maxima and minima

Looking horizontally from left to right in figure 3, one sees the changes produced by decreasing the aspect; most noticeable is the decrease in amplitude and the time shifts (leading to two lightcurve inversions and two partial inversions at the top right of the figure). The inversions are understood roughly as occurring when the illuminated part of the "true" maxima has a smaller area (as seen by the detector) than the illuminated part of the "true" minima. Looking vertically, one sees sometimes a noticeable change in amplitude with obliquity and sometimes changes in asymmetry. Looking diagonally (in groups of three), one sees the changes due to phase–usually small changes in amplitude with some asymmetries and time shifts.

AMPLITUDE-ASPECT RELATIONS

Figure 4 is the set of nine amplitude-aspect curves for the lightcurves from figure 3 (using secondary amplitudes to avoid reflectivity effects). The turnup in the curves at 90° obliquity and 40° and 60° phase is associated with

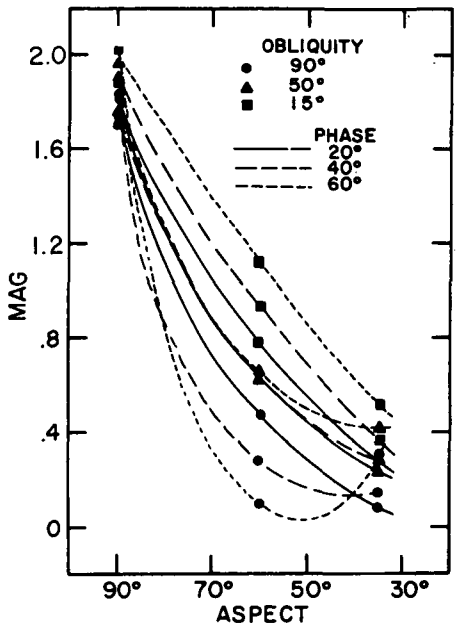

Figure 4.–Amplitude-aspect curves obtained from the secondary amplitudes of figure 3.

lightcurve inversions. (See fig. 3). Curves for the other models are similar but not exactly the same as these. It is clear, however, that there is no unique amplitude-aspect function for this or any of the models studied. Therefore, it is not possible, in general, to determine a rotation axis precisely by using a single amplitude-aspect function. Of course, approximations can be made; and they may be better if the phase angles are always small. However, the amplitude-aspect function is model dependent in an as-yet-unknown way.

COMPARISONS OF MODELS

Table I is a brief summary of the results of five comparisons of models. To see how differences in the shape affect the observed light variation, each model was compared with one having a different shape; finally, the lightcurves made at the same orientations were examined for differences in the characteristics described earlier. The changes in the light variation usually depend not only on the shape of the model, but also on aspect, obliquity, and phase. We cannot, for example, look at a single asteroid lightcurve and deduce the shape of the asteroid. Therefore, before comparisons can be made with actual observations, the orientation of the rotation axis in space must be known precisely ($\sim \pm 1°$). Probably the weakest point in our present method for obtaining the rotation axis (see Taylor[3]) is in accounting for differential time shifts in the maxima (or minima) that depend on aspect, obliquity, and phase. It may be possible to utilize the time shifts from the models to improve our determination of rotation axes. We notice also in table I that the presence of a third body axis is clearly evident in the change in brightness of the maxima as the aspect changes.

COMPARISON WITH TELESCOPIC OBSERVATIONS

Figure 5 shows the August 31, 1969, lightcurve of Geographos and also the average of the two model lightcurves from figure 3 that are closest to the calculated orientation of Geographos if its pole is at $\lambda_0 = 113°, \beta_0 = 84°$.

In the laboratory we were modeling direct rotation, but Geographos' rotation is retrograde. Making the necessary corrections to the lightcurve and moving the dark side to again follow the dark end, the model will reproduce the asymmetries in the minima; but the difference in the widths of the minima is still unexplained. We are currently developing a computer method of using the model data along with observed amplitudes to determine a pole, but results are not yet available. Other asteroids with large amplitudes (433 Eros, 624 Hektor, and possibly 15 Eunomia, 39 Laetitia, and 44 Nysa) might also be used for comparisons.

CONCLUSION

The extreme smoothness ($\leqslant 0.004$ mag) of all the model lightcurves is not usually seen in asteroid lightcurves, although asteroids with large light

[3]See p. 121.

TABLE I.—*Comparisons of Models*

Model compared with reference[a]	Observed changes in light variation relative to the reference model[b]			
	Amplitude	Shape of minima	Time shifts	Other
1. Same shape; cross-sectional area ratio 2.3 times larger	Larger by up to a factor of 2	Narrower, sharper, more asymmetry	Some larger shifts in maxima	Lightcurve inversion is possible at smaller phase angle.
2. Two tangent spheres of equal radii; 5 percent larger area ratio	Usually smaller	Narrower, sharper	Some smaller shifts in maxima, more in minima	
3. Both ends pointed (conical); ~5 percent larger area ratio	Somewhat larger; amplitude-aspect curves have less or opposite curvature	Complicated changes with less asymmetry	No significant change	Occasionally the minima are wedge-shaped.
4. One end pointed (conical); some brighter spots; 5 percent smaller area ratio	Primary and secondary amplitudes larger, except at 90° aspect	Wider minima with one resembling the reference and the other those of model 3 (above)	Some smaller shifts in maxima and minima	Primary and secondary minima are frequently interchanged.
5. Elongation along a second body axis 0.7 times the major axis; 3 percent larger area ratio at 90° aspect	Smaller, except at 90° aspect	Somewhat wider	Usually larger shifts in maxima and minima	Increase in brightness of the maxima as aspect decreases (up to 0.32 mag at 35° aspect).

[a]The reference model is a cylinder with hemispherical ends and a cross-sectional area ratio A_{max}/A_{min} of 1.9.
[b]These changes usually depend on the aspect, phase, and obliquity and therefore do not characterize all the lightcurves.

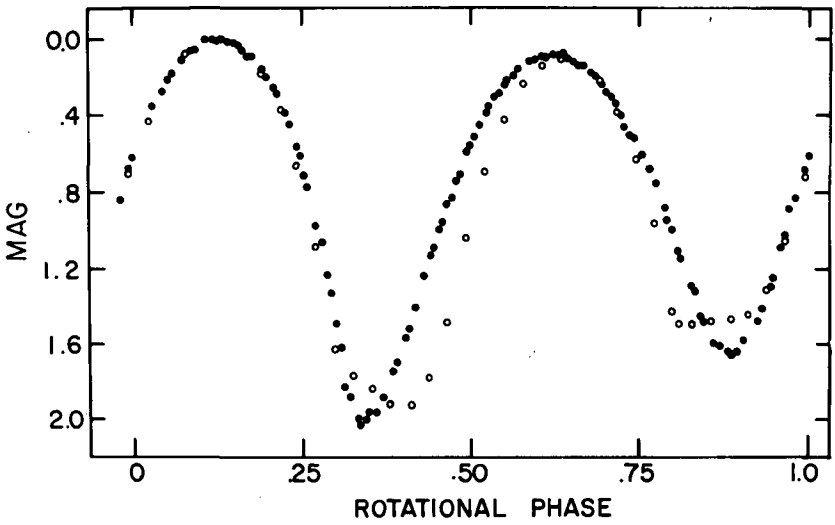

Figure 5.–Comparison of model to telescopic observations: • Geographos, August 31, 1969; o model whose lightcurves are in figure 3.

variations appear to have somewhat smoother lightcurves. Two models with rougher surfaces (about 5 and 20 percent deviations from an average dimension) were also observed. The roughest model produced the only deviation: a smooth tertiary hump seen in certain orientations near the minimum of light. A few lightcurves were also made using a very irregularly shaped and somewhat porous rock, and they show several small features with some indication of deviations from smoothness. More work needs to be done in modeling the surface texture, which is apparently the major source of small features in the lightcurves.

There is no unique amplitude-aspect function for any of the models studied, and this method should not be used for precise determinations of rotation axes. The differences in the amplitude-aspect function as well as in other characteristics of the lightcurves are partly due to the shape, but the orientation of the rotation axis must be precisely known–by photometric astrometry (see Taylor[4])–before the shape of an asteroid may be confidently determined.

ACKNOWLEDGMENTS

This work is supported by a grant from the National Geographic Society. I am also indebted to several of my colleagues for their help with the observations and especially to M. Howes who has helped extensively with the reductions.

---

[4]See p. 128.

REFERENCES

Coyne, G. V., and Gehrels, T. 1967, Interstellar Polarization. Astron. J. 72, 888.

Dunlap, J. L., and Gehrels, T. 1969, Lightcurves of a Trojan Asteroid. Astron. J. 74, 796-803.

Dunlap, J. L., and Gehrels, T. 1971, Minor Planets and Related Objects VIII. Astron. J., to be published.

Houten, C. J. van. 1963, Über den Rotationslichtwechsel der kleinen Planeten. Sterne Weltraum 2, 228-230.

Roach, F. E., and Stoddard, L. G. 1938, A Photoelectric Lightcurve of Eros. Astrophys. J. 88. 305-312.

DISCUSSION

BANDERMANN: Is there any obvious reason why the $|\Delta m|$ of successive minima in the lightcurves is usually larger than the $|\Delta m|$ of successive maxima?

DUNLAP: Perhaps small differences in surface reflectivity are relatively more important at low than at high levels of brightness.

ALFVÉN: I think laboratory work of this kind is very important. It is so healthy to see in the laboratory what is correct in theory and how many different solutions we can have. The theoretical models that are used always imply a number of assumptions that may not be applicable in nature.

624 HEKTOR: A BINARY ASTEROID?

A. F. COOK
Smithsonian Astrophysical Observatory

Dunlap and Gehrels (1969) have published lightcurves of the Trojan asteroid 624 Hektor. They proposed a conventional explanation in which Hektor is regarded as having the shape of a cigar. Two circumstances suggest, but do not prove, that Hektor is a binary asteroid. (1) The cigar shape at the conventional density of stony meteorites (3.7 g-cm^{-3}) appears to produce stresses that may well exceed the crushing strength of meteoritic stone. (2) The lightcurves exhibit an asymmetry changing with time that suggests librations of two ellipsoidal components. Observations are clearly required to look for these periodicities when we shall again be nearly in the plane of Hektor's revolution (or rotation) in 1973. An additional supporting lightcurve is desirable in 1972 and also in 1974. The periods of libration are probably nearly 1 day, if they exist, so that observations should be made from more than one geographic longitude in 1973. The present paper is an exposition on these considerations.

THE CIGAR-SHAPED MODEL

Dunlap and Gehrels (1969) employed a geometric albedo of 0.28 ± 0.14 and a cigar shape consisting of a right circular cylinder capped by two hemispheres at the ends. The radius of the cylinder and of the hemispheres is 21 km, and the height of the cylinder is 70 km. Mathematical convenience is served by replacement of this model by an ellipsoid of Jacobi with the same ratio of end-on to side-view cross sections. The ratio of the intermediate semiaxis to the largest semiaxis is as follows:

$$\frac{b}{a} = 0.32$$

A convenient graph for finding the ratio of the smallest semiaxis c to the largest has been published by Chandrasekhar (1965). His figure 2 (p. 902) yields

$$\frac{c}{a} = 0.23$$

The density of this ellipsoid at which equilibrium occurs so that no stresses are applied, i.e., so that the pressure is everywhere isotropic, can also be found

from another graph by Chandrasekhar (1965, fig. 3, p. 903). The abscissa in this case is Arccos $(c/a) = 77°$, whence the ordinate is

$$\frac{\Omega^2}{\pi G \rho_e} = 0.17$$

where Ω is the angular velocity of rotation,

$$\Omega = \frac{2\pi}{P}$$

P is the period of rotation (2.492×10^4 s according to Dunlap and Gehrels, 1969), and G is the universal constant of gravitation. Solution for the density ρ_e of the asteroid in equilibrium yields 1.7 g-cm^{-3}. It follows that if Hektor is a single body, either it is of lower density than a carbonaceous chondrite of type I or it is not in equilibrium.

STRESS IN THE CIGAR-SHAPED MODEL

Computation of a representative stress at the density of meteoritic stone is required to assess the viability of the Jacobi ellipsoid as a large meteoritic stone. Jardetzky (1958) provides the appropriate mathematical discussion. His equation (2.2.13) on page 31 can be transformed to read

$$\frac{\Omega^2}{G} = L_y - \frac{c^2}{b^2} L_z = L_x - \frac{c^2}{a^2} L_z = \frac{\pi \rho \Omega^2}{\pi G \rho} \tag{1}$$

where ρ without subscript refers to the actual density, and the potential takes the form

$$V = \frac{C'}{G} - \frac{1}{2}\left(L_x x^2 + L_y y^2 + L_z z^2\right) \tag{2}$$

where x is taken along the largest semiaxis, z along the shortest, and y along the intermediate one; the origin lies at the center of the ellipsoid; and C' is an arbitrary constant. Poisson's equation takes the form

$$\nabla^2 V = L_x + L_y + L_z = 4\pi\rho \tag{3}$$

Solution of equations (1), (2), and (3) for L_z, L_x, and L_y yields

$$L_z = 2\pi\rho \frac{1 - \Omega^2/\pi G\rho}{1 + c^2/b^2 + c^2/a^2} \tag{4}$$

$$L_x = \frac{c^2}{a^2} L_z + \pi\rho \frac{\Omega^2}{\pi G \rho} \tag{5}$$

$$L_y = \frac{c^2}{b^2} L_z + \pi\rho \frac{\Omega^2}{\pi G\rho} \tag{6}$$

The pseudopotential including the centrifugal term is

$$\frac{C_I}{G} = \frac{C'}{G} - \frac{1}{2}\rho \left[\left(L_x + \pi\rho \frac{\Omega^2}{\pi G\rho}\right)x^2 + \left(L_y + \pi\rho \frac{\Omega^2}{\pi G\rho}\right)y^2 + L_z z^2\right] \tag{7}$$

where C_I/G is the pseudopotential. The pressure p_s at the surface is given by

$$\begin{aligned} p_s &= C_{I_s} \\ &= C' - \frac{1}{2} G\rho \left[\left(L_x + \pi\rho \frac{\Omega^2}{\pi G\rho}\right)x_s^2 + \left(L_y + \pi\rho \frac{\Omega^2}{\pi G\rho}\right)y_s^2 + L_z z_s^2\right] \end{aligned} \tag{8}$$

$$\left(\frac{x_s}{a}\right)^2 + \left(\frac{y_s}{b}\right)^2 + \left(\frac{z_s}{c}\right)^2 = 1 \tag{9}$$

where x_s, y_s, z_s refer to a point on the surface.

At the equilibrium value of the density ρ_e, p_s vanishes all over the surface. We compute the difference due to a different value of ρ and consider only the differences in pressures along the principal axes, whence

$$\begin{aligned} \Delta p_{s_a} &= -\frac{1}{2} G(\rho - \rho_e)\left(L_x + \pi\rho \frac{\Omega^2}{\pi G\rho} a^2\right) \\ \Delta p_{s_b} &= -\frac{1}{2} G(\rho - \rho_e)\left(L_y + \pi\rho \frac{\Omega^2}{\pi G\rho} b^2\right) \\ \Delta p_{s_c} &= -\frac{1}{2} G(\rho - \rho_e) L_z c^2 \end{aligned} \tag{10}$$

In terms of a, b, c, and $\Omega^2/\pi G\rho$, these expressions become

$$\begin{aligned} \Delta p_{s_a} &= -\pi G\rho(\rho - \rho_e)\left(1 + \frac{a^2}{b^2} + \frac{a^2}{c^2}\right)^{-1}\left[1 + \left(\frac{a^2}{b^2} + \frac{a^2}{c^2}\right)\frac{\Omega^2}{\pi G\rho}\right]a^2 \\ \Delta p_{s_b} &= -\pi G\rho(\rho - \rho_e)\left(1 + \frac{a^2}{b^2} + \frac{a^2}{c^2}\right)^{-1}\left[1 + \left(\frac{b^2}{a^2} + \frac{b^2}{c^2}\right)\frac{\Omega^2}{\pi G\rho}\right]a^2 \\ \Delta p_{s_c} &= -\pi G\rho(\rho - \rho_e)\left(1 + \frac{a^2}{b^2} + \frac{a^2}{c^2}\right)^{-1}\left(1 - \frac{\Omega^2}{\pi G\rho}\right)a^2 \end{aligned} \tag{11}$$

Next we subtract the hydrostatic part or mean to find

$$\Delta p'_{s_a} = \frac{1}{3}\Omega^2(\rho - \rho_e)\left(\frac{1 + b^2/a^2 + b^2/c^2}{1 + a^2/b^2 + a^2/c^2} - 2\right)a^2$$

$$\Delta p'_{s_b} = \frac{1}{3}\Omega^2(\rho - \rho_e)\left(1 - 2\frac{1 + b^2/a^2 + b^2/c^2}{1 + a^2/b^2 + a^2/c^2}\right)a^2 \qquad (12)$$

$$\Delta p'_{s_c} = \frac{1}{3}\Omega^2(\rho - \rho_e)\left(1 + \frac{1 + b^2/a^2 + b^2/c^2}{1 + a^2/b^2 + a^2/c^2}\right)a^2$$

These are the hydrostatic pressures that would be required on the surface to keep the internal pressures isotropic. In their absence, an anisotropic pressure will appear at the center with signs opposite to those in equations (12). At $\rho = 3.7$ g-cm^{-3} as for meteoritic stone, we have

$$\left.\begin{aligned} -\Delta p'_{s_a} &= 7.6a^2 \\ -\Delta p'_{s_b} &= -3.3a^2 \\ -\Delta p'_{s_c} &= -4.6a^2 \end{aligned}\right\} \quad \text{nN-m}^{-2} \qquad (13)$$

(or $7.6 \times 10^{-8}\ a^2$, $-3.3 \times 10^{-8}\ a^2$, and $-4.6 \times 10^{-8}\ a^2$ dyne-cm^{-2}, respectively). This loading resembles that in a conventional unidirectional compression test of

$$P' \simeq 12 \text{ nN-m}^{-2} \qquad (14)$$

(or $1.2 \times 10^{-7}\ a^2$ dyne-cm^{-2}).

The cross sections in side view and end-on of Dunlap and Gehrels' (1969) model impose $a = 77$ km whence $P' \simeq 0.7$ MN-m^2 (7 bars), compared with a crushing strength of about 1 MN-m^{-2} (10 bars) for the Lost City meteorite (R. E. McCrosky, private communication, 1971). A geometric albedo of 0.14 (as for the brightest parts of the Moon) makes Hektor larger in dimension by a factor of $\sqrt{2}$, whence $P' \simeq 1.4$ MN-m^{-2} (14 bars). Finally, a geometric albedo of 0.07 (upper limit for the dark part of Iapetus according to Cook and Franklin, 1970) introduces a further factor of $\sqrt{2}$ in dimension and raises P' to about 3 MN-m^{-2} (30 bars). A large body like Hektor will have weak inclusions and thus have a lower bulk strength than a small body like the Lost City meteorite. Moreover, meteoritic bombardment will tend to induce failures as well. All this casts doubt on the model of Dunlap and Gehrels (1969) and suggests that a binary model may be more satisfactory.

THE BINARY MODEL

The lightcurves of Gehrels (Dunlap and Gehrels, 1969) are a heterogeneous lot obtained with different telescopes, photometers, and skies. The best quality in observations occurs at the largest and smallest amplitudes. The largest amplitude was observed on April 29 and May 1, 1968, with the 152 cm reflector at Cerro Tololo. The zero point of magnitude was obtained only on the second night. The smallest amplitude was observed on February 4, 1965, with the 213 cm reflector at Kitt Peak.

The author has carried out an analysis that can be called only a reconnaissance. An unusual amount of work has been required compared to the usual solution for an eclipsing binary. Interim light elements were derived to plot the lightcurves of 1965 and 1968 against phase. There is no evidence for any differences between successive half-periods, so each night's observations were plotted on a single half-period. A notable feature of the 1968 observations is an asymmetry such that the maxima occur 0.012 period early. The descent into the minimum is slower than the rise from it. In 1957 this asymmetry appears to be at the limit of detection but in the opposite direction. The 1957 observations are thin and were made at the Radcliffe Observatory, Pretoria, at the 188 cm reflector.

The most obvious explanation for the asymmetry is libration of the components about the radius vector joining them. This hypothesis can be tested by extensive observation at the next opposition in which Earth is near the plane of Hektor's revolution (or rotation).

The libration was taken into account in the rectification. The formula used for rectification of the intensity was

$$I^R = \frac{I}{[1 - z\cos^2(\theta - \theta_0)]^{1/2}} \tag{15}$$

where I is the observed intensity, I^R the rectified intensity, z the photometric ellipticity, θ the phase angle, and θ_0 the phase angle at which we look along the major axes of the components. We use here the standard preliminary model of two similar ellipsoids similarly situated. Rectification for phase was effected by the formula

$$\sin^2\Theta = \frac{\sin^2\theta}{1 - z\cos^2(\theta - \theta_0)} \tag{16}$$

where Θ is the rectified phase angle. Solution for z in the standard graphical plot of I^2 versus $\cos^2(\theta - \theta_0)$ employed

$$\bar{I}(\sin^2\theta) \equiv \tfrac{1}{2}[\bar{I}(\theta) + \bar{I}(\pi - \theta)] \tag{17}$$

and yielded

$$z = 0.745 \pm 0.015 \qquad \theta_0 = 0.012P = 4.32^\circ \tag{18}$$

Execution of the usual procedures using the tables of χ functions of Merrill (1950) produced the following solution:

$$l_0 = 0.777$$

$$k = 0.30 \pm 0.02$$

$$a_g = 0.42 \pm 0.04$$

$$i_r = 71^\circ \pm 2$$

where l_0 is the brightness at minimum in units of that outside eclipse, k is the ratio of radii of the components, a_g is the largest semiaxis of the larger component in units of the distance between the asteroids, and i_r is the inclination of the relative orbit in the rectified model in which the components are spheres. The most extreme solution pointing to the highest density of the components is that for equal bodies, $k = 1.00$. In this case $a_g = 0.38$ and $i_r = 70^\circ.1$.

The lightcurve for February 4, 1965, shows an apparent elliptic variability only with $z = 0.154 \pm 0.002$. The unit of intensity corresponds to an absolute magnitude of 7.63 compared with 7.70 for May 1, 1968. Combination of the results from 1968 and 1965 yields for the inclinations of the orbit and the ratios of principal axes the following results:

Year	*i*	
1965	$28^\circ.35$	$b/a = 0.493$
1968	$83^\circ.24$	$c/a = 0.454$

Here $k = 1.00$ has been chosen to present the most extreme case. The mean density of the components comes to 9.6 g-cm^{-3}. Correction for finite sizes of the components in ellipsoidal shape yields a drop of a few tenths, and adoption of $k = 0.60$ would push the density down to that of iron, about 8 g-cm^{-3}. Before one blithely proposes that Hektor is a binary composed of two solid iron ellipsoids, it seems only prudent to question the rectification, which is large. The extreme form of doing this is to consider a contact binary as a model.

THE CONTACT-BINARY MODEL

In the case of a contact binary, the rectification cannot be considered separately. In this reconnaissance, a start was made by assuming (1) that $\sin^2 \Theta_e \equiv 1$ where Θ_e denotes the rectified phase angle at external contact; (2) that the ratio of radii $k \equiv 1$; and (3) that the fractional depth of greatest eclipse $\alpha_0 \equiv 1$; i.e., that central eclipse occurred. This representation failed, so that two progressions away from this model were next considered. One such sequence of models had $k = 1$ but α_0 decreased successively. No models fitting the observations could be found. Next, a sequence of grazing annular and total

eclipses was tried ($\alpha_0 \equiv 1$), so that k was varied. This sequence yielded a satisfactory representation of the observations at $k = 0.80$:

Year	i	α_0	z
1965	31°.16	0.020	0.1403
1968	86°.27	1.000	0.5944

$$a_g = 0.5556$$

$$b/a = 0.635$$

$$c/a = 0.582$$

$$\rho = 2.4 \text{ g-cm}^{-3}$$

Correction for finite sizes of components reduced ρ to 2.0 g-cm^{-3}.

The two directions of Hektor in 1965 and 1968 lie some 110°.4 apart, whence it appears that the pole of revolution of the binary must lie near the plane of Hektor's heliocentric orbit. The librations will cause the epochs of the shallower minima to be not very reliable in derivations of this pole.

Better light elements have been derived by bootstrapping across successively longer intervals on the assumption that the pole lies in the plane of the orbit. The corresponding sidereal period is

$$P = 0^{d}.2884483 \pm 0.0000002$$

The ellipsoids can be replaced individually by two point masses of spheres to yield the same moment of inertia about the smallest semiaxis. Then the period of libration can be calculated in the field of the other represented as a point mass. The results indicate a period of libration of two to four periods of orbital revolution. The near equality of the heights of maxima in 1968 during two long nights at a 2 day interval strongly suggests periods of about 1 day for the librations.

FURTHER STUDIES NEEDED

Observations can only be planned efficiently if the above analysis is completed by using many values of the photometric ellipticity z for 1968. It is to be expected that there will be two groups of solutions—those at high densities described above and belonging to a narrow range of z near 0.745 and those at low densities and belonging to a wider range of z near 0.60. It is to be hoped that this latter group will reach up to or approach more conventional densities like that of meteoritic stone.

Observations will be needed in 1972, 1973, and 1974 to settle the choice between the cigar-shaped and binary models by seeking the periodicities in the librations and to improve the accuracy of the photometric solutions either by observation of annular and total eclipses or by observation of very deep partial

eclipses on either side of the orbital plane (or equatorial plane). This implies an extensive campaign in 1973 at one observatory coupled with an international campaign during the dark of the Moon closest to opposition. The best available range of photometric solutions will be required for intelligent planning of the extensive campaign at one observatory. The international campaign would be aimed at covering the suspected 24 hr periods of the librations. Good lightcurves at single epochs would be desirable in 1972 and 1974.

ACKNOWLEDGMENTS

It is a pleasure to acknowledge useful and extensive discussions with B. G. Marsden and F. A. Franklin.

REFERENCES

Chandrasekhar, S. 1965, On the Equilibrium and Stability of the Riemann Ellipsoids. Astrophys. J. 142, 890-921.

Cook, A. F., and Franklin, F. 1970, An Explanation of the Light Curve of Iapetus. Icarus 13, 282-291.

Dunlap, J. L., and Gehrels, T. 1969, Minor Planets III. Lightcurves of a Trojan Asteroid. Astron. J. 74, 796-803.

Jardetzky, S. 1958, Theories of Figures of Celestial Bodies. Interscience Pub., Inc. New York.

Merrill, J. E. 1950, Tables for Solution of Light Curves of Eclipsing Binaries. Contrib. no. 23, Princeton Univ. Observ.

DISCUSSION

HARTMANN: I wish to make a comment on irregular shapes of asteroids. Cook's evidence that Hektor would not retain an irregular shape rests on the crushing strength he assigns to the material. It appears that Cook's value of 1 MN-m^{-2} (10 bars), based on the Lost City chondrite, is unusually low. Wood (1963) lists compressive strengths of eight chondrites; they range from about 6 to 370 MN-m^{-2} (60 to 3700 bars) although Wood notes that some more crumbly chondrites are known. The one iron listed has a strength of about 370 MN-m^{-2}. Thus, according to the 0.7 MN-m^{-2} (7 bar) stress found by Cook for a Jacobi ellipsoid of Hektor's dimensions and chondritic density, the asteroid could be quite irregular.

How large an asteroid can be irregular? A simple estimate comes from the size of a nonrotating spherical asteroid whose central pressure P_c is just equal to the crushing strength. Under this condition the central core begins to be crushed and hence lacks rigidity. Larger asteroids would have a nonrigid interior and could thus deform to an equilibrium shape. For typical chondritic strengths we have

$$P_c = \frac{2\pi\rho^2 G}{3} r^2 = 1 \text{ to } 370 \text{ MN-m}^{-2} \text{ (10 to 3700 bars)}$$

Thus, the diameter = 46 to 880 km (if $\rho = 3.7$).

It is concluded that asteroids substantially larger than Hektor (42 by 112 km) can be irregular in shape. Such irregularity is indeed evidenced by lightcurves and is theoretically expected because many if not most asteroids are probably fragmentary pieces that have resulted from collisions.

DISCUSSION REFERENCE

Wood, J. A. 1963, Physics and Chemistry of Meteorites. The Moon, Meteorites, and Comets (eds., B. M. Middlehurst and G. P. Kuiper), ch. 12. Univ. of Chicago Press. Chicago.

Page intentionally left blank

ASTEROID CHARACTERISTICS BY RADAR

R. M. GOLDSTEIN
Jet Propulsion Laboratory

The techniques of radar offer a potentially powerful tool for the study of planetoids. It is a new approach, having been applied to extraterrestrial targets only recently in the history of astronomical study. Although the Moon was first, Venus has been observed by radar only since 1961. Since that time the techniques and capability of radar have evolved rapidly and many important new facts about Venus have been gathered. Further, the more distant and difficult targets, Mercury and Mars, have also yielded up secrets to radar probing. Finally, during the close approach of June 1968 Icarus itself was observed by radar from two different observatories (Goldstein, 1969; Pettengill et al., 1969). Review articles on radar studies of the planets are given in Shapiro (1968) and Goldstein (1970).

It is to be hoped that radar study of the asteroids will prove as fruitful as the study of the inner planets. However, asteroids present extra difficulties to radar as compared to the familiar planets. A diagram of the radar situation is given in figure 1. A tight beam of microwaves (0.1° is the current state of the

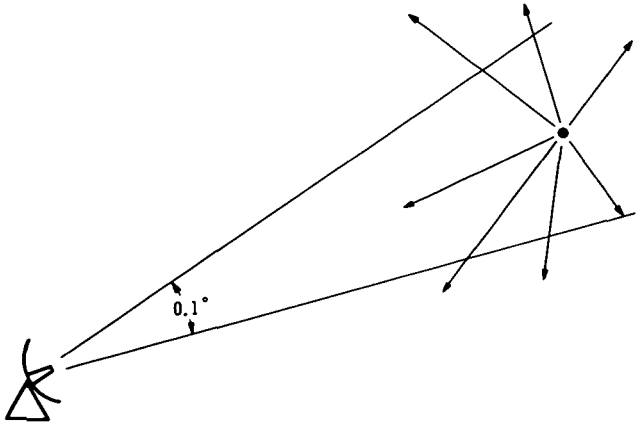

Figure 1.—Illustration of geometric difficulties of radar asteroid astronomy. The received power is extremely weak, and the antenna beam cannot resolve individual parts of the target.

art) is directed toward the target. However, only a minute fraction of the power is actually intercepted. Of that amount, most is dissipated by the surface as heat. The balance, which contains the desired information, is scattered more or less uniformly throughout the solar system. The echo power received by the antenna is incredibly small. For the Icarus measurements of 1968, the transmitted power was 450 kW; the echo power was 6×10^{-23} W. Thus the overriding problem of radar asteroid astronomy is one of signal-to-noise ratio (SNR).

The second important difficulty, related to the first, is angular resolution. It is necessary to be able to relate the echo to specific areas of the surface—to isolate different parts of the surface for separate study. It can be seen from the figure that angular resolution of the antenna is quite inadequate. However, radar commonly allows two dimensions to effect this separation: time delay and Doppler shift. Both of these dimensions consist of two parts: an orbital part, measured to the closest (or sub-Earth) point, and a part that relates other points on the surface to the sub-Earth point. Generally, the orbital part is accounted for by tuning, automatically, the radar receiver to track the sub-Earth point. This is analogous to sidereal drive on a telescope to hold the image still during a long time exposure. The contours of constant time delay and constant Doppler shift for the balance of the effect (for a spherical surface) are given in figure 2. For time delay the contours are circles, concentric about the sub-Earth point. The Doppler shift is caused by any rotation the target might have relative to the radar. The constant Doppler contours are also concentric circles, but seen edgewise from the radar.

Radar echoes from the inner planets have been analyzed into time-delay rings and into Doppler-shift rings and, in fact, both simultaneously. However, for asteroid study, only Doppler analysis has been used. The reason for this is the much weaker received power and the fact that narrowband signals are inherently easier to detect in the presence of noise. The narrowest band signals, of course, are those originating along a constant Doppler contour.

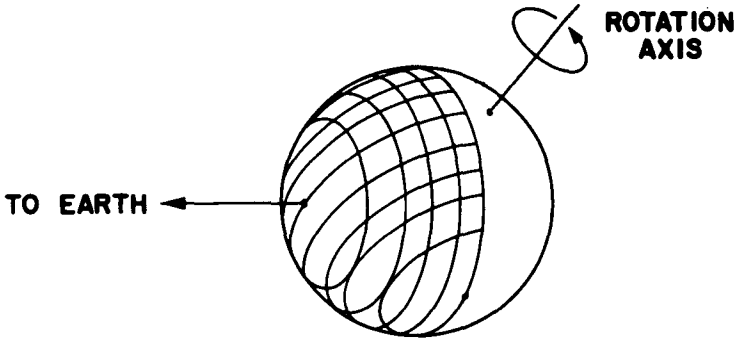

Figure 2.–Contours of constant time delay and of constant Doppler shift for a spherical target.

The most likely asteroid radar experiment, then, consists of transmitting a spectrally pure, monochromatic wave toward the target. The received signals are analyzed by a process such as the fast Fourier transform to yield the power spectrum of the echoes. This is equivalent to a scan across the disk with a narrow slit, parallel to Doppler contours. As usual, there is an essential compromise between high resolution (narrowness of the slit) and SNR.

A result of applying this technique to the planet Mercury is given in figure 3. These data were taken when Mercury was 0.6 AU distant, spinning such that the limb-to-limb bandwidth was 100 Hz. It required 1 hr of integration time (time exposure).

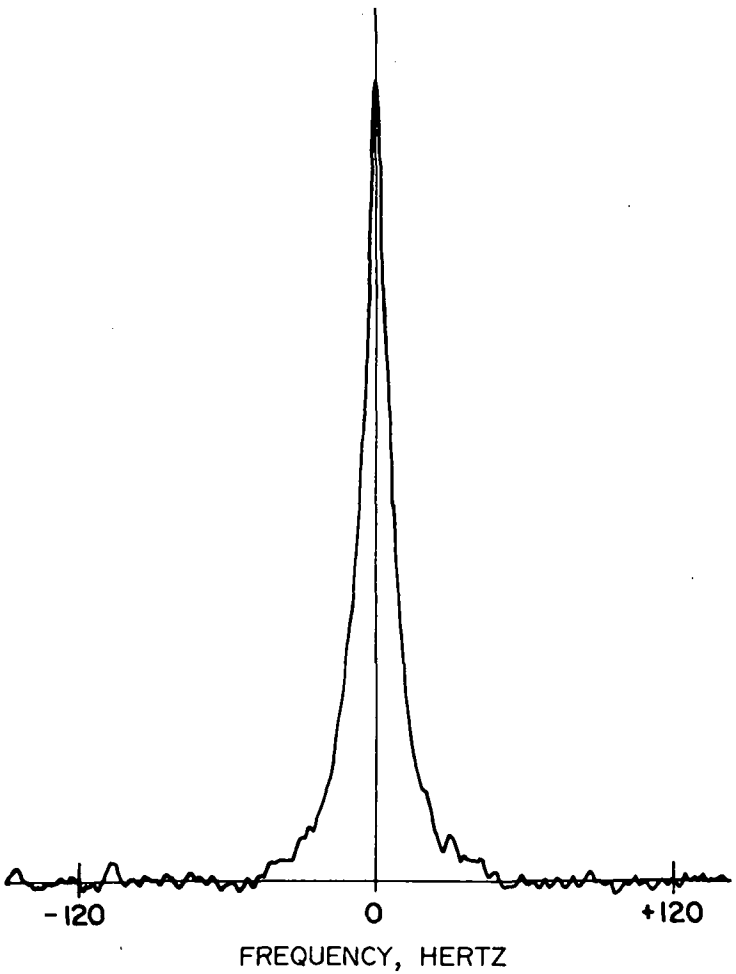

Figure 3.–Spectrogram of echoes from Mercury. Power density is plotted against Doppler frequency shift.

The center frequency of this spectrum is a direct measure of the relative velocity between Mercury and the radar, accurate to about 15 cm/s. Such data can be used to refine the orbit of an asteroid as it has been used for Venus. This is a bootstrap procedure, however, because knowledge of the orbit is needed to take the data. During the long time exposure, the receiver must be tuned continuously to keep the spectrum from moving, and hence blurring the data. For the weakest signals, appreciable blurring would render the signals undetectable. The bootstrapping converges very quickly if a fairly good orbit can be obtained in advance. For the Icarus radar experiment, a good orbit was obtained with the help of last-minute optical observations and reduction by Elizabeth Roemer.

The width of the spectrum at the base gives directly the line-of-sight velocity of the limbs, which equals the relative angular velocity, projected across the line of sight, times the target radius. When the SNR is good enough to detect the edges of the spectrum over an applicable arc as the asteroid passes Earth, the bandwidth data are sufficient to recover all three components of the spin vector and the radius. This is true because the Doppler broadening has two components: one due to spin and the other due to orbit-induced relative angular motion. The presumably known orbital part can be used to calibrate the effect of the spin.

The shape of the spectrum contains important information about surface slopes. For example, the Mercury spectrum of figure 3 is highly peaked at the center (although not so much as for Venus). This shows that most of the received power is reflected from regions near the sub-Earth point, where the Doppler shift is small. Hence the surface is relatively smooth, to a scale somewhat larger than the wavelength used (12.5 cm for the Goldstone radar). Under the assumption of a uniform surface, the spectrum can be converted uniquely to a backscattering function (Goldstein, 1964), which shows how the radar cross section of an average surface element varies with the angle of incidence. This backscattering function can be considered directly as the distribution of surface slopes. That is, the backscattering function of a surface element at a given angle represents that portion of the element which is perpendicular to the incident rays. Of course, the slope distribution, per se, gives no knowledge of the linear extent of any given slope.

Surface roughness can be tested to a scale smaller than the wavelength by a polarization technique. Right-handed circular polarized waves are transmitted. Because reflection from a smooth dielectric sphere reverses the sense, the receiver is usually set for left-handed polarization. A rough surface, however, will reflect signals equally into both polarizations. To measure this effect, right circular polarization is both sent and received. Figure 4 presents spectrograms from Venus and Mercury taken in this so-called depolarized mode at similar SNR's.

The high central peaks of these spectra have been suppressed by the polarization in much the same way as optical glare can be removed by polarized sunglasses. Furthermore, for Venus, the signal power has dropped by

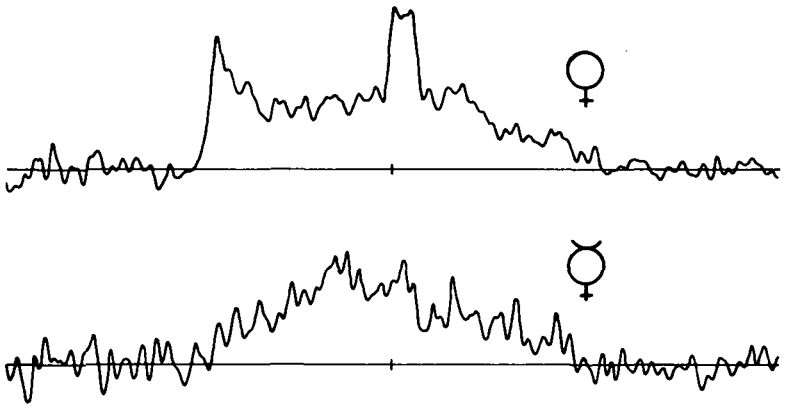

Figure 4.–Set of spectrograms taken in the depolarized mode. The upper curve is from Venus, the lower from Mercury. The individuality of the planets shows strongly here.

a factor of over 20, showing that most of the echo power had originated from the relatively smooth areas near the sub-Earth point. It is for this reason that the depolarized mode of radar observation has not yet been attempted for an asteroid. The power from Mercury, on the other hand, dropped only by a factor of 10, showing that Mercury is rougher (to the scale of a wavelength) than Venus.

Two very interesting features appear in the Venus data that do not appear in the Mercury data. These features were the first evidence that the surface of Venus, hidden under its cover of clouds, is not homogeneous. On the contrary, large topographic features exist on the surface, rotate with the planet, and appear year after year to radar view.

These features have high radar contrast to the surrounding areas, and have a much stronger ability to depolarize radar waves. It is not known whether they are mountains or craters or some other formation such as lava flows. Their existence, however, permits the rotation of Venus to be determined to very high precision. By tracking the Doppler frequency shift of these objects, a period of rotation for Venus of 243.0 days, retrograde, has been deduced. The direction of the spin axis is (or almost is) perpendicular to the orbital plane.

At first glance, the Mercury spectrum of figure 4 contains no significant features. However, a left-right (east-west) asymmetry can be seen, and the motion of this lesser feature has been used to determine the rotation period of Mercury to an accuracy of 0.5 percent.

The important thing is that, to radar, Venus is different from Mercury and, presumably, both are different from asteroids. The study of these differences can add to our knowledge of asteroids.

We return now to the problem mentioned earlier, the extreme weakness of echoes from an asteroid. The radar equation shows that the received power is proportional to $R^2\Delta^{-4}$ where R is the radius of asteroid and Δ is the

geocentric distance. Thus the small size of an asteroid compared to a planet reduces the received power by a factor of 10^6.

When considering the SNR, account must also be taken of the bandwidth of the echo and of the integration time t:

$$\mathrm{SNR} \simeq R^{3/2}\Delta^{-4}t^{1/2}\nu^{-1/2}$$

where ν is the perpendicular component of the velocity of rotation. For a calibration point, figure 5 is a spectrogram from Icarus, taken in June 1968 when the asteroid was 6.5×10^6 km from Earth. The spectrogram required 17 hr of integration.

As can be seen, this very noisy spectrogram cannot support much analysis. The edges of the spectrum are not distinguishable, so that it cannot be used to determine the rotation. The rotation, however, was measured with great precision optically (Gehrels et al., 1970), and the combination of the two data types is useful. A lower limit (0.5 km) was set to the radius of Icarus and an upper limit to the reflectivity. A surface model based on Mercury or Venus would not fit the data.

The close approach of Icarus was a rare opportunity for radar asteroid astronomy. The next weaker targets are the Jovian satellites Ganymede and Callisto, weaker than Icarus by a factor of 40. Next come the asteroids Vesta and Juno, down by an additional factor of 2. Another factor of 2 brings in Ceres and Pallas.

Radar capability continues to grow. The Goldstone radar is 5000 times stronger than when Venus was first detected in 1961. It is stronger by a factor of 6 than when the Icarus experiment was performed. Perhaps when Toro swings by in 1972 (an opportunity comparable to that of Icarus), much more of the potential of radar asteroid astronomy will be realized.

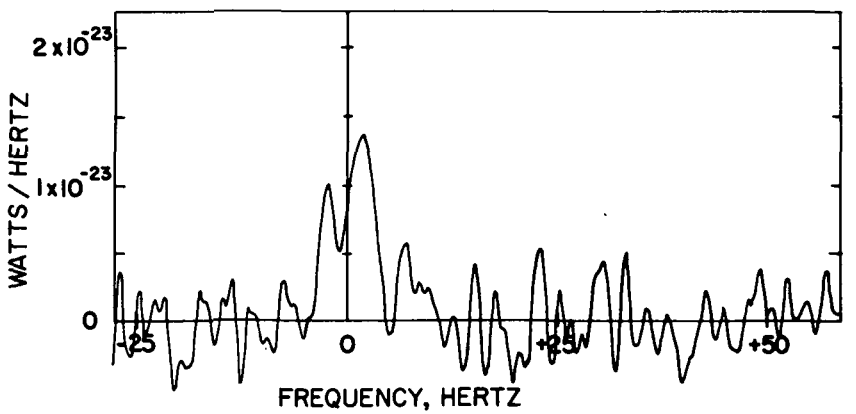

Figure 5.–Spectrogram of echoes from Icarus taken during closest approach of 1968.

REFERENCES

Gehrels, T., Roemer, E., Taylor, R. C., and Zellner, B. H. 1970, Asteroid (1566) Icarus. Astron. J. 75, 186-195.

Goldstein, R. M. 1964, Venus Characteristics by Earth Based Radar. Astron. J. 69, 12-18.

Goldstein, R. M. 1969, Radar Observations of Icarus. Icarus 10, 430.

Goldstein, R. M. 1970, Radio and Radar Studies of Venus and Mercury. Radio Science 5(2), 391.

Pettengill, G. H., Shapiro, I. I., Ash, M. E., Ingalls, R. P., Rainville, L. P., Smith, W. B., and Stone, M. L. 1969, Radar Observations of Icarus. Icarus 10, 432-435.

Shapiro, I. I. 1968, Planetary Radar Astronomy. IEEE Spectrum 5, 70.

DISCUSSION

CHAPMAN: After the anticipated improvement in the Arecibo dish, do you expect the larger asteroids such as Ceres to be detectable by radar?

GOLDSTEIN: The largest asteroids may just marginally be detected with the Goldstone (64 m) dish now, and they certainly should be detectable when Arecibo resurfaces within a few years.

Page intentionally left blank

DESCRIPTIVE SURVEY OF FAMILIES, TROJANS, AND JETSTREAMS

C. J. VAN HOUTEN
Sterrewacht te Leiden
Netherlands

The word "group" is so general that I would like to suggest that here it is used in its most general way: a group of asteroids is a collection of minor planets that have some feature in common. If we agree on this use of the word "group," then we can discern the following asteroidal groups:

(1) Groups that have a dynamical cause:
  (*a*) Trojans
  (*b*) Commensurability groups:
    (i) Hungaria group
    (ii) Hilda group
    (iii) Thule
(2) Groups that probably have no dynamical cause:
  (*a*) Hirayama families
  (*b*) Brouwer groups
  (*c*) Jetstreams

Because the topic of this colloquium is the physical studies of the asteroids, I shall here briefly review the physical studies made on these groups.

TROJANS

These are asteroids moving near the lagrangian points L_4 and L_5 of the Sun-Jupiter system. There are 15 numbered Trojans, but at fainter magnitudes than the limit of the ephemeris they are very numerous; it was shown that around L_5 there are 700 Trojans brighter than $B(a, 0) = 21.0$ (van Houten, van Houten-Groeneveld, and Gehrels, 1970). Their distribution as a function of absolute magnitude is similar to the normal asteroids. Rotation lightcurves of three Trojans were obtained (Gehrels, 1970) and they show relatively large amplitudes. The color measurements indicate a small ultraviolet excess (Gehrels, 1970), but the number of Trojans observed (2) is too small to be certain on this point. ($\overline{U-B} = 0.22$ of two Trojans against ≈ 0.40 of field asteroids.) The phase function of the Trojans will be discussed in my next

paper;[1] it looks as if the Trojan phase function is flatter than that of normal asteroids.

COMMENSURABILITY GROUPS

The members of these groups have values of semimajor axes that make their revolution period commensurate with that of Jupiter. The Hungaria group is found at the commensurability 2:9, the Hilda group at 2:3, and Thule at 3:4.

The Hungaria group has 15 numbered members, and the Palomar-Leiden survey (PLS) added nine more. No physical studies have been made on members of this group as yet.

The Hilda group has 23 numbered members and 10 additional members in the PLS. No physical studies have been made on members of this group as yet.

Thule is the only numbered asteroid found at this commensurability, and the PLS contributed no new members. A further remarkable fact about Thule is that both the eccentricity and inclination of its orbit are small (0.032 and 2°.3). It would be worthwhile to obtain a rotational lightcurve of this object because its amplitude may be small as well.

HIRAYAMA FAMILIES

If the numbered asteroids are plotted in a three-dimensional space using as coordinates the semimajor axis a, the proper inclination i', and the proper eccentricity e' (for the definition of the proper elements, see Brouwer and Clemence, 1961), then concentrations of asteroids are found that were called families by Hirayama. They are thought to be the remnants of a larger body after collision with a second body. Brouwer (1951) reinvestigated the families and adopted the following as definite: (1) Themis family; (2) Eos family; (3) Coronis family; (4) Maria family; (5) Phocaea family; and (6) Flora family, which Brouwer divided into four subfamilies. Except for the Phocaea family, all these families were recognized in the PLS. Moreover, five new families were found in the PLS, which were named the Nysa, Medea, Michela, Vesta, and Io families.

BROUWER GROUPS

The proper elements, as defined by Brouwer, still contain the secular terms, but in the sum of the longitudes of proper node λ_n' and proper perihelion λ_p' the first-order secular term cancels out. Brouwer, therefore, expected this sum to be approximately constant in the families, which turned out not to be the case. Nevertheless, he succeeded in finding small concentrations in the (a, i', e') space, for which this constancy of $\lambda_p' + \lambda_n'$ was more or less realized. They were named "groups" by Brouwer (1951). Kiang (1966) showed that in several cases Brouwer had selected the wrong quadrant for $\lambda_p' + \lambda_n'$, which makes Brouwer's criterion less convincing. Moreover, seven Brouwer groups were also

[1] See p. 184.

found in the PLS, three of them belonging to the new families. In none of these groups was the criterion of $\lambda_p' + \lambda_n' = \text{constant}$ fulfilled. It seems, therefore, better to regard the "Brouwer groups" as families, and disregard the criterion that Brouwer used for finding them. The average amplitude of the rotational lightcurves of family members is practically equal to those of the field asteroids. Also, no clear difference could be found between the colors of family members and field asteroids, although the fact that the four bluest asteroids observed thus far are all family members (see table I, taken from Gehrels, 1970) suggests that it may be fruitful to investigate this matter further.

TABLE I.–*Colors of the 4 Bluest Known Asteroids*

Asteroid no.	$B-V$, mag	$U-B$, mag	Family
2	0.65	0.26	Brouwer 28
16	.70	.24	Brouwer 13
44	.67	.22	Nysa family
268	.69	.29	Themis family

JETSTREAMS

These were introduced by Alfvén (1969) as concentrations in the (λ_p', λ_n') plane for family members. Alfvén found three in the Flora family and Arnold (1969) found several more. Moreover, one was found in the PLS, in the Nysa family. Kresák (this colloquium[2]) showed that the latter was caused by selection effects in the PLS material and suggested that the jetstreams found by Alfvén could be explained in a similar way. This matter should be investigated more closely.

REFERENCES

Alfvén, H. 1969, Asteroidal Jet Streams. Astrophys. Space Sci. 4, 84.

Arnold, J. R. 1969, Asteroid Families and "Jet Streams." Astron. J. 74, 1235.

Brouwer, D. 1951, Secular Variations of the Orbital Elements of Minor Planets. Astron. J. 56, 9.

Brouwer, D., and Clemence, G. M. 1961, Methods of Celestial Mechanics. Academic Press, Inc. New York.

Gehrels, T. 1970, Photometry of Asteroids. Surfaces and Interiors of Planets and Satellites (ed., A. Dollfus). Academic Press, Inc. London and New York.

Houten, C. J. van, Houten-Groeneveld, I. van, and Gehrels, T. 1970, Minor Planets and Related Objects. V. The Density of Trojans Near Preceding Lagrangian Point. Astron. J. 75, 659.

Kiang, T. 1966, Bias-Free Statistics of Orbital Elements of Asteroids. Icarus 5, 437.

[2]See p. 206.

Page intentionally left blank

PROPER ELEMENTS, FAMILIES, AND BELT BOUNDARIES

J. G. WILLIAMS
Jet Propulsion Laboratory

Families of asteroids were first found by Hirayama (1918, 1923, 1928). More recently Brouwer (1951) and Arnold (1969) have extended greatly the number of families known from the cataloged asteroids. The Palomar-Leiden survey (PLS) (van Houten et al., 1970), which mainly covered very faint, uncataloged objects, found several more families.

Except for the work of Hirayama (1918), which used osculating elements, all of the above studies looked for clusterings of the semimajor axis a, the proper eccentricities e', and proper inclinations i'. The calculation of proper elements involves using a theory of secular perturbations to remove the long-period, large-amplitude disturbances of the major planets. The theory used up to now (Brouwer and van Woerkom, 1950; Brouwer and Clemence, 1961) involved a low-order expansion in the eccentricities and inclinations. There is now a theory available (Williams, 1969) that will accurately handle much higher eccentricities and inclinations than before.

I am now applying this new theory to calculate improved proper elements. The job is only partly completed, but several interesting results have emerged. These preliminary results are based upon reductions for asteroids with $a < 2.61$ AU.

The theory may be used to calculate the closest approach between a major planet and an asteroid. When this is done for Mars, it is found that the density of asteroids drops sharply when one crosses into the region where an asteroid can encounter Mars. This effect can be seen in figure 1 where a histogram of the number of asteroids per 0.02 AU interval of the closest distance of approach to Mars is given. A negative distance means that the asteroid can pass that distance within the orbit of Mars and is subject to close encounters and eventual removal from the solar system by planetary collision or ejection. The evolution of planetary crossers was first discussed by Öpik (1963). There is a tail in the distribution for small negative distances. As one approaches the Mars crossing boundary from the negative side, the number of times the secular perturbations caused the orbits to intersect during the age of the solar system becomes fewer. Objects with small negative distances have very long lifetimes. The inner boundary of the asteroid belt in a, e', sin i' space is determined by the Mars crossing boundary. It is an almost inescapable conclusion that the belt

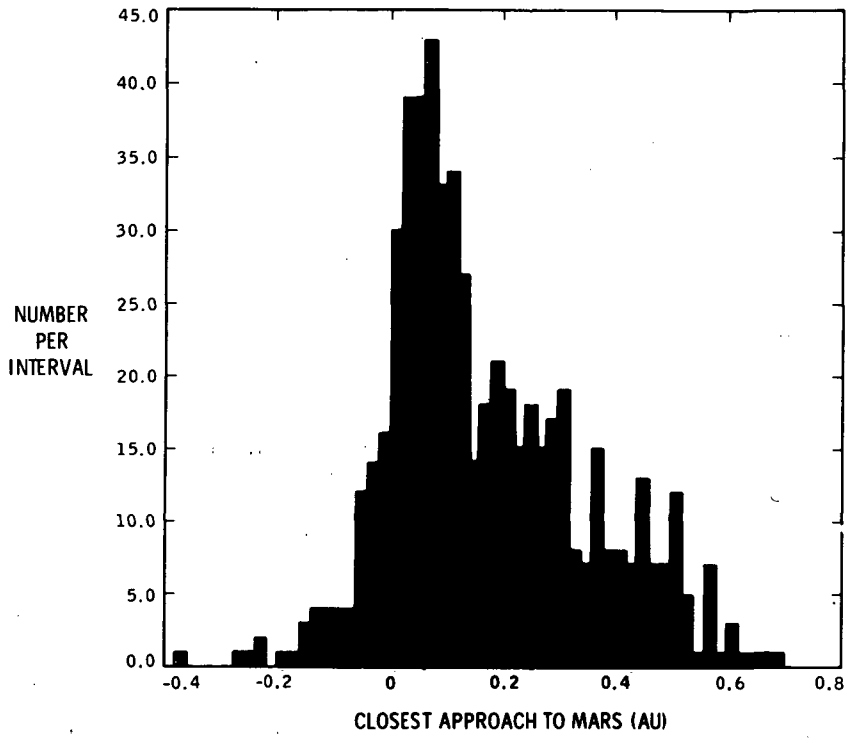

Figure 1.–Number of asteroids per 0.02 AU interval of the distance of closest approach to Mars. Negative distances are Mars crossers. Data are for belt asteroids with $a < 2.61$ AU.

once extended closer to the Sun and that only objects in stable or nearly stable orbits remain.

From the old theory it was known that there are strong resonances of the node rate $\dot{\Omega}$ and longitude of perihelion rate $\dot{\tilde{\omega}}$ at 1.94 and 2.03 AU, respectively, for $e' = i' = 0$. In the new theory these resonances form surfaces in a, e', sin i' space. It is found that there are very few asteroids in the vicinity of these resonance surfaces. In the vicinity of a resonance, the oscillations of e' and i' become very large and the Mars crossing boundary is pushed deeper into the belt. The resonances are not completely understood and it is not clear whether the displacement of the Mars crossing boundary is sufficient to explain all of the depopulation in the neighborhood of resonance surfaces.

Figure 2 shows a plot of proper sin i' against a for the cataloged asteroids that have been studied. Circles are used to denote Mars crossers. The high-inclination region at about 1.9 AU is the Hungaria region, and the one centered at 2.37 AU is the Phocaea region. The resonance that starts at 1.94 AU at $e' = i' = 0$ runs up between the Hungaria and Phocaea regions, whereas

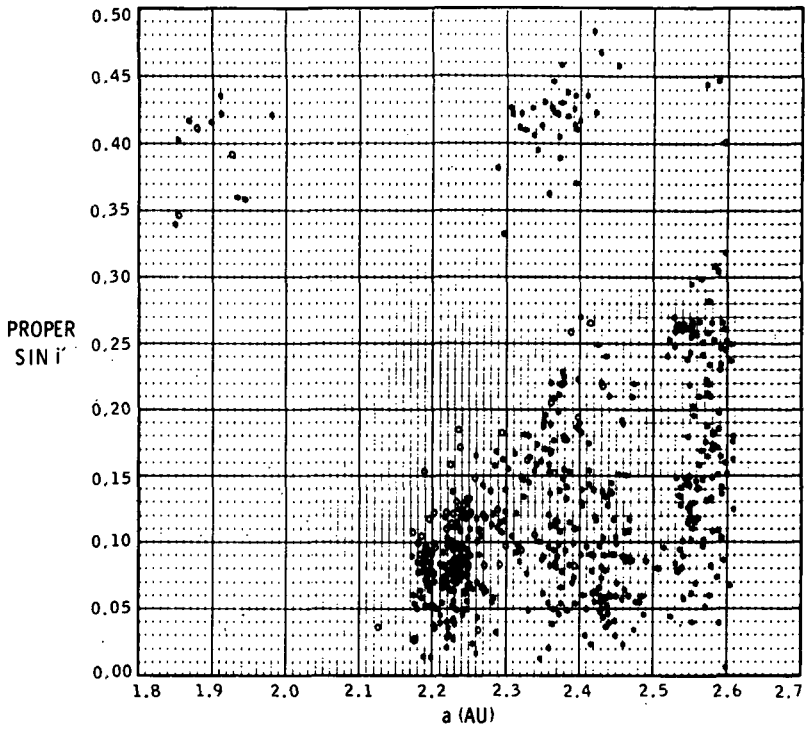

Figure 2.—Asteroid sin i' plotted against semimajor axes. Open circles are for objects that can encounter Mars during the age of the solar system. The two high-inclination regions are isolated from the main belt by secular resonances.

the one that starts at 2.03 AU runs between the Phocaea region and the main belt. A third strong resonance caps the belt off at about 30° inclination. The gap at 2.5 AU is the Kirkwood gap at the 3:1 commensurability with Jupiter. The Hungaria and Phocaea regions are not large families but segments of the belt isolated by resonances.[1] The former region contains one normal-sized family and the latter contains two.

Numerous families can be recognized in the data. Arnold's (1969) work is strongly confirmed. Many of the families are found to contain a relatively large object, and this large object is always at the edge of the family in a, e', sin i' space. These families with large objects would seem to be debris from a major cratering event on the large asteroid. The families without large objects presumably result from total disruption of the parent asteroid. The distinction between families with and without a large object is somewhat artificial. The two classes really merge. Of course, total disruption is the limiting case of

[1]See, however, p. 363 of PLS.

cratering. The above opinions obviously rely on the collision theory of the origin of asteroid families.

ACKNOWLEDGMENT

This work was one phase of research carried out at the Jet Propulsion Laboratory, California Institute of Technology, under Contract no. NAS 7-100, sponsored by the National Aeronautics and Space Administration.

REFERENCES

Arnold, J. R. 1969, Asteroid Families and Jet Streams. Astron. J. **74**, 1235-1242.

Brouwer, D. 1951, Secular Variations of the Orbital Elements of Minor Planets. Astron. J. **56**, 9-32.

Brouwer, D., and Clemence, G. M. 1961, Secular Perturbations. Methods of Celestial Mechanics, ch. 16, pp. 507-529. Academic Press, Inc. New York.

Brouwer, D., and van Woerkom, A. J. J. 1950, The Secular Variations of the Orbital Elements of the Principal Planets. Astron. Papers Amer. Ephemeris, vol. 13, pt. 2, pp. 85-107.

Hirayama, K. 1918, Groups of Asteroids Probably of Common Origin. Astron. J. **31**, 185-188.

Hirayama, K. 1923, Families of Asteroids. Jap. J. Astron. Geophys. **1**, 55-105.

Hirayama, K. 1928, Families of Asteroids. (Second Paper.) Jap. J. Astron. Geophys. **5**, 137-162.

Houten, C. J., van, Houten-Groeneveld, I. van, Herget, P., and Gehrels, T. 1970, Palomar-Leiden Survey of Faint Minor Planets. Astron. Astrophys. Suppl. Ser. **2**(5), 339-448.

Öpik, E. J. 1963, The Stray Bodies in the Solar System. Pt. 1. Survival of Cometary Nuclei and the Asteroids. Advances in Astronomy and Astrophysics, vol. 2, pp. 219-262. Academic Press, Inc. New York.

Williams, J. G. 1969, Secular Perturbations in the Solar System, pp. 1-270. Ph. D. Dissertation, UCLA.

DISCUSSION

MARSDEN: Does the 9:2 resonance with Jupiter (or 2:3 resonance with Mars) really have a decisive influence on the motions of the Hungaria asteroids?

WILLIAMS: These are only approximate commensurabilities and probably unimportant as far as the existence of these objects is concerned. Their mean motions spread over a large range, 1270 to 1410 arcsec/day, whereas the commensurabilities in question lie at 1346 and 1258 arcsec/day. The Jovian commensurability is of seventh order and should be very small, whereas Mars has such a small mass that it is hard for it to have a significant influence. Actually the Hungaria asteroids lie in a small island of stability between two of the secular resonances and the Mars crossing boundary. I think they demonstrate that the belt was once much larger but that Mars has swept out, by collisions and close approaches, the regions that are now empty.

BRATENAHL: The histogram of N versus a is remarkable in showing how sharply Mars defines the inner boundary of the asteroid belt. Do you have any estimate of the lifetime of Eros, and is that limited by an impact on Mars or on which planet?

WILLIAMS: The Mars crossers typically have lifetimes of 10^8 to 10^9 yr and may impact any of the terrestrial planets. If Eros could evolve into an Earth crosser through secular perturbations, then its lifetime might be an order of magnitude smaller.

ANONYMOUS: Can an explanation be given of the mechanism by which observational selection can give rise to an apparent jetstream?

WILLIAMS: I will give an example of a selection effect for the Flora family due to secular perturbations. These perturbations cause a bias in the eccentricities that has an approximately sinusoidal dependence on the longitude of perihelion and an amplitude of 0.05. This causes the average perihelion distance of 1.9 AU to have peak variations of ±0.1 AU. The objects with perihelia of 1.8 AU will be 0.7 mag brighter than those objects with perihelia of 2.0 AU, the two extremes being 180° apart in the sky. Because an asteroid is discovered in the vicinity of its perihelion, more small objects will be seen in the direction of the closer perihelia. Using the factor of 2.5 per mag for the differential number density from the PLS gives a factor of $2.5^{0.7} = 1.9$ in the ratio of the number of objects discovered at the two extremes. To be cataloged, an object must be seen at a minimum of three different oppositions. Because the discoveries at the different oppositions are usually independent of one another, the peak factor among cataloged objects will be $1.9^3 = 6.8$. Averaging the sinusoidal bias over a 180° range of longitude of perihelia, in the direction of the minimum perihelia, results in about four times as many cataloged objects as in the opposite half of the sky. Such a concentration would be considered to be evidence of a jetstream. There are also seasonal selection effects due to weather and altitude of the ecliptic.

The above is only an order of magnitude calculation, but it illustrates the severity of the selection effects among the cataloged asteroids fainter than mean opposition photographic magnitude 15.0.

Page intentionally left blank

THE PALOMAR-LEIDEN SURVEY

C. J. VAN HOUTEN
Sterrewacht te Leiden
Netherlands

The Palomar-Leiden survey (PLS) was set up as an extension to fainter magnitudes of the McDonald survey. The latter is, therefore, the more important survey as far as asteroid statistics are concerned. The main result of the PLS is that no clearcut differences exist between the fainter asteroids found in this survey and the numbered asteroids in the distribution functions of eccentricity, inclination, and semimajor axis and that the statistical relations found in the McDonald survey have a continuous extension in the PLS material. I would, therefore, propose not to summarize the results of the PLS, which would appear to be a tedious job, but to give here some new results that should properly have been included in the publication, but, for reasons of pressures to publish as soon as possible, were not.

AVERAGE DISTANCE TO THE ECLIPTIC PLANE AS A FUNCTION OF SEMIMAJOR AXIS

In the PLS a derivation is given of the density distribution perpendicular to the plane of the ecliptic, under the assumption that this distribution is independent of the distance to the Sun. Whether this was really the case was not checked. This is done here: the average value of $z_0 = a \sin i$ has been determined as a function of a, and this value is assumed to be proportional to the average distance of the asteroids to the plane of the ecliptic at a distance to the Sun equal to a. The results are given in table I and depicted in figure 1. It is seen that the assumption of constancy of $\overline{z_0}$ is wide off the mark; $\overline{z_0}$ varies approximately linearly with a, with the exception of a bulge near $a = 2.6$, which is caused by the new Io family. The value of z_0 at $a = 3.3$ is about four times as large as at $a = 2.2$.

This result shows that the average value of the orbital inclination is a function of the distance to the Sun, the nearby asteroids having, on the average, considerably smaller inclinations than those in the outer parts of the asteroid belt. It was checked that this is also the case for the numbered asteroids, so this result should not be new.

TABLE I.–$\overline{z_0}$ *Values for Various Sizes of the Semimajor Axis*

a	$\overline{z_0}$
2.15	0.14
2.25	.21
2.35	.22
2.45	.24
2.55	.42
2.65	.50
2.75	.38
2.85	.39
2.95	.46
3.05	.50
3.15	.60
3.25	.65

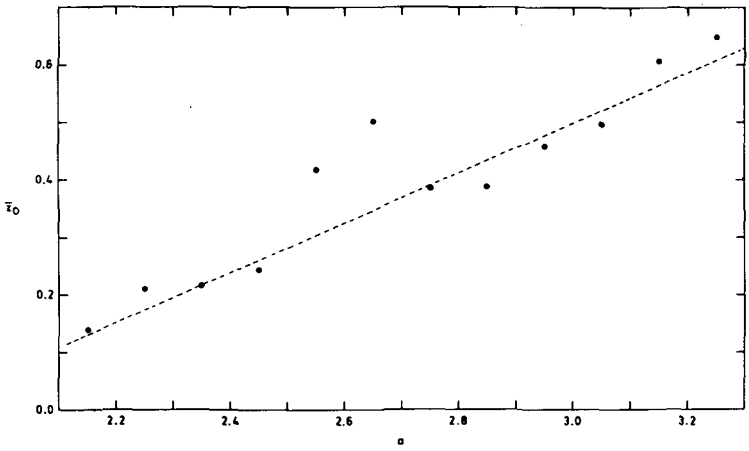

Figure 1.–$\overline{z_0} = \overline{a \sin i}$ as a function of a.

THE PHASE FUNCTION OF THE TROJANS

The average phase function of the *PLS* asteroids was shown to be of the form

$$F(\alpha) = 1.03T(\alpha) + 0.039|\alpha| - 0.05 \qquad (1)$$

in which $T(\alpha)$ is the opposition effect found for the brighter asteroids, α the phase angle, and $F(\alpha)$ is the brightness variation of the asteroid due to phase; it is zero at phase 4°.

In practice, the coefficient of $T(\alpha)$ was determined by only a limited number of asteroids that came close to the opposition point. Of these, the

Trojans played an important part; because of their slow motion and their large distance from the Sun, they were always observed at small phase angles. The maximum phase angle for a Trojan in the PLS is 6°.5. It follows that the Trojans contribute little to the linear part of the phase function, and heavily to the opposition effect. It is, therefore, surprising that most Trojans yielded negative residuals with respect to expression (1), as may be seen in table II. Here are listed the difference in brightness of the PLS Trojans in September and October 1960, due to phase, the corresponding values based on expression (1), and their difference, $O - C$.

TABLE II.—*Observed and Computed Phase Effect for PLS Trojans*

PLS no.	$(F_O - F_S)_{obs}$, mag	$(F_O - F_S)_{comp}$, mag	$O - C$, mag
2008	−0.02	0.14	−0.16
4139	−.02	.20	−.22
4523	+.20	.34	−.14
4572	+.18	.30	−.12
4596	+.46	.36	+.10
4655	+.20	.39	−.19
6020	+.31	.39	−.08
6540	+.44	.32	+.12
6541	+.43	.33	+.10
6581	+.27	.33	−.06
6591	+.28	.30	−.02
6629	+.44	.35	+.09
6844	−.19	.34	−.53

Apparently the phase function of the Trojans is flatter than that of the normal asteroids, which indicates a different surface structure. On the other hand, omission of the Trojans in the determination of the phase function will fairly certainly result in a larger value of the coefficient of $T(\alpha)$, so that both the opposition effect and the linear part of the phase function should be steeper for the PLS asteroids than for the numbered ones. This redetermination of $F(\alpha)$ for the PLS has not been made as yet.

DISCUSSION

KOWAL: On August 19 and 20, 1969, plates of the following lagrangian point of Saturn were taken at the Palomar 122 cm Schmidt telescope. The plates are 6.6° in diameter and were centered about 1°.5 north of the L_5 lagrangian point. No "Trojan" asteroids were found. It is estimated that any object brighter than about 19.5 mag would have been detected.

Because Gehrels (1957) has examined the *preceding* lagrangian point of Saturn with negative results, it can be stated with confidence that Saturn does not have any "Trojan" asteroids brighter than 19 mag.

DISCUSSION REFERENCE

Gehrels, T. 1957, Indiana Expedition to South Africa, April-June 1957. Astron. J. **62**, 244.

[*Editorial note: For further information regarding the PLS, see Kiang's paper, page 187; Kresák's paper, page 197; the "Discussion" following Dohnanyi's paper, page 292; and Lindblad's paper, page 337.*]

THE DISTRIBUTION OF ASTEROIDS IN THE DIRECTION PERPENDICULAR TO THE ECLIPTIC PLANE

T. KIANG
Dunsink Observatory
Ireland

For examining the steady-state distribution of asteroids in the direction perpendicular to the ecliptic plane (the z distribution), we shall assume all orbits to be circular. This assumption is incompatible with the north-south asymmetry found by Nairn (1965); but Kresak (1967) has shown that the asymmetry is caused by a combination of cosmic and human factors and is present only among fainter asteroids, $B(a, 0) > 16$, where the discovery is grossly incomplete. There is another perhaps even more cogent reason for using only the brighter asteroids: The easily understandable practice of confining asteroid hunting close to the ecliptic plane has meant that among the fainter objects, orbits with high inclinations are underrepresented (Kiang, 1966). Actually, in the range $14 < B(a, 0) < 15$ where, I estimate, the discovery is 95 percent complete, the sample of inclinations may already be somewhat biased in the same sense. One has to balance this risk, however, with the advantage of a much greater data size; and I shall use all the numbered asteroids with $B(a, 0) < 15$ as given in the 1962 *Ephemeris* volume (excluding 13 that are regarded as "lost").

A very welcome new set of data is provided by the Palomar-Leiden survey (PLS) (van Houten et al., 1970). In this case, important selection effects should and can easily be made. According to the authors (van Houten et al., 1970, p. 360), the area searched extends to a height of $5\overset{\circ}{.}9$ from the ecliptic. Consider all the orbits with the same radius a; for these, the search extends to a heliocentric latitude of $b = 5\overset{\circ}{.}9(a - 1)/a$. Although an orbit with inclination $i < b$ lies entirely within the latitudes $\pm b$, an orbit with $i > b$ has only the fraction

$$f_1 = f_1(i, a) = \frac{2}{\pi} \arcsin\left[\sin i \sin \frac{5\overset{\circ}{.}9(a - 1)}{a}\right] \qquad (1)$$

lying in the same range. Hence, as far as the shape of the distribution of i at a given a (in practice, within a small range Δa) is concerned, the correction factor is simply $1/f_1$. Expression (1) differs a little from expression (3) in the PLS paper (van Houten et al., 1970, p. 361), but appears to be more in line with the assumption of circular orbits.

Among numbered asteroids known at a given time, one always finds a positive correlation between a and i; this feature has been reported repeatedly, but the question whether this is due, at least in part, simply to the fact that Earth is inside the ring of asteroids has never been examined. Of course, even if the distribution of i is the same for all a, there will still be a systematic increase of the thickness of the system with increasing distance from the Sun. Here we shall concentrate on the z distribution at different intervals of a.

As may be seen from figure 1, the well-known Kirkwood gaps and other commensurability points divide the main belt ($2.0 < a < 3.8$) quite naturally into nine zones. These will be labeled zones 0 to 8 inclusive. The Hilda group, the Trojans, and the range $1.0 < a < 2.0$ will be labeled zones 9, T, and M (for Mars), respectively. Table I lists some statistics of the zones. The next-to-the-last column refers to the numbers of the largest asteroids ($B(1, 0) < 10$) found in the sample. These numbers are very likely to be complete, except the one in zone T. The last column gives the numbers of these objects per unit circle (in AU) of the ecliptic plane. These areal densities are only approximations to the average state of affairs at the corresponding distances from the Sun because of the strong radial asymmetry in the distribution in the ecliptic plane (Kresák, 1967). Because resonance effects obviously dominate the orbits and thus the

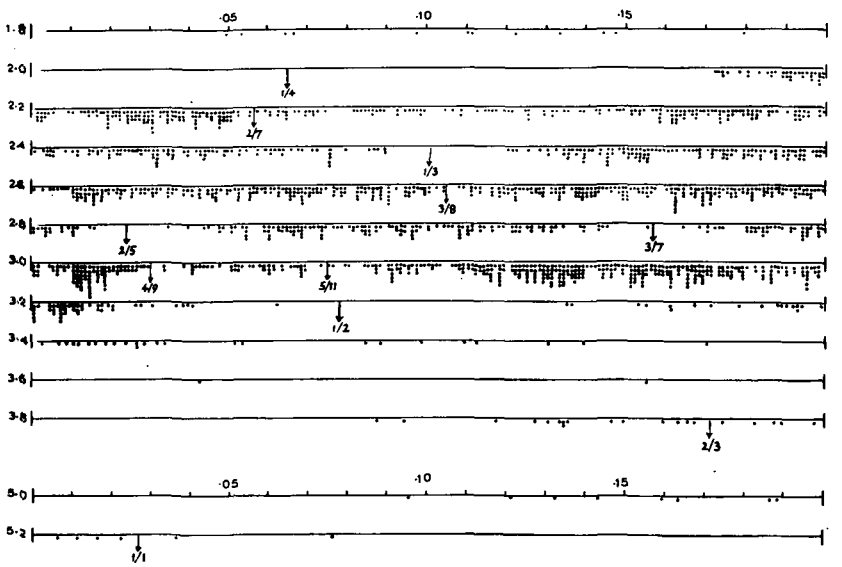

Figure 1.–Frequency distribution of semimajor axes of asteroids in intervals of 0.001 AU. Sample consists of the 1647 numbered asteroids given in the 1962 *Ephemeris* volume minus the 13 asteroids that are marked as "lost." The following five fall outside the diagram: 1566 Icarus, 1620 Geographos, 433 Eros, 279 Thule, and 944 Hidalgo with orbital radii a of 1.077, 1.244, 1.458, 4.282, and 5.794 AU, respectively. Commensurability points are marked with arrows, together with the ratios of periods (asteroid/Jupiter).

TABLE I.–*Division of the Ring of Asteroids Into 12 Zones*

Zone	Number of asteroids[a]	Observed limits, AU	Median a, AU	Median $B(a, 0) - B(1, 0)$	$B(1, 0) < 10$	
					Number	Number per unit circle of ecliptic plane
M	15	1.077 to 1.979	1.879	1.39	0	–
0	150	2.153 to 2.256	2.225	2.17	3	7
1	240	2.257 to 2.490	2.385	2.59	39	35
2	310	2.520 to 2.705	2.618	3.13	67	69
3	200	2.708 to 2.816	2.762	3.43	58	95
4	129	2.834 to 2.956	2.887	3.68	23	30
5	122	2.964 to 3.030	3.011	3.91	17	44
6	41	3.033 to 3.074	3.056	3.99	13	52
7	345	3.075 to 3.263	3.151	4.16	74	62
8	46	3.280 to 3.756	3.411	4.57	18	5
9	20	3.887 to 3.998	3.948	5.33	8	8
T	14	5.095 to 5.277	5.188	6.68	[b]11	[b]6
Total	1632	.....	.....	.....	331	.....

[a]Sample consists of all numbered asteroids given in the 1962 *Ephemeris* volume except 13 marked there as "lost," 279 Thule at $a = 4.282$ AU, and 944 Hidalgo at $a = 5.794$ AU.

[b]Multiply by 3.5 to correct for incompleteness of discovery.

spatial distribution of the Hilda and Trojan asteroids, and the asteroids in zone M are also rather special, the following discussion on the z distribution will be confined to zones 0 to 8 of the main belt.

The frequency distributions of i in zones 0 to 8 observed in the adopted sample of numbered asteroids are listed in table II. Let $n(\Delta i)$ be the number of objects in the interval Δi in a given zone; then the average number $n(\Delta b)$ of objects in an interval Δb of the heliocentric latitude, taken without regard to sign, in the same zone is calculated, in practice, according to the formula

$$n(\Delta b) = \sum_{\text{all } i} n(\Delta i) \cdot P(\Delta b, i) \tag{2}$$

where

$$P(\Delta b, i) = \Delta\left(\frac{2}{\pi} \arcsin \frac{\sin b}{\sin i}\right) \tag{3}$$

is the fraction of a circular orbit of inclination i that is included in the interval Δb. Now let $b_{0.5}$ and $b_{0.95}$ denote, respectively, the 50 percent point (the median) and the 95 percent point in the resulting b distribution; then the same percentage points in the corresponding z distribution are given by

$$z_{0.5} = a \sin b_{0.5} \tag{4}$$

$$z_{0.95} = a \sin b_{0.95} \tag{5}$$

In these expressions it is sufficiently accurate to set a equal to the appropriate median value shown in table I. The values $z_{0.5}$ and $z_{0.95}$ for each zone, together with their standard errors (s.e.), are listed in table II and are shown in figure 2 (the solid lines). Both show a steady increase with increasing distance from the Sun. Actually, $b_{0.5}$ and $b_{0.95}$ also show some increase with increasing a; but, of course, these increases are much less rapid and steady than the ones for $z_{0.5}$ and $z_{0.95}$.

We now examine the data of fainter asteroids provided by the PLS. The observed frequency distributions are listed in table III. They are corrected for the latitude cutoff as outlined above. The corrected individual frequencies are not shown; only their marginal totals S_1 are given. From the corrected i distribution in each zone except zone 8, which has too few objects for a proper determination, the values of $z_{0.5}$ and $z_{0.95}$ are derived as before; they are shown as broken lines in figure 2. Two effects are apparent: (1) The thickness of the system of fainter asteroids sampled by PLS also increases with increasing distance from the Sun, and (2) the thickness is noticeably less than that of the system of brighter asteroids at the same distance.

It should be remembered that the samples used here are, in one case strictly and in the other approximately, limited by $B(a, 0)$. If we note the actual differences between the solid and broken lines in figure 2 and the differences

TABLE II.–*Frequency Distribution of Inclinations and 50 and 95 Percent Points of z in Separate Zones*

[Data from numbered asteroids with $B(a, 0) < 15$]

i	i distributions for zones 0 to 8									Total
	0	1	2	3	4	5	6	7	8	
0° to 1°	2	1	–	2	–	1	–	3	–	9
1 to 2	2	5	3	2	5	–	1	5	1	24
2 to 3	2	8	8	5	5	1	–	10	1	40
3 to 4	3	9	7	6	5	1	2	10	1	44
4 to 5	4	7	7	9	3	2	–	7	3	42
5 to 7	15	21	27	17	6	6	3	8	2	105
7 to 9	5	18	16	24	6	7	5	21	1	103
9 to 11	–	19	15	27	9	16	2	19	4	111
11 to 13	–	5	28	8	9	7	3	13	1	74
13 to 15	–	5	18	15	8	6	1	16	2	71
15 to 19	–	4	20	15	9	3	10	28	3	92
19 to 23	–	3	2	4	2	2	–	14	7	34
23 to 27	–	7	5	5	2	1	–	8	1	29
27 to 35	–	–	4	1	–	1	–	–	–	6
Total	33	112	160	140	69	54	27	162	27	784
$z_{0.5}$	0.117	0.177	0.260	0.267	0.259	0.328	0.343	0.330	0.378	
s.e., ±	.025	.021	.024	.026	.048	.044	.074	.038	.117	
$z_{0.95}$	.269	.665	.770	.790	.802	.819	.894	1.007	1.235	
s.e., ±	.027	.114	.077	.081	.080	.122	.085	.095	.205	

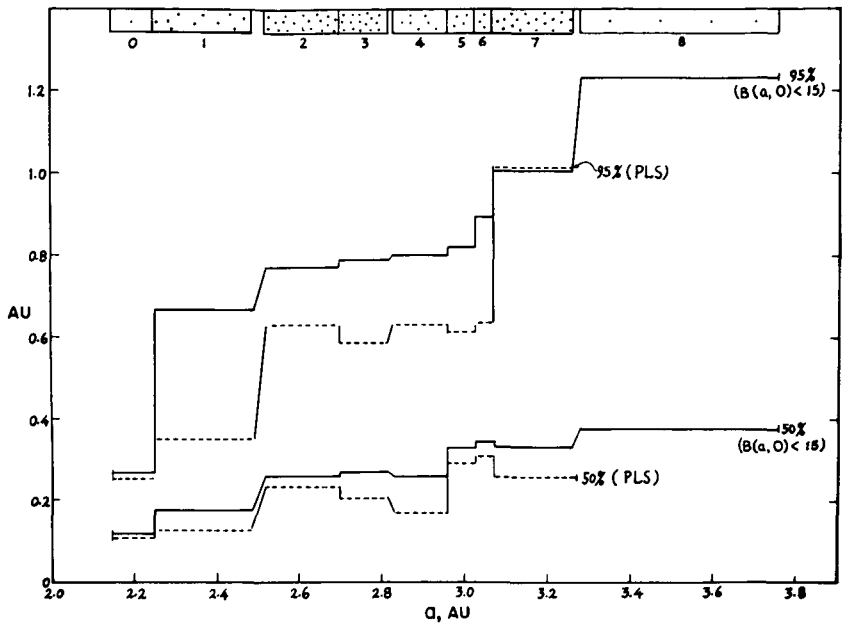

Figure 2.–The 50 and 95 percent points in the z distribution in nine intervals of the semimajor axis. Solid lines refer to numbered asteroids with $B(a, 0) < 15$, and broken lines to those found in the PLS. The "dominoes" along the top edge illustrate the areal densities of the largest asteroids given in the last column of table I.

$B(a, 0) - B(1, 0)$ listed in table I, we find that for a system of asteroids limited by constant $B(1, 0)$ (i.e., effectively down to certain physical size) there will be a rather reduced rate of increase in thickness with increasing distance. This, of course, assumes that effect (2) is real, which is by no means certain. The correction for the latitude cutoff is based on the value 5°.9 for the extension of the search area in PLS. Because vignetting is certainly present on the plates used in PLS, the effective extension may be less than 5°.9; thus the i distributions were undercorrected, leading to thickness estimates that are too low. This point should be examined in greater detail.

My conclusions are as follows:

(1) The thickness of the system of asteroids of the main belt increases steadily with increasing distance from the Sun. The 50 percent point in the z distribution increases from 0.12 at 2.2 to 0.38 at 3.5 (all values in AU), and the 95 percent point increases from 0.27 at 2.2 to 1.24 at 3.5.

(2) Less certainly, at a given distance from the Sun, the thickness is less for the system of smaller objects than for the system of larger ones.

These statements corroborate and amplify the conclusions on the proper inclinations reached earlier (Kiang, 1966).

TABLE III.—*Observed Frequency Distribution of Inclinations in Eight Zones*

[Data from class I orbits in the PLS]

i	i distributions for zones 0 to 8									S_0	S_1
	0	1	2	3	4	5	6	7	8		
0° to 1°	3	11	1	–	3	2	–	17	1	38	38
1 to 2	13	43	21	7	10	7	1	19	–	121	121
2 to 3	19	68	30	9	14	4	2	26	–	172	172
3 to 4	17	38	37	14	11	4	3	14	1	139	154
4 to 5	25	39	24	17	1	3	1	20	–	130	222
5 to 7	14	70	24	20	1	–	1	12	–	142	351
7 to 9	5	19	12	13	2	7	2	6	–	66	219
9 to 11	–	5	6	8	2	13	6	12	2	54	202
11 to 13	–	5	27	–	7	3	1	5	–	48	237
13 to 15	–	–	22	6	–	–	1	5	–	34	196
15 to 19	–	–	2	–	1	1	–	6	–	10	128
19 to 23	–	–	1	–	–	–	–	5	–	6	49
23 to 27	–	–	–	–	–	–	–	1	–	1	9
27 to 35	–	–	–	–	–	–	–	–	–	–	–
S_0	96	298	207	94	52	44	18	148	4	961	–
S_1	162	532	546	212	157	113	48	319	9	–	2098
$z_{0.5}$	0.105	0.124	0.237	0.206	0.171	0.291	0.307	0.259	–	–	–
$z_{0.95}$	.256	.351	.629	.585	.630	.611	.636	1.011	–	–	–

REFERENCES

Houten, C. J. van, Houten-Groeneveld, I. van, Herget, P., and Gehrels, T. 1970, Palomar-Leiden Survey of the Faint Minor Planets. Astron. Astrophys. Suppl. 2, 339-448.

Kiang, T. 1966, Bias-Free Statistics of Orbital Elements of Asteroids. Icarus 5, 437-449.

Kresák, L. 1967, The Asymmetry of the Asteroid Belt. Bull. Astron. Inst. Czech. 18, 27-36.

Nairn, F. 1965, Spatial Distribution of the Known Asteroids. Res. Inst. Rept. T-9, Astron. Sci. Center, Ill. Inst. Tech.

DISCUSSION

VAN HOUTEN (submitted after meeting): Formula (3) in the PLS is based on circular orbits. Kiang indeed found an error: ($a \cos i - 1$) should be ($a - 1$); fortunately, for most asteroids $\cos i \approx 1$.

Kiang's expression (1) should include the correction for the length of the arc traversed by the asteroid during the observation period, as explained in the PLS. The correct expression is

$$f_1 = \frac{2}{\pi}\left[\arcsin\left(a^{-1} \tan \frac{5°9}{a \sin i}\right) - \frac{1}{2}\Delta t n\right]$$

in which n is the mean daily motion of the asteroid and Δt the period over which the observations extend.

This additional correction term is only important for large inclinations, and therefore it is not certain how this influences the data derived by Kiang. For that reason a comparison is made in table D-I with my own results given in an earlier paper[1] in which $\bar{z}_0$ is given. This can be transformed into $\bar{z}$ by multiplication with a factor of 0.64. If the distribution of z is gaussian,

$$z_{0.5} = 0.84\bar{z} = 0.54\bar{z}_0$$

My values of $z_{0.5}$ were obtained by interpolation in table I of my paper.

It follows that no systematic difference exists between my values and those of Kiang for the first four zones; whereas for zones 5 through 8, Kiang's values appear about 6 percent too low. This difference is hardly meaningful.

Accordingly, Kiang's conclusion that the PLS asteroids are more concentrated toward the ecliptic than the numbered asteroids must be accepted as being correct. His tentative

TABLE D-I.–*Comparison of* $z_{0.5}$ *in the Eight Kiang Zones*

Kiang zone	van Houten, interpolated	Kiang	Difference
1	0.094	0.105	−0.011
2	.124	.124	.000
3	.248	.237	+.011
4	.205	.206	−.001
5	.226	.171	+.055
6	.258	.291	−.033
7	.270	.307	−.037
8	.329	.259	+.070

[1]See p. 183.

conclusion that vignetting effects may be the cause of this difference should be rejected on account of the small field effects of the Palomar 122 cm Schmidt plates. More likely the explanation should be sought in the remark made by Kiang (1966): "Large values of i are especially associated with values of the node around 90° . . . ." Because in the PLS the nodal values of the high-inclination asteroids cluster around 0° and 180°, it can be expected that the PLS material is deficient in minor planets with large inclination, which is in agreement with Kiang's conclusion.

DISCUSSION REFERENCE

Kiang, T. 1966, Bias-Free Statistics of Orbital Elements of Asteroids. Icarus 5, 437-449.

Page intentionally left blank

ORBITAL SELECTION EFFECTS IN THE PALOMAR-LEIDEN ASTEROID SURVEY

L. KRESÁK
Astronomical Institute of the Slovak Academy of Sciences
Bratislava, Czechoslovakia

The selection effects appearing in the list of minor planet orbits based on the Palomar-Leiden survey are discussed. In addition to purely geometrical effects produced by the limitation of the survey in time and position, the arrangement of orbits by perturbations plays an important role. Some apparent differences from the orbits of brighter asteroids can be easily explained. As an example of the operation of the selection effects, it is shown that the asteroidal jetstream believed to exist within the Nysa family is spurious.

The results of the Palomar-Leiden survey (PLS) (van Houten et al., 1970) will undoubtedly be, for years to come, the basic reference on the orbits of the faintest asteroids detectable by the present techniques. The PLS results provide an excellent counterpart to the list of numbered minor planets in the *Ephemeris* nearly as extensive and extended in the mass scale about three orders of magnitude lower. Although the accuracy of the orbits is insufficient for a recovery, it is quite satisfactory for statistical purposes. The only drawback is the inevitable limitation of the survey in time and position, which introduces selection effects rather different from those applying to the catalog of numbered asteroids. A correct appraisal of these effects is a prerequisite of any comparison of the two samples.

The important selection effect coming from the relation between absolute magnitude, mean distance, and mean opposition magnitude is common to both samples and will not be considered here. Selection effects special for PLS can be divided into two groups: those produced by the limitation of the survey in longitude (or time) and those produced by the limitation in latitude (or declination). Each of these consists of two components: one independent of the particular longitude interval covered by the survey and the other dependent on it.

In general, the former component produces primary effects, some of which have already been cited by the authors of the survey. Nevertheless, in some respects the latter component is also very significant, especially in the particular position of the survey areas chosen for PLS. The plates were taken, as in the previous McDonald survey, near the vernal equinox where a small

number of background stars makes the searches more efficient than in opposition areas of lower galactic latitude. By coincidence, this is at the same time the region of maximum clustering of asteroid perihelia due to the perturbational alinement of their lines of apsides to that of Jupiter. Moreover, the survey area is situated about midway between Jupiter's nodes on the ecliptic, approximately in the same longitude as the poles of the precessional motion of the orbital planes produced by secular perturbations. Plates centered on the ecliptic deviate here about 1° north from the great circle of the central plane of the asteroid belt. This deviation is not negligible compared with the 6° half-width of the strip covered by the survey.

In the following analysis of osculating elements, only first- and second-class orbits (1119 in number, $Q = 1$ and $Q = 2$ in table 7 of PLS) will be used. Where proper elements are introduced, the data are restricted to the first-class orbits only (967 asteroids of table 9 in PLS).

THE EFFECTS OF LIMITATION IN LONGITUDE

Because the detectability of an asteroid depends on its apparent brightness at the time of exposure, an immediate consequence of a time-limited survey is a preference for those asteroids that happen to be near their perihelia. This preference for mean anomalies near $M \cong 0°$, clearly borne out by the PLS catalog, should be reflected in the orbital elements as a maximum occurrence of the perihelion longitude $\pi \cong \lambda$, or about 0° to 30°, and a minimum at $\pi \cong \lambda + 180°$, or about 180° to 210°. The strength of this effect obviously depends on eccentricity e; it vanishes as e approaches zero.

The observed distribution of the perihelion longitudes of the PLS asteroids ($Q = 1$ and $Q = 2$) is shown in figure 1. The asymmetry is pronounced indeed, with about four times as many asteroids recorded near their perihelia as near their aphelia. As expected, the asymmetry decreases with decreasing eccentricity to a rather uniform distribution at $e < 0.10$. The only unexpected feature is the double maximum, with two lobes displaced about 30° to 40° on either side of the expected position. The reason for this duplicity is not quite clear. It may be noted that the errors in ω and π due to measuring errors would also tend to disperse π to both sides of $\pi = \lambda$ and $\pi = \lambda + 180°$. The importance of this effect should increase with decreasing e, in accordance with the edged outline of the distribution at $e < 0.15$. However, the angle of displacement appears too large for this interpretation as far as first- and second-class orbits are concerned.

The selection effect of a time-limited survey on perihelion longitudes can be eliminated if the actual plate limit (in apparent magnitude) is replaced by an artificial limit of mean opposition magnitude, up to which the search is essentially complete. Unfortunately, this considerably reduces the number of orbits available.

From figure 1(*b*) we see that asteroids with $m_0 > 19.0$ are those that contribute substantially to the asymmetry. Some traces of the effect remain

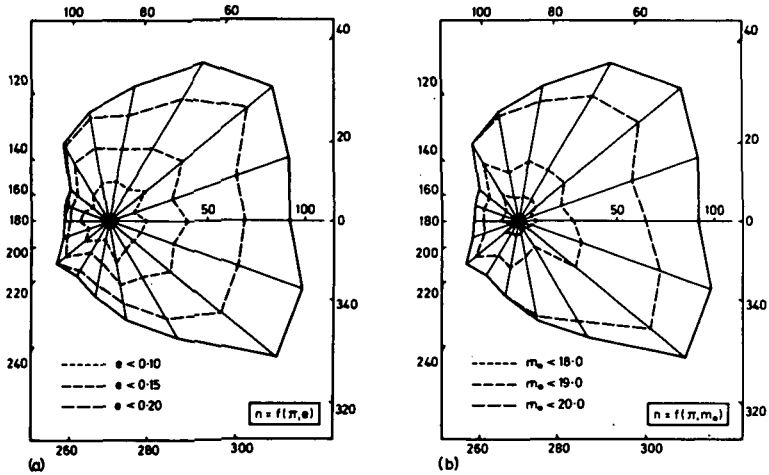

Figure 1.—Distribution of PLS asteroids in perihelion longitude π. (*a*) For different upper limits of eccentricity e. (*b*) For mean opposition magnitude m_0.

even at $m_0 < 19.0$. At $m_0 < 18.0$ some prevalence of $\pi \cong 90°$ over $\pi \cong 270°$ is indicated; however, the number of asteroids as bright as this is too small to justify any statistical conclusions.

One of the direct consequences of this selection effect is an apparent correlation between π and e, to be distinguished from the virtual correlation produced by the alinement of the lines of apsides by planetary perturbations. Orientation $\pi \cong \lambda$ prefers the detection of high-eccentricity orbits; orientation $\pi \cong \lambda + 180°$ prefers that of low-eccentricity ones. This effect is shown in figure 2, with characteristic values of eccentricities plotted in a polar diagram of perihelion longitudes.

The situation is complicated by the fact that the distribution in eccentricity is at the same time affected by the limitation of the survey in latitude. As already pointed out by van Houten et al. (1970), this limitation tends to eliminate the orbits of high inclinations, which are mostly associated with high eccentricities. On the other hand, the orbits closely alined to Jupiter's line of apsides, which are preferred in PLS by $\pi \cong \lambda$, are also generally above average in eccentricity. Thus the observed distribution of eccentricities in PLS is determined by the interplay of three fundamentally different effects; and without separating them one cannot compare the data with those on the numbered, brighter asteroids. One can only conclude that there is no evidence of any significant difference. At the level of median values, where the selection effects are not extraordinarily prominent, the resemblance of the two samples is very close: $e_{0.50} = 0.144$ for the numbered asteroids and $e_{0.50} = 0.147$ for the PLS. As we proceed to the high-eccentricity tail of the distribution, the elimination of the asteroids with high-eccentricity, high-inclination orbits by

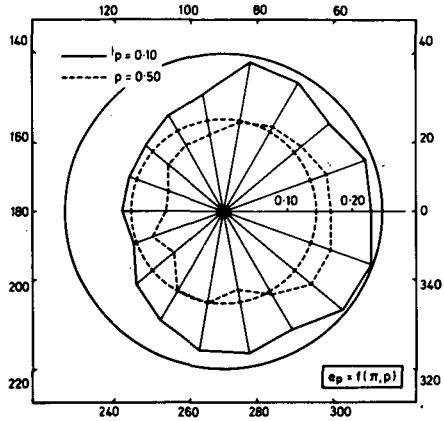

Figure 2.–Medians ($p = 0.50$) and limiting values of 10 percent occurrence ($p = 0.10$) of eccentricities of PLS asteroids plotted as a function of perihelion longitude π. The circles indicate comparative values obtained irrespectively of π from 1745 numbered asteroids.

the latitude effect becomes decisive and the proportion drops more rapidly in PLS than among the numbered asteroids. At the beginning of the 10 percent distribution tail, for which the values of $e_{0.10}$ are plotted in figure 2, the PLS data do not surpass the eccentricity $e_{0.10} = 0.247$ of the numbered asteroids even at $\pi = \lambda$.

The selection effects on the osculating perihelion longitude π obviously are reflected also in the corresponding proper element β, the difference between β and π being normally about 10°, and only rarely exceeding 30°. Thus the longitude limitation affects also the observed structure of the asteroid families in the β/γ plane.

As a result of the relationship between the proper elements and the osculating elements, a random distribution in β implies a prevalence of certain values of π. The resulting direction of maximum concentration of the osculating perihelia depends on the semimajor axis a. In the outer part of the asteroid belt a close alinement to Jupiter's line of apsides takes place. In the inner part, below $a = 2.64$, the deviation amounts to a few tens of degrees in the retrograde direction, but the maximum concentration is still not far from the PLS area. The elements π_0, e_0 corresponding to an orbit of zero proper eccentricity are given in table I for several values of a, which are medians from different asteroid samples. The sets of elements denoted "PLS" and "numbered asteroids" are composed of the median elements of each of these catalogs; the "center of the belt" is an ellipse passing through the median heliocentric distances of the 333 largest asteroids ($g < 10.0$) in different longitudes (Kresák, 1967). All asteroid families for which more than 20 members have been identified in PLS are included. The values of induced

TABLE I.–*Orbital Elements*

Asteroid samples	Elements						
	a	e	i	π_0	e_0	Ω_0	i_0
PLS	2.591	0.147	4°.15	350° ±	0.031±	92°	1°.03
Numbered asteroids	2.756	.144	8.40	6	.038	95	1.11
Center of the belt	2.850	.040	1.60	6	.037	96	1.15
Asteroid families (PLS):							
1 Themis	3.146	.163	1.87	9	.038	98	1.22
2 Eos	3.018	.073	9.50	8	.037	97	1.19
3 Coronis	2.885	.056	2.52	6	.037	96	1.16
6 Flora	2.231	.158	4.05	338	.048	57	.64
30 Vesta	2.311	.113	6.57	344	.042	75	.76
31 Michela	2.389	.187	1.42	349	.038	83	.86
32 Nysa	2.391	.187	2.41	349	.038	83	.86
33 Io	2.641	.182	12.76	0±	.035±	93	1.06
34 Medea	3.163	.135	4.62	9	.038	98	1.22

oscillations were interpolated from the table of Brouwer and Clemence (1961). The weighted means for the PLS asteroids are $\pi_0 = 354°$ and $e_0 = 0.038$.

It is evident that the degree of alinement to Jupiter's line of apsides is a function of the distribution in semimajor axes. The appreciable differences Δa and $\Delta\pi_0$ between PLS and the numbered asteroids may be due to a relative lack of faint asteroids at $a = 3.10$ to 3.20, as suggested by van Houten et al. (1970). However, the actual difference is likely to be smaller because the selection of faint asteroids near their perihelia is more efficient for smaller semimajor axes. On the other hand, the ecliptical longitude of the survey plates slightly favors asteroids of greater semimajor axes. Also the elimination of high-inclination objects by the limitation of PLS in latitude (to be discussed in the next section) may affect this difference, especially because of the tendency of asteroids to group into families with discrete values of proper inclination.

An important consequence of the radial asymmetry of the asteroid belt is that the distribution in geocentric distance of the asteroids located, and hence also the gain of the survey, varies with the ecliptical longitude covered. In the case of PLS, including Jupiter's perihelion, the conditions are optimum. The differences between the perihelion opposition magnitude m_P, the aphelion opposition magnitude m_A, and the mean opposition magnitude m_0 are expressed by

$$m_P - m_0 = 5 \log (1 - e) - 5 \log (a - 1) + 2.5 \log [1 + a^2(1 - e)^2 - 2a(1 - e)(1 - \sin^2 i \sin^2 \omega)^{1/2}] \quad (1)$$

$$m_A - m_0 = 5 \log (1 + e) - 5 \log (a - 1) + 2.5 \log [1 + a^2(1 + e)^2 - 2a(1 + e)(1 - \sin^2 i \sin^2 \omega)^{1/2}] \quad (2)$$

for statistical purposes we can insert $\sin^2 \omega = 0.5$.

Assuming the magnitude distribution found by van Houten et al. (1970),

$$\log N(m_0) = 0.39 m_0 + \text{const} \quad (3)$$

we can write the ratio ρ_1 of the number of asteroids observable at a perihelion opposition to that observable at an aphelion opposition as

$$\log \rho_1 = 0.39(m_A - m_P) \quad (4)$$

The actual relative numbers of asteroids detected in a survey will differ from this, both because of the Law of Areas maintaining the asteroids for a longer time in the remote part of their orbits and because of the variation of the effective field of view with distance. Neglecting the trailing effect, we have

$$\rho_2 = \frac{a - 1 - ea}{a - 1 + ea} \rho_1 \quad (5)$$

for the relative numbers of asteroids observable in the longitude of perihelion and aphelion, respectively, and

$$\rho_3 = \left(\frac{a - 1 - ea}{a - 1 + ea}\right)^2 \frac{1 + e}{1 - e} \rho_1 \tag{6}$$

for the relative gain in a survey restricted to a narrow strip along the ecliptic.

The values of $m_P - m_0$, $m_A - m_0$, ρ_1, ρ_2, and ρ_3 for selected types of orbits are listed in table II. The elements used for the computation are the same as in table I.

It must be emphasized that the validity of equation (4) for asteroid families is rather questionable; it appears probable that this distribution law holds only for the asteroidal "sporadic background." Nevertheless, in relatively narrow intervals of m_0 involved in the selection effects, it can be adopted as a rough approximation to show, at least, what bias in the observed structure of individual families can be expected.

The data of the third line of table II show the effect of opposition longitude on the total number of asteroids detected in PLS. If the alinement of the lines of apsides of faint asteroids is exactly the same as that of the bright ones, a repetition of the survey under equal conditions, but near the autumnal equinox instead of the vernal equinox, should reveal a total number of asteroids reduced by a factor of 1.26 (i.e., to 79 percent). Inversely, this repetition would yield decisive information on the actual degree of alinement, and would make it possible to determine the actual distribution of eccentricities from the differences in the relation between e and π (fig. 2) against that determined from PLS.

THE EFFECTS OF LIMITATION IN LATITUDE

The principal effects of this type, a strong preference for nodal longitudes $\Omega = \lambda \cong 0^\circ$ and $\Omega = \lambda + 180^\circ \cong 180^\circ$ and the elimination of orbits of higher inclination at other nodal longitudes, have already been pointed out by the authors of the PLS. The pronounced selection in Ω, as well as the gradual diminution of the effect with inclination approaching 0°, is clearly shown in figure 3(*a*). One important consequence that has not been considered is the transformation of this effect into the system of proper elements.

The poles of the precessional motion of most asteroidal orbits are inclined about 1° from the pole of the ecliptic in the direction north pole → vernal equinox → south pole → autumnal equinox. The weighted mean position of the plane perpendicular to this axis is defined by $\Omega = 88^\circ$ and $i_0 = 0^\circ.97$ for the PLS asteroids. The elements Ω_0, i_0 applying to different orbits, as determined from the median values of a using the table of Brouwer and Clemence (1961), are given in the last two columns of table I. The position of the nodes approximately 90° from the area of the PLS makes the data rather sensitive to this deviation. Although the distribution of osculating nodes Ω is essentially

TABLE II.—*Distribution Characteristics*

Asteroid samples	$m_P - m_0$	$m_A - m_0$	ρ_1	ρ_2	ρ_3
PLS	−0.94	0.77	4.61	2.83	2.34
Numbered asteroids	−.88	.74	4.29	2.71	2.29
Center of the belt	−.23	.22	1.49	1.32	1.26
Asteroid families (PLS):					
1 Themis	−.98	.79	4.92	3.02	2.58
2 Eos	−.40	.39	2.04	1.64	1.52
3 Coronis	−.32	.30	1.74	1.46	1.38
6 Flora	−1.10	.87	5.88	3.26	2.49
30 Vesta	−.73	.64	3.41	2.28	1.91
31 Michela	−1.29	.98	7.71	3.96	2.97
32 Nysa	−1.29	.98	7.70	3.95	2.96
33 Io	−1.15	.94	6.54	3.58	2.83
34 Medea	−.79	.67	3.72	2.49	2.19

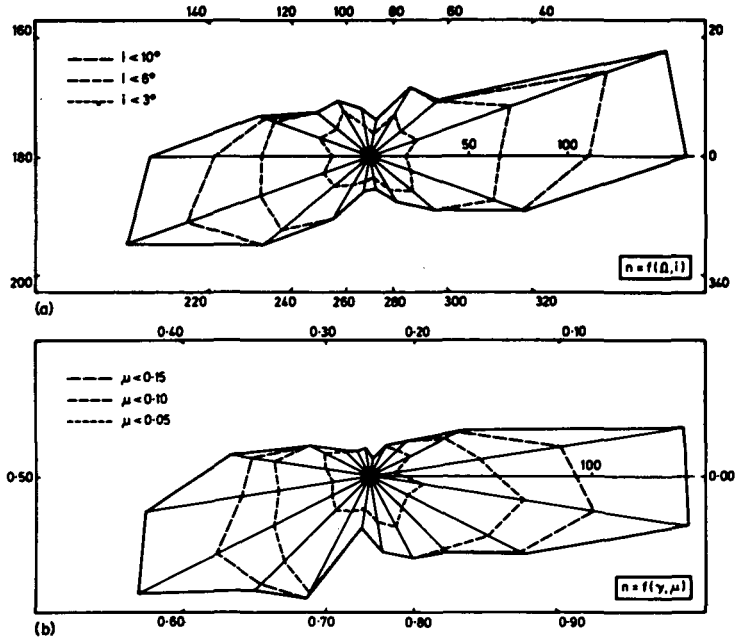

Figure 3.—Distribution of PLS asteroids. (*a*) In nodal longitude Ω for different upper limits of inclination i. (*b*) For the proper elements γ, μ.

symmetrical with respect to the ecliptical longitude of the survey area (fig. 3(*a*)), the distribution of proper nodes γ exhibits a displacement of the two maxima toward $\gamma = 0.75$. The first minimum near $\gamma = 0.25$ is considerably deeper (by a factor of 3) than the second minimum near $\gamma = 0.75$ (fig. 3(*b*)). In addition to the selection in the longitude of the proper perihelion, this effect can appreciably bias the observed structure of the asteroid families in the β/γ diagram, the occurrence of Brouwer's (1951) groups or Alfvén's (1969) jetstreams.

Although the distribution of the PLS asteroids in inclination is strongly affected by the limitation of the survey in declination, the median value of i being only one-half that found for the numbered asteroids (table I), some dependable information can be obtained even in this respect when selection effects are properly taken into account. It is obvious that the observed characteristic values of i (such as the median $i_{0.50}$ or the limit of the 10 percent occurrence tail $i_{0.10}$) should approach the correct value as Ω approaches, from both sides, $\Omega = \lambda$ and $\Omega = \lambda + 180°$. Because of the duration of the survey, which tended to eliminate objects of higher inclination from the first- and second-class sample (positions from two dark-of-the-Moon periods) even if they were located near their nodes, the correct value should not be reached even at $\Omega = \lambda$ and $\Omega = \lambda + 180°$. This is precisely what is shown in figure 4 where the whole polar diagrams of $i_{0.50}$ and $i_{0.10}$ lie within the

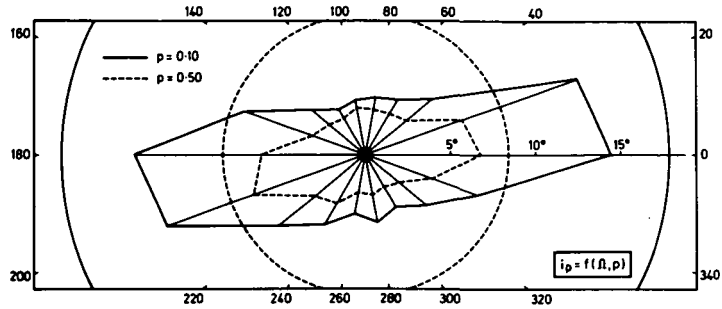

Figure 4.—Medians ($p = 0.50$) and limiting values of 10 percent occurrence ($p = 0.10$) of inclinations of PLS asteroids plotted as a function of nodal longitude Ω. The circles indicate comparative values obtained irrespectively of Ω from 1745 numbered asteroids.

circumference applying to the numbered asteroids, with a pronounced symmetry and extremes of about 80 percent of the latter. It is concluded that, with all probability, the actual distribution of faint asteroids in inclination does not differ at all from that of the bright objects.

The fact that the plane of greatest concentration of the asteroids, indicated by the proper elements, passed about 1° south of the center of the declination strip covered by the survey has some effect on the determination of the density gradient perpendicular to the central plane of the belt. However, because the displacement is only about one-tenth the distance at which the density drops to one-half, and the maximum is not very sharp (van Houten et al., 1970), this effect can be safely neglected in comparison with random sampling errors.

AN APPLICATION TO THE STRUCTURE OF ASTEROID FAMILIES

To illustrate the necessity of taking into account all the selection effects discussed here when the PLS data are used, we shall consider the existence of the asteroid jetstream within the Nysa family suggested by van Houten et al. (1970). This was the only jetstream detected in PLS. Having 77 members with first-class orbits, the Nysa family is the most abundant in the PLS data; it constitutes a twin system with the Michela family (26 members), differing only slightly in proper inclination. Van Houten et al. have found that a rectangle covering 22 percent of the β/γ diagram contains as much as 54 percent of the Nysa asteroids, and attribute this to the presence of a jetstream. In fact, the a priori probability of such a concentration in a random sample is less than one in a million. Nevertheless, it can be shown that the jetstream does not exist.

First, let us eliminate the longitude effect by constructing separate β/γ diagrams for different magnitude intervals. The result is shown in figure 5. We see that the concentration in β appears only with the incompleteness of the data ($m_0 > 19.0$) and becomes particularly prominent at $m_0 > 20.0$. This is

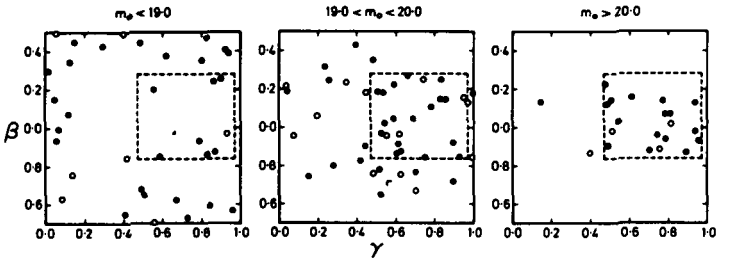

Figure 5.—The β/γ diagrams for the members of the twin asteroid family Nysa (black dots) and Michela (open circles). Dashed rectangles are the limits of the Nysa jetstream according to van Houten et al. (1970).

exactly the same selection effect as shown in figure 1. The excess around $\beta = 0$ is due to very faint asteroids that would be beyond the apparent magnitude threshold if they had not been moving near their perihelia in the area photographed.[1]

To explain all the irregularities, it remains to elucidate the relative avoidance of proper nodes at $0.2 < \gamma < 0.4$, appearing already at $m_0 < 19.0$. This effect is essentially identical with that shown in figure 3(*b*). The outer edges of the survey plates cut off the asteroids moving at a distance of more than 5°.9 from the ecliptic. The boundary can be represented in a polar diagram with coordinates Ω, i by parallel straight lines passing the pole ($i = 0$) at the distance ϑ in position angles $\Omega = \lambda + 90°$ and $\Omega = \lambda + 270°$. ϑ is given by

$$r \sin (5°.9 - \vartheta) = \sin 5°.9 \tag{7}$$

or, with a satisfactory approximation,

$$\vartheta = 5°.9\left(1 - \frac{1}{r}\right) \tag{8}$$

Inserting for r, in turn, the minimum perihelion distance $r = a(1 - e) = 1.81$, the median semimajor axis $r = a = 2.39$, and the maximum aphelion distance $r = a(1 + e) = 2.96$ of the Nysa family, we obtain the limits at which the selection effect begins to operate *A*, eliminates a majority of objects *B*, and eliminates all objects *C*. With regard to the selection in longitude (preference for $\pi \cong \lambda$), the effective limit that cuts off one-half of the asteroids passes somewhere between *A* and *B*.

---

[1]It has been shown elsewhere (Kresák, 1969) that a similar effect related to the alinement of the lines of apsides may produce spurious evidence of the existence of asteroidal jetstreams even among the numbered asteroids. As a matter of fact, all three jetstreams found by Alfvén (1969) within the Flora family have β near 0.

The Ω/i diagram for the Nysa and Michela families is plotted in figure 6. By the definition $\mu \simeq$ constant, the members of each family cluster on the circumference centered at the pole of precessional motion, which for $a = 2.39$ corresponds to $\Omega_0 = 83^\circ$ and $i_0 = 0^\circ.86$ (table I). The plate limits *A*, *B*, and *C* do not intersect the circumference of the Michela family, which is accordingly untouched by this selection effect. They also do not intersect the circumference of the Nysa family at $\Omega = \lambda + 270^\circ \simeq 280^\circ$ because of its eccentric position; but they do cut off a considerable part of it around $\Omega = \lambda + 90^\circ \simeq 100^\circ$. Transforming back to the proper element γ we find that the selection should have eliminated some members of the Nysa family at $0.15 < \gamma < 0.40$ (dotted part of the circle), with a loss exceeding 50 percent at $0.25 < \gamma < 0.30$. This is in excellent agreement with the position of the vertical gap in figure 5. Thus the observed structure of the Nysa family is fully explained and any indication of a jetstream disappears.

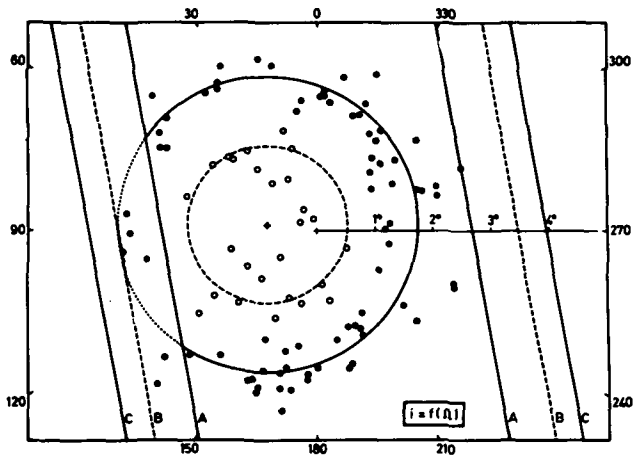

Figure 6.—Distribution of the members of the twin asteroid family Nysa (black dots) and Michela (open circles) in Ω and i. The center cross is the fundamental plane of the precessional motion of the orbits; the large circles are median values of proper inclination μ; the slanting lines are the mean limits of detection on PLS plates in perihelion *A*, at the mean heliocentric distance *B*, and in aphelion *C*.

Figure 6 also presents an interesting view on the relationships within the twin families Nysa and Michela. The latter is shown to fill rather uniformly, by the poles of the precessional motion, the circumference occupied by the former rather than to form another concentric ring. It is difficult to state whether there is also a similar outer halo composed of asteroids with higher proper inclinations because the selection effects of the PLS would have eliminated a great proportion of objects moving in such orbits.

REFERENCES

Alfvén, H. 1969, Asteroidal Jet Streams. Astrophys. Space Sci. 4, 84-102.

Brouwer, D. 1951, Secular Variations of the Orbital Elements of Minor Planets. Astron. J. 56, 9-32.

Brouwer, D., and Clemence, G. M. 1961, Methods of Celestial Mechanics, p. 527. Academic Press, Inc. New York.

Houten, C. J. van, Houten-Groeneveld, I. van, Herget, P., and Gehrels, T. 1970, Palomar-Leiden Survey of the Faint Minor Planets. Astron. Astrophys. Suppl. 2, 339-448.

Kresák, L. 1967, The Asymmetry of the Asteroid Belt. Bull. Astron. Inst. Czech. 18, 27-36.

Kresák, L. 1969, The Discrimination Between Cometary and Asteroidal Meteors. II. Orbits and Physical Characteristics. Bull. Astron. Inst. Czech. 20, 231.

DISCUSSION

VAN HOUTEN: Kresák argues that the number of asteroids found in the PLS is larger than the average value for a field of equal size along the ecliptic. This conclusion is based on a combination of the following points:

(1) There is a preferential orientation of asteroid perihelia in the direction of the perihelion of Jupiter's orbit.
(2) The PLS was taken in the direction of the perihelion of Jupiter's orbit.
(3) Asteroids are usually discovered near perihelion.

In his figure 1, Kresák shows that, indeed, there is a pronounced asymmetry in the distribution of perihelia for asteroids found in the PLS. This may give the impression that there is a large excess of PLS objects compared to those of the general field, supporting Kresák's conclusion mentioned above. But before this conclusion can be safely made, the PLS distribution of perihelia should be compared with that of the numbered asteroids. This comparison is shown in table D-I. The PLS material of 980 first-class orbits is compared with the data of Bauschinger (1901), who used the numbered minor planets 1 to 463, and Kiang (1966), who used 791 asteroids with $m_0 < 15$. The material is divided into four intervals; the first interval is centered on Jupiter's perihelion.

The results of Bauschinger and Kiang are practically identical; and they show that in the PLS there is a small excess, about 2 or 3 percent, of orbits oriented in the direction of Jupiter's perihelion. This excess is so small that it hardly influences the number statistics. Accordingly Kresák's result of a ratio of 1.26 of the asteroids near the vernal equinox compared to those near the autumnal equinox is far too large.

KRESÁK: A ratio of 1.26 of the two extremes corresponds to an excess of 12 percent in the direction of the PLS, and 10 to 11 percent in the first interval of table D-I, as

TABLE D-I.–*Comparison of the Distribution of Perihelia*

Intervals, $\omega + \Omega$	Distributions, percent		
	PLS	Bauschinger	Kiang
330° to 60°	40	38	38
60 to 150	23	24	24
150 to 240	11	14	15
240 to 330	26	24	23

compared with the average abundance along the ecliptic. Table D-I suggests a relative excess of 2/38 (i.e., 5 to 6 percent) in the first interval, and the differences in the ratios of the first to the third interval (3.6 for the PLS and 2.5 to 2.7 for the samples of numbered asteroids) appear rather significant. Thus the disagreement is not as bad as it appears to be at first glance. Moreover, the predicted ratio is based on the assumption that the actual degree of alinement is the same for bright and faint asteroids, which cannot be verified by a one-directional survey. The correlation between eccentricity and inclination, producing an additional latitudinal dispersion of asteroids in the direction of Jupiter's perihelion, might remove the remaining discrepancy. Anyway, a definitive solution of this complex problem can be obtained only from a comparison sample taken in the opposite direction.

DISCUSSION REFERENCES

Bauschinger, J. 1901, Tabellen zur Geschichte und Statistik der kleinen Planeten. Veröff. Königl. Astron. Recheninst. Berlin no. 16.

Kiang, T. 1966, Bias-Free Statistics of Orbital Elements of Asteroids. Icarus 5, 437-449.

PART II

ORIGIN OF ASTEROIDS
INTERRELATIONS WITH COMETS, METEORITES, AND METEORS

Page intentionally left blank

ASTEROIDAL THEORIES AND EXPERIMENTS

GUSTAF ARRHENIUS AND HANNES ALFVÉN
University of California, San Diego

Theories on the origin and evolution of asteroids are confronted with three types of experimental tests. The first refers to the dynamic state of the asteroids and consists of orbital and in some cases spin data for bodies as small as about 1 km. (There are reasons to assume that the size spectrum extends to very small objects but nothing is known about them.)

The second type consists of observations of the chemical and structural properties of objects fallen to Earth from space. Here the relationship to asteroids is much more tenuous. Nevertheless, the study of meteorites has provided important insight into the chemical evolution of small bodies in space. As long as one realizes that such data refer only to bodies of special structure, composition, velocity, and other orbital characteristics, they can be useful also for conjectures about asteroids.

The third source of information, also bearing indirectly on the structure and evolution of asteroids, is the lunar surface, which provides for the first time a display of the dynamic interaction between the surface of a celestial body and the space environment. To be applicable to the asteroidal environment, these results have to be scaled in a way that remains somewhat hypothetical.

BREAKUP AND ACCRETION IN THE ASTEROIDAL REGION

The mass in the asteroid region is small (fig. 1) and has not been collected into a small number of bodies as in the planetary regions. A similar situation seems to prevail in the satellite systems of Jupiter, Saturn (fig. 2), and Uranus, where analogous mass gaps are observed.

It is sometimes claimed that the present asteroid distribution has resulted from the explosion of one or a few larger bodies. Such an assumption meets with serious mechanical difficulties; some of these are examined below.

The distribution of particles in collectives such as the asteroidal and cometary jetstreams would appear to be a result of the two opposing processes of accretion and fragmentation. For reasons that are mainly historical, the emphasis has been placed mostly on the fragmentation process, which no doubt is important, but which alone cannot account for the observed distribution of bodies. One of the reasons for the biased interpretation is that

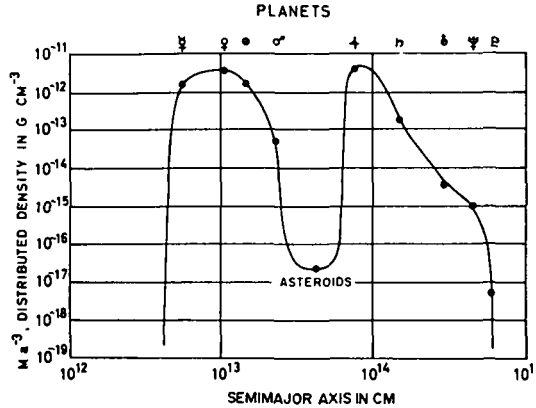

Figure 1.—Distributed density versus semimajor axis for the planets (from Alfvén and Arrhenius, 1970*a*).

for a long time we have seen the meteorites as direct evidence of breakup processes in space. In contrast, the processes responsible for accretion have been little known experimentally and theoretically until recently despite the realization that for larger bodies to break up, they must have first accreted.

Another reason for past emphasis of parent bodies of a size comparable to the Moon was the thought that high pressures and temperatures were needed to explain the phases observed in meteorites. These constraints may be largely relaxed as a result of recent experiments (Anders and Lipschutz, 1966; Arrhenius and Alfvén, 1971; Larimer, 1967; Larimer and Anders, 1967, 1970).

Until appropriate field and laboratory measurements on asteroidal properties can be made, appraisal of the rates of fragmentation and aggregation and their time evolution must be based on indirect evidence. Such evidence is provided primarily by distribution of asteroidal orbits, sizes, and spin states, and, in a more limited sense, by meteorites.

The observed distribution of spin periods (fig. 3) demonstrates the marked similarity in spin rate within a factor of 2 between most of those bodies in the

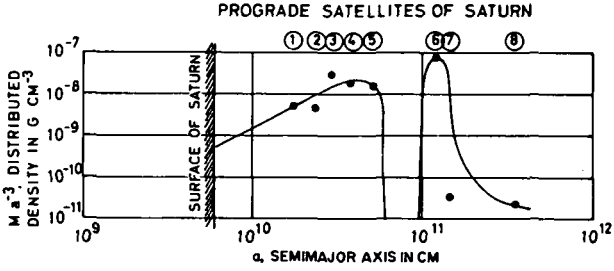

Figure 2.—Distributed density versus semimajor axis for the prograde satellites of Saturn.

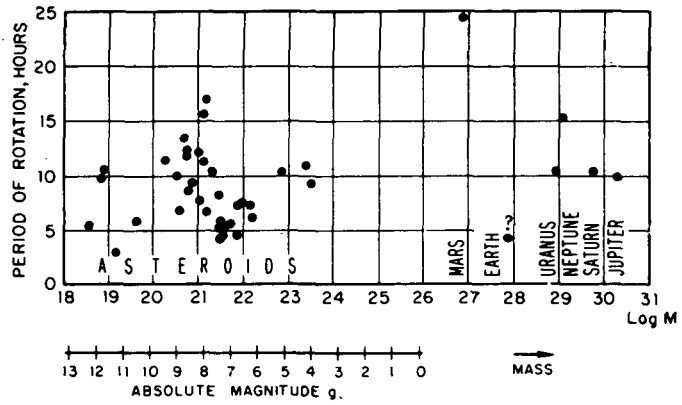

Figure 3.—Periods of axial rotation for the asteroids and some of the planets in relation to their masses (from Alfvén, 1964).

solar system that are unaffected by tidal braking. This isochronism of spin extends from small to large asteroids over the tidally undisturbed planets to the giant planets. If fragmentation played a major role after the accretion of the original bodies, one would expect to find, because of equipartition of rotational energy, a marked inverse dependence of spin period on size. This is obviously not the case despite the fact that observations extend over five orders of magnitude of mass. (Among the exceptions is the small asteroid Icarus with a spin period of only 2 hr; this high spin rate suggests that Icarus may be a fragment split off from a larger body.)

Another fact that is difficult to reconcile with extensive fragmentation in the upper range of presumed parent body sizes is that it becomes increasingly difficult to achieve a breakup by collision as the objects become larger. In the lunar size range, it would appear virtually impossible with the velocities allowed in the solar system.

ACCRETION PROCESSES

One reason why workers in the past concentrated on fragmentation and largely ignored accretion is that the nature of this latter process has remained enigmatic until recently. Electrostatic forces are effective at very small particle sizes (~10 cm) and small relative particle velocities (~10 cm/s), but rapidly become insignificant outside this range. Early in this century, it was also recognized that ices of various kinds could serve as bonding agents but only in a low-temperature regime such as outside the terrestrial planet region today.

For very large objects ($\sim 10^7$ cm) gravitational attraction is obviously the most important accretional force; however, it still remains a problem to account for the inception and continuation of growth of planetesimal embryos of such small size that the gravitational cross section is negligible.

Two recent developments may clarify this question. The first is the study of the focusing mechanism for gas and solid particles in asteroidal jetstreams (Alfvén, 1969, 1971; Baxter;[1] Danielsson;[2] Lindblad;[3] Trulsen[4]). This mechanism creates specific regions of high density and low relative velocities within the streams (Danielsson[2]) thus making net accretion possible.

The second is the recent exploration of the Moon. Consolidation of lunar particles appears to take place by three principal processes: (1) bonding by condensing silicate, sulfide, and metal vapor; (2) bonding by melts; and (3) shock lithification.

In the first process, impact vaporization gives rise to high-temperature gas clouds that form, upon condensation, filamentary bridging structures and surface deposits, cementing together particles originally loosely attached (figs. 4 and 5) and increasing the geometric capture cross section of individual grains (Asunmaa et al., 1970). Such silicate, sulfide, and metal vapor condensates are widespread on the lunar surface. The actual process of generation of a local plasma cloud by impact was recorded by the Apollo 12 suprathermal ion detector and the solar-wind spectrometer (Freeman et al., 1971; Snyder et al., 1971). This mechanism could be of major significance in the accretion of individual grains and grain clusters into larger embryos because the equipartition of motion between grains in space by collision would probably lead to recycling of much of the mass through the vapor state.

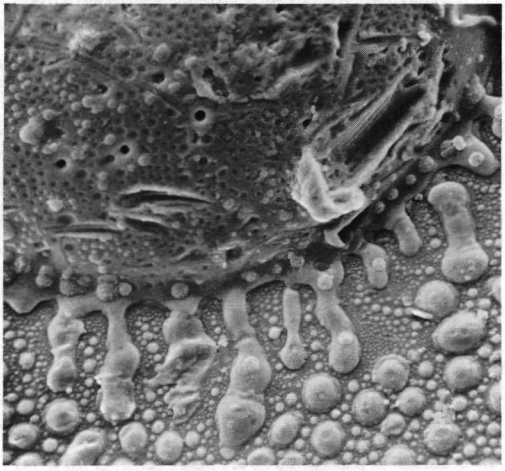

Figure 4.–Vapor condensate associated with deposition of glass splash on rock 12017. Original magnification: X 5000.

---

[1]See p. 319.
[2]See p. 353.
[3]See p. 337.
[4]See p. 327.

Figure 5.–Filament structures, presumably vapor deposits, bonding lunar particles to substrate crystal surface. Scanning electron micrograph taken at a magnification of X 10 000 (from Asunmaa et al., 1970).

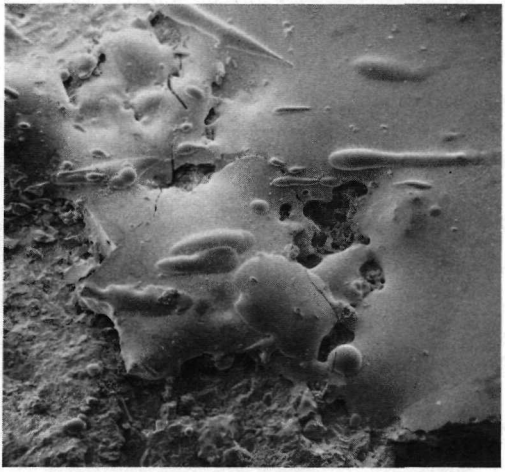

Figure 6.–Glass splash over friable breccia (rock 12017) from Oceanus Procellarum. Scanning electron micrograph taken at a magnification of X 50.

In the second process, certain types of impact generate silicate melts that splash over or permeate through loosely coherent material and cement it together. The resulting glass-bonded breccias and splash coatings are common in Oceanus Procellarum (fig. 6) and in Mare Tranquillitatis. (See also Morgan et al., 1971.)

In the third process, impact shock transforms loosely aggregated particles into cohesive clods that can attain large dimensions; e.g., the aggregates of boulder size found strewn over the Fra Mauro area (fig. 7).

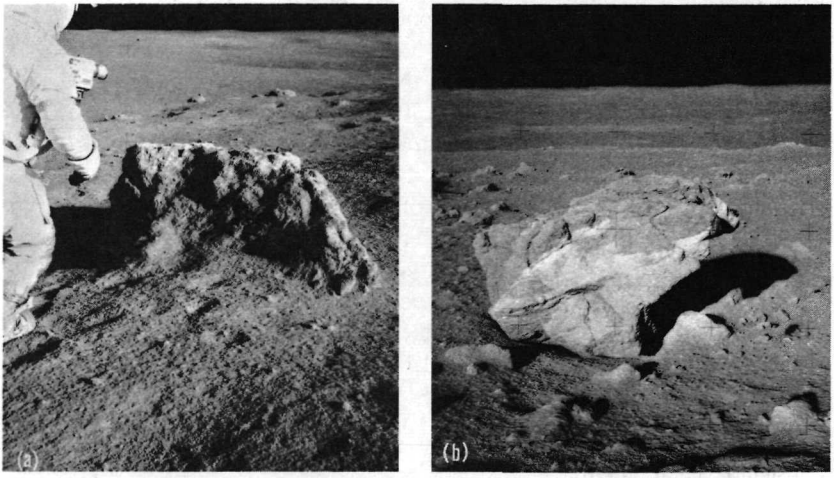

Figure 7.–Compacted aggregates of fine grained material at the Fra Mauro landing site. (a) NASA photograph AS14-68-9414. *(b)* NASA photograph AS14-68-9448.

The latter two mechanisms, of which the last is also recognized in meteorites, serve to compact material already aggregated. They could also be important in consolidating and compacting embryos already accreted but presumably would not assist in the accretion of single grains into clusters.

METEORITE PARENT ENVIRONMENT COMPARED TO LUNAR ENVIRONMENT

Observations of the lunar surface provided a first insight into the processes that modify solids exposed to the space environment. Qualitative similarities can be seen between the products of lunar surface processes and certain components of meteorites. It is possible that similar relationships may exist with the asteroids. In this context, the differences between lunar and meteoritic components are as important as the similarities because these differences give some indication of the scaling of properties between the lunar environment and the yet largely unknown environments where comets and asteroids were born.

Consolidation Processes

On the Moon, the melt-splash process is very extensive in some regions of the lunar regolith but in meteorites it appears to be very rare.

Chondrules

In the most common type of meteorites, the chondrites, chondrules are a major component. They have been interpreted as solidified molten droplets or

vapor condensates. On the Moon, chondrulelike objects occur but they are relatively rare. To explain the striking difference in abundance, Whipple[5] has suggested a sorting mechanism acting in the meteorite parent environment.

Those lunar glass bodies that are formed with free surfaces range in geometry from perfect spheres to teardrops, dumbbells, and rods. Analysis of physical and chemical characteristics of these bodies (Isard, 1971) suggests that they were formed by breakup in flight of thin jets of impact-melted glass from the lunar surface. In contrast, meteorite chondrules practically always occur as spheroidal shapes of varying complexity. Hence it would seem that there are considerable differences in the formation of flight-cooled impact glass on the Moon on one hand and chondrules in the precursor environment of meteorites on the other. It is difficult to explain these differences on the basis of gravitational or compositional effects.

Generation and Crystallization of Melts

The lunar igneous rocks were found by numerous investigators to show textural and chemical similarities to a specific type of meteorite, the basaltic achondrites. (See, for example, Arrhenius et al., 1970; Duke et al., 1970; Reid et al., 1970). However, these two types of objects have a distinctly different oxygen isotope composition (Taylor and Epstein, 1970) suggesting their origin in different environments.

Surface Irradiation

The frequently occurring grains in gas-rich meteorites that have been exposed to corpuscular irradiation in the range up to a few MeV, almost without exception show an all-sided exposure to this radiation (Lal and Rajan, 1969; Pellas et al., 1969; Wilkening et al., 1971). This has been interpreted by the discoverers of the phenomenon to be a result of exposure of the particles while they were freely suspended during the early stages of accretion. In contrast, such all-sided exposure is less common in the lunar regolith where a considerable fraction of particles, exposed to solar flare irradiation on the lunar surface, appear to have been irradiated mainly from one side before they were shielded by burial or a cohesive coating of fine dust.

One of the reasons for the occurrence of one-sided exposure of grains found on the lunar surface could be (Crozaz et al., 1970) that some of these grains received their irradiation while still part of exposed rock surfaces; the irradiated surfaces of these rocks subsequently would have disintegrated and the particles would have been transferred into the soil where shielding by material of the order of 10 to 30 μm thickness is sufficient to prevent further development of steep, high-density track gradients. The lack of the one-sided irradiation features in the achondrite crystals would then lead to the conclusion that in the parent environment of gas-rich achondrites, cohesive

---

[5]See p. 251.

rocks did not serve as a source of surface-exposed grains and hence probably were not present. To the extent that asteroids were formed in a way similar to these meteorite parent bodies, and provided that the mechanism proposed by Crozaz et al. is quantitatively important, similar conclusions would apply to the asteroidal precursor environment.

Another characteristic feature of the meteorite grains with direct surface exposure to corpuscular radiation is the gentleness of the process that has brought the grains together without destroying their highly irradiated surface skin (Wilkening et al., 1971), whereas other grains and aggregates in the same meteorite bear clear evidence of shock (Fredriksson and Keil, 1963; Wilkening et al., 1971).

At the time of the discovery of the skin implantation of low-energy cosmic-ray particles in grains now located in gas-rich achondrites (Eberhardt et al., 1965; Wänke, 1965), the isotropic distribution of impinging atoms, revealed by track techniques, was not known. Nor was the inhibited turnover behavior of aggregated particles in space yet known; this became evident only as a result of the lunar exploration (cf. the following section). Nonetheless, the perceptive suggestion was already at this stage made by Suess et al. (1964) that the irradiation took place while the individual particles were floating free in space, before their accretion into meteorite parent bodies. Lacking more direct evidence for this, and under the influence of the planetocentric reasoning of the time, the implantation process was relegated to surfaces of large bodies in most subsequent discussions.

The recent discovery of Lal and Rajan (1969) and of Pellas et al. (1969) returned the attention to the interesting alternative that the isotropic irradiation dates back to the largely unknown freeflight particle stage, preceding or concurrent with accretion. This interpretation avoids the difficulties associated with shielding at turnover of an accreted aggregate and is mechanically understandable in terms of theory and observation of particle streams in space (Alfvén, 1969, 1971; Alfvén and Arrhenius, 1970*a,b*; Danielsson;[6] Lindblad;[7] Trulsen[8]). It must be remembered, however, that predictions from meteorites and lunar sediments constitute extrapolations, and the lesson drawn from the Moon suggests caution in the reliance on prediction in complex natural systems. Meteorites cannot be expected to furnish well-defined information on surface-related problems because the critical interface between the parent body and space, even if it were represented and preserved in the fragments that are captured by Earth, is destroyed at the passage through the atmosphere. Hence, actual samples collected in a controlled fashion on asteroids and comets and returned to Earth would be of unique value for the reconstruction of their surface evolution and of the preaccretive history of the materials.

---

[6]See p. 353.
[7]See p. 337.
[8]See p. 327.

SURFACE PROPERTIES AND SOURCE MATERIALS OF ASTEROIDS

The question of the physical behavior of fine grained particle aggregates in space is crucial for reconstructing the accumulation of primordial grains into planetesimal embryos and, until direct studies are possible, for postulating the conditions on the surface of the asteroids. In the time preceding lunar exploration, widely divergent estimates were made, ranging from vacuum welding of solid particles into a crunchy aggregate, to dispersion of particles by repulsive electrostatic forces into highly mobile, fluffy dust. Actual observations on the Moon have provided the first factual information and show that finely divided dielectric materials exposed to the space environment form a relatively dense, cohesive aggregate but without perceptible cold contact welding.

This marked cohesion is probably the reason why, as discussed above, lunar soil particles do not appear to turn around freely in the exposed surface monolayer of grains and that, as a result, surface grains with isotropically irradiated skins are in the minority on the Moon. Because this effect would appear to be independent of gravitation, a similar situation is likely to prevail on the surfaces of asteroids, regardless of their size.

IMPORTANCE OF FIELD RELATIONSHIPS

The materials that make up the asteroids and comets may be found, wholly or in part, to be similar to those that we already know from meteorites. It has been suggested (Anders[9]) that such an identification would be an embarrassment to the exploration effort. On the contrary, this would make it possible for us to apply the large body of experience in meteoritics to the problems of primordial solar system history in a more realistic fashion than is possible at the present time.

The critical information to be obtained from asteroid missions concerns not only the materials from which the objects are constructed. The explorations of Earth and the Moon have demonstrated that it is equally or more important to establish also the field relationships of these materials and the physical properties of the whole body. Only controlled probing and sampling of the asteroids will make it possible to seriously approach the problems of the original mechanism and timing of accretion, the relative role of breakup, the sequence of formation of material units, the possible effects of differentiation before and after accretion, the internal and surface structure of the bodies, and their record of the history of the asteroidal and Martian region, the Earth-Moon system, and the Sun.

ACKNOWLEDGMENTS

The authors are grateful to the participants in the discussions at the Twelfth Colloquium of the International Astronomical Union in Tucson, Ariz., and for

[9]See p. 479.

further valuable criticism and comments from S. K. Asunmaa, A. Brecher, J. Z. Frazer, K. Fredriksson, D. Lal, D. Macdougall, and M. and J. Sinkankas.

Generous support from NASA is gratefully acknowledged.

REFERENCES

Alfvén, H. 1964, On the Formation of Celestial Bodies. Icarus **3**, 57.

Alfvén, H. 1969, Asteroidal Jet Streams. Astrophys. Space Sci. **4**, 84.

Alfvén, H. 1971, Apples in a Spacecraft. Science **173**, 522-525. An abbreviated version is in this book on p. 315.

Alfvén, H., and Arrhenius, G. 1970*a*, Structure and Evolutionary History of the Solar System, I. Astrophys. Space Sci. **8**, 338.

Alfvén, H., and Arrhenius, G. 1970*b*, Origin and Evolution of the Solar System, II. Astrophys. Space Sci. **9**, 3.

Anders, E., and Lipschutz, M. E. 1966, Critique of paper by N. L. Carter and G. C. Kennedy, Origin of Diamonds in the Canyon Diablo and Novo Urei Meteorites. J. Geophys. Res. **71**, 643.

Arrhenius, G., and Alfvén, H. 1971, Fractionation and Condensation in Space. Earth Planet. Sci. Lett. **10**, 253.

Arrhenius, G., Asunmaa, S., Drever, J. I., Everson, J., Fitzgerald, R. W., Frazer, J. Z., Fujita, H., Hanor, J. S., Lal, D., Liang, S. S., Macdougall, D., Reid, A. M., Sinkankas, J., and Wilkening, L. 1970, Phase Chemistry, Structure and Radiation Effects in Lunar Samples. Science **167**, 659.

Asunmaa, S. K., Liang, S. S., and Arrhenius, G. 1970, Primordial Accretion; Inferences From the Lunar Surface. Proc. Apollo 11 Lunar Sci. Conf. Geochim. Cosmochim. Acta **34**, suppl. **1**, vol. 3.

Crozaz, G., Haack, U., Hair, M., Maurette, M., Walker, R., and Woolum, D. 1970, Nuclear Track Studies of Ancient Solar Radiations and Dynamic Lunar Surface Processes. Proc. Apollo 11 Lunar Sci. Conf. Geochim. Cosmochim. Acta **34**, suppl. **1**, vol. 3, p. 2051.

Duke, M. B., Woo, C. C., Sellers, G. A., Bird, M. L., and Finkelman, R. B. 1970, Genesis of Lunar Soil at Tranquillity Base. Proc. Apollo 11 Lunar Sci. Conf. Geochim. Cosmochim. Acta **34**, suppl. **1**, vol. 1, p. 347.

Eberhardt, P., Geiss, J., and Grögler, N. 1965, Über die Verteilung der Uredelgase im Meteoriten Khor Temiki. Tschermak's Mineral. Petrogr. Mitt. **10**, 535.

Fredriksson, K., and Keil, K. 1963, The Light-Dark Structure in the Pantar and Kapoeta Stone Meteorites. Geochim. Cosmochim. Acta **27**, 717.

Freeman, J. W., Hills, H. K., and Fenner, M. A. 1971, Some Results From the Apollo XII Suprathermal Ion Detector. Proc. Apollo 12 Lunar Sci. Conf. Geochim. Cosmochim. Acta, to be published.

Isard, J. O. 1971, The Formation of Spherical Glass Particles on the Lunar Surface. Proc. Apollo 12 Lunar Sci. Conf. Geochim. Cosmochim. Acta, to be published.

Lal, D., and Rajan, R. S. 1969, Observations on Space Irradiation of Individual Crystals of Gas-Rich Meteorites. Nature **223**, 269.

Larimer, J. W. 1967, Chemical Fractionation in Meteorites–I. Condensation of the Elements. Geochim. Cosmochim. Acta **31**, 1215.

Larimer, J. W., and Anders, E. 1967, Chemical Fractionation in Meteorites–II. Abundance Patterns and Their Interpretation. Geochim. Cosmochim. Acta **31**, 1239.

Larimer, J. W., and Anders, E. 1970, Chemical Fractionation in Meteorites–III. Major Element Fractionations in Chondrites. Geochim. Cosmochim. Acta **34**, 367.

Morgan, J. W., Laul, J. C., Ganapathy, R., and Anders, E. 1971, Glazed Lunar Rocks: Origin by Impact. Science **172**, 556.

Pellas, P., Poupeau, G., Lorin, J. C., Reeves, H., and Audouze, J. 1969, Primitive Low-Energy Particle Irradiation of Meteoritic Crystals. Nature **223**, 272.

Reid, A. M., Frazer, J. Z., Fujita, H., and Everson, J. E. 1970, Apollo 11 Samples: Major Mineral Chemistry. Proc. Apollo 11 Lunar Sci. Conf. Geochim. Cosmochim. Acta **34**, suppl. **1**, vol. 1.

Snyder, C. W., Clay, D. R., and Neugebauer, M. 1971, An Impact-Generated Plasma Cloud on the Moon. Proc. Apollo 12 Lunar Sci. Conf. Geochim. Cosmochim. Acta **35**, suppl. **1**.

Suess, H. E., Wänke, H., and Wlotzka, F. 1964, On the Origin of Gas-Rich Meteorites. Geochim. Cosmochim. Acta **28**, 595.

Taylor, H. P., Jr., and Epstein, S. 1970, O^{18}/O^{16} Ratios of Apollo 11 Lunar Rocks and Minerals. Proc. Apollo 11 Lunar Sci. Conf. Geochim. Cosmochim. Acta **34**, suppl. **1**, vol. 2, p. 1613.

Wänke, H. 1965, Der Sonnenwind als Quelle der Uredelgase in Steinmeteoriten. Z. Naturforsch. A **20**, 946.

Wilkening, L., Lal, D., and Reid, A. M. 1971, The Evolution of the Kapoeta Howardite Based on Fossil Track Studies. Earth Planet. Sci. Lett. **10**, 334.

Page intentionally left blank

ON THE FORMATION OF THE ASTEROIDS

J. G. HILLS
University of Michigan

Recently Anders (1965) has shown that the smaller asteroids are over-abundant relative to their initial numbers because of the collisional fragmentation of larger asteroids. Allowing for this fragmentation, he has derived a reconstructed initial radius distribution. Although the reconstructed distribution only comprises a little more than 100 asteroids and consequently has a large statistical uncertainty as well as the uncertainty introduced by the reconstruction process, Anders finds that when displayed on a log-log plot, the distribution can be represented fairly well by a gaussian curve with a peak near radius $R = 30$ km. This work has basically been substantiated by Hartmann and Hartmann (1968), although Hartmann (1968) notes that a gaussian distribution underestimates the observed number of more massive asteroids. This suggests that the initial asteroid distribution function was probably broader than a gaussian function, but it still retains a distinct bell-like appearance.

In this paper we propose a simple model for the accretion of objects in the solar nebula that permits a straightforward calculation of their radius function. This fits the Anders reconstructed asteroid distribution, and it also predicts reasonably well the number of terrestrial planets. (The terrestrial planets are assumed to be asteroids that formed slightly earlier than their fellows and consequently captured most of the available solid material in the solar nebula. Subsequently the asteroids and terrestrial planets will collectively be called planetoids.) A number of consequences of our model are explored in this paper. A preliminary report on this theory has been published (Hills, 1970).

RADIUS FUNCTION

The calculation of the radius function of the planetoids requires some knowledge of the rate of formation of the seed bodies that initiated their accretion. From knowledge of other processes requiring the formation of seed bodies, it is probable that their formation was governed by a stochastic process. In this case, the rate of formation of the seed bodies was independent of time as long as the total mass accumulated in the planetoids remained much smaller than the amount of unaccreted material.

With the rate of formation of the seed bodies being independent of time, the number of planetoids with radii between R and $R + \Delta R$ is directly

proportional to the time necessary for the radius of a planetoid to grow from R to $R + \Delta R$. This requires a radius distribution function of the form

$$dN(R) = \frac{N_0' \, dR}{dR/dt} \tag{1}$$

where the constant of proportionality N_0' is the number of seed bodies formed per unit time in the nebula, and dR/dt is determined by the accretion equation. (See, e.g., Hartmann, 1968.)

$$\frac{dR}{dt} = \alpha \frac{\rho_a}{\rho_p} \frac{V}{4} \left(1 + \frac{8\pi G R^2 \rho_p}{3V^2} \right) \tag{2}$$

Here α is the sticking coefficient, ρ_a is the space density of the accretable material, ρ_p is the planetoid density, and V is the average preencounter velocity of the accreted particles relative to the planetoid. The equation is simplified by introducing a characteristic radius,

$$R_c = \left(\frac{3}{8\pi G \rho_p} \right)^{1/2} V \tag{3}$$

so that

$$\frac{dR}{dt} = \alpha \frac{\rho_a}{\rho_p} \frac{V}{4} \left[1 + \left(\frac{R}{R_c} \right)^2 \right] \tag{4}$$

R_c is the radius at which the accretion cross section of a planetoid is twice its geometric cross section.

Making use of the accretion equation, the radius distribution function becomes

$$dN(R) = \frac{N_0 \, dR/R_c}{1 + (R/R_c)^2} \tag{5}$$

where the new constant of proportionality is

$$N_0 = \frac{4 N_0' R_c}{\alpha V} \frac{\rho_p}{\rho_a} \tag{6}$$

Integrating equation (5), we find that the number of planetoids with radii equal to or less than R is

$$N(R) = N_0 \tan^{-1} \frac{R}{R_c} \tag{7}$$

As $R \to \infty$,

$$N(\infty) = N_0 \frac{\pi}{2} \tag{8}$$

Thus the number of planetoids is formally bound even if the radius of the largest one and the total mass of the system are not. This results from the

accretion cross section of the largest object formally growing much faster than its mass, which allows it to grow to infinite mass in a finite time if enough material is present. In a real system, the number of planetoids is similarly not determined by the total mass of the system but by the ratio of the time necessary for the largest object in the system to acquire most of its mass to the average time between the production of the seed bodies. Most of the mass in a typical planetoid system will be accumulated in the first one or two largest bodies.

In any actual system there is an upper limit R_{max} to the radius of the largest planetoid, but if $R_{max} \gg R_c$, then $N(\infty) \sim N(R_{max})$. If we mathematically allow $R \to \infty$ so that $N(\infty)$ is the total number of planetoids formed, the normalized integrated radius function is

$$N(R) = \frac{2}{\pi} N(\infty) \tan^{-1} \frac{R}{R_c} \tag{9}$$

and in differential form

$$dN(R) = \frac{2}{\pi} N(\infty) \frac{dR/R_c}{1 + (R/R_c)^2} \tag{10}$$

We note that R_c is the median radius of the planetoids.

To compare the theoretical radius distribution function with the Anders distribution we have to convert the former into one in units of $\ln R$. This yields

$$dN(\ln R) = \frac{2}{\pi} N(\infty) \frac{(R/R_c)\, d[\ln (R/R_c)]}{1 + (R/R_c)^2} \tag{11}$$

This function is plotted in figure 1. It is a serpentine curve and looks quasi-gaussian about the peak at $R = R_c$.

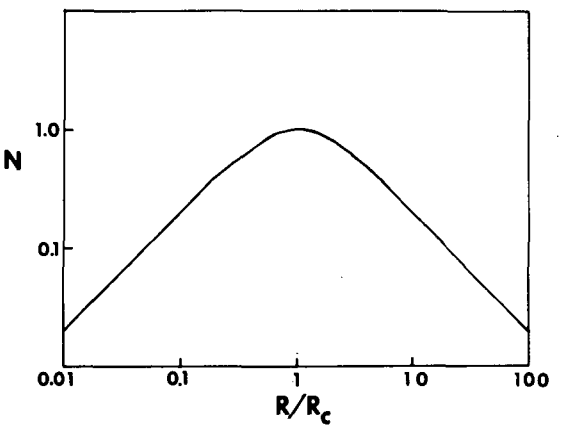

Figure 1.–Theoretical radius function of the planetoids.

The theoretical curve fits the reconstructed radius distribution to within the statistical errors if $R_c \sim 15$ km. This function is noticeably broader than a gaussian function. For the initial asteroid system, the radius of Ceres is R_{max}. We note in passing, that if we normalized the theoretical radius function to the reconstructed asteroid radius distribution, any planetoids with $R > R_{max}$ predicted by the theoretical relation can only have a mathematical and no physical significance.

With $R_c = 15$ km and $\rho_p = 3.6$ g/cm^3 for the asteroids we find by equation (3) that $V = 0.02$ km/s. The peak of Anders' (1965) proposed empirical function is $R_c \sim 30$ km with an error of about 50 percent. For $R_c = 30$ km, $V = 0.04$ km/s. We take $V = 2 \times 10^{-2}$ to 4×10^{-2} km/s as the likely range of V. This V was presumably due to large-scale turbulent motion in the solar nebula.

We shall now investigate some consequences of our theoretical model to shed more light on the planetoid formation process and to better test the validity of the theory by producing a larger body of results to check against observable data.

TOTAL NUMBER OF PLANETOIDS

Assuming that V was constant throughout the solar nebula allows the calculation of the total number $N(\infty)$ of planetoids formed in the region of the solar nebula now occupied by the terrestrial planets (terrestrial band). The total mass of a system of planetoids in which the largest body has a mass M_{max} is found by integrating equation (10). This gives

$$M_{total} = \int_0^{R_{max}} \frac{2}{\pi} N(\infty) \frac{4}{3} \pi R^3 \rho_p \frac{dR/R_c}{1 + (R/R_c)^2} \tag{12}$$

On completing the integration and rearranging terms, we find

$$N(\infty) = \frac{\pi (M_{total}/M_c)}{(M_{max}/M_c)^{2/3} - \ln [1 + (M_{max}/M_c)^{2/3}]} \tag{13}$$

where from equation (3)

$$M_c = \frac{4}{3} \pi R_c{}^3 \rho_p = \left(\frac{3}{32\pi G^3 \rho_p} \right)^{1/2} V^3 \tag{14}$$

Because $M_{max} \gg M_c$,

$$N(\infty) \sim \pi \frac{M_{total}}{M_{max}{}^{2/3} M_c{}^{1/3}} \tag{15}$$

We note that $N(\infty) \propto \rho_p{}^{1/6}$. This weak dependence of $N(\infty)$ on ρ_p makes rather immaterial whether we use $\rho_p = 3.6$ g/cm^3 as for chondrite meteorites or

$\rho_p = 5.5$ g/cm^3 as for Earth or Mercury in calculating $N(\infty)$. For the terrestrial band, $M_{\text{total}} = 2.0M_\oplus$ (total mass of present terrestrial planets and the asteroids) and $M_{\max} = 1.0M_\oplus$. With these values for the masses and $V = 0.02$ km/s, $N(\infty) = 3508$ for $\rho_p = 5.5$ g/cm^3 and 3269 for $\rho_p = 3.6$ g/cm^3; whereas for $V = 0.04$ km/s, $N(\infty) = 1752$ for $\rho_p = 5.5$ g/cm^3 and 1633 for $\rho_p = 3.6$ g/cm^3.

ACCRETED PLANETOIDS

Table I shows the normalized planetoid mass distribution functions for $\rho_p = 3.6$ g/cm^3 and turbulent velocities of 0.02 and 0.04 km/s. Note that the mass distributions are almost the same for masses greater than $10^{-5}M_\oplus$. One can show that the number of these more massive objects is similarly insensitive to ρ_p. Presumably, except for about 100 initial asteroids and their fragments, the smaller planetoids have been accreted by the four remaining terrestrial planets and the Moon.

From the table we find that about 15 percent of the mass of the original planetoid system was in objects less massive than Mercury, which implies that about 15 percent of the mass of Earth and the other terrestrial planets was accreted as small planetoids, whereas the remaining 85 percent was accreted as subplanetoid bodies, primarily clumps of dust. About one-third the mass of the accreted planetoids was in objects having sublunar masses and two-thirds was in objects having masses between that of the Moon and Mercury.

We may be concerned that a collision between a large planetoid in the latter group and a terrestrial planet could cause their mutual destruction. A breakup is expected if the preencounter total kinetic energy of the two objects relative to their center of mass is greater than their combined gravitational binding energies; i.e., for planetoids of uniform density, breakup requires that

$$\frac{1}{2}\mu V^2 > \frac{3}{5} G \left(\frac{M_1^2}{R_1} + \frac{M_2^2}{R_2} \right) \tag{16}$$

where $\mu = (M_1 M_2)/(M_1 + M_2)$, the reduced mass, and V is the relative velocity of the two objects prior to the encounter. An upper limit on V is probably its present value for interasteroidal collisions, 5 km/s (Piotrowski, 1953). After the terrestrial planets formed, their long-range gravitational perturbations increased V well above the 0.04 km/s maximum turbulent velocity in the solar nebula, but these forces were not likely to have had sufficient time before the accretion of most of the small planetoids to raise V much above its present interasteroidal value. Figure 2 shows the mass m of the smallest body required to cause the collisional breakup of a planetoid of mass M if $V = 5$ km/s and $\rho_p = 5.5$ g/cm^3 or 3.6 g/cm^3. We note that planetoids more massive than $0.026M_\oplus$ for $\rho_p = 5.5$ g/cm^3 and $0.033M_\oplus$ for $\rho_p = 3.6$ g/cm^3 are safe against breakup in collisions with all objects equal to or less massive than themselves. As the critical mass is less than half that of Mercury (for $\rho_p \sim 5.5$), it seems likely that all terrestrial planets were safe against collisional breakup.

TABLE I.–*Mass Function of the Planetoids*[a]

$\log \frac{M}{M_\oplus}$	Radius, km	Turbulent velocity					
		V = 0.02 km/s			V = 0.04 km/s		
		N_i	ΣN_i	$\frac{\Sigma \text{ mass}}{M_{\text{total}}}$	N_i	ΣN_i	$\frac{\Sigma \text{ mass}}{M_{\text{total}}}$
−17	0.02	2.7	2.3	–	0.67	0.6	–
−16	.03	5.8	5.0	–	1.5	1.3	–
−15	.07	12.5	10.9	–	3.1	2.7	–
−14	.16	27.0	23.4	–	6.7	5.8	–
−13	.34	58.1	50.4	–	14.5	12.6	–
−12	.73	124	108	1.6×10^{-11}	31.3	27.1	–
−11	1.58	261	233	2.9×10^{-10}	66.9	58.4	8.5×10^{-11}
−10	3.41	506	494	6.1×10^{-9}	140	125	1.6×10^{-9}
−9	7.35	756	1000	1.2×10^{-7}	267	265	3.2×10^{-8}
−8	15.8	699	1756	1.6×10^{-6}	384	533	6.1×10^{-7}
−7	34.1	422	2456	1.4×10^{-5}	338	916	8.3×10^{-6}
−6	73.5	210	2878	8.8×10^{-5}	198	1255	7.0×10^{-5}
−5	158	99.1	3088	4.5×10^{-4}	97.8	1453	4.1×10^{-4}
−4	341	46.1	3187	2.1×10^{-3}	46.0	1551	2.1×10^{-3}
−3	735	21.4	3233	1.0×10^{-2}	21.4	1597	9.9×10^{-3}
−2	1583	9.9	3254	4.6×10^{-2}	9.9	1618	4.6×10^{-2}
−1	3410	4.6	3264	.22	4.6	1628	.22
0	7346		3269	1.00		1633	1.00

[a] $M_{\max} = 1.0 M_\oplus$; $M_{\text{total}} = 2.0 M_\oplus$; $\rho_p = 3.6$ g/cm^3.

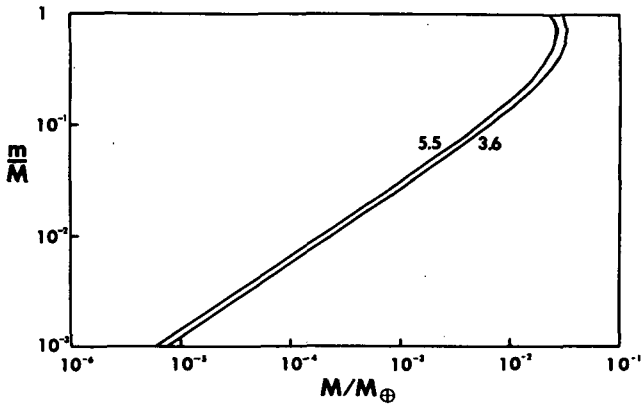

Figure 2.–In a collision between two planetoids having a preencounter relative velocity of 5 km/s, m is the minimum mass of the collision partner required to cause the breakup of a planetoid of mass M. We note that near the limit of M beyond which a planetoid is stable against breakup irrespective of m, m is double valued, which indicates that there is an upper as well as a lower limit on the m required for fragmentation. This results from the quadratic dependence of the gravitational potential energy on m and M.

Although a collision with a large fellow planetoid would not destroy a terrestrial planet, it would produce a drastic alteration in the direction of its rotational axis if the orbit of the planetoid did not lie in the equatorial plane of the planet.[1] A simple calculation shows that even single collisions with planetoids of lunar mass would easily account for the magnitude of the deviation of the equators of the terrestrial planets from the planes of their orbits. From the theoretical radius distribution function (table I) we see that Earth is likely to have accreted several such bodies.

COLLISIONAL FRAGMENTATION OF THE PLANETOIDS

Their small number [$N(\infty) \sim 2 \times 10^3$ to 3×10^3] indicates that the accretion of primary planetoids only produced a very small fraction of the observed lunar and Martian craters. As we shall see, likely agents for the production of most craters are the collisional fragments of a few primary planetoids of approximately lunar mass. We note from figure 2 that lunar-sized objects can be broken apart by collisions with bodies an order of magnitude less massive than themselves, whereas objects the size of Ceres can be broken up in collisions with bodies less than two orders of magnitude less massive than themselves. This extreme fragility of the asteroids suggests an explanation for their failure to coalesce into one body. If an object of $0.03M_{\oplus}$ or greater had formed in the asteroid belt, we would likely see only one object today.

---

[1]See p. 259.

The average number of fragmentation collisions that occur among a group of n planetoids before they are accreted by the planets is

$$N = \frac{K}{\sigma_p} \tag{17}$$

where

$$K = \sum_{j=1}^{n-1} \sum_{i=j+1}^{n} \sigma_{ij} = \frac{1}{2} n(n-1) < \sigma_{ij} > \tag{18}$$

Here σ_p is the total accretion cross section of the terrestrial planets for the average planetoid and σ_{ij} is the collision cross section for encounters between planetoids i and j. With $V = 5$ km/s, the collisional cross sections of sublunar planetoids are very nearly their physical cross sections. Thus

$$\sigma_{ij} \simeq \pi(R_i + R_j)^2 \tag{19}$$

Because the radius of the average sublunar planetoid is small compared with the radius S_i of a terrestrial planet, by conservation of energy and momentum we find

$$\sigma_p \simeq \sum_{i=1}^{4} S_i^2 \left[\left(\frac{W_i}{V} \right)^2 + 1 \right] \tag{20}$$

where W_i is the escape velocity from the ith planet. For $V = 5$ km/s, $\sigma_p = 1.5 \times 10^9$ km^2.

Table I indicates that there were 21.4 original planetoids in the mass range $0.001 M_\oplus$ to $0.01 M_\oplus$. These have radii between 735 and 1580 km for $\rho_p = 3.6$ g/cm^3. For these objects

$$< \sigma_{ij} > \simeq \pi(735 + 1580)^2 = 1.7 \times 10^7 \text{ km}$$

From equations (17) through (20) we find that $N = 2.4$. Thus it is highly likely that at least one fragmentation collision took place among the objects in this mass range with each collision causing the breakup of two objects.

The observed fragments produced by asteroidal collisions have an integrated radius function of approximately the form (Hartmann and Hartmann, 1968)

$$N(R) = \left(\frac{R_{max}}{R} \right)^2 \tag{21}$$

where $N(R)$ is the number of fragments with radii larger than R. The largest fragment, of radius R_{max}, has usually about one-half the initial mass of the fragmented planetoid. For the objects we have considered, R_{max} is typically 1000 km which implies the production of about 10^6 fragments with radii

greater than 1 km. This is three orders of magnitude larger than the number of primary planetoids, and it is quite adequate to account for the number of large lunar craters. Because $N(R)$ is very sensitive to R_{max}, we can expect that only the first one or two largest fragmented planetoids produced a majority of all the fragments. This result suggests that although most of the integrated mass in planetoids and their fragments accreted by a terrestrial planet or the Moon was in the form of a handful of very large unfragmented primary objects, the vast majority of crater-forming bodies were fragments of a few primary planetoids with initial masses on the order of that of the Moon. If meteorites are fragments of planetoids that were formed in the vicinity of Earth rather than objects that have diffused in from the asteroid belt, we can expect most of them to be from a few primary objects with masses on the order of that of the Moon.

Because the integrated cross-sectional area of the fragments of a planetoid is much larger than its initial cross-sectional area, one collisional fragmentation produces a chain reaction of further fragmentations. Thus, although the integrated mass in planetoids and their fragments that are being accreted by a planet per unit time decreases exponentially with time, an accelerating pace of further fragmentation actually causes the number of objects being accreted per unit time to increase. This is accompanied by a rapid decrease in the average mass of the individual fragments.

The integrated accretion cross section σ_p of the Jovian planets is about three orders of magnitude greater than that of the terrestrial planets. Consequently, if we apply the same arguments to the planetoids that formed in the region of the Jovian planets that we did to those in the terrestrial band, we find that no fragmentation collisions are likely to have occurred among these planetoids before they were accreted by the Jovian planets. Thus the surfaces of the satellites of the Jovian planets should not be scarred by the large number of impact craters that dominate the faces of the Moon and Mars; however, there may be some contamination in the case of the satellites of Jupiter due to the diffusion of fragments from the asteroid belt. It is hoped that this anticipated scarcity of craters can be tested by future space probes.

TEMPERATURE OF ACCRETION

It is desirable to know whether the temperature that a given planetoid attained during the course of accretion was sufficient to melt it and thereby allow the differentiation of a core of dense material. The minimum temperature maintained by a planetoid in the act of accreting material is one whereby the energy inflow due to accretion is just balanced by the loss of blackbody radiation, or

$$\frac{dE}{dt} = 4\pi R^2 \sigma (T^4 - T_0^4) = \frac{GM}{R}(4\pi R^2 \rho_p)\frac{dR}{dt} \tag{22}$$

Using the accretion equation to evaluate dR/dt and by minor algebra we find that

$$T = \left\{ \frac{\alpha G \rho_p \pi R^2 V \rho_a [1 + (R/R_c)^2]}{3\sigma} + T_0^4 \right\}^{1/4} \tag{23}$$

Here T_0 is the blackbody temperature of the planetoid in the absence of accretion.

To evaluate T we need to know ρ_a, the density of accretable material in the solar nebula. We have calculated this by assuming that the material presently in the terrestrial planets and asteroids, $M_{\text{total}} = 2M_\oplus$, was distributed uniformly in an annular sector of the solar nebula lying between 0.3 and 2 AU from the Sun. The turbulent velocity V determined the scale height of the dust above the plane of the nebula and consequently the density ρ_a in the plane. For $V = 0.02$ km/s, we find that $\rho_a = 1.6 \times 10^{-10}$ g/cm^3; whereas for $V = 0.04$ km/s, $\rho_a = 0.8 \times 10^{-10}$ g/cm^3.

To illustrate the dependence of T upon R, in figure 3 we have plotted this relation for a case in which $T_0 = 300$ K and planetoid densities ρ_p are 3.6 g/cm^3 and 5.5 g/cm^3. We note that if $T \geqslant 2T_0$, then T is practically independent of the particular T_0 chosen. We further note from the figure that Venus and Earth with $T \sim 3 \times 10^3$ K were probably the only terrestrial planets that thoroughly melted. Mercury and Mars with $T \sim 1100$ to 1800 K only partially melted. The Moon with $T \sim 600$ to 1000 K probably did not melt from accretion, and Ceres with $T \sim 303$ to 320 K was essentially accreted cold.

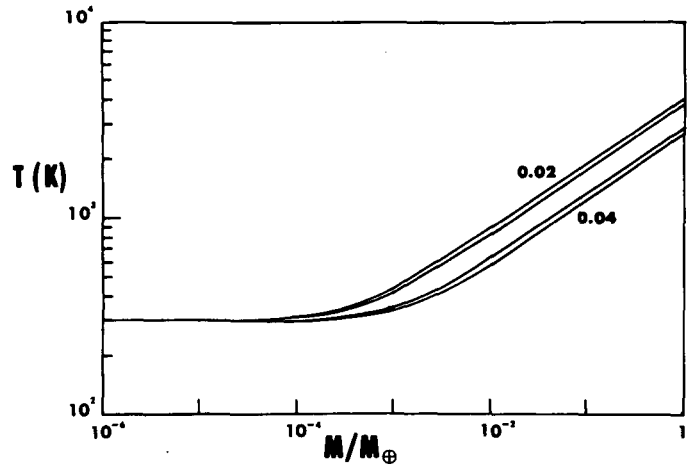

Figure 3.–Maximum temperatures attained by planetoids as the result of accretion. Curves are drawn for turbulent velocities of 0.02 and 0.04 km/s. The upper curve in each pair is for $\rho_p = 5.5$ g/cm^3 and the lower is for $\rho_p = 3.6$ g/cm^3.

TABLE II.—*Time (years) of Growth in the Solar Nebula*

$\log \frac{M_{max}}{M_\oplus}$	$\rho_p = 3.6$ g/cm^3		$\rho_p = 5.5$ g/cm^3	
	$V = 0.02$ km/s	$V = 0.04$ km/s	$V = 0.02$ km/s	$V = 0.04$ km/s
−17	2.3×10^3	2.3×10^3	3.0×10^3	3.0×10^3
−16	4.9	4.9	6.4	6.4
−15	1.0×10^4	1.0×10^4	1.4×10^4	1.4×10^4
−14	2.3	2.3	3.0	3.0
−13	4.9	4.9	6.4	6.4
−12	1.0×10^5	1.0×10^5	1.4×10^5	1.4×10^5
−11	2.2	2.3	3.0	3.0
−10	4.8	4.8	6.3	6.4
−9	9.7	1.0×10^6	1.3×10^6	1.4×10^6
−8	1.7×10^6	2.1	2.2	2.7
−7	2.4	3.5	3.0	4.5
−6	2.78	4.8	3.5	6.1
−5	2.98	5.6	3.70	7.0
−4	3.08	6.0	3.81	7.4
−3	3.12	6.16	3.86	7.63
−2	3.14	6.25	3.88	7.73
−1	3.151	6.28	3.895	7.77
0	3.155	6.30	3.900	7.79

Thus an Earth-type core is expected on Venus but probably not on any of the other terrestrial planets. Because of their low accretion temperatures, the asteroids can be expected to have preserved the chemical integrity of the material that they accreted. Thus future onsite inspections of asteroid fragments may yield valuable insight into the chemical and physical properties of the preplanetoid material and, consequently, insight into the chemical and thermal properties of the solar nebula during the time of planetoid formation.

TIME OF FORMATION

If the seed bodies were formed at a uniform rate in time, as has been assumed, the average number of planetoids with radii in some range R_1 to R_2 remained constant even in the presence of further accretion as long as the radius R_{max} of the most massive planetoid in the system was greater than or equal to R_2. Thus at any given time during the accretion of the planetoids, their radius distribution function was the same as given in table I up to radius R_{max}.

To find the time required for the radius of the largest planetoid in the system to grow to R_{max}, we integrate equation (4). This gives

$$t = \frac{(6\rho_p/\pi G)^{1/2}}{\rho_a \alpha} \tan^{-1} \frac{R_{max}}{R_c} \tag{24}$$

We note that, unlike the radius distribution function, this depends on the sticking coefficient α and the space density ρ_a of accretable material. Setting $R_{max} = \infty$, we see that formally a planet grows to infinite mass in a finite time

$$t_\infty = \frac{(6\rho_p/\pi G)^{1/2}}{\rho_a \alpha} \frac{\pi}{2} \tag{25}$$

This is the characteristic time for forming a planetary system. We further note that a planetoid takes only twice as long to grow to $R = \infty$ as to grow to $R = R_c$.

Table II tabulates t as a function of R_{max} for $\alpha = 1$ and previously calculated ρ_a values. The table shows that if $V = 0.02$ km/s, a planetoid only required about 8×10^4 yr to increase its mass from that of Ceres to that of Earth. This suggests that if a stable seed body had formed about 8×10^4 yr earlier in the asteroid belt, there might be a terrestrial planet there today. This small difference is less than 3 percent of the time required for a planetoid mass to grow to $1 M_\oplus$.

REFERENCES

Anders, E. 1965, Fragmentation History of Asteroids. Icarus 4, 399-408.

Hartmann, W. K. 1968, Growth of Asteroids and Planetesimals by Accretion. Astrophys. J. 152, 337-342.

Hartmann, W. K., and Hartmann, A. C. 1968, Asteroid Collisions and Evolution of Asteroidal Mass Distribution and Meteoritic Flux. Icarus 8, 361-381.

Hills, J. G. 1970, The Formation of the Terrestrial Planets. Bull. Amer. Astron. Soc. 2, 320.

Piotrowski, S. 1953, The Collisions of Asteroids. Acta Astron. Ser. A 5, 115-138.

Page intentionally left blank

THE RELATIONSHIP OF METEORITIC PARENT BODY THERMAL HISTORIES AND ELECTROMAGNETIC HEATING BY A PRE-MAIN SEQUENCE T TAURI SUN

C. P. SONETT
NASA Ames Research Center

Convincing evidence exists that meteoritic matter was reheated shortly after the initial condensation of the solar nebula for those meteorites thought to be derived from parent bodies. This evidence takes the form of cooling rates carefully determined from diffusion studies of the migration rate of Ni across kamacite-taenite boundaries in iron meteorites (Fish, Goles, and Anders, 1960; Goldstein and Ogilvie, 1965; Goldstein and Short, 1967; Wood, 1964). The notion that the irons condensed *directly* from the solar nebula requires that these measurements and the existence of large Widmanstätten figures be explained as a condensation event. This seems rather unlikely and, in any event, requires a far more complex explanation than heating and melting in a parent body.

The reheating episode and the need for melting at least the outer layers of the Moon early in the evolutionary time track of the solar system led Urey (1961) to propose the existence of a class of radionuclides that are now extinct and whose presence is postulated or inferred from the daughter products that follow naturally from the decay. In the case of ^{26}Al, this evidence is difficult to identify because the product of decay is ^{26}Mg, which is naturally abundant. Recently, Schramm et al. (1970) determined an upper bound from the examination of feldspars in terrestrial, lunar, and meteoritic samples. They found that the contribution of ^{26}Al to parent body heating would have been unimportant at the time of solidification. Additionally ^{244}Pu and ^{129}I are known to have existed in the solar nebula because trace quantities of the Xe daughter products have been found and Pu fission tracks have been observed (Fleischer, Price, and Walker, 1968; Reynolds, 1963). Nevertheless, the amounts of these fossil nuclides do not appear to have been enough to yield the requisite level of heating. Such ancillary matters as the storage time in the solar nebula are important. Long before the parent bodies condensed to the point where heat could be stored, there would have been appreciable decay that would not contribute to the heating. An additional criticism of the fossil nuclide hypothesis (in terms of heating) is that if serious mixing of the fossil components in the original nebula took place and if parent bodies were to have

been melted, then the inner planets would also have experienced this process (Sonett, 1969*b*). Although the early thermal history of Earth is well masked, the same does not appear to be true of the Moon. If the Moon were formed at a position in the solar system where the mixing requirements were met, then it is difficult to understand why the Moon would not have been completely melted very early. The present evidence does not support such an extreme thermal history but, in fact, suggests that the deep interior was only partially melted at best. The electromagnetic evidence from the Apollo 12 magnetometer suggests a condition in which only the outer several hundred kilometers, corresponding to a mantle, were melted (Dyal et al., 1970; Sonett et al., 1971*c,d*). Thus unless substantial fractionation of the fossil radionuclide component of the primitive solar nebula took place, the hypothesis of fossil nuclide heating must be regarded as only marginally plausible.

We have examined an alternative hypothesis for early heating of the meteoritic parent bodies. This mechanism is based upon ohmic heating by a primordial sun endowed with high spin, a reasonable magnetic field, and an extreme outflow of plasma that might be loosely characterized as a solar wind. These conditions conform generally to those postulated for T Tauri stars and also form a self-consistent chronology because T Tauri stars are thought to be of approximately 1 solar mass in an early postcondensation stage (Sonett, 1969*a,b;* Sonett, Colburn, and Schwartz, 1968; Sonett et al., 1970).

The process of ohmic heating is based upon the generation of electrical currents deep within the body by the action of the interplanetary magnetic field and the solar wind. Electrical currents flow as a result of excitation from the interplanetary magnetic and electric fields, corresponding to a transverse electric (TE) and transverse magnetic (TM) excitation of the body (Schubert and Schwartz, 1969; Sonett et al., 1971*a;* Sonett et al., 1971*b,c*). Detailed calculations have been carried out for the case of steady-state (time-independent) TM excitation. The detailed results of this work have been reported elsewhere and only the final conclusions are given here. These are shown in figure 1 and indicate the peak temperature reached for a representative set of parent body radii, starting temperature T_0, and solar spin decay "time constant" δ. The latter is incorporated into a subroutine for solar spin damping so that the sun evolves toward the present epoch spin rate while starting at a higher value. Figure 1 shows three basic regimes for the heating process. The left side of the diagram shows the radiation damped cases where losses from the body into space limit the peak temperature. The peak value is achieved in very short times, characteristically some 5×10^5 yr, after which radiative losses dominate and the body cools. The other extreme is given by the case where the heating is joule dominated and radiative losses are important only near the surface. In this range of sizes, the heating varies approximately as $1/R^2$ where R is the body radius. The intermediate cases are governed by more complex phenomena involving lack of saturation. Saturation means that the formation of a bow shock wave ahead of the body is inhibited by the small

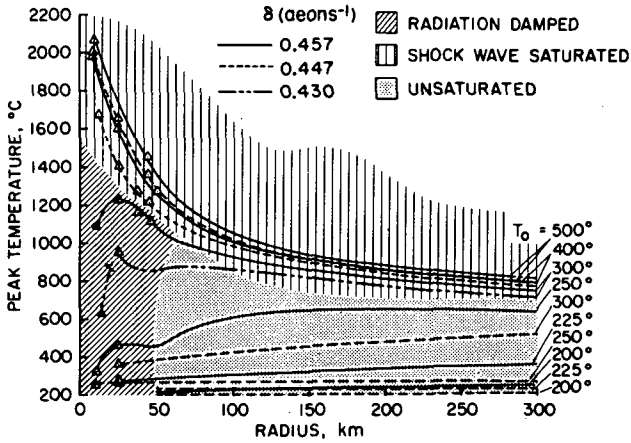

Figure 1.–Peak core temperatures of bodies ranging in size from 10 to 300 km radius using a bulk electrical conductivity function for basalt-diabase (Parkhomenko, 1967), and for various uniform starting temperatures and a variable solar spin rate. The latter is identified with the solar magnetic field time constant δ shown above the graph. The largest value corresponds to a starting field of 2.3 mT (23 G) and a centrifugally limited sun; the other values correspond respectively to spin rates of 150 and 80 times the present value. The computer runs carried the computation to 10^6 yr; thus for the smaller bodies that were eventually overwhelmed by radiative losses, the peak temperature is attained early (i.e., about 5×10^5 yr) and the triangles correspond to this time rather than 10^6 yr as in the case of the larger bodies, which are not radiation damped. The heating calculation shown here is for the TM mode and does not include either TE heating or any addition due to fossil nuclides. (Adapted from Sonett et al., 1970).

electrical current. In these cases the $1/R^2$ dependence is voided because it depends exclusively upon the process of saturation where the total planetary current is determined by mechanical pressure effects in turn governed by the radius of the body, other parameters being equal. Details of the heating are shown in figures 2 and 3. The physical behavior is given in the references.

The calculations reported here are determined by a wide set of parameters including the surface temperature, which is required because the TM mode currents pass through the surface of the body (Sonett et al., 1970). On the other hand, the TE mode does not carry this restriction. Calculations are underway to determine the effects of coupled TE-TM heating. Generally, it can be said that the addition of the TE mode will increase the heating, although special conditions may prevail during part of the cycle where the two conflict.

A rudimentary example of TE mode heating can serve to illustrate the conditions required for this case. To melt a parent body requires on the order of 10^4 J/g of matter. To do this in about 10^6 yr (an upper bound for TM heating) would require that the energy input into the body correspond to about 100 μW-m^{-3} (3×10^{-3} ergs/cm^3-s). The target area of a planet is given

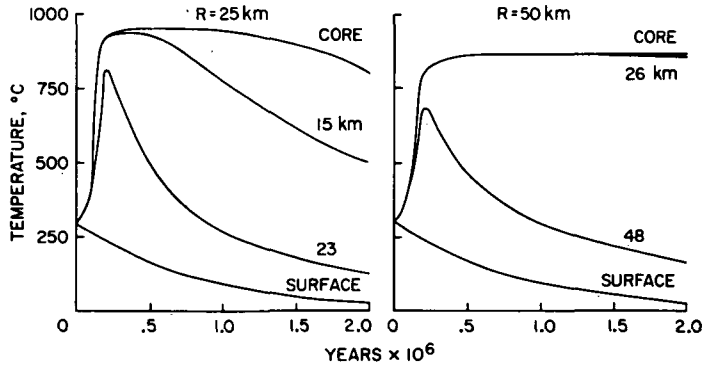

Figure 2.–The detailed chronology of parent bodies having radii R = 25 and R = 50 km subject to TM heating alone. The figure shows the temperature versus time at different levels in the bodies measured inward from the surface. It is seen that the surface follows the space temperature closely; at 2 km depth the temperature rises rapidly at first followed by a strong loss of heat, while the core for R = 25 km shows only a small decline after 1 million yr and for R = 50 km shows no loss in that time. These calculations are for basalt-diabase (Parkhomenko, 1967), T_0 = 300° C, and a spin decrement δ = 0.447.

by πR^2 whereas the volume is $(4/3)\pi R^3$; thus the field amplitude requirement is given by the condition that

$$\frac{B^2}{2\mu}\frac{v}{R} = 10^{-4}$$

where B is the peak value of the field amplitude, v the speed of the solar wind, and R the radius of the body. This equation is a statement of the intercepted flux per unit volume of the body, under the assumption that the incident hydromagnetic radiation is *wholly* adsorbed through joule heating. Then $B \sim 0.03$ mT (0.3 G). This value can be compared to the strength of the basic spiral field for TM heating. For a centrifugally limited sun with a maximum permissible starting magnetic field of 2.3 mT (23 G) yielding the final present epoch spin (assuming an exponential decay in the magnetic field), the field strength at 3 AU at the onset is of an order of 8 μT (80 mG). Thus the disturbance field is considerably greater than the steady component, and the interplanetary magnetic field can be characterized as turbulent. This condition is not in conflict with the extrapolation of conditions thought to exist in the emissions from T Tauri stars. The postulated conditions for the steady component of the field can easily be modified upwards because the present model is conservative with respect to the starting magnetic field. Spectroscopic evidence of fields associated with T Tauri stars is limited by turbulence broadening so that the observational threshold is on the order of 1 dT (10^3 G),

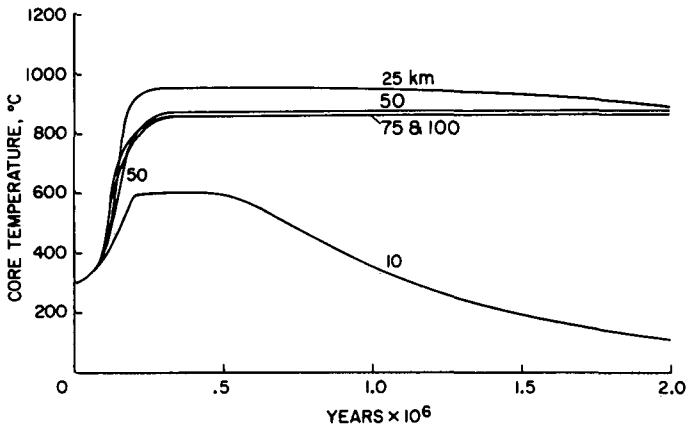

Figure 3.—The core temperature versus time for bodies ranging in size from 10 to 100 km using TM heating solely. The smallest body (R = 10 km) shows the effect of radiative loss to space most strongly while the larger bodies show little or no effect in 2 million yr. The material assumed, starting temperature, and spin decrement are the same as for figure 2.

more than two orders above our estimate. Increase of the starting field can substantially increase the interplanetary electric field that drives the TM mode although saturation effects must be considered where the formation of a bow shock wave inhibits further heating. Nevertheless, for those cases where the onset of the bow wave is absent, an additional component of TM heating can be expected; and, in any event, the heating is not expected to be diminished by the saturation process. Then the spiral structure can be preserved even in the presence of an extremum in the time-dependent part of the field, though this is not an essential part of the model.

The conclusions to be drawn from this note are perhaps even more important in regard to the early Sun than for the question of planetary heating. For the absence of an adequate explanation of the Ni-Fe phases using radiogenic sources means that the electrical hypothesis becomes more compelling; this in turn requires certain critical conditions to be placed upon the early pre-main sequence Sun. These are essentially the high spin rate, modest to large magnetic field, and the presence of a substantial efflux of plasma, representative of T Tauri stars. All this is in accord with contemporary models of the early evolution of the solar system where condensations from a primordial cloud accompanied by a Hayashi-like contraction of the Sun are implied.

REFERENCES

Dyal, P., and Parkin, C. W. 1970, Electrical Conductivity and Temperature of the Lunar Interior From Magnetic Transient Response Measurements. NASA TM X-62012. J. Geophys. Res., in press.

Fish, R. A., Goles, G. G., and Anders, E. 1960, The Record in the Meteorites. III: On the Development of Meteorites in Asteroidal Bodies. Astrophys. J. 132, 243.

Fleischer, R. L., Price, P. B., and Walker, R. M. 1968, Identification of Pu^{244} Fission Tracks and the Cooling of the Parent Body of the Toluca Meteorite. Geochim. Cosmochim. Acta 32, 21.

Goldstein, J. I., and Ogilvie, R. E. 1965, The Growth of the Widmanstätten Pattern in Metallic Meteorites. Geochim. Cosmochim. Acta 29, 893.

Goldstein, J. I., and Short, J. M. 1967, Cooling Rates of 27 Iron and Stony-Iron Meteorites. Geochim. Cosmochim. Acta 31, 1001.

Parkhomenko, E. I. 1967, Electrical Properties of Rocks. Plenum Press, Inc. New York.

Reynolds, J. A. 1963, Xenology. J. Geophys. Res. 68, 2939.

Schramm, D. N., Tera, F., and Wasserburg, G. J. 1970, The Isotopic Abundance of ^{26}Mg and Limits on ^{26}Al in the Early Solar System. Earth Planet. Sci. Lett. 10, 44.

Schubert, G., and Schwartz, K. 1969, A Theory for the Interpretation of Lunar Surface Magnetometer Data. The Moon 1, 106.

Sonett, C. P. 1969*a*, Fractionation of Iron: A Cosmogonic Sleuthing Tool, I, Radioisotope Heating. Comments Astrophys. Space Phys. 1, 6.

Sonett, C. P. 1969*b*, Fractionation of Iron: A Cosmogonic Sleuthing Tool, II, Heating by Electrical Induction. Comments Astrophys. Space Phys. 1, 41.

Sonett, C. P., Colburn, D. S., and Schwartz, K. 1968, Electrical Heating of Meteorite Parent Bodies and Planets by Dynamo Induction From a Pre-Main Sequence T Tauri Solar Wind. Nature 219, 924.

Sonett, C. P., Colburn, D. S., Schwartz, K., and Keil, K. 1970, The Melting of Asteroidal-Sized Bodies by Unipolar Dynamo Induction From a Primordial T Tauri Sun. Astrophys. Space Sci. 7, 446.

Sonett, C. P., Dyal, P., Colburn, D. S., Smith, B. F., Schubert, G., Schwartz, K., Mihalov, J. D., and Parkin, C. W. 1971*b*, Induced and Permanent Magnetism on the Moon: Structural and Evolutionary Implications. Highlights of Astronomy 1970 (ed., C. De Jager), in press. D. Reidel. Dordrecht.

Sonett, C. P., Dyal, P., Parkin, C. W., Colburn, D. S., Mihalov, J. D., and Smith, B. F. 1971*a*, Whole Body Response of the Moon to Electromagnetic Induction by the Solar Wind. Science 172, 256.

Sonett, C. P., Schubert, G., Smith, B. F., Schwartz, K., and Colburn, D. S. 1971*c*, Lunar Electrical Conductivity From Apollo 12 Magnetometer Measurements: Compositional and Thermal Inferences. Proc. Apollo 12 Lunar Sci. Conf. Geochim. Cosmochim. Acta 35, suppl. II:

Sonett, C. P., Smith, B. F., Colburn, D. S., Schubert, G., Schwartz, K., Dyal, P., and Parkin, C. W. 1971*d*, Lunar Electrical Conductivity Profile. Nature 230, 359.

Urey, H. C. 1961, The Origin of the Moon and Its Relationship to the Origin of the Solar System. Proc. Symp. 14 IAU. Academic Press, Inc. New York.

Wood, J. A. 1964, The Cooling Rates and Parent Planets of Several Iron Meteorites. Icarus 3, 429.

DISCUSSION

ALFVÉN: It is difficult to see how your mechanism works. You assume that the current is given by the conductivity of the body. Instead, would not the lack of charged particles transferring the current to and from the body be the limiting factor? If so, the energy released by ohmic heating must be small compared to the heating due to direct solar-wind impact on the body.

SINGER: Have you investigated the torque produced in the parent body by the interaction of the induced magnetic moments and the external field?

SONETT: This calculation has not been carried out. It was suggested earlier (Sonett et al., 1970) that fields of the magnitude indicated would have completely despun parent

bodies. Then if the asteroids are their residues, they should not be spinning today. Repeated collisions, however, could cause spin up where the total ensemble spin angular momentum is zero but both prograde and retrograde spins are present.

SINGER: For one of your modes of heating, it is necessary for currents to flow between the solar wind and the body. Will photoelectrons suffice?

SONETT: It seems most likely that photoelectron emission from the negative hemisphere and positive ion collection on the other hemisphere would suffice for the steady-state TM mode that I discussed. A value of nearly 10^{-3} A/m^2 is given for peak photocurrent (Sonett et al., 1970). The use of the photocurrent mechanism to supply current carriers means, however, that the mechanism is restricted to the sunlit hemisphere, whereas the calculations are for cylindrical symmetry. However, I do not think that the error introduced by the restriction to the sunlit hemisphere is severe.

DISCUSSION REFERENCE

Sonett, C. P., Colburn, D. S., Schwartz, K., and Keil, K. 1970, The Melting of Asteroidal-Sized Bodies by Unipolar Dynamo Induction From a Primordial T-Tauri Sun. Astrophys. Space Sci. 7, 446.

Page intentionally left blank

PRELIMINARY RESULTS ON FORMATION OF JETSTREAMS BY GRAVITATIONAL SCATTERING

R. T. GIULI
NASA Manned Spacecraft Center

Alfvén and Arrhenius (1970) have considered the development and stability of jetstreams by collisional interactions among grains; and they propose that in a jetstream environment, grains may collect and adhere to form self-gravitating embryos. Gravitational attraction of smaller particles by these embryos may then lead to a net accretion because high relative approach speeds, which could erode or break up embryos, have been minimized during the formation of the jetstream.

As an embryo grows, the synodic orbital frequencies between it and the particles it attracts become greater than the collision frequencies among these particles and between these particles and the rest of the jetstream. At this point, the embryo rather than the primordial jetstream will determine both the orbital parameters a, e, and i that the particles near the embryo adopt and the distribution of the particles among these orbits. The question is, will the redistribution of particle orbits by embryos remove particles from the jetstream?

Figure 1 illustrates schematically how streams of particles are attracted to impact an embryo in a two-dimensional model developed by Giuli (1968*a*,*b*). Calculations for a three-dimensional model have been made, and they qualitatively support the results for the two-dimensional model. The dotted lines represent elliptical particle orbits as seen in a rotating coordinate system centered on a massless embryo. The coordinates rotate with the same period as the embryo's orbital period. As mass is added to the embryo, it attracts some of the particles of given a and e to impact, and it gravitationally scatters other particles from their former (a, e) orbits and places them in different (a', e') ones. The impact cross section of the embryo is greatest for those orbits that provide impacting particles with impact speeds v_i at or near the embryo escape speed v_e. There is a well-defined relation between a and e for impacting orbits with $v_i/v_e = \text{const} = 1$, say, such that, if the dotted lines in figure 1 represent (a_{max}, e_{max}) for these orbits, then all impacting orbits with $v_i = v_e$ are contained within the two regions defined by the inner and outer extremes of the dotted lines.

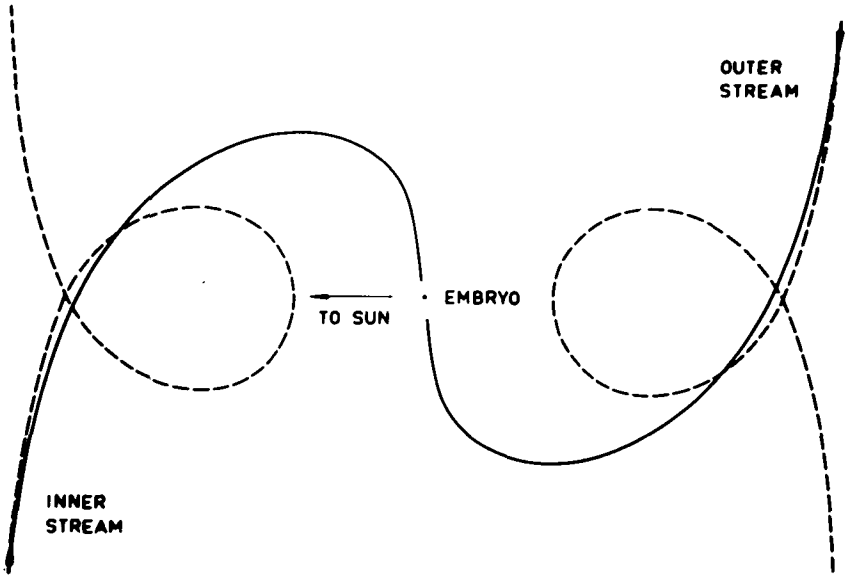

Figure 1.–Schematic illustration of particle streams gravitationally attracted to an embryo in the two-dimensional model developed by Giuli (1968*a*,*b*).

Calculations show that particles on impacting orbits with given v_i/v_e that do not impact on a given "pass" by the embryo will be scattered back into orbits with different (a', e') that are also impacting orbits with the same value of v_i/v_e, or else will be scattered into orbits with greater (a'', e'') that will eventually become impacting orbits with the same v_i/v_e as soon as the embryo becomes massive enough to reach them. In other words, if a particle is ever on an impacting orbit with given v_i/v_e, it remains on *some* orbit with the *same* v_i/v_e until it impacts, no matter how many times it is scattered before impact occurs. Spatially this means that, as the embryo grows, the particles that it does not capture on a given pass are shoved outward into more distant locations in the primordial jetstream, where they may be captured on succeeding passes. In two dimensions, the two "scattering jetstreams" (denoted by the inner and outer extremes of the two dotted lines in fig. 1) recede into the surrounding "viscous jetstream." The region between the scattering jetstreams is mostly devoid of particles; the regions outside are populated by the primordial jetstream particles; and the regions in the scattering jetstreams contain both primordial particles and particles relocated from the inner regions. Therefore, we expect the scattering jetstreams to have higher particle density than the viscous jetstream. In three dimensions, we expect the scattering jetstream to be a toroidal annulus of enhanced particle density, enclosing a tube of diminished particle density. In the center of the tube is the embryo.

Thus we see that the traditional (two-body) concept of an embryo growing by sweeping out a tube of matter of ever-increasing cross section is actually a valid concept, although the mechanics are rather involved.

Because the scattering jetstream is itself stable (particles are either stored or captured), the presence of embryos in primordial jetstreams does not destroy their stability.

REFERENCES

Alfvén, H., and Arrhenius, G. 1970, Structure and Evolutionary History of the Solar System, I. Astrophys. Space Sci. 8, 338-421.

Giuli, R. T. 1968*a*, On the Rotation of the Earth Produced by Gravitational Accretion of Particles. Icarus 8, 301-323.

Giuli, R. T. 1968*b*, Gravitational Accretion of Small Masses Attracted From Large Distances as a Mechanism for Planetary Rotation. Icarus 9, 186-190.

DISCUSSION

DOHNANYI: Have you had a chance to consider the influence on your accretion rates of competing processes; e.g., planetary perturbations, the Poynting-Robertson effect, and lifetime due to collisional breakup or erosion?

GIULI: No. We do not consider accretion rates in this model. To do that would require an estimate of the particle density during planet formation. That consideration will be an elaboration to the model.

SINGER: Is there a simple dimensional argument that can be put forth to explain the qualitative nature of the results for the gravitational accretion theory?

GIULI: Because the numerical integrations do display the asymptotic development of rotation with mass so dramatically, I feel strongly that there should be a simple explanation. As yet I have not found it.

ALFVÉN: One can show that if accretion occurs for any size body for which the total angular momentum contributed by the accreted material is some constant fraction of the angular momentum contributed by a particle that grazes the body tangentially with the body's escape speed, then the rotation speed acquired by the body is proportional to the square root of the body's density. Giuli's calculations show that the asymmetry of the impacts give about 1 percent of the tangential angular momentum for all masses.

WHIPPLE: It seems to me we are putting too much emphasis on the assumption that the process of formation of bodies produces a particular rotation rate. The limitation on rotation rates is density, not mass, and the solid bodies of the solar system have a small range of densities. The reason the observed rotation rates appear to cluster around certain values is that accumulation processes tend to give rapid rotation rates. Those bodies that tried to form with much higher rotation rates were disrupted and are not observed. Some bodies that were formed with lower rotation rates are observed. Forces that change rotation rates thus may destroy the bodies or reduce rotation rates, leading to the observed distribution.

GIULI: Getting back to Singer's question, and elaborating somewhat on Alfvén's comment: The rotational angular momentum per unit mass (specific angular momentum) contributed by an impacting particle that grazes a body with the body's escape speed (or with some factor of the escape speed) is easily shown to vary as the two-thirds power of the mass of the body, for a given body density. If any accretion process adds matter to an embryo in such a way that the sum of the contributions of specific angular momentum of added matter is some constant C times the two-thirds power of the embryo mass, then it is easy to show analytically that the asymptotic development of rotation rate with mass is an inevitable result, along with the period-density relation stated above by Alfvén. These

points are developed by Giuli (1968*a*, *b*). The gravitational accretion calculations provide this relation between contributed angular momentum and embryo mass, for any particular body that grows with constant mean density, at any distance from the Sun. This fact is true over at least the seven orders of magnitude of mass for which I did the calculations. This is a result of the fact that the geometry of the impacting particle trajectories scales linearly with the radius of the body. I have no simple explanation of why this should be the case, but probably it is connected with the fact that all embryo masses for which I did the calculations were small compared to the solar mass. (The largest embryo mass considered was Jupiter's mass.) I should mention that one failure of the current model is that it gives a different value of C for the different bodies of the solar system. Fish (1967) and Hartmann and Larson (1967) have shown that most of the bodies of the solar system have the same value of C over a mass range of 11 orders of magnitude.

UREY: MacDonald was the first to consider the relation between specific angular momentum and mass, and he obtained a power of 0.83 rather than two-thirds. This came about because he included Mars. The value two-thirds applies only if all terrestrial planets are excluded. Is this justifiable?

GIULI: Mercury, Venus, and Earth are excluded because of the apparent tidal effects upon their rotation rates subsequent to their formation. Mars is a very serious problem. If no subsequent process has affected Mars' rotation rate, and if Mars and the other bodies have formed by the same process, then the validity of the present gravitational accretion model as representing the process of formation may be in doubt. On the other hand, the present model can explain a retrograde rotation for, e.g., Venus if some peculiar condition restricted the eccentricity of heliocentric particle orbits in Venus' vicinity to low values during its growth.

HAPKE: The final rotation state of the body after accretion is strongly influenced by the initial density distribution in the nebula. This follows from consideration of the conservation of angular momentum and is independent of the details of the accretion process. Consider small particles in orbit about the proto-Sun that later condense into a larger body. The material initially inside the final orbit will have been moved outward during accretion and the material outside will have moved inward. The orbital angular momenta of both sets of particles will have changed in opposite senses. In general, the net change will not be zero, and thus the orbital angular momentum difference will show up as the spin angular momentum of the body. The direction and amplitude of the rotation depends on the original density distribution and final orbit.

GIULI: Perhaps. I am currently investigating the question of whether an embryo captures particles from their primordial heliocentric orbits or redistributes them before capture. The current investigation suggests that the latter situation applies to most of the captured particles. Also, the work of Trulsen[1] suggests that an intermediate particle state may occur before embryo formation; namely, a viscous jetstream that modifies the primordial particle distribution over the distances of interest.

DISCUSSION REFERENCES

Fish, F. F., Jr. 1967, Angular Momenta of the Planets. Icarus 7, 251-256.

Giuli, R. T. 1968*a*, On the Rotation of the Earth Produced by Gravitational Accretion of Particles. Icarus 8, 301-323.

Giuli, R. T. 1968*b*, Gravitational Accretion of Small Masses Attracted From Large Distances as a Mechanism for Planetary Rotation. Icarus 9, 186-190.

Hartmann, W. K., and Larson, S. M. 1967, Angular Momenta of Planetary Bodies. Icarus 7, 257-260.

MacDonald, G. J. F. 1963, The Internal Constitutions of the Inner Planets and the Moon. Space Sci. Rev. 2, 473-557.

[1]See p. 327.

ACCUMULATION OF CHONDRULES ON ASTEROIDS

FRED L. WHIPPLE
Smithsonian Astrophysical Observatory
and
Harvard College Observatory

It is suggested that aerodynamic forces played a significant role in the selective accumulation of chondrules on asteroids moving with respect to the gas in a primeval solar nebula. Particles smaller than millimeter chondrules would sweep by an asteroid moving in a critical velocity range, whereas larger particles could be accumulated by impact. Theory and calculation cover the case of subsonic velocity and asteroidal diameter up to 50 km for a nebula density up to 10^{-6} g/cm^3, or higher for smaller asteroids.

Chondrules, roughly millimeter spherules found abundantly in many meteorites, have long been aptly described in Eucken's (1944) terms as products of a "fiery rain" in a primeval solar system nebula. Chondrules are clearly mineral droplets that have cooled rapidly, some showing evidence of supercooling. On the basis of the quantitative loss of volatile elements, Larimer and Anders (1967) deduced that chondrules were formed in an ambient temperature of some 550 K. Because melting temperatures are roughly 1300 K greater, some violent heating mechanism must have been involved. Noteworthy is a suggestion by Wood (1963) that the quick heating was produced by shock waves in a primitive solar nebula. Volcanic and impact processes have been suggested, as has the pinch effect in lightning (Whipple, 1966).

Whatever the source of droplet formation, a major evolutionary problem concerns the high abundance of chondrules among several classes of meteorites; in some the percentage of chondrules exceeds 70 percent by mass. Accepting the concept that meteorites are broken fragments of asteroids that were originally accumulated from solids in a gaseous solar nebula, one's credulity is taxed by the added assumption that a substantial fraction of the solid material should have been in the form of spherules. Thus, the purpose of this paper is to explore the possibility that chondrules may have been selectively accumulated on some asteroidal bodies, thereby eliminating the undesirable supposition that chondrules constituted a major fraction of the dispersed solids in any part of the nebula.

Almost axiomatic is the assumption that the accumulation process for smaller asteroids essentially ceased when the solar nebula was removed,

presumably by the effect of the solar wind from the newly formed Sun in its brilliant Hayashi phase (Hayashi et al., 1960). Possibly the largest asteroids can still continue to grow in vacuum conditions, but the relative velocities of particle impact on asteroids less than perhaps a hundred kilometers in dimension would be generally dissipative rather than accumulative because of the low velocities of escape against gravity.

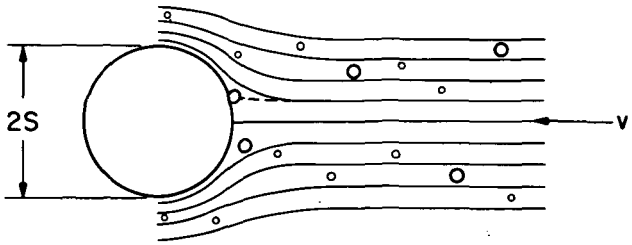

Figure 1.–Flow pattern in which larger particles may strike the moving body. S = radius of sphere.

While the solar nebula was present, however, small bodies moving through the gas would have exhibited aerodynamic characteristics. At a given body velocity and gas density, solid particles having a mass-to-area ratio below a certain value would be carried around the body by the inertia and viscosity of the gas currents so as not to impinge or accumulate on the moving body (fig. 1). The physical conditions for certain such accumulation processes will be established in the following sections of this paper.

IMPACT OF SMALL PARTICLES ON A SPHERE MOVING THROUGH A GAS

Taylor (1940) dealt with this basic problem for a cylinder. Langmuir and Blodgett (1945) derived numerical results by theory and calculation for cylinders, wedges, and spheres moving through air containing water droplets or icy spheres. Fuchs (1964) and Soo (1967) summarized the subject for subsonic flow and included both theoretical and experimental results by various investigators. Probstein and Fassio (1969) investigated "dusty hypersonic flows." The transonic case has apparently not been attacked seriously. The following discussion is based on the presentations by Langmuir and Blodgett augmented by the summaries by Fuchs and Soo.

A sphere of radius S is assumed to move at velocity v through a gas of density ρ and viscosity η containing in suspension small spheres of radius s and density ρ_s. The gas viscosity is given by the classical approximation

$$\eta = \frac{1}{2} vL\rho \tag{1}$$

where L is the mean free path of the atoms or molecules, assumed to be neutral.

Because the flow about the forward surface of the moving body is relatively streamlined at rather high values of the Reynolds number, the reference Reynolds number R_e is calculated for the small particles and given by the expression

$$R_e = \frac{2s\rho v}{\eta} \tag{2}$$

The applicable Reynolds number is reduced greatly from this value because the small particles will not be thrown violently into the full velocity of the gasflow v, except perhaps near the stagnation point. As will be seen, the relatively small value of the applicable Reynolds number permits the application of the simple Stokes' law of particle drag at values of v far above those for which the law might intuitively appear to be valid. Because the Stokes force F on a sphere of radius s moving at a velocity v_s through a gas

$$F = 6\pi\eta s v_s \tag{3}$$

is independent of the gas density when $L < s$, the impact equation for particles impinging on the larger sphere of radius S is widely applicable in a solar nebula where the density cannot be accurately specified. The Stokes approximation begins to fail significantly for $R_e > 10$, but the drag force is overestimated only by about a factor of 3 at $R_e = 10^2$. (See Probstein and Fassio, 1969.) An inertia parameter ψ is defined as

$$\psi = \frac{s^2 \rho_s v}{9\eta S} \tag{4}$$

which is the ratio of the inertia force to the viscous force for small particles in the stream. Theory and experiment show (fig. 2) that particles of radius $< s$ do not impact the sphere for $\sqrt{\psi} < 0.2$ for potential flow and 0.8 for viscous flow.

At higher values of R_e, when Stokes' law deteriorates, the behavior of the impact changes as a function of another parameter ϕ defined by

$$\phi = \frac{R_e^2}{2\psi} = \frac{18\rho^2 v S}{\rho_s \eta} \tag{5}$$

Figure 2 illustrates the changes in impact efficiency for values of ϕ up to $\phi = 10^4$. Note that the limiting value of $\sqrt{\psi}$, initiating the impacts, is nearly independent of ϕ, whereas the efficiency of impact is not greatly dependent on ϕ. Hence limiting conditions for impaction of particles of radius s, on a sphere of radius S, up to R_e somewhat less than 10^2, can be confidently given by equation (4) when $\psi_{limit} \sim 0.04$.

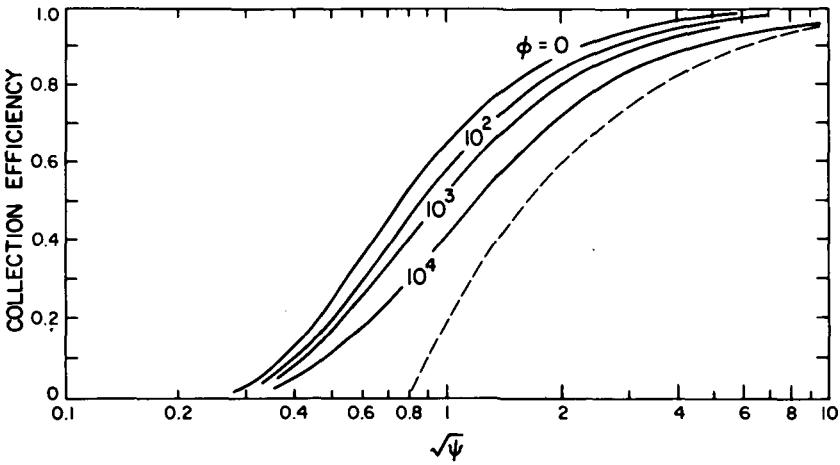

Figure 2.–Collection efficiency versus inertia parameter ψ as function of parameter ϕ. *Dotted curve: viscous flow.*

Let us then assume that chondrules have a radius of 0.05 cm and decide that particles of 1/3 this radius (diameter 1/30 cm) should not impact our asteroid of radius S moving at velocity v_l through the primeval nebula of viscosity η. Then $s = 1/60$ cm, $\sqrt{\psi} = 0.2$, and

$$v_l = \frac{0.36\eta}{s^2 \rho_s} S = 432\eta S \approx 0.069S \tag{6}$$

if we take ρ_s as 3 g/cm^3; employ cgs units; and adopt a "solar mix" of primeval gas with mass distribution $X_{\mathrm{H}} = 74$ percent, $Y_{\mathrm{He}} = 24$ percent, and $Z_{\mathrm{other}} = 2$ percent, hydrogen being in the form of neutral molecules at a temperature of 550 K. The viscosity becomes approximately

$$\eta = 1.6 \times 10^4 \text{ dyne-s-cm}^{-2}$$

Numerical values for equation (6) are given in table I.

TABLE I.–*Numerical Values for Equation (6)*

Diameter asteroid, 2S, km	Limiting velocity v_l, km/s	R_e
0.1	0.0034	0.04
1.0	.034	.4
10.0	.34	4.0
100.0	3.4?	40.0

DISCUSSION OF RESULTS

Before drawing conclusions from the first two columns of table I, we must check to see that the Reynolds numbers involved are not too high for the Stokes extrapolation to be valid; i.e., $R_e < 10^2$. This check involves an assumption as to the density near the plane of the solar nebula in the asteroid belt, say at 2.5 AU. Few theorists place the gas pressure here much greater than 1 kN/m^2 (10^{-2} atm). (See, for example, Cameron, 1962.) For a central mass equal to the Sun and allowing for the gravitational attraction of the gas itself, we find the corresponding density, $\rho \sim 5 \times 10^{-7}$ g/cm^3, and the surface density integrated perpendicular to the plane throughout the nebula some 3×10^5 g/cm^2, or about 1/30 solar mass per square astronomical unit. The Reynolds number (eq. (2)) is then given at $s = 1/60$ cm by $R_e = 11 \times 10^{-5}\, v$ cm/s, values of which are tabulated in the third column of table I, safely within our limits for asteroids up to 100 km in diameter. The limiting velocity, however, becomes supersonic at $v_l \sim 1.8$ km/s. Hence the condition of subsonic velocity limits our present conclusions to asteroids less than about 50 km in diameter.

The condition of molecular mean free path not exceeding the limiting dimensions of the chondrules restricts the theory to $\rho > 10^{-8}$ g/cm^3, a somewhat higher density than is sometimes assumed for the solar nebula in the asteroid belt. It is evident that a more complete theory is needed to cover the case of low densities in the solar nebula and that the transonic case should be developed before the present suggestion for the selective accumulation of chondrules by asteroids can be wholeheartedly accepted. The latter situation probably requires numerical analysis.

The case of lower density can be roughly approximated by means of Epstein's law of drag (see, e.g., Kennard, 1938), which, for mean free paths that are large compared with the dimension of the body, gives a drag force roughly $\rho/3\rho_c$ that of Stokes' law, where ρ_c is the critical gas density at which the mean free path of the molecules equals the dimension of the body. Because ψ varies inversely as the drag force, the critical value of ψ for accumulation in equation (4) will also vary approximately as $\rho/3\rho_c$ for relatively low gas densities. Hence the limiting velocity in equation (6) and in table I can be corrected as to order of magnitude by a factor of $\rho/3\rho_c$, or about $\rho \times 10^7$ g-cm^{-3}, for $\rho < 10^{-8}$ g-cm^{-3}.

The simple solution involving Stokes' law covers a considerable range of possible physical conditions and fairly reasonable ranges for planetoid velocities. In equation (6) the square of the radius of the limiting particle size varies inversely as the velocity and directly as the radius of the asteroid or planetoid. This indicates that the process of selective accumulation is fairly sharply defined in particle size when measured by velocity or size of the planetoid. If the process of chondrule formation (e.g., by lightning) is inherently limited for large dimensions, but not at small dimensions, the aerodynamic selection factor could frequently produce a fairly narrow range in

chondrule dimensions. Furthermore, extremely small chondrules could easily lose their identity in some meteorites by chemical differentiation during subsequent heating of the asteroid. Together, upper limits to dimensions in chondrule formation, a selective accumulation process, and perhaps some partial differentiation seem capable of relieving the theorist from the undesirable postulate that chondrules once constituted a sizable fraction of the mineral content in any part of the solar nebula.

Note that aerodynamic forces will prevent the accumulation of finely divided minerals on planetoids in motion with respect to the gaseous medium, thus greatly reducing the accumulation rates calculated on the basis of simple cross-sectional areas and velocities.

REFERENCES

Cameron, A. G. W. 1962, The Formation of the Sun and Planets. Icarus **1**, 13-74.

Eucken, A. T. 1944, Über den Zustand des Erdinnern. Naturwiss. **32**, 112-121.

Fuchs, N. A. 1964, The Mechanics of Aerosols, ch. 4. Macmillan Co. New York.

Hayashi, C., Jugaku, J., and Nishida, M. 1960, Models of Massive Stars in Helium-Burning Stage. Astrophys. J. **131**, 241-243.

Kennard, E. H. 1938, Kinetic Theory of Gases, p. 310. McGraw-Hill Book Co., Inc. New York.

Langmuir, I., and Blodgett, K. B. 1945, Mathematical Investigation of Water Droplet Trajectories. General Electric Res. Lab. Rept. RL-225. (1948, J. Meteorol. **5**, 175.)

Larimer, J. W., and Anders, E. 1967, Chemical Fractionations in Meteorites–II. Abundance Patterns and Their Interpretation. Geochim. Cosmochim. Acta **31**, 1239-1270.

Probstein, R. F., and Fassio, F. 1969, Dusty Hypersonic Flows. Fluid Mechanics Lab. Pub. 69-2, MIT. Cambridge.

Soo, S. L. 1967, Fluid Dynamics of Multiphase Systems, ch. 5. Blaisdell Publ. Co. Waltham, Mass.

Taylor, G. I. 1940, Notes on Possible Equipment and Techniques for Experiments on Icing on Aircraft. R&M no. 2024, Aeronautical Res. Comm. London.

Whipple, F. L. 1966, Chondrules: Suggestion Concerning the Origin. Science **153**, 54-56.

Wood, J. A. 1963, On the Origin of Chondrules and Chondrites. Icarus **2**, 152-180.

THE ALINEMENT OF ASTEROID ROTATION

JOSEPH A. BURNS
Cornell University

Data have been accumulating since the beginning of this century that indicate that most, if not all, large asteroids have periodic lightcurves. The variations that are seen have periods of the order of several hours and can be understood as being caused by bodily rotation, accompanied by changes in shape and/or surface properties. Because corresponding color changes are usually absent, the former explanation of a variation in cross section is probably the correct one.

The lightcurves of the asteroids do not exhibit photometric beat phenomena and, as Kopal (1970) has argued, this indicates that the rotation is about only one axis. In point of fact, the pole of the rotation axis can be determined from observations.[1] The principle behind interpreting these observations is easily understood: If, for simplicity, we assume that an asteroid orbits in the ecliptic and that its brightness is proportional to the surface area seen, then any variation in brightness (after corrections for distance and phase effects have been made) must correspond to a variation in the projected surface area. There will be no change in the brightness variation over one *orbital* period if the rotation pole is normal to the orbit plane, for then the differences in surface area seen over one *rotation* period are the same everywhere on the orbit. On the other hand, the maximum changes in surface area and, hence, the maximum brightness variation will occur when the rotation pole lies in the orbit plane; intermediate variations will correspond to intermediate positions. So, by observing the variation in the magnitude of the brightness over one orbital period, one can evaluate the longitude and latitude of the asteroid's rotation pole. An approximate technique, based on this idea but using only a few observations, has been applied to many asteroids in a series of papers primarily by Kuiper and Gehrels with others. (See Dunlap and Gehrels, 1969; Gehrels, 1967; Gehrels and Owings, 1962; Gehrels et al., 1970; Vesely;[2] and Wood and Kuiper, 1962.) The results, which could be further refined, indicate that the rotation axes may be clustered in ecliptic longitude and that almost all asteroids have large obliquities; the only one of the 15 or so whose rotation

[1]See p. 127.
[2]See p. 133.

axis lies more than 20° from the ecliptic is the large and nearly spherical Vesta (Gehrels et al., 1970) whose pole appears to be at about 65° ecliptic latitude.

The result that the rotation is about only one axis is truly surprising. According to rigid body dynamics, only when a principal axis lies along the direction defined by the body's angular momentum vector **H** will there be no precession. Otherwise, the principal axis system xyz fixed to the body should freely precess about **H**. We define $C > B > A$ to represent the moments of inertia about the z, y, and x axes, respectively, and consider as an example the case where the angular velocity $\boldsymbol{\omega}$ lies near the maximum axis z of inertia. Then the precession has an angular velocity $(\alpha\delta)^{1/2}\omega_z$ where

$$\alpha = \frac{C - B}{A} \qquad \delta = \frac{C - A}{B}$$

Furthermore

$$\left(\frac{\omega_x}{\omega_z}\right)^2 \sim \alpha \qquad \left(\frac{\omega_y}{\omega_z}\right)^2 \sim \delta$$

(Symon, 1960). For typical asteroid shapes, α and δ range from 10^2 to 10^{-2} and thus the free precession will occur on a time scale that is within an order of magnitude or two of the rotation time scale; in other words, it would be observable if it existed and $\boldsymbol{\omega}$ were not closely alined with **H**.

Dynamics also tells that the rotation will be stable only if it is about z, the axis of maximum moment of inertia, or x, the minimum axis. Observations are in agreement with this: The asteroids appear to be spinning about the maximum axis. This latter fact indicates that energy dissipation may be taking place because convergence of the maximum axis with **H** generally will occur whenever energy is dissipated internally in a quasi-rigid body (Pringle, 1966).

Kopal (1970) has argued that the absence of any precession indicates that the asteroids could not have arisen from collisions because then one should expect a random distribution of their angular momenta with respect to their body axes; thus he believes asteroids must have been formed in their present alined state. We wish to present a different interpretation of the peculiar alinement phenomenon.

We will present directly below calculations showing that at least a few major impacts should have taken place on the large asteroids after their formation. Such collisions will change each asteroid's **H** and will, in general, misaline **H** from $\boldsymbol{\omega}$. Thus, even if the rotation axes were perfectly alined originally, precession of some asteroids should be observed today. Because it is not seen, an alining mechanism must be (or must have been) at work if the collision calculations are correct. This idea receives some further support from the unusual ordering of the orientations of the rotation axes that itself speaks of an alinement process; it is quite difficult to explain Gehrels' large obliquities and the clustering in ecliptic longitude without some such process.

Before discussing possible alining mechanisms, let us first consider the collision process. Collisions between at least small asteroids are generally

believed to be still occurring; they are frequently invoked as a mechanism to provide material for the zodiacal dust cloud and for some meteorites. To find the number n of asteroids that are large enough to measurably affect the angular momenta of the visible asteroids, we recall that a collision between two bodies of masses m and M will change the angular momentum of the M body on the order of Rmv, where R is a mean radius and v is the impact velocity. The impact does not change the initial orientation of the asteroid but does instantaneously affect ω and **H**; **H** swings in space through an angle of the order of $mv/M\omega R$ radians. Taking an average relative velocity of 5 km/s, about one-third the Kepler orbit speed (Wetherill, 1967), $R = 40$ km and $2\pi/\omega = 5$ hr, collisions with bodies of $m/M > 3 \times 10^{-4}$ will cause **H** to rotate on the average by more than 5°. These collisions should produce a perceptible precession; for $R = 40$ km there will be 10^4 to 10^5 particles capable of producing this precession (Allen, 1963).

An asteroid's mean collision time scale τ can be approximated by a particle-in-a-box calculation: We consider that all the asteroids move within a torus of elliptical cross section whose volume V is approximately

$$2\pi\bar{a}\pi(\bar{a}\sin\bar{I})(2\bar{a}\bar{e}) \quad \text{or} \quad \sim 5 \times 10^{40}\ \text{cm}^3$$

where $\bar{a}$, $\bar{e}$, and $\bar{I}$ are, respectively, the mean semimajor axis, the mean eccentricity, and the mean inclination of the visible asteroids (Allen, 1963). Now τ is found by dividing the torus volume by the number of possible colliding particles multiplied by the collision cross section times the average velocity difference between two asteroids; i.e., the v from above. So

$$\tau = \frac{V}{vn\pi R^2} \tag{1}$$

or 10^8 to 10^9 yr. The results of more detailed work (Anders, 1965; Hartmann and Hartmann, 1968; Wetherill, 1967) agree quite well with this rough calculation. If present densities have existed throughout the past, most asteroids having a mean radius $R = 40$ km will have been struck many times during their lifetimes by particles massive enough to change their **H** by at least 5°. Larger particles will be so affected less frequently; τ for a 100 km body is just about the age of the solar system. Thus it is more likely that a medium-size asteroid should be seen precessing than a very large one. Naturally the current photometric data are primarily of the larger asteroids with many having radii about 100 km and only several with $R < 50$ km. The arguments presented here would be strengthened if data could be obtained on more medium-size asteroids.

We now wish to discuss briefly some factors that may affect the final rotation of an asteroid; namely, the influence of melting, aerodynamic drag, internal damping, and electromagnetic dissipation.

Asteroid melting during the Sun's T Tauri phase, as postulated by the unipolar generator mechanism of Sonett et al. (1970; see Sonett's paper in this

volume[3]), would have a profound effect on the asteroid's rotational properties. In fact, with complete melting there would be perfect alinement along the major principal axis; this complete melting would, however, symmetrize the body and this is not seen today. The effects of partial internal melting are difficult to discern at this time but they should produce an immediate partial alinement and accelerate any damping mechanisms. However, this melting would occur early in the evolution of the solar system (if at all) and thus, many of the misalining collisions postulated above will take place subsequently. Hence the alinement seen today apparently cannot be ascribed to a melting that occurred eons ago.

Dissipative aerodynamic torques have been shown to sometimes have a stabilizing effect on the rotation of satellites. Johnson (1968), using many simplifying assumptions and a complicated analysis, has given a stability criterion for cylindrical satellites in terms of a ratio of moments of inertia and body dimensions; applying this to uniform density bodies shows that they always tend to aline themselves along the minimum axis in the presence of aerodynamic torques. The decay time is very long, even in Earth's atmosphere. Although we might expect similar effects due to dust interactions to occur on asteroids, they should be very small; however, Johnson's idealized analysis leaves much to be desired and the problem needs to be studied further.

Let us now discuss internal damping mechanisms. Recently Kopal (1970) has dealt with the damping arising from the most obvious force, gravity. We consider the same problem in a somewhat different manner. The period of the forced precession of an axially symmetric asteroid due to the gravitational torque exerted by a disturbing body of mass μ is

$$P = \frac{4\pi r^3 C\omega}{3G\mu(C - A)\cos\epsilon} \tag{2}$$

where r is the distance between the bodies, ϵ is the asteroid's obliquity, and G is the universal gravitational constant (Kaula, 1968). If the disturbing body is the Sun, this is of the order of $\omega/(n^2 J_2 \cos\epsilon)$ where $J_2 = (A - C)/MR^2$ and n is the asteroid's orbital mean motion. Using reasonable values of the variables, P is 10^7 or 10^8 yr—far too long to be observed. One can use equation (2) to find a period of similar magnitude for the precession caused by Jupiter. Because the rate of damping of the precessional motion should occur with a time scale of at least an order or two greater than P, we find, in agreement with Kopal (1970), that Jovian-solar effects most likely cannot account for the alinement.

Prendergast (1958) in a brief conference report has summarized unpublished calculations on the internal damping of energy in a mechanism that is driven by the free precessional motion; this work was pointed out to me at this colloquium by G. P. Kuiper. Prendergast's persuasive physical arguments and his results will be repeated here. In a freely precessing body each element that

[3]See p. 239.

lies off the instantaneous rotation axis will have an elastic strain as a result of the instantaneous centrifugal acceleration. The elastic strain energy stored by any element in a freely precessing body will change as the instantaneous rotation axis moves through the body. The total strain energy will decrease because each element is in a varying stress field and, thus, loses energy by internal damping. The lost energy ultimately comes from the rotational kinetic energy. As mentioned above, the body accommodates this loss by alining its major principal axis with **H** so as to minimize its energy while conserving angular momentum. At this last stage, the axis of rotation is then fixed in the body so that the strains are constant in time and dissipation by this mechanism ceases. The decay times found by Prendergast are of the order of 10^5 yr. This appears to be the alining mechanism we seek; however, unless the calculations themselves become available, one must withhold absolute judgment.

We now ask, is there a dynamical reason that accounts for the observational indication, according to Gehrels' work, that a possible alinement of the rotation axes lies near the ecliptic? (We will ignore Vesta because its free precession time will be very long as a result of its sphericity and any precession it may have will not be observable.) Because the ecliptic is, in some sense, defined by the presence of a planar interplanetary magnetic field, one might seek a mechanism that involves electromagnetic dissipation of energy. Davis and Greenstein (1951) have proposed such a mechanism, using paramagnetic absorption, to explain the polarization of starlight by alining the rotation axes of elongated dust grains with the interstellar magnetic field. This mechanism, when applied to an orbiting body, will cause alinement with the plane of the magnetic field **B**. The time scale over which this phenomenon takes place is $0.1\ \chi'' B^2/\omega R^2$, where χ'' is the imaginary part of the complex susceptibility of the asteroid. Unhappily, this is many orders of magnitude too large to explain the alinement with the ecliptic.

In conclusion, we would like to review briefly the arguments that have been presented. It has been shown that most visible asteroids have suffered at least one major collision in their lifetime and that this collision should have caused subsequent free precession of the asteroid. Because such precession is not observed, mechanisms were sought that would produce alinement. Internal damping, as proposed by Prendergast (1958), seems to account for the body's alinement with the rotation axis. Although the search for an ecliptic alinement mechanism has been unsuccessful, such an alinement mechanism must exist (particularly for the small asteroids) and must have a time scale that is short in comparison with the age of the solar system. The presence of an alining process means that one cannot infer the primordial asteroid rotations from observations made today.

ACKNOWLEDGMENTS

I thank Dr. J. Veverka for assistance with all aspects of this presentation and D. McAdoo for reading a preliminary manuscript.

REFERENCES

Allen, C. W. 1963, Astrophysical Quantities, p. 152. Second ed., Athlone Press. London.
Anders, E. 1965, Fragmentation History of Asteroids. Icarus 4, 399-409.
Davis, L., Jr., and Greenstein, J. L. 1951, The Polarization of Starlight by Aligned Dust Grains. Astrophys. J. 114, 206-240.
Dunlap, J. L., and Gehrels, T. 1969, Minor Planets III. Lightcurves of a Trojan Asteroid. Astron. J. 74, 796-803.
Gehrels, T. 1967, Minor Planets. I. The Rotation of Vesta. Astron. J. 72, 929-938.
Gehrels, T., and Owings, D. 1962, Photometric Studies of Asteroids. IX. Additional Light Curves. Astrophys. J. 135, 906-924.
Gehrels, T., Roemer, E., Taylor, R. C., and Zellner, B. H. 1970, Minor Planets and Related Objects. IV. Asteroid (1566) Icarus. Astron. J. 75, 186-194.
Hartmann, W. K., and Hartmann, A. C. 1968, Asteroid Collisions and Evolution of Asteroidal Mass Distribution and Meteoritic Flux. Icarus 8, 361-381.
Johnson, K. R. 1968, Effect of Dissipative Aerodynamic Torque on Satellite Rotation. J. Spacecr. Rockets 5, 408-413.
Kaula, W. M. 1968, An Introduction to Planetary Physics, p. 183. John Wiley & Sons, Inc. New York.
Kopal, Z. 1970, The Axial Rotation of Asteroids. Astrophys. Space Sci. 6, 33-35.
Prendergast, K. H. 1958, The Effects of Imperfect Elasticity in Problems of Celestial Mechanics. Astron. J. 63, 412-415.
Pringle, R., Jr. 1966, On the Stability of a Body With Connected Moving Parts. AIAA J. 4, 1395-1404.
Sonett, C. P., Colburn, D. S., Schwartz, K., and Keil, K. 1970, The Melting of Asteroidal-Sized Bodies by Unipolar Dynamo Induction From a Primordial T Tauri Sun. Astrophys. Space Sci. 7, 446-488.
Symon, K. R. 1960, Mechanics, p. 454. Second ed., Addison-Wesley Pub. Co., Inc. Reading, Mass.
Wetherill, G. W. 1967, Collisions in the Asteroid Belt. J. Geophys. Res. 72, 2429-2444.
Wood, H. J., and Kuiper, G. P. 1962, Photometric Studies of Asteroids. X. Astrophys. J. 137, 1279-1285.

DISCUSSION

DOHNANYI: It seems to me that the influence of impacts on the rotation rate and axis of an asteroid is sensitive to the particular failure mode of the asteroid during such inelastic collisions. If an asteroid is hit by an object large enough to cause a catastrophic collision, a spherical shell of debris, concentric with the (spherical) target asteroid will most likely be ejected from it. There may then be an opportunity for momentum multiplication during such a process with corresponding implications on the realinement of the spin axis of the surviving core.

BURNS: The mass loss and angular momentum change resulting from a catastrophic collision–or, for that matter, from any hypervelocity impact–are difficult to predict. Certainly these quantities will depend strongly upon the particular mode of failure that occurs; i.e., on how much matter is ejected following a collision and *how* that matter is ejected.

However, the important point, insofar as this presentation is concerned, is that many collisions with relatively small bodies will appreciably misaline the angular momentum vector from the body's spin axis, causing noticeable precession. This misalinement will occur also in the remnants of catastrophic collisions. Furthermore, one can expect that the given expression for the change in the angular momentum direction will be of the right order of magnitude as long as the surviving core retains much of the body's original mass. Of course, most collisions are not catastrophic in the sense we are talking about here and in fact the middle-sized collisions should determine how the angular momentum vector changes direction for most bodies.

FRAGMENTATION AND DISTRIBUTION OF ASTEROIDS

JULIUS S. DOHNANYI
Bellcomm, Inc.

As a result of mutual inelastic collisions, frequent on a geologic time scale, the mass distribution of asteroids undergoes constant change. Using a simplified velocity distribution for asteroids, the redistribution of their masses caused by collisions can be mathematically modeled as a stochastic process and the distribution of asteroidal masses can then be obtained as the solution. This paper is a review of recent progress on this problem.

The most detailed discussion of this problem considers the influence of the following collisional processes on the asteroidal mass distribution: (1) loss of asteroids by catastrophic breakup, (2) creation of new objects from the fragments of a catastrophically disrupted one, (3) erosive reduction in the masses of individual asteroids, and (4) erosive creation of new objects (i.e., production of secondary ejecta during erosive cratering by projectiles not large enough to catastrophically disrupt the target object). The main result is that after a sufficiently long period of time the population of asteroids may reach a quasi-steady-state distribution, regardless of the initial distribution. This final distribution is a product of a slowly decreasing function of time by a power law of index 11/6 for masses smaller than the largest asteroids. For the largest asteroids, an additional factor is included that expresses the influence on the distribution of the absence of masses larger than those observed. The observed distribution of bright asteroids from the McDonald asteroidal survey and that of faint ones from the Palomar-Leiden asteroidal survey are each individually consistent with the theoretical distribution, although they differ from each other by a numerical factor.

As a result of mutual inelastic collisions, frequent on a geologic time scale, the distribution of asteroids is constantly changing. We shall, in this paper, discuss the influence these collisions have on the mass distribution of belt asteroids and compare the results with observation.

Ideally, one would consider the mass and orbital elements of each asteroid and establish their origin from precise calculations. This method has been employed by Anders (1965); making the usual assumption that the members of each Hirayama (1923, 1928) family are collisional fragments of some parent object, Anders (1965) has reconstructed the original parent objects and, subtracting the fragments, has estimated the hypothetical initial distribution of asteroids. Hartmann and Hartmann (1968) further studied this problem; they suggested that the present distribution may indeed have evolved, under the influence of collisional fragmentation, from Anders' (1965) estimated initial

distribution. Alfvén (1964*a,b*, 1969), on the other hand, discussed the origin of asteroids making the alternate assumption that asteroids in Hirayama families constitute original jetstreams. (Also see Kuiper, 1953.)

In view, however, of the fact that next to nothing is known about the distribution of asteroids too faint to be observed, and much still remains to be learned about those cataloged, it appears worthwhile to employ statistical methods to improve our understanding of some of the gross properties of the population of asteroids. Ideally, one would like to combine the distribution of orbital elements for asteroids with their mass distribution in a complete statistical analysis. This difficult problem can be simplified by two methods:

(1) Studying the distribution of the masses of asteroids using an assumed spatial (and velocity) distribution
(2) Studying the asteroidal population by using precise spatial and velocity distributions combined with an assumed mass distribution (Wetherill, 1967).

This second method has its basis on Öpik's (1951, 1963, 1966) statistical treatment of the dispersal of stray objects by planetary (gravitational) perturbations, and in its most highly developed form has been applied to asteroids by Wetherill (1967).

In this paper we shall limit our attention to method (1). Method (2) is, however, complementary to method (1), because a complete analysis would employ a combination of both methods; i.e., a joint mass, velocity, and position distribution.

Method (1) is the physical and mathematical modeling of a population of objects that undergo mutual inelastic collisions. Such collisions take place with an assumed mean encounter velocity, and the larger of the colliding masses may completely shatter (catastrophic collision) or it may lose a modest fraction of its mass (erosive collision) depending on the relative size of the other colliding object.

The result is a process by which the masses of individual objects in the population decrease with time because of erosion and by which some objects are violently destroyed from time to time. Redistribution of the comminuted debris produced during erosive and catastrophic collisions constitute a particle creation mechanism. A correct modeling of these processes would enable one to describe the evolution of the distribution of these colliding masses.

Piotrowski (1953) has derived a mathematical expression for the rate at which asteroids disappear because of catastrophic collisions and the rate at which the number of asteroids in any given mass range changes because of the erosive reduction of their masses caused by the cratering collisions with relatively small objects. He did not include the particle creation resulting from fragmentation during collisions and his analysis therefore is restricted to cases in which the replenishment (i.e., feedback) of the population by comminuted fragments is insignificant.

Jones (1968) has studied the evolution of the mass distribution of asteroids using a more detailed model; the contribution of fragmentation was considered but later discarded because the size of the fragments produced during collisions was taken to be insignificantly small.

Dohnanyi (1969) (see also Dohnanyi, 1967*a,b,c;* 1970*a*) has discussed a model that includes the influence on the distribution of asteroidal masses of the following collisional processes:

(1) Disappearance of asteroids because of catastrophic breakup
(2) Reappearance of new asteroids from the fragments of catastrophically disrupted ones
(3) Progressive change in the number of asteroids in any given mass range caused by the gradual reduction of asteroidal masses by erosive cratering of small projectile particles
(4) Reappearance, as tiny asteroids, of secondary ejecta produced during erosive cratering

Numerical values for all parameters were taken from experiment and observation, wherever possible; and a particular solution of a simple power-law type was obtained, under the provision that the distribution could be assumed stationary.

The study was continued (Dohnanyi, 1970*b*), and it was found that the mass distribution of asteroids may indeed approach a stationary form, regardless of initial conditions, after a sufficiently long time period has elapsed. The uniqueness of the solution obtained in Dohnanyi (1969) was considered, and it was found to be the only analytic solution that can be expanded into a power series in m, for masses m far from the limiting masses of the distribution. An approximate solution for large asteroids was also obtained.

Hellyer (1970) has also examined this problem; he considered large asteroids and small ones separately. For small asteroids he studied the influence on the mass distribution of fragmentation and his treatment is comparable to that in Dohnanyi (1969, 1970*b*) except that it is less detailed but mathematically much shorter.

Because of their completeness compared with earlier work, we shall, in what follows, give a review of these studies (Dohnanyi, 1969, 1970*b*). Most of the earlier work can readily be discussed by comparing it with special cases of these studies.

OBSERVATIONAL EVIDENCE

McDonald Asteroidal Survey[1]

In their survey of asteroids at the McDonald Observatory (the McDonald survey (MDS)), Kuiper et al. (1958) obtained statistical data for the brighter

[1] Currently under revision; see van Houten in the "Discussion" following this paper.

asteroids up to a limiting apparent magnitude of 16. The observation covered the asteroid belt over all longitudes and a 40° width in latitude. The absolute photographic magnitudes of 1554 asteroids were obtained in half-magnitude intervals together with correction factors for estimating the true number of asteroids in each magnitude interval, based on the completeness of the survey.

To estimate the masses of asteroids, we assume a geometric albedo of $0.2 \times 3^{\pm 1}$ and material density of 3.5×10^3 kg/m^3. The upper limit on the geometric albedo represents a completely white smooth surface and the lower limit corresponds to basalt. The nominal value of 0.2 is the mean of the estimated geometric albedos of the asteroids Ceres, Pallas, Juno, and Vesta. (See, e.g., Sharonov, 1964.) The result is

$$\log_{10} m = 22.67 \pm 0.72 - 0.6g \tag{1}$$

where m is the mass, in kilograms, of a spherical asteroid with absolute photographic magnitude g (i.e., relative photographic magnitude at a distance of 1 AU from both Earth and the Sun). A measure of the uncertainty due to albedo is indicated.

The observational material of MDS is presented in figure 1. Plotted in this figure are the cumulative number of observed asteroids (solid histogram) as well as the probable true number of asteroids (dashed line histogram) versus absolute photographic magnitude g, as given by MDS. The curve is complete up to $g = 9.5$; i.e., the observed number of these objects is believed to equal the true number. Above $g \gtrsim 9.5$ the difference between the true and the observed number of asteroids, based on the completeness of the survey, has been tabulated in MDS (also see Kiang, 1962); the dashed line histogram in figure 1 is their mean value.

The solid curve in figure 1 is the cumulative number $N(m)$ of asteroids larger than m

$$N(m) = \int_m^{M_\infty} f(M)\, dM \tag{2}$$

as a function of mass m (or g) obtained in Dohnanyi (1969). In that study, we took $M_\infty = 1.86 \times 10^{20}$ kg corresponding to $g = 4$ and

$$f(m) = 2.59 \times 10^{16}\, m^{-1.837} \tag{3}$$

where the numerical (normalization) factor is empirical and the numerical value of the exponent was theoretically obtained for relatively small (faint) asteroids. It can be seen that there is close agreement between theory and the statistical results of MDS.

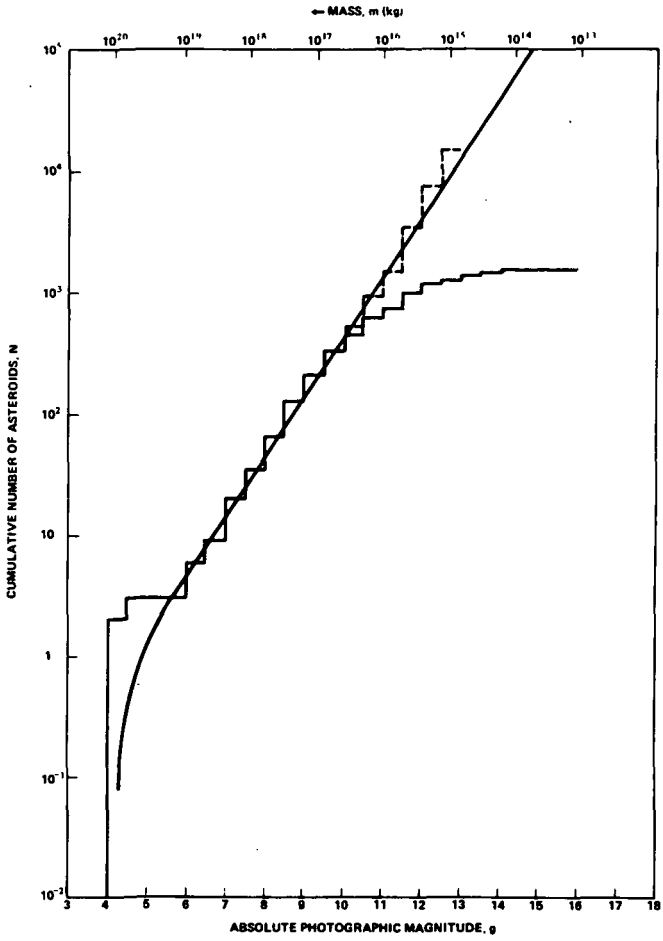

Figure 1.–Cumulative number of asteroids having an absolute photographic magnitude g or smaller (i.e., mass m or greater), obtained by the MDS. Observed value = solid line histogram; probable value = dashed line histogram; earlier theory (Dohnanyi, 1969) = solid curve.

Palomar-Leiden Survey

A series of observations of faint asteroids with limiting apparent magnitudes of less than 20 was made by van Houten et al. (1970) at Hale Observatories (Mount Palomar) (the Palomar-Leiden survey (PLS)). The angular area covered was only 18° by 12° and a compilation of the estimated number of faint asteroids as a function of absolute magnitude, in the range $11 \leqslant g \leqslant 17$, was prepared. Whereas in the MDS results, the number of asteroids found is believed to be complete up to an absolute magnitude of about $g = 9.5$, in the

case of the PLS results, the number of observed asteroids needs to be corrected for completeness for all values of g because of the smaller area covered (about 1 percent of the MDS area). Thus, to estimate the total number of faint asteroids in the entire asteroid belt as a function of absolute magnitude g, the PLS data have to be extrapolated over the large regions not covered by the survey.

The result is displayed in figure 2, a plot of the cumulative number of asteroids having an absolute magnitude g or greater (per half-magnitude intervals) obtained by MDS and PLS, as indicated. It can be seen that the two curves display the same trend, i.e., the shapes of the two distributions are identical, but that the MDS results are almost an order of magnitude higher than corresponding PLS results, and likewise for their respective extrapolations. It was pointed out in the PLS report that this discrepancy may be due to the method of estimating completeness factors in MDS. Because the true cause for this discrepancy has not yet been given, we shall avoid combining the results of MDS with those of PLS and will consider them separately.

In figure 3, we plot the cumulative number of asteroids from PLS as a function of absolute magnitude g and seek to represent the results by an empirical formula of the form

$$N(m) = Am^{-\alpha+1} \tag{4}$$

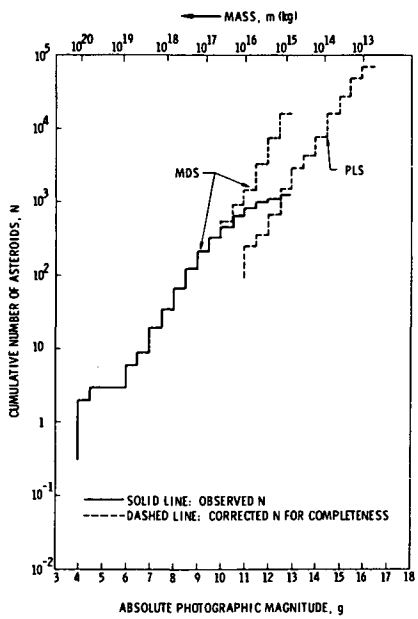

Figure 2.–Cumulative number of asteroids obtained by the MDS and the PLS. Solid line is the observed number; dashed line is the corrected number for completeness.

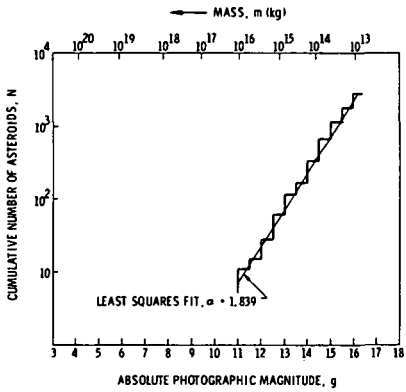

Figure 3.–Cumulative number N of the PLS asteroids with a least-squares fit to N.

where $N(m)$ is the cumulative number of asteroids having masses of magnitude m or greater and A is a constant. A least-squares fit to the data of equation (4) gives

$$\alpha = 1.839 \tag{5}$$

which, in view of uncertainties, can be regarded as identical to the theoretical result (eq. (3)) of $\alpha = 1.837$ obtained in Dohnanyi (1969) and found to represent very well the MDS results. (If the five objects too bright for measurement in the iris photometer employed by PLS are included, one obtains $\alpha = 1.815$; i.e., an insignificant difference of 0.024 for magnitudes $g \geqslant 11$.)

Kessler (1969) has studied the joint distribution of magnitudes, radial distance from the Sun, and heliocentric longitudes of the cataloged asteroids. It appears, from his results, that equations (4) and (5) are good representations of his overall results (NASA SP-8038, 1970).

Recent work by Roosen (1970) indicates that the counterglow may be caused, almost entirely, by particles in the asteroid belt. We may therefore have direct evidence that the distribution of minor planets extends to the size range of micrometeoroids. (See Dohnanyi, 1971.)

We shall, in the remainder of this paper, discuss the manner in which power-law distributions of the types in equations (3), (4), and (5) arise.

IMPACT MECHANICS

Mean Impact Velocity

When two asteroidal objects collide, the damage done to the colliding bodies depends on, besides other factors, the magnitude of the relative velocity of the two colliding objects. A statistical treatment of asteroidal collisions should,

therefore, include the velocity distribution function as well as the mass distribution of the colliding masses. We shall, however, confine our attention to the influence of collisions on the mass distribution, using a mean encounter velocity. Such a simplified approach leads to a model that is mathematically tractable, as we shall see later. An alternate approach, in which the velocity distribution is modeled using Monte Carlo techniques but using an assumed mass distribution, has been given elsewhere. (See Wetherill, 1967, for a review and references.)

Consider two asteroidal objects with masses M_1 and M_2. Using a simple molecules-in-a-box approach, kinetic theory tells us that the expected number of times these two objects collide per unit time is

$$\pi(R_1 + R_2)^2 \frac{\bar{v}}{V_0} \tag{6}$$

where R_1 and R_2 are the effective radii of the two objects, $\bar{v}$ is the mean encounter velocity, and V_0 is the effective volume of the asteroid belt.

Using the distribution of the inclinations and eccentricities for known asteroids, I have estimated (Dohnanyi, 1969) the rms encounter velocity with the estimated dispersion as

$$\sqrt{\overline{v^2}} \approx 5 \pm 5 \qquad \text{km/s} \tag{7}$$

in agreement with Piotrowski's (1953) estimate of 5 km/s. The distribution of encounter velocities appears to be rather broad and individual encounter velocities may vary considerably as suggested by equation (7).

Comminution Law

Collisions at impact velocities of several kilometers per second are inelastic and result in fragmentation. Gault et al. (1963) have fired projectiles into effectively semi-infinite basalt targets at very high velocities over a range not exceeding 10 km/s and over a range of projectile kinetic energies from 10 to 10^4 J. The result of the impact was the production of a crater and the ejection of crushed material. The total ejected mass M_e was found to be proportional to the projectile kinetic energy and the size distribution of the ejecta could be approximated by a power-law distribution.

We, therefore, choose (Dohnanyi, 1969) a comminution law of the form

$$g(m; M_1, M_2)\, dm = C(M_1, M_2) m^{-\eta}\, dm \tag{8}$$

where $g(m; M_1, M_2)\, dm$ is the number of fragments in the mass range m to $m + dm$ created when a projectile object M_1 strikes a larger target object of

mass M_2. The factor $C(M_1, M_2)$ is a function of the colliding masses and η is a constant,

$$\eta \approx 1.8 \tag{9}$$

for semi-infinite targets. (See Hartmann, 1969, for a survey.)

Using the fact that mass is conserved during impact, it is readily shown that

$$C(M_1, M_2) = (2-\eta) M_e M_b{}^{\eta-2} \tag{10}$$

where M_e is the total ejected mass and M_b is the upper limit to the mass of the largest fragment.

Erosive and Catastrophic Collisions

We shall presently distinguish between two different types of collisions depending on the mass M_1 of the projectile compared with the mass M_2 of the target. For

$$M_1 \ll M_2 \tag{11}$$

the target mass is effectively infinite and Gault's (Gault et al., 1963) results apply. These collisions we shall denote as erosive; clearly, during erosive collisions the projectile craters out a relatively minor amount of mass, leaving the large target mass otherwise intact.

For these collisions, M_e is proportional to the projectile mass M_1 (Gault et al., 1963) and we write (Dohnanyi, 1969), for basalt targets,

$$M_e = \Gamma M_1 \qquad \Gamma \approx 5v^2 \tag{12}$$

with the impact speed v expressed in kilometers per second. (See Marcus, 1969, for a detailed discussion.)

The upper limit to the mass of the largest fragment is given by

$$M_b \simeq \frac{M_e}{\lambda} \qquad \lambda \simeq 10 \tag{13}$$

If the target mass M_2 is not effectively infinite, then some projectile masses will be sufficiently large to catastrophically disrupt the target. Not much is known about the precise relationship between the target mass M_2 and the smallest projectile mass M_1 necessary for catastrophic disruption of M_2 or about the precise nature of the catastrophic failure mode of colliding objects with arbitrary sizes, shapes, and physical composition.

Experiments (Moore and Gault, 1965) with basalt targets conducted at relatively low impact velocities in the range of 1.4 to 2 km/s imply that a target mass M_2 about 50Γ times the projectile mass or smaller will be catastrophically disrupted. The failure mode of the spherical target consists in the separation of a spherical shell of debris leaving an approximately spherical core behind as the largest fragment.

More recent experiments (Gault and Wedekind, 1969) on finite glass targets indicate a failure mode in which, in addition to a crater having a size determined by equation (12) for semi-infinite targets, a spall fragment on the surface of the spherical target opposite the point of impact will be produced. Both glass and basalt targets are seen to have comparable failure modes; the difference is that the basalt target fails by the production of a spall engulfing most of the spherical surface of a spherical target M_2, whereas the glass sphere target fails by the formation of a spall opposite the impact.

In both cases the distribution of fragments can be represented reasonably well by a formula of the form of equation (8). The total ejected mass is now given by

$$M_e = M_1 + M_2 \tag{14}$$

for catastrophic collisions, and the largest target mass M_2 catastrophically disrupted by M_1 will be taken as $M_2 = \Gamma' M_1$. Thus,

$$M_2 \leqslant \Gamma' M_1 \tag{15}$$

for catastrophic collisions, and

$$M_2 \geqslant \Gamma' M_1 \tag{16}$$

for erosive collisions.

The quantity Γ' is difficult to estimate precisely; combining results by Gault et al. (1963), Moore and Gault (1965), and Gault and Wedekind (1969), we may write

$$\begin{aligned} \Gamma' &\approx 50\Gamma \qquad \text{for basalt} \\ \Gamma' &\approx 10^3\Gamma \qquad \text{for glass} \end{aligned} \tag{17}$$

The large difference in these numbers is due mainly to the differences in the catastrophic failure modes between basalt and glass. Less energy is needed to detach a spall from a glass sphere than to detach a spherical shell of fragments from a basalt sphere.

The limit of the mass of the largest fragment for catastrophic collisions can be taken as

$$M_b = \frac{M_2}{\lambda'} \tag{18}$$

This formula is an idealization because for catastrophic collisions the size of the largest fragment should be approximately inversely proportional to the collisional kinetic energy. This relation defines the expected size of the largest fragment during an average catastrophic collision. For a more detailed definition of M_b we can take

$$M_b = \frac{{M_2}^2}{\lambda_0 M_1}$$

where M_b is inversely proportional to M_1 and λ_0 is a constant. The main effect of this refinement on the subsequent analysis (unpublished) is to add further detail without, however, altering the main conclusions. We therefore choose to retain the mathematically simpler but physically less correct definition of M_b (eq. (18)). Collecting formulas, we have

$$g(m; M_1, M_2)\, dm = (2-\eta)\Gamma^{\eta-1}\lambda^{2-\eta} {M_1}^{\eta-1} m^{-\eta}\, dm \qquad M_2 \geqslant \Gamma' M_1 \quad (19)$$

for erosive collisions, and

$$g(m; M_1, M_2) = (2-\eta)(M_1 + M_2){M_2}^{\eta-2}(\lambda')^{2-\eta} m^{-\eta}\, dm \quad M_2 < \Gamma' M_1 \quad (20)$$

for catastrophic collisions.

COLLISION EQUATION

Collisions between asteroids must undoubtedly affect their mass distribution. To gain insight into this problem, we give a precise mathematical model of the evaluation of the asteroidal mass distribution under the influence of mutual inelastic collisions.

Let $f(m, t)\, dm$ be the number density per unit volume of asteroids in the mass range m to $m + dm$ at time t. Clearly, $f(m, t)\, dm$ will change in time because of (1) erosion, (2) removal by catastrophic collisions of objects in this mass range, and (3) creation of fragments into this mass range by the erosive or catastrophic collisions of larger objects.

Assuming a uniform spatial distribution throughout the asteroid belt, one can write a continuity equation for the number density $f(m, t)$:

$$\frac{\partial f(m,t)}{\partial t}\, dm = dm \left.\frac{\partial f}{\partial t}\right|_{\text{erosion}} + dm \left.\frac{\partial f}{\partial t}\right|_{\text{catastrophic collisions}} + dm \left.\frac{\partial f}{\partial t}\right|_{\text{catastrophic creation}} + dm \left.\frac{\partial f}{\partial t}\right|_{\text{erosive creation}} \quad (21)$$

Here $[\partial f(m, t)/\partial t]\, dm$ is the time rate of change of the number density per unit volume of asteroids in the mass range m to $m + dm$ because of all the collisional processes listed on the right-hand side of the equation. The individual terms on the right-hand side of equation (21) are discussed below.

Erosion

The first term on the right-hand side of equation (21) is the contribution of the erosive reduction in the particle masses; i.e., the reduction in the number of particles with given mass because much smaller erosive projectiles crater out minor amounts of mass from these particles.

It has been shown in Dohnanyi (1969) that

$$\left.\frac{\partial f}{\partial t}\right|_{\text{erosion}} = -\frac{\partial}{\partial m}\left[f(m, t)\frac{dm}{dt}\right] \tag{22}$$

where

$$\frac{dm}{dt} = -\Gamma K \int_{\mu}^{m/\Gamma'} Mf(M, t)(M^{1/3} + m^{1/3})^2\, dM \tag{23}$$

is the mass lost per unit time by an object having a mass m that is being "sandblasted" by erosive collisions, and where

$$K = \left(\frac{3\pi^{1/2}}{4\rho}\right)^{2/3} \bar{v} \tag{24}$$

The parameter μ is the smallest mass permitted to be present by radiation pressure. Although objects may be present that are smaller than the limiting small mass blown away by radiation pressure as determined by geometric optics, we shall not concern ourselves with this problem. We shall assume that masses smaller than μ are either absent or simply do not participate in the collisional processes considered here.

The expression for dm/dt in equation (23) can be seen to be correct because the amount of mass per unit time lost by m because of erosive collisions with particles in the mass range M to $M + dM$ is, using equations (6) and (12),

$$-\Gamma M[R(M) + R(m)]^2 f(M, t)\, dM = -K\Gamma M(M^{1/3} + m^{1/3})^2 f(M, t)\, dM \tag{25}$$

and the right-hand side of equation (23) is just the contribution to $\dot{m}$ of all erosive projectiles; i.e., all projectiles with masses smaller than m/Γ' (cf. eq. (16)).

The contribution of this erosive reduction of the masses to the distribution $\partial f/\partial t|_{\text{erosion}}$ is then seen to be correctly given by equation (22), because $\dot{m}f(m, t)$ is the one-dimensional flux of particles in "mass space" and the right-hand side of equation (22) is the negative divergence of the flux in mass space. The net contribution of $\partial f/\partial t|_{\text{erosion}}$ may be positive or negative, depending on whether more masses are eroded into the range m to $m + dm$ than are eroded out of this range per unit time, or vice versa. (See Dohnanyi, 1967*b*, for a detailed derivation.)

Catastrophic Collisions

The second term on the right-hand side of equation (21) is the contribution of catastrophic collisions to the evolution of the population. It is (Dohnanyi, 1969),

$$dm \left.\frac{\partial f(m, t)}{\partial t}\right|_{\text{catastrophic collisions}} = -Kf(m, t)\, dm \int_{m/\Gamma'}^{M_\infty} f(M, t)(M^{1/3} + m^{1/3})^2\, dM \quad (26)$$

where M_∞ is the largest mass present.

This equation is readily derived because the number of collisions per unit volume of space and unit time $\delta^2 n$ between spherical particles with masses in the range M_1 to $M_1 + dM_1$ and M_2 to $M_2 + dM_2$ is (cf. eqs. (6) and (25))

$$\delta^2 n = K(M_1{}^{1/3} + M_2{}^{1/3})^2 f(M_1, t) f(M_2, t)\, dM_1 dM_2 \quad (27)$$

The total number per unit volume and unit time of catastrophic collisions that objects with masses in the range m to $m + dm$ experience is then given by the integral $\delta^2 n$ over the permissible limits, which is just equation (26). The range of values for the dummy integration variable M, $m/\Gamma' \leqslant M \leqslant M_\infty$ is seen to include all mass values that would completely disrupt m during an inelastic collision (cf. eq. (15)).

Creation by Catastrophic Collisions

We shall presently derive an expression for the creation per unit volume and unit time of objects in the mass range m to $m + dm$ by the catastrophic disruption of larger objects.

We first note that the number of fragments in the mass range m to $m + dm$ created by the catastrophic disruption of two objects having masses M_1 and M_2

is given by equation (20). The number of collisions $\delta^2 n$ per unit volume of space and unit time between two spherical objects with masses in the range M_1 to $M_1 + dM_1$ and M_2 to $M_2 + dM_2$ is given by equation (27). Hence, combining these, we obtain the number of fragments in a mass range m to $m + dm$ created per unit time and volume by catastrophic collisions between masses in the range M_1 to $M_1 + dM_1$ and M_2 to $M_2 + dM_2$ (with $M_2 > M_1$):

$$g(m; M_1, M_2)\, dm\, \delta^2 n = m^{-\eta}\, dm(2-\eta)(\lambda')^{2-\eta} M_2^{\eta-2}(M_1 + M_2) \times K(M_1^{1/3} + M_2^{1/3})^2 f(M_1, t) f(M_2, t)\, dM_1\, dM_2 \quad (28)$$

This expression is valid for

$$m \leqslant \frac{M_2}{\lambda'} \quad (29)$$

because m cannot exceed the mass of the largest fragment produced by the catastrophic collision of M_1 with M_2 (cf. eq. (18)).

Integrating expression (28) over all permissible masses M_2 and M_1, we obtain the contribution of this creation process to equation (21):

$$\left.\frac{\partial f(m, t)}{\partial t}\right|_{\text{catastrophic creation}} = K(2-\eta)(\lambda')^{2-\eta} m^{-\eta} \int_{\lambda' m}^{M_\infty} dM_2 \times \int_{M_2/\Gamma'}^{M_2} dM_1\, M_2^{\eta-2}(M_1 + M_2)(M_1^{1/3} + M_2^{1/3})^2 f(M_1, t) f(M_2, t) \quad (30)$$

which is the desired expression.

Creation by Erosive Collisions

Using the same reasoning as the one employed in the derivation of equation (30), we can obtain the corresponding expression for the erosive creation of objects into the mass range m to $m + dm$. Combining the comminution law for erosive collisions, equation (19), with the differential frequency of these collisions $\delta^2 n$ and integrating, over all permissible masses M_1 and M_2, we obtain

$$\left.\frac{\partial f(m, t)}{\partial t}\right|_{\text{erosive creation}} = K(2-\eta)\Gamma^{\eta-1}\lambda^{2-\eta} m^{-\eta} \int_{\lambda m/\Gamma}^{M_\infty/\Gamma'} dM_1 \times \int_{\Gamma' M_1}^{M_\infty} dM_2\, M_1^{\eta-1}(M_1^{1/3} + M_2^{1/3})^2 f(M_1, t) f(M_2, t) \quad (31)$$

This completes the derivation of the explicit form of $\partial f(m, t)/\partial t$, equation (21).

SOLUTION FOR SMALL MASSES

Asymptotic Solution

The general solution of the collision equation (eq. (21)) is difficult to obtain. We shall, however, seek an asymptotic solution valid after a long period of time of the creation of the asteroids.

Specifically, we seek a solution of the form

$$f(m, t) \simeq a_0(m) + \frac{a_1(M)}{t} + \frac{a_2(m)}{t^2} + \ldots \tag{32}$$

valid when t becomes very large. We substitute equation (32) into equation (21) and equate the coefficients of like powers of t to zero.

Using equations (21), (22), (26), (30), and (31) we get, for $a_0(m)$,

$$0 = K\Gamma \frac{\partial}{\partial m}\left[a_0(m)\int_{\mu}^{m/\Gamma'} Ma_0(M)(M^{1/3} + M^{1/3})\,dM\right]$$

$$- Ka_0(m)\int_{m/\Gamma'}^{M_\infty} a_0(M)(M^{1/3} + M^{1/3})^2\,dM + K(2 - \eta)(\lambda')^{2-\eta}m^{-\eta}$$

$$\times \int_{\lambda' m}^{M_\infty} dM_2 \int_{M_2/\Gamma'}^{M_2} dM_1\, {M_2}^{\eta-2}(M_1 + M_2)({M_1}^{1/3} + {M_2}^{1/3})^2 a_0(M_1)a_0(M_2)$$

$$+ K(2 - \eta)\Gamma^{\eta-1}\lambda^{2-\eta}m^{-\eta}\int_{\lambda m/\Gamma}^{M_\infty/\Gamma'} dM_1$$

$$\times \int_{\Gamma' M_1}^{M_\infty} dM_2\, {M_1}^{\eta-1}({M_1}^{1/3} + {M_2}^{1/3})^2 a_0(M_1)a_0(M_2) \tag{33}$$

which is the equation for the steady-state solution (cf. Dohnanyi, 1969; 1970*b*).

A time-independent solution of equation (21) is not valid because

$$\lim f(m, t) = 0 \qquad t \to \infty \tag{34}$$

in the absence of sources. We, therefore, take $a_0(m)$ to be a slowly varying function of time, satisfying equation (34), and approximately satisfying equation (33). This argument requires that the creation and destruction terms

on the right-hand side of equation (21) balance each other. It is, however, clear that for masses

$$m > \frac{M_\infty}{\lambda'} \tag{35}$$

no particle creation is possible because the upper limit of the largest fragment during a catastrophic collision involving M_∞ is smaller than m. Equation (32) can therefore be valid only if

$$a_0(m) = 0 \qquad \frac{M_\infty}{\lambda'} \leqslant m \leqslant M_\infty \tag{36}$$

and we have, therefore, a different solution for the distribution of large masses.

Solution in a Power Series of m for Small Masses

The power series solution to the leading terms of the steady-state equation, equation (33), is (Dohnanyi, 1969; 1970*b*)

$$a_0(m) = Am^{-\alpha} \tag{37}$$

where A is a constant and the population index α is

$$\alpha = \frac{11}{6} \tag{38}$$

The leading terms in equation (33) are those describing particle creation and destruction by catastrophic collisions caused by the impact of projectile particles whose masses and geometric cross sections are negligibly small compared with the target objects.

The contribution of erosion to the steady-state process, equation (33), is a minor one. The contribution of $\partial f/\partial t|_{\text{erosion}}$ (cf. eqs. (21) and (22)) is negative; i.e., the number of objects in the mass range m to $m + dm$ will decrease because of the erosive reduction of particle masses when the distribution is given by $\alpha = 11/6$ (eq. (38)). This happens because for a power-law-type distribution, $\partial f/\partial t|_{\text{erosion}}$ (eq. (22)) is positive for $\alpha > 4/3$.

It is interesting to note that when $\alpha = 11/6$, the leading terms of $\partial f/\partial t|_{\text{erosion}}$ and $\partial f/\partial t|_{\text{erosive creation}}$ cancel each other out.

If the comparatively small contribution of terms associated with the mass and size of the projectile during catastrophic collisions as well as the contribution of erosive processes are included in equation (33), the value of α is not appreciably different from 11/6. It was found (Dohnanyi, 1969) that at

mean impact velocities ranging from 1 to 20 km/s and values for the comminution index η (eq. (8)) ranging from 1.7 to 1.9, numerical solutions for α ranged from 1.841 at 1 km/s to 1.835 at 20 km/s mean impact velocity.

It therefore follows that the steady-state solution is rather insensitive to changes in the physical parameters. This solution represents a population whose evolution is mainly controlled by the catastrophic destruction of objects in a given mass range, and by the creation of fragments in this same mass range by catastrophic disruption of larger masses. These two competing processes cancel each other in a steady-state population described by the solution of equation (33).

SOLUTION FOR LARGE MASSES

Very Large Masses

For the largest masses, creation by fragmentation cannot be very effective and the number of these asteroids decreases with time. The collision equation (21) becomes correspondingly simplified.

Specifically, for masses in the range

$$\frac{M_\infty}{\lambda'} \leqslant m \leqslant M_\infty \tag{39}$$

i.e., for masses greater than the largest fragment when M_∞ is disrupted, no creation by fragmentation is possible. If the number density of asteroids in this mass range is denoted by $F(m, t)$ and the number density for masses $m \leqslant M_\infty/\lambda'$ is denoted by $f(m, t)$, we have, using equations (21) and (26)

$$\frac{\partial F(m, t)}{\partial t} = -KF(m, t)\left[\int_{m/\Gamma'}^{M_\infty/\lambda'} f(M, t)(M^{1/3} + m^{1/3})^2\, dM + \int_{M_\infty/\lambda'}^{M_\infty} F(M, t)(M^{1/3} + M^{1/3})^2\, dM\right] \tag{40}$$

where

$$\lambda' < \Gamma' \tag{41}$$

The contribution of erosion has been dropped because the largest asteroids have a sufficiently strong gravitational field to retain most of the secondary ejecta produced during erosive cratering (Marcus, 1969; Hartmann, 1968).

The most important feature of equation (40) is the strong coupling between the solutions $F(M, t)$ and $f(m, t)$ for $\lambda' \ll \Gamma'$. Because Γ' is of the order of 10^3 to 10^5, depending on whether we assume asteroids to be more similar to basalt

spheres or to glass spheres and because λ' is about 1, we conclude that, for asteroids,

$$\lambda' \ll \Gamma' \tag{42}$$

If, however, we make the opposite assumption and let

$$\lambda' \to \frac{M_\infty}{\mu} \tag{43}$$

i.e., all collisional fragments somehow just go away as do masses smaller than μ, we obtain the equation

$$\frac{\partial F(m, t)}{\partial t} = - KF(m, t) \int_{M_\infty/\Gamma'}^{M_\infty} F(M, t)(M^{1/3} + m^{1/3})^2 \, dM \tag{44}$$

This equation, first posed for asteroids by Piotrowski (1953), has received attention by a number of authors. Piotrowski found that equation (44) can be solved approximately if we separate variables and let

$$F(m, t) = \rho(m)T(t) \tag{45}$$

The result is

$$F(m, t) \approx T(t)m^{-5/3} \tag{46}$$

and has the property that the total cross-sectional area of asteroids having masses in the range m_1 and m_2 is proportional to $\ln (m_1/m_2)$ and therefore independent of m_1 or m_2.

The stability of the solution, equation (46), has been discussed by Piotrowski (1953) and in greater detail by Marcus (1965); they conclude that once the population reaches a distribution of the form of equation (46), it is stable.

Jones (1968) examined the problem when Γ' is small and λ' is large; i.e., a case similar to the one defined by equation (43). He also obtained an approximate solution of the form of equation (46).

More recently, Hellyer (1970), in an effort to obtain separate solutions for large and small asteroids, discussed Piotrowski's equation (44) and again verified the approximate solution, equation (46).

Unfortunately, there are difficulties associated with the application of equation (44) and its particular solution, equation (46), for asteroids as has also been pointed out by Hartmann and Hartmann (1968). First, equation (44) is incorrect, unless it is assumed that in a collision the colliding objects are virtually atomized (eq. (43)) and hence their fragments do not contribute to the population of smaller objects (cf. eq. (40)). This assumption is in contrast

with results of experiments on laboratory-sized objects and there appears to be evidence (Anders, 1965) that large asteroids break up into a spectrum of debris that significantly contributes to the population of observed asteroids. It is indeed probable that most asteroids are collisional fragments (Anders, 1965; Dohnanyi, 1969). Thus it appears that equation (44) is not a good mathematical model for asteroidal collisions.

Even if the physical applicability of equation (44) could somehow be maintained, it is difficult to interpret the significance of the approximate particular solution in equation (46). Because Piotrowski's equation (eq. (44)) is a partial differential equation, its solution must include an arbitrary function. Physically, this is an obvious consequence of the fact that one should be able to prepare a fairly arbitrary initial distribution that should satisfy equation (44) at some point of time. No evidence has yet been advanced for the existence of an initial distribution, other than the solution equation (46) itself, which would approach the $m^{-5/3}$ power-law distribution. In short, there appears to be no evidence that equation (46) is indeed an asymptotic solution valid after some long period of time has elapsed since creation.

Asymptotic Solution for Long Times

In this section, we shall derive an asymptotic form for the distribution of large asteroids valid after some long period of time has elapsed since their creation.

We shall take

$$\lambda' = 1 \tag{47}$$

which means that the mass of the target object becomes the upper limit to the mass of the largest fragment; i.e., the "threshold" of the failure mode is included. (The *expected* size of the largest fragment is naturally smaller than the target object.)

Using this relation (eq. (47)) in the continuity equation for the largest asteroids, equation (40), we see that the second integral on the right-hand side vanishes with $\lambda' \cong 1$. We also must include the contribution $\partial F(m, t)/\partial t|_{\text{catastrophic creation}}$ (eq. (30)) to $\partial F(m, t)/\partial t$ (eq. (40)), because the largest fragment of a catastrophic process involving a large asteroid may still be within the size range of the largest asteroids. We may therefore write

$$\frac{\partial F(m, t)}{\partial t} = -KF(m, t)\int_{m/\Gamma'}^{M_\infty} F_p(M, t)(M^{1/3} + m^{1/3})^2\, dM + K(2-\eta)m^{-\eta}$$

$$\times \int_m^{M_\infty} dM_2 \int_{M_2/\Gamma'}^{M_2} dM_1\, M_2{}^{\eta-2}(M_1 + M_2)(M_1{}^{1/3} + M_1{}^{1/3})^2$$

$$\times F(M_1, t)F_p(M_2, t) \tag{48}$$

where the subscript p has been attached to $F(m, t)$ to denote the number density of the smaller (i.e., projectile) asteroids.

Each of the two asteroidal surveys, MDS and PLS, suggests a power-law-type population

$$f(m) \approx Am^{-11/6} \tag{49}$$

For such populations, the dominant contribution to catastrophic collisions (both the creation and removal term) is caused by the collision of projectile objects having masses of the order of M/Γ', with target objects having masses M. (See Dohnanyi, 1969.)

Because Γ' is a large number of several orders of magnitude, we shall take as a first approximation to equation (48):

$$F_p(m, t) \approx a_0(m, t) = A(t)m^{-\alpha} \qquad \alpha = \frac{11}{6} \tag{50}$$

where a_0 is the solution for the steady-state distribution of small objects, equation (37). Furthermore, a_0 is taken here as a function of t that varies slowly compared with $a_1/t + a_2/t^2 + \ldots$ in equation (32), which are here treated as transients.

Substitution of equation (50) for $F_p(m, t)$ in equation (48) yields a linear equation for $F(m, t)$. Retaining the leading terms in this linearized equation, one can solve it for $F(m, t)$ and thereby obtain a first approximation for the distribution of large asteroids. This was done in Dohnanyi (1970*b*) with the result

$$F(m, t) = A(t)m^{-11/6}\left[1 - \left(\frac{m}{M_\infty}\right)^{1/6}\right]^{6(2-\eta)-1} \tag{51}$$

where

$$A(t) = A_0\left[1 + M_\infty^{-\alpha+5/3}K(\Gamma')^{\alpha-1}\,\frac{A_0(t - t_0)}{\alpha - 1}\right]^{-1} \tag{52}$$

A_0 is the value of A when the time parameter t equals t_0.

We now let t_0 denote the present time and A_0 the present value of $A(t)$; we have (cf. Dohnanyi, 1969),

$$A(t) = A_0\left[\frac{1 + (t - t_0)}{\tau_\infty}\right]^{-1} \tag{53}$$

where τ_∞ is the mean time between catastrophic collisions of the largest objects M_∞(cf. Dohnanyi, 1969), if the latter could survive these collisions. It was estimated (Dohnanyi, 1969) that

$$\tau_\infty \sim 10^9 \text{ yr} \tag{54}$$

Combining equations (53) and (54), we see that, according to the present model, it will take on the order of 3×10^9 yr for the number of asteroids to decrease to one-half its present value. $A(t)$ cannot, of course, be extrapolated backward over long periods of time because it is a first approximation to the distribution of asteroids a long time after their creation.

The first approximation of $F(m, t)$ given by equation (51) has the property that it goes over into $a_0(m, t)$; i.e., into $A(t)m^{-11/6}$ for sufficiently small m. Thus

$$F(m, t) \approx A(t)m^{-11/6} \qquad m \ll M_\infty \tag{55}$$

as can readily be seen from equation (51).

DISCUSSION OF RESULTS

Physical Significance of the Stationary Solution ($\alpha \approx 11/6$)

It is difficult to give a simple physical argument that would demonstrate, from first principles only, that $\alpha \approx 11/6$ is the obvious solution to the collision equation (eq. (21)). It has, however, been shown in Dohnanyi (1969) that the total amount of mass $\dot{M}_{12}$ crushed catastrophically per unit time by projectile masses in any finite range m_1 to m_2 is

$$\dot{M}_{12} \approx \int_{m_1}^{m_2} AM^{-\alpha}\, dM \int_M^{\Gamma' M} M_2 K M_2^{2/3} A M_2^{-\alpha}\, dM_2$$

$$= \frac{KA^2(\Gamma')^{-\alpha+8/3}}{(-\alpha+8/3)(-2\alpha+11/3)} \left(m_2^{-2\alpha+11/3} - m_1^{-2\alpha+11/3}\right) \tag{56}$$

when $\alpha \neq 11/6$ and $m_2 \leqslant M_\infty/\Gamma'$, and

$$\dot{M}_{12} = \frac{KA^2(\Gamma')^{-\alpha+8/3}}{-\alpha+8/3} \ln \frac{m_2}{m_1} \tag{57}$$

when $\alpha = 11/6$ and $m_2 \leqslant M_\infty/\Gamma'$.

In these equations only the leading terms have been retained, treating projectiles as point particles and disregarding grazing collisions.

We now consider equations (56) and (57) in more detail. It can readily be seen that if $\alpha > 11/6$, then $\dot{M}_{12}$ will mainly depend on m_1 if the logarithmic interval m_2/m_1 is sufficiently large; i.e., $\dot{M}_{12}$ depends on the particular value of m_1 but is insensitive to m_2. The converse is true for $\alpha < 11/6$; for sufficiently large m_2/m_1, $\dot{M}_{12}$ depends on the particular value of m_2 and not on m_1. Thus, for a sufficiently large logarithmic interval m_2/m_1, practically all mass is crushed by the smallest projectile objects in the interval for $\alpha > 11/6$ and practically all mass is crushed by the biggest projectile masses in the interval for $\alpha < 11/6$. For $\alpha = 11/6$, however, $\dot{M}_{12}$ does not depend on the particular value of either m_1 or m_2 but only on their ratio m_2/m_1. Therefore, the total mass crushed per unit time in the asteroidal belt depends, mainly, on the particular value of the limiting masses of the distribution, μ or M_∞, depending on whether $\alpha < 11/6$ or $\alpha > 11/6$, respectively; whereas for $\alpha = 11/6$ the mass production is constant for fixed logarithmic intervals of projectile masses m_2/m_1 and is independent of the limiting masses μ and M_∞ in a first order of approximation.

Relative Importance of the Various Collisional Processes

The result $\alpha = 11/6$ is valid when only the leading terms of equation (21) are retained. A more detailed treatment has to consider the influence of higher order terms, as well. This was done in Dohnanyi (1969) for a distribution of this type

$$f(m) = Am^{-\alpha} \tag{58}$$

and for masses m that are far from the limiting masses μ and M_∞.

Figures 4 and 5 are plots, in units of $(KA^2m^{-2\alpha+5/3})^{-1}$, of the number of particles per unit mass, volume, and time removed (or created) by the individual collisional processes and their sum for two different average collisional velocities, as indicated. The population index of the crushed fragments during each collision η is taken to be the experimental value 1.8. The value of α at which the curve representing the sum of all processes crosses the horizontal axis (i.e., the value of α at which the individual processes add up to zero) is the solution for α of equations (33) and (37).

It can be seen, from figures 4 and 5, that the particle creation term is significant only for values of α lower than about 1.9 and that the influence of the erosive reduction of the masses dominates for higher values of α. The individual processes and their sums exhibit remarkably similar trends; the values of α at which steady state is reached is $\alpha = 1.841$ in figure 4 and 1.835 in figure 5. It can be seen, from these figures, that the steady-state distribution is determined by the balance of the catastrophic creation and collision processes. Because, however, it is readily shown that the contribution of erosive creation is at most on the order of $\Gamma/\Gamma' \approx 1/50$ times the similar contribution of catastrophic processes, we may conclude that erosion has only a minor effect on the steady-state distribution.

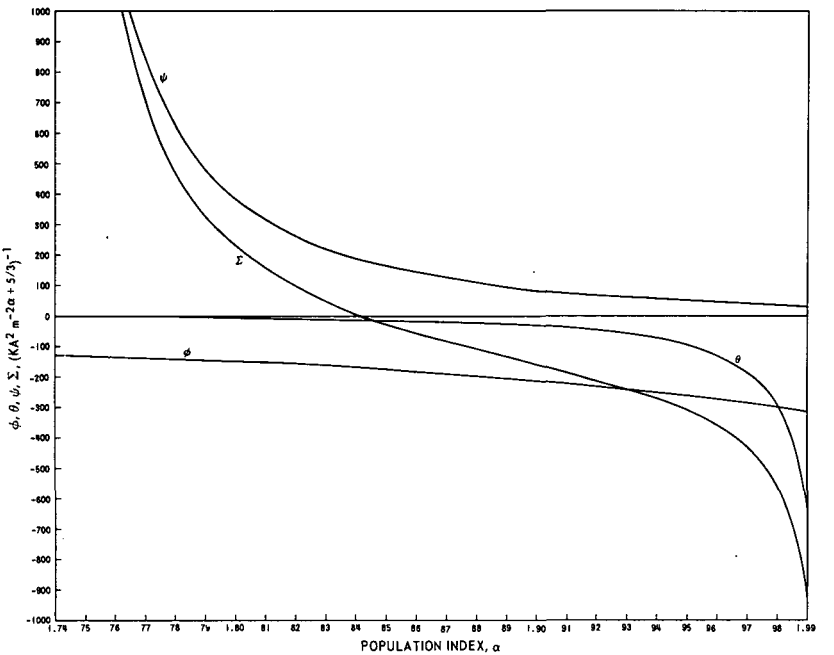

ψ = rate of change in the number of particles because of particle creation by fragmentation of larger objects
ϕ = rate of change in the number of particles because of catastrophic collisions
θ = rate of change in the number of particles because of erosion
$\Sigma = \theta + \phi + \psi$

Figure 4.–Rate of change of the number of particles in units of $(KA^2m^{-2\alpha+5/3})^{-1}$ per unit time and unit mass range as a function of the population index α. $\eta = 1.8$; $V = 1$ km/s; and $\Gamma \approx 5$.

Because the material parameter Γ is greater by a factor of 400 in figure 5 than in figure 4, we conclude that the value of α at which steady state is reached and the relative trends of the individual collisional processes are insensitive to the material parameters. The same holds for η, because a modest variation in η was found in Dohnanyi (1969) to produce no significant departures.

Distribution of the Largest Asteroids

The influence of some of the higher order terms on the solution of equation (21) was studied in Dohnanyi (1969). (Also see the previous section of this paper.) We now consider the influence of the limiting largest mass M_∞ on the solution of equation (21). This was discussed in Dohnanyi (1970*b*) and the section entitled "Solution for Large Masses" in this present paper.

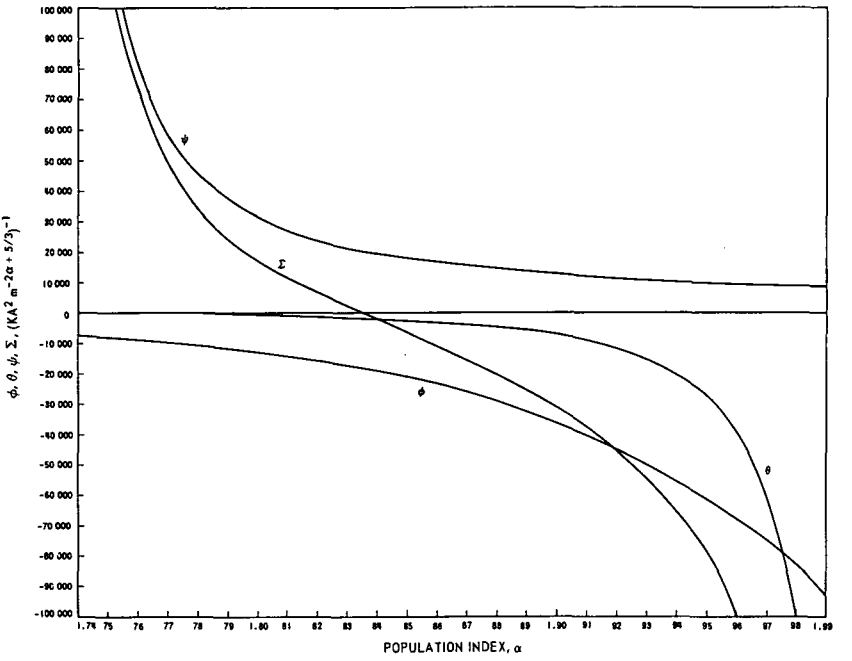

Figure 5.–Rate of change of the number of particles in units of $(KA^2m^{-2\alpha+5/3})^{-1}$ per unit time and unit mass range as a function of the population index α. $\eta = 1.8$; $V = 20$ km/s; and $\Gamma = 2000$.

The main result is that in the neighborhood of the limiting largest mass M_∞, the number density of asteroids is approximately

$$f(m, t) \approx A(t)m^{-11/6}\left[1-\left(\frac{m}{M_\infty}\right)^{1/6}\right]^{6(2-\eta)-1} \tag{59}$$

where $A(t)$ is given by equation (52). Equation (59) is valid only if a long period of time has elapsed since the creation of the asteroids and if any indication of the initial distribution has been lost.

Figure 6 is a plot of the cumulative number of the MDS asteroids from figure 1 together with the theoretical value

$$N(m, t) = \int_m^{M_\infty} f(M, t)\, dM \tag{60}$$

where f is given by equation (59). Plots of N for several different values for η are included; M_∞ is taken to be 1.86×10^{20} kg ($g = 4$) and A has been so chosen that $N(m, t)$ is made to coincide with observations at $g = 9$.

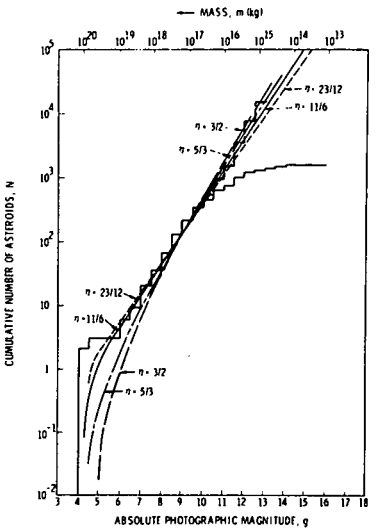

Figure 6.–Cumulative number of asteroids having an absolute photographic magnitude g or smaller (i.e., mass m or greater). Observed value = solid line histogram (MDS); probable value = dashed line histogram (MDS); theoretical value for different values of the fragmentation parameter, as indicated.

It can be seen from figure 6 that the higher values of η (11/6 and 23/12) provide the best agreement between theory and observation. The curve for $\eta = 5/3$ is still reasonably good, but for $\eta = 3/2$ the agreement with observation begins to deteriorate. For values of η less than 5/3, the number of large asteroids is underestimated by theory.

Erosion Rates

The rate $\dot{R}$ at which the effective radius of an asteroid decreases with time because of erosive collisions has been estimated by Dohnanyi (1969). The result is plotted in figure 7 and a systematic error of about a half order of magnitude may be present because of the uncertainties in the albedo alone. Because gravitational attraction has not been considered, $\dot{R}$ is an overestimate for large asteroids that retain much of the secondary ejecta produced during erosive cratering (Marcus, 1969; Hartmann, 1968).

The most conspicuous feature of the plot in figure 7 is that $\dot{R}$ is not a constant but a function of the mass of the asteroid undergoing erosion, because erosion is not due alone to collisions with minute particles but also to collisions with all masses up to m/Γ', where m is the mass of the target object being eroded. Because the population index α is here less than 2, the total mass eroded away from a given object by collisions with microparticles is much less than the mass eroded away by larger objects. Hence we expect that asteroidal surfaces are not smooth but are pock marked by relatively large craters.

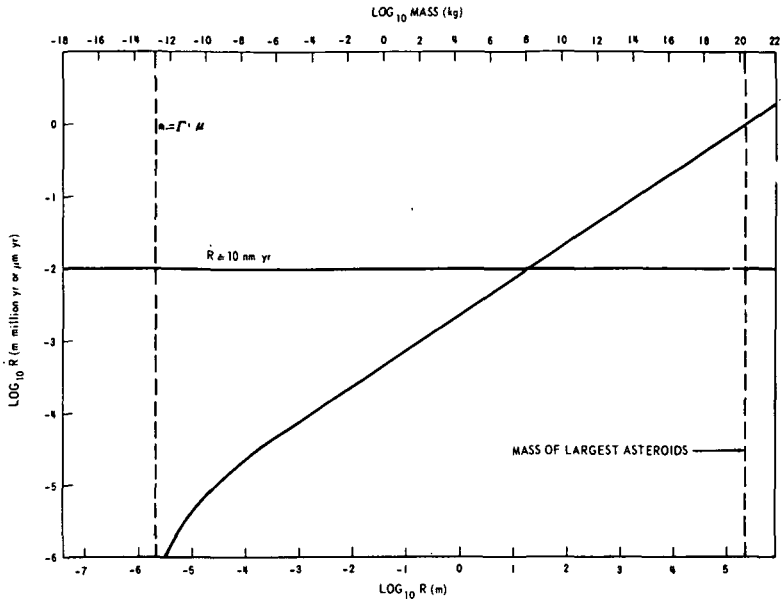

Figure 7.–Statistical rate of change because of erosion of the particle radius in meters per million years (or micrometers per year) as a function of particle mass (or particle radius). The horizontal line corresponds to a linear erosion rate of 10 nm/yr.

Values for $\dot{R}$ in figure 7 for small masses are not realistic because the influence of collisions with cometary meteoroids and spallation by cosmic rays has not been included. These processes have been estimated by Whipple (1967) to give rise to an erosion rate not exceeding about 10 nm/yr for stones. This upper limit is indicated in figure 7 as a horizontal line. Although Whipple's estimate applied to objects with orbits intersecting Earth's orbit, his upper limit is still meaningful for particles in the asteroidal belt if the erosive effect of cometary meteoroids in the asteroidal belt is taken to be comparable to, or lower than, the effect near Earth.

Lifetimes

Lifetimes of asteroids as a function of their masses and effective radii have been estimated in Dohnanyi (1969) and are plotted here in figure 8.

The lifetime with respect to catastrophic collisions is taken as the mean time between collisions of an object with mass m and other objects with masses greater than m/Γ':

$$\tau_{cc} = \left[K \int_{m/\Gamma'}^{m_\infty} AM^{-\alpha}(m^{1/3} + M^{1/3})^2 \, dM \right]^{-1} \tag{61}$$

An uncertainty due to albedo of about half an order of magnitude is present, in addition to other uncertainties.

The value of τ_{cc} for the largest asteroids is on the order of 10^9 yr (fig. 8). It can be seen, from figure 8, that the lifetime of the six largest asteroids with masses $m \geqslant 10^{19}$ kg is about 4×10^9 yr or longer and therefore these may have survived since the time of their creation. The other asteroids have shorter lifetimes τ_{cc} and may therefore be collisional fragments.

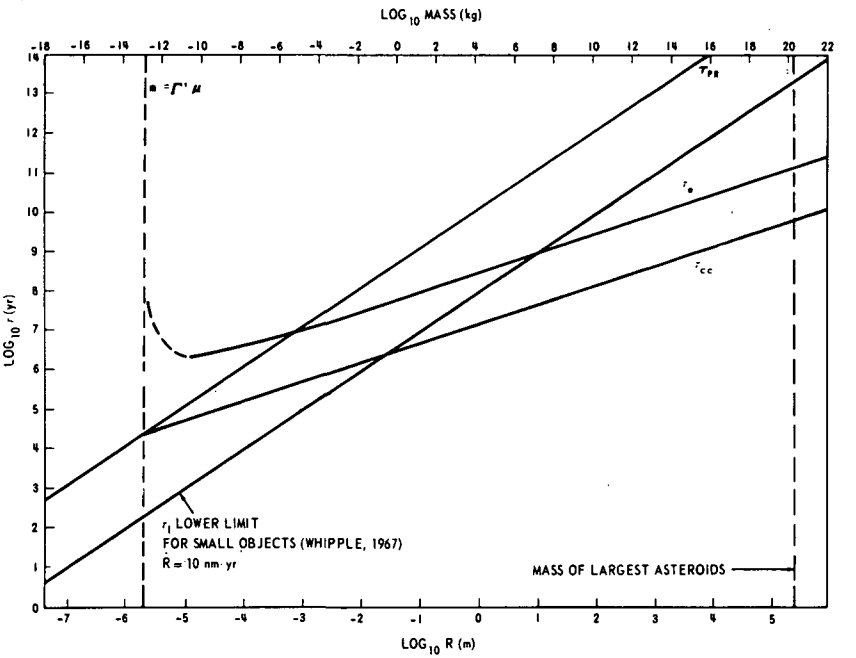

Figure 8.–Double logarithmic plot of particle lifetimes in years as a function of particle masses in kilograms (or particle radii in meters).

Using a more detailed spatial and velocity distribution, Wetherill (1967) has calculated collisional probabilities and obtained values comparable to but smaller than the values that a randomly distributed asteroid population (particle-in-a-box) would imply. He also estimated τ_{cc} for a 1 m diameter object for a number of assumed mass distributions. He considered (Wetherill, 1967, table 7) population indexes in the range $\alpha = 5/3$ to $\alpha = 1.8$; corresponding values of τ_{cc} were then computed for $\Gamma' = 10^2$, 10^3, and 10^4. Because these population indexes are lower than the steady-state value of $\alpha \approx 11/6$, the values in Dohnanyi (1969) for τ_{cc} are correspondingly shorter. The difference is about an order of magnitude in τ_{cc}.

The lifetime with respect to erosion (i.e., erosive reduction of the particle mass) can be obtained when the expression for $\dot{m}$ (eq. (23)) is integrated. The result is, from Dohnanyi (1969),

$$\tau_e = \frac{(\Gamma')^{1/6}}{\Gamma K A}\left[(\sqrt{2}-1)\, m^{1/6} + (\Gamma'\mu)^{1/6} \ln \frac{\sqrt{2}\, m^{1/6} - (\Gamma'\mu)^{1/6}}{m^{1/6} - (\Gamma'\mu)^{1/6}}\right] \quad (62)$$

where the erosive lifetime τ_e of an object was taken to be the time required to erode it to one-half its initial radius and where $\alpha = 11/6$ was used. The logarithmic term is significant for masses approaching the value $\Gamma'\mu$, as can be seen from figure 8, τ_e becoming infinitely long for masses $m \leqslant \Gamma'\mu$. This happens because erosion stops for these small particles and all collisions they experience are catastrophic.

We also plot, in figure 8, the particle lifetimes with respect to the Poynting-Robertson effect (Robertson, 1936) τ_{PR} and the lower limit of the lifetime of small objects τ_l due to the influence of cometary meteoroids and cosmic rays estimated by Whipple (1967). Here the definition of τ_l is similar to that of τ_e; i.e., it is the time for erosion of an object to one-half its radius. τ_{PR} is the time required for an object to traverse radially one-half of the asteroidal belt, because of the Poynting-Robertson effect. It can be seen, from the figure, that catastrophic collisions dominate the lifetime of the particles greater than about 10^{-5} kg (or 1 mm in radius). Smaller particles may be subject to erosion by cometary particles to an extent that this mechanism dominates.

CONCLUSIONS

Using a stochastic model of asteroidal collisions, their mass distribution has been estimated. The results individually agree with the observed distribution of bright asteroids (MDS) and faint asteroids (PLS). After correction for completeness, the MDS and PLS distributions are similar in form but differ from each other by a numerical factor. Until this difficulty is resolved, some uncertainty remains in the precise form of the distribution of bright asteroids. Subject to this reservation, we may conclude that the mass distribution of most asteroids has reached (i.e., relaxed into) a stationary form that is independent of the original distribution and is a power-law function with index $\sim 11/6$ for faint asteroids.

The influence of catastrophic collisions dominates the evolution of the population; erosion plays a minor part. The influence of the Poynting-Robertson effect becomes dominant, however, for particles with masses of 10^{-10} g or smaller.

Whereas the particle lifetimes, erosion rates, collision probabilities, and other derived quantities of physical interest are expected to be self-consistent, uncertainties in the albedo of asteroids and in other parameters introduce an

appreciable systematic error; the numerical values of these quantities should therefore be regarded as order of magnitude approximations.

ACKNOWLEDGMENTS

Thanks are due to D. E. Gault for important suggestions and to T. Gehrels for helpful discussions.

REFERENCES

Alfvén, H. 1964*a*, On the Origin of Asteroids. Icarus **3**, 52-56.

Alfvén, H. 1964*b*, On the Formation of Celestial Bodies. Icarus **3**, 57-62.

Alfvén, H. 1969, Asteroidal Jet Streams. Astrophys. Space Sci. **4**, 84-102.

Anders, E. 1965, Fragmentation History of Asteroids. Icarus **4**, 398-408.

Dohnanyi, J. S. 1967*a*, Collisional Model of Meteoroids. The Zodiacal Light and the Interplanetary Medium (ed., J. L. Weinberg), pp. 315-319. NASA SP-150.

Dohnanyi, J. S. 1967*b*, Bellcomm Rept. TR-340-3.

Dohnanyi, J. S. 1967*c*, Collisional Model of Asteroids and Their Debris. Paper presented at Int. Symp. Phys. Dyn. Meteors (Tatranska Lomnica, Czech.).

Dohnanyi, J. S. 1969, Collisional Model of Asteroids and Their Debris. J. Geophys. Res. **74**, 2531-2554.

Dohnanyi, J. S. 1970*a*, On the Origin and Distribution of Meteoroids. J. Geophys. Res. **75**, 3468-3493.

Dohnanyi, J. S. 1970*b*, Mass Distribution of Asteroids. Bellcomm TM-70-2015-6.

Dohnanyi, J. S. 1971, Micrometeoroids. Trans. Amer. Geophys. Union, in press.

Gault, D. E., Shoemaker, E. M., and Moore, H. J. 1963, Spray Ejected From the Lunar Surface by Meteoroid Impact. NASA TN D-1767.

Gault, D. E., and Wedekind, J. A. 1969, The Destruction of Tektites by Micrometeoroid Impact. J. Geophys. Res. **74**, 6780-6794.

Hartmann, W. K. 1968, Growth of Asteroids and Planetesimals by Accretion. Astrophys. J. **152**, 337-342.

Hartmann, W. K. 1969, Terrestrial, Lunar, and Interplanetary Rock Fragmentation. Icarus **10**, 201-213.

Hartmann, W. K., and Hartmann, A. C. 1968, Asteroid Collisions and Evaluation of Asteroidal Mass Distribution and Meteoritic Flux. Icarus **8**, 361-381.

Hellyer, B. 1970, The Fragmentation of the Asteroids. Mon. Notic. Roy. Astron. Soc. **148**, 383-390.

Hirayama, K. 1923, Families of Asteroids. Jap. J. Astron. Geophys. **1**, 55-93.

Hirayama, K. 1928, Families of Asteroids, 2. Jap. J. Astron. Geophys. **5**, 137-162.

Houten, C. J. van, Houten-Groeneveld, I. van, Herget, P., and Gehrels, T. 1970, Palomar-Leiden Survey of Faint Minor Planets. Astron. Astrophys. Suppl. Ser. **2**, 339-448.

Jones, J. 1968, The Mass Distribution of Meteoroids and Asteroids. Can. J. Phys. **46**, 1101-1107.

Kessler, D. J. 1969, Spatial Density of the Known Asteroids in the Ecliptic Plane. NASA TM X-58026.

Kiang, T. 1962, Asteroid Counts and Their Reduction. Mon. Notic. Roy. Astron. Soc. **123**, 509-519.

Kokott, W. 1970, The Dust Population in the Asteroid Belt. Paper presented at the 13th COSPAR Plenary Meeting (Leningrad).

Kuiper, G. P. 1953, Note on the Origin of Asteroids. Proc. Nat. Acad. Sci. 39, 1159-1161.

Kuiper, G. P., Fujita, Y., Gehrels, T., Groeneveld, I., Kent, J., Van Biesbroeck, G., and Houten, C. J. van, 1958, Survey of Asteroids. Astrophys. J. Suppl. Ser. **3**, 289-428.

Marcus, A. H. 1965, Positive Stable Laws and the Mass Distribution of Planetesimals. Icarus 4, 267-272.

Marcus, A. H. 1969, Speculations on Mass Loss by Meteoroid Impact and Formation of the Planets. Icarus 11, 76-87.

Moore, H. J., and Gault, D. E. 1965, The Fragmentation of Spheres by Projectile Impact. Astrogeologic Studies, U.S. Geol. Survey Annu. Progress Rept., pp. 127-150.

NASA SP-8038. 1970, Meteoroid Environment Model–1970 (Interplanetary and Planetary).

Öpik, E. J. 1951, Collision Probabilities With the Planets and the Distribution of Interplanetary Matter. Proc. Roy. Irish Acad. 54, 165-199.

Öpik, E. J. 1963, The Stray Bodies in the Solar System, 1. Survival of Cometary Nuclei and the Asteroids. Advan. Astron. Astrophys. 2, 219-262.

Öpik, E. J. 1966, The Stray Bodies in the Solar System, 3. The Cometary Origin of Meteorites. Advan. Astron. Astrophys. 4, 301-336.

Piotrowski, S. 1953, The Collisions of Asteroids. Acta Astron. Ser. A 5, 115-138.

Robertson, H. P. 1936, Dynamical Effects of Radiation in the Solar System. Mon. Notic. Roy. Astron. Soc. 97, 423-438.

Roosen, R. G. 1970, The Gegenschein and Interplanetary Dust Outside the Earth's Orbit. Icarus 13, 184-201.

Sharonov, V. V. 1964, The Nature of the Planets. Israel Program for Scientific Translation. Jerusalem.

Wetherill, G. W. 1967, Collisions in the Asteroid Belt. J. Geophys. Res. 72, 2429-2444.

Whipple, F. L. 1967, On Maintaining the Meteoritic Complex. Smithson. Astrophys. Observ. Special Rept. 239, 2-45. (Also available in NASA SP-150, pp. 409-426.)

DISCUSSION

VAN HOUTEN: I wish to comment on figure 2 of Dohnanyi's paper. In this figure, the cumulative number of asteroids, as a function of absolute magnitude, is shown for MDS and PLS. In the overlapping part, the MDS values are approximately 10 times as large as the PLS values. This discrepancy could be traced to the following causes:

(1) The correction factors for incompleteness in table 15 of MDS in group III ($3.0 < a < 3.5$) are incorrect; the correct values are given in table D-I.

(2) Dohnanyi apparently used table 5 of PLS for the computation of his cumulative numbers of PLS asteroids. But to this table should be added the objects that were too bright for measurement in the iris photometer; these are five in total.

TABLE D-I.–*MDS Correction Factors*

g	$3.0 < a < 3.5$			$2.0 < a < 3.5$		
	N_{obs}	N_{min}	N_{max}	N_{obs}	N_{min}	N_{max}
9.75.....	39	39	40	114	114	115
10.25.....	64	65	69	150	151	155
10.75.....	93	121	143	180	208	231
11.25.....	78	137	169	184	246	288
11.75.....	77	220	320	168	334	453
12.25.....	45	250	450	150	418	661
12.75.....	17	255	472	138	568	913

After these corrections, and using the average of N_{max} and N_{min} for the MDS value as Dohnanyi did, the comparison between MDS and PLS becomes as given in table D-II.

The MDS values are still about twice as large as the PLS values, after these corrections. But the comparison is based on only 12 objects in the PLS. The statistical uncertainty of this number is such that maybe not too much importance should be attached to this difference.

TABLE D-II.—*Comparison Between MDS and PLS*

	Number of asteroids	
$g <$ –	MDS	PLS
11.25.....	961	505
11.75.....	1355	600
12.25.....	1895	912
12.75.....	2635	1704

DOHNANYI: If the five objects, too bright for photometry in PLS, are included, the resulting change in figure 2 is not significant for the purposes of my present study. A least-squares fit for asteroids with $g \geqslant 11$ gives a new population index $\alpha = 1.815$, which does not significantly differ from the previous value of $\alpha = 1.839$ that I have obtained earlier.

The maximum and minimum probable number of asteroids was estimated in MDS. No such quantitative estimate is given in PLS even though large correction factors affecting every asteroid observed in PLS were employed in extrapolating the relatively small sample of PLS to the rest of the asteroid belt. Large nonlinear corrections that have been applied are particularly visible when comparing figures 9 and 11 in PLS. The maximum in distribution of inclinations (fig. 9, PLS) is near 3° whereas the average inclination for cataloged asteroids is about 10° (Watson, 1956). The simple method based on several assumptions for estimating the completeness factors due to the inclination cutoff in PLS may be especially vulnerable to systematic error. The large correction factors employed for the small number of high-inclination orbits may be subject to noise because the number of these asteroids probably fluctuates in time. (See Nairn, 1966.)

Assuming that the PLS results are free from the type of difficulties that led van Houten to revise the MDS data, uncertainties in PLS data do still exist. Without a quantitative estimate of these uncertainties it might be arbitrary and misleading to connect the PLS results with those of the MDS without further comment at this time.

VAN HOUTEN: N_{max} and N_{min} in table 15 of MDS should not be regarded as the maximum and minimum probable number of asteroids. They are simply numbers derived from two different extrapolations of the $\log N(m_0)$ relation. They should be compared with the PLS to see whether any of them approximates the real numbers. This comparison yields the results given in table D-III (cf. table 14 of MDS). It is seen that at $p_0 > 18$ even the use of equation (7) results in values that are too small. Fortunately the incompleteness corrections of the MDS were not extended to such faint magnitudes. Their lower limit is $p_0 = 17$, and here the PLS value is indeed between equations (6) and (7) (from which N_{min} and N_{max} were derived, respectively).

A check is possible on the correctness of the correction factors for the declination cutoff, used in the PLS. The corrected values should reproduce the same distribution of asteroids with respect to the ecliptic as was found in the MDS. (See fig. D-1.) It was shown in the PLS that one strip of the MDS yielded 1.90 times as many asteroids as a PLS strip for the same limiting magnitude; moreover it was found in the MDS that 10 percent of the

TABLE D-III.—*Comparison of MDS Extrapolations and PLS values*

p_0	Equation (6)	Equation (7)	PLS
17.....	1990	3700	3240
18.....	3240	8300	11500
19.....	4940	18600	28200

NOTE.—The mean photographic opposition magnitude is defined in the MDS.

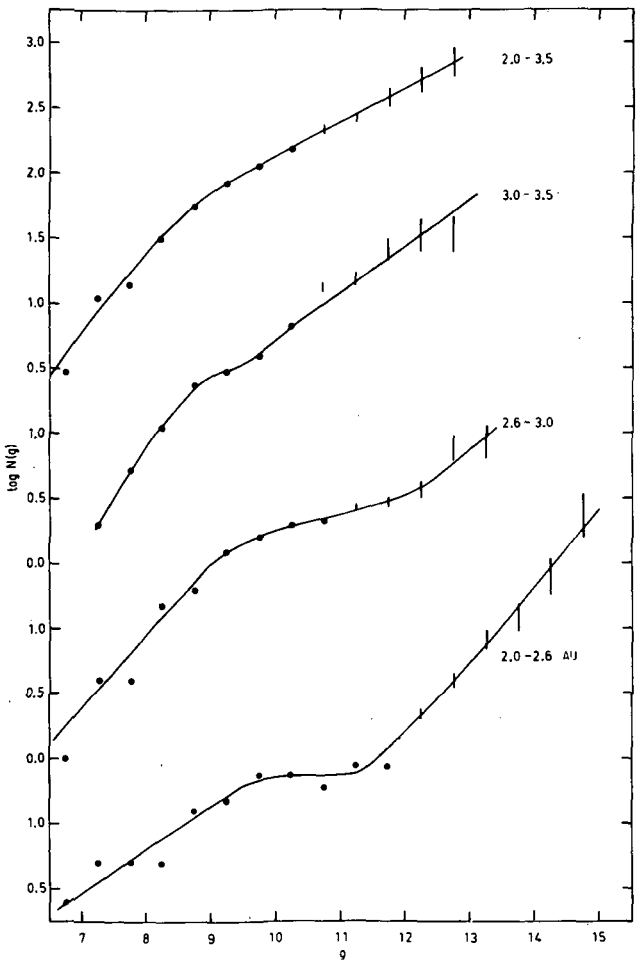

Figure D-1.—MDS frequency distribution of absolute magnitudes g for three distance zones and their sum. This was originally figure 5 of the MDS; revised by I. van Houten-Groeneveld.

asteroids at a given opposition fall outside the MDS region. Therefore the comparison between MDS and PLS indicates that the correction factor for the inclination cutoff, integrated over the three distance groups, should be 1.10 times 1.90, or 2.09.

Using the approximation of circular orbits, the correction factors for the inclination cutoff for the three distance intervals separately were found to be 1.94, 2.42, and 2.45, respectively. The numbers of objects in the three distance groups are 52, 29, and 19 percent of the total (first-class orbits used only). This results in an integrated correction factor for the inclination cutoff of 2.18. The two numbers differ by only 4 percent. This shows that the correction factors for the inclination cutoff, as used in the PLS, are completely satisfactory.

The correction factor used to extend the PLS field to the whole sky depends on the size of the PLS field, which is accurately known. This correction factor cannot give rise to any inaccuracy.

In short, I do not see any reason to suppose that systematic errors are present in the PLS results. The accuracy of the PLS material is probably better than the MDS because the photometric material was larger, every asteroid being measured about six times, and because accurate reductions to absolute magnitude were available. Therefore I do not share Dohnanyi's reluctance to combine the two surveys. According to me, such a combination is completely justified.[2]

DISCUSSION REFERENCES

Nairn, F. 1966, Spatial Distribution and Motion of the Known Asteroids. J. Spacecr. Rockets 3, 1438-1440.

Watson, F. G. 1956, Between the Planets. Harvard Univ. Press. Cambridge.

[2]For additional information on the PLS, the reader is referred to van Houten's paper, p. 183.

Page intentionally left blank

REMARKS ON THE SIZE DISTRIBUTION OF COLLIDING AND FRAGMENTING PARTICLES

LOTHAR W. BANDERMANN
University of Hawaii

This paper is concerned with some aspects of determining the evolution of the size distribution of a finite number of mutually colliding and fragmenting particles such as the asteroids or interplanetary dust. If $n(m, t)$ is the number of particles per unit volume per mass interval at time t, then $\dot{n} = dn/dt$ is the rate at which that number changes with time. This rate can be calculated if the laws are known according to which the colliding bodies erode one another and fragment and if the influence of collisions on the motion of the particles is known. To reduce the complexity of the problem, one assumes that the speed of approach between the bodies is always the same v_{coll} and that they, as well as the debris, occupy a fixed volume ("particles in a box"). Only collisions between two bodies are considered, and the way in which erosion and fragmentation occurs at a given value of v_{coll} depends only on their masses. The particles are assumed to be spherical. One is particularly interested in stationary states (i.e., cases where n can be factored into independent functions of t and m):

$$n(m, t) = T(t) \cdot \phi(m)$$

and in steady states (i.e., where $dT/dt = 0$). Steady states can of course be reached only over limited ranges of m because no particles are supplied from outside to the system. Even for very simple assumed fragmentation laws, the equation for $\dot{n}$ is extremely complicated, being of a multiple integro-differential type, and analytical solutions can be found (sometimes) for very restricted mass ranges and even then only by making some rather drastic approximations.

A simpler problem—namely, where the probability of destruction of a particle is independent of the total number and the mass distribution of the other particles in the system—was solved by Filippov (1961). Assuming that the probability is proportional to a power of the mass and that the size distribution of the fragments of a particle is given by a power law, he derived a formula by which the asymptotic ($t \to \infty$) solution for n can be calculated. In the collision problem, the probability of the collision depends on the relative

numbers of other particles, and the size distribution of the fragments and erosion products depend on the masses of the colliding components. By neglecting the role of debris in further collisions, Piotrowski (1953) found a stationary solution with $\phi \propto m^{-5/3}$. Dohnanyi (1969), who did consider the role of debris in the evolution of the distribution, derived analytically a steady-state solution with $\phi \propto m^{-11/6}$, applicable to particles with intermediate sizes. Hellyer (1970) subsequently concluded that Piotrowski's law applies only to large masses when one considers the role of debris; i.e., to masses not covered by Dohnanyi's law. More recently, Dohnanyi (1970) has investigated the evolution of the large particles in a mass distribution, in particular, those particles that are not created by collisions of others; and he has concluded that their distribution function approaches asymptotically the $m^{-11/6}$ law. To appreciate the significance of these results, let us look at the equation for n and at the fragmentation laws themselves.

There are two types of collisions. In *erosive* collisions the target mass M is very much greater than the projectile mass μ. (We assume that $M > \mu$.) As a result of the collision, a small amount of matter M_e is eroded from the target mass M. For hypervelocity collisions that occur between asteroids as well as between interplanetary dust particles, $M_e \gg \mu$. Because $M_e \propto \mu$ (as experiments confirm (Gault, Shoemaker, and Moore, 1963)), for sufficiently large values of μ/M, the mass M will be disrupted. Those are *explosive* collisions.

The $m^{-11/6}$ law is determined almost exclusively by explosive collisions. The threshold projectile mass is equal to M/Γ', where the parameter Γ' depends on v_{coll}. A first approximation of the mass distribution of collisional debris derived from either type of collision is

$$\frac{dN}{dm} = Cm^{-\eta}\, dm \tag{1}$$

where $\eta < 2$. For erosive collisions, $\eta \cong 1.8$, $M_e = \Gamma\mu$, and the largest debris has a mass $M_b = \Lambda\mu$; Γ, Γ', and Λ are much greater than unity. These relations complete the erosive fragmentation law.

In the case of explosive collisions, the corresponding relations are much less well known, except $M_e = M + \mu$ in this case; η is perhaps somewhat less than 1.8 (Gault, Shoemaker, and Moore, 1963; Gault and Wedekind, 1969). A relation for M_b is unknown. Dohnanyi (1969) initially assumed M_b to be proportional to μ. This leads to absurd consequences, however; and he more recently suggested (Dohnanyi, 1970) that $M_b = \lambda M$, where $\lambda < 1$.

It may be worthwhile at this time to consider qualitatively how the value of M_b is affected by increasing or decreasing the masses M and μ. The kinetic energy in the center-of-mass rest frame is, per unit mass of the colliding particles,

$$E \propto \left(\frac{M}{\mu} + 2 + \frac{\mu}{M}\right)^{-1}$$

(See table I.) It appears that the entries in the first column of table I are inconsistent. Although the energy per unit mass in the center of mass increases sharply by increasing the projectile mass while keeping the target the same, the largest debris remains the same even though the decimation of the target must be increasingly severe. It is true, of course, that part of the energy is used for vaporization and for acceleration of fragments; glancing collisions may lead to a different M_b than head-on collisions. But these effects are difficult to assess. It seems more reasonable to me to assume that M_b decreases with increasing μ, perhaps as follows:

$$M_b = \lambda M \left(\frac{M}{\mu}\right)^{\delta} \tag{2}$$

where $\lambda < 1$ and, perhaps, $\delta \ll 1$. In such a case, we must require $\lambda(\Gamma')^{\delta} \leqslant 1$. The fragmentation laws for the two types of collisions are then given in table II.

Experiments indicate that Γ, Γ', and Λ are proportional to $v_{\text{coll}}{}^2$. We expect λ to decrease with increasing v_{coll}. If the smallest and largest masses in the system are $m_<$ and $m_>$, respectively (particles with $m < m_<$ in the case of the asteroid belt and interplanetary dust may be lost by the action of solar radiation pressure and radiation drag), the equation for $\dot{n}$ is

$$\dot{n}(m, t) = -\kappa n(m, t) \int_{\max(m_<,\, m/\Gamma')}^{m_>} (m^{1/3} + \mu^{1/3})^2 n(\mu, t)\, d\mu$$

$$-\kappa \frac{d}{dm}\left[n(m, t)\Gamma \int_{m_<}^{m/\Gamma'} n(\mu, t)\mu(\mu^{1/3} + m^{1/3})^2\, d\mu\right]$$

$$+\kappa \int_{\max(m_<,\, m/\Lambda)}^{m/\Gamma'} n(\mu, t)\, d\mu \int_{\Gamma'\mu}^{m_>} (\mu^{1/3} + M^{1/3})^2 \frac{dN}{dm} n(M, t)\, dM$$

$$+\kappa \int_{\max[m_<,\, m/\lambda(\Gamma')^{\delta}]}^{m_>} n(\mu, t)\, d\mu$$

$$\times \int_{\max[\mu,\, (m/\lambda)^{1/(1+\delta)}\mu^{\delta/(1+\delta)}]}^{\min(m_>,\, \mu\Gamma')} (\mu^{1/3} + M^{1/3})^2 \frac{dN}{dm} n(M, t)\, dM \tag{3}$$

The first and last terms are due to explosive collisions, the others to erosive collisions. The second term gives the change in n caused by gradual erosion of large particles. (See Dohnanyi, 1969, for detailed discussions of collision equations.)

There are two ways to go about solving equation (3): substituting trial solutions of the stationary type, for instance, or starting with an initial

TABLE I.–*Effect of* M *and* μ *on Elements in a Collision System*

Element	$M>\mu$			$M=\mu$
	M constant, μ increasing	μ constant, M increasing	M/μ constant, M and μ increasing	M and μ increasing
M_e	Increases	Increases	Increases	Increases
E	Increases	Decreases	Constant	Constant
$M_b \propto M$	Constant	Increases	Increases	Increases

TABLE II.–*Fragmentation Laws*

Collisions	M_e	M_b	C
Erosive, $\mu<M/\Gamma'$	$\Gamma\mu$	$\Lambda\mu$	$(2-\eta)\Lambda^{\eta-2}\Gamma\mu^{\eta-1}$
Explosive, $\mu>M/\Gamma'$	$M+\mu$	$\lambda M(M/\mu)^{\delta}$	$(2-\eta)\lambda^{\eta-2}(M+\mu)M^{(\eta-2)(1+\delta)}\mu^{(2-\eta)\delta}$

distribution $n(m, 0)$ and recomputing again and again by determining Δn for a given interval Δt. Because the right-hand side of equation (3) does not contain t in explicit form, a stationary solution suggests itself naturally:

$$\frac{dT/dt}{T^2} = -\frac{\kappa}{\phi}\left[\phi(m)\int_{\max(m_<, m/\Gamma')}^{m_>} (m^{1/3} + \mu^{1/3})^2\,\phi(\mu)\,d\mu + \ldots\right] \quad (4)$$

The power law $\phi \propto m^{-11/6}$ can be found by setting $\delta = 0$, substituting a trial function $\phi \propto m^{-\alpha}$, setting the constant in equation (4) to zero (steady state), restricting α to a narrow range of possible values (in anticipation of the result), evaluating the integrals in equation (4), and discarding all but the two largest terms obtained for values of m in the intermediate range. (See Dohnanyi, 1969.)

This procedure, however, raises questions concerning the uniqueness and stability of the solution and its relation to the general solution of equation (3); these questions I feel have not yet been answered satisfactorily. Quite strangely, the solution $\phi \propto m^{-\alpha}$ does not seem to reflect any of the physics going into the problem (represented by the parameters Γ, etc.). Note also that the value of α is very little different from the power index of the fragment size distribution η (assumed to be equal to 1.8 for the above solution). This makes it impossible to decide, for instance, if the present asteroidal size distribution reflects the effects of the collisions having taken place over eons or the initial distribution formed quite recently in the fragmentation of a larger parent body. Another disadvantage is the lack of information about the actual

evolution from a given initial distribution n. One would like to know, for instance, how long it takes to reach the steady state. There is no information about the large and the small particles. The solution for T derived from equation (4) is of course just the asymptotic solution; therefore the initial development cannot be found by seeking a stationary solution for n. Finally, a collision equation (3) for particles with a narrow mass range (several orders of magnitude rather than several ten) does not lend itself to the above analysis. Instead, a numerical solution must be found by actually following the evolution of a distribution on a computer as it changes in the course of time, trying several sets of collision parameters Γ, etc.

A computational approach to solving the problem has the great advantage of allowing us to consider more accurate (and therefore often mathematically more complex) descriptions of the experimental data from which we build the fragmentation laws.[1] The power-law substitution for $\phi(m)$ obviously is suggested by the fact that the collision probability of particles M and μ is proportional to $(M^{1/3} + \mu^{1/3})^2$ and also by the form of the suggested distribution of fragments. Other functions render an analytical approach all but hopeless. Just as analytical approaches are beset with special problems, so are computational ones. In the latter, n becomes the number of particles with a fixed mass m and is therefore an integer; however, when considering large ranges of mass, the number of the smallest particles is too large to be handled as an integer even on large computers such as the IBM 360, which the author used. Also, the time interval is discrete; and therefore one works with fractional events, noninteger numbers of particles, and, in general, nonconservation of total mass. If the chosen time interval is too large, then, in effect, the same particle is destroyed several times and debris is created from nonexistent particles. If it is too small, the evolution proceeds much too slowly (the computations become excessively expensive); if too large, then details in the evolution are lacking.

Some of the inaccuracy inherent in the numerical solution for $n(m, t)$ is balanced, however, by the great uncertainty in the fragmentation laws. The particles are not really spherical, of homogeneous composition, nor colliding head on at the same v_{coll}; and their occupied volume changes in the course of time for various reasons besides the effects of the collisions themselves. Mass is

---

[1] I find that the impact experiment data of Gault and others (Gault, Shoemaker, and Moore, 1963; Gault and Wedekind, 1969) are better represented by

$$\log \int^{M} m\, dN(m) = \text{const} + A \log m + B(\log m)^2$$

The simple power law for dN/dm is obtained by setting $B=0$. Otherwise one obtains a rather complicated form for dN/dm:

$$\frac{dN}{dm} = \text{const}\, m^{A-2}(A + 2B \log m) m^{B \log m}$$

indeed actually lost from the system in the forms of both gas and very small particles, which are ejected from the system by radiation pressure or radiation drag. Finally, a collision does not necessarily lead only to erosion and fragmentation but could cause some aggregation of matter, though this is probably a minor effect.

I have recently begun numerical studies of the evolution of the particle size distribution under collisions, using an IBM 360 computer. Details of this program will be published elsewhere, and I would like to describe at this time some of the results. I first chose a narrow mass range (seven orders of magnitude) and assumed Dohnanyi's form of the fragmentation law ($\delta = 0$; $M_b = \lambda M$) with $\Gamma' = 5000$, $\Gamma = 100$, $\Lambda = 10$, and $0.1 < \lambda < 1$. The ratio of masses m_i and m_{i+1} was set equal to $10^{0.1}$, and the number of the largest particles was 10. Various initial distributions n were used. All were power laws suggested by the results of Dohnanyi and others. The time interval was adjusted during the program so that a "visible" change in n could be detected. The number of collisions between two given species of particles as well as the number of particles created by collisions were rounded to integers using a random number generator and a uniform probability distribution on (0, 1). This rounding insured that no "ghost" particles and/or fragments appeared in the problem, and it was, of course, necessary because of the discrete masses m_i of the program. The total mass decreased with time because debris with a mass less than a certain mass m_1 was presumed to be lost from the system. Under these conditions, I found that, regardless of the value of λ or of the initial distribution, particles with intermediate sizes were immediately and, eventually, greatly diminished in number as compared with very small or very large particles. A stationary state was reached eventually in this size range that was fairly well represented by a power law with index $\alpha \cong 3$. Because the number of particles of all sizes eventually decreased with time, the particles with intermediate size eventually disappeared altogether leaving a bimodal size distribution. For $\delta = 1$, the loss of particles with intermediate masses occurred without first reaching a stationary state described above. The two modes of the final distribution were not at any time given by power laws. The preliminary result of studies of the collisions between masses ranging over 30 orders of magnitude (corresponding to asteroidal radii from 10 μm to 100 km) gave a quite different result. I found that the number of very large particles is quickly diminished in relation to intermediate size or small particles.

These results must be tested by further calculations using many sets of parameters and initial distributions before it becomes worthwhile to formulate them in a more quantitative manner. I should like to mention, nevertheless, that the results suggest the existence of a bimodal size distribution for interplanetary dust: some small particles, some large particles, but nothing in between, to put it in simple words. This may explain some of the disagreement concerning the dust size distribution as determined by different experiments (e.g., polarimetry versus particle-impact counting).

ACKNOWLEDGMENT

This research was supported by NSF Grant GA-10 883.

REFERENCES

Dohnanyi, J. S. 1969, Collisional Model of Asteroids and Their Debris. J. Geophys. Res. 74, 2531.

Dohnanyi, J. S. 1970, Mass Distribution of Asteroids. Bellcomm TM-70-2015-6.

Filippov, A. F. 1961, Theory of Probability, vol. 6, p. 275.

Gault, D. E., Shoemaker, E. M., and Moore, H. J. 1963, Fragments Ejected From Lunar Surface by Meteoroid Impact Analyzed on Basis of Studies of Hypervelocity Impact in Rock and Sand. NASA TN-D 1767.

Gault, D. E., and Wedekind, J. A. 1969, The Destruction of Tektites by Micrometeoroid Impact. J. Geophys. Res. 74, 6780.

Hellyer, B. 1970, The Fragmentation of the Asteroids. Mon. Notic. Roy. Astron. Soc. 148, 383.

Piotrowski, S. 1953, The Collisions of Asteroids. Acta Astron. Ser. A 5, 115-138.

DISCUSSION

DOHNANYI: It is my experience that attempts to solve the collision equation of my model by successive approximations may involve convergence difficulties. I wonder if this is responsible for the differences in our results?

BANDERMANN: If the time interval Δt for the successive steps is chosen reasonably small, then I have found little or no dependence of the eventual evolution of the distribution on Δt, although the first few steps may show a strange behavior of the distribution.

Page intentionally left blank

INTERNAL CONSTITUTION AND MECHANISMS OF ASTEROID FRAGMENTATION

AVIVA BRECHER
University of California, San Diego

It has been generally assumed in the past that the fragmentation of asteroidal bodies and the production of meteorites are solely the result of collision events. (See Dohnanyi, 1969; Hartmann and Hartmann, 1968; Wetherill, 1967.)

A possible mechanism of noncollisional fragmentation will be proposed below, its proper framework of applicability will be defined, and evidence suggesting and supporting its existence will be adduced. Briefly, it is shown that the presence of even trace amounts of hydrogen in meteoritic metal phases (Edwards, 1955) may have caused the parent bodies of iron meteorites to undergo, spontaneously, delayed brittle fracture under the action of prolonged slow stresses, the imprint of which has been recorded in the phase structure of meteorites (Baldanza and Pialli, 1969). This phenomenon, termed "hydrogen embrittlement," has been amply documented in the literature on the metallurgy of ferrous metals (Bernstein, 1970; Tetelman, 1969).

INTERNAL CONSTITUTION OF ASTEROIDAL BODIES

Inferences on the internal constitution of asteroids are based on several lines of evidence.

First, an *average density* can be obtained if independent determinations of the mass and diameter of the body are made. Such data exist for Vesta and Ceres, yielding $\rho \sim 5 \pm 1$ g/cm^3 in the latest estimate by Schubart.[1] These densities are compatible with a high content of metallic nickel/iron, corresponding on the average to mesosideritic or pallasitic ($\rho \sim 5$ g/cm^3) composition (~50 percent by volume of meteoritic Ni/Fe).

Second, recent spectral reflectivity data (Chapman, Johnson, and McCord;[2] McCord, Adams, and Johnson, 1970) may yield information on the *surface composition* of the asteroids. The identification of the ferromagnesian silicate pyroxene on Vesta and the similarity of the overall spectrum to that of basaltic

[1]See p. 33.
[2]See p. 51.

achondrites do not rule out a high metal content for Vesta because basaltic achondrites (stony meteorites) are similar in composition to the silicate component of mesosiderites (stony iron meteorites). The possibility of high metal content is supported also by the fairly high density inferred for Vesta and is consistent with its very high albedo (Hapke[3]). Compositional differences between Ceres, Pallas, and Vesta are also apparent in spectral reflectivity data (McCord, Adams, and Johnson, 1970). This may be the rule in the asteroid belt, rather than the exception, as Levin (1965) suggested. An expectation of compositional diversity arose with the study of meteorites, which provides the largest body of evidence brought to bear, by implication, on the structure and composition of asteroidal bodies. The view that meteorites originated in asteroidal bodies (Anders, 1964) is entirely consistent with the assumption that many observed properties of meteorites are primordial and thus reflect the conditions prevailing during the condensation and accretion of small bodies in the solar system (Anders, 1964; Arrhenius and Alfvén, 1971). Such an assumption is particularly important with regard to metallic (Ni/Fe) phases in all meteorites, which have been used extensively and exclusively to determine cooling rates and parent body sizes (Buseck and Goldstein, 1968; Goldstein and Short, 1967; Powell, 1969; Wood, 1964; Wood, 1967).

It was recently shown (Fricker, Goldstein, and Summers, 1970) that for very slowly cooled classes of meteorites such as the pallasites (0.5 to 2 K/10^6 yr) or mesosiderites (~0.1 K/10^6 yr) the parent body size cannot be specified uniquely and may be larger than asteroidal. In any case, the cooling rates of various classes of meteorites alone provide a strong argument against an origin of stony irons in the same (differentiated) parent body with iron or stony meteorites (Buseck and Goldstein, 1968; Fricker, Goldstein, and Summers, 1970; Powell, 1969). Sizes of iron meteorite parent bodies, however, based on cooling rates of 0.5 to 500 K/10^6 yr, encompass the range 10 to ~450 km in radius and are still compatible with observed sizes of asteroids, although the models are inadequate for discrimination between a "core" or a "raisin" origin (Fricker, Goldstein, and Summers, 1970; Levin, 1965).

The evidence from meteorites clearly suggests an origin in a multiplicity of parent bodies (required by the existence of discrete chemical groups and different cooling rates for various classes of meteorites, as well as by the scatter in cooling rates within a class) of relatively large sizes (as required by slow cooling rates and by the large-scale continuity of Widmanstätten patterns in iron meteorites), which were fragmented in a few, discrete, large events (as indicated by the conspicuous clustering of cosmic-ray ages). (See Anders, 1964; Hartmann and Hartmann, 1968.)

Mass balance arguments (Arnold, 1965), as well as the longer cosmic-ray exposure ages of iron meteorites, make an origin of these objects in fairly massive asteroids compatible with most evidence to date. Yet the study of size

---

[3]See p. 67.

and mass distributions of various groups of asteroids (Anders, 1965; Brecher and Alfvén, 1969-70; Hartmann and Hartmann, 1968) indicates that very few major collision events have altered the reconstituted primordial distribution and that the long collision lifetimes ($\tau > 10^9$ yr for $m > 10^{18}$ kg) preclude frequent collisional disruption of massive bodies; moreover, secondary collisions are also less frequent than expected (Dohnanyi, 1969), as reflected in the relatively narrow spread in cosmic-ray exposure ages of meteorite classes (Anders, 1964; Anders, 1965; Arnold, 1965; Hartmann and Hartmann, 1968).

An interesting alternative to their destruction in collision events can be conjectured for some massive parent bodies of iron meteorites (with a low probability of collisional destruction but with a considerable amount of strong Ni/Fe) and for parent bodies with a mesosideritic or pallasitic structure; i.e., with the metal (Ni/Fe) phase continuous in three dimensions conferring structural strength. It involves spontaneous brittle failure of the parent body due to hydrogen embrittlement of the Ni/Fe phases.

HYDROGEN EMBRITTLEMENT AND THE PRODUCTION OF IRON METEORITES

In a recent study of the mechanical properties of iron meteorites, Gordon (1970) found the internal structure of about 150 samples to have preserved surprising perfection over large dimensions for bodies presumed to have resulted from violent collisions. Moreover, no evidence was found of the large-scale plastic deformation or ductile fracture expected on the basis of shock loading experiments on the Odessa iron. He concluded that the iron meteorites appear to have formed in brittle fracture events; yet the metal of the Gibeon octahedrite was remarkably ductile and strong. Moreover, no tendency was found in the samples studied for preferential fracture along octahedral planes nor for embrittlement due to inclusions. The fact that the meteoritic metal was not intrinsically brittle (and it did not become brittle at any testing temperature down to 100 K) forced Gordon to conclude that "a mechanism of embrittlement must function for all meteorites having a Widmanstätten structure if these are to be considered fragments of a larger metal mass." Unable to find such a mechanism, he assumed that small, meteorite-size masses of Ni/Fe must have been embedded in intrinsically brittle silicates.

A well-known embrittling agent of ferrous metals is gaseous hydrogen, and the phenomenon of hydrogen embrittlement has been extensively reviewed. (See Barth and Steigerwald, 1970; Bernstein, 1970; Groeneveld, Fletcher, and Elsea, 1966; Nelson, Williams, and Tetelman, 1971; Tetelman, 1969.) The loss in ductility caused by the introduction of hydrogen into Ni/Fe alloys to levels of a few parts per million is *not* detectable under impact loading conditions (i.e., at collisions), but only at very low strain rates of $\dot{\epsilon} < 0.05$ per minute (Tetelman and McEvily, 1967) and under static or sustained stresses. Thus, the susceptibility of meteoritic metal to structural hydrogen embrittlement could

not have been detected at the relatively high strain rates ($\dot{\epsilon} < 0.3$ per minute) in Gordon's (1970) tests. Nor is the hardness or the yield strength of iron meteorites affected by the presence of hydrogen, so that data available for the Gibeon (Gordon, 1970), Odessa, Sikhote-Alin, Canyon Diablo, and Henbury irons and for the Brenham pallasite (Baldanza and Pialli, 1969; Knox, 1970) may reflect the intrinsic, structure-dependent properties of meteoritic Fe/Ni alloy phases (Baldanza and Pialli, 1969, table 1). The presence of hydrogen, however, reduces the fracture strength so that microcracks can start to propagate unstably after an incubation time during which the internal hydrogen reaches a critical configuration (Tetelman, 1969). Thus the body undergoes seemingly spontaneous brittle fracture, often after having withstood previous dynamic impacts or high loads. The incubation time before failure is relatively insensitive to stress level but is sensitive to stress rate. The embrittlement is promoted not only by low strain rates or prolonged quasi-static loading but also by concentration gradients in hydrogen.

The physical picture of hydrogen embrittlement is briefly that of local stress fields in the metal lattice caused by screened protons at interstitial sites, by atomic H pinned at defects and grain interfaces, and even by H_2 molecules recombined in internal voids. The amounts sufficient to cause brittle failure in steel can be less than 1 ppm by weight of average H content. Details about solubility in the α and γ phases of Ni/Fe, and about the possible mechanisms of embrittlement will be given elsewhere (Brecher, 1971). Suffice it to say that a variety of environments can supply the internal and/or external hydrogen necessary for brittle fracture of a metal body, such as corrosive atmospheres of H_2S and H_2O (which may have existed at various stages of the formation of meteorites), fields of accelerated protons implanting hydrogen such as the solar wind, or partially ionized and dissociated low-pressure interplanetary gas media containing atomic hydrogen as an important constituent (Arrhenius and Alfvén, 1971; Nelson, Williams, and Tetelman, 1970). The seed of self-destruction may have been planted in parent bodies of iron meteorites at birth as hydrogen was occluded during the grain condensation and growth stages, in the presence of abundant hydrogen. Moreover, continuous surface implantation of solar-wind protons may have provided the local hydrogen pressure gradients and local strains known to initiate microcracks and thus may have promoted failure by brittle fracturing under unstable crack propagation.

Is there evidence for the presence of hydrogen in iron meteorites? The old work on thermal release patterns of gases reported by Farrington (1915) showed that hydrogen was the most abundant gas phase released from iron meteorites at levels of 3 to 55 ppm; by chemical methods, Nash and Baxter (1947) detected minimal levels of a few tenths of a part per million of H_2. More sophisticated determinations by Edwards (1953, 1955) revealed surprisingly high levels of hydrogen in iron meteorites (up to ~33 ppm average content, and up to ~55 ppm in the fine-grained fraction), leading Edwards (1955) to conclude that the hydrogen "must have been originally incorporated during the formation of the meteorites." The H/D ratios typical of iron

meteorites (Edwards, 1953, 1955) in comparison with terrestrial steels seem to exclude terrestrial contamination as the source of hydrogen.

MORE SUPPORTING EVIDENCE

Supporting evidence for the conjectured brittle failure of parent bodies of iron meteorites can be drawn from several areas of research.

One area is the study of preterrestrial deformation effects in meteorites (Axon, 1969; Baldanza and Pialli, 1969). For example, in their study of "dynamically" deformed structures in irons and chondrites, Baldanza and Pialli found extensive evidence that "shear forces of a slow character" acted to distort the phase structure in irons, and concluded that "the pressure was related to a slow dynamic event and temperature was confined to relatively low values." Such effects are not expected in collisional shock events. Moreover, the recrystallization observed mainly along faults (indicating local loss in ductility, i.e., embrittlement), "shear fractures," and "deformation due to prolonged stress action" seem to fit well the path leading to hydrogen brittle failure, as does the history formulated for these meteorites (culminating in the production of "split" bodies, when conditions of low temperatures were attained). It is remarkable that the critical range of temperature for failure due to molecular hydrogen is 173 to 373 K (Bernstein, 1970), thus bracketing the values relevant for iron meteorites at 1 AU (~363 K) to 3 AU (~223 K). Moreover, in the presence of atomic hydrogen, brittle failure occurs over a wider range of low temperatures (Nelson, Williams, and Tetelman, 1971), whereas "hydrogen cathode charging" of steels (which is equivalent to solar-wind implantation of hydrogen) is known to cause irreversible brittle failure at levels of 5 to 8 ppm of H_2 even at 77 K (Barth and Steigerwald, 1970).

Another significant fact is the presence of very high levels of hydrogen ($\sim 8.4 \times 10^{-2}$ cm^3/g) in some gas-rich meteorites (Lord, 1969) as well as proton contents of 4×10^{19} to 2×10^{20} per gram found in various chondrites (Chatelain et al., 1970), all being accountable by $\sim 10^4$ equivalent irradiation years at 1 AU in typical solar-wind proton fluxes of $\sim 3 \times 10^8$ $cm^{-2}\text{-}sec^{-1}$ ($E > 1$ keV). Not only is the hydrogen effectively implanted by solar wind into the grain surfaces (possibly prior to their aggregation (Lord, 1969) or while suspended in jetstreams (Arrhenius and Alfvén, 1971; Trulsen, in this book[4])), but it also is released mostly above ~700 K from stones (Lord, 1969), whereas in irons it can be held as "residual hydrogen" to above 1000 K (Johnson and Hill, 1960). In Apollo 11 Moon material (Fireman, D'Amico, and De Felice, 1970), a hydrogen concentration gradient was found to exist in rocks, and the abundant hydrogen content of the lunar soil (1.2 cm^3/g) was only in part attributable to solar wind, thus suggesting that some primordial hydrogen was retained.

---

[4]See p. 327.

The solar wind therefore could establish in surface layers a local concentration gradient of hydrogen and an equivalent quasi-static internal stress known to facilitate an eventual fracture of the parent body. It also could establish a trapping layer for hydrogen at irradiation-caused or other defects and dislocations close to the surface.

Can the evidence of shock in some iron meteorites (Jaeger and Lipschutz, 1967; Jain and Lipschutz, 1969) rule out the occurrence of noncollisional fragmentation? It seems that it cannot do so because shock of mild to moderate levels appears to be limited to certain groups of iron meteorites (such as the group III octahedrites, which also cluster in cosmic-ray ages at $\sim 650 \times 10^6$ yr). Other groups, like the hexahedrites, show no evidence of shock; unshocked octahedrites, although randomly distributed among the Ga-Ge groups, also seem to exhibit peaks in their cosmic-ray age distribution at 200 to 500 and 800 to 1000×10^6 yr, suggesting a formation in noncollisional discrete events (Jain and Lipschutz, 1969; Voshage, 1967). Even some group III octahedrites, like Henbury and Cape York, are apparently unaltered; although they are believed to have been mildly shocked (at 130 to 400 kb levels).

There are at least two massive, well-studied finds of iron meteorites that appear to have undergone spontaneous brittle failure prior to entering the atmosphere. They are Gibeon (Bethany) in Southwest Africa and Cape York in Greenland. Nininger (1963) remarks that in the case of Gibeon, more than 50 irons totaling 15×10^3 kg were recovered. The fact that all were strongly ablated and that the scatter ellipse covered an area of several hundred square miles indicated that Gibeon meteorites arrived as a "preatmospheric swarm." Similarly, the giant Greenland irons (specimens weighed 36, 3.5, 3, and 0.4×10^3 kg) were scattered widely over ~ 250 km^2 and seemed to have traveled as a "swarm" along the same orbit without suffering any further fragmentation upon entering the atmosphere. In contrast, in the large fall of Sikhote-Alin, several thousand fragments resulting from atmospheric fragmentation were scattered within less than 2.5 km^2 and exhibited a wide range of sizes from grains to several tons. In both Gibeon, whose mechanical properties suggested to Gordon (1970) the formation in a brittle fracture event, and in Cape York, hydrogen was found at levels of ~ 7 and ~ 25.5 ppm, respectively (Edwards, 1955). One could thus assume that, in the presence of internal hydrogen and under repeated stress and intense solar-wind bombardment at ~ 1 AU perihelion approach, brittle failure of the parent body might have occurred and that the pieces were not dispersed considerably from the common orbit in this gentle type of preatmospheric fragmentation. The time of the fragmentations may be indicated by the fairly long cosmic-ray ages of iron meteorites.

This type of seemingly spontaneous splitting of a parent body has been well known to occur in comet nuclei at perihelion approach when unusual stresses on compact nuclei could facilitate unstable cracking. Such fragmentation was observed, for example, in the comets Biela (1826), Olinda (1860), Taylor

(1916I), which split in two, and the large comet 1882III, which split into six pieces. In these cases, the centrifugal force about the Sun at perihelion approach and/or the intense irradiation by the solar wind may have aided in disrupting the nucleus (Dauvillier, 1963). The propensity of Eros to disrupt and fragment was also noted during its 1931 close approach to Earth (Dauvillier, 1963). In view of the possibly compact, rigid bodylike nature of some comet nuclei (Whipple, 1963) and of the plausibility of a cometary origin for at least some classes of meteorites (see paper by G. W. Wetherill in this volume[5]), and in the light of a possible evolution of some comets into asteroidal objects (see paper by B. G. Marsden in this volume[6]), the splitting of comet nuclei into a few large pieces may be highly suggestive of a mechanism for low-energy fracture.[7]

CONCLUSIONS

It has been shown previously that the mechanical properties of iron meteorites (Gordon, 1970) required their production in brittle fracture breakup events. It was suggested above that the excess hydrogen found in iron meteorites (Edwards, 1955) is likely to be the necessary embrittling agent. A survey of the metallurgy of hydrogen embrittlement (Barth and Steigerwald, 1970; Bernstein, 1970; Groeneveld, Fletcher, and Elsea, 1966; Nelson, Williams, and Tetelman, 1971; Tetelman, 1969) indicated that an iron meteorite parent body could suffer delayed brittle fracture under the action of low rate (accumulated or periodic) stresses whose imprint was found in the metal phase structure (Axon, 1969; Baldanza and Pialli, 1969). Such fracture would occur when the internal hydrogen distribution has reached a critical configuration, which could facilitate rapid propagation of cracks. Two large groups of iron meteorites (Gibeon and Cape York), which are thought to have arrived as preatmospheric swarms, were found to contain sufficient amounts of hydrogen to have been produced in brittle fracture (noncollisional) fragmentation of their parent bodies.

REFERENCES

Anders, E. 1964, Origin, Age and Composition of Meteorites. Space Sci. Rev. 3, 583.

Anders, E. 1965, Fragmentation History of Asteroids. Icarus 4, 399.

Arnold, J. R. 1965, The Origin of Meteorites as Small Bodies. III–General Considerations. Astrophys. J. 141, 1548.

Arrhenius, G., and Alfvén, H. 1971, Fractionation and Condensation in Space. Earth Planet. Sci. Lett. 10, 253.

Axon, H. J. 1969, Pre-Terrestrial Deformation Effects in Iron Meteorites. Meteorite Research (ed., P. M. Millman), p. 796. D. Reidel. Dordrecht.

---

[5]See p. 447.

[6]See p. 413.

[7]*Note added in press:* An alternative mechanism for low-energy fracture of iron meteorite parent bodies has just been proposed by H. L. Marcus and P. W. Palmberg (1971) in J. Geophys. Res. 76, 2095.

Baldanza, H., and Pialli, G. 1969, Dynamically Deformed Structures in Some Meteorites. Meteorite Research (ed., P. M. Millman), p. 806. D. Reidel. Dordrecht.

Barth, C. F., and Steigerwald, E. A. 1970, Evaluation of Hydrogen Embrittlement Mechanisms. Met. Trans. 1, 3451.

Bernstein, I. M. 1970, The Role of Hydrogen in the Embrittlement of Iron and Steel. Mater. Sci. Eng. 6, 1.

Brecher, A. 1971, Hydrogen-Embrittlement and Implications for the Production of Iron Meteorites, in preparation.

Brecher, A., and Alfvén, H. 1969-70, Size and Mass Distributions of Families, Jet Streams and "Bachelor" Asteroids. (Unpublished)

Buseck, P. R., and Goldstein, J. I. 1968, Pallasitic Meteorites: Implications Regarding the Deep Structure of Asteroids. Science 159, 300.

Chatelain, A., Kline, D., Kolopus, J. L., and Weeks, R. A. 1970, Electron and Nuclear Magnetic Resonance of Three Chondritic Meteorites. J. Geophys. Res. 75, 5681.

Dauvillier, A. 1963, Cosmic Dust, p. 60. G. Newnes. London.

Dohnanyi, J. S. 1969, Collisional Model of Asteroids and Their Debris. J. Geophys. Res. 74, 2531.

Edwards, G. 1953, Hydrogen and Deuterium in Iron Meteorites. Proc. Conf. Nucl. Processes Geol. Settings, p. 48.

Edwards, G. 1955, Isotopic Composition of Meteoritic Hydrogen. Nature 176, 109.

Farrington, O. C. 1915, Meteorites, p. 190. Univ. of Chicago Press. Chicago.

Fireman, E. L., D'Amico, J. C., and De Felice, J. C. 1970, Tritium and Argon Radioactivities in Lunar Material. Science 167, 566.

Fricker, P. E., Goldstein, J. I., and Summers, A. L. 1970, Cooling Rates and Thermal Histories of Iron and Stony-Iron Meteorites. Geochim. Cosmochim. Acta 34, 475.

Goldstein, J. I., and Short, J. M. 1967, The Iron Meteorites, Their Thermal History and Parent Bodies. Geochim. Cosmochim. Acta 31, 1733.

Gordon, R. B. 1970, Mechanical Properties of Iron Meteorites and the Structure of Their Parent Planets. J. Geophys. Res. 75, 439.

Groeneveld, T. P., Fletcher, E. E., and Elsea, A. R. 1966, Review of Literature on Hydrogen Embrittlement. Special Report to NASA (NAS 8-20029).

Hartmann, W. K., and Hartmann, A. C. 1968, Asteroid Collisions and Evolution of Asteroidal Mass Distribution and Meteoritic Flux. Icarus 8, 361.

Jaeger, R. R., and Lipschutz, M. E. 1967, Implications of Shock Effects in Iron Meteorites. Geochim. Cosmochim. Acta 31, 1811.

Jain, A. V., and Lipschutz, M. E. 1969, Shock Histories of Hexahedrites and Ga-Ge Group III Octahedrites. Meteorite Research (ed., P. M. Millman), p. 826. D. Reidel. Dordrecht.

Johnson, E. W., and Hill, M. L. 1960, The Diffusivity of Hydrogen in α-Iron. Trans. Met. Soc. AIME 218, 1104.

Knox, R., Jr. 1970, The Yield Strength of Meteoritic Iron. Meteoritics 5, 63.

Levin, B. J. 1965, Origin of Meteorites. Planet. Space. Sci. 13, 243.

Lord, H. C. 1969, Possible Solar Primordial Hydrogen in the Pesyanoe Meteorite. Earth Planet. Sci. Lett. 6, 332.

McCord, T. E., Adams, J. B., and Johnson, T. V. 1970, Asteroid Vesta, Spectral Reflectivity and Compositional Implications. Science 168, 1445.

Nash, L. K., and Baxter, G. P. 1947, The Determination of Gases in Terrestrial Irons and Steels. J. Amer. Chem. Soc. 69, 2534.

Nelson, H. G., Williams, D. P., and Tetelman, A. S. 1971, Embrittlement of a Ferrous Alloy in a Partially Dissociated Hydrogen Environment. Metallurg. Trans. 2, 953-959.

Nininger, H. H. 1963, Meteorite Distribution on the Earth. The Solar System (eds., B. M. Middlehurst and G. P. Kuiper), vol. IV, p. 162. Univ. of Chicago Press. Chicago.

Powell, B. N. 1969, Petrology and Chemistry of Mesosiderites–I. Textures and Composition of Nickel-Iron. Geochim. Cosmochim. Acta 33, 789.

Tetelman, A. S. 1969, The Mechanism of Hydrogen Embrittlement in Steel. Fundamental Aspects of Stress Corrosion Cracking (eds., R. W. Staehle, A. J. Forty, and D. van Rooyen), pp. 446-464. Nat. Assoc. Corrosion Engs. Houston.

Tetelman, A. S., and McEvily, A. J., Jr. 1967, Fracture of Structural Materials, p. 456. John Wiley & Sons, Inc. New York.

Voshage, H. 1967, Bestrahlungsalter und Herkunft der Eisenmeteorite. Z. Naturforsch. A 22, 477.

Wetherill, G. W. 1967, Collisions in the Asteroid Belt. J. Geophys. Res. 72, 2429.

Whipple, F. L. 1963, On the Structure of the Cometary Nucleus. The Solar System (eds., B. M. Middlehurst and G. P. Kuiper), vol. IV, ch. 19. Univ. of Chicago Press. Chicago.

Wood, J. A. 1964, Cooling Rates and Parent Planets of Several Iron Meteorites. Icarus 3, 429.

Wood, J. A. 1967, Chondrites: Their Metallic Minerals, Thermal Histories and Parent Planets. Icarus 6, 1.

DISCUSSION

DOHNANYI: Have you had a chance to examine this problem to see if a critical object size exists beyond which the fragments would tend to stick together? It seems that there should be a critical size where gravity is strong enough to keep the fragments together despite other perturbations.

BRECHER: It is difficult to appraise such a critical object size without making very particular assumptions about the size, density, fragmentation spectrum, and orbit of the body, as well as about the mode of disruption and the type of forces (self-gravitation, tidal, solar-wind dynamic pressure, torques, etc.) acting at breakup.

Order of magnitude estimates for 10^3 kg sized pieces of meteoritic iron seem to indicate that they may be kept in contact by mutual gravitational attraction, if the perturbations acting on them are less than ~1 μN/kg (~10^{-4} dyne/g). Compared to the solar gravitation of 6 mN/kg (0.6 dyne/g) at 1 AU, tidal forces exerted by the Sun and Earth, which are ~10^{-13} and ~10^{-18} N/kg-m (~10^{-13} and ~10^{-18} dyne/g-cm), respectively, for 1 AU approach, or ~10^{-10} and ~10^{-15} N/kg-m (~10^{-10} and ~10^{-15} dyne/g-cm) for 0.1 AU approach, may be neglected. Similarly, rotational instability will not prevail over mutual gravitation of such 10^3 kg sized chunks, if the rotation period of the body was initially larger than 1 hr. This holds for asteroids, whose spin periods range from 2 to ~10 hr.

But the solar-wind dynamic pressure, at the present 1 AU flux of kiloelectron volt protons, would suffice to transfer a momentum of ~5×10^4 g-cm/s per unit area, allowing a body with a 1 m^2 area to acquire a velocity of ~5 m/s after only 10 million yr of "storage" in a geocentric orbit (Arnold, 1965); if iron meteorites were stored in such an orbit during the ~500 million yr that have elapsed since breakup, different surface areas of fragments may have led to considerable scatter velocities.

Compare the above to the extremely small initial differential velocities of ~2×10^{-7} cm/s inferred for the presumed members of the Cape York "preatmospheric swarm" from the dimension (~25 km) of their scatter ellipse (Nininger, 1963), if breakup occurred 500 million yr ago. It seems that some cohesive forces (cold welding), or the gentle fracture mode, may have allowed some fragments to hold together in spite of dispersive perturbations. For a 10^5 kg body, the escape velocity is only ~0.2 cm/s and, indeed, it is hard to see how 10^3 kg sized chunks could have had smaller scatter velocities at breakup. (I thank Dr. Anders for pointing out this fact.) One could only hope that, just as for asteroidal families assumed to form by collisional breakup, extremely long lifetimes

(~2.2 billion yr) against dispersal were found (Anders, 1965), similarly long lifetimes may hold for smaller fragments resulting from noncollisional fracture modes.

DISCUSSION REFERENCES

Anders, E. 1965, Fragmentation History of Asteroids. Icarus **4**, 399.

Arnold, J. R. 1965, The Origin of Meteorites as Small Bodies. III—General Considerations. Astrophys. J. **141**, 1548.

Nininger, H. H. 1963, Meteorite Distribution on the Earth. The Solar System (eds., B. M. Middlehurst and G. P. Kuiper), vol. IV, p. 162. Univ. of Chicago Press. Chicago.

MOTION OF SMALL PARTICLES IN THE SOLAR SYSTEM

HANNES ALFVÉN
Royal Institute of Technology
Stockholm

Unlike planets and satellites, smaller bodies in the solar system, like asteroids, comets, and meteoroids, are affected by nongravitational forces due to collisions, viscosity, and in some cases electromagnetic forces. The way such forces change the orbits of the bodies seems not to have been analyzed until recently. For example, it is generally believed that collisions between asteroids will make their orbits spread over an increasing volume of space and that collisions inside meteor streams will make their cross sections increase. At least under certain conditions the reverse is true, as shown by the papers of Baxter[1] and Trulsen[2] at this symposium. Furthermore, besides the usual picture of meteoroids being emitted by comets, we should also discuss the reverse process; viz, comet formation by bunching in a meteor stream.

We shall discuss a very simple model to illustrate the manner in which celestial mechanics works in a special case.

Suppose a number of particles ("apples") are enclosed in a spacecraft that is orbiting in a circle of radius r_o around a central body with mass M_c. We assume that both the spacecraft and the particles have a mass so small that their mutual gravitation is negligible. Hence, the particles orbit around the central body in Kepler ellipses (neglecting the case in which particles are stuck to the wall of the spacecraft). Seen from the spacecraft they will perform oscillations, which sooner or later will be damped by collisions with the walls or with each other. We may also assume that the spacecraft contains some gas so that eventually all relative motions are damped.

When this state is reached, all particles must move in circles located in the plane of the spacecraft's orbit for the same reasons that cause the Saturnian rings to be flat. However, unlike the rings, all of the particles must move with the same period because of their location inside the spacecraft. This means that their orbital radii all must equal the orbital radius r_o of the center of gravity of the spacecraft. Hence, all of the particles will be located on a straight line (or, more accurately, on a small part of a circular arc) through the center of gravity,

[1]See p. 319.
[2]See p. 327.

pointing in the direction of motion. Let this line be the y axis of an orthogonal coordinate system. Let the x axis point in the radial direction and the z axis in the axial direction. Suppose that we displace one of the particles a distance z in the axial direction. The gravitation $\kappa M_c r^{-2}$ from the central body will then have a z component $f_z = -\kappa M_c r^{-3} z$ not compensated for by the centrifugal force. Hence, the particle will describe harmonic oscillations in the z direction with a period equal to the orbital period. This is just another way of saying that the orbital plane of the particle has an inclination $\neq 0$.

Further, a displacement in the x direction will produce a similar oscillation with the same period. (This oscillation, however, is coupled with an oscillation that has a double amplitude in the y direction. In the x, y plane, the particle describes an "epicycle" that is an ellipse with the y axis twice the x axis.) This means that the eccentricity is $\neq 0$.

Hence, seen from the spacecraft, the particles move parallel to the x, z plane as if they were subject to an *apparent attraction* that is transverse to the motion

$$\mathbf{f}_a = -\frac{\kappa M_c}{r_o^3} \cdot \boldsymbol{\rho}$$

with $\rho = (x^2 + z^2)^{1/2}$. This force acts perpendicular to the velocity of the spacecraft and tends to bring all particles to the y axis, a result that is achieved when the oscillations are damped.

The phenomena described here are strongly related to the jetstream producing effects that are analyzed by Baxter and by Trulsen.

Suppose that the motion we have considered is perturbed by the gravitation of a small body passing not very far from the spacecraft. Under certain conditions, which have been discussed elsewhere (H. Alfvén, 1971), the perturbation is such as to make all of the alined particles move toward the center of gravity of the spacecraft. In certain special cases, the result is that all of the particles will reach this point at the same moment. This means that besides the apparent transverse attraction there may also be, under certain conditions, an apparent *longitudinal* attraction (although this term is not very accurate).

It is possible that similar phenomena may bunch a large number of grains in a meteor stream in such a way as to produce a comet.

REFERENCE

Alfvén, H. 1971, Apples in a Spacecraft. Science **173**, 522-525.

DISCUSSION

DOHNANYI: What do you feel is the basic difference between a jetstream and a meteor stream?

ALFVÉN: The terminology here is always difficult. You can use the word "jetstream" for the theoretical conception of streams formed by viscosity effects acting on particles

moving in Kepler orbit. Then the question arises whether meteor streams and asteroid streams really are caused in this way. I think that there are strong arguments for this, but it is not proved yet and cannot be proved until we know the densities of the small particles in these streams. For the formation of such a stream, there must be enough interaction among the particles, or between them and a gas, or some kind of similar effect must be present.

WHIPPLE: Dr. Schatzman (1953) worked out this problem several years ago using a large number of particles for a loose comet nucleus. Generally, the particles eventually come together. However, the time constant is the vital weakness in a jetstream theory applied either to the asteroid belt or to a meteor stream in the solar system today. Other minor forces, such as the Poynting-Robertson effect, planetary perturbations, and collisions with extraneous fast moving bodies with loss of fine particles and gases, have time to act and destroy the possibility of coagulation in such a jetstream.

ALFVÉN: The time constant is of interest for the application, but there is not enough information to support Dr. Whipple's general statement.

DISCUSSION REFERENCE

Schatzman. 1953, La Physique des Comètes. Liège Symp., pp. 313-323. Louvain.

Page intentionally left blank

JETSTREAM FORMATION THROUGH INELASTIC COLLISIONS

DAVID C. BAXTER AND WILLIAM B. THOMPSON
University of California, San Diego

An inelastic collision integral is used in a Boltzmann-type equation for a distribution of particles in Kepler orbits. A Fokker-Planck equation is found that leads to radial density clustering.

It has been suggested that in a cloud of grains moving in Kepler orbits in a gravitational field, inelastic collisions will cause the grains to form groups having similar orbits, called jetstreams (Alfvén, 1970). One would expect that a jetstream already formed would contract into a tighter jetstream (Trulsen[1]) because the jetstream would lose total energy because of the inelasticity of collisions, whereas the total angular momentum would be conserved. The grains would move toward a circular orbit because circular orbits have the lowest energy E_0 for a given angular momentum L (fig. 1). We consider the question of whether jetstreams will form from an initially smooth distribution function.

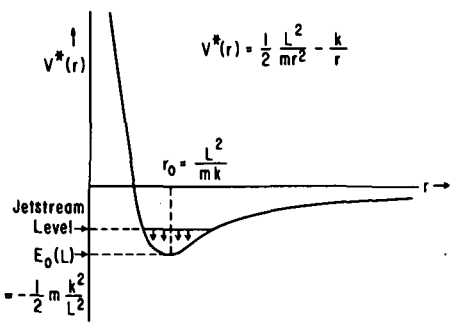

Figure 1.–A jetstream can be thought of as a group of particles filling an effective potential well $V^*(r)$, which arises from gravitational and centrifugal forces. As the particles lose energy E in inelastic collisions, they concentrate at the bottom of the well. m = mass of a single grain.

[1]See p. 327.

THE MODEL

The essential feature of this suggestion is the inelasticity of the collisions. Accordingly, we look at a particularly simple model with particularly simple inelastic collisions; i.e., perfectly inelastic collisions in which colliding particles stick together. We avoid the consideration of accretion of particles by considering the final velocities of colliding particles to be arbitrarily close while the particles maintain their distinct identities. We consider one species of particles moving in coplanar Kepler orbits.

Particles in an arbitrary distribution of exactly circular orbits would never collide, so such a distribution would be stationary (fig. 2). A thermal equilibrium distribution

$$f(r, \theta, p, L) = A \exp\left[-\beta\left(\frac{p^2}{2m} + \frac{L^2}{2mr^2} - \frac{k}{r}\right) - \alpha L\right] \tag{1}$$

yields a radial density distribution

$$n(r) = \iiint f \, d\theta dp dL$$

$$= A(2\pi)^2 \frac{mr}{\beta} \exp\left(\beta \frac{k}{r} + \frac{mr^2\alpha}{2\beta}\right) \tag{2}$$

which diverges exponentially at $r = 0$ and $r = \infty$, where r and θ are polar coordinates, p and L are the corresponding canonical momenta (radial and angular momentum, respectively), m is the mass of a single grain, and $\Phi(r) = -k/r$ is the gravitational potential energy. A distribution with minimum

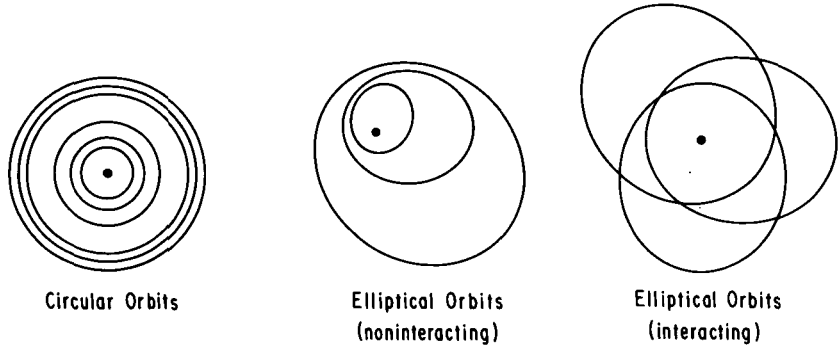

Figure 2.–Particles in circular orbits (or in nonintersecting orbits with $\epsilon \neq 0$) experience no collisions. Collisional evolution only occurs when these elliptical orbits intersect. Kepler orbit: $\Phi(r) = -k/r$.

energy for a given total angular momentum would be one in which a single grain, having all the angular momentum and almost no energy, moves very slowly in an orbit with very large radius, whereas all the other particles collapse into the central body.

We consider an initial distribution that depends arbitrarily on angular momentum, has orbits of generally small eccentricity, and is axisymmetric:

$$f_0(r, \theta, p, L) = A(\epsilon_0)F(L) \exp \frac{-\epsilon^2}{\epsilon_0{}^2} \tag{3}$$

where

$$\epsilon^2(r, p, L) = \frac{p^2/2m + L^2/2mr^2 - k/r + mk^2/2L^2}{mk^2/2L^2}$$

is the spatial eccentricity of an orbit that passes through the point (r, θ, p, L) in phase space, and $-mk^2/2L^2$ is the energy of a circular orbit with angular momentum L. We assume that essentially all of the particles are orbiting in the same direction. We use a smooth function $F(L)$ so that

$$F(L + \delta L) \simeq F(L) + \delta L \frac{dF}{dL} + \frac{\delta L^2}{2} \frac{d^2F}{dL^2} \tag{4}$$

(where $\delta L = 0(\epsilon L)$) is a valid expression. We can rewrite equation (3) as

$$f_0 = \tilde{A}F(L) \exp [-\beta(L)E] \tag{5}$$

which has a superficial resemblance to the equation for thermal equilibrium. Note that the initial axisymmetry demands that the final state will be axisymmetric (i.e., only circular jetstreams are possible). We will also have to consider the functions

$$h(L) = \iiint f \, dr d\theta dp \simeq (2\pi)^2 \epsilon_0{}^2 \frac{L}{2} AF(L) \tag{6}$$

$$A(\epsilon_0) = N \left(\iiiint f \, dr d\theta dp dL \right)^{-1}$$

$$= N \left[\int h(L) \, dL \right]^{-1} \tag{7}$$

where $h(L)$ is the density in angular momentum space, $A(\epsilon_0)$ is the normalization constant, and N is the total number of grains.

THE CALCULATION

We wish to find a differential equation that describes the evolution of $h(L)$, the distribution function in angular momentum space. The equation describing the time evolution of the phase space distribution function is

$$\frac{df}{dt} = \frac{\partial f}{\partial t} + \mathbf{v} \cdot \frac{\partial f}{\partial \mathbf{x}} + \mathbf{a} \cdot \frac{\partial f}{\partial \mathbf{v}} = I(f, f) \tag{8}$$

where $\mathbf{x}$ is the position vector, $\mathbf{v} = d\mathbf{x}/dt$, $\mathbf{a} = d\mathbf{v}/dt$, and $I(f, f)$ is the collision integral. Our initial distribution f_0, being a function of constants of the motion only, is stationary in the absence of collisions. We assume that the mean free path is long compared with the orbital path so that collisions are treated as a perturbation, whence

$$f = f_0 + \delta f \tag{9}$$

where δf is the perturbation distribution caused by collisions. Linearizing equation (8) we get

$$\frac{df}{dt} = \frac{d\delta f}{dt} = I(f_0, f_0) \tag{10}$$

The collision integral for completely inelastic collisions is

$$I(f, f) = -\iint \frac{\sigma}{r}(g)|g| \left[f(r, \theta, p, L) f(r, \theta, p + p', L + L') - f\left(r, \theta, p - \frac{p'}{2}, L - \frac{L'}{2}\right) f\left(r, \theta, p + \frac{p'}{2}, L + \frac{L'}{2}\right) \right] dL' dp' \tag{11}$$

where p' and L' are relative momenta between colliding grains,

$$g = \left[\left(\frac{p'}{m}\right)^2 + \left(\frac{L'}{mr}\right)^2 \right]^{1/2} \tag{12}$$

is the relative speed between the two grains, and $\sigma(g)$ is the collisional cross section. (Note that a (p, L); $(p + p', L + L')$ collision scatters a particle out of the phase space volume element at (r, θ, p, L) and a $(p - p'/2, L - L'/2)$; $(p + p'/2, L + L'/2)$ collision scatters two particles into a phase space volume element at (r, θ, p, L).)

Inserting equation (3) into equation (11), Taylor-expanding $F(L)$, assuming that $\sigma(g)$ is a constant, and integrating over p' and L', we get

$$\frac{df}{dt}(r, \theta, p, L) = \epsilon_0{}^2 mk \frac{\sigma}{r} \sqrt{\frac{\epsilon_0{}^2 k}{mr}} A^2$$

$$\times \left\{ EF^2(L) + \frac{\epsilon_0{}^2 L^2}{8} B \left[F(L) \frac{d^2F}{dL^2} - \left(\frac{dF}{dL} \right)^2 \right] \right\} \exp\left(- \frac{2\epsilon^2}{\epsilon_0{}^2} \right)$$

$$- \left[CF^2(L) + \left(D\delta L + G \frac{\epsilon_0 L}{2} \right) \frac{dF^2}{dL} \right.$$

$$+ \frac{1}{2} \left(H\delta L^2 + J\delta L \frac{\epsilon_0 L_0}{2} + K \frac{\epsilon_0{}^2 L_0{}^2}{4} \right) \frac{d^2F^2}{dL^2}$$

$$\left. + \frac{1}{2} \left(M\delta L^2 + N\delta L \frac{\epsilon_0 L_0}{2} + P \frac{\epsilon_0{}^2 L_0{}^2}{4} \right) \left(\frac{dF}{dL} \right)^2 \right] \exp\left(- \frac{\epsilon^2}{\epsilon_0{}^2} \right) \quad (13)$$

where $\delta L = L - L_0$; $L_0 = \sqrt{mkr}$ is the angular momentum of the circular orbit at radius r; E and B are constants; and C, D, G, N, J, K, M, N, and P are polynomials in ϵ/ϵ_0 with coefficients of order unity. The expressions $\epsilon_0{}^2 mk$ and $\sqrt{\epsilon_0{}^2 k/mr}$ can be thought of as effective available relative momentum space and mean relative velocity, respectively. To find

$$\frac{dh}{dt} = \iiint \frac{df}{dt} \, dr d\theta dp = \iiint I(f_0, f_0) \, dr d\theta dp \quad (14)$$

we transform (r, p) to (ϵ^2, χ) where χ is the orientation of the major axis of the ellipse through the point (r, θ, p, L) in phase space:

$$r = \frac{L^2}{mk} [1 + \epsilon \cos(\theta - \chi)]^{-1}$$

$$p = \frac{mk}{L} \epsilon \sin(\theta - \chi) \quad (15)$$

The Jacobian is

$$\frac{\partial(r, p)}{\partial(\epsilon^2, \chi)} = -\frac{L}{2}\,[1 + \epsilon\cos(\theta - \chi)]^{-2}$$

so

$$\frac{dh}{dt} = 2\pi\frac{L}{2}\int \frac{d\epsilon^2 d\theta}{(1 + \epsilon\cos\theta)^2}\,\frac{df}{dt}$$

$$= -2\pi{\epsilon_0}^2 mk\sigma\sqrt{\frac{{\epsilon_0}^2 k}{mr_0}}\,\frac{L}{2}\,A^2{\epsilon_0}^2$$

$$\times\left\{aF^2(L) + \frac{\epsilon_0 L}{2}\,b\,\frac{dF^2}{dL} + \frac{{\epsilon_0}^2 L^2}{8}\left[c\,\frac{d^2F^2}{dL^2} + d\left(\frac{dF}{dL}\right)^2\right]\right\} \tag{16}$$

where a, b, c, and d are polynomials in ϵ_0. Because the total number of particles and the total angular momentum are conserved, we have

$$\int\frac{dh}{dt}\,dL = 0 \qquad \int L\frac{d}{dt}h(L)\,dL = 0 \tag{17}$$

with the result that

$$a = b = 0 \tag{18}$$

therefore

$$\frac{dh}{dt} = -\pi{\epsilon_0}^2 m^2 k^2 \sigma\epsilon_0 k\,\frac{{\epsilon_0}^4}{8}\,c\,\frac{d^2}{dL^2}A^2F^2 \tag{19}$$

It can be shown that $c > 0$. Using equation (6), we find that

$$\frac{dh}{dt} = -\frac{{\epsilon_0}^3 m^2 k^3 \sigma}{32\pi^3}\,c\,\frac{d^2}{dL^2}\left(\frac{h^2}{L^2}\right) \tag{20}$$

CONCLUSION AND INTERPRETATION

Equation (20) looks something like a diffusion equation with a negative diffusion coefficient. Thus $h(L)$ grows at maxima of $L^{-2}h^2(L)$ and decreases where $L^{-2}h^2(L)$ is at a minimum as shown in figure 3(a). Note that this

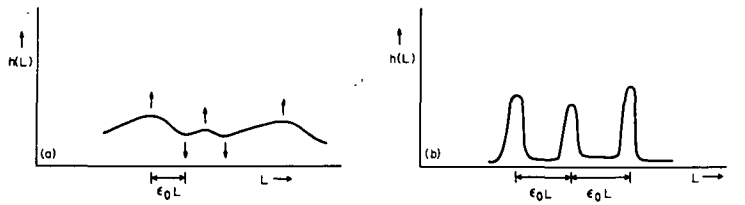

Figure 3.–(*a*) Initial smooth distribution function with local maxima separated by approximately $\epsilon_0 L$. (*b*) A distribution function in which most of the particles are in groups, separated in angular momentum by about $\epsilon_0 L$.

equation will never allow $h(L)$ to become negative. The fastest growth is experienced by the narrowest peaks. These fine scale peaks eventually dominate the distribution function, and the particles concentrate at the angular momenta where the narrowest peaks were originally, as in figure 3(*b*). We initially used a distribution function that was smooth on a scale length $\epsilon_0 L$ (i.e., initial peaks in $F(L)$ and, consequently, in $h(L)$ and $h^2(L)$ were separated in angular momentum by distances $\epsilon_0 L$). Because ϵ_0 is small compared to unity, L is slowly varying by comparison and peaks in $L^{-2}h^2(L)$ are separated by $\epsilon_0 L$. Thus grains concentrate in orbits separated in angular momentum by $\epsilon_0 L$; these jetstreams must be circular because of the initial axisymmetry of our distribution. As the grains lose energy because of inelastic collisions, the orbits themselves become more circular.

A finer grain distribution function would have finer scale peaks, but our result would not necessarily apply in that case because the calculation depended critically on the Taylor expansion of the original distribution. The fine scale peaks might evolve into distinct subjetstreams, or they might merge into a single jetstream.

Now consider what effect this has on the radial density distribution. Because the radius of a circular orbit is related to its angular momentum by

$$r = \frac{L^2}{mk} \tag{21}$$

then the radial separation is given by

$$\frac{\delta r}{r} = 2\frac{\delta L}{L} = 2\epsilon_0 \tag{22}$$

(In our solar system $\delta r/r$ is roughly 0.4 to 0.6 corresponding to $\epsilon_0 \cong 0.25 \pm 0.05$ (Jeans, 1944).)

There are many other properties that may influence the collisional evolution of an orbiting cloud of grains. Although we have neglected size, shape, and

mass differences among grains, effects of rotational degrees of freedom, self-gravitation, actual accretion, or even shattering of particles, our calculation indicates that the inelasticity tends to cause jetstreams.

ACKNOWLEDGMENTS

We wish to thank H. Alfvén for his suggestions and encouragement.

This work was supported in part by the United States Atomic Energy Commission, contract no. AT(04-3)-34 PA 85-13.

REFERENCES

Alfvén, H. 1970, Jet Streams in Space. Astrophys. Space Sci. 6, 161.

Jeans, J. H. 1944, The Universe Around Us, pp. 237-238. Fourth ed., Cambridge Univ. Press. London.

COLLISIONAL FOCUSING OF PARTICLES IN SPACE CAUSING JETSTREAMS

JAN TRULSEN
University of Tromsø

Jetstreams probably played an important role at an intermediate stage of the formation of the solar system (Alfvén and Arrhenius, 1970). A jetstream is defined here as a collection of grains moving in neighboring elliptical orbits around a central gravitating body and with the dynamics modified by the action of complicated collision processes among the grains themselves.

Three main types of collisions will take place in such a stream. Hypervelocity impacts will lead to fragmentation of the grains involved. At lower impact velocities, the particles will retain their identities after the collision even if they might be deformed to some degree depending on impact velocity and internal structure of the grains. With still lower impact velocity, accretion can take place, the grains sticking together after collision to form larger grains. A common feature of these collision processes are that they will be partially inelastic. A certain fraction of the kinetic energy of the colliding particles will be spent on changing their internal structure. The internal kinetic energy in an isolated jetstream thus will tend to decrease with time. The mass spectrum of the grains also will vary during the lifetime of a stream, the probability for accretive processes increasing with time.

Qualitative arguments for the collisional focusing effect leading to the formation of streams have been given by Alfvén. The most important points in his argument are

(1) Two orbits after a collision will be more similar than before because of the loss of kinetic energy.
(2) Because of the central force field, a particle having collided with a stream is not easily lost from the stream. It will always return to the place where it last collided, thus making it subject to new collisions with particles in the stream.

As a first step toward a quantitative theory, the idealized situation of a jetstream of identical spherical grains will be studied. Collisions leading to fragmentation and accretion will be neglected together with the self-gravitational effect of the stream. The distribution of grains in the stream will be described by a distribution function $f(\mathbf{r}, \mathbf{v}, t)$ in the six-dimensional phase

space. The first problem is to construct a kinetic equation describing the evolution of this distribution function due to the motion in the central gravitational field and to the mutual collisions.

The equations of motion of a single particle in a central gravitational force field are

$$\dot{\mathbf{r}} = \mathbf{v} \qquad \dot{\mathbf{v}} = -\frac{\mathbf{r}}{r^3} \tag{1}$$

The orbits for bound particles are ellipses with the central body at one of the focal points. Time and length units have been chosen such that the orbital period in an ellipse with a semimajor axis equal to unity is 2π time units.

The rate of change of the distribution function due to the motion in the gravitational field is

$$\left(\frac{\partial f}{\partial t}\right)_{\text{motion}} = -\mathbf{v} \cdot \frac{\partial f}{\partial \mathbf{r}} + \frac{\mathbf{r}}{r^3} \cdot \frac{\partial f}{\partial \mathbf{v}} \equiv \Lambda f \tag{2}$$

If the effect of collisions is described by a nonlinear operator C,

$$\left(\frac{\partial f}{\partial t}\right)_{\text{coll}} = C[f, f] \tag{3}$$

the complete kinetic equation takes the form

$$\frac{\partial f}{\partial t} = \left(\frac{\partial f}{\partial t}\right)_{\text{motion}} + \left(\frac{\partial f}{\partial t}\right)_{\text{coll}} = \Lambda f + C[f, f] \tag{4}$$

Already Boltzmann gave the form of the collision operator for the case of number-conserving elastic collisions (Chapman and Cowling, 1960). Because we are interested in partially inelastic collisions, a somewhat modified expression is needed.

DERIVATION OF COLLISION OPERATOR

The details of a collision process are described in figure 1. A collision takes place as soon as the distance between the centers of two particles is equal to their diameter D. The direction between the centers at impact is given by the impact vector $\mathbf{k}$ which is a unit vector. Particles 1 and 2 have velocities $\mathbf{v}_{1b}$ and $\mathbf{v}_{2b}$ before the collision. Afterward, the corresponding velocities are $\mathbf{v}_{1a}$ and $\mathbf{v}_{2a}$.

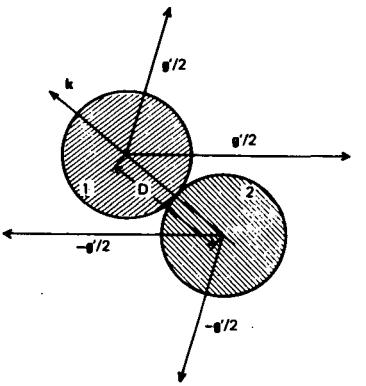

Figure 1.—Details of a collision event. k is impact vector, g and g′ are relative velocities before and after the impact, respectively.

Conservation of momentum requires that

$$v_{1b} + v_{2b} = v_{1a} + v_{2a} \tag{5}$$

Kinetic energy is not conserved. To simplify the problem, we do not care what happens to this lost energy by simply prescribing the amount lost in a given collision by the relation

$$v_{1b}^2 + v_{2b}^2 + \tfrac{1}{2}[(\beta - 1)^2 - 1]\,[(v_{1b} - v_{2b}) \cdot \mathbf{k}]^2 = v_{1a}^2 + v_{2a}^2 \tag{6}$$

Here β is a restitution parameter describing varying degrees of inelasticity. It is allowed to take any value in the range (1, 2). The upper limit, $\beta = 2$, corresponds to elastic collisions. For the lower limit, $\beta = 1$, a head-on collision will be completely inelastic. The amount of energy lost decreases as the collision takes place more and more off axis, and in the limit of a grazing collision there is no energy loss.

Proceeding in a manner similar to the derivation of the classical Boltzmann operator, the following form of the collision operator can be derived from equations (5) and (6):

$$C[f, f] = D^2 \int d\mathbf{v}' \int (\mathbf{v}' - \mathbf{v}) \cdot \mathbf{k} \left[\frac{f(\bar{\mathbf{v}}) \cdot f(\bar{\mathbf{v}}')}{(\beta - 1)^2} - f(\mathbf{v}) \cdot f(\mathbf{v}') \right] d\mathbf{k} \tag{7}$$

$$(\mathbf{v}' - \mathbf{v}) \cdot \mathbf{k} > 0$$

Here the explicit $\mathbf{r}$ and t dependence of the distribution function was suppressed and

$$\bar{\mathbf{v}} = \mathbf{v} + \tfrac{1}{2}\frac{\beta}{\beta - 1}(\mathbf{v}' - \mathbf{v}) \cdot \mathbf{kk}$$
$$\bar{\mathbf{v}}' = \mathbf{v}' - \tfrac{1}{2}\frac{\beta}{\beta - 1}(\mathbf{v}' - \mathbf{v}) \cdot \mathbf{kk} \tag{8}$$

The operator (eq. (7)) reduces to the Boltzmann operator for the case $\beta = 2$. The apparent singularity of equation (7) as the extreme case $\beta = 1$ is approached is not real. For the product $f(\bar{\mathbf{v}})f(\bar{\mathbf{v}}')$ to be nonvanishing, both $\bar{\mathbf{v}}$ and $\bar{\mathbf{v}}'$ must lie inside the support of f in velocity space. This requires the quantity $(\mathbf{v}' - \mathbf{v}) \cdot \mathbf{k}$ to be of order $\beta - 1$. Thus we get one factor $\beta - 1$ from the volume element in velocity space and one from the factor $(\mathbf{v}' - \mathbf{v}) \cdot \mathbf{k}$ already present in the integrand, making the operator (eq. (7)) tend toward a finite limit as $\beta \to 1$.

Entropy arguments through Boltzmann's H theorem play an important role in the discussion of the classical Boltzmann equation. With elastic collisions, the entropy source function is always positive except for local thermodynamic equilibrium (LTE) distributions where it vanishes. For the motion in a central gravitational force field with a nonvanishing total angular momentum, however, it is not possible to construct a time-independent, physically relevant state from LTE distributions. For a physically relevant situation, the average flow velocity should increase with decreasing distance from the central body if all the grains are moving in the prograde direction. If, on the other hand, an LTE distribution function is substituted into the time-independent kinetic equation, the only allowed average velocity goes as $\mathbf{U} = \mathbf{r} \times \boldsymbol{\omega}$ where $\boldsymbol{\omega}$ is a constant vector; that is, a fixed body rotation with a velocity increasing with increasing distance from the center (Chapman and Cowling, 1960). This result does not imply, however, that the system would not evolve asymptotically toward a time-independent final state. An additional possibility is that the collisions tend to make themselves less important by making the individual orbits more and more parallel, the whole system evolving toward a Saturnian ring configuration.

For the case of inelastic collisions, we no longer have a description of a closed system. We do not have a description of what happens to the lost kinetic energy. No extension of the H theorem has been given for this case. In a way, the kinetic energy function plays the role of Boltzmann's H function, giving the allowed direction of evolution of the system. Again, the only time-independent state of the system is the singular state consisting of parallel individual orbits only.

THE INITIAL RATE OF CHANGE PROBLEM

The most usual way of extracting information about a system by linearizing the equations of motion around a time-independent equilibrium state is hardly

of interest here for two reasons. We have already seen that this state is rather singular. Further, accretion would probably play a crucial role long before this state is approached. A complete analytic study of the dynamics seems out of the question at the present time. A more modest undertaking is to study an initial rate of change problem. How will the system start to change from a prescribed initial state $F(\mathbf{r}, \mathbf{v})$?

The crucial point now is to choose initial states that make it possible to extract interesting properties of the system. Because we are interested in the influence of collisions on the dynamics, $F(\mathbf{r}, \mathbf{v})$ should be chosen to be a time-independent solution of the collisionless kinetic equation; that is, F should satisfy $\Lambda F = 0$. Any function depending on $\mathbf{r}$ and $\mathbf{v}$ through only time-independent constants of motion for a central gravitational force field satisfies this requirement. Such constants are (Danby, 1962)

$$a = \frac{r}{2 - rv^2}$$

$$\mathbf{L} = \mathbf{r} \times \mathbf{v} \tag{9}$$

$$\mathbf{P} = -(\mathbf{r} \times \mathbf{v}) \times \mathbf{v} - \frac{\mathbf{r}}{r}$$

being the semimajor axis, the angular momentum vector, and the perihelion vector, respectively. Only five of these constants are independent because the following two relations exist between them:

$$\mathbf{P} \cdot \mathbf{L} = 0 \qquad \mathbf{L}^2 = a(1 - \mathbf{P}^2) \tag{10}$$

The collisions give rise to an additional mass flux in the stream. If $\delta f(\mathbf{r}, \mathbf{v}, t)$ designates the deviation of the distribution function from the initial distribution, this flux is given by

$$\delta(n, \mathbf{U}) = \int \mathbf{v} \delta f(\mathbf{r}, \mathbf{v}, t)\, d\mathbf{v} \tag{11}$$

which can be shown to equal

$$\delta(n, \mathbf{U}) = -\tfrac{1}{2}t^2 \frac{\partial}{\partial \mathbf{r}} \cdot \Phi + O(t^3) \tag{12}$$

where

$$\Phi = \int \mathbf{v}\mathbf{v}\, C[F, F]\, d\mathbf{v}$$

$$= \frac{\beta}{48} \pi D^2 \int g[\beta g^2 \mathbf{1} + 3(\beta - 4)\mathbf{g}\mathbf{g}] f(\mathbf{v}) f(\mathbf{v}')\, d\mathbf{v}\, d\mathbf{v}' \tag{13}$$

with $\mathbf{g} = \mathbf{v}' - \mathbf{v}$.

NUMERICAL RESULTS AND DISCUSSION

For the special case of an azimuthally symmetric stream, the six-dimensional velocity integration in equation (13) was evaluated numerically. For this case, F does depend only on a, $\mathbf{P}^2$, and L_z; and it is enough to study the situation in one cross section of the stream. Instead of a, $\mathbf{P}^2$, and L_z, the distribution function could also be expressed in terms of a, $e^2 = \mathbf{P}^2$, and $\cos i$, where i is inclination and e eccentricity.

The results for a series of distribution functions of the type

$$F(a, e^2, \cos i) \propto (a_2 - a)(a - a_1)(e_0{}^2 - e^2)(\cos^2 i - \cos^2 i_0)$$

for $a_1 < a < a_2$, $e < e_0$, and $i < i_0$ are presented below. The values for the parameters a_1, a_2, e_0, and i_0 were chosen to be

$$a_1 = 0.8 \qquad a_2 = 1.2$$

and

Case I:	$e_0 = 0.35$	$i_0 = 7°$
Case II:	$e_0 = 0.35$	$i_0 = 13°$
Case III:	$e_0 = 0.20$	$i_0 = 13°$
Case IV:	$e_0 = 0.10$	$i_0 = 13°$

The distribution functions were normalized such that the number of particles in the stream are the same for each case.

In figure 2 the density profile corresponding to case I along a radius in the equatorial plane of the stream is plotted. The shape of the profile is the same for the other cases except that it gets narrower with decreasing value of the maximum eccentricity e_0.

The kinetic pressure tensor takes a diagonal form in a spherical coordinate system. In figure 3, the three pressure components over density are plotted. The pressure in the azimuthal direction $P_{\phi\phi}$ is less than the two transverse pressure components. This is a general result, valid for all distribution functions that have been studied. By varying the maximal eccentricity and inclination, the ratio of the two transverse pressure components can be varied.

A general property of the collisions is to try to make the pressure tensor more isotropic. This gives rise to a most unusual property of the jetstream configuration that can be seen in figure 4. Here the mass flux vector $\delta(n, \mathbf{U})$ is plotted for two points in a cross section of the stream, at $r = 0.9$ and $r = 1.1$ and at the same distance above the equatorial plane, represented by the broken line. The flux vector is plotted for three different values of the restitution parameter β: $\beta = 2$, which is the elastic case; $\beta = 1$, which is the opposite extreme; and $\beta = 1.5$, the intermediate value. The x's indicate the density maximum in the stream.

Consider the extreme cases I and IV, the former characterized by an excess pressure in the radial direction, the latter by an excess pressure in the polar

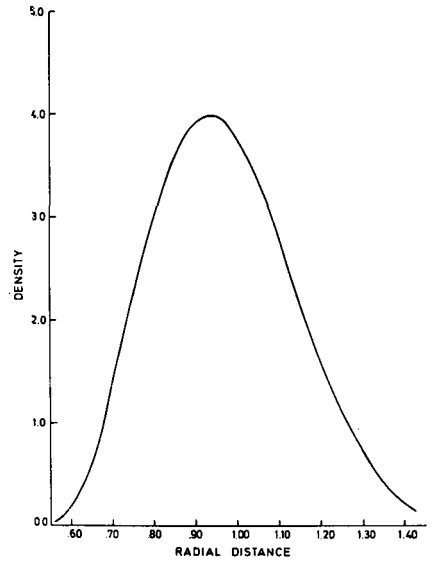

Figure 2.–Particle density in the stream along a radius vector in the symmetry plane of the stream, case I; arbitrary units.

direction. Common physical experience tells that if a system wants to eliminate excess pressure, it has to expand in some way. This is a statement of the Boyle-Marriotte ideal gas law. The jetstream behaves in the opposite manner. It eliminates excess pressure by contracting.

This can be understood from a consideration of the individual orbits in the stream. The central force field has the property of twisting these orbits very effectively. A particle that is on the bottom of the stream at one side will be on the top on the other side. A particle in a high-eccentricity orbit that is on the inner side of the stream at one time will be on the outer side half a period later. The pressure component in the polar direction is generated mainly by the orbits having the highest inclination. If the stream expands in this direction, this means that the distribution of inclinations must get wider. This again implies that the polar pressure increases. Thus for case I, to take care of the deficit in the polar pressure, the stream expands in this direction, contracting in the radial direction. Case IV represents the opposite case. Here the stream expands in the radial direction while contracting in the polar direction to eliminate excess pressure in the polar direction. Note that whereas an expansion or contraction in the polar direction is mainly an effect in inclination alone, the similar process in the radial direction is a more complicated phenomenon depending on the distribution of both eccentricity and the semimajor axis.

The effect of inelasticity always is to make the stream approach a more narrow configuration relative to the corresponding elastic case. This is in

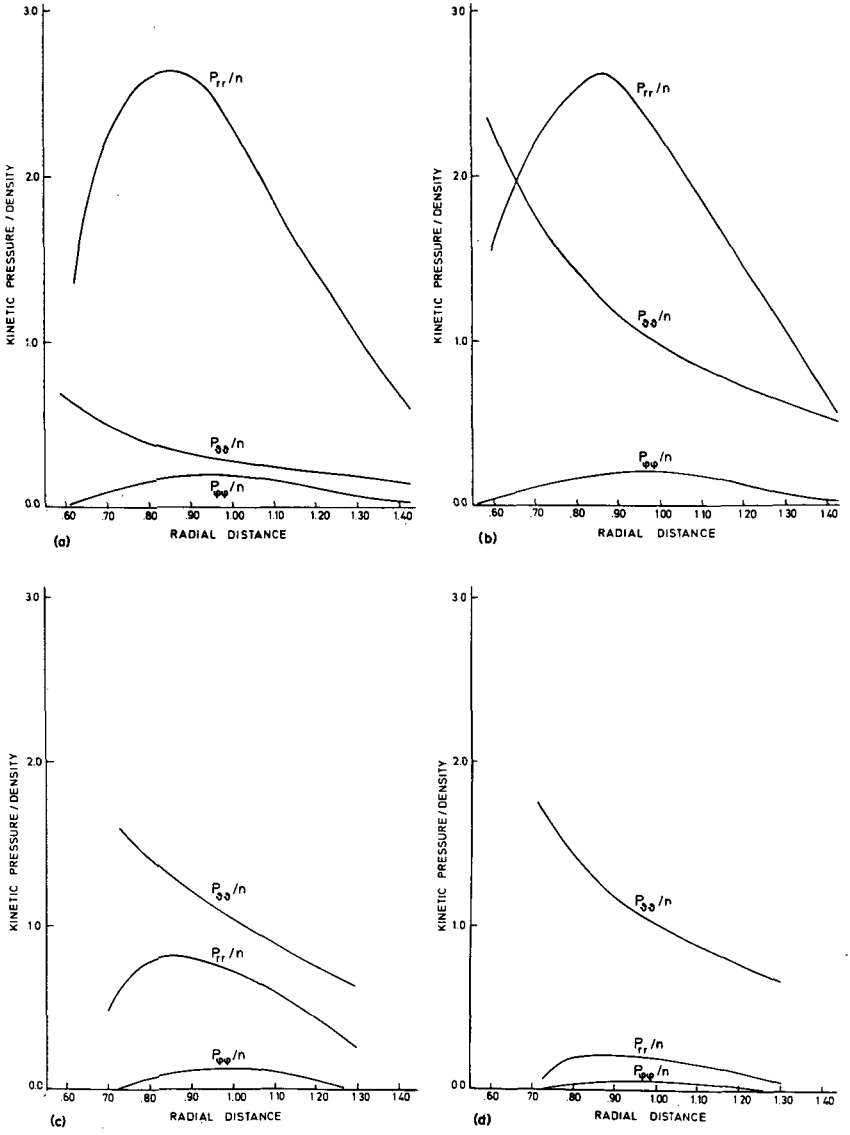

Figure 3.–Ratio of the three pressure components over density along a radius vector in the symmetry plane of the stream. (*a*) Case I. (*b*) Case II. (*c*) Case III. (*d*) Case IV. The same arbitrary units are used for all cases.

accordance with qualitative arguments. The degree of inelasticity, however, will have a varying degree of importance depending on details of the distribution function. For certain situations this parameter will determine whether the stream will expand or contract. Case II is such an example.

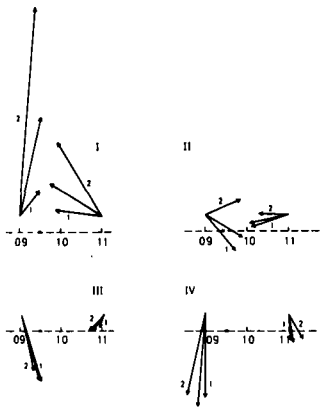

Figure 4.–Collision-induced mass flux at two points in a cross section of the stream for the four different cases studied. The broken line indicates the symmetry plane; the x's indicate the density maximum in the stream. The flux vectors are drawn for the three values 1.0, 1.5, and 2.0 of the restitution parameter β. The vectors belonging to the two extreme cases are indicated by 1 and 2, respectively.

To estimate the time interval for which this type of analysis is valid, the ratio of the average mean free time between collisions to the average orbital period for the particles in the stream must be evaluated. This ratio is not a simple relation between particle diameter, mass, and volume of the stream, for instance. To a large degree it depends on the details of the distribution function. It is clear that this ratio increases rapidly as the particle diameter increases if the mass in the stream and the form of the distribution function are kept constant. According to the arguments presented above, this ratio will also increase with time, reducing the importance of collisions.

Results from an initial rate of change study should be interpreted with care because transient effects from a specific choice of initial state could easily mask important properties of the system. For our case, the above pattern was repeated for all distribution functions studied. Numerous questions, however, were not treated. Can instabilities develop in the stream? Is there a preferred profile the stream will try to reach? To what degree will the final state depend on initial state and on the degree of inelasticity? Answers to several of these and similar questions will hopefully be obtained from numerical simulations of jetstreams in the near future.

REFERENCES

Alfvén, H., and Arrhenius, G. 1970, Origin and Evolution of the Solar System, I. Astrophys. Space Sci. 8, 338.

Chapman, S., and Cowling, T. G. 1960, The Mathematical Theory of Non-Uniform Gases. Cambridge Univ. Press. London.

Danby, J. M. A. 1962, Fundamentals of Celestial Mechanics. Macmillan Co. New York.

Page intentionally left blank

A STUDY OF ASTEROID FAMILIES AND STREAMS BY COMPUTER TECHNIQUES

B. A. LINDBLAD
Lund Observatory
and
R. B. SOUTHWORTH
Smithsonian Astrophysical Observatory

A study of asteroid orbits is made to determine if there exist groupings of similar orbits in the asteroid population. A computer program based on Southworth's D *criterion for similarity in meteor orbits is used. The program successfully sorted out the asteroid families listed by Hirayama, Brouwer, and van Houten et al. A number of new families were detected, several of which appear to be more significant than the minor Brouwer families. Asteroidal streams (jet-streams) are studied and a list of such streams is presented.*

It is well known that the distribution of orbital elements among the minor planets is nonrandom. The frequency distribution of the semimajor axis a exhibits gaps corresponding to commensurabilities with Jupiter. Hirayama (1918, 1928) has shown the existence of families; i.e., groups of asteroids with almost equal values of the orbital elements a, e, and i. Brouwer (1951), who restudied this problem using the proper elements, has added several new families. Arnold (1969) introduced computer methods in the classification of families and found additional families among the numbered asteroids. Alfvén (1969, 1970) has drawn attention to the fact that within the Flora family there exist groups of orbits that exhibit similarity also in the orbital elements ω and Ω.

The orbital elements of about 1700 numbered minor planets are published in the standard asteroid *Ephemeris* (1970). Orbital elements of some further 2000 minor planets from the Palomar-Leiden survey (PLS) have recently been reported by van Houten et al. (1970). In the PLS material, van Houten et al. have verified a number of the Hirayama and Brouwer families. Four new families were discovered.

The PLS considerably increased the number of orbits available for study, and a comprehensive search in the data will probably reveal additional families and streams. The purpose of the present paper is to make such a search with the use of computer techniques.

STREAM DETECTION PROGRAM

D Criterion

The problem of classification based on orbital similarity is well known in meteor astronomy, where the study of meteor streams has necessitated the use of sophisticated computer techniques for the detection and classification of streams. The basis for our stream detection program is Southworth and Hawkins' (1963) criteria for orbital similarity, which for low-inclination orbits may be written

$$D(M, N)^2 = (e_N - e_M)^2 + (q_N - q_M)^2 + \left(2 \sin \frac{i_N - i_M}{2}\right)^2 + \sin i_M \sin i_N$$

$$\times \left(2 \sin \frac{\Omega_N - \Omega_M}{2}\right)^2 + \left(\frac{e_M + e_N}{2}\ 2 \sin \frac{\Omega_N + \omega_N - \Omega_M - \omega_M}{2}\right)^2$$

where M and N represent two orbits to be compared and a, e, i, ω, and Ω are the customary notations for the orbital elements. The stream detection program computes $D(M, N)$ for all possible pairs in the sample under study. If $D(M, N)$ is below a certain stipulated value D_s, the program considers these two orbits as forming a stream. In the continued comparison process, more and more orbits are grouped into the stream. The program finally lists the meteor streams and their members, their mean orbit, and the deviation of each stream member from the mean stream orbit. An extensive survey of photographic meteor orbits using this stream detection program has been made by Lindblad (1971).

The Southworth D criterion is an objective method of classification on the basis of the orbital elements; i.e., it selects concentrations in five-dimensional (q, e, i, ω, Ω) space. The reason for using the perihelion distance q instead of the semimajor axis a is that the perihelion distance q for meteor orbits is better defined than a. In adapting the method to asteroid orbits, we did not consider it necessary to modify the original program. The main problem encountered in our study was how to determine the appropriate rejection level D_s.

Data Sample and Data Preparation

Present and proper orbital elements for 1697 numbered asteroids and for 1232 PLS asteroids were available on cards. The 1697 numbered asteroids have well-defined orbits, and the entire data sample was used in our study. Of the PLS orbits, 28 were excluded because they are already included in the 1697 numbered asteroid sample. In the PLS, the investigators assigned each individual orbit a quality class. The 977 orbits of highest quality (type 1) were used by van Houten et al. in their study of asteroid families. The same data

sample is used by us in the family searches described below. In our stream searches, a slightly larger data sample was desirable and orbits of types 2 and 3 were also included. The number of PLS orbits studied for streams was 1232.

DISTRIBUTION OF ORBITAL ELEMENTS

A comparison of the 1697 numbered asteroid orbits and the 1232 PLS orbits of types 1 through 3, using the present-day elements, showed that the distribution functions of orbital elements differ in the two data samples.

The distribution of inclination i is markedly different in the two populations, with an almost complete cutoff in the PLS data at about 20°. This is to be expected because the PLS was limited to the immediate neighborhood of the ecliptic. It follows that high-inclination families, as a rule, will not be detected in the PLS.

Figure 1 depicts the distribution of the longitude of the node in the two data samples. The numbered asteroid sample shows an almost random distribution of Ω, whereas asteroids of the PLS exhibit strong maxima at nodal values near 20° and 200°. Hence, asteroid streams with mean nodal values near

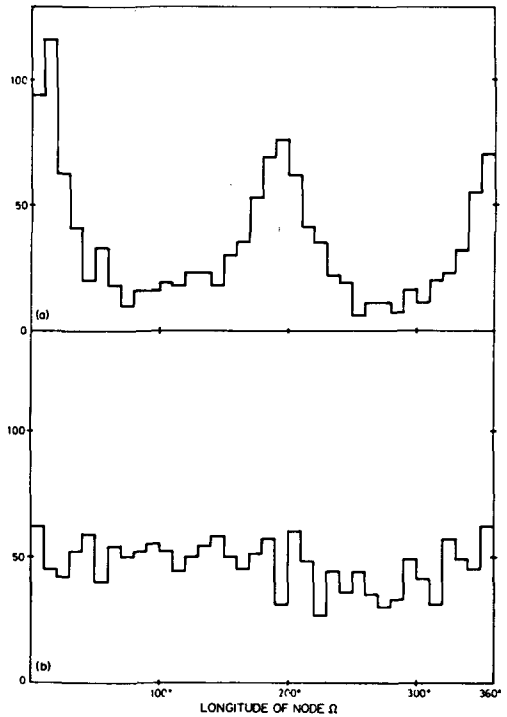

Figure 1.–Distribution of the longitude of the node. (*a*) PLS asteroids; N = 1232. (*b*) Numbered asteroids; N = 1697.

110° and 290° may be difficult to detect in the PLS material. In practice this may not be a serious restriction, however, because the asteroidal streams detected by us show a fairly large scatter in Ω.

FAMILIES AMONG NUMBERED ASTEROIDS

Rejection Level D_S

The degree of orbital similarity within the asteroid population is far higher than in the meteor population, and no direct inference from the meteor studies can be made as to the correct numerical value of D_S to use in a family search. In addition, the mathematical definition of D_S is different because only three orbital elements are involved. A trial and error method was therefore adopted. The mean $D(M, N)$ was first computed for the Brouwer families 1, 2, and 3. The mean $D(M, N)$ was found to be 0.045, 0.026, and 0.017, respectively, if only the proper elements a, e', and i' are considered. A D_S value between 0.015 and 0.030 thus appears reasonable. Numerically this D_S value is about one-tenth of that encountered in meteor studies.

For the family searches in the asteroid population, the deck of proper elements was used and constant values of ω' and Ω' were introduced on the cards. The numbered asteroid sample was searched for families at four different rejection levels, $D_S = 0.015, 0.018, 0.020$, and 0.025. The purpose of the study was to investigate at which D_S value the best possible agreement with Brouwer's original family classification was obtained. In the comparison, interest was focused mainly on families 1 through 9.

It was found that the search at $D_S = 0.020$ gave the best agreement with Brouwer, and this D_S value was therefore adopted as the rejection level. The search at $D_S = 0.020$ accepted 48 of the 53 members listed by Brouwer as family 1, considered four as belonging to a satellite family and one as a nonfamily member. In families 2 and 3 the search accepted 57 out of 58 and 33 out of 33 members, respectively.

Previously Known Families

The computer search at $D_S = 0.020$ classified the 1697 numbered asteroids into 25 previously known (Brouwer) families and 198 new families. The total number of asteroids listed as family members was 1026. However, a very large number of the new families have only two or three members and may be considered as chance groupings in the data. If these families are rejected, we find that 652 asteroids belong to families. Thus approximately 40 percent of the numbered asteroid population are in families.

Table I details how the known Brouwer family members were classified by our search at $D_S = 0.020$. Of the 458 asteroids listed by Brouwer as belonging to families, 380 appear as family members in our search. Table I is directly compiled from the computer output without involvement of any "personal

TABLE I.—*Classification of Brouwer Family Members*

Brouwer family no.	Number of asteroids in family	Asteroids in satellite families	Total number of asteroids	Remarks	Number of asteroids (Brouwer)
1	48	4	52		53
2	57	0	57		58
3	33	0	33		33
4	7	10	17		17
5	3	5	8	High inclination	25
6	22	1	23		23
7	61 } 119	1 } 3	62 } 122		62
8	8	0	8	6 through 9 combined	9
9	28	1	29		31
10	0	0	0		0
11	2	0	2	High inclination	6
12	2	3	5		6
13	0	0	0		7
14	2	0	2		8
15	3	3	6		6
16	4	3	7	Arnold 66	8
17	2 } 5	2 } 8	4 } 13	17 and 18 combined	10
18	3	6	9		12
19	5	0	5		7
20	6	2	8	Arnold 70	8
21	3	4	7	Arnold 71	7
22	3	5	8	Arnold 72	8
23	2	0	2		5
24	5	2	7	Arnold 74	9
25	6	4	10	Arnold 75	11
26	4	0	4	Arnold 76	8
27	5	0	5	Arnold 77	8
28	0	0	0	High inclination	6
29	0	0	0	High inclination	7
Total	324	56	380		458

judgment" or "manual handling." The first column gives the family number according to Brouwer. The second column lists the number of Brouwer members in each family according to our search at $D_s = 0.020$. Members of a Brouwer family assigned by our search to a satellite family–or to other groupings–appear in column 3. Column 4 gives the total number of Brouwer family members assigned by our search to families. Any remaining Brouwer family members were rejected. The total number of Brouwer family asteroids involved in the compilation is listed in column 6.

The original Hirayama families 1 through 4 are well represented and have very nearly the same members as in Brouwer's study. The outstanding case is family 3 where all 33 members are classed the same as in Brouwer's study. In contrast, the high-inclination family 5 has suffered losses. This is not unexpected, considering that we used the same rejection level D_s for all orbits irrespective of the inclination value. In a graphical search, it would have been natural to vary the similarity criteria depending on the density of points. If we had searched the sample of high-inclination orbits separately at a less rigorous rejection level, the high-inclination Brouwer family 5 could no doubt have been retained in almost its original form.

As expected, the Flora group is the largest family detected in our search. It contained 160 members, of which 119 are listed by Brouwer and 41 are new identifications. Three of Brouwer's Flora members were assigned to other families and three were rejected. The Flora group is often subdivided, after Brouwer, into four separate families, 6 through 9. There was no clear indication of such a separation in our study. Integrity of the Flora group was investigated by making additional searches at lower D_s values (stricter rejection levels). The use of a stricter rejection level reduced the number of members in the Flora group, but it was in no case possible to disentangle the separate families 6 through 9. Our computer output lists the members within each family in order of inclination. Inspection of the list shows that at all levels of D_s the division lines separating the various Flora families are arbitrarily set at certain inclination values.

Table I shows that 16 out of 19 Brouwer families with numbers 11 through 29 are detected. With the exception of families 17 and 18, all are listed as separate families. In general, the minor families have fewer members in our study than in Brouwer's. Most of the minor families are divided into two or sometimes three subgroups. The frequent existence of subgroups indicates that many of the Brouwer families 11 through 29 are fairly loose associations of orbits. Brouwer appears to have used a more liberal rejection level in classifying these groups than in the study of families 1 through 9.

It is interesting to note that families 16, 20, and 24 were detected by van Houten et al. in the PLS. Family 24, however, was incorporated by them into the Nysa family (van Houten family 32). Arnold, in his study of the numbered asteroids, revised family 24 and introduced a new family 74. This family is essentially the Nysa family of van Houten et al. The Nysa family is thus also discernible in the numbered asteroid population.

Significance of Small Families

In a large data sample, it is to be expected that a number of small-sized families are due to chance. This problem was studied by making searches in samples of random orbits. It was found that more than 50 percent of the two- and three-member families and about 30 percent of the four-member families are spurious groupings in the data. In accordance with these results, only Brouwer families 19, 20, 24, 25, and 27 are considered as statistically significant groupings among the small families.

New Families

A number of previously unknown or poorly studied families were identified by the search at $D_S = 0.020$. The largest new family found had 21 members. There also were 15 new families with from 5 to 11 members. These families are not detailed here. The majority of them appear in a subsequent search in the total asteroidal sample (table III).

The largest new family detected in the numbered asteroid population is the Io family with 21 members. The mean $D(M, N)$ for this group is 0.023. It should be considered as a rather loose association of orbits. This family includes asteroid 85 Io, but it appears to be distinctly different from the Io family detected by van Houten et al. in the PLS.

Arnold's Family Classification

Our discussion has mainly emphasized a comparison with Brouwer's classification. Arnold's computer study will be referred to only briefly. Arnold qualitatively confirmed the major Brouwer families. Several of the minor families, however, were extensively modified in his study.

Our search at $D_S = 0.020$ listed as separate groups nearly all the Brouwer families 1 through 29. However, it is evident from table I (column 3) that some members of the Brouwer families were assigned to other families, or to altogether new groups. By way of illustration, two members of family 24 were incorporated into a new family (Fortuna) and two were rejected altogether. In the present search, the Fortuna group consisted of eight members, five of which were included in Arnold 82. Several similar groupings were studied and were identified with Arnold's new families. At the four-or-more-member level, Arnold families 66, 67, 69, 73, 76, 82, 84, 85, and 90 were discernible, whereas families 72, 86, and 87 were divided into two about-equal-sized groups. Arnold family 70 was divided by our search into several small-sized families, each of low significance.

FAMILIES AMONG THE PLS ASTEROIDS

The PLS data were searched for families by van Houten et al. (1970) using 977 orbits of type 1. The same data sample was used by us, thus allowing a direct comparison between the searches.

The numerical value of D_S is known to be a function of sample size and the precision of the orbital elements. In a family search, D_S should vary inversely as the cube root of the sample size, if the samples are otherwise similar. If $D_S = 0.020$ is accepted as the rejection level in the numbered asteroid population, a rejection level of

$$D_S = 0.020 \left(\frac{1697}{977}\right)^{1/3} = 0.024$$

would have been appropriate for the somewhat smaller PLS sample. However, the stronger concentration to the ecliptic plane suggests a lower D_S value because the density of observed orbits corresponds to a larger sample. Because of this truncation effect, we are inclined to use about the same D_S value as in the numbered asteroid sample. In order not to prejudice the choice, computer searches were made at four rejection levels, $D_S = 0.017$, 0.018, 0.019, and 0.020.

Our study showed that at the stricter rejection levels the recognized families often were split into two or three subgroups. The searches at $D_S = 0.019$ and $D_S = 0.020$ provided reasonable agreement with the classification of van Houten et al. The finally adopted rejection level was $D_S = 0.019$. This level is, perhaps, slightly on the conservative side.

Previously Known Families

Table II compares the classification of van Houten et al. with that of our search at $D_S = 0.019$. Table headings are similar to those of table I. It is seen that 214 out of 386 orbits are classified in the same manner, whereas 110 orbits are assigned to satellite families or to other groups. Inspection of families 1 through 3 suggests that the classification boundaries used by van Houten et al. are slightly wider than those of Brouwer.

The newly introduced families 30, 33, and 34 were readily identified by our search, although about half of their members were assigned to smaller satellite families. Families 4 and 12, with very few members in the PLS sample, were not found in our study at $D_S = 0.019$. Nor were they found in the search at $D_S = 0.020$. Family 33 was split into several groups, two of which were related to Brouwer 19 and 20 and a third which appeared to be related to the Io family introduced by us (table III). These results again indicate that the limits of the van Houten families in general are wider than those of the Brouwer study.

In the classification of the PLS orbits, the newly found Michela-Nysa group (van Houten families 31 and 32) presented some problems. The Michela and Nysa families represent two fairly close groupings, which our search could not disentangle. The division line between the two families appears to be one of inclination much in the same way as in the Flora group. Our investigation

TABLE II.—*Classification of Family Members in the PLS Data*

van Houten family no.	Number of asteroids in family	Asteroids in satellite families	Total number of asteroids	Remarks	Number of asteroids (van Houten)
1	40	16	56		63
2	5	10	15		23
3	28	2	30		32
4	0	0	0		0
5	0	0	0		0
6 to 9	16	19	35		36
12	0	0	0		7
16	4	2	6		10
25	0	4	4	Incorporated in 31 and 32	7
27	2	0	2		8
30	14	13	27		28
31	14 } 86	7 } 11	21 } 97	Combined with 32	26
32	72 }	4 }	76 }		77
33	8	18	26		37
34	11	15	26		32
Total	214	110	324		386

produced more members in the Michela-Nysa group than found by van Houten et al. The search at $D_S = 0.019$ listed 181 members in the combined Michela-Nysa group. Of these, 97 were included among the 103 members ascribed to the Michela-Nysa families by van Houten et al. The properties of the Michela-Nysa families deserve further detailed study.

New Families

The search at $D_S = 0.019$ produced a number of previously unknown families or groups. These have not yet been fully investigated and therefore are not detailed here. The more important families were detected in a subsequent search in the total asteroid sample (table III).

FAMILY SEARCHES IN TOTAL SAMPLE

The number of orbits available for study in the combined numbered/PLS asteroid sample was 2674. Of the PLS orbits, 22 of type 1 were excluded because they are already included in the 1697 numbered asteroid sample. The total number of orbits used in the study was 2652. As previously, proper elements were used.

Rejection Level

The appropriate rejection level to use in the family search was estimated as follows. From the relations

$$D_S = 0.020\left(\frac{1697}{2652}\right)^{1/3} = 0.017 \quad \text{and} \quad D_S = 0.019\left(\frac{977}{2652}\right)^{1/3} = 0.014$$

a rejection level slightly smaller than 0.014 or 0.017 may be estimated. Searches were made at four different levels, $D_S = 0.011$, 0.012, 0.013, and 0.014. The investigations at $D_S = 0.011$ and 0.012 separated and identified the low-inclination families but gave a far too severe rejection level for the moderate- and high-inclination groups. Family 2 Eos was split into two groups. The search at $D_S = 0.013$ gave adequate separation of the Brouwer families and this rejection level therefore was adopted. The adopted D_S value again was chosen conservatively.

Previously Known Families

The results of the search at $D_S = 0.013$ were compared with the classifications of Brouwer and van Houten. Families identified were 1 through 9, 16, 18 through 22, 25, 27, and 30 through 34. Family 24 was incorporated into the Nysa group. Families 11 through 15, 17, 23, and 26 were not detected in the total sample; i.e., at the chosen, stricter, rejection level their members were classified as nonfamily objects.

TABLE III.–*New Families*

No.	Family name	Number of members	Mean[a] $D(M, N)$	Members	Remarks[b]
35	Fortuna	6 (4)	0.010	19, 21, 138, 557, 1012, 1190 (1076, 1358, 2552, 4087)	A82
36	Pawlowia	6	.010	1007, 2058, 4641, 6584, 6653, 6700	Related to L39
37	Una	6	.010	160, 847, 1228, 2568, 4030, 4117	A86
38	Arcadia	7 (1)	.005	1020, 1352, 1726, 2088, 2598, 6059, 6554 (272)	A86, very concentrated
39	Nemesis	7 (5)	.011	125, 128, 301, 4058, 4609, 6323, 6646 (58, 380, 1135, 2740, 4863)	Part of A87
40	Merxia	7 (1)	.012	808, 1662, 2615, 4054, 4095, 4633, 4781 (4592)	.....
41	Hecuba	6	.011	108, 1107, 1209, 4214, 4529, 6575	Related to vH34
42	Mathilda	5 (3)	.012	253, 869, 1178, 1525, 1555 (505, 1277, 5578)	A84, loose association
43	Valda	7	.010	262, 518, 678, 1391, 4591, 6038, 6744	.....
44	Dora	7 (4)	.009	668, 1427, 1734, 2142, 4010, 4013, 6045 (479, 638, 2540, 4040)	.....
.....	Io	11	.013	85, 141, 390, 888, 1313, 1329, 1431, 1458, 1499, 2802, 6523	A69? Loose association, separate from vH33

[a]Computed from orbital elements a, e', and i'.

[b]A, L, and vH stand for Arnold, Lindblad, and van Houten, respectively.

New Families

Table III lists those new families that had six or more members detected by the search. The first and second columns give the numbers and names suggested for these families, the third and fourth columns give the number of members and the mean value of $D(M, N)$ at the rejection level $D_s = 0.013$. The individual members are given in column 5. Numbers above 2000 refer to the PLS asteroids. Parentheses indicate additional members obtained at the rejection level $D_s = 0.014$. Column 6 lists the family number given by Arnold (1969) to these groupings.

The new families have been named after bright asteroids occurring within their boundaries, and have been numbered 35 through 44 in continuation of the numbering of van Houten et al. It is seen that the new families have members in both data samples studied by us. Further, it should be mentioned that the new families (table III) were also detected in the separate searches in these two samples.

The mean $D(M, N)$ listed in table III is a measure of the concentration within an asteroid family, a low $D(M, N)$ value implying a high degree of concentration. For most families, $D(M, N)$ is of the order of 0.010. This value is lower than that found in our study for the majority of the Brouwer families.

In addition to the families reported in table III, a large number of minor groups were detected by the search. It is believed that a number of the new four- and five-member families are significant, but there is an increasing probability as we proceed to small-sized groups that the associations are due to chance. Subsequent studies may very well give reasons to include some of the smaller groups in an extended listing of families. It is also possible that a future study will revise upward the rejection level D_s, thus allowing more members in the families reported in table III.

ASTEROIDAL STREAMS

An asteroidal stream (jetstream) is defined as an assembly of orbits showing similarity in all five orbital elements a, e, i, ω, and Ω. For the purpose of the study of streams, the present-day elements will be used. From a geometrical point of view, the asteroidal streams are analogous to the meteor streams. Southworth and Hawkins' D criterion can thus be used without modification to search for similar orbits once the rejection level D_s is determined.

Very little information is at present available as to the size and number of streams in the asteroidal population. Alfvén (1969) found three separate streams, denoted A, B, and C, among the members of the Flora family. The statistical significance of these groupings has been discussed by Danielsson (1969). Some additional streams have been listed by Arnold (1969).

Lacking more detailed information, the investigator is faced with the problem of setting the rejection level D_s more or less arbitrarily. Test runs in the numbered asteroid population indicated that D_s values in the range 0.050

to 0.060 gave a reasonable number of streams and provided confirmation of the known streams in the Flora family. Similar results were obtained in test runs in the PLS data.

For the study in the total asteroid population, we rather conservatively have chosen $D_S = 0.044$. The search at this rejection level produced 81 streams with two members, 12 streams with three members, and 36 streams with four or more members. The number of asteroids in streams was 647 out of a total of 2929 orbits. Thus at the rejection level $D_S = 0.044$, approximately 22 percent of the asteroid population was placed in streams.

Table IV lists those streams detected in our search that had seven or more members. In nearly all cases, these streams were detected independently in searches both in the numbered asteroid population and in the PLS data. The possibility that these streams are caused mainly by selection effects peculiar to the PLS therefore appears unlikely.

Alfvén's jetstreams A and C are detected. Alfvén's stream B was discernible, but was split into two groups, one with five and one with four members. At the adopted acceptance level of table IV, these groupings were rejected. The tendency of asteroids to aline their lines of apsides with Jupiter's is well known. An interesting situation occurs in Alfvén's jetstream A, where the search at $D_S = 0.044$ split stream A into two groups of orbits having their lines of apsides oriented roughly symmetrically with respect to Jupiter's perihelion. A similar geometry exists in the Coronis and Denone streams, which also form two sets of orbits symmetrical with respect to the apsidal line of Jupiter's orbit.

The streams listed by Arnold (1969) were compared with our streams (table IV). Only three orbits were common to both searches. The reason for this poor agreement is not known. As can be seen from the definition of $D(M, N)$, the D criterion favors orbits that have their major axes alined. For low-inclination streams, this condition can be met even if there exist rather large differences in ω and Ω. It is possible that the stream search program of Arnold did not emphasize the alinement of the orbital major axis.

The statistical significance of the streams listed in table IV was investigated by making stream searches in random samples. In one search in the combined population, we found, besides numerous two- and three-member streams, four streams with four members, one stream with five members, and one with seven members. It follows that the majority of four-, five-, and six-member streams found in the real sample are significant groupings, and thus could have been included in an extended version of table IV.

The asteroidal streams represent concentrations within the recognized families of Themis, Coronis, Flora, and Nysa. The streams consist of family members that have a similar orientation of the orbital major axis. It is interesting to note that there are preferred directions of alinement. Figure 2 depicts the distribution of the longitude of perihelion π in the 647 stream orbits. Maxima in the distribution are evident at about $\pi = 50°$ and 320°. The

TABLE IV.—*Asteroidal Streams (Jetstreams)*

Preliminary stream name	Number of members	Mean[a] $D(M, N)$	Family no.	Members	Remarks
Rosa	11	0.055	1	223, 461, 621, 946, 1003, 1674, 4776, 6582, 6634, 6725, 6745	–
Janina	8	.035	1	383, 515, 1074, 1576, 1615, 1687, 2523, 4602	–
Coronis	7	.033	3	158, 243, 993, 1079, 1570, 2549, 4122	–
Denone	10	.034	3	215, 761, 1100, 1128, 1289, 1363, 1497, 1635, 2560, 4521	–
Elvira	8	.036	3	263, 277, 832, 962, 1350, 1442, 4036, 4593	–
Lacrimosa	17	.071	3	208, 321, 452, 658, 720, 975, 1029, 1223, 4545, 4626, 4661, 4893, 6044, 6546, 6555, 6632, 6636	Loose assoc.; doubtful stream
Anahita	19	.058	6, 32	270, 315, 939, 960, 1682, 1699, 2084, 2716, 4065, 4171, 4227, 4663, 6061, 6063, 6074, 6097, 6098, 6189, 7595	–
Nephele	14	.049	1	431, 468, 492, 767, 938, 1073, 1082, 1383, 1445, 2547, 2757, 4590, 4896, 6587	–
Hertha	9	.037	32	135, 1493, 2035, 2164, 4009, 4015, 4078, 6080, 9093	–
Gisela	10	.040	6, 7	244, 296, 352, 703, 1120, 1335, 1422, 1494, 4637, 6199	Alfvén A
–	7	.035	6	810, 1150, 2526, 2659, 2679, 4578, 6619	Alfvén A
Eriphyla	15	.053	3	462, 811, 1010, 1245, 1336, 1423, 1725, 2522, 2567, 2581, 6534, 6542, 6565, 7631, 7633	–
Lucretia	8	.035	7, 8	281, 915, 935, 1016, 2168, 4014, 4537, 6110	Alfvén C

[a]Computed from orbital elements a, e, i, ω, and Ω.

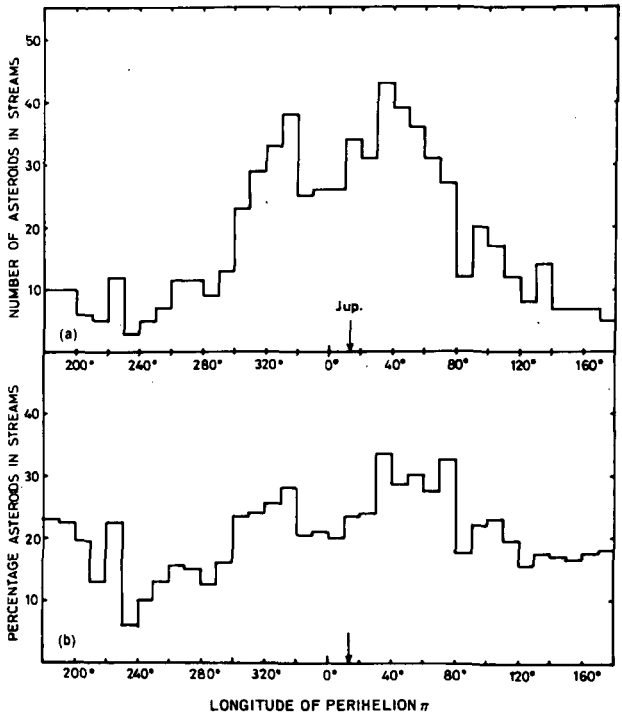

Figure 2.—Distribution of the longitude of the perihelion in 647 stream orbits. (*a*) Number. (*b*) Percentage.

overall distribution (fig. 2(*a*)) is symmetric with respect to a weighted mean longitude of perihelion $\pi = 12^{\circ}.5$, which agrees closely with the longitude of perihelion in the Jupiter orbit. It is evident that Jupiter plays a predominant role in the orbital history of most of these asteroidal streams.

ACKNOWLEDGMENTS

The authors are indebted to Dr. J. R. Arnold and Drs. van Houten for kindly placing at our disposal card decks of the present and proper elements of the numbered asteroids and PLS asteroids. One of us (Lindblad) is indebted to Professor H. Alfvén for many helpful and stimulating discussions. This work has been partly supported by grants 204-43 and 204-44 from the Swedish Natural Science Research Council and by NASA contract NSR 09-015-033.

REFERENCES

Alfvén, H. 1969, Asteroidal Jet Streams. Astrophys. Space Sci. 4, 84-102.
Alfvén, H. 1970, Jet Streams in Space. Astrophys. Space Sci. 6, 161-174.
Arnold, J. 1969, Asteroid Families and Jet Streams. Astron. J. 74, 1235-1242.

Brouwer, D. 1951, Secular Variations of the Orbital Elements of Minor Planets. Astron. J. 56, 9-32.

Danielsson, L. 1969, Statistical Arguments for Asteroidal Jet Streams. Astrophys. Space Sci. 5, 53-58.

Hirayama, K. 1918, Groups of Asteroids Probably of Common Origin. Astron. J. 31, 185-188.

Hirayama, K. 1928, Families of Asteroids. Jap. J. Astron. Geophys. 5, 137-162.

Houten, C. van, Houten-Groeneveld, I. van, Herget, P., and Gehrels, T. 1970, Palomar-Leiden Survey of Faint Minor Planets. Astron. Astrophys. Suppl. Ser. 2, 339-448.

Lindblad, B. 1971, Two Computerized Stream Searches Among Meteor Orbits. Smithson. Contrib. Astrophys. 12, in press.

Southworth, R., and Hawkins, G. 1963, Statistics of Meteor Streams. Smithson. Contrib. Astrophys. 7, 261-285.

THE PROFILE OF A JETSTREAM

*LARS DANIELSSON**
University of California, San Diego

The jetstream concept was introduced by Alfvén in 1969. Since then, the subject has been studied from various aspects by Danielsson (1969), Arnold (1969), Alfvén and Arrhenius (1970), Lindblad and Southworth,[1] and Trulsen.[2] In an attempt to define a jetstream, we may say that it is a group of objects moving in space with almost identical orbits. The largest objects in the jetstream may have any size, but the group must include a vast number of very small objects and their density must be large enough for the objects to interact. This means that collisions between the particles give rise to viscosity in the stream. Other interactions (e.g., by electromagnetic forces) are not excluded a priori.

The meteor streams, or at least some of them, seem to have a constitution that is not in conflict with this definition. As far as asteroid streams are concerned, we know nothing. However, one might assume that the observed size spectrum of asteroids can be extrapolated to smaller objects. (We, of course, do introduce a great uncertainty if we extrapolate all the way to the size of micrometeoroids.) The best assumption we can make about the distribution of the orbital elements for the subvisual objects is that it is similar to that of the visual bodies.

With these ideas as a background, Alfvén (1969) studied the classical Hirayama families among the asteroids to see whether there existed any clustering in the two orbital parameters that were not included in the analysis by Hirayama. Alfvén thus claimed to have found three streams in the Flora family, which were called Flora A, B, and C.

By essentially the same principle, Arnold (1969) searched all of the main asteroidal belt for streams. An important difference was that Arnold considered all five orbital parameters at the same time; his technique was to enclose each asteroid in turn in a five-dimensional "rectangular" box with predetermined sides and to count the number of asteroids in each box. If the number was "large," a stream was considered located.

---

*On leave from Royal Institute of Technology, Stockholm, Sweden.

[1]See p. 337.
[2]See p. 327.

Lindblad and Southworth[3] used a different and in principle better method to find streams. They employed a five-dimensional distance formula originally derived by Southworth and Hawkins (1963) to find the distances between meteor orbits. By this method they located a great number of asteroid streams; many of them, however, have very few members.

Unfortunately these three works, notably the last two, do not agree very well; i.e., they generally do not find the same streams. One may raise the question of the statistical significance of the observed streams. This is a very difficult problem. (See discussion in a later paragraph of this paper.) In an earlier investigation, it was claimed that the streams Flora A and C are statistically significant (Danielsson, 1969). The value of this work is limited, however, because it did not consider the full five-dimensional problem. The significance of Arnold's streams is impossible to determine. His method for finding groups gives, contrary to what he claims (Arnold, 1969, pp. 1235 and 1236: "probability . . . 10^{-100}"), nothing on which to base a judgment. It is likely, however, that at least the groups with many ($\geqslant 10$) members are significant. The same should be true for Lindblad's investigation. In both these works, the method used is tested on synthetic distributions of the orbital elements. The disagreement of the results also can be attributed to the difference in the methods.

SIMILARITY OF ORBITS

Two orbits are similar if their orbital elements differ little from each other or, in other words, if the distance between the points representing the orbits in the five-dimensional orbit space is short. The methods used so far are based on estimates according to this principle. A shortcoming of Arnold's method is that the parameters enter independently of each other. The formula used by Lindblad and Southworth is an empiric expression found to work well for meteor streams; i.e., by choosing a suitable value for the orbit "distance," the formula will include members of the stream and exclude nonmembers as determined by the classical technique. Because, however, the classical technique is four-dimensional, one cannot be sure that the five-dimensional formula tested in this way is appropriate. It is also well known that the individual objects of a meteor stream may be very far apart when they are far from the neighborhood of Earth. One can say that the formula is insensitive to variations of the eccentricity (whereas it is oversensitive to variations in the perihelion longitude). This may be well motivated for meteor streams because the uncertainty in the determination of the eccentricity is quite large. It seems doubtful whether this formula is the best possible for stream searches among main belt asteroid orbits.

To estimate an average distance D between two orbits one might calculate instead the actual distance between the intersections of two orbits with a

[3]See p. 337.

heliocentric meridian plane as a function of longitude $d(\lambda)$ to get the quantity

$$D^2 = \frac{1}{2\pi}\int_0^{2\pi} d^2(\lambda)\, d\lambda$$

$d(\lambda)$ is a good approximation of the shortest distance from a point on one of the orbits to the other orbit for moderate eccentricities and inclinations. If terms of the order $e^{4-q} \sin^q i$ and smaller are neglected, the result is

$$D^2 = a_1^2(1 - e_1^2) + a_2^2(1 - e_2^2) - a_1a_2(2 - e_1^2 - e_2^2)$$
$$+ \tfrac{1}{2}[e_1^2a_1^2 + e_2^2a_2^2 - 2e_1e_2a_1a_2 \cos(\lambda_{p_2} - \lambda_{p_1})]$$
$$+ \tfrac{1}{2}a_1a_2[\sin^2 i_1 + \sin^2 i_2 - 2 \sin i_1 \sin i_2 \cos(\lambda_{n_2} - \lambda_{n_1})] \quad (1)$$

where λ_p and λ_n are the longitudes of perihelion and ascending node, respectively. The terms are arranged so as to emphasize their geometrical interpretation. The advantages with this formula over the one Lindblad uses are mainly that it gives an average value of the distance between two orbits and that this distance is expressed in normal length units, AU. Admittedly, the averaging can be done in different ways. The method used here is probably the easiest.

THE FLORA STREAMS

The Flora A, B, and C streams now can be redefined according to formula (1). Let us specify that all objects in Flora A with mutual distances less than 0.15 AU according to equation (1) be retained and let us in addition include all other asteroids that fulfill the same requirements. Present elements are used throughout. Four objects will then be added and six excluded to make Flora A contain asteroids 244, 703, 827, 836, 1037, 1120, 1335, 1422, 1494, and 1536. A mean orbit of these 10 orbits is defined by the mean values of each orbital element; the average distance to this mean orbit is less than 0.1 AU for all the members. It might seem that the average distance 0.1 AU is quite large, but it must be remembered that this is a distance in a five-dimensional space and that the probability of finding some neighboring orbit within this distance of a random orbit depends on the five-dimensional density n_5 of the asteroids:

$$P(D_{1,2} \leqslant d) = 1 - e^{-n_5 d^5}$$

With the present definition, all three Flora streams appear as clusters of orbits with 10, 9, and 10 members, respectively. So far nothing is known about the statistical significance of these clusters.

The quantity $n_5 d^5$ is best estimated through experiment; it is found to be 1.0 for $d = 0.10$ AU in the inner region of the main belt.

GEOMETRICAL PROPERTIES OF SOME ASTEROID STREAMS

We are not only interested in the statistical significance of a certain pattern in the distribution of the orbital parameters but even more in the geometrical properties of a group (stream). Figures 1 and 2 show the geometrical profile of Flora A. Figure 1 shows the intersections of the individual orbits with a heliocentric meridional plane as this plane makes one cycle around the ecliptic polar axis. The four groups of curve symbols show the intersection points for the longitudes 90°, 180°, 270°, and 355°/360°. Figure 2 shows the same curves but now in relation to the intersection of the mean orbit, which is stationary at the origin of this plot.

From the phase markings in figure 1, it is concluded that the orbits remain rather well collimated through the cycle and that they seem to have two "focusing" points at 110° and 290°. Figure 2 shows that at the extremes of the orbit a stream member can be as much as 0.11 AU from the mean orbit. The average distance of a stream member from the mean orbit according to equation (1) varies between 0.046 and 0.082 AU.[4]

In studying the evolution of the asteroids, their mutual collisions are of fundamental importance. The focusing points may be of particular interest because the probability for collisions is largest in these regions. At the longitude 290°, for example, seven members of Flora A intersect the plane within an area $\Delta r \times \Delta z = 0.070 \times 0.035$ (AU)^2, where r is the distance from

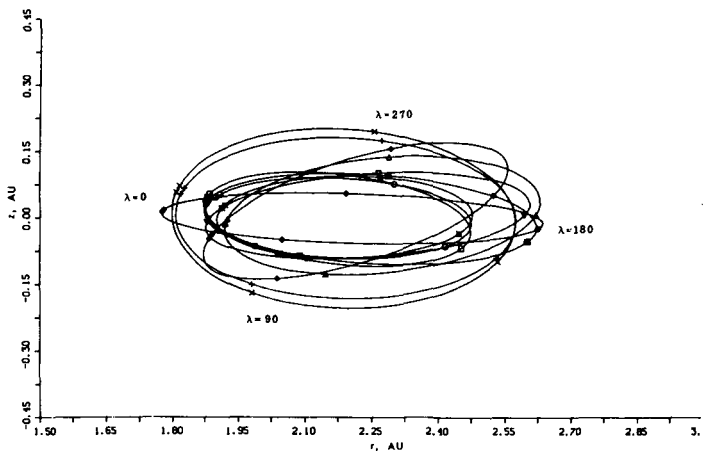

Figure 1.–Intersections of the 10 individual orbits of Flora A with a heliocentric meridional plane as this plane makes one cycle around the ecliptic polar axis. A curve symbol for each asteroid is plotted for λ = 90°, 180°, 270°, and 355°/360°.

[4]It is not known whether it is possible to find an orbit with the average distance to the other orbits always smaller than 0.5 × 0.15 = 0.075 AU by means of the approximate formula used here.

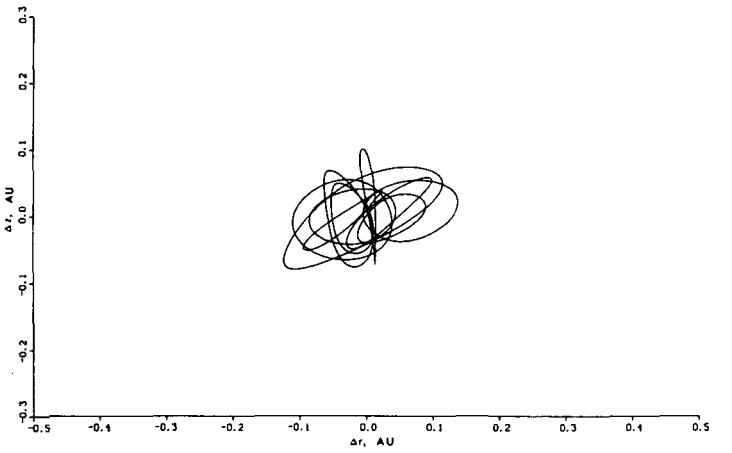

Figure 2.–Flora A orbits in relation to their mean orbit. The scale of the plot is chosen the same as in figures 3 and 4 for comparison.

the Sun and z is the distance from the ecliptic plane. It can be estimated that a random area of this size should be intersected by two or three orbits out of the total 1700; this particular area is in fact intersected by nine orbits (i.e., seven Flora A orbits and two others). Their relative velocities at the focus range from 0.2 to 1 km/s, which is 1 to 5 percent of the orbital velocities. The relative velocity between asteroids that by chance come close to each other is typically in the range 5 to 8 km/s.

Approximately the same holds for the other focusing point in Flora A and for the two focusing points in Flora C, whereas the Flora B stream is not as well focused anywhere.

This demonstrates that there are regions in space where the density of orbits is considerably larger than expected and where the relative velocities are substantially smaller than expected.

In the investigations made so far, the Flora A stream is unique because it is the only stream that can be recognized in a comparison between Arnold's and Lindblad's works. However, the three versions of Flora A do not contain exactly the same members. A comparison of the three corresponding stream profiles may then reveal something about the geometrical properties of the methods used in selecting them. Plots analogous to those in figures 1 and 2 have been prepared for these streams; namely, Arnold's stream J-1 with 32 members and Lindblad's stream 21 with 15 members (Lindblad, 1970, private communication).[5] Similar plots have also been made for two other streams of

[5]The stream numbers used in this paragraph refer to Lindblad's preliminary results. He later used a larger rejection level for $D(M, N)$ than in the work presented elsewhere in this volume.

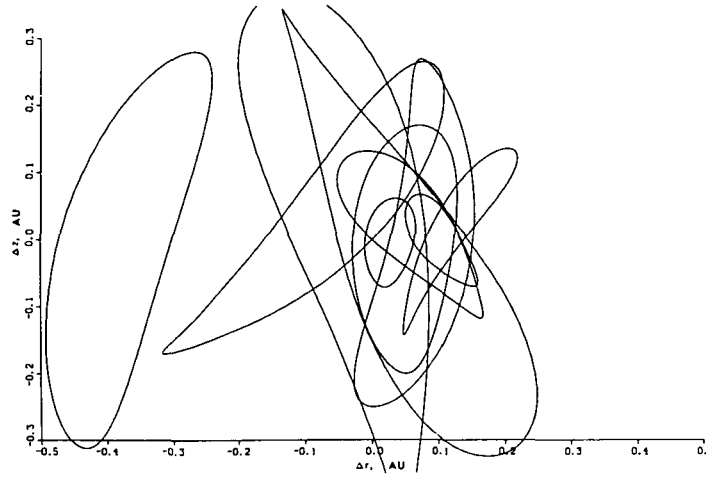

Figure 3.–The 10 orbits of stream J-6 (Arnold) in relation to their mean orbit.

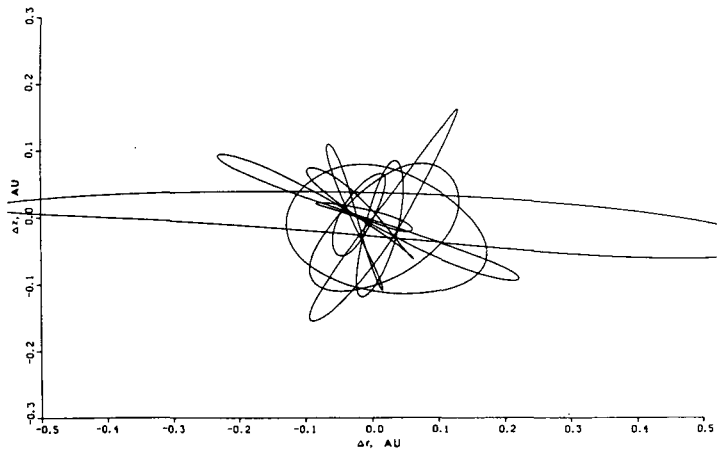

Figure 4.–Ten orbits of stream 2 (Lindblad) in relation to their mean orbit. (The four members most distant to the mean orbit are excluded.)

the same size as Flora A; namely, stream J-6 (Arnold) and stream 2 (Lindblad). (The latter stream was reduced from 14 to 10 members by omitting the four members with the largest value of $D(M, N)$ according to the formula used by Lindblad.) The plots of the orbits relative to their mean orbits for the two latter streams are shown in figures 3 and 4. The distance to the mean orbit is about twice as large for Lindblad's streams and about 10 times larger for Arnold's streams compared to Flora A, B, or C. Further, this investigation does not show any focusing regions, either in Lindblad's or in Arnold's streams.

COMET GROUPS

Another observed phenomenon might be included in a survey of jetstreams; namely, what is often called comet groups. From a statistical point of view these are probably insignificant because very few members (2 to 4) are included in each group (except for the Sun-grazing group). The only reason for mentioning them here is that if comets are considered to accrete from jetstreams (meteor streams) one could as easily imagine a stream developing several condensations.

STATISTICAL REMARKS

An important problem as far as the statistics are concerned is to decide whether "observed streams" are real or not. Hence, we want to estimate the probability (risk) that a certain property of the observed distribution is a result of a Poisson process. This probability is the level of significance of our conclusions concerning, for example, jetstreams. The problem thus formulated is a very difficult one (see the appendix for a simple example), which has never been solved in an analytic way (with the exception of the example given in the appendix). For general references on this type of problem, see Kendall and Moran (1963, chs. 2 and 5) and Roach (1968, ch. 4). Analytical methods described in the first of these works could possibly be employed, but this would be quite difficult and it is not at all certain that the result would be useful. A remaining possibility is to test synthetic distributions for the property under consideration (Roach, 1968; Danielsson, 1969). This test has to be done, of course, on a substantial number of synthetic distributions because the significance of such a test only can be determined from the distribution of the studied property among these synthetic distributions. In the present case, even making synthetic distributions is a complicated task.

Thanks to the Palomar-Leiden survey (PLS) (van Houten et al., 1970), which represents an additional, independent sample of asteroids, we can get an indication concerning the reality of our jetstreams if we find them here also. The value of this test is limited because of the observational selection of the PLS; essentially the test has to be confined to streams of low inclination. Nine hundred and thirty-one well-determined orbits (class I) have been investigated. The three Flora streams do appear also in the PLS material; however, these clusters of orbits are much less noticeable here. Within a distance $D = 0.10$ AU of the mean orbits of Flora A, B, and C, there are four, five, and three objects in the new material. At the same time, the density in this region of the five-dimensional space is twice as large in the new material as in the old. (This fact is found by experiment.) Because the mean orbits of Flora A, B, and C can be regarded as random points in relation to the PLS sample, one would expect them to have two (experimentally found average) neighbors within 0.10 AU if the distributions were random. It is obvious that the significance of each individual stream tested in this way is not overwhelming. If the streams are

tested together, one finds that the risk that they all are a result of a Poisson process is about 1 percent.

CONCLUSIONS

By means of the new definition of an average distance between celestial orbits (eq. (1)) asteroid streams can be defined. So far only the three streams in the Flora family, Flora A, B, and C (Alfvén, 1969), have been studied (and redefined) by this method. It is found that the orbits of the members in these streams are well collimated everywhere along their path in contrast to previously defined streams. Furthermore, two of the streams show marked focusing regions where a majority of the orbits come very close together and where the relative velocities are an order of magnitude smaller than between randomly coinciding asteroid orbits.

From the point of view of jetstream physics, the best definition of a jetstream might be connected more closely with regions where the density of orbits is high and at the same time the relative velocity is low. This argument is not quite in line with the one leading to the distance formula used here. Maybe a weight function, giving more weight to those parts of two orbits where the distance is smallest, should be included in the integration leading to equation (1). In view of this argument, the classical way to determine a meteor stream would be quite good. According to this, a meteor stream is defined by the geocentric quantities of radiant, velocity, and date.

The statistical significance of the studied streams, admittedly, is shown far from satisfactorily. More work is required on this problem.

APPENDIX–PROPERTIES OF A POISSON PROCESS

The need to estimate the probability that a certain property of an observed distribution can be expected to appear in one realization of a Poisson process arises frequently in works of the present type. Because this is a very difficult task and misconceptions concerning the fundamental character of this problem are not rare in the literature of nonspecialized disciplines, this comment is considered worthwhile.

Any of the above discussed methods for finding clusters of similar orbits among the asteroids can serve as an example. In some way, the number of neighbors to an orbit (a point in a five-dimensional space) is determined; and if this number is "large," an orbit cluster is considered located. By "large" number is meant that the probability of finding the same cluster in a random distribution should be small. However, one has to be very careful as to what can be expected in a random (Poisson) distribution. It gives an entirely false result to regard an observation of a certain large cluster of this kind as a random observation. Thus probabilities according to the formula

$$P(X = k) = \frac{n^k e^{-n}}{k!} \tag{A-1}$$

are completely irrelevant in our case. (n and k are the uniform average and actually observed number of members in the cluster.)

As earlier pointed out (see above and Danielsson, 1969) the problem of finding an analytical expression for the probability of coming across a certain cluster in a random distribution is in reality a very difficult one. It seems to have been solved only for a very special one-dimensional case (Ajne, 1968). The formulation of the problem should be as follows: Given a random distribution with n members, what is the probability of observing a cluster of k members in some volume of suitably chosen size and location (k being considerably larger than the uniform average)?

The problem will be illustrated by two examples:

(1) Let five points be randomly distributed on the perimeter of a circle. The probability that all of them occur on one side of a given (in advance) diameter is of course $2^{-5} = 0.031$. The probability that all of them can be located on one side of a suitably chosen diameter can be calculated according to a formula deduced by Ajne from straightforward combinatorial analysis: for $2k-n > 0$,

$$P(X \geqslant k) = 2^{1-n}(2k - n) \sum_{j=0}^{\infty} \left(\frac{n}{j(2k-n)+k} \right)$$

With $k = n = 5$, then $P(X = 5) = 5 \times 2^{-4} = 0.31$; i.e., 10 times more likely than in the first case.

(2) Consider the alleged asteroidal cluster Flora B as studied by Danielsson (1969). In a two-dimensional area, where only one point would be found on an average, seven were observed. If the area had been randomly located, the probability for this occurrence in a Poisson distribution would be $(e \cdot 7!)^{-1} = 7 \cdot 10^{-5}$.

To estimate the actual probability under the proper formulation of the problem, 100 synthetic random distributions were made to simulate the observed population. Seven points were observed in the given area, suitably located, 26 times. Thus the probability was estimated to be 0.26. More than seven points were observed three times so that the probability of finding seven or more points was 0.29.

It is clear that formula (A-1) can be wrong by very many orders of magnitude when the number of points is large. For example, the probability 10^{-100} mentioned by Arnold (1969, p. 1236) may very well be wrong by a factor of 10^{90} or more.

ACKNOWLEDGMENTS

The author is indebted to Prof. Hannes Alfvén for initiating this project and to Lynne Love for help with the computer work.

This work has been supported by grants from NASA (NASA NGR-05-009-110) and The Swedish Council for Atomic Research (AFR 14-89).

REFERENCES

Ajne, B. 1968, A Simple Test for Uniformity of a Circular Distribution. Biometrika 55, 343.

Alfvén, H. 1969, Asteroidal Jet Streams. Astrophys. Space Sci. 4, 84.

Alfvén, H., and Arrhenius, G. 1970, Origin and Evolution of the Solar System, I. Astrophys. Space Sci. 8, 338.

Arnold, J. 1969, Asteroid Families and Jet Streams. Astron. J. 74, 1235.

Danielsson, L. 1969, Statistical Arguments for Asteroidal Jet Streams. Astrophys. Space Sci. 5, 53.

Houten, C. J. van, Houten-Groeneveld, I. van, Herget, P., and Gehrels, T. 1970, Palomar-Leiden Survey of Faint Minor Planets. Astron. Astrophys. Suppl. 2, 339-448.

Kendall, M. G., and Moran, P. A. P. 1963, Geometrical Probability. Griffin & Co. London.

Roach, S. A. 1968, The Theory of Random Clumping. Methuen & Co. London.

Southworth, R., and Hawkins, G. 1963, Statistics of Meteor Streams. Smithson. Contrib. Astrophys. 7, 261-285.

DISCUSSION

WILLIAMS: Were observational selection effects considered in judging the significance of jetstreams?

DANIELSSON: The problem of observational selection certainly needs to be investigated very carefully to determine whether the asteroid streams are real or not. One can probably assume that asteroids of absolute magnitude (visual) $g < 12$ are unbiased with respect to observational selection. In a paper examining the Flora family (Danielsson, 1969) I have shown that if the asteroids with $g \geqslant 12$ are excluded, one of the streams (Flora C) remains statistically significant. Selecting the largest asteroids of the family in this way, of course, meant a substantial reduction of the number of members.

UREY: Are the jetstream particles the result of a collision in which the components that were produced remained in neighboring orbits?

DANIELSSON: The appearance of focusing points could possibly be the result of a collision, but this must then have been a very recent (10^4 to 10^5 yr) event because the phases of these orbits are very quickly spread out.

UREY: Do the geometrical properties you describe support a model based on fragmentation?

DANIELSSON: The geometrical properties that I have described do not tell you anything directly about accretion or fragmentation. However, as far as I can see, the well-collimated streams with focusing regions would have a very short lifetime unless there were some viscous force in the stream producing and maintaining these properties. Thus, if these geometric characteristics are found to be common for most of the streams, it would indicate the existence of such a force. This in turn would probably favor an accretion model.

DISCUSSION REFERENCE

Danielsson, L. 1969, Statistical Arguments for Asteroidal Jet Streams. Astrophys. Space Sci. 5, 53.

SPATIAL DISTRIBUTION OF INTERPLANETARY DUST

ROBERT G. ROOSEN
NASA Goddard Space Flight Center

Interplanetary dust can be defined as solid particles outside Earth's atmosphere in the size range larger than a molecule and smaller than an asteroid. It is studied by a number of quite different techniques. For Earth-based observers, these techniques include measurement of the brightness and polarization of the interplanetary light,[1] optical radar studies of particles entering the upper atmosphere, photographic and radar meteor observations, study of meteorites, and various methods of collecting dust particles in the atmosphere, in ice cores, and in deep sea sediments. Observations made from spacecraft include some interplanetary light observations and measurements of individual particles by means of microphones, penetration sensors, and collection experiments. These observational techniques are described by Millman (1969) and Bandermann (1969).

EARTH-ASSOCIATED DUST?

At the beginning of the last decade it was generally considered probable—if not certain—that interplanetary dust was concentrated at a number of preferred locations in the near-Earth environment. In particular, Whipple (1961) reported evidence for a high concentration of dust near Earth with a maximum concentration with respect to the average interplanetary medium perhaps as high as 10^5 (the so-called geocentric dust cloud (GDC)). Kordylewski (1961) reported that he had observed concentrations of dust (the so-called libration clouds) associated with the quasi-stable triangular Earth-Moon libration points L_4 and L_5 (fig. 1). He further stated, "The surface intensity of the libration clouds is a little less in their opposition than that of the Gegenschein[2] [counterglow]." Also, there was a widespread belief that the

[1]"Interplanetary light" has been suggested by Roosen (1971*a*) as a general term to describe all light scattered (or emitted) by interplanetary material. It includes the zodiacal light, which by definition is concentrated toward the plane of the ecliptic, the counterglow, which is a weak brightening in the antisolar direction, and also the light known to come from high ecliptic latitudes, up to and including the ecliptic poles.

[2]*Editorial note:* The responsibility for replacing "Gegenschein" with "counterglow" is entirely mine; I thank Dr. Roosen for accepting this change, which he did reluctantly and only because it had already been made when he received galley proofs.—T. Gehrels.

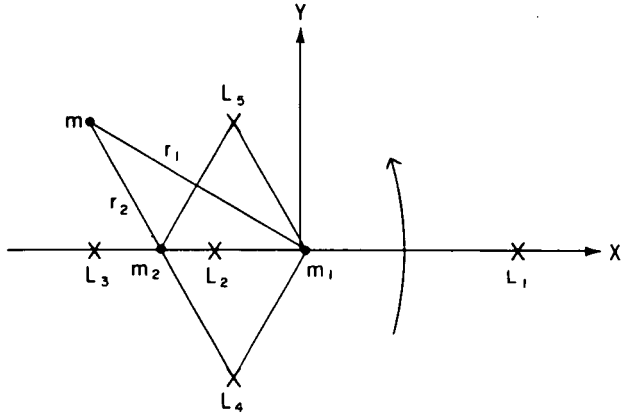

Figure 1.—Geometry for the restricted three-body problem showing schematically the positions of the libration (or equilibrium) points. The arrow indicates the direction of rotation of the system. In the Gyldén-Moulton counterglow hypothesis, m_1 is the Sun, m_2 is Earth, and the dust cloud is at the libration point L_3. For the Earth-Moon libration clouds, m_1 is Earth, m_2 is the Moon, and the dust clouds are near L_4 and L_5. See van de Kamp (1964) or Szebehely (1967) for further discussion.

counterglow was due to a collection of dust around the L_3 libration point in the Sun-Earth system (fig. 1). This suggestion was first made by Searle (1882), but it is generally attributed to Gyldén (1884) and Moulton (1900). It also was thought that the counterglow might be due to an Earth's dust tail populated by lunar ejecta (Brandt and Hodge, 1961).

All of these suggestions were quite controversial, and in the last 10 yr a prodigious amount of work has been done to test their validity. It now seems safe to say that they are all wrong.

Numerous theoretical investigations were carried out to find a justification for the existence of a GDC. The most complete was a series of papers by Lautman, Shapiro, and Colombo (1966) who considered a number of physical processes including gravitational focusing, Jacobi capture, meteor-Moon collisions, and sunlight-pressure air-drag capture. They found that, under any set of reasonable assumptions, none of these mechanisms lead to a significant concentration of material. Peale (1967, 1968) has made an excellent analysis of many dynamical and observational investigations and has set an upper limit of 1 percent on any geocentric contribution to the interplanetary light.

Evidence for concentrations of material associated with the Earth-Moon libration points has been sought photographically and photoelectrically by Morris, Ring, and Stephens (1964); Wolff, Dunkelman, and Haughney (1967); Roosen (1966, 1968); Bruman (1969); and Weinberg, Beeson, and Hutchison (1969). None of these workers found any evidence for lunar libration clouds. The last mentioned study concluded that any brightness enhancement due to lunar libration clouds must be less than 0.5 percent of the background

brightness. This is 200 times fainter than the brightness reported by Kordylewski (1961).

Roosen (1969, 1970) has investigated the Earth-associated theories for the counterglow using the fact that they require such a concentration of material near Earth that Earth's shadow would be visible in the center of the counterglow. Because the shadow was not visible to within an accuracy of 1 percent, dust accumulated at the L_3 libration point in the Sun-Earth system can account for no more than 1.2 percent of the counterglow's light. Because the hypothetical dust and gas tails are assumed to have a 3° westward displacement from the antisolar point, the base of the tail in either case would be quite close to Earth (inside the umbra). The lack of a shadow indicates that less than 1 percent of the counterglow light is produced by a dust or gas tail.

We can conclude, therefore, that to within an observational limit of 1 percent, there is no evidence for accumulations of material in the near-Earth environment. Thus, for the purposes of this discussion, we can assume that essentially all of the interplanetary dust is in heliocentric orbits.

RADIAL DISTRIBUTION

A large number of models of interplanetary dust distribution have been built based on observed interplanetary light isophotes and the assumption that the radial distribution of material could be described by a simple power law R^{-p} where R is heliocentric distance. Examples of these can be found in Sandig (1941), Allen (1946), van de Hulst (1947), Fesenkov (1958), Beard (1959), Giese (1962), Ingham (1962-63), Gindilis (1963), Gillett (1966), Aller et al. (1967), Singer and Bandermann (1967), Divari (1967, 1968), Giese and Dziembowski (1967), Powell et al. (1967), Southworth (1967), and Bandermann (1968). Values of p ranging from 0.1 to 3.5 were derived or assumed for the various models.

Southworth (1964) and Bandermann (1968) have shown that if the interplanetary dust is due to cometary debris, then Poynting-Robertson drag causes the dust concentration to vary as R^{-1} for $R < q$ and as $R^{-2.5}$ for $R > q$, where q is the comet's perihelion distance. Essentially all of the comets that have been suggested as sources of interplanetary dust are short-period comets with perihelia less than 1 AU. In particular, Whipple (1967) has stated that "over the past several thousand years" comet Encke with $q = 0.338$ has been "quite probably the major support for maintaining the quasi-equilibrium of the zodiacal cloud." Thus, dust from these comets would be expected to follow an $R^{-2.5}$ law outside Earth's orbit. Dust from a cloud of particles injected with perihelia greater than 1 AU would follow an R^{-1} law as long as the injection is a steady-state mechanism (i.e., a large cloud was not injected fairly recently).

Thus the assumption that the radial density follows an inverse power law is based on very reasonable physical arguments. However, Roosen (1969, 1970) has shown that these assumed distributions require such a concentration of

material near Earth that Earth's shadow should be visible in the center of the counterglow. Such a shadow is not observed (fig. 2), and hence the spatial density of reflecting material must *increase* at some distance outside Earth's orbit. The source suggested by Roosen is the asteroid belt, and figure 3 shows the relative density of reflecting material that results. The curves for R^{-p} contributions are upper limits based on the lack of an observed shadow to an accuracy of 1 percent. Note that this result does not say anything about the source or distribution of interplanetary dust inside Earth's orbit. However, models based on an R^{-p} distribution of material outside Earth's orbit are incorrect.

There exists yet another source of information on the radial distribution of interplanetary dust; that is, impact measurements made by two Mariner and two Pioneer spacecraft. Alexander et al. (1965) found that over the heliocentric distance range 0.72 to 1.56 AU the interplanetary dust density was roughly constant. This result is based on two impacts measured by Mariner 2 (Alexander, 1962) and 215 impacts measured by Mariner 4. Berg (1971, personal communication) reports that Pioneers 8 and 9 have ranged in heliocentric distance from 0.75 to 1.1 AU and have measured a total of over 150 impacts. His preliminary analysis also indicates that the interplanetary dust particle density is constant in that range of distances. It is immediately apparent that the number of impacts measured is too small for an R^{-1} distribution to be detected. However, an $R^{-2.5}$ distribution should be detectable. Hence the $R^{-2.5}$ distribution can be questioned on yet another ground.

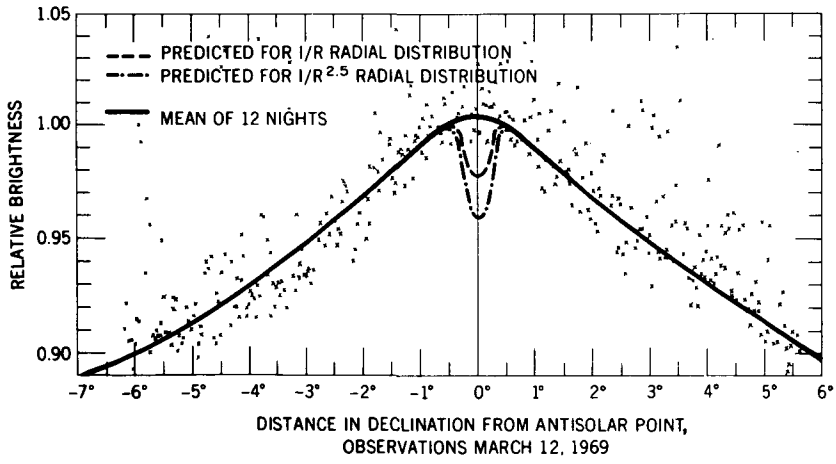

Figure 2.—Brightness curves predicted for two possible radial distributions of interplanetary dust. The points are from observations made on a single night. The points that lie well above the mean curve are due to faint stars passing through the field of view. Data are from Roosen (1969, 1970).

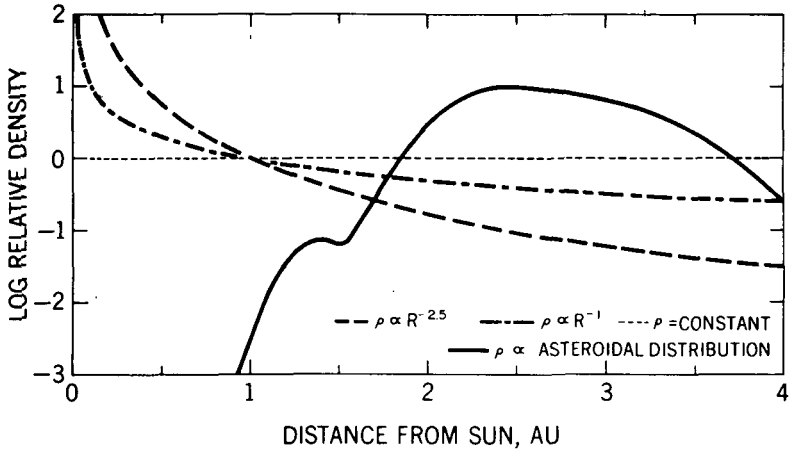

Figure 3.—Relative spatial densities for four possible radial distributions of material. The R^{-p} curves are upper limits with respect to the asteroidal distribution set by Roosen (1969, 1970).

There is an additional simple test to distinguish between the cometary and asteroidal hypotheses (Roosen, 1969, 1970). It requires that a photometer on a space probe traveling toward the outer solar system monitor the counterglow brightness. If the counterglow is due to asteroidal debris, its brightness will remain almost constant until the probe goes further than 2 AU from the Sun. If, on the other hand, cometary debris produces the counterglow, the observed brightness will steadily decrease, and the counterglow will only appear to be a tenth as bright at 2 AU as it is when seen from Earth's distance.

DISTRIBUTION OF INCLINATIONS

Bandermann (1968) and Singer and Bandermann (1967) fit a series of models to the interplanetary light observations reported by Smith, Roach, and Owen (1965) and found that the number of interplanetary dust particles with a given inclination i was best described by a function of the form

$$n(i) = K \sin i \exp(-3i)$$

This result was generally confirmed by Zook and Kessler (1968). Results of this type, however, are based on a faulty assumption.

The radial distribution assumed by Bandermann and Singer was proportional to $R^{-1.5}$. This means that most of the brightness contribution at elongations greater than 90° is assumed to come from material relatively close to Earth. Let us examine the situation at an elongation of 180°. From figure 4 we see that the closer to Earth the material is, the larger the geocentric latitude

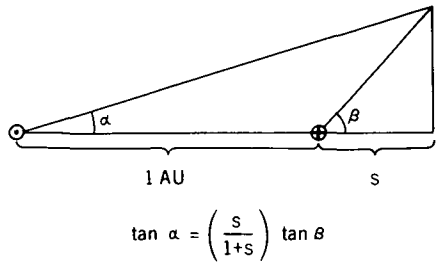

Figure 4.–The relation between the geocentric latitude β and the heliocentric latitude α at elongation 180°.

β at which one must look to see particles with a given heliocentric latitude α. In fact,

$$\tan \beta = \frac{1+s}{s} \tan \alpha$$

where s is the projection into the ecliptic plane of the distance of the material from Earth. As an example, let us look at two cases: (1) $s = 0.3$, the distance within which 50 percent of the counterglow brightness would arise for material distributed according to an $R^{-1.5}$ power law, and (2) $s = 1.5$, the mean distance for an asteroidal contribution. In case 1, in order to see a particle at a heliocentric latitude α of 5°, the observer must look at a geocentric latitude β of 21°. For case 2, β is 8° (fig. 5). In effect what this means is that if the $R^{-1.5}$

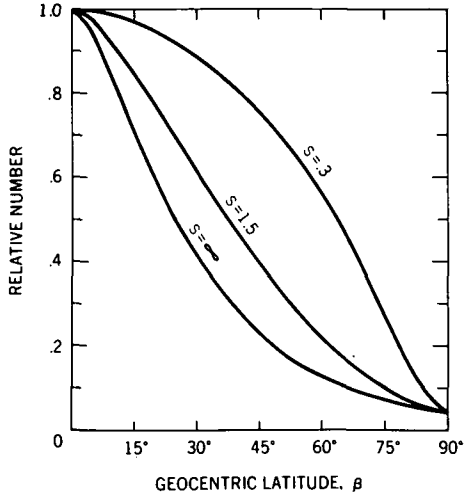

Figure 5.–Spatial density of material at 180° elongation as a function of geocentric ecliptic latitude for various values of s, the projected mean distance of the material from Earth, and Singer and Bandermann's distribution of inclinations.

law is assumed, the distribution of particle density can decrease steeply with increasing α and still yield the relatively gently sloping observed brightness curve (fig. 5).

As we have already seen, however, the main contribution to the counterglow brightness cannot come from material close to Earth and may come, in fact, from material in the asteroid belt. Until the radial distribution of interplanetary dust is known more accurately, therefore, the orbital inclinations of the dust particles cannot be deduced in this manner.

However, the facts that the observed brightness at high ecliptic latitudes is relatively large (Smith et al., 1965) and that there is a slow decrease in particle concentration with increasing latitude observed in the counterglow seem to imply that the average dust particle inclination must be at least some tens of degrees. This is higher than the average inclinations of the numbered asteroids or short-period comets, but that is not surprising (Roosen, 1969).

ORIGIN OF THE MATERIAL

Discussions of the origin of the interplanetary dust make the necessary assumption that the distribution of dust is in a steady-state condition; i.e., the sources and sinks for the dust are in equilibrium. This means that there must be a continuous injection of small particles into the interplanetary dust cloud because the Poynting-Robertson effect, destructive collisions, sputtering, planetary perturbations, and other dissipative processes make the mean lifetime of the small particles that most likely produce the interplanetary light much less than a million years. (See, e.g., Bandermann, 1968; Whipple, 1967.) Somewhere around 10^4 kg/s of small particles must be continually injected into the interplanetary dust cloud to maintain its quasi-equilibrium (Whipple, 1967). Possible origins for the interplanetary dust that have been suggested (Vedder, 1966) include cometary debris, asteroidal debris, and interstellar grains.

Harwit (1964), Bandermann (1969), and Bandermann and Wolstencroft (1970) have examined the mechanisms for capture of interstellar dust and have found that none of them is sufficiently effective to produce a sensible contribution to the interplanetary dust cloud. Harwit suggests that there may be a contribution from dust particles that remained in the outer solar system when comets were formed that is now "drizzling" into the inner solar system. Although the work on the radial distribution of the dust by Roosen (1969, 1970) would seem to disallow this hypothesis, the possibility that there is a large concentration of dust from this source outside the "Jupiter gravitational barrier" cannot at this time be ruled out completely.

At present, however, there seems to be general agreement that the dust is due to either cometary or asteroidal debris (or a combination of both; see the paper by Whipple in this volume[3]). A firm decision as to which of these

[3]See p. 389.

sources produces most of the interplanetary dust seems to be extremely remote at this time. Indeed, much of IAU colloquium number 13, *The Evolutionary and Physical Problems of Meteoroids,* will be devoted to this question. However, it is proper here to discuss a few of the more general approaches that have been taken.

One way to approach this problem is to examine the rate of production of interplanetary dust by the various mechanisms. There have been a number of papers written on this subject. Whipple (1967), for instance, presented a model wherein the interplanetary dust cloud is produced and replenished entirely by debris from short-period comets, and asteroidal debris makes no contribution. Harwit (1963) found that, although the amount of dust produced by comets was insufficient to maintain the equilibrium concentration of the interplanetary dust cloud, asteroidal collisions could produce sufficient debris. (The injection rate, however, would be extremely variable because most of the debris must be produced in very rare collisions between the largest asteroids.) Bandermann (1968) and Gillett (1966) also found that comets could not produce enough material, but asteroidal debris was quite sufficient. See also the discussion by Dohnanyi (1969). It seems apparent that too many uncertainties are involved in the calculations to allow a definitive solution to be reached by this approach.

The radial distribution arguments discussed earlier seem to imply that most of the interplanetary dust outside Earth's orbit is asteroidal in origin. There are a number of apparently valid objections, however, to the suggestion that all interplanetary dust comes from the asteroid belt.

First, the correlation of photographic meteors with cometary orbits (e.g., Jacchia, 1963) shows that comets do produce dust particles with elliptical orbits. (Most of the dust from comets immediately escapes from the solar system (Harwit, 1963).) It is intriguing that these correlations disappear for very faint meteors (Elford, 1965), but this effect may well be indicative of the lifetimes of the particles or the perturbing forces acting on them rather than indicative of their origin (Dohnanyi, 1970).

Another strong argument against the existence of asteroidal debris intersecting Earth's orbit in large quantities is the apparent low density of observed meteors (Jacchia, 1963). However, the densities derived from the observations depend on a raft of assumptions (primarily the luminous efficiency), and the trend in recent years has been to revalue the densities much higher than originally thought (Baldwin and Sheaffer, 1971).

Another problem with an asteroidal origin for interplanetary dust inside Earth's orbit is to find a mechanism by which the dust can be brought in past Earth without a shadow being observable.

In any case, it would appear to be safe at this time to state that both asteroids and comets contribute to the interplanetary dust cloud, but the exact contributions have yet to be determined.

REVIEWS

Reviews discussing in situ measurements, meteor observations, and interplanetary light observations have been published by Whipple (1959), Kaiser (1962), Hawkins (1964), Vedder (1966), Singer and Bandermann (1967), and Bandermann (1969). Reviews of in situ measurements have been published by Alexander et al. (1963), McCracken and Alexander (1968), and Kerridge (1970). A review of optical meteor observations is given by Jacchia (1963). Zodiacal light observations and models are discussed by Ingham (1962-63) and Divari (1964). Langton (1969) has discussed the meteoroid hazard question. Also, as part of NASA's meteoroid hazard study, estimates of interplanetary dust parameters have been compiled by Cour-Palais (1969) and Kessler (1970). The classical identification of components of the light of the night sky has been described by Mitra (1952) and Roach (1964).

Roosen and Wolff (1969) have discussed the status of lunar libration clouds. An extensive review on the counterglow was presented by Roosen (1969, 1971*a*). Weinberg (1967*a*) has summarized observations of the interplanetary light and collected an unannotated bibliography on that subject. An unannotated bibliography on meteoroids has also been prepared by Dohnanyi (1971). An annotated bibliography on interplanetary dust was collected by Hodge et al. (1961), and one on the counterglow was produced by Roosen (1971*b*). The proceedings of two recent conferences on interplanetary dust have been edited by Weinberg (1967*b*) and Hawkins (1967). Kresák and Millman (1968) edited the proceedings of a symposium on the physics and dynamics of meteors, and Millman (1969) edited the proceedings of a symposium on meteorite research.

REFERENCES

Alexander, W. M. 1962, Cosmic Dust. Science **138**, 1098-1099.

Alexander, W. M., McCracken, C. W., and Bohn, J. L. 1965, Zodiacal Dust: Measurements by Mariner IV. Science **149**, 1240-1241.

Alexander, W. M., McCracken, C. W., Secretan, L., and Berg, O. E. 1963, Review of Direct Measurements of Interplanetary Dust From Satellites and Probes. Space Res. 3, 871-917.

Allen, C. W. 1946, The Spectrum of the Corona at the Eclipse of 1940 October 1. Mon. Notic. Roy. Astron. Soc. **106**, 137-150.

Aller, L. H., Duffner, G., Dworetsky, M., Gudehus, D., Kilston, S., Leckrone, D., Montgomery, J., Oliver, J., and Zimmerman, E. 1967, Some Models of the Zodiacal Cloud. The Zodiacal Light and the Interplanetary Medium (ed., J. L. Weinberg), pp. 243-256. NASA SP-150.

Baldwin, B., and Sheaffer, Y. 1971, Ablation and Breakup of Large Meteoroids During Atmospheric Entry. J. Geophys. Res. **76**, 46-53.

Bandermann, L. W. 1968, Physical Properties and Dynamics of Interplanetary Dust. Ph. D. Dissertation. Univ. of Maryland.

Bandermann, L. W. 1969, Interplanetary Dust. Lectures in High-Energy Astrophysics (eds., H. Ogelman and J. R. Wayland), pp. 137-165. NASA SP-199.

Bandermann, L. W., and Wolstencroft, R. D. 1970, Three-Body Capture of Interstellar Dust by the Solar System. Mon. Notic. Roy. Astron. Soc. **150**, 173-186.

Beard, D. B. 1959, Interplanetary Dust Distribution. Astrophys. J. **129**, 496-506.

Brandt, J. C., and Hodge, P. W. 1961, Lunar Dust and the Gegenschein. Nature **192**, 957.

Bruman, J. R. 1969, A Lunar Libration Point Experiment. Icarus **10**, 197-200.

Cour-Palais, B. G. 1969, Meteoroid Environment Model–1969 (Near Earth to Lunar Surface). NASA SP-8013.

Divari, N. B. 1964, Zodiacal Light. Sov. Phys. Usp. **7**, 681-695.

Divari, N. B. 1967, On Some Models of Zodiacal Cloud. Astron. Vestn. **1**, 103-109. (Also available as NASA CR-86679 (1967).)

Divari, N. B. 1968, A Meteor Model for the Zodiacal Cloud. Sov. Astron. AJ **11**, 1048-1052.

Dohnanyi, J. S. 1969, Collisional Model of Asteroids and Their Debris. J. Geophys. Res. **74**, 2531-2554.

Dohnanyi, J. S. 1970, On the Origin and Distribution of Meteoroids. J. Geophys. Res. **75**, 3468-3493.

Dohnanyi, J. S. 1971, Meteoroids. Trans. Amer. Geophys. Union, in press.

Elford, W. G. 1965, Incidence of Meteors on the Earth Derived From Radio Observations. Smithson. Contrib. Astrophys. **11**, 121-131. (Also NASA SP-135, 1967)

Fesenkov, V. G. 1958, Zodiacal Light as the Product of Disintegration of Asteroids. Sov. Astron. AJ **2**, 303-309.

Giese, R. H. 1962, Light Scattering by Small Particles and Models of Interplanetary Matter Derived From the Zodiacal Light. Space Sci. Rev. **1**, 589-611.

Giese, R. H., and Dziembowski, C. v. 1967, On Optical Models Approximating Observations of the Zodiacal Light Outside the Ecliptic. The Zodiacal Light and the Interplanetary Medium (ed., J. L. Weinberg), pp. 271-276. NASA SP-150.

Gillett, F. C. 1966, Zodiacal Light and Interplanetary Dust. Ph. D. Thesis, Univ. of Minnesota.

Gindilis, L. M. 1963, The Gegenschein as an Effect Produced by the Scattering of Light From Particles of Interplanetary Dust. Sov. Astron. AJ **6**, 540-548.

Gyldén, H. 1884, On a Particular Case of the Problem of Three Bodies Bull. Astron. **1**, 361-369.

Harwit, M. 1963, Origins of the Zodiacal Dust Cloud. J. Geophys. Res. **68**, 2171-2180.

Harwit, M. 1964, Origins of the Zodiacal Dust Cloud II. Ann. N.Y. Acad. Sci. **119**, 68-71.

Hawkins, G. S. 1964, Interplanetary Debris Near the Earth. Ann. Rev. Astron. Astrophys. **2**, 149-164.

Hawkins, G. S., ed. 1967, Meteor Orbits and Dust. Smithson. Contrib. Astrophys. **11**. (Also NASA SP-135, 1967.)

Hodge, P. W., Wright, R. W., and Hoffleit, D. 1961, An Annotated Bibliography on Interplanetary Dust. Smithson. Contrib. Astrophys. 5(8), 85-111.

Hulst, H. C. van de. 1947, Zodiacal Light in the Solar Corona. Astrophys. J. **195**, 471-488.

Ingham, M. F. 1962-63, Interplanetary Matter. Space Sci. Rev. **1**, 576-588.

Jacchia, L. G. 1963, Meteors, Meteorites, and Comets: Interrelations. The Moon, Meteorites, and Comets. The Solar System (eds., Middlehurst and Kuiper), vol. IV, pp. 774-798. Univ. of Chicago. Chicago.

Kaiser, T. R. 1962, Meteors and the Abundance of Interplanetary Matter. Space Sci. Rev. **1**, 554-575.

Kamp, P. van de. 1964, Elements of Astromechanics. W. H. Freeman & Co. San Francisco.

Kerridge, J. F. 1970, Micrometeorite Environment at the Earth's Orbit. Nature **228**, 616-619.

Kessler, D. J. 1970, Meteoroid Environment Model–1970 (Interplanetary and Planetary). NASA SP-8038.

Kordylewski, K. 1961, A Photographic Search of the Libration Point L_5 in the Earth-Moon System. Acta Astron. **11**, 165-169.

Kresák, L., and Millman, P. M., eds. 1968, Physics and Dynamics of Meteors. Springer Pub. Co. New York.

Langton, N. H. 1969, The Meteoroid Hazard to Spacecraft. Space Res. Tech. **1**, 143-169.

Lautman, D. A., Shapiro, S. I., and Colombo, G. 1966, The Earth's Dust Belt: Fact or Fiction? J. Geophys. Res. **71**, 5695-5741.

McCracken, C. W., and Alexander, W. 1968, Interplanetary Dust Particles. Introduction to Space Sciences (ed., W. N. Hess), second ed., pp. 447-499. Gordon & Breach, Science Pub. New York.

Millman, P. M., ed. 1969, Meteorite Research. D. Reidel. Dordrecht.

Mitra, S. K. 1952, The Upper Atmosphere, second ed., p. 485. Asiatic Society. Calcutta.

Morris, E. C., Ring, J., and Stephens, H. G. 1964, Photographic and Photoelectric Investigations of the Earth-Moon Libration Regions L_4 and L_5 From Mt. Chacaltaya Bolivia. Astrogeologic Studies, Annual Progress Report, pt. D, August 25, 1962, to July 1, 1963, pp. 71-74. U.S. Geological Survey.

Moulton, F. R. 1900, A Meteoric Theory of the Gegenschein. Astron. J. **21**, 17-22.

Peale, S. J. 1967, The Zodiacal Light and Earth-Orbiting Dust. The Zodiacal Light and the Interplanetary Medium (ed., J. L. Weinberg), pp. 337-342. NASA SP-150.

Peale, S. J. 1968, Evidence Against a Geocentric Contribution to the Zodiacal Light. J. Geophys. Res. **73**, 3025-3033.

Powell, R. S., Woodson, P. E., III, Alexander, M. A., Circle, R. R., Konheim, A. G., Vogel, D. C., and McElfresh, T. W. 1967, Analysis of All Available Zodiacal-Light Observations. The Zodiacal Light and the Interplanetary Medium (ed., J. L. Weinberg), pp. 225-241. NASA SP-150.

Roach, F. E. 1964, The Light of the Night Sky; Astronomical, Interplanetary, and Geophysical. Space Sci. Rev. **3**, 512-540.

Roosen, R. G. 1966, A Photographic Investigation of the L_5 Point in the Earth-Moon System. Contrib. McDonald Obs. Ser. 2(9). (Also Sky and Telescope **32**, 139 (1966).)

Roosen, R. G. 1968, A Photographic Investigation of the Gegenschein and the Earth-Moon Libration Point L_5. Icarus **9**, 429-439. (See also erratum in Icarus **10**, 352 (1969).)

Roosen, R. G. 1969, The Gegenschein. Ph. D. Dissertation. Univ. of Texas.

Roosen, R. G. 1970, The Gegenschein and Interplanetary Dust Outside the Earth's Orbit. Icarus **13**, 184-201.

Roosen, R. G. 1971*a*, The Gegenschein. Rev. Geophys. Space Phys., in press.

Roosen, R. G. 1971*b*. An Annotated Bibliography on the Gegenschein. Icarus, in press.

Roosen, R. G., and Wolff, C. L. 1969, Are the Libration Clouds Real? Nature **224**, 571.

Sandig, H. U. 1941, The Spatial Distribution of the Zodiacal Light Material. Astron. Nachr. **272**, 1-24.

Searle, A. 1882, On Certain Zodiacal Phenomena. Astron. Nachr. **102**, 263-266.

Singer, S. F., and Bandermann, L. W. 1967, Nature and Origin of Zodiacal Dust. The Zodiacal Light and the Interplanetary Medium (ed., J. L. Weinberg), pp. 379-397. NASA SP-150.

Smith, L. L., Roach, F. E., and Owen, R. W. 1965, The Absolute Photometry of the Zodiacal Light. Planet. Space Sci. **13**, 207-217.

Southworth, R. B. 1964, The Size Distribution of the Zodiacal Particles. Ann. N.Y. Acad. Sci. **119**, 54-67.

Southworth, R. B. 1967, Phase Function of the Zodiacal Cloud. The Zodiacal Light and the Interplanetary Medium (ed., J. L. Weinberg), pp. 257-270. NASA SP-150.

Szebehely, V. 1967, Theory of Orbits. Academic Press, Inc. New York and London.

Vedder, J. F. 1966, Minor Objects in the Solar System. Space Sci. Rev. 6, 365-414.
Weinberg, J. L. 1967*a*, Summary Report II on Zodiacal Light, July 1967. Hawaii Inst. Geophys.
Weinberg, J. L., ed. 1967*b*, The Zodiacal Light and the Interplanetary Medium. NASA SP-150.
Weinberg, J. L., Beeson, D. E., and Hutchison, P. B. 1969, Photometry of Lunar Libration Regions. Bull. Amer. Astron. Soc. 1, 368.
Whipple, F. L. 1959, Solid Particles in the Solar System. J. Geophys. Res. 64, 1653-1664.
Whipple, F. L. 1961, The Dust Cloud About the Earth. Nature 189, 127-128.
Whipple, F. L. 1967, On Maintaining the Meteoritic Complex. The Zodiacal Light and the Interplanetary Medium (ed., J. L. Weinberg), pp. 409-426. NASA SP-150.
Wolff, C., Dunkelman, L., and Haughney, L. C. 1967, Photography of the Earth's Cloud Satellites From an Aircraft. Science 157, 427-429.
Zook, H. A., and Kessler, D. J. 1968, The Zodiacal Light and Meteoroid Measurements. Trans. Amer. Geophys. Union 49.

DISCUSSION

DUBIN: The shadow of Earth in the counterglow (and near-Earth dust) is not expected to be observed at all altitudes. You imply that because the shadow could not be observed, the dust of the counterglow is in the vicinity of the asteroid region and that the satellite results of dust measurements near Earth could not be correct. What is the lowest altitude for which the shadow measurements may be applied?

ROOSEN: The shadow technique that I used (Roosen, 1970) is useful only above about 6000 km. In the direction in which I was looking, material below that altitude would have been in Earth's umbra and hence could not contribute to the counterglow brightness.

DUBIN: The atmosphere extends to several hundred kilometers. It is doubtful that this measurement would work close in where the airglow would interfere. A source of the near-Earth measurements has been identified from the disintegration of the Prairie Network meteoroids, for example.

ROOSEN: As I have already mentioned, Peale (1968) has summarized a number of very convincing arguments against a near-Earth geocentric dust cloud.

DUBIN: Another point in regard to interstellar particles is the discovery of the penetration of the interstellar wind that has been made by Bertaux and Blamont (1971), and by Thomas and Krassa (1971). The results indicate that a hydrogen wind detected by resonant excitation in Lyman alpha penetrates into the solar system to a distance between 3 and 7 AU. Such an interstellar wind should be accompanied by interstellar grains that, accordingly, should also be able to penetrate into the asteroid region and may contribute to the counterglow without showing an Earth shadow. You indicated that there would be no contribution from interstellar dust based on a recent publication of Bandermann?

ROOSEN: I think that Dr. Bandermann should answer that.

BANDERMANN: The publication by Bandermann and Wolstencroft (1970) is concerned with the gravitational capture of interstellar dust into the solar system by a single encounter with a planet, rather than with the penetration of dust contained in a gas cloud colliding with the solar system, which involves gas-dust coupling and solar-wind interaction. These authors found a total capture rate of ≤ 10 kg/s for interstellar dust densities of 3×10^{-26} g/cm^3 and compared this rate with the estimated rate of loss from the zodiacal cloud, $\sim 1 \times 10^3$ kg/s. They did not calculate the contribution by captured dust to the zodiacal light or counterglow surface brightness.

DISCUSSION REFERENCES

Bandermann, L. W., and Wolstencroft, R. D. 1970, Three-Body Capture of Interstellar Dust by the Solar System. Mon. Notic. Roy. Astron. Soc. 150, 173-186.

Bertaux, J. L., and Blamont, J. E. 1971, Evidence for a Source of an Extraterrestrial Hydrogen Lyman-Alpha Emission–The Interstellar Wind. Astron. Astrophys. **11**(2), 200-217.

Peale, S. J. 1968, Evidence Against a Geocentric Contribution to the Zodiacal Light. J. Geophys. Res. 73, 3025-3033.

Roosen, R. G. 1970, The Gegenschein and Interplanetary Dust Outside the Earth's Orbit. Icarus 13, 184-201.

Thomas, G. E., and Krassa, R. F. 1971, OGO 5 Measurements of the Lyman Alpha Sky Background. Astron. Astrophys. **11**(2), 218-233.

Page intentionally left blank

PHYSICAL PROPERTIES OF THE INTERPLANETARY DUST

MARTHA S. HANNER
Dudley Observatory

The interplanetary dust may be composed of cometary material, interstellar grains, debris from asteroidal collisions, primordial material formed by direct condensation, or contributions from all of these sources. Before we can determine the origin of the dust, we need to know its physical nature, spatial distribution, and the dynamical forces that act on the particles. The spatial distribution and dynamics are separately treated in this symposium by Roosen.[1] We discuss here the physical characteristics of the dust particles: their size distribution, chemical composition, physical structure, and optical properties.

Data on these properties can be obtained from particle collections, impact craters, thin-film penetrations, acoustic detectors, and the zodiacal light. The results obtained from various methods have been reviewed by Singer and Bandermann (1967) and Bandermann (1968). We shall concentrate on discussing the information that can be derived from observations of the zodiacal light.

ZODIACAL LIGHT MODELS

The zodiacal light provides information on the average properties of the interplanetary dust over a large volume of space. Analysis of the brightness and polarization of the zodiacal light yields, in principle, the large-scale size distribution, spatial distribution, and optical properties of the scattering particles. The optical properties, in turn, contain information on the composition and physical structure of the dust particles.

Figure 1 illustrates the basic scattering geometry. Particles in the volume element at P, at a distance r from the Sun, scatter sunlight through an angle θ into the line of sight along PE. The contribution to the observed brightness from all the particles in the volume element at P will be

$$dI_\lambda(\epsilon) = \frac{E_0 {R_0}^2}{r^2} d\Delta \int_{a_1}^{a_2} n(a, r) F_\lambda(a, \theta)\, da \qquad (1)$$

---

[1]See p. 363.

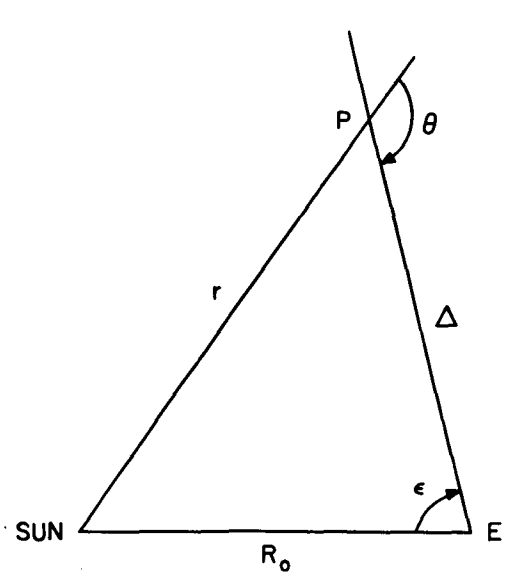

Figure 1.–Basic scattering geometry for the zodiacal light.

where

E_0 = solar flux at 1 AU
R_0 = 1 AU
$n(a, r)$ = particle size and spatial distribution
a_1, a_2 = the lower and upper limits to the particle size distribution
$F_\lambda(a, \theta)$ = angular scattering function for particles of radius a

The total surface brightness at an elongation ϵ from the Sun will be the integral of $dI(\epsilon)$ over the line of sight

$$I_\lambda(\epsilon) = E_0 R_0{}^2 \int_{\Delta=0}^{\infty} \int_{a_1}^{a_2} \frac{n(a, r)}{r^2} F_\lambda(a, \theta)\, da d\Delta \qquad (2)$$

In practice, there is no simple way of separating the parameters in equation (2). The size distribution can be expected to be a function of r because the dynamical forces acting on the dust depend on particle dimension as well as density. The scattering functions themselves may vary with distance from the Sun because solar radiation can alter the optical properties of the dust particles. The interplanetary material is probably a mixture of several components having different relative concentrations in different parts of the solar system. Cometary and asteroidal debris, for example, would not be injected at the same solar distance.

The approach that has generally been applied has been to choose a form for $F_\lambda(a, \theta)$, assume that the particle size distribution is independent of the spatial distribution, and adopt a functional form for each that is based either on convenience, on the results of dynamical calculations, or on other observational evidence, such as data from acoustic and penetration experiments or extrapolation of meteor fluxes. Models of the brightness and polarization of the zodiacal light are then computed and the model parameters adjusted until a fit with the observations is obtained. Even if a good fit is achieved, there is, of course, no guarantee that the model so obtained is unique, and a variety of models have been found to represent the data about equally well. Reviews of theoretical work have been given by Blackwell, Dewhirst, and Ingham (1967), Elsässer (1963), and others.

The earliest models, which assumed an isotropic scattering function, made it necessary to postulate a high particle concentration near the Sun to account for the steep increase in brightness in the *F* corona. Allen (1946) and van de Hulst (1947) independently showed that the brightness distribution in the *F* corona can be accounted for by diffraction without having to assume large numbers of dust particles close to the Sun. Ingham (1961) and Blackwell, Ingham, and Petford (1967) also treated the scattering function as a diffraction component plus a reflection component in deriving the albedo and the spatial distribution from coronal observations. Separating the scattering function into reflection and diffraction components is valid at all scattering angles for particles much larger than the wavelength. At small scattering angles, the diffraction component will be adequate for spherical particles a few micrometers in size at optical wavelengths. Diffraction will predict too steep a rise in intensity in the forward direction for particles less than 1 μm in size. (See van de Hulst, 1957, and Giese, 1961.)

With the introduction of high-speed computers, many authors have generated models using Mie theory to compute the scattering functions. The most extensive calculations have been carried out by Giese (1961), Giese and Siedentopf (1962), Giese (1963), and Giese and Dziembowski (1967). Similar studies have been done by Little, O'Mara, and Aller (1965); Elsässer and Schmidt (1966); Aller et al. (1967); Powell et al. (1967); and Hanner (1970).

COMPARISON OF THEORY AND OBSERVATION

Most of the observations available for comparison with theoretical models are restricted to the ecliptic plane. Even here there are wide discrepancies among the results of different observers, due in part to the difficulties in correcting for atmospheric scattering and in separating the zodiacal light from the airglow and integrated starlight. These problems have been discussed by Weinberg (1970). The most extensive published data on the distribution of the zodiacal light brightness away from the ecliptic are by Smith, Roach, and Owen (1965). Their observations were made at only one wavelength, so that models that fit their data at 530 nm cannot be tested over a wide wavelength

range. Ingham and Jameson (1968) and Jameson (1970) observed the brightness and polarization at 510 nm in regions away from the ecliptic.

Model calculations indicate that the polarization is a more sensitive discriminant than the intensity in determining the optical properties and size distribution of the dust particles. The maximum observed polarization P_{max} in the ecliptic (about 23 percent at 530 nm) occurs near $\epsilon = 70°$ (Weinberg, 1964). For a reasonably smooth spatial distribution, regardless of the exact form, a maximum near $\epsilon = 70°$ implies a maximum polarization at scattering angles near 90°. On the basis of Mie theory, the maximum polarization occurs near $\theta = 90°$ (and thus $\epsilon = 70°$) only if a significant number of particles have radii on the order of 0.1 μm or less. This is true for both dielectric and metallic particles. For $n(a) \propto a^{-p}$ this means $p \geqslant 4$ and $a_1 \lesssim 0.1$ μm. When the particle size distribution is weighted toward larger radii, Mie theory predicts the following changes:

(1) Metals: P_{max} shifts to smaller scattering angles ($\theta < 90°$).
(2) Ices ($m \sim 1.3$): P_{max} shifts to larger angles ($\theta \sim 130°$ to 150°).
(3) Silicates ($1.5 \leqslant m \leqslant 1.75$): Large amounts of negative polarization occur over a wide range of scattering angles.

Thus, a fit to the observed polarization in the ecliptic plane with a single-component model requires that the scattering particles be predominantly of radius $a \lesssim 0.1$ μm.

Both Giese and Dziembowski (1967) and Aller et al. (1967) found that the single-component model ($m = 1.3$) giving the best fit to the intensity and polarization in the ecliptic did not match the data of Smith, Roach, and Owen away from the ecliptic. Giese and Dziembowski proposed a two-component model consisting of silicates and iron particles, $n(a) \propto a^{-2.5}$. By adjusting the cutoff sizes and the relative concentration of the two components, they were able to produce a polarization maximum near 70° and to improve the fit to the observed brightness perpendicular to the ecliptic.

The presence of negative polarization near the antisolar direction has been discussed by Weinberg and Mann (1968). They find that the polarization reversal occurs near $\epsilon = 165°$ at 508 nm and shifts toward smaller elongation at longer wavelength. Mie theory predicts negative polarization at large scattering angles for dielectric particles less than 1 μm in size consisting of either ices or silicates. The negative polarization extends over a wider range of scattering angles at larger refractive index. For refractive index $m = 1.3$, the appropriate choice of size and spatial distribution can produce a neutral point near $\epsilon = 165°$ at 508 nm. However, for a power-law size distribution, the position of the neutral point shifts to larger ϵ at longer wavelength.

The published observational data have limited coverage in both space and time as well as a limited range in wavelength. In spite of the amount of effort that has been expended in analyzing these observations, very few definitive conclusions can be drawn regarding the physical nature of the dust particles. On the theoretical side, too much emphasis has been placed on adjusting

mathematical parameters to fit a specific idealized model to a limited set of observations. We must take a broader approach and ask what qualitative features can be used to discriminate between different kinds of scattering particles and what observational data will be most valuable for this purpose.

The wavelength dependence of polarization is a critical parameter in determining the size range and physical nature of the dust particles. More extensive data are needed from a good ground-based site, covering the entire sky over a wide range of wavelengths.

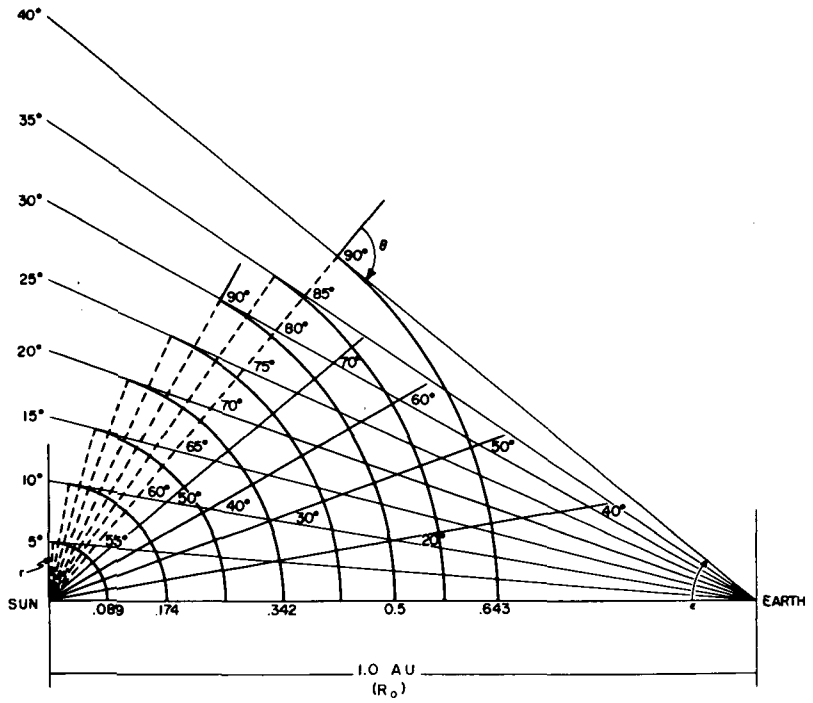

Figure 2.–Variation of scattering angle and solar distance along line of sight as a function of elongation (J. L. Weinberg, personal communication).

Ground-based observations have several limitations, however. Corrections for tropospheric scattering and airglow emission are uncertain. The ultraviolet and infrared spectral regions cannot be observed. Observations outside of eclipse are restricted to $\epsilon \geqslant 30°$. Figure 2 shows the region of space sampled by the line of sight for a series of elongation angles. It can be seen that at $\epsilon = 30°$ we can get no information about the region closer than 0.5 AU to the Sun. It is therefore important to obtain detailed observations from satellites to supplement the ground-based data. The following types of observations are of particular value.

Observations in the Ultraviolet

The scattering properties of small particles depend on the quantity $2\pi a/\lambda$. Thus in the ultraviolet the particles "look" larger, and a better discrimination between different size distributions will be possible. We would expect the $I_\lambda(\epsilon)$ curve to have a steeper slope in the ultraviolet at $\epsilon < 90°$ and the position of maximum in the $P_\lambda(\epsilon)$ curve to shift. Assuming Mie theory provides at least a qualitative indication of the particle scattering properties, we expect the maximum polarization to shift toward larger ϵ if the particles are dielectric (ices or silicates) and toward smaller ϵ if the particles are metallic. The two-component model of Giese and Dziembowski would show a broadened maximum or perhaps a double maximum. Negative polarization may appear either at small angles or near the backscatter direction depending on the particle sizes and refractive index. The larger a/λ also means that effects of shape and surface irregularities will show up more strongly in the ultraviolet.

More fundamentally, many materials have a change in their optical properties in the ultraviolet region (Taft and Philipp, 1965; Field, Partridge, and Sobel, 1967). Thus it is important to search for "signatures" of certain materials by studying the wavelength variation of the intensity and polarization in the ultraviolet. The interstellar extinction curve, for example, shows a bump near 220 nm (Stecher, 1965). The presence of unusual features in the zodiacal light at 220 nm could have interesting implications in relating the interplanetary and interstellar grains.

Observations at Small Elongations

The importance of relating observations of the F corona and the zodiacal light has been stressed by van de Hulst (1947), Blackwell and Ingham (1967), and many others. Observations of the F corona made during eclipse are difficult to relate to zodiacal light data, for almost no data exist in the intervening region. The region at small ϵ is critical for several reasons:

(1) The change in slope of $I_\lambda(\epsilon)$ with λ ($5° \leqslant \epsilon \lesssim 50°$) provides information on the size of the scattering particles.
(2) The amount and direction of polarization, particularly in the ultraviolet, may indicate the nature of the particles because certain materials and certain sizes show negative polarization at small scattering angles.
(3) Comparison of the observed brightness at small ϵ with theoretical models may give information on the extent of a dust-free zone surrounding the Sun (Elsässer, 1970).
(4) Particles close to the Sun may show a change in their optical properties as a result of radiation damage.
(5) The size distribution may be modified by sputtering and vaporization (Singer and Bandermann, 1967).

Simultaneous Satellite and Ground-Based Observations

The large body of ground-based data would become more valuable if accurate methods of correcting for tropospheric scattering and airglow emission can be developed. Simultaneous observations from the ground and from a satellite using similar instruments and wavelength bands can provide direct information on the effects of Earth's atmosphere. Such observations should be carried out over an extended period of time so that effects of variation in airglow emission and possible variations in the zodiacal light can be evaluated.

Infrared Observations

Observations in the infrared at small ϵ can provide information on the thermal properties of the dust particles and the extent of the dust-free zone surrounding the Sun (Peterson, 1963, 1964; Harwit, 1963). Eclipse observations at 2.2 and 3.5 μm have been obtained by Peterson and MacQueen (1967) that show a maximum at 4.0 and a secondary peak at 3.5 solar radii (distance from the center of the Sun). Satellite data can provide more extensive coverage in space and time.

SCATTERING BY IRREGULAR PARTICLES

Many of the theoretical models of the zodiacal light brightness and polarization used to draw conclusions concerning the particle size distribution and composition have been based on the scattering functions for smooth, homogeneous, spherical particles, whereas the dust particles gathered in collection experiments are generally irregular, even fluffy in appearance (Hemenway et al., 1967; Hemenway and Hallgren, 1970; Hemenway et al., 1970). The assumption is implicitly made that an extended size distribution of randomly oriented, irregular particles will scatter light in the same manner as the same size distribution of spheres. There are little experimental data available for particles of size $a \sim \lambda$ with which to test the validity of this assumption.

Donn and Powell (1962) have studied the scattering by a size distribution of zinc oxide crystals, $m = 2.01$, which grow in the form of spikes. They found that the scattering characteristics for a size distribution of such particles could be represented by a distribution of much smaller spheres with $m = 2.01$ or moderately smaller spheres with refractive index as low as 1.2. Their work and other research on irregular particles have been summarized by Powell et al. (1967), who conclude that the scattering by a size distribution of large-volume particles such as cubes can be described by a size distribution of spheres very close to the real size distribution. They find that the angular dependence of the intensity and polarization at different wavelengths can be duplicated by the same distribution of spheres. For small-volume particles such as needles and fourlings, the equivalent size distribution of spheres that matches their data at

one wavelength will not fit at another wavelength. In addition, the sizes of the spheres will be much smaller than the characteristic lengths of the actual particles.

Holland and Gagne (1970) measured the scattering matrix for a polydisperse system of silica particles smaller than 1 μm, $m = 1.55$. Their data for the matrix elements S_{11} and S_{22} at 546 nm are reproduced in figure 3 (Holland, 1969). The solid curve was computed from Mie theory for the observed size distribution. Mie theory fits the data fairly well at small scattering angles, but it predicts a steep rise toward the backscatter direction that is absent in the laboratory data. Data for $S_{12} = S_{21}$ indicate that the polarization is positive at $\theta \lesssim 160°$, whereas Mie theory predicts negative polarization. There is, however, an indication that the polarization changes sign near 160° at 546 nm and near 150° at 486 nm. The position of the neutral point varies with wavelength in the opposite direction from the shift observed by Weinberg and Mann in the zodiacal light.

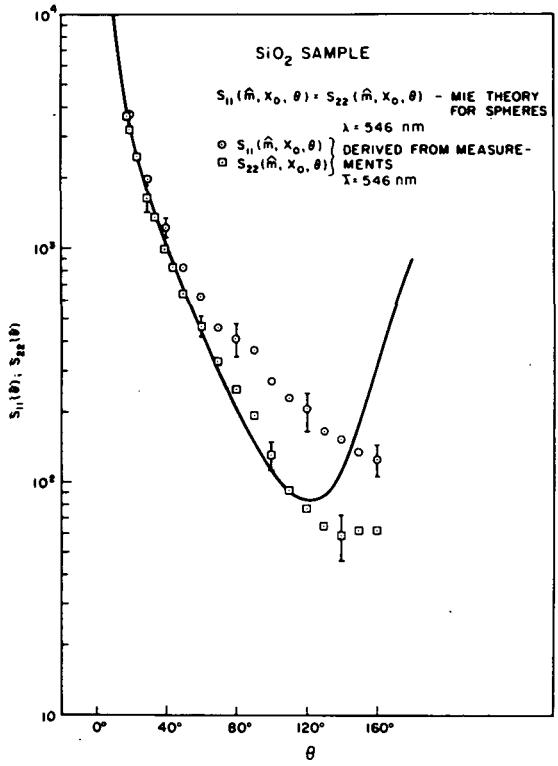

Figure 3.–Variation of matrix elements $S_{11}(\theta)$ and $S_{22}(\theta)$ with scattering angle θ. Solid line is theoretical curve computed from Mie theory (Holland, 1969, fig. 6). $\hat{m}$ = refractive index; X_0 = size distribution parameter.

The scattering properties of nonspherical particles also can be studied by microwave scattering from scaled particle models (Greenberg, Pedersen, and Pedersen, 1961). Greenberg, Wang, and Bangs (1971) have found that the measured extinction for particle models with roughened surfaces differs widely from the extinction by smooth spheres. Microwave scattering data over the whole range of scattering angles for many values of a/λ are needed before we can conclude whether the peculiar scattering patterns observed for individual particles average out to resemble scattering by spheres over an extended size distribution.

Scattering functions can be computed analytically for the case of long cylinders (Kerker, 1969; Lind, 1966). Detailed comparison of the scattering functions for spheres and cylinders, and possibly ellipsoids, can provide useful information on the effects of particle shape. For example, there is a significant change in the polarization, even for an extended size distribution, when the angle between the cylinder axis and the incident radiation is varied. However, the polarization by randomly oriented cylinders with $n(a) \propto \exp[-5(a/0.5)^3]$ was quite similar to that for spheres with the same size distribution (Hanner, 1969).

The limitations of Mie theory and the importance of computing zodiacal light models for nonspherical particles have been emphasized by Greenberg (1970). Richter (1966) has discussed experimental phase functions and polarization curves for irregular particles over the size range 10^{-6} to 10 cm.

CONCLUSION

The zodiacal light data sample the average properties of the interplanetary dust particles over a large volume of space. Intensity and polarization measurements in the ultraviolet and infrared, together with the wavelength dependence of polarization throughout the visible spectral region, will provide information on the physical nature and size distribution of the dust particles. However, we cannot expect to obtain a complete model of the interplanetary dust from zodiacal light observations alone. The data will be most valuable when combined with the results of particle collections and other methods used to study in detail the physical properties of individual particles.

Giese and Dziembowski (1969) and Giese (1970) have discussed the value of zodiacal light observations from space probes in determining the spatial distribution of the interplanetary dust. Zodiacal light experiments will be included on both the Helios inner solar system probes and the Pioneer F and G asteroid-Jupiter probes.

ACKNOWLEDGMENTS

It is a pleasure to thank Dr. J. L. Weinberg for his interest and his helpful discussions. This research has received support from NSF grant GA-12400 and NASA grant NGR 33-017011.

REFERENCES

Allen, C. W. 1946, The Spectrum of the Corona at the Eclipse of 1940 October 1. Mon. Notic. Roy. Astron. Soc. **106**, 137.

Aller, L. H., Duffner, G., Dworetsky, M., Gudehus, D., Kilston, S., Leckrone, D., Montgomery, J., Oliver, J., and Zimmerman, E. 1967, Some Models of the Zodiacal Cloud. The Zodiacal Light and the Interplanetary Medium (ed., J. L. Weinberg), pp. 243-256. NASA SP-150.

Bandermann, L. W. 1968, Physical Properties and Dynamics of Interplanetary Dust. Ph. D. Thesis. Univ. of Maryland.

Blackwell, D. E., Dewhirst, D. W., and Ingham, M. F. 1967, The Zodiacal Light. Advances in Astronomy and Astrophysics (ed., Z. Kopal), vol. 5, p. 1. Academic Press, Inc. New York.

Blackwell, D. E., and Ingham, M. F. 1967, Toward a Unification of Eclipse and Zodiacal-Light Data. The Zodiacal Light and the Interplanetary Medium (ed., J. L. Weinberg), pp. 17-21. NASA SP-150.

Blackwell, D. E., Ingham, M. F., and Petford, A. D. 1967, The Distribution of Dust in Interplanetary Space. Mon. Notic. Roy. Astron. Soc. **136**, 313.

Donn, B., and Powell, R. S. 1962, Angular Scattering From Irregularly Shaped Particles With Application to Astronomy. Electromagnetic Scattering (ed., M. Kerker), p. 151. Pergamon Press, Inc. New York.

Elsässer, H. 1963, The Zodiacal Light. Planet. Space Sci. **11**, 1015.

Elsässer, H. 1970, The Zodiacal Light: Space Observations. Space Research X. (eds., T. M. Donahue, P. A. Smith, and L. Thomas), p. 244. North-Holland Pub. Co. Amsterdam.

Elsässer, H., and Schmidt, T. 1966, Rayleigh-Teilchen ($a < 10^{-5}$ cm) im interplanetaren Raum? Z. Naturforsh. A **21**, 1116.

Field, G. B., Partridge, R. B., and Sobel, H. 1967, Effects of Absorption Spectra of Ices on the Ultraviolet Extinction by Interstellar Grains. Interstellar Grains (ed., J. M. Greenberg and T. P. Roark), p. 207. NASA SP-140.

Giese, R. H. 1961, Streuung elektromagnetischer Wellen an absorbierenden und dielektrischen Kugelförmigen Einzelteilchen und an Gemischen solcher Teilchen. Z. Astrophys. **51**, 119.

Giese, R. H. 1963, Light Scattering by Small Particles and Models of Interplanetary Matter Derived From the Zodiacal Light. Space Sci. Rev. **1**, 589.

Giese, R. H. 1970, Model Computations Concerning Zodiacal Light Measurements by Space Missions. Paper presented at COSPAR, 13th meeting (Leningrad).

Giese, R. H., and Dziembowski, C. v. 1967, On Optical Models Approximating Observations of the Zodiacal Light Outside the Ecliptic. The Zodiacal Light and the Interplanetary Medium (ed., J. L. Weinberg), pp. 271-276. NASA SP-150.

Giese, R. H., and Dziembowski, C. v. 1969, Suggested Zodiacal Light Measurements From Space Probes. Planet. Space Sci. **17**, 949.

Giese, R. H., and Siedentopf, H. 1962, Optische Eigenschaften von Modellen der interplanetaren Materie. Z. Astrophys. **54**, 200.

Greenberg, J. M. 1970, Models of the Zodiacal Light. Space Research X (eds., T. M. Donahue, P. A. Smith, and L. Thomas), p. 225. North-Holland Pub. Co. Amsterdam.

Greenberg, J. M., Pedersen, N. E., and Pedersen, J. C. 1961, Microwave Analog to the Scattering by Nonspherical Particles. J. Appl. Phys. **32**, 233.

Greenberg, J. M., Wang, R. T., and Bangs, L. 1971, Extinction by Rough Particles and the Use of Mie Theory. Nature (London) Phys. Sci. **230**, 110-112.

Hanner, M. S. 1969, Light Scattering in Reflection Nebulae. Ph. D. Thesis. Rensselaer Polytechnic Institute.

Hanner, M. S. 1970, Zodiacal Light Models Based on Scattering by Silicate Particles. Paper presented at Amer. Astron. Soc. Meeting (Boulder, Colo.).

Harwit, M. 1963, Infrared Appearance of Different Zodiacal Light Cloud Models. Paper presented at the 12th Int. Colloq. Astrophys. Inst. (Liege, Belgium).

Hemenway, C. L., and Hallgren, D. S. 1970, Time Variation of the Altitude Distribution of the Cosmic Dust Layer in the Upper Atmosphere. Space Research X (ed., T. M. Donahue, P. A. Smith, and L. Thomas), p. 272. North-Holland Pub. Co. Amsterdam.

Hemenway, C. L., Hallgren, D. S., and Coon, R. E. 1967, High Altitude Balloon-Top Collections of Cosmic Dust. Space Research VII (ed., R. L. Smith-Rose), p. 1423. North-Holland Pub. Co. Amsterdam.

Hemenway, C. L., Hallgren, D. S., Laudate, A. T., Patashnick, H., Renzema, T. S., and Griffith, O. K. 1970, A New High Altitude Balloon-Top Cosmic Dust Collection Technique. Paper presented at COSPAR, 13th meeting (Leningrad).

Holland, A. C. 1969, The Scattering of Polarized Light by Polydisperse Systems of Irregular Particles. NASA TN D-5458.

Holland, A. C., and Gagne, G. 1970, The Scattering of Polarized Light by Polydisperse Systems of Irregular Particles. Appl. Opt. 9, 1113.

Hulst, H. C., van de. 1947, Zodiacal Light in the Solar Corona. Astrophys. J. 105, 471.

Hulst, H. C., van de. 1957, Light Scattering by Small Particles. John Wiley & Sons, Inc. New York.

Ingham, M. F. 1961, Observations of the Zodiacal Light From a Very High Altitude Station IV. The Nature and Distribution of the Interplanetary Dust. Mon. Notic. Roy. Astron. Soc. 122, 157.

Ingham, M. F., and Jameson, R. F. 1968, Observations of the Polarization of the Night Sky and a Model of the Zodiacal Cloud Normal to the Ecliptic Plane. Mon. Notic. Roy. Astron. Soc. 140, 473.

Jameson, R. F. 1970, Observations and a Model of the Zodiacal Light. Mon. Notic. Roy. Astron. Soc. 150, 207.

Kerker, M. 1969, The Scattering of Light and Other Electromagnetic Radiation. Academic Press, Inc. New York.

Lind, A. C. 1966, Resonance Electromagnetic Scattering by Finite Circular Cylinders. Ph. D. Thesis. Rensselaer Polytechnic Institute.

Little, S. J., O'Mara, B. J., and Aller, L. H. 1965, Light Scattering by Small Particles in the Zodiacal Cloud. Astron. J. 70, 346.

Peterson, A. W. 1963, Thermal Radiation From Interplanetary Dust. Astrophys. J. 138, 1218.

Peterson, A. W. 1964, Thermal Radiation From Interplanetary Dust II. Distribution of the Dust. Ann. N.Y. Acad. Sci. 119, 72.

Peterson, A. W., and MacQueen, R. M. 1967, Infrared Observations of Thermal Radiation From Interplanetary Dust at the Eclipse of November 12, 1966 (abstract). The Zodiacal Light and the Interplanetary Medium (ed., J. L. Weinberg), p. 89. NASA SP-150.

Powell, R. S., Woodson, P. E., III, Alexander, M. A., Circle, R. R., Konheim, A. G., Vogel, D. C., and McElfresh, T. W. 1967, Analysis of all Available Zodiacal Light Observations. The Zodiacal Light and the Interplanetary Medium (ed., J. L. Weinberg), pp. 225-241. NASA SP-150.

Richter, N. B. 1966, The Photometric Properties of Interplanetary Matter. Quart. J. Roy. Astron. Soc. 3, 179.

Singer, S. F., and Bandermann, L. W. 1967, Nature and Origin of Zodiacal Light. The Zodiacal Light and the Interplanetary Medium (ed., J. L. Weinberg), p. 379. NASA SP-150.

Smith, L. L., Roach, F. E., and Owen, R. W. 1965, The Absolute Photometry of the Zodiacal Light. Planet. Space Sci. 13, 207.

Stecher, T. P. 1965, Interstellar Extinction in the Ultraviolet. Astrophys. J. 142, 1683.

Taft, E. A., and Philipp, H. R. 1965, Optical Properties of Graphite. Phys. Rev. 138A, 197.

Weinberg, J. L. 1964, The Zodiacal Light at 5300Å. Ann. Astrophys. 27, 718.
Weinberg, J. L., 1970, Current Problems in the Zodiacal Light. Space Research X (eds., T. M. Donahue, P. A. Smith, and L. Thomas), p. 233. North-Holland Pub. Co. Amsterdam.
Weinberg, J. L., and Mann, H. M. 1968, Negative Polarization in the Zodiacal Light. Astrophys. J. 152, 665.

DISCUSSION

BANDERMANN: Purely photometric, spectroscopic, polarimetric observations of the zodiacal light will not lead to definite answers about the physical properties of the particles. One must try to consider *all* the different types of evidences (zodiacal light as well as impact counts, deep sea sediments, etc.) and then look for collaboration toward an answer.

ON THE AMOUNT OF DUST IN THE ASTEROID BELT

FRED L. WHIPPLE
Smithsonian Astrophysical Observatory
and
Harvard College Observatory

Calculations of upper limits to the quantity of small particles in the asteroid belt are based on (1) the brightness of the counterglow coupled with observations and theory for the zodiacal cloud near Earth's orbit and (2) the destruction and erosion of asteroidal particles as they spiral toward the Sun because of solar radiation via the Poynting-Robertson effect. These calculations place the likely upper limit on asteroidal space particle density at the order of 5 to 10 times and the hazard to space vehicles at 2 to 4 times those near Earth's orbit. No such evidence indicates, however, that the hazard from small particles is actually much greater in the asteroid belt.

Observations near Earth, coupled with theory, can provide some upper limits to the quantity of small particles in the asteroid belt, which may possibly be hazardous to space vehicles venturing into that region. Measures of the counterglow and the zodiacal cloud of particles in the neighborhood of Earth's orbit provide a basis for one such limit. The destruction or erosion of particles by impact as they spiral from the asteroid belt inward toward the Sun under the influence of solar radiation by the Poynting-Robertson effect provide another limiting calculation. These limits are discussed in the sections that follow.

THE COUNTERGLOW

The brightness of the counterglow limits the quantity of dust that may be present in the asteroid belt. Roosen (1969, 1971)[1] shows that the counterglow cannot arise from any source within a million or so kilometers of the Earth because of the Earth's shadow in sunlight on backscattering particles. His observations indicate that the counterglow reaches a peak intensity exactly at the antisolar point in the plane of the ecliptic (Earth's orbit) and not in the fundamental plane of the solar system where the asteroids tend to move. This fact weakens his conclusion that the light of the counterglow is reflected from the asteroid belt and not from the zodiacal cloud, which provides the fine material we observe as meteoritic dust near Earth and meteors in Earth's atmosphere.

[1]Also see p. 363.

Roosen does not discuss the backscattering properties of dust but it is well known that rough materials tend to have peak reflection at exactly 180° backscatter. It follows from simple diffraction optics that the counterglow peak cannot be filled by particles of diameter much less than 100 μm (some 200 wavelengths of visual light) for a peak of diameter ¼° to ½°.

From the distribution of particle sizes in the zodiacal cloud (Whipple, 1967) derived from space probes and meteors, we can calculate the effective surface area for backscatter. The derived space density near Earth's orbit is some 2×10^{-22} g-cm^{-3} and the flux on the surface of a nongravitating sphere is 1.6×10^{-16} g-cm^{-2}-s^{-1}. Integrating the apparent area of the particles πs^2, where s is the radius, for $s > 50\ \mu$m, I find the apparent area per unit volume for zodiacal particles near Earth,

$$A_0 = 1.3 \times 10^{-20}\ \text{cm}^{-1}$$

The effective fractional area for backscattering of sunlight, referred to total reflection near Earth, becomes

$$\text{effective area} = \int_{R=0}^{\infty} A_0 \left(\frac{R_0}{R_0 + R} \right)^{2+n} dR \qquad (1)$$

where R_0 = 1 AU, R = distance from Earth, and n represents the inverse power law of zodiacal cloud density with solar distance r, or r^{-n}.

The total effective fractional area for reflection in the antisolar direction then becomes $A_0 R_0 (1+n)^{-1}$ for $n \geqslant 0$. Let us then assume that the density of the zodiacal cloud falls off as r^{-1}, inversely as the solar distance. The total effective fractional area of the zodiacal cloud becomes $A_0 R_0/2$ or 0.97×10^{-7}, compared to a perfect backscattering surface near Earth.

Let us further assume that the zodiacal particles backscatter like the average surface of the Moon. The apparent visual magnitude of the Moon at opposition is -12.70 mag (Allen, 1963), covering an area of 0.212 deg^2, or -14.38 mag-deg^{-2}. Our calculated effective fractional area at 1 AU of 0.97×10^{-7} corresponds to a magnitude loss of 17.5 mag, bringing the apparent surface brightness calculated for the counterglow to

$$17^{\text{m}}.5 - 14^{\text{m}}.4 = +3^{\text{m}}.1\ \text{deg}^{-2}$$

or 580 tenth magnitude stars per square degree, 1.1 mag brighter than the commonly adopted value of 200 10 mag stars deg^{-2}.

First note that the meteoritic flux rate of 1.6×10^{-16} g-cm^{-2} is confirmed by Keays et al. (1970) and Ganapathy et al. (1970) by analysis of trace elements on the Moon, their values being, respectively, 1.2×10^{-16} and 1.3×10^{-16} g-cm^{-2}. The use of their mean value coupled with our

distribution function would reduce the discrepancy by only 0.3 mag. The adopted mean velocity of 15 $km\text{-}s^{-1}$ is a reasonable velocity with which to correct to space density, even though the value is not precisely measured.

That zodiacal particles backscatter like the Moon is, of course, an ad hoc hypothesis. As cometary debris they should be porous and perhaps even darker than surface lunar material. Thus our fair success in predicting the brightness of the counterglow suggests strongly, at least, that few additional reflective sources are needed; perhaps none are needed.

Thus the asteroid belt need contain only enough dust to produce, say, one-half the light in the counterglow, or perhaps a negligible amount. At a mean solar distance of some 2.5 AU the surface brightness for the same reflective area would be reduced by a factor of 6.2. If the asteroid belt is 1 AU thick at the same space reflectivity as zodiacal dust near Earth, the reduction factor for the reflective area would increase by a factor of about 2 as compared to our calculations above. The presumed higher density of asteroid dust, say 3.0 $g\text{-}cm^{-3}$ as compared to perhaps 0.5 $g\text{-}cm^{-3}$ for cometary dust, would increase the corresponding mass by a factor of 3.0/0.5 = 6. The albedo of asteroid dust would surely exceed that of cometary dust, but the factor is unknown. Let us call it 2.

If we combine the factors of the last paragraph to predict the density of meteoritic material in the asteroid belt, averaged over a 1 AU radial distance to produce ½ the light of the counterglow, we find the factors ½ (brightness), 6.2 (distance), ½ (for 1 AU), 6 (density), and ½ (albedo), assuming the same distribution function of particle size as for the zodiacal cloud. Thus we should not expect the asteroid belt to exceed near-Earth space in particle mass by a factor of more than about 5, leading to a space density $< 1.0 \times 10^{-21}$ $g\text{-}cm^{-3}$. The Poynting-Robertson effect of solar radiation momentum exchange with small particles in the asteroid belt should tend to bring in the dust from the major concentration of asteroids and to reduce this maximum calculated density.

SPACE EROSION AND THE POYNTING-ROBERTSON EFFECT

As the Poynting-Robertson effect (Robertson, 1937) causes asteroidal particles to spiral in toward the Sun, space erosion from particle impacts in space will tend to destroy and to reduce the radii of the asteroidal particles. For convenience let us express the space erosion in terms of reduction in radius of the particles

$$\frac{ds}{dt} = -\frac{\epsilon}{r^2} \tag{2}$$

where ϵ is the erosion rate in centimeters per year at Earth's orbit and r is the solar distance measured in astronomical units. The r^2 term arises from an assumed falloff of particle density as r^{-1} and velocity of impact as $r^{-1/2}$.

The Poynting-Robertson effect differentiated gives for the time dt (years) to reduce a circular orbit of radius vector r AU by dr the equation

$$dt = -2C\rho s r\, dr \tag{3}$$

where $C = 0.7 \times 10^7$ to give t in years, ρ is particle density in grams per cubic centimeter, and the spherical radius s is given in centimeters.

Equations (2) and (3) combine to give

$$\frac{ds}{s} = 2C\epsilon\rho \frac{dr}{r} \tag{4}$$

The lunar landings give values for ϵ at the lunar surface from nuclear track studies by Crozaz et al. (1970),

$$1 \times 10^{-8} < \epsilon < 10 \times 10^{-8} \text{ cm-yr}^{-1}$$

and from micrometeoritic craters by Hörz, Hartung, and Gault (1970),

$$2 \times 10^{-8} < \epsilon < 4 \times 10^{-8} \text{ cm-yr}^{-1}$$

The suggested value of

$$\epsilon = 3 \times 10^{-8} \text{ cm-yr}^{-1}$$

is considerably smaller than that adopted by the author (Whipple, 1967) from the cosmogenic ages of stony meteorites. The actual value for a particle in space should, indeed, be greater than that for lunar rocks because the latter are partially protected by a thin layer of dust from the smallest particles of the zodiacal cloud.

Let us, however, adopt as a minimum erosion rate in space the values

$$\epsilon = 3 \times 10^{-8} \text{ cm-yr}^{-1}$$

$$C = 0.7 \times 10^7 \text{ yr}$$

$$\rho = 3 \text{ g-cm}^{-3}$$

to derive from equation (4) the numerical result

$$\frac{ds}{s} > 1.3 \frac{dr}{r} \tag{5}$$

Hence from equation (5) an asteroid particle released in circular orbit at $r = 2.5$ AU would be reduced to less than 1/6 in radius and less than 1/200 in mass by the time it had reached Earth's orbit. Its surface area would have been reduced to less than 1/30 of its original value. Thus we see that an assumed

total particle space density in the asteroid belt of five times that in the near-Earth zodiacal cloud would be reduced to $5 \times (2.5)^3 \times 0.005$ or <0.4 the total space density of the zodiacal cloud by the time the particles reached Earth's orbit. Thus it seems quite possible that the hazard to a space vehicle from small meteoritic particles might exceed that near Earth's orbit by a factor of 5 or 10 for mean space density, reduced by a factor of 1/2.5 for velocity, or two to four times greater.

The minimal hazard from larger particles, capable of producing serious damage but not contributing significantly to the zodiacal cloud, might be somewhat greater in the asteroid belt than near Earth's orbit, but not by a large factor. Calculations for these larger particles should be based on Dohnanyi's (1967, 1969, and 1970)[2] thorough study of the theoretical distribution function for asteroidal bodies.

REFERENCES

Allen, C. W. 1963, Astrophysical Quantities, p. 145. Athlone Press. Univ. of London.

Crozaz, G., Haack, U., Hair, M., Maurette, M., Walker, R., and Woolum, D. 1970, Nuclear Track Studies of Ancient Solar Radiations and Dynamic Lunar Surface Processes. Proc. Apollo 11 Lunar Sci. Conf. Geochim. Cosmochim. Acta **34**, Suppl. 1, vol. 3, pp. 2051-2080.

Dohnanyi, J. S. 1967, Mass Distribution of Meteors. Astrophys. J. **149**, 735-737.

Dohnanyi, J. S. 1969, Collisional Model of Asteroids and Their Debris. J. Geophys. Res. **74**, 2531-2554.

Dohnanyi, J. S. 1970, On the Origin and Distribution of Meteoroids. J. Geophys. Res. **75**, 3468-3493.

Ganapathy, R., Keays, R. R., and Anders, E. 1970, Apollo 12 Lunar Samples: Trace Element Analysis of a Core and the Uniformity of the Regolith. Science **170**, 533-535.

Hörz, F., Hartung, J. B., and Gault, D. E. 1970, Micrometeorite Craters on Lunar Rock Surfaces. Lunar Sci. Inst. Contrib. no. 9.

Keays, R., Ganapathy, R., Laul, J. C., Anders, E., Herzog, G. F., and Jeffery, P. M. 1970, Trace Elements and Radioactivity in Lunar Rocks: Implications for Meteorite Infall, Solar-Wind Flux and Formation Conditions of Moon. Science **167**, 490-493.

Robertson, H. P. 1937, Dynamical Effects of Radiation on the Solar System. Mon. Notic. Roy. Astron. Soc. **97**, 423-438.

Roosen, R. G. 1969, The Gegenschein. Doctoral Dissertation, Univ. of Texas.

Roosen, R. G. 1971, Earth's Dust Cloud. Nature **229**, 478-480.

Whipple, F. L. 1967, On Maintaining the Meteoritic Complex. The Zodiacal Light and the Interplanetary Medium (ed., J. L. Weinberg), NASA SP-150, pp. 409-426.

[2]Also see p. 263.

Page intentionally left blank

ARE METEORS A TOOL FOR STUDYING THE ASTEROIDS? OR VICE VERSA?

R. E. McCROSKY
Smithsonian Astrophysical Observatory

The bulk of the comments I made at the colloquium are to be found in two recent papers (McCrosky and Ceplecha, 1970; McCrosky et al., 1971). The following summary is offered in place of a full text.

Most interpretations of all meteor data rely on knowledge of the relationship (luminous efficiency) between mass and luminosity. Discussions of recent experiments made to determine the luminous efficiency are found in papers by Ayers et al. (1970) and Becker and Friichtenicht (1971). Faint meteor phenomena can be understood if the meteoroids are weak, low-density ($\rho_m \approx 0.25$ g/cm^3) "fluff balls" such as can be expected on the basis of Whipple's comet model (Jacchia, 1955; Jacchia et al., 1967). Alternative explanations, not requiring low densities, have been offered. Jones and Kaiser (1966) propose thermal shock of strong, high-density material as a fragmentation mechanism. Allen and Baldwin (1967) and Baldwin and Allen (1968) have reanalyzed Jacchia's data in terms of phenomena observed in the laboratory in simulated reentry experiments. Here, a high-density meteoroid froths and thereafter behaves as a low-density body. They also revise the luminosity law to account for blackbody radiation of refractory material. McCrosky and Ceplecha (1970) show that neither of these alternative explanations can apply to large bodies and, using photographic observations of bright fireballs, they defend Jacchia's original proposal for all meteors.

The mechanism for producing *large*, low-density meteoroids is unknown. The comet model places limits on the size of the body that can be carried away by comet outgassing. Whipple (1967) suggests that large, weak material might be of asteroidal origin ("half-baked" asteroids) and perhaps closely related to, or equivalent to, carbonaceous chondrites. However, Ceplecha (1968) shows that among the small bodies there exist at least two classes, A and C, distinguishable from the observations. Class C is apparently of lower density. Class A might be similar to carbonaceous chondrites (McCrosky and Ceplecha, 1970). Members of both classes are clearly associated with comets through comet-meteor shower associations. Cook (1970) expands Ceplecha's analysis and finds evidence that class A material comes from old comets or comet interiors whereas class C is the material from the outer shell.

The analysis of the in-flight photographic data of the recovered meteorite, Lost City, by McCrosky et al. (1971) points out the possibility of the substantial errors in previous density determinations if bodies of the flattened shape of Lost City are common. It is not reasonable, however, to use this argument to explain every case of fireballs that seem to have structures or densities unlike meteorites.

The most accurate and/or most comprehensive list of orbits for photographic meteors are presented in the following papers: for faint meteors, papers by Jacchia and Whipple (1961), Hawkins and Southworth (1961), and McCrosky and Posen (1961); for orbits of meteors of intermediate brightness, Whipple (1954); and for fireballs, McCrosky (1968). However, the reader should also see Kresák (1970) for discussion of possible important observational biases in these data. The half dozen cases known to be high-density material (asteroidal) or with flight characteristics thought to be appropriate for such material are given, with references, in McCrosky et al. (1971).

The problem of producing Earth-crossing orbits for asteroidal material is left to another speaker. The question of whether such material is evident among photographic meteors has most recently been extensively discussed by Kresák (1969). Convincing arguments are used to divide the meteors into pure cometary (II) and cometary plus asteroidal (I) groups. Kresák proposes certain evolutionary tracks (due to Jupiter perturbation, collision, or radiation pressure) from asteroidal orbits to Earth-crossing orbits and investigates group I meteors for statistically significant subgroups compatible with this evolution. A number of unexpected and unexplained relationships emerge but none can be immediately applied as a criterion for asteroidal origin. Either it is not yet possible to formulate the problem sufficiently well or the group I orbits are heavily contaminated by material of cometary origin.

REFERENCES

Allen, H. J., and Baldwin, B. S., Jr. 1967, Frothing as an Explanation of the Acceleration Anomalies of Cometary Meteors. J. Geophys. Res. 72, 3483-3496.

Ayers, W. G., McCrosky, R. E., and Shao, C.-Y. 1970, Photographic Observations of 10 Artificial Meteors. Smithson. Astrophys. Observ. Spec. Rept. 317.

Baldwin, B. S., Jr., and Allen, H. J. 1968, A Method for Computing Luminous Efficiencies From Meteor Data. NASA TN D-4808.

Becker, D. G., and Friichtenicht, J. F. 1971, Measurement and Interpretation of the Luminous Efficiencies of Iron and Copper Simulated Micrometeors. Astrophys. J. 166, 699-716.

Ceplecha, Z. 1968, Discrete Levels of Meteor Beginning Height. Smithson. Astrophys. Observ. Spec. Rept. 279.

Cook, A. F. 1970, Discrete Levels of Beginning Height of Meteors in Streams. Smithson. Astrophys. Observ. Spec. Rept. 324.

Hawkins, G. S., and Southworth, R. B. 1961, Orbital Elements of Meteors. Smithson. Contrib. Astrophys. 4(3), 85-95.

Jacchia, L. G. 1955, The Physical Theory of Meteors. VIII Fragmentation as Cause of the Faint-Meteor Anomaly. Astrophys. J. 121, 521-527.

Jacchia, L. G., Verniani, F., and Briggs, R. E. 1967, An Analysis of the Atmospheric Trajectories of 413 Precisely Reduced Photographic Meteors. Smithson. Contrib. Astrophys. 10(1), 1-139.

Jacchia, L. G., and Whipple, F. L. 1961, Precision Orbits of 413 Photographic Meteors. Smithson. Contrib. Astrophys. 4(4), 97-129.

Jones, S., and Kaiser, T. R. 1966, The Effects of Thermal Radiation, Conduction and Meteoroid Heat Capacity on Meteoric Ablation. Mon. Notic. Royal Astron. Soc. 133, 411-420.

Kresák, L. 1969, The Discrimination Between Cometary and Asteroidal Meteors. I. The Orbital Criteria. II. The Orbits and Physical Characteristics of Meteors. Bull. Astron. Inst. Czech. 20, 177-188, 231-251.

Kresák, L. 1970, On the Orbits of Bright Fireballs. Bull. Astron. Inst. Czech. 21, 1-9.

McCrosky, R. E. 1968, Orbits of Photographic Meteors. Physics and Dynamics of Meteors (eds., L. Kresák and P. M. Millman), pp. 265-279. D. Reidel. Dordrecht.

McCrosky, R. E., and Ceplecha, Z. 1970, Fireballs and the Physical Theory of Meteors. Bull. Astron. Inst. Czech. 21, 271-296.

McCrosky, R. E., and Posen, A. 1961, Orbital Elements of Photographic Meteors. Smithson. Contrib. Astrophys. 4(2), 15-84.

McCrosky, R. E., Posen, A., Schwartz, G., and Shao, C.-Y. 1971, Lost City Meteorite–Its Recovery and Comparison With Other Fireballs. J. Geophys. Res. 76(17), 4090-4108.

Whipple, F. L. 1954, Photographic Meteor Orbits and Their Distribution in Space. Astron. J. 59, 201-217.

Whipple, F. L. 1967, On Maintaining the Meteoritic Complex. The Zodiacal Light and the Interplanetary Medium (ed., J. L. Weinberg), pp. 409-426. NASA SP-150. (Also Smithson. Astrophys. Observ. Spec. Rept. 239.)

DISCUSSION

KENKNIGHT: If you were to heat the outside layer of a meteorite, would it not tend to break up at lower stresses? Furthermore, are not the remnants we test in the lab anomalously strong because they have endured the atmospheric entry forces?

McCROSKY: Thermal inertia and ablation govern the heating of a meteorite. The characteristic depth of heating–the depth at which the temperature decreases by $1/e$–is a few millimeters. This temperature gradient does induce a tensile stress in the center of the body, but it cannot cause the breakup of large bodies.

As to your second question, I agree entirely that the atmosphere introduces a selection effect. However, the degree of atmospheric crushing required to produce the anomalous deceleration in meteors is, I think, unreasonable. In many cases the body must be broken into hundreds or thousands of fragments high in the atmosphere.

Page intentionally left blank

THE MARTIAN SATELLITES

S. FRED SINGER
Department of the Interior

The Martian satellites are some of the most interesting and accessible objects in the solar system, and therefore worth studying or even visiting. As small bodies, on the order of kilometers in diameter (see table I), they may have experienced no internal heating or volcanism, and could therefore be original condensations in the solar system. They may thus be the only remnants of the original planetesimals.

An additional point of interest is that they are the only satellites in the inner part of the solar system—Earth's Moon is generally assumed to be a sister planet. As such, their study could illuminate one of the important differences between the inner and outer parts of the solar system.

Let us assume first that Phobos and Deimos were formed when Mars was formed, that they constitute original planetesimal material, that their orbits have not changed. The orbits are nearly circular and equatorial, like those of many satellites of the outer planets. Kuiper (1956) has also pointed to certain regular relations between satellite masses and distances.

However, we note some peculiarities. First, that Deimos is located at 6.9 Martian radii, which is just beyond the synchronous orbit limit of Mars. We also note that Phobos is located at 2.8 Martian radii, which is just near the Roche limit.

We may therefore consider the alternative possibility that Phobos and Deimos are captured planetesimals, asteroids (i.e., fragments of larger bodies), or captured cometary nuclei. Any of these three possibilities would give us a valid reason for direct examination of the Martian satellites. But how were they captured? Clearly not in an initially dense atmosphere that then conveniently disappeared. This would not explain why the inclinations are so close to zero. This leaves tidal capture followed by tidal evolution as a distinct possibility.

If we start with the present orbits and calculate the orbits backward in time using a tidal perturbation in which the bulge position depends in magnitude and *sign* on the relative angular velocity of the satellite and of Mars, we obtain results that suggest that both Phobos and Deimos started with highly eccentric orbits and might have been captured (Singer, 1968). It is interesting to note in figure 1 that the orbital evolution of an original parabolic orbit can proceed

TABLE I.–*Properties of Martian Satellites*

Satellites	Observed quantities				
	Distance from Mars at mean opposition	Sidereal period	i	e	Visual magnitude (at opposition)
Phobos	9 400 km 25″	$0^d.319$	1°.8	0.019	11.5
Deimos	23 500 km 1′2″	$1^d.262$	1°.4	.003	13.0

Satellites	Derived quantities					
	Radius, km	Mass,[a] g	Orbital velocity, km/s	Orbital period, hr	Surface gravity, cm/s^2	Escape velocity, cm/s
Phobos	8	7.16×10^{18}	2.14	7.65	0.745	1100
Deimos	4	8.96×10^{17}	1.35	30.6	.372	550

NOTE.–*Some characteristics for the planet Mars* (Öpik, 1962): radius, 3310 km; density, 4.23 g/cm^3; mass, 10.7 percent of that of Earth; surface gravity, 390 cm/s^2; escape velocity, 5.1 km/s; and rotation period, 24^h37^m.

[a]Assumed density = 3.34 g/cm^3.

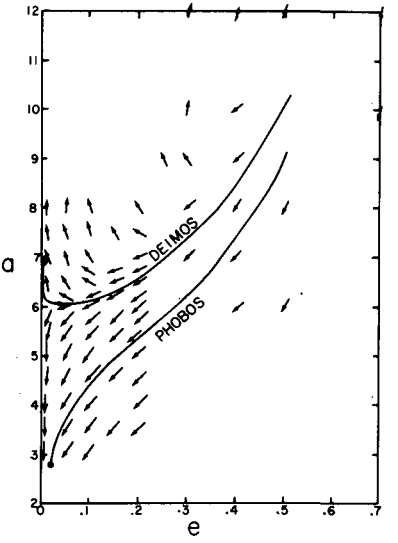

Figure 1.–Orbit evolution, due to tidal forces, of the Martian satellites Phobos and Deimos plotted in a, e space. At present, Phobos has a semimajor axis of 2.8 Mars radii and an eccentricity of 0.019 and Deimos has a semimajor axis of 6.9 Mars radii and an eccentricity of 0.003. The arrows are plotted so that $\tan \Theta = (da/dt)/(de/dt)$. Starting with orbits of large a and e, evolution proceeds toward smaller values. An interesting bifurcation phenomenon develops leading to satellites of the Deimos class spiraling outward and of the Phobos class spiraling inward. The calculations were performed to illustrate an extension of classical tidal theory in which dissipation is taken to be frequency dependent.

either toward a Phobos-type orbit, which must then shrink into the planet, or toward a Deimos-type orbit, which will be permanently captured.

Unfortunately, however, tidal capture is quite improbable for objects of the small mass of Deimos and Phobos, and, further, the time scale of evolution is of the order of 30 billion yr and therefore much too long. One way of overcoming these objections would be to assume extremely large internal dissipation for Mars, but that does not seem realistic. Or we could assume that Phobos and Deimos were initially much more massive objects and therefore more easily captured, and that they lost their mass gradually or more recently. Perhaps the most likely explanation is that Mars captured into a prograde orbit a large object, either a comet or a solid object, that through tidal evolution soon crashed into the surface of Mars. But before the crash, Phobos and Deimos were split off and they still survive. Phobos, however, may not survive for much more than 10 million yr.

This suggestion would solve the capture problem and time-scale problem as well. More calculations are needed and will be carried out in the near future. A great advantage of this explanation is that it is consistent with an origin of

Earth's Moon by capture (Singer, 1968), and also with the nearly zero angular momentum of Venus explained by capture of a moon into a retrograde orbit (Singer, 1970). In general, these suggestions fit in well with Urey's picture of the existence of many moon-sized bodies in the inner solar system (Urey, 1952).

One might like to verify the suggestion advanced here in three different ways: (1) by direct examination of the satellites, (2) by looking for subvisual satellites, and (3) by examining the Martian surface for unusual craters in the equatorial plane that are remnants of the original big object that crashed.

REFERENCES

Kuiper, G. P. 1956, On the Origin of the Satellites and the Trojans. Vistas in Astronomy (ed., Arthur Beer), vol. 2, pp. 1631-1666. Pergamon Press. New York.

Öpik, E. J. 1962, Atmosphere and Surface Properties of Mars and Venus. Progress in Astronautical Sciences (ed., S. F. Singer), vol. 1, pp. 261-342. North-Holland Pub. Co. Amsterdam.

Singer, S. F. 1968, The Origin of the Moon and Geophysical Consequences. Geophys. J. Roy. Astron. Soc. **15**, 205-226.

Singer. S. F. 1970, How Did Venus Lose Its Angular Momentum? Science **170**, 1196-1198.

Urey, H. C. 1952, The Planets: Their Origin and Development. Yale Univ. Press. New Haven, Conn.

DISCUSSION

KUIPER: There was a meeting in 1953 where I gave a paper (Kuiper, 1956) on the universal relation of satellite masses in terms of the primary. This relation is of such a nature that the Mars satellites have exactly the right masses for their distance. Therefore, it was my conclusion that the close satellites of Mars, Jupiter, and Saturn were formed essentially where they are now. These systems have not been appreciably disturbed. I think it is out of the question that these are captured asteroids; there is no relation between the two.

BANDERMANN: How do you explain the very short lifetime of Phobos?

KUIPER: The notion that Phobos has a short lifetime was based on erroneous observations at the Naval Observatory some 20 yr ago.

KAULA: Pertinent to the lifetime problem of Phobos, it seems extremely probable that the tidal evolution has been hung up at various stages at commensurabilities with longitudinal variations in the Martian gravitational field. The torque exerted by the tidal bulge of such a tiny satellite is plausibly much less than the torque by the fixed irregularities in the Martian mass distribution:

$$\frac{m}{r}\frac{\partial U_T}{\partial \lambda} < \frac{m}{r}\frac{\partial U_{lmpq}}{\partial \lambda} \quad \text{or} \quad U_T < U_{lmpq}$$

where m, r, and λ are Phobos' mass, radial coordinate, and longitude, and the potential functions are

$$U_T = kG\frac{mR^5}{r^6} \times \frac{3}{4} \sin 2\delta_T$$

$$U_{lmpq} = \frac{GM^*}{a}\left(\frac{R}{a}\right)^l F_{lmp}(i) G_{lpq}(e) J_{lm} \cos\left[(l-2p)\omega + (l-2p+q)M + m(\Omega - \theta - \lambda_{lm})\right]$$

where a, e, i, ω, Ω, and M are Kepler elements; M^*, R, and θ are mass, radius, and the reference meridian sidereal time of Mars; k is the tidal Love number of Mars; G is the gravitational constant; J_{lm} and λ_{lm} are the amplitude and phase angle of a spherical harmonic term in Mars' gravitational field; $F_{lmp}(i)$ and $G_{lpq}(e)$ are polynomials dependent on the indices l, m, p, and q (Kaula, 1966); and δ_T is the lag angle and sin $2\delta_T$ is equal to $1/Q$, the dissipation factor.

Commensurability other than 1:1 depends on either the eccentricity or inclination of Phobos. For 3:1, commensurability dependent on the inclination seems plausible: $lmpq = 3310$, which results in

$$kG\frac{mR^5}{r^6} \times \frac{3}{4}\frac{1}{Q} < \frac{GM^*R^3}{a^4}(f \sin i)J_{33}$$

where f is a factor from $F_{331}(i)$ of order 1/10. Thence

$$fJ_{33} \sin i > k\frac{m}{M^*}\left(\frac{R}{a}\right)^2\frac{1}{Q}$$

where k is about 0.08; m/M^*, 10^{-9}; a/R, 3; and Q, 100 to 1000. Therefore

$$J_{33} \sin i \gtrsim 10^{-13}$$

J_{33} would likely be of a magnitude intermediate between Earth's and the Moon's, say 3×10^{-6}. So the inclination i of Phobos does not have to differ much from zero for this sort of coupling to occur.

The above term would be one of several terms dependent on either nonzero i ($p \neq 0$) or nonzero e ($q \neq 0$). As long as the commensurability is maintained, a is unchanged, but i and e will continue to decrease. Hence the torque due to the combination of terms may pass through zero, and Phobos will slip out of the commensurability. Furthermore, if there is any significant tectonic activity in Mars, the J_{lm} values will change.

HARTMANN: In analyzing the Mariner '69 photos of Martian craters, I have considered the question of whether we can account for Martian craters by considering only the present-day asteroids or whether we need to consider the early intense accretionary phase of bombardment by preasteroidal particles. There appear to be three marginal items of supporting evidence for the former:

(1) Craters from diameters of 50 to 200 km are not saturated on the Martian surface as would be expected if we could see all the way back to the time of accretion.

(2) This flat spot or undersaturation in the crater counts corresponds to asteroids in the diameter range of 6 to 25 km, which is where the McDonald survey, the Palomar-Leiden survey (PLS), and the list of Mars crossers all show a flat spot in their diameter distributions. This flat spot divides what Kuiper has called the fragments from the larger original accretions. (See fig. D-1.) Thus, there is marginal evidence that we actually see the fossil imprint of the asteroid mass distribution when we look at Martian craters.

(3) Using Anders' calculated half-life for Mars-crossing asteroids and then calculating back 4×10^9 yr, we get approximately the observed number of Martian craters within a factor of 3. This means that the present-day Mars-crossing population is approximately sufficient to account for the Martian craters without invoking the early accretionary bombardment.

According to this picture, Martian craters that we now see were caused by already-fragmented Mars-crossing asteroids. The initial mass distribution, such as discussed

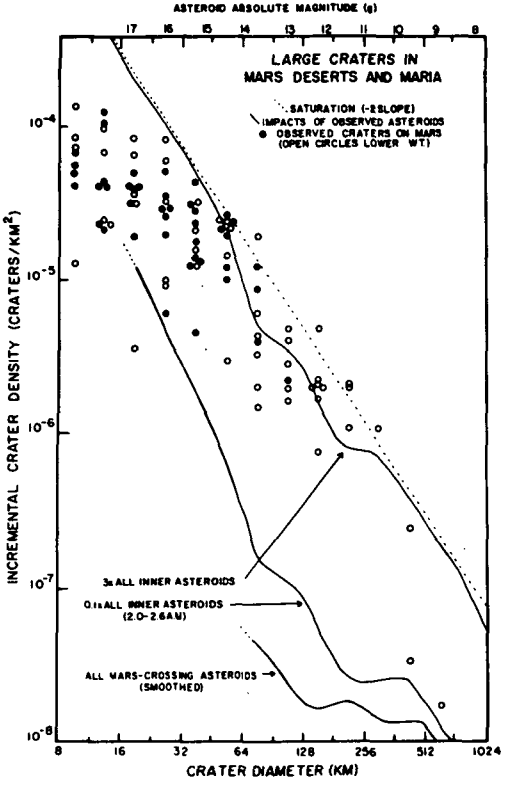

Figure D-1.—Diameter distribution of craters of Mars compared with diameter distribution predicted for craters formed from asteroids in the PLS (upper two solid curves) and present-day Mars-crossing asteroids (lowest curve). Upper solid and dashed curves show how saturation effects would truncate the Mars crater distribution. Nonetheless, the Mars crater counts from 50 to 200 km show a marginal trace of the "flat spot" in the asteroid size distribution, suggesting Mars craters are caused by impacts of Mars-crossing asteroids over the last 4 aeons.

by Hills,[1] had already been disturbed, which is reasonable because the original mass distribution probably would have been changed by fragmentation by the time Mars had accreted. It does leave one interesting point: We apparently do not see all the way back to the beginning of Mars' history (i.e., to its accretionary phase), as seems to be the case with the Moon.

LINDBLAD: Alfvén (Alfvén and Arrhenius, 1970) has suggested that an asteroidal belt may exist in the Jovian satellite system. By analogy with the formation of our planetary system it appears likely that an asteroid or "minor-moon" belt exists between the orbits of the Jovian satellites Amalthea (no. 5) and Io (no. 1). It is suggested that a special effort be made during a Grand Tour Jupiter flyby mission to detect such a belt, and measure parameters of interest; i.e., particle spatial density, size, and composition.

---

[1]See p. 225.

A Jupiter-Saturn-Pluto mission with a Jupiter flyby trajectory passing about 100 000 km inside the orbit of the satellite Io would be desirable for the Jovian "asteroid belt" experiment.

According to a recent JPL study, it is feasible to intercept the Jovian satellites Io, Ganymede, and Callisto in one single 1977 flyby mission. However, it is known that these satellites are rather similar in their physical characteristics. Alfvén (1971, private communication) has pointed out the desirability of including in the flight plan (if feasible) also a near encounter with one of the outer Jovian satellites (nos. 6, 7, and 10). It is suggested that feasibility studies for a Jupiter flyby mission including one of the outer Jovian satellites as well be considered.

A similar situation may exist in the Saturnian satellite system where a concentration of small particles may exist between satellites 5 and 6.

DISCUSSION REFERENCES

Alfvén, H., and Arrhenius, G. 1970, Structure and Evolution of the Solar System. Astrophys. Space Sci. 8, 338.

Kaula, W. M. 1966, Theory of Satellite Geodesy. Blaisdell Pub. Co. Waltham, Mass.

Kuiper, G. P. 1956, On the Origin of the Satellites and the Trojans. Vistas in Astronomy (ed., Arthur Beer), vol. 2, pp. 1631-1666. Pergamon Press. New York.

Page intentionally left blank

TROJANS AND COMETS OF THE JUPITER GROUP

EUGENE RABE
Cincinnati Observatory

In a recent paper (Rabe, 1970), I suggested that at least some comets of the Jupiter group may have originated from the relatively dense Trojan clouds that, according to a recent survey by the van Houtens and Gehrels (1970), seem to be associated with the equilateral points L_4 and L_5 of the Jupiter orbit. This suggestion was inspired by the finding that the periodic comet Slaughter-Burnham has been captured (or perhaps recaptured) into unstable or temporary "Trojan" librations lasting approximately 2500 yr and by the circumstance that the Jacobi "constants" of most Jupiter group comets have values between 3.0 and 2.5, or just in that range which would also be occupied by all known and unknown Trojans associated with Jupiter in stable or unstable librations involving heliocentric eccentricities up to about 0.5 and inclinations as large as 30°. Moreover, it is well known that nearly all comets of the Jupiter group are able to approach Jupiter rather closely, thus providing the possibility for such drastic orbital changes as temporary capture into, or escape from, librational motion of the Trojan type. All, presumably stable, orbits of actual Trojan planets presently known have eccentricities e not exceeding 0.15, but we also know that stable *short*-period librations with much larger e values do exist in the restricted Sun-Jupiter problem, so that even in the real, nonrestricted situation there should be a possibility for corresponding librations with these more substantial short-period components. These librations may be unstable but may have long lifetimes nevertheless. The case of P/Slaughter-Burnham has proved that such motions are indeed possible, even with an e as large as 0.52.

The Jacobi integral is valid only in the restricted three-body problem, but the experience from many numerical integrations indicates that in the real Sun-Jupiter elliptic problem, with $e' \sim 0.05$, the Jacobi "constant" C from the approximating Tisserand criterion,

$$C = \frac{1}{a} + 2\sqrt{a}\cos\phi\cos I \tag{1}$$

with

$$\cos I = \cos i \cos i' + \sin i \sin i' \cos(\Omega - \Omega') \tag{2}$$

tends to vary only within relatively narrow limits, as long as the osculating elements used in evaluating equation (1) do not belong to some moment at which the small body in question is inside of Jupiter's gravitational "sphere of action." In equations (1) and (2), a is the semimajor axis of the Trojan's or comet's heliocentric orbit expressed in units of the mean Sun-Jupiter distance, ϕ is related to e through $e = \sin \phi$, and I denotes the orbital inclination relative to the Jupiter orbit as computed from the respective ecliptical inclinations i and i' and nodes Ω and Ω' according to equation (2). The prime symbol denotes the elements of Jupiter.

For the overwhelming majority of all minor planets, $C > 3$ and $a < 1$. To the exceptions with $C < 3$ belong all the known Trojans (because of their small deviations from $a_0 = a' = 1$ in combination with nonvanishing I and e), several members of the Hilda family with their also relatively large a values of the order of 0.8, and some asteroids with smaller values of a but with such exceptionally large values of e or/and I, as to enable the second term of the right-hand side of equation (1) to become sufficiently small. If the auxiliary angle γ is introduced through

$$\cos \gamma = \cos \phi \cos I \tag{3}$$

equation (1) can be solved to express $\cos \gamma$ as a function of the nearly constant C and of the variable a. Assuming that at some time the value $a_0 = 1$ can be attained by a, in consequence of Jupiter's perturbing action, the resulting function $\cos \gamma$ reduces to

$$\cos \gamma_0 = \frac{1}{2}(C - 1) \tag{4}$$

This equation contains the well-known statement that the attainment of $a_0 = 1$, and thus a "crossover" from $a < 1$ to $a > 1$ or vice versa, is impossible if $C > 3$. Clearly, $C > 3$ leads to $\cos \gamma_0 > 1$ and thus to either $\cos \phi > 1$ or $\cos I > 1$, if not to both inequalities together. Actually, because terms of the order of Jupiter's mass, $\mu \sim 0.001$, have been neglected in equation (1), even if applied to the restricted problem with $e' = 0$, the subsequent equation (4) proves the impossibility of crossovers only for C values that exceed 3.000 by amounts larger than some quantity of order μ. Conservatively, one may require $C > 3.01$. Considering also Jupiter's orbital eccentricity $e' \sim 0.05$, however, in conjunction with the resulting slight variability of C (as evidenced in many relevant numerical integrations), the critical C limit for the possible occurrence of $a_0 = 1$ has to be increased even more. Indications are that the effective limit (in the absence of significant perturbations from other major planets) lies near $C = 3.03$. It also appears that for any asteroids or comets within $3.00 < C < 3.03$, any crossovers would tend to happen through temporary capture into *satellite* rather than Trojan status, as evidenced by the C values that one finds for the many sets of elements a, e, and I obtained by Hunter (1967) in his work on satellite/asteroid transfers. For any *comets* with

C values close to 3.00, the possibility of temporary satellite capture must definitely be considered together with that of temporary Trojan-type librations. For nearly all Jupiter group comets, however, one finds $C \leqslant 2.97$; therefore, satellite captures become rather unlikely. Such C values fall into the range typical for Trojan librations (as low as $C = 2.673$ for 1208 Troilus, among the known Trojan planets). Comets, however, may pass through $a_0 = 1$ in most cases, of course, without getting caught into temporary oscillations of a within the narrow boundaries $0.95 \leqslant a \leqslant 1.05$ required for Trojan-type librations (Rabe, 1970).

Because the Jupiter group comets as well as the Trojans are able, practically by definition, to experience crossovers through $a_0 = 1$, it should, of course, be expected that the C distributions of both groups will overlap. On the other hand, all known Trojans vary their osculating a values within the rather narrow limits $0.97 \leqslant a \leqslant 1.03$, whereas the Jupiter comets attain a values as small as 0.44 (P/Encke) and as large as 1.38 (P/Oterma). For the eccentricities, the observed upper limit $e = 0.15$ for the Trojans has already been mentioned, whereas the comets considered here have e values up to 0.85. Only the inclinations I have similar distributions in both groups, with a very few being somewhat larger than 30° in each category. On the basis of their significantly different a and e distributions, however, it would not be surprising to find rather different C distributions, too, with a similarly narrow overlap as in a and e. As repeatedly mentioned, though, there is an *extensive* overlap of the two C distributions, suggesting a close dynamical affinity of the two groups of bodies. The principal purpose of this paper is the computation and presentation of a sufficiently large number of individual C values, as well as of some related quantities that are of interest with regard to possible conjectures concerning a dynamical relationship between Trojans and Jupiter group comets.

For the 15 numbered Trojan planets, the elements needed in equations (1) and (2) have been taken from the Leningrad *Ephemeris* volume for 1971, except for those of the not yet listed newest member 1749 Telamon, which are given in Minor Planet Circular 3019. For 38 comets of the Jupiter group rather approximate but for the present purpose sufficiently accurate elements were taken from Marsden's (1967) tabulation of such comets with a values presently (~1965) inside Jupiter's $a' = 1$. Three other comets were added, without any attempt to achieve completeness: P/Oterma (Astron. J. **66**, 248), P/Schwassmann-Wachmann 1 (Astron. J. **66**, 268), and P/Slaughter-Burnham (Acta Astron. **18**, 419). Finally, the quite exceptional minor planet 944 Hidalgo was also included here for the sake of comparison. For the total of 57 objects, the computed C values are listed in decreasing order in table I, together with the "crossover parameter" γ_0 from equation (4). Of the basic elements a, e, and I, only e has been listed, under the heading e_1, so that it may be compared with the e_0 given in the last column, which is the largest possible value of e at crossover in connection with $a = 1$. Because equation (3) has to be satisfied also when $\gamma = \gamma_0$, this maximum e_0 would occur only in conjunction with $I = 0$, whereas the also possible maximum I ($a = 1$, $\phi = 0$) $= \gamma_0$ would

TABLE I.—*The Jacobi Constant* C *and Related Quantities for Trojans and Selected Jupiter Group Comets*

Comet or Trojan	C	γ_0 ($a = 1$)	e_1	e_0 ($a = 1, I = 0$)
Oterma	3.00	0°	0.25	0.00
Schwassmann-Wachmann 2	3.00	0	.38	.00
1143 Odysseus	2.986	–	.093	–
1647 Menelaus	2.986	–	.028	–
659 Nestor	2.980	–	.110	–
1749 Telamon	2.974	–	.111	–
Encke	2.97	9	.85	.16
Tempel 1	2.97	10	.52	.17
Schwassmann-Wachmann 1	2.97	10	.14	.17
1173 Anchises	2.961	–	.136	–
Tempel 2	2.96	11	.55	.19
884 Priamus	2.955	–	.120	–
Whipple	2.95	13	.35	.23
Johnson	2.94	14	.38	.24
588 Achilles	2.939	–	.148	–
Neujmin 2	2.92	16	.58	.28
de Vico-Swift	2.91	17	.52	.29
Reinmuth 2	2.91	17	.46	.29
Brooks 2	2.90	19	.50	.32
1172 Äneas	2.895	–	.102	–
624 Hektor	2.892	–	.025	–
Ashbrook-Jackson	2.89	19	.40	.33
1404 Ajax	2.880	–	.113	–
Forbes	2.87	21	.55	.35
1437 Diomedes	2.859	–	.046	–
Kopff	2.85	22	.56	.37
Holmes	2.85	22	.38	.38
617 Patroclus	2.844	–	.141	–
911 Agamemnon	2.843	–	.067	–
Tempel-Swift	2.84	23	.54	.40
Wirtanen	2.84	23	.54	.40
Reinmuth 1	2.84	23	.49	.40
Tuttle-Giacobini-Kresák	2.83	24	.64	.41
Grigg-Skjellerup	2.82	24	.66	.41
Harrington	2.81	25	.56	.42
Wolf-Harrington	2.79	26	.54	.44
Harrington-Abell	2.79	27	.52	.45
1583 Antilochus	2.745	–	.054	–
Daniel	2.74	29	.55	.49
Faye	2.74	30	.58	.49
d'Arrest	2.73	30	.61	.50
Arend-Rigaux	2.72	30	.60	.51
Wolf	2.72	31	.39	.51
Slaughter-Burnham	2.71	31	.50	.52
Arend	2.70	32	.53	.53
Pons-Winnecke	2.69	32	.64	.54
1208 Troilus	2.673	–	.092	–

TABLE I.—*The Jacobi Constant* C *and Related Quantities for Trojans and Selected Jupiter Group Comets*—Concluded

Comet or Trojan	C	γ_0 ($a = 1$)	e_1	e_0 ($a = 1, I = 0$)
Perrine-Mrkos	2.67	33	.64	.55
Comas Solá	2.67	34	.58	.55
Finlay	2.63	35	.70	.58
Borrelly	2.60	37	.60	.60
Honda-Mrkos–Pajdušáková	2.56	39	.82	.63
Biela	2.54	40	.76	.64
Schaumasse	2.49	42	.71	.66
Brorsen	2.47	43	.83	.68
Giacobini-Zinner	2.46	43	.73	.68
944 Hidalgo (non-Trojan minor planet for comparison)	2.07	58	.65	.85

require $e = 0$. It is well known that I as well as e may undergo large variations during close approaches to Jupiter, so that the possibility of a near-zero inclination I after some approach cannot be excluded. Normally, though, I will not become very small; and, consequently, the related crossover eccentricity e satisfying equation (3) will be smaller than the listed maximum e_0. No e_0 values have been computed for the 15 numbered Trojans, because it may be assumed that they move in stable libration orbits and do not experience close approaches to Jupiter. We know that their e and I values vary only rather moderately during the small long-period oscillations of a, so that the formal computation of e_0 for $I = 0$ would make no physical sense. If they would be computed and given, they would fall right into the systematic trend of this last column in table I, because the listing is in order of C, and e_0 and γ_0 are functions of C alone. To facilitate the separate recognition of Trojans and comets in table I, the γ_0 values of the Trojans have been omitted as well.

It is seen from table I that even the numbered and presumably stable Trojans have C values that extensively overlap those of the Jupiter comets. It is very likely that most of the at least several hundred additional Trojans (van Houten et al., 1970) fall into about the same range, $2.67 \leqslant C < 3.00$, simply because of their probably stable association with the equilateral points. Of the 41 comets in table I, 34, or 83 percent, also have C values between 2.67 and 3.00. For those contemplated unstable or escaped Trojans with initial e values exceeding 0.15, the related C values could easily be as small as 2.5; therefore, there could be a complete overlap of the ranges of C values for the comets and Trojans. Of particular interest are the e_0 values of the 41 comets. Most of them are much smaller than the associated e_1 values; therefore, in connection with the suggested Trojan origin of such comets, the related values of e for $a = 1$ should be in quite reasonable agreement with the e range that is permissible by

dynamical considerations for librational motions of the Trojan type. First, the actual crossover values of e will normally be smaller than the maximum e_0; and, second, on the theoretical side, we know that in the restricted Sun-Jupiter case, even stable librations of short period may involve e values near 0.64. In the one known case of temporary librations, for P/Slaughter-Burnham, such motion actually occurs with $e \sim 0.52$.

When the possibility of Trojan origin for some Jupiter group comets was first suggested (Rabe, 1970), the detailed features of the reverse event of capture into libration for P/Slaughter-Burnham were interpreted as indicating a rather small probability of such capture for any given comet because, in most cases, the large perturbations in a during the required Jupiter approach will tend to overshoot the apparently necessary entry conditions. Such probability considerations have no bearing on the contemplated escapes from librations of an unstable nature. The only requirement seems to be that the original Trojan clouds had to be large enough to permit the formation and growth of condensations even near the fringes of librational stability.

When Oort (1950) discussed the proposed existence of a very distant cloud of comets surrounding the solar system, he suggested that these bodies might actually be unstable escapees from the original minor planet belt between Mars and Jupiter. It appears now that, at least for the Jupiter comets, the escape from the two Trojan clouds provides a much simpler and more direct mechanism of asteroid transfer into cometary motion, without the need of moving these bodies first to the remote fringes of the solar system, and of then recapturing them in a complicated chain of dynamical events. It should be noted again, as in Rabe (1970), that the similarity of the anomalous distributions of the perihelion longitudes of the Trojans and of the Jupiter group comets lends further support to their proposed common origin. Also, the complete absence of retrograde orbits would automatically be accounted for by such an origin of these comets. The relatively large masses of some Trojans can no longer be considered as an argument against a common origin, because the van Houtens and Gehrels (1970) have found that the frequency of the Trojans increases greatly with decreasing magnitude.

REFERENCES

Houten, C. J. van, Houten-Groeneveld, I. van, and Gehrels, T. 1970, Minor Planets and Related Objects. V. The Density of Trojans Near the Preceding Lagrangian Point. Astron. J. **75**, 659-662.

Hunter, R. B. 1967, Motions of Satellites and Asteroids Under the Influence of Jupiter and the Sun. II. Asteroid Orbits Close to Jupiter. Mon. Notic. Roy. Astron. Soc. **136**, 267-277.

Marsden, B. G. 1967, One Hundred Periodic Comets. Science **155**, 1207-1213.

Oort, J. H. 1950, The Structure of the Cloud of Comets Surrounding the Solar System, and a Hypothesis Concerning Its Origin. Bull. Astron. Inst. Neth. **11**, 91-110.

Rabe, E. 1970, Orbital Characteristics of Comets Passing Through the 1:1 Commensurability With Jupiter. Proc. IAU Symp. no. 45, Motion, Orbit Evolution and Origin of Comets. Leningrad.

EVOLUTION OF COMETS INTO ASTEROIDS?

B. G. MARSDEN
Smithsonian Astrophysical Observatory

There has long been speculation as to whether comets evolve into asteroidal objects. On the one hand, in the original version of the Oort (1950) hypothesis, the cometary cloud was supposed to have formed initially from the same material that produced the minor planets; and an obvious corollary was that the main physical difference between comets and minor planets would be that the latter had long since lost their icy surfaces on account of persistent exposure to strong solar radiation (Öpik, 1963). However, following a suggestion by Kuiper (1951), it is now quite widely believed that, whereas the terrestrial planets and minor planets condensed in the inner regions of the primordial solar nebula, icy objects such as comets would have formed more naturally in the outer parts, perhaps even beyond the orbit of Neptune (Cameron, 1962; Whipple, 1964*a*). Furthermore, recent studies of the evolution of the short-period comets indicate that it is not possible to produce the observed orbital distribution from the Oort cloud, even when multiple encounters with Jupiter are considered (Havnes, 1970). We must now seriously entertain the possibility that most of the short-period orbits evolved directly from low-inclination, low-eccentricity orbits with perihelia initially in the region between, say, the orbits of Saturn and Neptune, and that these comets have never been in the traditional cloud at great distances from the Sun.

On the other hand, there is also the extreme point of view that comets completely disintegrate after only a few passages near the Sun. This feature was present in the original Whipple (1950) icy-conglomerate comet model, principally on account of the widespread assumption that the frequent and complete disappearance of comets was an observed fact. Twenty yr ago, 44 comets were known to have been observed at more than one perihelion passage, but 10 of these (i.e., 23 percent) were regarded as lost, having failed to appear at several of their recent returns. The number of more-than-one-appearance comets has now risen to 59; and 5, if not 6, of those lost have been found, reducing the proportion of those lost to only 7 or 8 percent. Two of the comets were found by accident, but the reduced percentage is mainly a demonstration of what can be done when modern computational and observational techniques are applied to the problem (Klemola, 1965; Kowal, 1970*a,b;* Marsden, 1963; Roemer, 1964, 1968; Schubart, 1965); and there is

every expectation of our being able to reduce the percentage of lost comets even further.

Closely related to this is the question of secular brightness decrease. Straightforward use of the observational data cataloged by Vsekhsvyatskij (1958), and the assumption that a decrease in the total brightness of a comet is accompanied by one in the radius of the nucleus, reveals the startling possibility that 60 percent of the known periodic comets will cease to exist by the end of the present century (Whipple, 1964*b;* Whipple and Douglas-Hamilton, 1966). Because of changing observational methods, it is extremely difficult to correlate estimates of cometary brightness by different observers at different times in history. Periodic fluctuations in brightness, sometimes rendering a comet systematically brighter or fainter for a whole apparition, further confuse the issue. In any case, variation in the total brightness of a comet does not necessarily give any information about variation in nuclear brightness, which is what we need to know.

The most reliable information about cometary decay is probably that furnished by the modern investigations on the nongravitational anomalies in the motions of periodic comets (Marsden, 1969, 1970*a;* Yeomans, 1971). There is some uncertainty concerning the effective velocity of the escaping matter, but the mass loss rates obtained (Sekanina, 1969), less than 0.1 to about 1 percent per revolution, are quite consistent with the values derived from theoretical studies on the sublimation of the ice (Huebner, 1967).

Thus a comet should survive at least 100 passages within 1 AU of the Sun, and 1000 passages or more might be more typical. Decay takes place; but the point at issue is whether the sublimation results in shrinkage of the nucleus and complete dispersal of the comet's meteoric material or whether, as the nucleus loses its volatiles, it evolves into an object that, to all outward appearances, is indistinguishable from a minor planet. Some comets are often remarkably asteroidal in appearance. In particular, P/Arend-Rigaux and P/Neujmin 1 have consistently appeared asteroidal–except during their discovery apparitions when they were relatively close to Earth and careful scrutiny revealed very slight, but definite cometary activity. It has not been possible to detect nongravitational effects in the motions of these two comets, which means that the effects must be at least two orders of magnitude smaller than those for more typical comets. Furthermore, it is observed that the nongravitational effects on several comets, very notably P/Encke, are systematically diminishing with time, strongly suggesting reduction in the rate of mass loss and evolution toward objects like P/Arend-Rigaux and P/Neujmin 1. A cometary nucleus whose radius is decreasing linearly with time, on the other hand, should in its later stages show a progressive *increase* in these nongravitational effects (Sekanina, 1969).

A certain amount of insight into the relationship between comets and minor planets is provided by a comparison of their orbits. Criteria have been developed (Kresák, 1967; Whipple, 1954) for distinguishing asteroidal and cometary orbits; however, we feel that the single most important factor is the

aphelion distance Q. Because no comet has $Q < 4.1$ AU, we shall restrict ourselves to those minor planets with $Q > 3.9$ AU, or about 5 percent of all the numbered objects. Among the comets, we shall consider just those of more than one appearance and $Q < 15$ AU. The outstanding difference between the comets and the minor planets is that the former are continually passing near Jupiter–half of them have been within half an astronomical unit at some time during the past half century–whereas the latter do not. The 32 minor planets having a large Q and perihelion distances q of less than 2.4 AU are listed in table I in order of decreasing Q. There are also 63 minor planets with $q > 2.4$ AU, of which 60 percent belong to the Trojan and Hilda groups (and none of the other 40 percent has $Q > 4.1$ AU). The Trojan and Hilda minor planets are prevented from approaching Jupiter on account of libratory situations. The same is true of 279 Thule (which has a nearly circular orbit at 4.3 AU from the Sun), the second and third entries in the table (1373 Cincinnati and 1362 Griqua), and the final entry (887 Alinda). Appropriate interaction of orbital eccentricity, inclination, and sometimes mean distance also seems to keep the other minor planets, except for 944 Hidalgo, away from Jupiter. For a detailed discussion, see Marsden (1970*b*).

With this single exception, and so far as we can tell, the numbered minor planets are unable to pass within 1.1 AU of Jupiter; and in the absence of any nongravitational effects, their orbits are essentially stable for an interval that can very conservatively be taken as within 10 000 yr of the present time. As for Hidalgo, soon after its discovery it passed only 0.9 AU from Jupiter and in 1673 it passed less than 0.4 AU away. Among the comets, all but two have

TABLE I.–*Numbered Minor Planets With* $q \leqslant 2.4$ *AU and* $Q \geqslant 3.9$ *AU*

Minor planet	q, AU	Q, AU	Minor planet	q, AU	Q, AU
944 Hidalgo	2.0	9.6	965 Angelica	2.3	4.0
1373 Cincinnati	2.3	[a]4.5	880 Herba	2.0	4.0
1362 Griqua	2.2	[b]4.4	612 Veronika	2.3	4.0
225 Henrietta	2.4	4.3	1317 Silvretta	2.4	4.0
1006 Lagrangea	2.0	4.3	719 Albert	1.2	4.0
814 Tauris	2.2	4.1	1537 1940 QA	2.1	4.0
1036 Ganymed	1.2	4.1	717 Wisibada	2.3	4.0
1477 Bonsdorffia	2.3	4.1	372 Palma	2.4	4.0
1099 Figneria	2.2	4.1	1093 Freda	2.3	4.0
1474 Beira	1.4	4.1	882 Swetlana	2.3	4.0
1672 1935 BD	2.3	4.1	1625 The NORC	2.4	3.9
680 Genoveva	2.2	4.1	664 Judith	2.4	3.9
886 Washingtonia	2.2	4.0	931 Whittemora	2.4	3.9
794 Irenaea	2.2	4.0	1508 1938 UO	1.6	3.9
778 Theobalda	2.3	4.0	1134 Kepler	1.4	3.9
747 Winchester	2.0	4.0	887 Alinda	1.1	3.9

[a]Because of libration, extremes are 4.4 and 5.2.

[b]Because of libration, extremes are 4.0 and 4.4.

passed within 0.9 AU of Jupiter during the past 200 years. The two exceptions are the asteroidal comets P/Arend-Rigaux and P/Neujmin 1, neither of which has passed near Jupiter for about 1000 years. The relative stability of their orbits, in particular the fact that the perihelion distances cannot for at least a millennium have had significantly larger values than now, means that these two comets have long been subject to strong solar radiation, and considerable aging should certainly have taken place. Many of the other comets not unreasonably had larger perihelion distances only a few centuries ago, and until these distances dropped below 2.5 to 3.0 AU there would have been little deterioration. One cannot exclude the possibility that Hidalgo is an ordinary minor planet ejected recently into its rather unstable orbit through collision with some other minor planet, but there is at least as much justification for supposing that it is physically an object very similar to the two exceptional comets. It certainly will be very desirable to have appropriate physical observations made of Hidalgo at its next return to perihelion in 1976-77.

Although P/Arend-Rigaux and P/Neujmin 1 (and probably Hidalgo) may look and behave very much like conventional minor planets, it does not seem probable that they will continue to survive indefinitely. If the future lifetime of a defunct cometary nucleus were as long as that of a typical stony or iron asteroid, we should expect to find very many more asteroidal objects with only relatively stable, or even completely unstable, orbits. The Palomar-Leiden survey (van Houten et al., 1970) did not reveal any. The only minor planets having $Q > 4.1$ AU were intrinsically fainter members of the Trojan and Hilda groups, and their orbits are presumably stable.

Sekanina (1969, 1971*a*) has attempted to explain the decrease and accelerated rate of decrease of the nongravitational effects on P/Encke in terms of a nuclear model consisting of a porous meteoric matrix with ices embedded uniformly inside it. During each revolution about the Sun the ices in the surface layer are sublimated out; the remaining volatiles then diffuse throughout the nucleus and restore the uniform distribution without any reduction in the total volume. This model describes the observed history of P/Encke very well and suggests that the comet will evolve into an asteroidal object about 60 yr from now. Extrapolation into the past, however, yields an unacceptably small proportion of meteoric material for the time, at least 700 revolutions ago, when the comet's aphelion distance would have been large enough for Jupiter to perturb the comet into something like its present orbit. Sekanina has therefore proposed a core-mantle model for the nucleus, the porous, ice-embedded matrix being surrounded by an envelope of free ices and loose dust particles. He supposes that the mantle of P/Encke finally evaporated during the two centuries or so before discovery; until shortly before then, the comet would have behaved much like a pure icy nucleus, with the nongravitational effects constant or *increasing* very slightly in magnitude. With this model, capture by Jupiter can be pushed back to at least 1200 revolutions ago, more in line with data on the evolution of the associated Taurid meteor streams (Whipple and Hamid, 1952).

Our more recent investigations have revealed a few cases where the nongravitational effects on comets do seem to be increasing slightly with time, or indeed to change sign. We have tended to regard this as an apparent effect, incidental to the real systematic decrease in the magnitude of the force, and arising merely on account of long-term changes in the inclination of a comet's equator to its orbit (Marsden, 1971*a*) or as a consequence of precession of the nucleus (Sekanina, 1971*b*).

It could be, however, that the increases are real. Sekanina[1] envisages newly captured comets as generally having nuclei that, at least in their outer regions, have a great deal of free ice. Some of them would evolve as we have discussed. Others, lacking significant cores, would show increases and perhaps even sudden changes in their nongravitational parameters; eventually they would completely disperse.

It is hard to judge which, if either, of these courses represents the "main sequence." There is certainly something unusual about the two almost defunct comets P/Arend-Rigaux and P/Neujmin 1. They were last in the vicinity of Jupiter 900 and 1200 yr ago, respectively. Just as we wonder what has become of those short-period comets that were last near Jupiter 2000 and 5000 yr ago and more, we must question the absence of comets that last passed within the critical distance of 0.9 AU between 200 and 900 yr ago. This indicates either that the cores of these comets (and Hidalgo) are unusually large or that the majority of comets are coreless. As already noted, however, recent experience shows that lost comets have an excellent recovery rate, suggesting that most cometary nuclei do have small cores. P/Biela, one of the comets that Sekanina supposes has completely disintegrated, is, of course, one of the four, or possibly five, comets of more than one appearance that are still lost. P/Brorsen may also be a coreless comet that has disintegrated. No searches have been made for either comet since the 19th century, and observers should certainly not be discouraged from trying to recover a small asteroidal remnant of P/Biela at its favorable return later this year (Marsden, 1971*b*). P/Tempel-Swift is still lost, but the possibility of recovering it is now hampered by the fact that its perihelion distance—and thus its minimum apparent magnitude—has significantly increased. Searches have been made in recent months for P/Neujmin 2; it was not found, which suggests that it was within 2 days of the prediction, but more than 2 mag fainter than predicted, or up to 5 days from the prediction but more than 1 mag fainter (E. Roemer, Z. M. Pereyra, and C. Kowal, personal communications). The fifth comet, P/Tempel 1, may possibly have been recovered in 1967 (Roemer, 1968), but confirmation will not be possible until it returns again next year.

The indication that the cores of most cometary nuclei are small naturally leads us to discuss the Apollo group, tiny asteroidal objects with $q < 1$ AU and discovered only because they pass close to Earth. By estimating the probabilities of their collisions with Earth and other inner planets, Öpik (1963)

[1]See p. 423.

concluded that they could not have existed in their present state since the origin of the solar system. Deflection of ordinary minor planets by collision or through perturbations by Mars appears to be insufficient for producing them, so he supposed that they were ex-comets whose aphelion distances had been decreased to their present values by the nongravitational effects that once would have been acting. There is the problem, however, that all the Apollos have aphelion distances smaller than that of P/Encke (and presumably that of P/Encke will not be decreasing much further). This is certainly a severe difficulty in the case of the objects with $Q < 3.5$ AU, although coordination of the nongravitational effects with the systematic perturbations by Jupiter when the comets pass through mean motion resonances can be of assistance (Sekanina, 1971*c*).

In table II we list, in order of decreasing Q, the Apollo objects and also the so-called Amor objects (having perihelion distances slightly greater than 1 AU). Except for two very uncertain objects, the table is complete for numbered and unnumbered minor planets currently found to have $q \leqslant 1.15$ AU. Only the first two objects, each of which is kept away from Jupiter because of a libration, have Q in the range included in table I. In addition to q, Q, the orbital eccentricity e, the orbital period P, the orbital inclination i, and the absolute magnitude $B(1, 0)$, we have noted whether there seem to be associated meteors (Sekanina, 1970) and short-term light variations (Gehrels et al., 1970; E. Roemer, K. Tomita, and T. Gehrels, personal communications). Large light variation can almost certainly be regarded as indicating a deflected, conventional minor planet; a small variation and, to a lesser extent, associated meteors might be considered as indications of cometary origin.

We conclude that 433 Eros and 1620 Geographos are very probably planetary, and this is also rather probable for 1968 AA. If any of the objects are of cometary origin, they are most likely to be among the first five entries in the list, although there also exists the enigmatic possibility of cometary origin for 1566 Icarus, small though its aphelion distance may be. Deflection of ordinary minor planets into Apollo orbits is perhaps not as much of a problem as it was thought to be: consider the enormous number of planets of the Hungaria group, on the inner fringe of the main belt (with mean distances of 1.95 AU), indicated by the Palomar-Leiden survey (van Houten et al., 1970). Accurate photometric studies of all the Apollo and Amor minor planets are much to be encouraged. Among the unnumbered objects, only 1968 AA has been observed at two approaches to Earth, although there will be a good opportunity for recovering Apollo itself later this year. Adonis will come within 0.20 AU of the Earth in 1977. Past searches for 1953 EA, 1948 EA, and 1960 UA have not been adequate; and these objects should be pursued more extensively on appropriate occasions in the future. The orbits of the remaining four objects are more uncertain.

Přibram, one of the two meteorites with well-determined orbits, had the surprisingly large aphelion distance of 4.1 AU, which might be suggestive of

TABLE II.–*Apollo and Amor Objects* ($q \leqslant 1.15$ *AU*)[a]

Objects	*q*, AU	*Q*, AU	*e*	*P*, yr	*i*	*B*(1, 0)	Meteors	Light variation
1953 EA	1.03	4.0	0.59	4.0	21°	19.6		
887 Alinda	1.15	3.9	0.54	4.0	9	16.3		Small
1948 EA	0.89	3.6	0.60	3.4	18	16.6		
1960 UA	1.05	3.5	0.54	3.4	4	18.1		
1936 CA Adonis	0.44	3.3	0.76	2.6	1	18.6	Yes	
1580 Betulia	1.11	3.3	0.49	3.2	52	15.7		
1968 AA	1.06	3.2	0.51	3.2	24	16.6	Maybe	Large
1221 Amor	1.08	2.8	0.44	2.7	12	19.2		
1937 UB Hermes	0.62	2.7	0.62	2.1	6	18.1	Maybe	
1627 Ivar	1.12	2.6	0.40	2.6	8	14.2		
1950 DA	0.84	2.5	0.50	2.2	12	16.1		
1971 FA	0.56	2.4	0.62	1.8	22	16.3		Large
1932 HA Apollo	0.65	2.3	0.56	1.8	6	15.6	Maybe	
1950 LA	1.08	2.3	0.36	2.2	26	14		
1566 Icarus	0.19	2.0	0.83	1.1	23	17.6	Maybe	Small
1685 Toro	0.77	2.0	0.44	1.6	9	16.3		
1959 LM	0.83	1.9	0.38	1.6	3	14		
433 Eros	1.13	1.8	0.22	1.8	11	12.4		Large
1620 Geographos	0.83	1.7	0.34	1.4	13	16.0		Large

[a]See table I of Roemer (p. 644) for current observational status.

cometary origin. This meteorite, a crystalline chondrite (Tuček, 1961), passed only 1.3 AU from Jupiter 6 yr before it collided with Earth, and similar approaches occurred previously at intervals of about 70 yr.

We cannot exclude the possibility of cometary origin for some of the large-Q objects listed in table I. The three librating objects, for example, could be ex-comets that were trapped in libration when the nongravitational forces ceased. (This same explanation is not likely for the Hildas, Thule, and the Trojans because their perihelion distances are too large for the nongravitational effects to have been significant.) Photometric and other physical studies are most desirable, particularly for these three and the objects with q significantly smaller than 2 AU (719 Albert is lost, unfortunately; but we may add the single-apparition object 1963 UA, which has $q = 1.2$ AU and $Q = 4.0$ AU, and should be recoverable in 1976). If we decrease the limiting Q to 3.6 AU, the following interesting objects may be included: 132 Aethra ($q = 1.6$, $Q = 3.6$), 475 Ocllo (1.6, 3.6), 699 Hela (1.5, 3.7), 898 Hildegard (1.7, 3.7), and 1009 Sirene (1.4, 3.8; lost).

REFERENCES

Cameron, A. G. W. 1962, The Formation of the Sun and Planets. Icarus **1**, 13-69.

Gehrels, T., Roemer, E., Taylor, R. C., and Zellner, B. H. 1970, Minor Planets and Selected Objects. IV. Asteroid (1566) Icarus. Astron. J. **75**, 186-195.

Havnes, O. 1970, The Effect of Repeated Close Approaches to Jupiter on Short-Period Comets. Icarus **12**, 331-337.

Houten, C. J. van, Houten-Groeneveld, I. van, Herget, P., and Gehrels, T. 1970, Palomar-Leiden Survey of Faint Minor Planets. Astron. Astrophys. Suppl. **2**, 339-448.

Huebner, W. F. 1967, Diminution of Cometary Heads Due to Perihelion Passage. Z. Astrophys. **65**, 185-193.

Klemola, A. R. 1965, Periodic Comet de Vico-Swift (1965e). IAU Circ. 1914.

Kowal, C. T. 1970*a*, Periodic Comet du Toit-Neujmin-Delporte (1970i). IAU Circ. 2264.

Kowal, C. T. 1970*b*, Periodic Comet Jackson-Neujmin (1970k). IAU Circ. 2277.

Kresák, L. 1967, Relation of Meteor Orbits to the Orbits of Comets and Asteroids. Smithson. Contrib. Astrophys. **11**, 9-34.

Kuiper, G. P. 1951, On the Origin of the Solar System. Astrophysics (ed., J. Hynek), pp. 357-424. McGraw-Hill Book Co., Inc. New York.

Marsden, B. G. 1963, On the Orbits of Some Long-Lost Comets. Astron. J. **68**, 795-801.

Marsden, B. G. 1969, Comets and Nongravitational Forces. II. Astron. J. **74**, 720-734.

Marsden, B. G. 1970*a*, Comets and Nongravitational Forces. III. Astron. J. **75**, 75-84.

Marsden, B. G. 1970*b*, On the Relationship Between Comets and Minor Planets. Astron. J. **75**, 206-217.

Marsden, B. G. 1971*a*, Nongravitational Effects on Comets: The Current Status. IAU Symp. no. 45, in press.

Marsden, B. G. 1971*b*, New Light on Biela's Comet. Sky and Telescope **41**, 84-85.

Oort, J. H. 1950, The Structure of the Cloud of Comets Surrounding the Solar System, and a Hypothesis Concerning its Origin. Bull. Astron. Inst. Neth. **11**, 91-110.

Öpik, E. J. 1963, The Stray Bodies in the Solar System. Pt. 1. Survival of Cometary Nuclei and the Asteroids. Advances in Astronomy and Astrophysics (ed., Z. Kopal), vol. 2, pp. 219-262. Academic Press, Inc. New York.

Roemer, E. 1964, Periodic Comet Holmes (1964i). IAU Circ. 1876.

Roemer, E. 1968, Periodic Comet Tempel 1. IAU Circ. 2121.

Schubart, J. 1965, Periodic Comet Tempel-Tuttle (1965i). IAU Circ. 1926.
Sekanina, Z. 1969, Dynamical and Evolutionary Aspects of Gradual Deactivation and Disintegration of Short-Period Comets. Astron. J. 74, 1223-1234.
Sekanina, Z. 1970, Dynamics of Meteor Streams and New Asteroid-Meteor and Comet-Meteor Associations. Bull. Amer. Astron. Soc. 2, 217-218.
Sekanina, Z. 1971*a*, A Model for the Nucleus of Encke's Comet. IAU Symp. no. 45, in press.
Sekanina, Z. 1971*b*, Rotation Effects in the Nongravitational Parameters of Comets. IAU Symp. no. 45, in press.
Sekanina, Z. 1971*c*, Dynamical Evolution of Extinct Comets. Bull. Amer. Astron. Soc. 3, 271.
Tuček, K. 1961, Multiple Fall of Příbram Meteorites Photographed. 2. Morphological and Mineralogical Composition of the Meteoritic Stones of Příbram. Bull. Astron. Inst. Czech. 12, 196-207.
Vsekhsvyatskij, S. K. 1958, Fizicheskie Kharakteristiki Komet. Gosudarstvennoe Izdatel'stvo Fiziko-Matematicheskoj Literatury. Moskva. (Also available as NASA TT F-80, 1964.)
Whipple, F. L. 1950, A Comet Model. I. The Acceleration of Comet Encke. Astrophys. J. 111, 375-394.
Whipple, F. L. 1954, Photographic Meteor Orbits and Their Distribution in Space. Astron. J. 59, 201-217.
Whipple, F. L. 1964*a*, Evidence for a Comet Belt Beyond Neptune. Proc. Nat. Acad. Sci. USA 51, 711-718.
Whipple, F. L. 1964*b*, Brightness Changes in Periodic Comets. Astron. J. 69, 152.
Whipple, F. L., and Douglas-Hamilton, D. H. 1966, Brightness Changes in Periodic Comets. Mem. Soc. Roy. Sci. Liège Ser. 5, 12, 469-480.
Whipple, F. L., and Hamid, S. E. 1952, On the Origin of the Taurid Meteor Streams. Roy. Observ. Helwan Bull. 41.
Yeomans, D. K. 1971, Nongravitational Forces Affecting the Motions of Periodic Comets Giacobini-Zinner and Borrelly. Astron. J. 76, 83-86.

Page intentionally left blank

A CORE-MANTLE MODEL FOR COMETARY NUCLEI AND ASTEROIDS OF POSSIBLE COMETARY ORIGIN

ZDENEK SEKANINA
Smithsonian Astrophysical Observatory

Arguments for a long time have been brought forward in support of the idea that the minor planets with orbits approaching Earth's orbit might be of cometary origin. Our feeling is that before such hypotheses are considered for any particular object, it is necessary to prove that differences in physical appearance and dynamical behavior between a typical asteroid of the Apollo or Albert types and a typical short-period comet can be interpreted in terms of cometary evolution.

In this paper, we discuss models of cometary nuclei, transition of an object from cometary phase into asteroidal phase, and specific asteroidal objects that may be of cometary origin.

PHYSICAL MODEL

Nongravitational (NG) activity in a comet essentially measures the rate of mass output from the nucleus in units of the nuclear mass. An obvious method of studying the NG effects, therefore, is to test various models of mass transfer in the nucleus and the related mass loss rate from the nucleus.

The most obvious possibility is to consider a cometary nucleus composed of freely deposited ices (upper part of fig. 1), which gradually shrinks at a constant rate. The NG effects increase in proportion to the decreasing nuclear dimensions as the comet passes through the *early* phase (E) into a *fading* phase (F). The free ice model finally sublimates out completely, leaving no compact debris whatsoever.

Dynamical calculations (e.g., Marsden, 1969, 1970) show that, by contrast, for most comets the NG activity tends to decrease rather than increase with time on a secular scale. Such behavior can be explained in terms of a core-mantle model. This model is composed of a porous core of nonvolatile materials surrounded by an icy envelope. The envelope may be contaminated by loosely distributed solid grains. Secular variations in the NG activity of a core-mantle comet is schematically represented in the lower part of figure 1. The icy shell, of considerable thickness in the *early* phase, gradually sublimates under the effects of solar radiation; the diameter of the nucleus decreases as

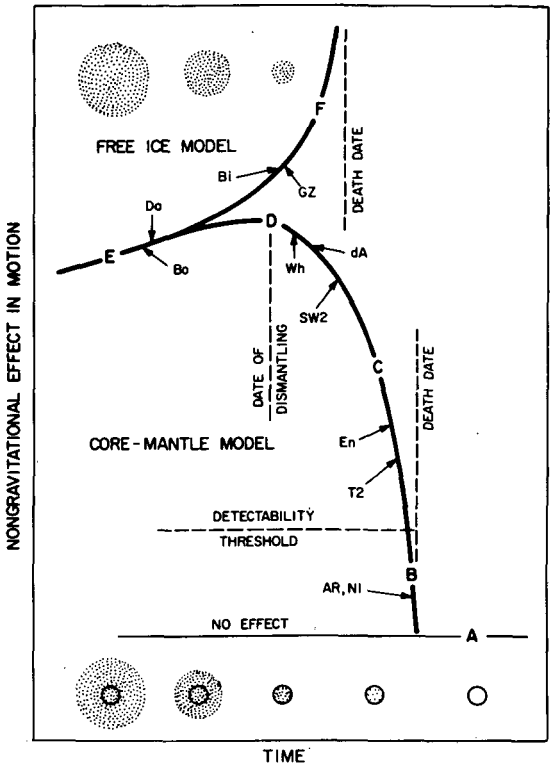

Figure 1.—Evolution of cometary nuclei and NG activity. Evolution of the free ice model is outlined in a sequence of schematic pictures at the top of the figure, that of the core-mantle model at the bottom. Dotted areas of various density show the degree of concentration of ices, empty area within a circle marks the presence of solid materials only. Secular variations in the NG effects on the free ice model are represented by the upper curve, those on the core-mantle model by the lower curve. Present approximate locations of several short-period comets are indicated by arrows and the following abbreviations: GZ, Giacobini-Zinner; Bi, Biela (in the first half of the 19th century); Bo, Borrelly; Da, Daniel; Wh, Whipple; dA, d'Arrest; SW2, Schwassmann-Wachmann 2; En, Encke; T2, Tempel 2; AR, Arend-Rigaux; and N1, Neujmin 1.

the comet approaches the *dismantling* phase (D). NG effects are relatively large and reach their maximum before the date of dismantling. At this point solid materials start extending over the nuclear surface in the form of a rigid, continuous matrix whose tensile strength is high enough to withstand pressure from activated ices below; the comet no longer loses substantial amounts of dust. Reduction in the nuclear radius is stopped, free evaporation of volatiles is replaced by their activated diffusion through the pores of the solid core, and the mass output is reduced more significantly. Because the dismantling process is accompanied by increasing lag effects in the direction distribution of mass ejection, the dynamical effects of output deficit are partly or completely

compensated, and the magnitude of NG forces may vary in a fairly smooth though complicated way in the D phase. More energy is spent on heating deeper layers of the core, so that the average nuclear temperature increases secularly. The comet passes through its *core* phase (C), the NG effects decreasing progressively. The ability of the nucleus to regenerate icy supplies at the surface gradually weakens. Physical activity becomes less regular, and the reactivation mechanism of the comet *breaks down* (phase B). NG effects are no longer detectable, and the comet is stellar or almost stellar in appearance. Finally the object, a chunk of solid materials, is completely deactivated and enters the ultimate *asteroidal* phase (A). The comet becomes a minor planet. Consequently, the core-mantle model is of interest from the point of view of possible cometary origin of some minor planets.

DYNAMICAL EVOLUTION

The Apollo and Albert type objects have aphelia well inside Jupiter's orbit. Practical calculations show that after one or more successive close approaches to Jupiter a comet can occasionally be captured into an eccentric orbit with aphelion Q as small as 4.5 or 4.6 AU. If, in addition, the revolution period of the comet in the new orbit slightly exceeds 3:1 (perihelion q about 0.5 AU) or 5:2 (perihelion slightly over 1 AU) resonance with Jupiter and if the comet has a fairly strong NG acceleration, we get the most favorable conditions for the comet to escape from disastrous encounters with Jupiter forever. The NG acceleration reduces the comet's aphelion distance approximately at a rate of $(4/3)a(\dot{\mu}/\mu)$ (AU per revolution), where a is the semimajor axis, μ the corresponding daily mean motion, and $\dot{\mu}$ the NG change of the latter per revolution. For a comet with $q = 0.5$ AU, $Q = 4.5$ AU, and secular acceleration of 0.1 day per revolution per revolution, the NG aphelion reduction rate amounts to 0.006 AU per century. The abovementioned conditions insure no close approach to Jupiter for, statistically, almost 200 revolutions after the capture. During this interval of time, the total NG decrease in the comet's aphelion distance can be estimated at almost 0.05 AU, a rather significant amount. Perturbations due to moderate approaches to Jupiter can increase, under favorable circumstances, the rate of reduction of the aphelion distance even more.

The above scheme includes implicitly a transition of the comet through a 3:1 or 5:2 resonance with Jupiter. A discussion of Marsden's experimentation with hypothetical NG forces in the motion of 887 Alinda suggests that a secular acceleration of about 0.04 day per revolution per revolution would be sufficient to overpower the coupling of the 3:1 resonance libration. Therefore, in the absence of close encounters with Jupiter, the NG acceleration of a moderate magnitude is dominant, over very long intervals of time, in reducing systematically the comet's aphelion distance. When the nucleus is completely depleted of volatile materials, the NG mechanism stops. The final aphelion distance depends on the original structure and dimensions of the comet's

nucleus. The core-mantle model provides a possibility of estimating the lifetime of a comet in its short-period orbit in terms of physical constants of the nucleus and the difference in aphelion distance between the time of capture and the death date.

NUCLEAR CORE IN AN ACTIVE COMET

The core-mantle model was designed with the aim of putting the interpretation of the NG effects in periodic comets on a quantitative basis and of following—also quantitatively—how a comet can possibly turn into a minor planet. The model proved successful in fitting very satisfactorily the secular variations in NG activity of periodic comet Encke over the past 150 yr (Sekanina, 1971). The model can be handled mathematically very easily, but more work should be done on its physics. The dismantling phase may particularly appear to be troublesome because of severe changes in the physical properties of the surface layer and, correspondingly, in the mass-output and heat-delay mechanisms.

A completely coreless nucleus is probably fictitious. However, a comet with a tiny solid core should behave in much the same manner. Its nucleus can be expected to have lower tensile strength, so that it obviously can be subject to catastrophic events more easily than a comet with a more sizable core. On the other hand, the secular fading of an almost coreless comet is likely to proceed more slowly than for a comet with a massive core.

Dynamically, the most important difference between the two models is in the sign of Marsden's B_2 coefficient (defined as a logarithmic derivative of the NG transverse component with time): the icy model cannot explain any positive B_2, whereas the core-mantle model cannot explain any B_2 more negative than about -0.01, a value that is extremely hard to detect in practice. In other words, one cannot distinguish between the two models unless B_2 is well determined and clearly different from zero.

A slightly or moderately negative B_2 may suggest that the comet has a tiny nuclear core. Of the comets with reliably known NG parameters, P/Biela and P/Giacobini-Zinner seem to be the most likely candidates. (See fig. 1; Marsden and Sekanina, 1971; and Yeomans, 1971.) The Přibram meteorite might be, with its typically cometary orbit, an example of what possibly remains from an almost coreless comet.

A strongly negative B_2 (say, -0.3 or more) is troublesome to explain in any case. In terms of the coreless icy model it means that the nucleus is already almost completely disintegrated; such a comet, however, would be barely visible. We therefore tend to believe that a strongly negative B_2 (and also a strongly positive B_2, unless confirmed by independent runs covering many revolutions) is caused by a sudden impulse on the comet's nucleus, possibly as a result of its collision with a cosmic projectile. Such "jumps" have been detected in the motion of P/Perrine-Mrkos, P/Schaumasse, and P/Giacobini-Zinner (Marsden, 1969, 1970; Yeomans, 1971) and may have also occurred in

the motion of P/Honda-Mrkos-Pajdušáková, P/Biela, and P/Forbes (Marsden, 1969; Marsden and Sekanina, 1971).

TRANSITION FROM COMETARY PHASE INTO ASTEROIDAL PHASE

The shape of the curve of NG activity varies from comet to comet. Specifically we note that a comet newly captured by Jupiter does not necessarily start its way across the graph in the E phase. The nuclear core could have already been dismantled by the time of capture, even if the comet had originally an icy envelope but had spent a very long time (at least, say, several thousand years) in low eccentricity orbits at solar distances comparable to that of Jupiter.

Similarly, the comet does not necessarily progress all the way down to complete deactivation. The regular course of events can be interrupted, for example, by expulsion of the comet back into a distant orbit if close approaches to Jupiter are not avoided. We must admit that some comets can undergo the capture-expulsion process several times during their lifetimes.

Therefore, only a small fraction of comets currently located on the core-mantle branch of evolution turn ultimately into minor planets. P/Arend-Rigaux and P/Neujmin 1 are apparently on the verge of the asteroidal phase, and both P/Encke and P/Tempel 2 are likely to reach the phase in a few tens of revolutions.

To see, on the other hand, whether the minor planets of the Apollo and Albert types could be extinct cometary nuclei, we have applied the core-mantle model to all of these objects that have perihelion distance smaller than 1.5 AU. We have found that nine of them may be of cometary origin. They are listed in table I. The cutoff at 1.5 AU has been applied because of the dimensions of Mars' orbit. Öpik (1963) has shown that about one-half of the original

TABLE I.–*Potential Extinct Cometary Nuclei Among Apollo and Albert Objects*

Object	Present orbit		Radius, km		Lifetime in cometary phase, yr
	q, AU	*Q*, AU	Present	Original	
Adonis	0.44	3.30	0.55	60	30 000
1953 EA	1.03	3.99	.3	3	3 000
Alinda	1.15	3.88	1.5	30	30 000
Albert	1.19	3.98	1.2	15	15 000
Ganymed	1.21	4.10	18.6	130	120 000
1963 UA	1.24	4.05	2.4	20	20 000
Beira	1.39	4.07	6.9	60	60 000
Kepler	1.43	3.93	2.3	40	45 000
Sirene	1.44	3.82	1.1	35	40 000

population of asteroidal objects crossing Mars survived since the time of origin of the solar system. The objects outside Mars' orbit (and well inside Jupiter's) must have collisional lifetimes much longer than the age of the solar system. There is, therefore, no point in attempting to prove their cometary origin.

The NG reduction in the aphelion distance, integrated over the comet's lifetime in the exposed orbit, amounts to less than 1 AU for objects with $q \geqslant 1$ AU and less than 1.5 AU for Adonis. Consequently, the mechanism cannot explain orbits with aphelia smaller than 3 AU and only exceptionally those smaller than 3.5 AU, unless the objects are allowed to have been originally huge bodies (more than several hundred kilometers in radius). For the same reason, Apollo itself was not found a likely candidate for this process, and also the strange orbit of Icarus cannot be explained solely by the effect of the NG mechanism.

Although it is difficult to give any specific figures at present, it is felt that the process of "permanent" capture of a comet into an eccentric orbit inside that of Jupiter is completed very rarely, and, therefore, the number of asteroids of the Apollo and Albert types that evolved in this way should be rather limited.

ACKNOWLEDGMENT

The writer's thanks belong to Dr. B. G. Marsden for a countless number of very valuable discussions about various aspects of the comet-asteroid relationships that helped to improve the quality of this paper.

REFERENCES

Marsden, B. G. 1969, Comets and Nongravitational Forces II. Astron. J. **74**, 720-734.

Marsden, B. G. 1970, Comets and Nongravitational Forces III. Astron. J. **75**, 75-84.

Marsden, B. G., and Sekanina, Z. 1971, Comets and Nongravitational Forces IV. Astron. J. **76**, in press.

Öpik, E. J. 1963, The Stray Bodies in the Solar System. Pt. I. Survival of Cometary Nuclei and the Asteroids. Advan. Astron. Astrophys. **2**, 219-262.

Sekanina, Z. 1971, A Model for the Nucleus of Encke's Comet. IAU Symp. no. 45.

Yeomans, D. K. 1971, Nongravitational Forces in Comet Giacobini-Zinner. IAU Symp. no. 45.

INTERRELATIONS OF METEORITES, ASTEROIDS, AND COMETS

EDWARD ANDERS
University of Chicago

Most meteorites come from a small number of parent bodies (6 to 11), with radii mainly between 100 and 300 km. The most likely sources of meteorites are seven asteroid families between 1.9 and 2.8 AU, whose eccentricities and inclinations are high enough to permit their collisional debris to cross the orbit of Mars. Comets are too small and too numerous to serve as a source of the major meteorite classes, but they may well be an important source of micrometeorites and carbonaceous chondrites.

Asteroids and comets are the two most plausible sources of meteorites. However, there is as yet no agreement on the relative importance of the two. Some authors believe that the great majority of meteorites come from comets (Öpik, 1965, 1968; Wetherill, 1968*a*). Others argue that they come mainly from asteroids (Anders, 1964; Wood, 1968). Let us review the principal clues to the nature of meteorite parent bodies, as obtained from the meteorites themselves.

NUMBER AND SIZE OF METEORITE PARENT BODIES

Irons

Wasson has shown in an impressive series of papers (Wasson, 1969, 1970, and earlier publications cited therein) that most iron meteorites fall into 11 discrete groups, differing from each other in chemical composition and structure. In four-dimensional composition space (Ga, Ge, Ir, and Ni) these groups form very compact, well-defined clusters. Many of these clusters can also be recognized by other criteria, such as radiation age and shock effects (Jaeger and Lipschutz, 1967; Voshage, 1967). The observed infall rate of these meteorites requires a source at least 1 to 100 km^3 in extent; and it therefore seems highly probable that each group represents either a separate parent body, or a sizable, compositionally distinct region within a parent body.

Clues to the size of these bodies have been obtained from the Widmanstätten pattern of iron meteorites. The formation of this pattern, long a subject of controversy, is now well understood, thanks to the work of Wood

(1964), Goldstein and Doan (1971), and Goldstein and Ogilvie (1965). As a result of this understanding, it has been possible to estimate cooling rates of iron meteorites through the range in which the pattern formed, 700 to 300 C. The results for nearly 300 iron meteorites and pallasites range from 0.4 to 500 K/million yr, with the majority of values lying between 1 and 10 K/million yr (table I).

These metallographically determined cooling rates are a direct clue to the size of the parent bodies, because the cooling rate of a planetary object is a sensitive function of size. Fricker et al. (1970) have shown that the above cooling rates correspond to radii between 10 and 500 km, with most values lying between 100 and 300 km. Some of Wasson's groups show little spread in cooling rates, which suggests that they come from a (nearly isothermal) core. Others show a nearly tenfold variation, which may imply that they are derived from a series of isolated iron pools extending from the center to the surface (Urey, 1966). At cooling rates less than 7 K/million yr, the radius depends strongly on whether the outer layers of the body are compositionally uniform or differentiated, with radioactive elements concentrated near the surface. Two different radii are therefore given in table I, for the uniform and differentiated cases.

The cooling rates have been confirmed by an independent method: fission-track measurements in the Toluca iron meteorite (Fleischer et al., 1968). By measuring tracks from extinct, 82 million yr ^{244}Pu in three minerals differing in track retention temperatures, Fleischer et al. obtained three points on a cooling curve for Toluca. The cooling rate found, $1.1^{+0.6}_{-0.3}$ K/million yr, agrees well with the metallographically determined value, 1.6 ± 0.6 K/million yr

TABLE I.–*Parent Bodies of Iron Meteorites*

Chemical group[a]	Cooling rate,[b] K/million yr	Number of members	Radius, km[c]		Radiation age,[d] million yr
			Uniform body	Differentiated body	
I	1 to 3.5	87	150 ±30	230 ±70	900
IIA	.....	29	.....	.....	⩽100
IIB	.....	11	.....	.....	1000
IIC	100 to 250	7	25 ±5	25 ±5	.....
IID	1 to 2	6	165 ±15	260 ±40	~1000
IIIA	1.5 to 10	24	170	250	700
IIIB	1 to 2	14	165 ±15	260 ±40	700
IIIC	2 to 5	5	130 ±10	180 ±40	700
IIID	2 to 5	5	130 ±20	180 ±40	200
IVA	7 to 90	16	100	110	400
IVB	2 to 20	7	150	220	Variable

[a]Wasson (1969, 1970, and earlier publications cited therein.)
[b]Goldstein and Short (1967*a*).
[c]Fricker et al. (1970).
[d]Voshage (1967).

(Goldstein and Short, 1967*b*). Although a few uncertainties remain, the metallographic cooling rates for iron meteorites are probably reliable to within a factor of 2 to 3.

The actual number of parent bodies involved may be as small as six. Though the subgroups IIIA to IIID are chemically distinct from each other, the differences are not drastic and in fact were not noticed until very precise analyses became available. Perhaps all came from the same body. All give essentially the same radius *r;* at least three of the four were produced in a single collision, judging from their common radiation age of ~700 million yr and the ubiquity of strong shock effects (Jaeger and Lipschutz, 1967). Similarly, IIA, B, and D may come from a single body. Assuming independent bodies for I, IIC, IVA, and IVB, we are thus left with only six bodies. Apparently more than 80 percent of all iron meteorites came from 11 bodies at most (possibly as few as six), of which all but 1 were larger than 100 km in radius.

Chondrites

According to chemical criteria, chondrites are divided into five groups (table II). The hiatuses separating these groups are not as wide as those for irons, and hence there is less reason to conclude, on *chemical* grounds, that only five parent bodies are involved. Here we must rely on other evidence.

Among the meteorites in table II, the L-chondrites stand out in having a preponderance of short K-Ar and U-He ages, discordant between 1 and 4 aeons, but becoming concordant at ~0.5 aeon. These short ages are correlated with shock and reheating symptoms. Detailed analysis of the data suggests that at least two-thirds of these meteorites were involved in a major collision 520 ± 60 million yr ago, which caused partial or complete outgassing of ^{40}Ar and ^{4}He (Anders, 1964; Heymann, 1967; Taylor and Heymann, 1969).

TABLE II.—*Classification of Chondrites*

[Van Schmus, 1969]

Chemical group	$\frac{Fe_{metal}}{Fe_{total}}$	Fe/Si	Mg/Si	$\frac{Fe^{2+}}{Fe^{2+} + Mg^{2+}}$, percent[a]	Known falls
E, enstatite	0.80±0.10	0.83±0.32	0.79±0.06	0 to 2	11
H }	.63±.07	.83±.08	.96±.03	16 to 20	225
L } ordinary[b]	.33±.07	.59±.05	.94±.03	22 to 26	273
LL }	.08±.07	.53±.03	.94±.03	27 to 31	39
C, carbonaceous	Low	.83±.08	1.05±.03	33	36

[a]Atom percentage of Fe^{2+} in principal ferromagnesian silicate ($(Mg, Fe)SiO_3$ in enstatite chondrites and $(Mg, Fe)_2SiO_4$ in all others).

[b]The symbols H, L, and LL refer to total iron content, and stand for high, low, and low-low, respectively.

If this is true, then the L-chondrites come mainly from one or at most two bodies. Because L-chondrites are the most abundant class of meteorites now falling on Earth, it seems that the majority of chondrites, like the irons, come from a small number of bodies: probably no more than 10, perhaps as few as five. The total number of bodies need not be greater than perhaps six because some chondrites and irons may come from the same body. For example, the outgassing time of L-chondrites, 520 ± 60 million yr, is rather close to the radiation age of group III irons, 600 to 700 million yr (Voshage, 1967), and the systematic errors in the two dating methods are large enough to admit the possibility that both refer to the same event. Chemical resemblances between these two classes are sufficiently great to permit an origin in the same body.

Wänke (1966) and Öpik (1968) have questioned the reality of the 520 million yr event, and the conclusion that most L-chondrites come from a single parent body. They suggest that the meteorite parent body was hot enough throughout its history to cause ^{4}He to partition between solid and pore space. On breakup, the ^{4}He in the pores would escape, leaving only a fraction of the total ^{4}He in the meteorite. If this fraction happened to be 8 percent, an *apparent* U-He age of 520 million yr would result.

However, this explanation appears to be untenable. It does not account for the fact that U-He ages of 0.5 aeon are sometimes associated with concordant K-Ar ages of 0.5 aeon, and sometimes with discordant values as high as 3 aeons. It predicts a correlation between U-He age and porosity that is not observed, and yet fails to explain the correlation between U-He or K-Ar age and shock effects that is observed. (This correlation has been confirmed by several authors: Carter et al., 1968; Christophe, 1969; Taylor and Heymann, 1969; Van Schmus and Ribbe, 1968; Wood, 1967.) Finally, the reality of the 520 million yr outgassing event has been confirmed by the ^{40}Ar/^{39}Ar method (Turner, 1969). Stepwise heating of six L-chondrites with nominal K-Ar ages from 1.0 to 1.85 aeons showed that the least retentive ^{40}Ar sites in each meteorite had been completely outgassed in a single event 500 ± 30 million yr ago; the higher ages for the bulk meteorites represent incomplete outgassing of the more retentive sites. Two other L-chondrites gave shorter ages (305 ± 30 million yr), implying partial or complete outgassing at a later time.

The size of the chondrite parent bodies can be estimated again from cooling rates, as for the irons. Wood (1967) has shown that most ordinary chondrites have cooled through 500 K at rates between 2 and 10 K/million yr. These limits correspond to depths of 40 to 150 km in bodies of $R \geqslant 150$ km and 20 to 80 km in bodies of $R \geqslant 90$ km. Similar cooling rates, 5 to 9 K/million yr, have been estimated from ^{129}Xe diffusion (Manuel et al., 1968). They are also supported by various estimates of cooling times. (See Anders, 1971, for discussion and references.) It would seem that the parent bodies of ordinary chondrites were of about the same size as those of the irons.

There are a few skeletons in this closet, however. Unequilibrated chondrites of three chemical groups and type III carbonaceous chondrites gave lower

cooling rates, 0.2 to 1 K/million yr, corresponding to depths of 70 to 150 km in bodies $\geqslant$400 km in radius. This is about the size of Ceres; and though one cannot rule out the possibility that another Ceres-sized asteroid once existed but was destroyed, it does not seem very plausible that this one body should be the source of the least recrystallized, most primitive meteorites, and from four chemically distinct classes at that. Perhaps the metallographic method becomes unreliable in systems containing stony phases in addition to metal. Exceedingly low cooling rates were obtained for two other silicate-containing classes: pallasites, 0.4 K/million yr, and mesosiderites, 0.1 K/million yr. The latter corresponds to a temperature drop of only 450 K during the entire age of the solar system.

POSSIBLE CANDIDATES

Comets

Comets are too numerous and too small to serve as the principal source of meteorites. Öpik (1965) has estimated the number of extinct, short-period comets with aphelion distance smaller than 4.94 AU as 2×10^4 to 10^5. A significant fraction of these must have perihelia less than 1 AU. Even if one assumes that only a special subset of this population (e.g., low-velocity objects) can contribute meteorites, the resulting number far exceeds the apparent number of meteorite parent bodies, about 6 to 10. Available estimates of comet sizes (Roemer, 1971; Whipple, 1963) show them to be one to two orders of magnitude smaller than the meteorite parent bodies. Larger comets undoubtedly exist, but it is difficult to see how one giant comet, disrupted 520 million yr ago, could furnish half of Earth's meteorite influx. It is also hard to reconcile the fragility and high volatile content of comets with the prolonged high-temperature history of meteorite parent bodies and with the texture, chemistry, and mechanical strength of meteorites.

Asteroids

At first sight, the small number of meteorite parent bodies would seem to be incompatible with an asteroidal origin because asteroids, too, are very numerous. More than 4000 are known and at least 10 times as many undiscovered ones are thought to exist in the telescopically observable size range alone. However, two factors very greatly reduce this number. To change a typical asteroidal orbit into a meteoritic one, an acceleration of about 6 km/s is required. Cratering theory and experiments show that only a minute fraction of the ejecta in a hypervelocity impact can be accelerated to this velocity, and because half the total energy appears as heat, such material will be vaporized. The absence of lunar basalts from Earth's meteorite collections shows that acceleration of rocks to $\geqslant$2.4 km/s is indeed a very improbable process. Thus the majority of asteroids cannot contribute to Earth's meteorite influx.

One group of asteroids that does not fall under this limitation is the Mars-crossing asteroids (Anders, 1964). Traversing the main part of the asteroid belt during every revolution, they suffer impacts from time to time. The debris, being ejected with low velocities, will move in similar, Mars-crossing orbits, but with slightly different periods. Consequently it soon spreads out in a toroid along the orbit of the parent body. Secular perturbations further disperse the fragments; and in a steady state, some of them are always in orbits intersecting the orbit of Mars. Close encounters with Mars reorient the velocity vectors of the debris (Arnold, 1965; Öpik, 1951), leading to Earth-crossing orbits in a fraction of cases. Thus Mars-crossing asteroids can serve as a source of meteorites.

The number of Mars asteroids, 34 according to the 1964 *Ephemeris* volume, is somewhat larger than the apparent number of meteorite parent bodies. However, 21 of these, comprising 98 percent of the mass and 92 percent of the cross section, belong to four Hirayama families (Anders, 1964). Thus the number of original Mars asteroids is indeed of the same order as the number of meteorite parent bodies.

Let us see how the picture changes when we make more optimistic assumptions about the escape of meteorites from the asteroid belt. Some asteroids of high inclination that are not Mars crossing at present will periodically become so, owing to secular perturbations (e.g., Pallas; Smith, 1964). Data are not available for most asteroids of interest, and would, moreover, not be quite appropriate for their debris, which moves in slightly different orbits. To obtain some sort of *upper limit* on the number of asteroids that can contribute meteorites, let us calculate **U**, the velocity relative to a hypothetical circular orbit at the same semimajor axis a (Öpik, 1951):

$$U^2 = 2\left(1 - \sqrt{1 - e^2}\cos i\right)$$

The components of **U** in the x, y, and z directions are

$$U_x = e$$

$$U_z = \sqrt{1-e^2}\sin i$$

$$U_y = \sqrt{1-e^2}\cos i - 1 = \text{const}$$

Minimum perihelion $q_{\min}$ is reached when **U** is reoriented such that U_z and $i = 0$, causing e to reach $e_{\max}$. At each value of a, only debris from asteroids with U greater than some minimum value has a chance of reaching the orbit of Mars, and then only in the doubly favorable case that perturbations cause U_z to approach zero and cause the node to occur at or near minimum perihelion.

Whether such reorientation can actually take place is completely uncertain. One must appeal to unknown or ill-understood effects; e.g., higher order terms in secular perturbations or commensurabilities with Jupiter. However, it may be significant that the asteroids with highest eccentricities (719, 887, 1036,

6344) occur near the 1/3 commensurability, $a = 2.50$ AU. Perhaps a substantial reorientation of **U** takes place when a is close to a major commensurability. Because all Mars-crossing asteroid families have a within 0.2 AU of the 1/3, 1/4, or 2/5 commensurabilities, some fraction of their ejecta will have commensurable orbits. They will certainly be subject to strong Jupiter perturbations, perhaps of the required kind.

[*Note added after colloquium:* There now exists some support for these speculations. Williams[1] has found, using his new theory of secular perturbations, that several resonance surfaces exist in a, e', $\sin i'$ space in the inner asteroid belt. Any object in the vicinity of these resonances will experience very large oscillations in e and i, which of course favor attainment of a Mars-crossing orbit. Interestingly, each of the high-velocity asteroid families in figure 1 adjoins one or more of these resonance surfaces. A significant fraction of their collisional debris thus will be thrown into these resonance regions, where the postulated reorientation of **U** may take place. Williams' resonances may thus be the long-sought factor permitting change of highly inclined to highly eccentric orbits.]

The distribution of U is illustrated in figure 1 for the inner half of the asteroid belt. The minimum value of U required to reach $q = 1.700$ AU (a value part way between the present and maximum aphelion of Mars) is indicated by the solid line. Asteroids lying above the line are potential sources of Mars-crossing debris under the above, optimistic assumptions.

Nearly one-tenth of all asteroids have $q_{\min}$ less than 1.700 AU. Yet the number of potential meteorite parent bodies has not increased greatly. Many of the newly added asteroids are less eccentric but otherwise bona fide members of Mars-crossing families 5, 29, 30, and 31.[2] Others fall within the boundaries of these families on a U versus a plot, but have e' and i' outside the family limits. They are either interlopers or former members whose elements were changed by Mars encounters.

Only three new families appear on this graph. The cluster at 1.9 AU, though quite disperse on an a, e', i' plot, is fairly compact on a U, a plot. Nine additional members of this cluster were discovered by van Houten et al. (1970), who referred to it as the "Hungaria group." Family 28, including 2 Pallas, becomes marginally Mars crossing every 10^4 yr (Smith, 1964) but its velocity is high enough to give a potential $q_{\min}$ as small as 1.10 AU if $i = 0$. In fact, family 30 may have been derived from family 28 by a partial reorientation of **U**. Family 17 is a very marginal case, but has been included for the sake of completeness.

---

[1]See p. 177.

[2]The status of family 31 is in some jeopardy. Anders (1965) suggested that it might be related to the Flora families, 6 to 9. Arnold (1969) has questioned its reality on the grounds that it constitutes only a twofold enhancement of asteroid density in a, e', i' space over the general "background." Van Houten et al. (1970) have assigned number 31 to another family, not being aware of the previous assignment.

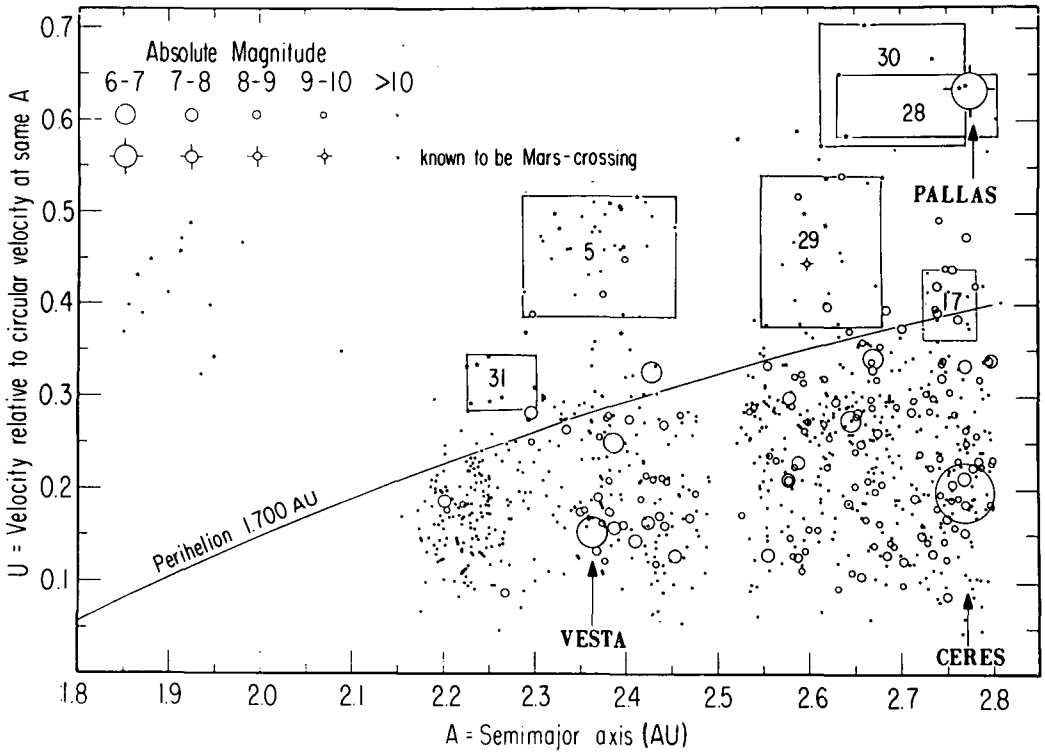

Figure 1.–The curve represents the critical condition for achieving a Mars-crossing orbit. Asteroids lying above this line either have Mars-crossing orbits or are potentially capable of ejecting debris into such orbits if secular perturbations reorient U so as to make *i* small and allow the node to occur at perihelion. Most of these actually or potentially Mars-crossing asteroids are members of six numbered Hirayama families or the Hungaria group at 1.9 AU.

Only a few nonfamily asteroids fall above the $q = 1.700$ AU line, most of them by very marginal amounts. The only sizable objects are 18 Melpomene at 2.296 AU (possibly related to family 31), 6 Hebe at 2.426 AU, 247 Eukrate at 2.741 AU, and 148 Gallia at 2.771 AU. A list of actual or potential Mars crossers is given in table III. Original radii were reconstructed according to Anders (1965), using data for the first 1651 numbered asteroids from the 1964 *Ephemeris* volume. A geometric albedo of 0.12, as for Ceres, was assumed, resulting in the magnitude-radius relationship

$$\log R = 3.385 - 0.200g$$

We see that the reconstructed family asteroids (table III) are only about one-half as large or one-eighth as massive as the meteorite parent bodies (table I). This is not surprising, because the family asteroids now visible represent but a fraction of the original population. If we ascribe the discrepancy to loss of 7/8 of the members by dispersal or deflection to terrestrial space, the combined half-life for these processes must be on the order of 1 to 2 aeons, depending on the age of the family. This is roughly consistent with the half-lives found in Monte Carlo calculations, and with Dohnanyi's (1969) estimated lifetimes for collisional destruction of asteroids 10 to 20 km in radius. The half-lives may be longer if the albedo of the asteroids is smaller than assumed. A value of 0.065, as for Phobos (Smith, 1970), would reduce the mean discrepancy in mass to a factor of ~3 and would lengthen the half-life accordingly.

We note in passing that the two most massive objects in table III, 2 Pallas and 6 Hebe, are not extensively broken up, and hence probably cannot serve as

TABLE III.—*Actual and Potential Mars-Crossing Asteroids*

Family	Number of members	Representative member	a, AU	q, AU	q_{min},[a] AU	U	R_0, km
Hungaria	23	1235 Schorria	1.910	1.617	1.060	0.457	[b]11
31	9	1204 Renzia	2.264	1.596	1.592	.300	[c]71
5 Phocaea	34	1310 Villigera	2.392	1.538	1.219	.507	[b]53
30 Aethra	4	1036 Ganymed	2.658	1.216	.910	.703	[b]28
29 Desiderata	7	1134 Kepler	2.683	1.432	1.289	.539	[b]53
17	11	36 Atalante	2.749	1.924	1.576	.437	[b]85
28 Pallas	6	2 Pallas	2.772	2.123	1.103	.635	245
Hebe	1	6 Hebe	2.426	1.934	1.646	.326	116

[a]For zero inclination.

[b]Highly fragmented.

[c]Including 18 Melpomene; without this asteroid, R_0 would be 5 km and the classification changed to highly fragmented.

sources of iron meteorites. Most or all irons in each group apparently came from the deep interiors of their parent bodies (Fricker et al., 1970). But if the dispersal-deflection half-life is as short as 1 to 2 aeons, some older families may have been decimated, fragmented, and dispersed beyond recognition. Their remains are presumably hidden in the nonfamily background in figure 1.

Thus far we have relied entirely on planetary perturbations to extract meteorites from the asteroid belt, neglecting the effect of ejection velocity. Actually, it appears that ejection velocity was an important factor in at least one case, the group III irons. Jaeger and Lipschutz (1967) have noted that group III irons, without exception, are shocked to >13 GN/m^2 (130 kb), often to >75 GN/m^2 (750 kb). Shock pressures of this order correspond to free-surface velocities of 1 to 3 km/s; and the fact that no lightly shocked members are found in group III (in contrast to other groups) suggests that high shock pressures, and the concomitant acceleration, were essential to the escape of these meteorites from the asteroid belt. Jaeger and Lipschutz propose that the parent body of group III was a ring asteroid not crossing the orbit of Mars. Only its high-velocity ejecta had a chance of achieving a Mars-crossing orbit, the essential prerequisite for deflection into terrestrial space.

Various objections have been raised to Mars asteroids as the principal source of meteorites. Öpik (1965, 1968) has pointed out that their mean lives for deflection into Earth-crossing orbits, 10^9 to 10^{10} yr, are far longer than the radiation ages of stony meteorites, 2×10^4 to 6×10^7 yr. He maintains that such short capture times are completely unattainable for debris from Mars asteroids. However, it is important to make a distinction between *mean* capture times for a large population and *actual* capture times for individual objects. On the Mars asteroid model, the radiation age T is the sum of two intervals: t_1, from ejection of the meteorite from its parent body to deflection into an Earth-crossing orbit, and t_2, from achievement of the first Earth-crossing orbit to actual capture by Earth. Both t_1 and t_2 are exponentially distributed about the *mean* lives for the two processes, τ_1 and τ_2, and, because the most probable values of t_1 and t_2 in an exponential distribution are zero, small values of T are not at all inconsistent with large values of τ_1 and τ_2. One can also prove this by recognizing that the toroidal debris stream associated with each Mars asteroid is analogous to a meteor stream. Typically, orbits of planet and stream intersect for a few centuries during each 10^4 yr oscillation in e and i. If the stream is continuous, some objects will be captured or deflected during each revolution as the planet crosses the stream. Because the distribution of radiation ages along the stream is random, the objects deflected will include some very young ones.

Arnold (1965) and Wetherill (1967, 1968*a*) objected to a Mars asteroid origin mainly on the grounds that it would give a preponderance of long ages, in the range 10^8 to 10^9 yr. In principle, such long ages could be suppressed by collisional destruction of meteorites, but a careful analysis of the problem seemed to show that the density of dust and rubble in the asteroid belt was too

low to give a short enough lifetime against collisional destruction; e.g., 10^7 yr. However, there is good reason to believe that the destruction lifetime is indeed on this order. Dohnanyi (1969) has reexamined the problem using an improved mass distribution function and cratering relations. He obtains mean destruction lifetimes of 3 to 10 million yr for objects 10 to 100 cm in diameter. Mazor et al. (1970) and Herzog (1970) have pointed out the curious fact that the radiation age distributions of meteorites show cutoffs related to crushing strength: ~15 million yr for the friable carbonaceous chondrites, ~60 million yr for all other stones, ~200 million yr for stony irons, and ~2 billion yr for irons. It appears that the age distribution is indeed governed by collisional destruction. Cutoffs of exactly the right order have been produced in Monte Carlo calculations, using a destruction lifetime of 10 million yr (Mellick and Anders, unpublished).

Of course, if the majority of stony meteorites are destroyed by collisions, a correspondingly more intense source is needed to maintain the meteorite flux observed on Earth (10^5 to 10^6 kg/yr). The potential reservoir, from figure 1, is probably on the order of 10^{19} to 10^{20} kg, so that even an extraction efficiency as low as 10^{-2} to 10^{-3} would suffice to maintain this flux for 10^9 to 10^{10} yr. However, if the correlations of ω (the argument of perihelion) and e noted by Wetherill (1968*a*) prevent node and perihelion from coinciding even over periods of $>10^7$ yr, and even for ejecta, then there may indeed be a problem.

Another observation to be explained is the predominance of p.m. falls among the chondrites. Wetherill (1968*b*, 1969) has pointed out that this requires a large orbit of low inclination. Moreover, the meteorite must be captured by Earth during the first few passes, otherwise a decreases, i increases, and the a.m./p.m. asymmetry is lost. Wetherill suggested that a special class of low-velocity, short-period, cometary orbits with aphelia near Jupiter would be suitable because objects in such orbits, if not quickly captured by Earth, are soon eliminated by Jupiter. However, it is difficult to envision circumstances where this type of orbit would dominate over more conventional short-period cometary orbits with higher geocentric velocities and/or smaller aphelia. It seems that the a.m./p.m. asymmetry can be equally well explained by the asteroidal model if collisional destruction is invoked to prevent "evolution" of the orbit by repeated close encounters with Earth. With a destruction lifetime of 3 to 10 million yr (Dohnanyi, 1969), meteorites will be captured by Earth in the first few passes, if at all.

An unsolved problem still remaining is the relatively high frequency of meteorites with high geocentric velocities, $U_e = 0.5$ to 0.7. Data are limited and of variable quality, but it appears from the available information on photographic and visual meteorite orbits (Millman, 1969), dense ("asteroidal") meteors, and Apollo asteroids that perhaps one-third of all meteorites have velocities in this range. Monte Carlo calculations for all Mars asteroid families give such velocities in much lower abundance (Anders and Mellick, 1969;

Mellick and Anders, unpublished). In principle, the required acceleration could be achieved by an appulse to Jupiter, but such appulses lead to crossings and subsequent rapid elimination of the object. Perhaps commensurabilities or other factors stabilize some types of large orbit long enough for Earth capture to compete with Jupiter ejection. A theoretical investigation of this problem would be very desirable.

COMETARY CONTRIBUTION TO THE METEORITE FLUX

If most meteorites come from Mars asteroids, where then is the cometary debris? Three major clues are available: meteors, Apollo asteroids, and meteoritic material on the Moon.

Meteors

It appears that the majority of photographic meteors, including the Prairie Network fireballs, are of cometary origin (McCrosky[3]). An asteroidal component seems to be present (Ceplecha, 1966; Kresák, 1969*a,b*) but is clearly subordinate in this mass range.

Apollo Asteroids

The Apollo asteroids seem to fall into two groups differing in geocentric velocity (table IV). Anders and Arnold (1965) suggested that the low-velocity group was asteroidal and the high-velocity group, cometary. Some support for this division has been obtained by Gehrels and his associates. The "cometary"

TABLE IV.—*Apollo Asteroids*
[Wetherill and Williams, 1969]

Asteroid	*a*, AU	U_e	*R*, km
1620 Geographos[a]	1.244	0.393	1.62
1685 Toro	1.382	.443	2.82
1950 DA	1.695	.451	1.02
Hermes	1.29	.481	.39
1948 EA	2.261	.536	2.95
Apollo	1.48	.569	.39
1959 LM	2.155	.624	2.45
Adonis	1.97	.852	.15
1580 Betulia	2.195	.978	1.86
1566 Icarus[b]	1.078	.995	.54
Comet Encke	2.22	1.002	

[a]Axial ratio is 3.4 (Gehrels et al., 1970).
[b]Axial ratio is 1.1 (Gehrels et al., 1970).

[3]See p. 395.

object 1566 Icarus shows only a minor variation ($\leqslant$0.24 mag) in its lightcurve, implying a nearly spherical shape, to $\leqslant$10 percent (Gehrels et al., 1970). According to Dohnanyi (1969), an object 0.54 km in radius, situated in the asteroid belt, has a lifetime of only 2.5×10^8 yr against collisional destruction. It seems inconceivable that an object as small as Icarus could have maintained its spherical shape for 4.5 aeons if it had resided in the asteroid belt during that time. Oort's comet belt, on the other hand, would be an acceptable, relatively collision-free place of storage.

The asteroidal object 1620 Geographos, on the other hand, has a strongly elongated shape, with axial ratio 3.4:1 (Gehrels et al., 1970). This is entirely reasonable for an object that spent its entire life in the asteroid belt.

If geocentric velocity is accepted as the criterion, three of the objects in table IV are cometary and seven asteroidal. (Comet Encke must be omitted because its discovery was aided by its light emission.) On a mass basis, the cometary contribution would seem to be smaller than 30 percent, but in view of the limited statistics, not much can be made of this trend.

Moon

A number of trace elements (Au, Ir, Bi, Te, etc.) are enriched in Apollo 11 lunar soils and breccias relative to igneous rocks, apparently reflecting addition of a meteoritic component (Ganapathy et al., 1970). From the abundance pattern it appears that this component consists largely of primitive, "carbonaceous-chondrite-like" material. The amount is about 1.9 percent, corresponding to an average influx rate of 4×10^{-9} g-cm^{-2}-yr^{-1}. This agrees within a factor of 3 with a similar estimate for Earth, based on the Ir and Os content of Pacific and Indian Ocean sediments (Barker and Anders, 1968).

Apollo 12 soils collected some distance away from craters showed a very similar pattern, whereas those collected on crater rims gave a different pattern, resembling fractionated meteorites (irons, ordinary chondrites) in their low abundance of Bi, for example (Laul et al., 1971).

Six different impacts have thus far been characterized, and it seems that five of them were caused by fractionated meteorites (table V). On the basis of these

TABLE V.–*Meteorite Impacts on Moon*

[Laul et al., 1971]

Event	Crater diameter, km	Projectile composition
12017 Glass	?	Primitive
Bench Crater	.07	Fractionated
Head Crater	.13	Fractionated
Surveyor Crater	.18	Fractionated
10085 Anorthosite	?	Fractionated
Copernicus?	91	Fractionated

limited statistics, it appears that fractionated material dominates among the larger (>1 kg) bodies falling on both Earth and the Moon. Primitive material, on the other hand, seems to dominate among the subkilogram objects that are apparently responsible for the uniform blanket of C1-like material covering the Moon and for fireballs or meteors on Earth.

Probably the primitive component consists mainly of the debris of spontaneously disintegrating comets, with an unknown asteroidal contribution. Comets are rich in volatiles and hence almost certainly are of primitive composition. However, any material accreted at temperatures below ~400 K is likely to have this composition. An additional source of such material may thus be asteroids from the outer part of the belt and the surface layers of all asteroids.

ORIGIN OF METEORITES

Great efforts have been made to understand the chemical and thermal history of meteorites, starting with Urey's (1952, 1954) classic papers. It appears that the observed chemical fractionations, involving some 55 elements, are due to only four basic processes that occurred in the solar nebula during cooling from high temperatures. I have reviewed the subject in a recent paper (Anders, 1971) and will therefore merely summarize the model that best accounts for the evidence (fig. 2). Degree of condensation is plotted on the ordinate; and degree of retention, on the abscissa.

(1) An early condensate, containing refractory elements (Ca, Al, Ti, U, Th, lanthanides, Pt metals, etc.) was partially lost from ordinary and enstatite chondrites.

(2) After condensation of the remaining material to grains of 10^{-5} to 10^{-6} cm, some of the nickel-iron was lost, at a temperature around 700 K. During this and the following stages, the enstatite chondrites apparently found themselves in a more reducing environment, perhaps a gas phase of $C/O \geqslant 0.9$.

(3) During or after the metal loss, about 30 to 80 percent of the condensate was remelted to millimeter-sized droplets by local heating events on a time scale of seconds to minutes (probably electric discharges; Whipple, 1966). Volatiles were lost from the remelted material.

(4) The unremelted, fine-grained material continued to take up volatiles from the nebula (Pb, Bi, Tl, In, etc.) and accreted with the remelted material. Accretion took place at $P = 10^{-4\pm2}$ atm and falling temperatures, as indicated in figure 2. The values for carbonaceous and enstatite chondrites are only rough estimates.

The five principal chondrite classes were affected by these processes to a markedly different extent. Carbonaceous chondrites were generally affected least, and enstatite chondrites, most. Presumably this reflects differences in place and time of formation. If we only knew the original location of their

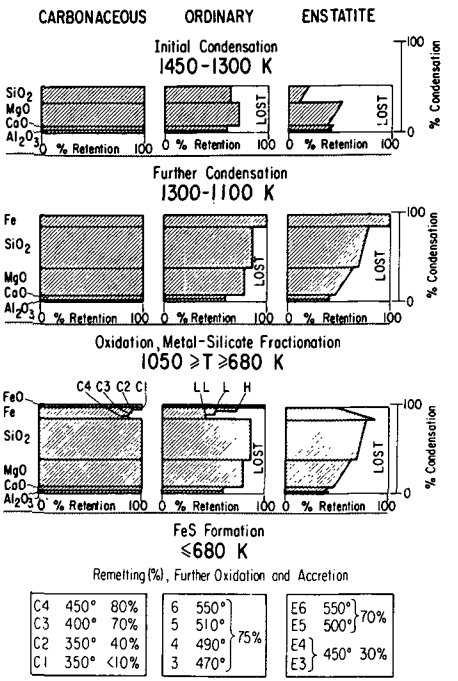

Figure 2.–Proposed outline of chondrite formation in a cooling solar nebula (Larimer and Anders, 1970). Shaded areas represent condensed phase at end of each stage. Fraction condensed is shown on ordinate; amount remaining after fractionation, on abscissa. Four partial fractionations seem to have taken place: (1) loss of initial condensate at ~1300 K, (2) loss of metal at ~700 K, (3) remelting at ~500 to 600 K, and (4) accretion at 350 to 550 K. The three main chondrite classes presumably represent three to five different regions of the inner solar nebula. Boxes at bottom of figure give estimated accretion temperatures of each petrologic type and percent remelted, volatile-poor materials. Numbers refer to petrologic types within each chondritic class.

parent bodies, we could correlate all this information with heliocentric distance, and thus reconstruct the chemical and thermal history of the inner solar nebula in considerable detail.

ACKNOWLEDGMENTS

I am indebted to Michael S. Lancet and Rudy Banovich for the preparation of figure 1. This work was supported in part by the U.S. AEC Contract AT(11-1)-382 and NASA Grant NGL 14-001-010.

REFERENCES

Anders, E. 1964, Origin, Age, and Composition of Meteorites. Space Sci. Rev. 3, 583-714.
Anders, E. 1965, Fragmentation History of Asteroids. Icarus 4, 399-408.
Anders, E. 1971, Meteorites and the Early Solar System. Ann. Rev. Astron. Astrophys. 9, 1-34.

Anders, E., and Arnold, J. R. 1965, Age of Craters on Mars. Science 149, 1494-1496.

Anders, E., and Mellick, P. J. 1969, Orbital Clues to the Nature of Meteorite Parent Bodies. Meteorite Research (ed., P. M. Millman), ch. 47, pp. 560-572. D. Reidel. Dordrecht.

Arnold, J. R. 1965, The Origin of Meteorites as Small Bodies. II. The Model. Astrophys. J. 141, 1536-1547.

Arnold, J. R. 1969, Asteroid Families and "Jet Streams." Astron. J. 74, 1235-1242.

Barker, J. L., Jr., and Anders, E. 1968, Accretion Rate of Cosmic Matter From Iridium and Osmium Contents of Deep-Sea Sediments. Geochim. Cosmochim. Acta 32, 627-745.

Carter, N. L., Raleigh, C. B., and DeCarli, P. S. 1968, Deformation of Olivine in Stony Meteorites. J. Geophys. Res. 73, 5439-5461.

Ceplecha, Z. 1966, Classification of Meteor Orbits. Bull. Astron. Inst. Czech. 17, 96-98.

Christophe, Michel-Lévy, M. C. 1969, Comparaison de Certains Aspects de la Structure Microscopique des Chondrites Avec Leur Âge Apparent de Rétention Gazeuse. C. R. Acad. Sci. Paris 268, 2853-2855.

Dohnanyi, J. S. 1969, Collisional Model of Asteroids and Their Debris. J. Geophys. Res. 74, 2531-2554.

Fleischer, R. L., Price, P. B., and Walker, R. M. 1968, Identification of Pu^{244} Fission Tracks and the Cooling of the Parent Body of the Toluca Meteorite. Geochim. Cosmochim. Acta 32, 21-31.

Fricker, P. E., Goldstein, J. I., and Summers, A. L. 1970, Cooling Rates and Thermal Histories of Iron and Stony-Iron Meteorites. Geochim. Cosmochim. Acta 34, 475-491.

Ganapathy, R., Keays, R. R., Laul, J. C., and Anders, E. 1970, Trace Elements in Apollo 11 Lunar Rocks: Implications for Meteorite Influx and Origin of Moon. Proc. Apollo 11 Lunar Sci. Conf. Geochim. Cosmochim. Acta 34, suppl. 1, 1117-1142.

Gehrels, T., Roemer, E., Taylor, R. C., and Zellner, B. H. 1970, Minor Planets and Related Objects. IV. Asteroid (1566) Icarus. Astron. J. 75, 186-195.

Goldstein, J. I., and Doan, A. S., Jr. 1971, The Effect of Phosphorus on the Formation of the Widmanstätten Pattern in Iron Meteorites. Geochim. Cosmochim. Acta 35, in press.

Goldstein, J. I., and Ogilvie, R. E. 1965, The Growth of the Widmanstätten Pattern in Metallic Meteorites. Geochim. Cosmochim. Acta 29, 893-920.

Goldstein, J. I., and Short, J. M. 1967*a*, The Iron Meteorites, Their Thermal History, and Parent Bodies. Geochim. Cosmochim. Acta 31, 1733-1770.

Goldstein, J. I., and Short, J. M. 1967*b*, Cooling Rates of 27 Iron and Stony-Iron Meteorites. Geochim. Cosmochim. Acta 31, 1001-1023.

Herzog, G. F. 1970, A Revised Radiation Age for Norton County Meteorite. Paper presented at National Fall Meeting, Amer. Geophys. Union (San Francisco).

Heymann, D. 1967, On the Origin of Hypersthene Chondrites: Ages and Shock-Effects of Black Chondrites. Icarus 6, 189-221.

Houten, C. J. van, Houten-Groeneveld, I. van, Herget, P., and Gehrels, T. 1970, Palomar-Leiden Survey of Faint Minor Planets. Astron. Astrophys. Suppl. Ser. 2, 339-448.

Jaeger, R. R., and Lipschutz, M. E. 1967, Implications of Shock Effects in Iron Meteorites. Geochim. Cosmochim. Acta 31, 1811-1832.

Kresák, L. 1969*a*, The Discrimination Between Cometary and Asteroidal Meteors–I. The Orbital Criteria. Bull. Astron. Inst. Czech. 20, 177-188.

Kresák, L. 1969*b*, The Discrimination Between Cometary and Asteroidal Meteors–II. The Orbits and Physical Characteristics of Meteors. Bull. Astron. Inst. Czech. 20, 232-251.

Larimer, J. W., and Anders, E. 1970, Chemical Fractionations in Meteorites–III. Major Element Fractionations in Chondrites. Geochim. Cosmochim. Acta 34, 367-388.

Laul, J. C., Morgan, J. W., Ganapathy, R., and Anders, E. 1971, Meteoritic Material in Lunar Samples: Characterization From Trace Elements. Proc. Apollo 12 Lunar Sci. Conf. Geochim. Cosmochim. Acta 35, suppl. 1.

Manuel, O. K., Alexander, E. C., Jr., Roach, D. V., and Ganapathy, R. 1968, ^{129}I-^{129}Xe Dating of Chondrites. Icarus 9, 291-304.

Mazor, E., Heymann, D., and Anders, E. 1970, Noble Gases in Carbonaceous Chondrites. Geochim. Cosmochim. Acta 34, 781-824.

Millman, P. M. 1969, Astronomical Information on Meteorite Orbits. Meteorite Research (ed., P. M. Millman), ch. 45, pp. 541-551. D. Reidel. Dordrecht.

Öpik, E. J. 1951, Collision Probabilities With the Planets and Distribution of Interplanetary Matter. Proc. Roy. Irish Acad. Sect. A 54, 165-199.

Öpik, E. J. 1965, The Stray Bodies in the Solar System. Part II. The Cometary Origin of Meteorites. Adv. Astron. Astrophys. 4, 301-336.

Öpik, E. J. 1968, The Cometary Origin of Meteorites. Irish Astron. J. 8, 185-208.

Roemer, E. 1971, Long-Focus Observations. Paper presented at 3d Ann. Meeting, Div. Planet. Sci., Amer. Astron. Soc. (Tallahassee).

Smith, A. J., Jr. 1964, A Discussion of Halphen's Method for Secular Perturbations and Its Application to the Determination of Long Range Effects in the Motions of Celestial Bodies. Pt. 2. NASA TR R-194.

Smith, B. A. 1970, Phobos: Preliminary Results From Mariner 7. Science 168, 828-830.

Taylor, G. J., and Heymann, D. 1969, Shock, Reheating, and the Gas Retention Ages of Chondrites. Earth Planet. Sci. Lett. 7, 151-161.

Turner, G. 1969, Thermal Histories of Meteorites by the ^{39}Ar-^{40}Ar Method. Meteorite Research (ed., P. M. Millman), ch. 34, pp. 407-417. D. Reidel. Dordrecht.

Urey, H. C. 1952, Chemical Fractionation in the Meteorites and the Abundance of the Elements. Geochim. Cosmochim. Acta 2, 269-282.

Urey, H. C. 1954, On the Dissipation of Gas and Volatilized Elements From Protoplanets. Astrophys. J. Suppl. Ser. 1(6), 147-173.

Urey, H. C. 1966, Chemical Evidence Relative to the Origin of the Solar System. Mon. Notic. Roy. Astron. Soc. 131, 199-223.

Van Schmus, W. R. 1969, The Mineralogy and Petrology of Chondritic Meteorites. Earth Sci. Rev. 5, 145-184.

Van Schmus, W. R., and Ribbe, P. H. 1968, The Composition and Structural State of Feldspar From Chondritic Meteorites. Geochim. Cosmochim. Acta 32, 1327-1342.

Voshage, H. 1967, Bestrahlungsalter und Herkunft der Eisenmeteorite. Z. Naturforsch. A 22, 477-506.

Wänke, H. 1966, Meteoritenalter und verwandte Probleme der Kosmochemie. Fortschr. Chem. Forsch. 7, 322-408.

Wasson, J. T. 1969, The Chemical Classification of Iron Meteorites–III. Hexahedrites and Other Irons With Germanium Concentrations Between 80 and 200 ppm. Geochim. Cosmochim. Acta 33, 859-876.

Wasson, J. T. 1970, The Chemical Classification of Iron Meteorites–IV. Irons With Ge Concentrations Greater Than 190 ppm and Other Meteorites Associated With Group I. Icarus 12, 407-423.

Wetherill, G. W. 1967, Collisions in the Asteroid Belt. J. Geophys. Res. 72, 2429-2444.

Wetherill, G. W. 1968*a*, Dynamical Studies of Asteroidal and Cometary Orbits and Their Relation to the Origin of Meteorites. Origin and Distribution of the Elements (ed., L. H. Ahrens), pp. 423-443. Pergamon Press. Oxford.

Wetherill, G. W. 1968*b*, Time of Fall and Origin of Stone Meteorites. Science 159, 79-82.

Wetherill, G. W. 1969, Relationships Between Orbits and Sources of Chondritic Meteorites. Meteorite Research (ed., P. M. Millman), ch. 48, pp. 573-589. D. Reidel Dordrecht.

Wetherill, G. W., and Williams, J. G. 1969, Evaluation of the Apollo Asteroids as Sources of Stone Meteorites. J. Geophys. Res. 73, 635-648.

Whipple, F. L. 1963, On the Structure of the Cometary Nucleus. The Moon, Meteorites, and Comets. Vol. IV of The Solar System (eds., B. M. Middlehurst and G. P. Kuiper), pp. 639-664. Univ. of Chicago Press. Chicago.

Whipple, F. L. 1966, A Suggestion as to the Origin of Chondrules. Science 153, 54-56.
Wood, J. A. 1964, The Cooling Rates and Parent Planets of Several Iron Meteorites. Icarus 3, 429-460.
Wood, J. A. 1967, Chondrites: Their Metallic Minerals, Thermal Histories, and Parent Planets. Icarus 6, 1-49.
Wood, J. A. 1968, Meteorites and the Origin of Planets. McGraw-Hill Book Co., Inc. New York.

COMETARY VERSUS ASTEROIDAL ORIGIN OF CHONDRITIC METEORITES

GEORGE W. WETHERILL
University of California, Los Angeles

Much of what we know about the early history of the solar system has been learned from the study of meteorites. This results from the fact, demonstrated by isotopic age measurements, that all of the various classes of stone and iron meteorites were formed 4.6×10^9 yr ago within a short period of time, probably less than 100 million yr in duration. This is also the age of Earth and the Moon and may be presumed to be the time of formation of the solid bodies in the solar system. Measurements of the products of the decay of the extinct radioactive isotopes ^{129}Xe and ^{244}Pu show, furthermore, that the formation of these solid bodies occurred within 100 million yr of the time of separation of the solar nebula from interstellar matter. Except for physical fragmentation into smaller bodies, the chemical and mineralogical composition of most meteorites has been essentially unaltered since this time during the formation interval of the solar system.

This situation contrasts with that found on Earth, where geological processes have essentially erased the record of the first 25 percent of Earth's history. The Moon is now known to be intermediate between Earth and meteorites in this regard. Although the record of the Moon's early history is preserved to a much greater extent than that of Earth, significant formation of lunar rocks occurred at least as recently as 3.3×10^9 yr ago. Although the best preserved record of the early history of the solar system is to be found in the meteorites, these data are difficult to interpret because, unlike rocks from Earth and the Moon, we have no definite information regarding the sources in the solar system of these rocks that are now colliding with Earth. Were such information to become available, the role of meteorites would become fully equivalent to that of lunar samples in experimental studies of the origin of the solar system.

SUMMARY OF EARLIER WORK

From the work of Öpik (1951) we know that neither the meteoritic fragment nor its parent body can have been in its present Earth-crossing orbit for the entire history of the solar system. This is because these orbits are stable

with respect to planetary impact or ejection from the solar system for no more than 100 million yr. From the cosmic-ray-exposure ages we also know that the meteorite was broken from a larger body late in the history of the solar system. These facts require us to find some place in the solar system where we can "store" the larger body from which the meteorite was fragmented for most of the solar system's history, and then we must find a way to transfer more recently either the fragment or the parent body itself from its "storage place" into an Earth-crossing orbit, from which further fragmentation and collision with Earth are possible.

The problem of identifying the source of meteorites can therefore be approached from the point of view of finding an appropriate storage place. The surfaces of a planetary body such as Mars or the Moon have been proposed, but are very unlikely to be satisfactory. It is hard to see how a fragment of meteoritic size can be accelerated to planetary escape velocities without complete destruction, or without at least experiencing shock metamorphism far exceeding that found in most meteorites.

For this reason, as well as others, smaller bodies are more promising candidates. The two principal types of smaller bodies in the solar system are the comets and the asteroids. The associated storage spaces are the cometary cloud of Oort and the asteroid belt, respectively. No other associations of small bodies and storage places are known at present; it is conceivable that in the outer solar system there are additional unobservable families of small bodies of some kind. However, it seems most fruitful to give first consideration to known classes of bodies, rather than to entirely speculative ones.

We have insufficient knowledge of the chemical or mineralogical composition, or for that matter, even the mean density of comets and asteroids to permit identification of any class of meteorites with these bodies on the basis of data of these kinds. Also, because the chemistry and mineralogy of the meteorites has been fixed since some time during the formation of the solar system, it is possible that the establishment of this chemistry and mineralogy preceded the time at which the present parent bodies were formed. Consequently, it is very difficult to make even plausible arguments concerning the kind of objects that could be derived from comets or asteroids without far more understanding than we possess regarding the processes by which these objects were formed.

It is possible that identification of meteorites with their sources must await in situ analyses and other studies by suitable spacecraft. However, prior to such studies, there is a body of dynamical evidence bearing on this problem that can prove valuable in making plausible inferences regarding this identification and that can provide reasonable hypotheses useful in planning such missions. Application of dynamical data to this problem has been described (Arnold, 1965*a,b;* Öpik, 1966; Wetherill, 1968*a,b;* Wetherill, 1969). The purpose of this report is to update this earlier work and describe the progress that has been made in the last few years.

As discussed in these earlier reports, it may be expected that there will be a relationship between the distribution of orbits from which meteorites impact Earth and the orbit of their source. At the time the meteorite was fragmented from a larger body, its initial orbit was approximately that of the larger body, because the large unshocked fragments surviving the fragmentation event will have a low velocity in the center-of-mass reference frame. However, these initial orbits will not be identical; and, with the passage of time, they will evolve into a distribution of orbits, some of which will be Earth crossing ones from which meteorites will be derived. The approach that has been taken is to consider various source orbits or "initial orbits" and see which, if any, of these evolve into orbits distributed in such a way as to correspond to the observed data. It is also necessary that the time interval between the fragmentation event that starts the "cosmic-ray clock" and Earth impact be in agreement with cosmic-ray-exposure ages, and furthermore, that any acceptable source provide a mass yield in accord with the observed meteorite flux.

The observed data consist of the time of fall of several hundred meteorites, the apparent radiants and exposure ages of about 100, and a very few complete orbits, only two of which can be considered well determined, Přibram and Lost City. Only for the most abundant class of meteorites, the chondrites, are these observed data sufficiently complete to be useful. In addition, orbits have been determined for a large number of bright fireballs falling within the Prairie Network. (See McCrosky, 1967.) These data for chondrites and fireballs are shown in figures 1 through 4.

In my previous studies (Wetherill, 1968*a,b;* 1969), I have considered initial orbits corresponding to those of the Moon, the Earth-crossing Apollo asteroids,

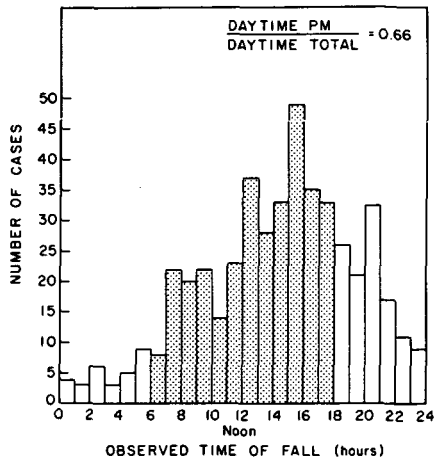

Figure 1.—Observational data for time of fall of chondritic meteorites. Dotted area indicates daytime falls, when social biases are of lesser importance.

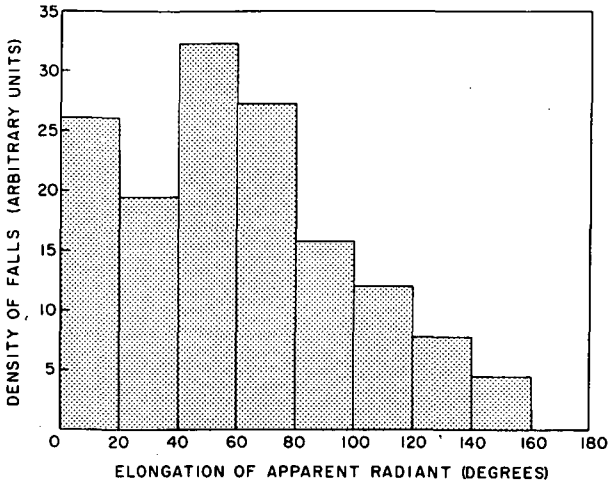

Figure 2.–Observed distribution of 133 chondrite radiants.

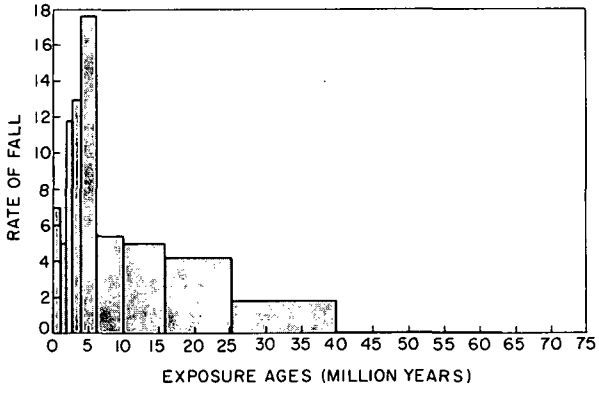

Figure 3.–Observed distribution of chondrite exposure ages.

the Mars-crossing asteroids, typical ring asteroids, Hilda and Trojan asteroids, various short-period comets, and long-period comets. The evolution of these orbits was calculated by use of a revised version of the Monte Carlo method developed by Arnold (1965*a*,*b*), and the distribution of the observable quantities calculated from those orbits terminating with Earth impact. Comparison of the calculated and observed data showed that none of these sources yielded data that agreed with the observed data. In fact, it was shown that only an initial Earth-crossing orbit with perihelion near Earth, aphelion near Jupiter (i.e., ~4.5 AU), and low inclination would be satisfactory. Calculated exposure ages for such a source are shown in figure 5. The difficulty

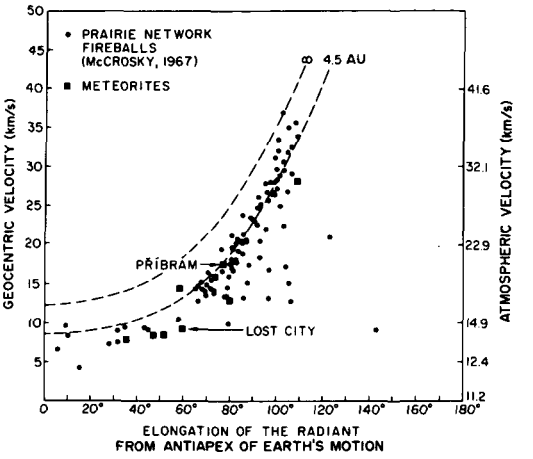

Figure 4.–Observed distribution of geocentric velocities and radiants for Prairie Network fireballs (circles) and the better determined meteorite orbits (squares). The curve marked ∞ is the boundary between elliptic and hyperbolic orbits; the other curve is the locus of relatively low-inclination orbits with aphelia at 4.5 AU.

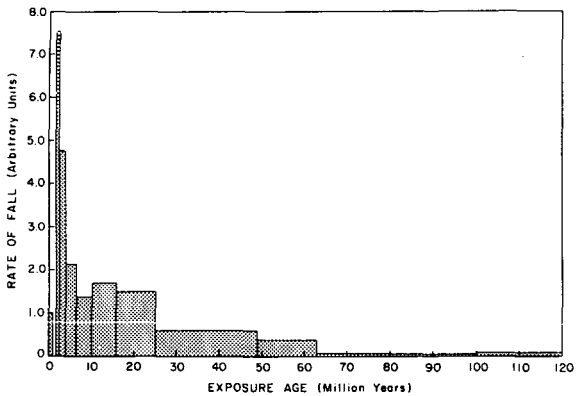

Figure 5.–Calculated distribution of exposure ages for a starting orbit resulting in Earth impacts corresponding to the low-velocity component of the Prairie Network flux. Aphelion = 4.50 AU, perihelion = 1.01 AU, inclination = 2°. This dynamically determined distribution is very similar to that observed for chondrites, except for those few with exposure ages greater than 50 million yr. These will probably be removed by collisional destruction.

with this orbit is that no family of bodies with such orbits is known. It was suggested (Wetherill, 1969) that a more plausible model would be one in which the observed data were augmented by a component of higher velocity bodies that fail to survive passage through Earth's atmosphere.

RECENT DEVELOPMENTS

Work done on this problem during the last 2 yr has confirmed and extended these earlier conclusions. In particular, no satisfactory way has been found for removing from the principal belt of asteroids a significant quantity of relatively unshocked material on the necessary time scale. Other asteroidal sources continue to appear unsatisfactory. The principal new developments during the last 2 yr are the recognition of the fact that the Prairie Network fireball data agree very well with the results predicted for short-period comets of Jupiter's family (and not for other possible sources) and the experimental work of Gault (1969) showing that finite-sized bodies can be broken into fragments much more readily than semi-infinite targets.

It now appears very likely that the Prairie Network fireballs are derived from short-period comets or possibly from related bodies having the same orbital history but less visible as a consequence of containing a smaller fraction of volatile matter. In any case, the identification of the fireballs with these comets shows that objects hundreds of kilograms in mass are associated with these bodies, only a small fraction of which mass can be volatile matter. Consequently, in at least this sense there must be "dead comets," as discussed by Öpik (1963).

COMETS AS SOURCES OF FIREBALLS AND CHONDRITES

In figure 4, the Prairie Network results are plotted on a diagram where the ordinate is the geocentric velocity and the abscissa is the elongation of the geocentric radiant (corrected for zenith attraction). The scale on the ordinate at the left is the geocentric velocity prior to acceleration by Earth's gravitational field; that at the right is the actual velocity at which the body enters the atmosphere with its velocity augmented by Earth's gravitational field. Values of the elongation of the radiant near 0° correspond to objects of low inclination that are near their perihelion, when they are moving more rapidly than Earth and are overtaking Earth. Values near 180° correspond to the opposite situation: bodies near their aphelion; i.e., with orbits within that of Earth. The curve marked ∞ is the boundary between elliptic heliocentric orbits and hyperbolic orbits not bound to the solar system. The other curve bounds the regions for which objects of low inclination (i.e., $\lesssim 15°$) have their aphelia greater or less than 4.5 AU. Orbits plotted to the right of this curve have aphelia less than 4.5 AU and have escaped Jupiter's "sphere of influence" but nevertheless are still subject to strong perturbations by Jupiter. The exact position of this boundary is slightly dependent on the inclination, but for the values of the inclination actually observed, this is not significant.

The Prairie Network fireball points are seen to be displaced along the 4.5 AU curve over a wide range of geocentric velocities. This is characteristic of bodies whose orbital evolutions have been primarily determined by proximity to Jupiter. In contrast to this, a body crossing only Earth's orbit will tend to

preserve a constant geocentric velocity as a consequence of the approximate conservation of its kinetic energy in geocentric coordinates at the point of close approach to Earth. Such a body will evolve horizontally on a diagram of this kind, resulting in frequent high values of the elongation of the radiant. On the other hand, the Jupiter perturbations tend to conserve the same quantity in Jupiter's frame of reference, resulting in a wide spread of geocentric velocities, as exhibited by the Prairie Network fireballs. This is the essential reason why predicted data for bodies with initial Earth-crossing orbits well inside Jupiter's orbit, such as most asteroidal sources, fail to agree with the Prairie Network data.

There are several possible meteorite sources whose orbital evolution is dominated by Jupiter. These are the short-period comets of Jupiter's family and collision ejecta from the Hilda ($a \sim 4.0$ AU) and Trojan ($a \sim 5.0$ AU) families of asteroids. Ejecta from the latter two sources that are not stabilized by the commensurability stabilizing the asteroid orbits themselves will be strongly perturbed by Jupiter but will seldom achieve perihelia within that of Earth. The low Jovicentric velocity of these bodies may lead to Jupiter capture; more probably, interaction with the eccentric components of Jupiter's velocity will accelerate the object into Saturn crossing, and ultimately to ejection from the solar system.

The orbits of the short-period comets will evolve in a somewhat different way. If their perihelia are initially not too distant from Earth's orbit (i.e., 1 to 2 AU), Jupiter perturbations acting near their aphelia will frequently move the perihelia just inside Earth's orbit. Following this, close approaches to Earth will occasionally move the aphelia within 4.5 AU. Escape from Jupiter's sphere of influence may also be aided by nongravitational accelerations, as discussed by Marsden (1968). Although most cometary orbits will suffer the fate of ejection from the solar system (as was the case for the Hilda and Trojan asteroidal ejecta), a small but significant fraction of short-period comet orbits will evolve so that their aphelia are ~4.5 AU and their perihelia ~1 AU. From such orbits, meteoroids with the orbital characteristics of the Prairie Network fireballs are derived. If, as proposed by Öpik (1963), there is a residual nonvolatile portion of the comet remaining after the volatile gases, which cause the comet to be visible, have evaporated after ~1000 yr, this nonvolatile component will comprise a "dead comet" that will still have, in many cases, a dynamical lifetime of 10^6 to 10^7 yr. This model fits the observed dynamical and physical properties of the Prairie Network fireballs, and no other source has proven to be satisfactory. Predicted data calculated by the Monte Carlo method for residua from comet Neujmin 2 are shown in figure 6, and are seen to resemble closely the distribution found observationally for the fireballs (fig. 4). Similar results are found for any orbit with aphelion within Jupiter's orbit and perihelion less than about 2.0 AU. About 10 percent of the observed short-period comets fulfill these criteria; the remainder will give similar points but with greatly reduced mass yields. The results of similar Monte Carlo

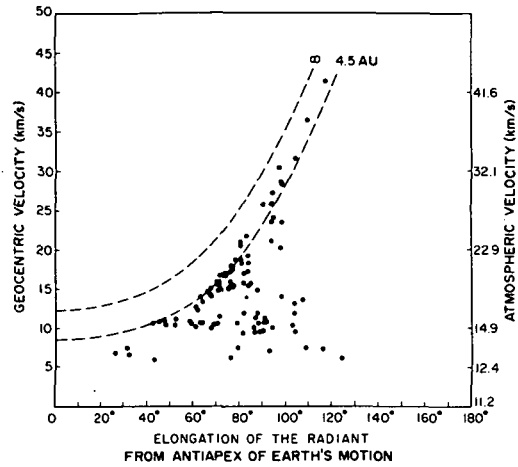

Figure 6.–Calculated distribution of geocentric velocities and radiants for Earth impacts resulting from a starting orbit equivalent to the observed short-period comet Neujmin 2. Aphelion = 4.79 AU; perihelion = 1.32 AU; inclination = 10.6°; and Earth impact efficiency = 0.24 percent. Earth impacts requiring more than 30 million yr have been removed because these bodies would probably be destroyed by collisions in the asteroid belt. Inclusion of these events would not affect the distribution very much.

calculations for several other comets are being published elsewhere (Wetherill, 1971).

From this work it is believed that not only are most of the smaller meteors of cometary origin, as has been known for a long time, but also the massive objects observed by the Prairie Network. Consequently, essentially all of the extraterrestrial flux on Earth is derived from comets. There remains the question of whether the meteorites and the chondrites in particular can be identified with this source. It would not be expected that objects with initial atmospheric velocities greater than about 20 km/s would survive passage through the atmosphere unless they are unusually large. Therefore it may be anticipated that only the lower velocity component of the data shown in figure 4 would be represented in the material reaching Earth. From figure 4 it may be noted that almost all of these low-velocity bodies have elongations of the radiant less than 90°. This is in accord with the observational data for chondrites (fig. 2) and also leads to the correct distribution of fall times (fig. 1).

The calculated exposure ages would also be similar to those of figure 5. The interpretation of the exposure age for a cometary source depends on the comet model employed. If it is thought that chondrites are buried within the volatile matter of the comet and become separated following the loss of the volatile matter, then the exposure age would start immediately after this loss. As mentioned above, the time (~1000 yr) required for loss of the volatile matter

is small compared to the exposure age and can therefore be neglected. On the other hand, it could also be that the cometary core is a solid piece of chondritic material hundreds of meters in dimension, the interior of which will be initially shielded from cosmic rays. This model then is in many ways equivalent to an Apollo asteroid source in that the meteorites are derived from a dense, nonvolatile body in an Earth-crossing orbit. Unlike the observed Apollo asteroids, these bodies will predominantly have aphelia near 4.5 AU. As discussed elsewhere (Wetherill and Williams, 1968), it is quite likely that Apollo asteroids with large aphelia have escaped detection, and as Öpik (1963) has argued, it is also probable that even the observed Apollo asteroids are cometary cores. If these statements are accepted, therefore, this model of the cometary source becomes identical to an Apollo asteroid model for the origin of chondrites and would also be acceptable as the source of Prairie Network fireballs.

There is evidence that at least the present flux of chondrites is derived from a small number of sources. The most compelling evidence of this kind is that a large number of hypersthene chondrites appear to have experienced a common shock impact within the last 500 million yr (Heymann, 1967). As discussed elsewhere (Gopalan and Wetherill, 1971), this event is not well dated and could have occurred during the last 50 million yr. Therefore, these data are not in themselves strong evidence against a cometary origin of chondrites, but do support the second alternative discussed above; i.e., derivation of chondrites from large comet cores rather than from many small pieces.

In summary, when one includes the effect of the atmosphere as a velocity filter, it turns out that short-period comets satisfy the dynamical requirements for chondrites as well as for fireballs.

Probably the principal difficulty in identifying the chondrites with the fireballs is that the typical fireball apparently has a density lower than that of chondrites and tends to disintegrate in the atmosphere more readily than expected for chondrites. The Lost City meteorite had an aerodynamically determined density higher than that of a typical fireball; on the other hand, Příbram was a typical fireball, with a calculated density, if anything, lower than average. Some evidence for associating typical fireballs with at least one class of chondrites is provided by Revelstoke, a type I carbonaceous chondrite recovered following the disintegration of a very large fireball corresponding to an incident mass of hundreds of megagrams, most of which failed to penetrate the atmosphere. The question of the association of more dense stones with the more friable material of a typical fireball remains open.

The identification of possible sources for the highly differentiated meteorites, the achondrites and irons, is more difficult because of the paucity of dynamical data available for these bodies. The high exposure ages of iron meteorites are probably indicative of an asteroidal origin, although a completely satisfactory theory of their mode of derivation from the asteroid belt remains to be developed.

COLLISIONAL DESTRUCTION

The other major development in the last few years has been the experimental work of Gault (1969) on the fragmentation of finite-sized targets.

It has long been recognized that meteoritic bodies will undergo collisions with asteroidal debris and cometary meteors and will thereby be reduced in mass. Earlier calculations (Wetherill, 1967) showed that "space erosion" by micrometeorite bombardment was probably of minor importance. However, these same calculations showed that total destruction by a single impact of the meteorite in space might be sufficiently probable to play a minor role in limiting the observed exposure ages of chondrites to a few tens of millions of years. This higher probability for total destruction is in large measure a consequence of the fact that fragmentation of a finite-sized body can result from hypervelocity collision with much smaller masses. Cratering experiments indicate that collisions in the asteroid belt between small and large bodies should produce craters on the larger body, the mass ejected from the crater into space being about 100 times the mass of the projectile. However, for somewhat larger projectiles, additional damage to the target results from shock waves traversing the body and reflecting from the bounding surfaces. In the earlier calculations (Wetherill, 1967) it was estimated that this effect might increase the ratio of ejected mass to projectile mass to about 10^4 for the case when this additional damage was just sufficient to fragment the target into a number of pieces.

The experiments of Gault have now shown that ratios of ejected to projectile mass as high as 10^6 are possible. The effect of this new result on cosmic-ray-exposure ages has been evaluated by computing the probability of destruction of bodies in various orbits by collision with a population of objects with orbits distributed similarly to the observed asteroids and periodic comets. Several assumptions were made regarding the total mass and population index of the colliding asteroidal and cometary bodies, based on meteor observations and theoretical studies of fragmentation in the asteroid belt (Dohnanyi, 1970). The effect of the relative velocity of the two colliding bodies was taken into consideration not only insofar as it affects the probability of collision, but also in accordance with its effect on the strength of the collision by use of Gault's experimental result that kinetic energies of 10^2 to 10^3 J/kg (10^6 to 10^7 ergs/g) will suffice to completely fragment finite-sized bodies.

The results of these calculations are that total destruction by asteroidal fragments and cometary meteors are of comparable importance and that either may predominate, depending on the exact assumptions made regarding the flux of the colliding bodies. For fragmentation energies of 10^2 J/kg (10^6 ergs/g), a body 50 cm in radius will have a mean lifetime of about 10 million yr. This result is not very sensitive to the orbit assumed for the body. Uncertainties in the flux could easily cause the quantity to be in error by a factor of 10. Fragmentation energies of 10^3 J/kg (10^7 erg/g) will increase the lifetime to

about 100 million yr. In addition, it is possible that meteorite lifetimes may be limited by rotational bursting (Paddack, 1969).

The consequence of these results is that it now seems likely that total destruction by collision will prevent meteorites from having very large cosmic-ray-exposure ages. For the calculations based on the cometary source, this is a secondary effect. In this case, the cosmic-ray-exposure ages will be primarily controlled dynamically; the probability of these objects surviving ejection from the solar system by Jupiter perturbations for more than ~25 million yr is not large anyway. The effect of collisional destruction will be to cut off the high exposure age "tail" on figure 5 and bring the calculated results into even better agreement with the observed data.

For asteroidal sources, the effect is greater because for collision lifetimes as short as 10^7 yr it is no longer possible to obtain the long exposure ages calculated for meteorites derived from Mars-crossing asteroids and, to a lesser extent, from Earth-crossing Apollo asteroids. This does not, however, increase the plausibility of deriving asteroids from these sources. Fragments of objects moving in orbits similar to the observed Mars-crossing or "Mars-grazing" asteroids will have their initial perihelia barely within Mars' aphelion. Multiple perturbations involving elapsed times of the order of 10^9 yr will be required to perturb this initial orbit into an Earth-crossing orbit. By this time, collisional destruction will have eliminated all of the fragments. If the initial distribution of Mars-crossing orbits were a random one, about 1 percent of the fragments would be perturbed into Earth-crossing orbits sufficiently rapidly to avoid destruction. However, as pointed out above, the distribution of initial orbits is a very special one, and a distinct delay on the order of 10^9 yr is involved prior to appearance of the fragments in Earth-crossing orbits.

This difficulty of survival can be avoided by theories in which chondrites are derived from Apollo asteroids as a result of partial or complete fragmentation of the asteroid as it passes through the asteroid belt. In this case, the fragments are produced directly in Earth-crossing orbits and no delay of the type discussed above occurs. As discussed earlier in this paper, the most plausible cometary model is a theory of this kind in which the "Apollo asteroids" are cometary cores with aphelia near 4.5 AU. Alternative Apollo asteroid theories in which they are derived from ring asteroids or from Mars-crossing asteroids are less satisfactory. A short lifetime for collisional destruction removes the objection to theories of this kind raised previously (Wetherill and Williams, 1968) that predicted exposure ages are far too long. At the same time, this makes it more difficult to reconcile the other observations with the results predicted for such a model.

The large observed excess of radiants less than 90° requires that most Earth impacts occur while the meteorites are near their perihelion. This fact in turn requires that a large fraction of the meteorites be produced immediately after the Apollo asteroid is perturbed into Earth crossing. With the passage of time, the Apollo asteroid will be perturbed by Earth and Venus into orbits for which

its aphelion is near Earth as frequently as its perihelion. This tends to produce a symmetric distribution of radiants for low-velocity bodies, and an excess of radiants greater than 90° for higher velocity bodies. This has always been a problem with theories of this kind. Short collisional lifetimes aggravate this difficulty by relatively deemphasizing fragments produced when the Apollo asteroid first becomes Earth crossing in favor of those produced later after the perihelion of the source has become randomized.

SUMMARY

These calculations indicate excellent agreement between observed and predicted orbits of Prairie Network fireballs, if it is assumed that fireballs are derived from remnants of short-period comets of Jupiter's family. No such satisfactory agreement has been found for any other proposed source. The distribution of radiants and time of fall observed for chondrites will also be reproduced by this source, provided that consideration is given to the fact that Earth's atmosphere will permit low-velocity bodies to survive but will destroy high-velocity bodies. Again, no other proposed source has been found to be adequate.

It now appears likely that the mean lifetime of chondrites is limited to $\sim 10^7$ yr by the high probability of complete fragmentation following impact by smaller bodies. This improves the agreement between the observed cosmic-ray-exposure ages and those predicted for a cometary source. This also requires some modification of the earlier discussions of alternative sources but does not result in their becoming more satisfactory.

Note added in proof: Recent work by P. Zimmerman and the author shows that it is possible to inject fragments of the size of small asteroids into the 2:1 Kirkwood gap. Although the resulting libration will enable the body to avoid Jupiter, a meteorite-sized fragment ejected at a velocity of about 200 m/s as a result of a collision can escape the libration region and be in an orbit similar to those of the short-period comets, as discussed in this paper. This mechanism has not yet been sufficiently quantitatively evaluated in order to learn its importance as a source of meteorites.

REFERENCES

Arnold, J. R. 1965*a*, The Origin of Meteorites as Small Bodies, 2, The Model. Astrophys. J. **141**, 1536-1547.

Arnold, J. R. 1965*b*, The Origin of Meteorites as Small Bodies, 3, General Considerations. Astrophys. J. **141**, 1548-1556.

Dohnanyi, J. S. 1970, On the Origin and Distribution of Meteoroids. J. Geophys. Res. **75**, 3468-3493.

Gault, D. E. 1969, On Cosmic Ray Exposure Ages of Stone Meteorites (abstract). Meteoritics **4**, 177.

Gopalan, K., and Wetherill, G. W. 1971, Rubidium-Strontium Studies on Black Hypersthene Chondrites: Effects of Shock and Reheating. J. Geophys. Res., in press.

Heymann, D. 1967, On the Origin of Hypersthene Chondrites: Ages and Shock Effects of Black Chondrites. Icarus **6**, 189-221.

McCrosky, R. E. 1967, Orbits of Photographic Meteors. Smithson. Observ. Special Rept. 252.

Marsden, B. G. 1968, Comets and Non-gravitational Forces. Astron. J. 73, 367-379.
Öpik, E. J. 1951, Collision Probabilities With the Planets and the Distribution of Interplanetary Matter. Proc. Roy. Irish Acad. Sect. A 54, 164-199.
Öpik, E. J. 1963, Survival of Comet Nuclei and the Asteroids. Adv. Astron. Astrophys. 2, 219-262.
Öpik, E. J. 1966, The Stray Bodies in the Solar System, 2, The Cometary Origin of Meteorites. Adv. Astron. Astrophys. 4, 302-336.
Paddack, S. J. 1969, Rotational Bursting of Small Celestial Bodies: Effects of Radiation Pressure. J. Geophys. Res. 74, 4379-4381.
Wetherill, G. W. 1967, Collisions in the Asteroid Belt. J. Geophys. Res. 72, 2429-2444.
Wetherill, G. W. 1968*a*, Time of Fall and Origin of Stone Meteorites. Science 159, 79-82.
Wetherill, G. W. 1968*b*, Dynamical Studies of Asteroidal and Cometary Orbits and Their Relation to the Origin of Meteorites. Origin and Distribution of the Elements (ed., L. Ahrens), pp. 423-443. Pergamon Press. New York.
Wetherill, G. W. 1969, Relationships Between Orbits and Sources of Chondritic Meteorites. Meteorite Research (ed., P. M. Millman), pp. 573-589. D. Reidel. Dordrecht.
Wetherill, G. W. 1971, Origin and Age of Chondritic Meteorites. Vinogradov 75th Anniv. Vol. Moscow. In press.
Wetherill, G. W., and Williams, J. G. 1968, Evaluation of the Apollo Asteroids as Sources of Stone Meteorites. J. Geophys. Res. 73, 635-648.

DISCUSSION

KESSLER: I have always been leary of comparing observational data from two different sources. For example, the probability of observing a fireball of a given mass may vary as something like velocity to the third or fourth power, whereas the probability of observing an asteroid or comet in space may be inversely proportional to velocity. The results would be to reduce the relative number of high-velocity fireballs and perhaps increase the number of high-velocity asteroids or comets. I am wondering if you considered these selection effects; and, if so, what effects they would have on your conclusions.

WETHERILL: There are only a few comets known with aphelia between 4.5 and 5 AU. However, whether there are more or less is minor in importance. Any of these will evolve in such a way as to give a similar distribution on the velocity-elongation diagram. Whether there are strong biases in the Prairie Network can best be answered by McCrosky.

McCROSKY: The bias is in favor of observing higher velocity objects.

WHIPPLE: I question the large radii obtained by Wood and Goldstein. How can one have very much confidence in the radiation loss on a body which we know so little about? The outer surfaces of asteroids could have very low thermal conductivity and prevent heat loss. Consequently the interior could have been much hotter and the bodies would have been considerably smaller. It is very hard to know what value to put in.

ANDERS: Fricker considered a thin surface layer but it was not significant. If you make it thick enough it will be significant.

ARRHENIUS: There is another way to approach this discrepancy; that is, by the rather large uncertainties in the cooling rates. The diffusion coefficients that are used are extrapolated from higher temperatures, and there are rather large uncertainties. Another one is based on the fact that minor components such as phosphorus and hydrogen will increase the diffusion rate. All this would work in the direction of making the size of the body smaller.

WETHERILL: I would like to say something about this question of large bodies. I do not see any compelling reason for not believing that asteroidal and cometary masses are distributed in a similar way. Most of the asteroidal mass is in a few large bodies, and hence these few large bodies might be expected to contribute most asteroidal fragments. In the

same way, most of the cometary fragments could be derived from a few large comets rather than a large number of small ones.

UREY: It seems to me that the rather large objects must have been present in the primitive solar nebula and that they collided with the planets during their accumulation. In this way the tilt of the axes of the planets from the vertical to the ecliptic plane can be accounted for; and, in fact, the reverse rotation of Venus and the tilt of the axes of Earth, Mars, Uranus, and others with the exception of Jupiter must have originated in this way. I have suggested that many lunar-sized objects were present. It has been discussed by Marcus, Safranov, and, more recently, by Singer. The particular case of Uranus was called to my attention by Gold quite some years ago.

KENKNIGHT (submitted after meeting): Although comets might be attractive for meteors and some chondrites, the chemistry of the achondrite meteorites strongly suggests origin on, or in association with, a large enough body to have been strongly heated at origin. The chemistry and mineralogy of achondrites suggest a magmatic relation to material of the chondrite type. The structure and composition of the brecciated achondrites suggest histories as complicated as lunar surface breccias, including magmatic differentiation, brecciation or surface effusion, recrystallization, and further brecciation (Duke and Silver, 1967). Wasson and Wai (1970) give 11 reasons for believing the enstatite chondrites and enstatite achondrites form a systematic sequence driven by a heat source external to the parent body that was increasing with time and sufficiently intense to cause partial melting of silicates. The occurrence of gas-rich achondrites and the specific pattern of enrichment in C, Ni, Br, and Bi in addition to the noble gases in these achondrites suggests (Mazor and Anders, 1967; Müller and Zahringer, 1966) that carbonaceous chondrite material was added as an impurity at a parent body surface and then incorporated in a breccia during impact. These conditions at or near a meteorite parent body surface are consistent with the identification of the surface reflectivity of Vesta in the earlier paper by Chapman, Johnson, and McCord[1] with a eucritic achondrite, Nuevo Laredo.

WETHERILL: KenKnight's statement covers a very wide amount of territory in a very few sentences, some of which I agree with, some of which I do not. Therefore, I will confine my remarks to his first sentence, which may be taken to represent a summary of the remainder. I agree that the chemistry of the achondritic meteorites strongly suggests origin in a large enough body to have been strongly heated at the time of its formation. The same is true of the metamorphosed chondrites for that matter. On the other hand, we do not know if asteroids were strongly heated at the time of their formation, nor do we know that the cores of the comets were not. We do know that this heating took place during the formation interval of the solar system; and, therefore, an understanding of the very complex processes that took place in this interval is necessary to discuss these questions in a meaningful way. I am not convinced that any of us know that much about it, even though some people purport to.

DISCUSSION REFERENCES

Duke, M. B., and Silver, L. T. 1967, Petrology of Eucrites, Howardites, and Mesosiderites. Geochim. Cosmochim. Acta **31**, 1637-1665.

Mazor, E., and Anders, E. 1967, Primordial Gases in the Jodzie Howardite and the Origin of Gas-Rich Meteorites. Geochim. Cosmochim. Acta **31**, 1441-1456.

Müller, O., and Zahringer, J. 1966, Chemische Unterschiede bei Uredelgashaltigen Steinmeteoriten. Earth Planet. Sci. Lett. **1**, 25-29.

Wasson, J. T., and Wai, C. M. 1970, Composition of the Metal, Schreibersite, and Perryite of Enstatite Achondrites and the Origin of Enstatite Chondrites and Achondrites. Geochim. Cosmochim. Acta **34**, 169-184.

---

[1]See p. 51.

IS WATER ICE THE MAJOR DIFFERENCE BETWEEN COMETS AND ASTEROIDS?

A. H. DELSEMME
University of Toledo

The nature of the volatile phase in comets has never been established from observations. Although water was likely to be its major constituent, evidence was still circumstantial. It is shown here that water evaporation quantitatively explains not only the brightness of the hydrogen and hydroxyl halos observed by the OAO for the two bright comets of 1970, but also, which is much more convincing, it explains their brightness dependence on the heliocentric distance.

The existence of a volatile phase, whatever it is, seems to be, of course, the major chemical difference between a "normal" cometary nucleus and a standard asteroid. This idea was used by Whipple (1950) to build his icy-conglomerate model, which explained in a qualitative way the nature of the so-called nongravitational forces acting on comet Encke. However, the chemical nature of this icy phase has not yet been positively identified. Therefore, the nongravitational force theory, developed for many comets by Marsden (1968, 1969), suffers from having no physicochemical model able to describe, in particular, the dependence of the acting force on the heliocentric distance.

The only molecule of the icy phase that cannot be reasonably doubted is water. There are many circumstantial reasons that I will not try to review again here. They range from the type of chemical considerations that were so successfully introduced by Urey into the study of the solar system and its origin, up to the recent observations of the hydrogen and hydroxyl halos by the OAO for the two bright comets of 1970 (Blamont, 1970; Code, Houck, and Lillie, 1970), to which I have just learned that we should add comet Encke. Previously, I have shown (Delsemme, 1971) that water evaporation explains the right order of magnitude of the brightnesses of the two halos. The major uncertainty comes from our ignorance of the albedo (or of the radius) of the cometary nucleus concerned. The right order of magnitude is reached if the albedo is between 0.10 and 0.90. It is obvious that when the albedo is larger than that, the energy absorbed diminishes drastically and the ices do not vaporize enough any more.

This shows how such an argument heavily depends on the model adopted. The other arguments for water are of an even more circumstantial nature and could be turned around easily. For instance, OH and H could be described as free radicals from the nucleus, using the ideas independently proposed by Haser (1955) and by Donn and Urey (1956). In this case, Levin's (1943, 1948) ideas on desorption could still be used.

Of course, the large brightness of the two halos makes these ideas rather unlikely. On the other hand, OH and H could come from one or several other molecules more complex than water. This cannot be ruled out because we still do not know very much about either the early chemical history of the cometary nucleus or the hypothetical parent molecules of the other free radicals observed in the cometary heads.

A new quantitative argument for the presence of water can be developed from the observed brightness dependence on the heliocentric distance of the hydrogen and hydroxyl halos. It is based on Code's (1971) observations, in particular of comet 1969g. On the log brightness versus log heliocentric distance diagram, the eight observed points draw a perfectly straight line for OH. For the Lyman-α emission, seven of the nine observed points also draw a straight line. Two points that are lower than the straight line are explained by Code as a spurious effect that is clearly understood (telluric reabsorption of part of the halo light because of the geometry). The slope for both OH and H is exactly the same. Code mentions a dependence on distance to -5.8 power. In the preprint kindly communicated later by Dr. Code, I find a slope $n = -5.9 \pm 0.1$. Because it is almost exactly 6, I propose here that the emission of light by the hydrogen and hydroxyl halos is in each case a three-step process in which each step shows, at least in a first approximation, an inverse square law dependence. The three steps proposed are

(1) Vaporization of water snows from the cometary nucleus
(2) Photodissociation of the water molecule into H and OH
(3) Photoexcitation of H and OH by absorption of the solar continuum

The production rate of H_2O vapor by the first process depends on the total energy flux absorbed by the cometary snows, which varies as the inverse square law if the temperature of the cometary snows does not vary. The correction introduced by the temperature dependence on the vaporization rate of the snows gives a slope that is not exactly 2, but remains a constant at heliocentric distances smaller than 1.3 AU. The slope is between -2.15 and -2.05 depending on the accepted values for the snow albedos in the visible and in the infrared (Delsemme and Miller, 1971). An average value of -2.1 therefore can be used. It remains true for all types of snow.

The photodissociation described in the second step depends, of course, on the photon flux, which also follows the inverse square law. This photodissociation can be obtained by absorption of the solar flux, either in the first or in the

second continuum of water (McNesby and Okabe, 1964), giving reactions (1) or (2), respectively:

$$H_2O + h\nu \rightarrow H(^2S) + OH(X^2\Pi) \quad (1)$$

$$H_2O + h\nu \rightarrow H(^2S) + OH(A^2\Sigma^+) \quad (2)$$

As the two continua overlap, the ratio of the rates of the two processes is not known with accuracy; but the first one must strongly predominate because there is much more energy available in the solar spectrum between 180 and 140 nm than between 140 and 115 nm.

For the third step, H and OH must be distinguished. H is produced in the ground state and must therefore absorb a solar photon again, introducing the third dependence on the inverse square law, before emitting Lyman-α radiation.

The same third step is followed by the OH molecules produced by reaction (1) in the ground state. But if they were produced by reaction (2) in their excited state, they would bypass the third step and immediately radiate the molecular band $A^2\Sigma^+ \rightarrow X^2\Pi$.

Provided that the heliocentric distance of the comet does not vary too much during the time of flight of the molecules or atoms through the whole coma (which is almost always true) and provided that the optical depth effects do not vary too much during the range of distances covered, because the global brightness in Lyman-α light (or in OH light) is practically proportional to the production rate of the H atoms (or of the OH radicals) in their excited state, one has

$$B \propto Zf^2 \propto r^{-6.1} \qquad r < 1.3 \text{ AU}$$

where Z is the production rate of molecules by vaporization, f is the photon flux of the Sun, and r is the heliocentric distance. If H_2O were dissociated by process (2) only, the exponent of r would still be 6.1 for H (Lyman α) but would be 4.1 for OH.

The observation of the slope $n = -5.9 \pm 0.1$, both for H and OH, seems to point out that process (1) is overwhelming and, by the same token, confirms for the first time in a more quantitative way the likely presence of water ices or snows in comets and the three-step mechanism of production of OH and H. It seems very difficult to keep a three-step mechanism by using something other than water. Direct desorption of radicals would give a two-step process with $n = 4$ or less. Dissociation of larger molecules would give, by and large, at least one more step for either H or OH. When better observations are known, it is hoped that mechanisms of this type will explain the physical processes and the origin of the other radicals observed in cometary heads. On the other hand, the evaporation of water could be used with more confidence to provide a physical meaning in Marsden's formulation of the nongravitational force.

ACKNOWLEDGMENTS

I thank Dr. Code for an early communication of his results. This work was made possible by grant GP-17712 of the National Science Foundation.

REFERENCES

Blamont, J. 1970, Observation de l'Émission d'Hydrogène Atomique de la Comète Bennett. C. R. Acad. Sci. Paris **270**, 1581-1584.

Code, A. D. 1971, Symp. on Recent Observations of Comets, AAS Div. Planet. Sci. (Tallahassee).

Code, A. D., Houck, T. E., and Lillie, C. F. 1970, Comet Tago-Sato-Kosaka (1961g). Central Bureau Astron. Telegrams, IAU Circ. 2201.

Delsemme, A. H. 1971, Symp. on Recent Observations of Comets, AAS Div. Planet. Sci. (Tallahassee).

Delsemme, A. H., and Miller, D. C. 1971, Physico-Chemical Phenomena in Comets. III. The Continuum of Comet Burnham. Planet. Space Sci. 9, in press.

Donn, B., and Urey, H. C. 1956, On the Mechanism of Comet Outbursts and the Chemical Composition of Comets. Astrophys. J. **123**, 339-342.

Haser, L. 1955, La Conservation des Radicaux Libres à Basse Température et la Structure des Noyaux des Comètes. C. R. Acad. Sci. Paris **241**, 742-743.

Levin, B. F. 1943, Astron. Zh. **20**, 37.

Levin, B. F. 1948, Dependence of the Variation in Brightness of Comets on Their Solar Distance. Astron. Zh. **25**, 246.

McNesby, J. R., and Okabe, H. 1964, Vacuum Ultraviolet Photochemistry. Advances in Photochemistry (ed., W. A. Noyes et al.), vol. 3, p. 157. Wiley-Interscience. New York.

Marsden, B. G. 1968, Comets and Nongravitational Forces I. Astron. J. **73**, 367-379.

Marsden, B. G. 1969, Comets and Nongravitational Forces II. Astron. J. **74**, 720-734.

Whipple, F. 1950, A Comet Model. I. The Acceleration of Comet Encke. Astrophys. J. **111**, 375-394.

STRUCTURE OF COMETS AND THE POSSIBLE ORIGIN OF FAINT ASTEROIDS

V. VANÝSEK
Charles University
Prague

It is shown that very old and still active icy-conglomerate or "clathrate" cometary nuclei may exist at the outer boundary of the asteroidal belt and belong to the group of relatively stable "outer" short-period comets of which only a small fraction have been discovered or recognized as cometary objects.

The search for these comets among very faint asteroids with the mean motion $\mu \leqslant 600''$, and the study of their behavior could be very important to our knowledge about the final stage of cometary nuclei.

The study of the processes involved in the formation of the solar system requires some attention to the physical structure of comets, as has been emphasized by many authors in the last two decades. It appears to be a logical procedure to follow the formation of comets as a link to a better understanding of the processes that occurred in the early stages of the solar system because it is highly probable that comets represent the remnants in which preplanetary matter is preserved.

The comets are "soft" bodies and, unlike other sizable objects in the solar system, undergo relatively very fast changes. The outflow of gases and dust from cometary nuclei, bright outbursts, and splitting of comets are indisputable evidences of processes that lead to complete disintegration or to considerable changes of the structure of the nucleus in the time range, which depends on the perihelion distance, original mass, and orbital period.

The mean lifetime of a cometary nucleus need not be necessarily considered as the lifetime of its entire existence but as the time range in which such a body possesses the ability to produce observable typical cometary phenomena, which distinguish the cometary appearance from the asteroidal one. Besides complete disintegration, the asteroidal appearance might be another possible final stage of a cometary nucleus. The existence of asteroids like Icarus, Geographos, Apollo, Adonis, and Hermes or the Hilda group supports this idea, which has been discussed by many authors in the past.

It is evident, however, that the final stage of a cometary nucleus is determined by its composition and structure, as well as by the formation

process. What is the final stage (is it the starlike appearance of exhausted remnants of the nuclei or is it complete disintegration) is one of the most significant questions concerning the evolution of comets.

The high abundance of neutral hydrogen in the cometary atmosphere, confirmed by observations of the resonance Lyman-α radiation and strong O-O bands of OH of recent bright comets (Code and Houck, 1970), indicates that hydrogen compounds are dominant constituents of the cometary nuclei. The most probable precursor of atomic hydrogen and hydroxyl is H_2O.

Although there is still lack of direct evidence of the presence of water in comets,[1] the 20 yr old icy-conglomerate model proposed by Whipple (1950, 1951) and modified by Urey (1952), Donn and Urey (1957), and recently by Delsemme and Miller (1970) seems to be the best approach to the real composition of the cometary nuclei.

The homogeneous icy-conglomerate nucleus undergoes complete disintegration. On the other hand, the "dead" nucleus requires a more complicated initial structure of comets. The possibility of some kind of stratification in the nucleus is supported by the fact that the "new" comets (according to Oort's terminology) or those with low frequency of perihelion passages produce large amounts of nonvolatile material and gases, a fact that is not typical of short-period comets. This may imply that the young nucleus is surrounded by a loose layer of dust and ice grains. This loose layer requires a lower amount of energy for evaporation than deeper parts of nuclei and it easily produces a very extensive dust-gaseous coma.

One can assume either the nonvolatile material surrounded by the mantle of volatile material or the increasing compactness of a matrixlike structure of the nonvolatile material toward the center of the nucleus.

As was shown by Whipple and Stefanik (1965), the radioactive heating of an icy-conglomerate nucleus can transfer the volatile material such as CH_4 from the center to the surface layers. The condensed CH_4 can form a brittle shell easily breakable by the heat shock shortly before the first approach to the perihelion. This breakage can be observed as a splitting of the nucleus and seems to be very typical for the "new" comets (Harwit, 1968; Pittich, 1971; Stefanik, 1965).

On the other hand, we have little knowledge about the behavior of the "dying" comets.[2] The often-studied secular changes of comet P/Encke must be interpreted with precaution because this object is not quite typical among short-period comets.

Comets in the transient stage, with nearly depleted nuclei, are probably more numerous just at the mean heliocentric distances beyond which a comet nucleus can survive without considerable diminution of the original mass.

---

[1] See, however, p. 461.

[2] See p. 427.

If t_0 is the mean lifetime for a nucleus in the circular orbit at the heliocentric distance $r = 1$ AU, then the lifetime $t = t(r)$ at $r > 1$ is given approximately by the relation

$$\frac{t}{t_0} = \frac{z_0}{z_r} \tag{1}$$

where z_0 and z_r are vaporization rates at corresponding heliocentric distances, defined by

$$z_r = p(2\pi m T_r)^{-1/2} \tag{2}$$

where $p = p(T)$, the saturated vapor pressure; m is the mass; and T_r is temperature which holds for the energy balance equation

$$F_0 r^{-2} \alpha = \sigma T_r^4 \epsilon + z_r L \tag{3}$$

where F_0 is solar energy flux at $r = 1$, α and ϵ are coefficients of absorptivity and emissivity of the nucleus, and $L = L(T)$ is the latent heat of vaporization. The vaporization rates for various homogeneous nuclei composed from various constituents were computed by Huebner (1965).

The t for a comet in the elongated elliptical orbit must be computed as a cumulative effect of the vaporization and restitution of the volatile material in surface layers before and after perihelion passages. However, for a comet in a less eccentric orbit, formula (1) can be used with the average value of r.

Figure 1 shows the relative lifetime t/t_0 of a nucleus composed of H_2O, CO_2, and CH_4 as a function of the heliocentric distance. The nucleus is

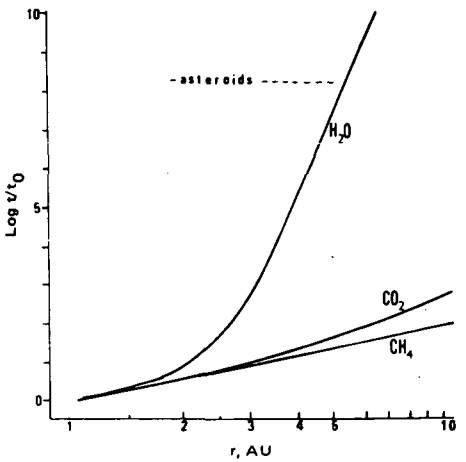

Figure 1.—The relative lifetime t/t_0 for ices of some simple compounds as a function of the heliocentric distance. The extension of the asteroidal belt is marked.

supposed to be a spherical rotating body with the albedo 0.1 in a circular orbit. (The effect of possible collisions in the asteroidal belt and the influence of the corpuscular solar radiation are not considered, therefore the value of $\log t/t_0$ in $r = 2.5$ to 3.5 AU might be somewhat overestimated.)

The curve for the H_2O ice model can be used with good approximation for an icy lattice of the clathrates, as far as the hydrocarbons and radicals are only a minor contamination in the ordinary ice. If the mean production rate of a periodic comet is about 10^{29} to 10^{30} molecules s^{-1}, the real mean value of t_0 ranges between 10^3 and 10^4 yr, depending on the initial mass, frequency of perihelion passages, and the lifetime for an icy-conglomerate nucleus at $r \simeq 3.5$, which is on the order of 10^8 to 10^9 yr. Even if this value seems to be somewhat unrealistically high, there is no doubt that the nucleus of a typical comet will be preserved for a very long time if it orbits beyond the asteroidal belt in the period that does not make simple commensurability ratios to Jupiter's mean motion.

Kresák (1965, 1971) pointed out that commensurabilities in the system of short-period comets with typical eccentricities frequently mean drastic changes in orbits because of the repetition of the close approach to Jupiter (which is not the case in asteroidal systems). Particularly the 1:2 ratio commensurability is "forbidden" as can be demonstrated by the outstanding gaps near the mean motion $\mu = 600''$. According to Kresák, the commensurability gap 1:2 separates a compact "outer" group of comets from "inner" comets with a higher eccentricity of orbits and short perihelion distances. The "inner" comets have a short life and represent only a small fraction of the existing number of objects classified generally as short-period comets.

Therefore, if the icy-conglomerate or "clathrate" models are correct, a large number of the active comet nuclei with the mean motion $\mu < 590''$ remain undiscovered until now, even if they are potentially observable as asteroidlike objects.

As one such example, the case of comet P/Oterma might be noted; it was a starlike object of the 17th to 19th magnitude before the last change of the orbit with orbital elements resembling those of an asteroidal orbit (e.g., 153 Hilda). Because of a change in its orbit in 1962, the comet became very faint and practically unobservable. Bouška (1965), using the $r^{-6.8}$ law for the brightness, obtained apparent magnitudes 22 to 27 mag; i.e., beyond detectability. However, when the gas production fades out, the r^{-2} law is more realistic and the nucleus with low activity of an Oterma-type comet might be still detectable with large Schmidt telescopes. Moreover, the brightness outbursts, very typical for the giant comet Schwassmann-Wachmann 1, could be assumed as general behavior of comets at larger heliocentric distances. These outbursts (or surges) mean a considerable increase in brightness, and the comet becomes an easily observable object for a long time interval. As was shown recently by Pittich (1969), there exist at least 40 cases where comets appear to have suddenly increased their brightness shortly before their discovery. The

increase of brightness occurs even at large heliocentric distances. In addition to comet Schwassmann-Wachmann 1, 10 other cases with at least one outburst are known.

The frequency of the outbursts increases with the decrease of brightness amplitudes, and the nonperiodic changes in magnitudes of very faint starlike comets with asteroidal appearance might be expected as very typical.

The search for old but still partly active cometary nuclei among very faint asteroids would appear to be a worthwhile program, especially among the asteroids of the Palomar-Leiden survey. Because of the differences in cometary and asteroidal orbits, one can assume that some families and streams (in the sense of Alfvén's streams) of long-life comets with asteroidal appearance exist and can be distinguished from asteroids not only by occasional brightness flares but also by the grouping of orbital elements.

REFERENCES

Bouška, J. 1965, The Collisions of Asteroids. Bull. Astron. Inst. Czech. **16**, 358.

Code, A. D., and Houck, T. E.1970, OAO Observations of Comet 1969g and Comet 1969i. Bull. AAS **2**, 321.

Delsemme, A. H., and Miller, D. C. 1970, Physico-Chemical Phenomena in Comets. II. Gas Adsorption in the Snows of the Nucleus. Planet. Space Sci. **18**, 717-730.

Donn, B., and Urey, H. C. 1957, Chemical Heating Processes in Astronomical Objects. Mém. Soc. Roy. Sci. Liège Ser. **4**, vol. 18, pp. 124-132.

Harwit, M. 1968, "Spontaneously" Split Comets. Astrophys. J. **151**, 789-790.

Huebner, W. F. 1965, Über die Gasproduktion der Kometen. Z. Astrophys. **63**, 22-34.

Kresák, L. 1965, On Two Aspects of Evolution of Short-Period Comets. Mém. Soc. Roy. Sci. Liège Ser. **5**, vol. 12, pp. 459-467.

Kresák, L. 1971, The Dividing Line Between Cometary and "Asteroidal Orbits." The Motion, Evolution of Orbits and Origin of Comets, IAU Symp. 45. D. Reidel. Dordrecht. In press.

Pittich, E. M. 1969, Sudden Changes in the Brightness of Comets Before Their Discovery. Bull. Astron. Inst. Czech. **20**, 251-292.

Pittich, E. M. 1971, The Motion, Evolution of Orbits and Origin of Comets, IAU Symp. 45. D. Reidel. Dordrecht. In press.

Stefanik, R. P. 1965, On Thirteen Split Comets. Mém. Soc. Roy. Sci. Liège Ser. **5**, vol. 12, pp. 29-32.

Urey, H. C. 1952, The Planets. Yale Univ. Press. New Haven.

Whipple, F. L. 1950, A Comet Model. I. The Acceleration of Comet Encke. Astrophys. J. **111**, 375-394.

Whipple, F. L. 1951, A Comet Model. II. Physical Relations for Comets and Meteors. Astrophys. J. **113**, 464-474.

Whipple, F. L., and Stefanik, R. P. 1965, On the Physics and Splitting of Cometary Nuclei. Mém. Soc. Roy. Sci. Liège Ser. **5**, vol. 12, pp. 33-52.

Page intentionally left blank

PART III

POSSIBLE SPACE MISSIONS AND FUTURE WORK

Page intentionally left blank

ARGUMENTS FOR A MISSION TO AN ASTEROID

H. ALFVÉN and G. ARRHENIUS
University of California, San Diego

GROUPS OF ASTEROIDS

With respect to their orbital parameters, the known asteroids fall into different groups:

(1) *Main belt asteroids* orbit between Mars and Jupiter. Most of them have semimajor axes a in the range $2.0 < a < 3.5$ AU.

(2) *Asteroids outside the main belt* form a number of different groups, such as the Trojans, Hildas, etc.

(3) *Mars-crossing asteroids* are bodies with low a values and perihelia inside the Martian orbit; in several cases they are inside Earth's orbit. They are the closest neighbors in space of the Earth-Moon system. A list of them is given by Marsden, table II.[1] We select from these the ones with eccentricities in the range 0.2 to 0.4; they will be referred to as the Eros group, named after its largest member. The arguments for a mission to an asteroid refer especially to the Eros group as a first target.

SPECIFIC INTEREST OF ASTEROID EXPLORATION

Access

Of the celestial bodies yet discovered, our closest neighbors in space, except for the Moon, are members of the Apollo and Amor groups. One of them, Icarus, passed very close to Earth in 1968.

A flyby mission to members of these groups would be relatively simple, but probably not very rewarding because their relative velocities when close to Earth are very high, on the order of 30 km/s. A rendezvous and soft landing is for this reason a technically difficult project.

Of all the translunar celestial bodies, the Eros asteroids are the easiest to reach and therefore would be more favorable objects for investigation. They have eccentricities that are definitely lower than the other Apollo and Amor asteroids (although still rather high), and their relative velocities when close to

[1]See p. 419.

Earth are reasonably small (some < 5 km/s). This means that they are not very difficult objects with which to rendezvous by means of a soft unmanned landing or—in the future—a manned landing.

If space activity is planned as a stepwise penetration into outer space, a mission to an Eros asteroid is a logical second step after the lunar landings.

An Almost Unknown Group of Bodies

Very little is known about the asteroids. Except for Ceres and Vesta, almost nothing is known about their mass, density, bulk chemical composition, structure, or albedo. Polarimetric and infrared measurements have given some information on their surface properties. Regular light variations indicate that they spin with periods on the order of 3 to 15 hr.

As compared to the planets, the asteroids have attracted very little interest. The reason seems to be simply that so little is known about them. There is a priori no reason why a small body like an asteroid should be less interesting than a body as big as a planet. On the contrary, the small bodies probably have recorded and preserved more information about the early history of the solar system than the planets and satellites, which actively destroy their own record.

The asteroids traditionally have been considered to be fragments of one or several "exploded planets," but this view encounters serious difficulties (e.g., it cannot adequately explain the distribution of orbits). Moreover, it is reasonable to assume that they were accreted by the same process as planets and that the assembly of asteroids is similar to the "planetesimal" state preceding the formation of planets. As such they would be products of concurrent accretion and breakup processes. The development of theories for either one of these processes encounters the difficulty that we know next to nothing about the collective behavior of a population of orbiting small bodies of asteroid size.

Asteroids: Celestial Bodies of Unique Size

The observed asteroids form a group of bodies that in size are intermediate between planets and meteoroids. We may take a diameter of 3000 km (about the size of the Moon) as a lower limit for a planetary object, 3 km as representing an Eros asteroid, and 3 m as the size of meteorites from which we have gained our information about meteoroids (fig. 1). With these values, the masses of the Eros group of asteroids differ by a factor of 1 billion from those of the planets, and also by a factor of 1 billion from the masses of meteorites.

Hence the Eros asteroids, which we are particularly considering here, *form a group about in the middle of a vast gap of 18 orders of magnitude in the mass spectrum of celestial bodies.*

It should be remembered that natural satellites and comets also are located in the same gap. Our knowledge of these is also very deficient, but they are more distant in space than the Eros asteroids. Our hope of filling this gap in the near future is connected with missions to members of this latter group.

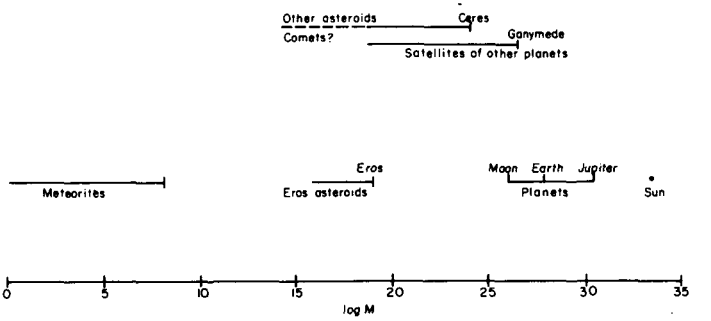

Figure 1.—Mass spectrum of bodies in the solar system. Lower group: Bodies which have been explored are (1) meteorites that have fallen to Earth and (2) the Moon and planets that have been targets of space missions. The Eros asteroids are located in the middle of a gap of almost 20 orders of magnitude between the meteorites and the planets. Upper group: Other bodies, more difficult to explore.

It is sometimes claimed that the region of the mass spectrum which the asteroids occupy is unimportant. In reality there are a number of fundamental questions that can be solved only by a closer study of this region. One of these questions is how the accretion of planets took place, because the accreting embryos (or planetesimals) must have passed through this range. Furthermore, in this mass region, the accretive process must change its character from nongravitational to predominantly gravitational. Exploration of the Moon has demonstrated that all new material accreting on bodies of this large size impacts with such a high energy that practically all traces of the original structure are obliterated.

The Relations Between Asteroids, Comets, and Meteoroids

The observed asteroids are probably only samples of a large population of bodies, most of which are subvisual.

The orbit distribution of the subvisual asteroids is unknown. Attempts have been made to estimate the size distribution theoretically; but there is no observational confirmation, and the theories involve a number of uncertain hypotheses. A genetic connection between meteoroids and some asteroids is likely to exist, but because the gap in the mass spectrum between these groups of bodies is of the order of magnitude of millions or billions, the connection is necessarily uncertain.

It has been claimed that from studies of meteorites we can obtain all the scientific information about asteroids (and comets) that is needed, and that space missions to these bodies hence are unnecessary at the present time. "Poor man's space research," consisting of analysis of meteorites that automatically fall to Earth, is thus sometimes thought to be a satisfactory substitute for real space missions.

The determination of the orbits of meteorites, which now is beginning to supplement the chemical and mineralogical studies of these objects, is certainly very important for the exploration of the meteoroid population. Existing results make it clear, however, that meteorites constitute a highly biased sample that is far from representative of the small bodies in space. These show a much wider range of orbital and structural characteristics than those of meteorites, which depend on low relative velocities and high cohesive strength to survive passage through the atmosphere. In fact, only a very small fraction ($< 10^{-3}$) of the groups of bodies that intersect Earth's orbit are sufficiently tough and slow to be collected on the ground for analysis. Of the small fraction of meteoroids that thus can be studied, many have broken up and all have suffered serious damage by surface heating and ablation. This completely destroys the loose material and the skin, which contain the record of the low-energy space irradiation. The ablation also makes it difficult to take full advantage of the higher energy exposure record in meteoroids.

It is possible that the meteorites are related to some groups of asteroids (especially the Apollo group) and to the comets, but these relations badly need observational confirmation. It is doubtful whether there is any direct connection with main belt asteroids, because it is very difficult to deflect these bodies into Earth-crossing orbits. The Eros asteroids are intermediate. Some of them are Earth-crossing, and may be associated with meteors, some are not. A clarification of these questions is possible only with increased knowledge of asteroids.

There is a possibility of finding soft-landed cosmic dust and meteoroids preserved on the surface of asteroids because their gravitation is so small and because alteration by impact gardening proceeds at a much lower rate than previously inferred (Arrhenius et al., 1971). Hence, asteroid investigations may also clarify the in-space structure of these materials.

Both the comets and the natural satellites of other planets are very interesting objects, some in the same mass range as asteroids. In comparing missions to asteroids with missions to comets or satellites, one can give good arguments for consideration of the latter two classes of bodies. However, the technical difficulties connected with scientifically rewarding missions to these bodies are very much larger at the present time.

Eros Asteroids as Space Probes Clarifying the History of Earth-Moon System

Investigation of an Eros asteroid could give us an important point of reference for clarifying the history of the Earth-Moon system. For example, an event like the heating of the Moon 3.5 billion yr ago can either be associated with some event specific to the development of the Earth-Moon system (for example, the capture of the Moon) or it could possibly be produced by some external cosmic phenomenon affecting this whole region of space. If the thermal history of Eros asteroids is clarified, a decision between these alternatives is possible.

The Eros Asteroids and the Early History of the Moon

The asteroids may also contribute in another respect to the clarification of the early history of the Moon. Some of the Eros asteroids come very close to Earth with reasonably low velocities. There is a possibility that the precapture orbit of the Moon was similar. Hence, the history of the Moon may be related to some of the Eros asteroids. For example, it is possible that some of them are planetesimals that escaped accretion by the planet Moon. If this type of relationship exists, there should be a direct connection between these asteroids and the bodies that produced the lunar craters when impacting on the Moon.

The First Undifferentiated Bodies To Be Investigated

Both Earth and the Moon are large enough for high-temperature planetary evolution including volcanism and radial differentiation. This means that it is impossible to draw any certain conclusions about their bulk chemical composition from studies of samples from their surfaces.

Among the asteroids we are much more likely to find materials that have never been melted since the accretion. Although degassing and partial melting by shock have modified parts of them, gravitational separation is ineffective in the mass range covered by the Eros asteroids. If some are fragments of larger bodies, the internal constitution of these could be determined from the fragments. Their composition and structure may in part be similar to some types of meteorites. However, the loose surface deposits (which must necessarily be found locally) and the exposed hard rock surfaces must have characteristics that have never been sampled in meteorites or on the Moon. This surface layer is likely to contain a unique record of the accretion and ablation processes active in the planetesimal environment. In general, the exploration of asteroids would provide the real configuration and interrelation of the component materials (which may be of known or unknown type) and hence for the first time a direct record of how the most primitive bodies develop in the solar system. No new minerals in a strict sense were found on the Moon, yet their configuration and alteration provided completely new and largely unpredicted information.

In contrast to the planets and to the Moon, the Eros asteroids may supply us with planetesimal matter in a very primitive state. This does not mean that they are samples of homogeneous "primordial" matter because the proportions of condensable elements in the primordial plasma most likely have undergone significant fractionation during the emplacement and condensation processes. However, we would approach the primordial state one step farther.

ACKNOWLEDGMENTS

In preparing this review, we have profited from the discussion at this colloquium. Support from NASA grants NGL-05-009-154 and NGL 05-009-002 is gratefully acknowledged.

REFERENCE

Arrhenius, G., Liang, S., Macdougall, D., Wilkening, L., Bhandari, N., Bhat, S., Lal, D., Rajagopaln, G., Tamhane, A. S., and Venkatavaradan, V. S. 1971, The Exposure History of the Apollo 12 Regolith. Proc. Apollo 12 Lunar Sci. Conf. Geochim. Cosmochim. Acta **35**, suppl. 1.

REASONS FOR NOT HAVING AN EARLY ASTEROID MISSION

EDWARD ANDERS
University of Chicago

Let me first emphasize the area of agreement with Professor Alfvén. I, too, believe that the asteroids are of very great scientific interest; great enough to justify space missions some day. What we differ on is the timing and target selection for these missions (Alfvén and Arrhenius, 1970, and in this volume[1]). I look upon space missions as a tremendously expensive way of obtaining scientific data, which should not be attempted until all available alternatives are exhausted. Ground-based research on asteroids and meteorites is nowhere near exhaustion; on the contrary, it is moving at an impressive pace. If we maintain this pace for another decade or two, we will not only have answered most of the questions posed for an *early* mission, but will be able to come up with a more worthwhile, more informative mission.

Harold Urey once said that meteorites are the only samples of extraterrestrial matter delivered to our doorstep free of charge. Although some people will disagree, I think there is more than a slight chance that most meteorites come from the asteroid belt. It would be tremendously embarrassing to our entire profession if it turned out after a mission to Eros that pieces of Eros (erotic meteorites?) have been reposing in our museums all along. I say "embarrassing" because I think it is well within our powers to trace each group of meteorites to its parent body in the sky. What makes the problem tractable is the small number of objects to be matched up: 6 to 11 meteorite parent bodies and about 7 asteroid families. Each successful match reduces the number of combinations remaining. Let me outline some possible approaches.

ORBITAL CLUES

Arnold's (1965) Monte Carlo method makes it possible to trace meteorites to their parent bodies, by comparing observed meteorite orbits with computer-generated sets for various possible parent bodies. Wetherill (1968, 1969) has made major improvements in the model, and others are undoubtedly feasible. Once a way has been found to treat distant interactions with Jupiter, the model will have reached a degree of realism at which meaningful comparisons with observed meteorite orbits can be made.

[1]See p. 473.

Observational material is still scarce; the Prairie Network and the Czechoslovak All Sky Camera Network have thus far yielded orbits for only two meteorites. But similar networks are being built in Canada and Germany, and there is hope that progress in this area will quicken. At least several dozen of the older visual orbits appear to be salvageable (Levin and Simonenko, 1969; Millman, 1969) and additional criteria are available for eliminating the remaining 15 to 20 percent doubtful ones in Millman's selection.

It would be premature to claim any identifications on the basis of the present data. But figures 1 to 3 show that different meteorites and asteroids are readily distinguishable from one another on appropriate plots. The Monte

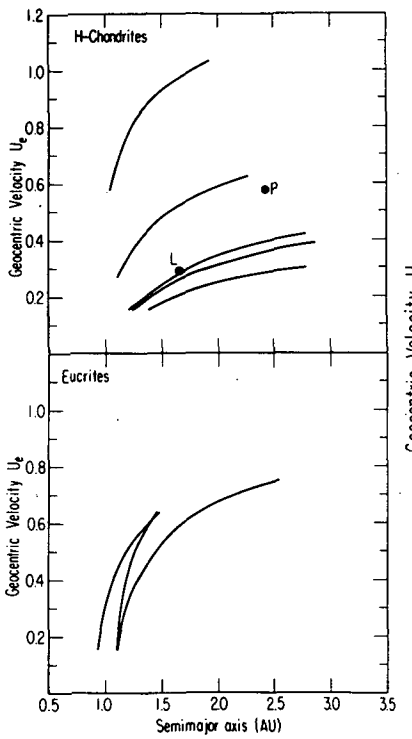

Figure 1.–Observed meteorite orbits. Photographic orbits for Přibram *P* and Lost City *L* are indicated by black circles; visual orbits (Millman, 1969, and personal communication) are indicated by curves representing loci of plausible U_e-a combinations. Eucrites appear to have systematically smaller orbits.

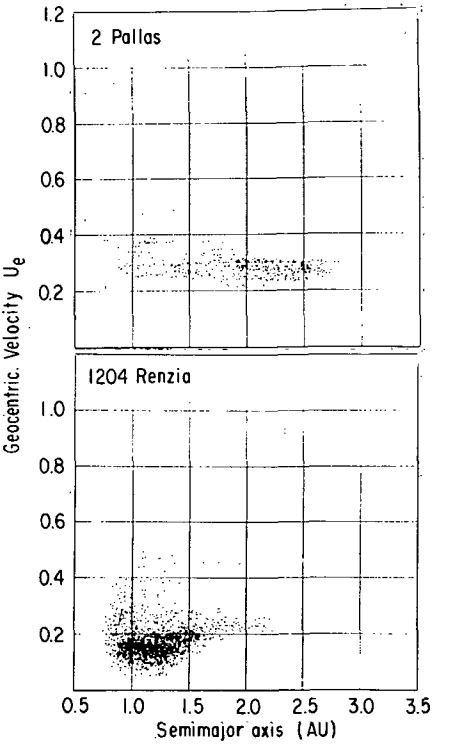

Figure 2.–Monte Carlo orbits of meteorites (Mellick and Anders, unpublished). Both were calculated on the assumption that the inclination drops to a small value whenever the meteorite reaches a near 2.50 AU (1/3 commensurability with Jupiter), and that the mean life for collisional destruction is 1×10^7 yr. Meteorites from Renzia have systematically smaller a and lower U_e than those from Pallas.

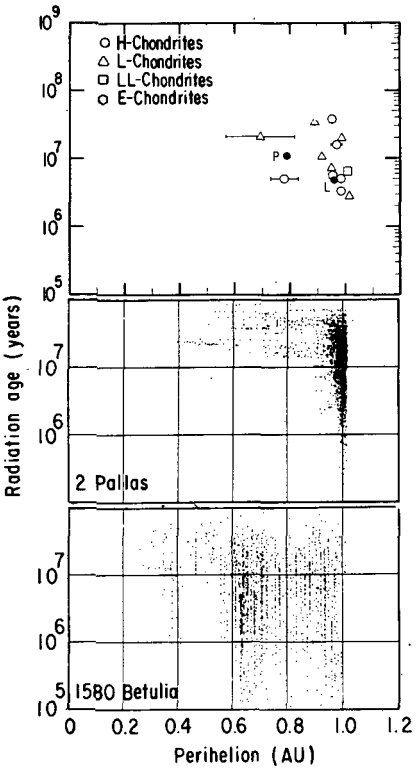

Figure 3.–Radiation age versus perihelion q. Perihelia of chondrites and Pallas-derived meteorites tend to be close to 1 AU, decreasing slightly with increasing radiation age. This is true of all Mars-crossing asteroid families, as long as older meteorites are eliminated by collisional destruction, with mean life of 10^7 yr. For Betulia and other initially Earth-crossing parent bodies, smaller perihelia appear from the very beginning. Open symbols represent visual orbits; black symbols, photographic orbits of the H-chondrites Pribram *P* and Lost City *L*.

Carlo orbits were calculated on the "optimistic" assumption that geocentric velocity **U** is occasionally reoriented by Jupiter perturbations when the semimajor axis a reaches a major commensurability (Anders[2]). Williams'[3] newly discovered resonances suggest that such an assumption is not grossly unrealistic. As the model is further refined, definite identifications ought to be possible.

Some of the parameters most useful in such comparisons can be obtained from sources other than photographic orbits. Perihelia often can be estimated with surprisingly good accuracy from visual observations. Small perihelia (less than 0.5 to 0.7 AU) can be inferred from loss of cosmogenic gases. Some meteorite classes (e.g., H-chondrites) show such gas losses more frequently than others; and because they also show a preference for a.m. falls, they probably have orbits with small a and small q (Wänke, 1966).

Geocentric velocities can also be estimated from the ablation loss, which in turn can be determined from measurement of charged particle tracks or cosmogenic radioactivities (Bhandari, 1969).

[2]See p. 434.
[3]See p. 177.

Finally, some meteorites have radiation ages less than 1 million yr. They are not likely to have experienced any close encounters with Earth prior to impact and thus probably struck Earth from a relatively "unevolved" orbit. Such an orbit should be easy to trace to that of the parent body. If the parent body was Earth-crossing, the two orbits should be identical; if it was Mars-crossing, they should differ by only a single Mars deflection. Sooner or later such a meteorite will be recovered by one of the camera networks. In fact, Lost City, with a radiation age of only 5 million yr, did not intersect Earth's orbit for much of the past 0.5 million yr, according to calculations by Lowrey (1970). Thus it may be suitable for this kind of analysis.

OPTICAL AND CHEMICAL CLUES

McCord et al. (1970) and Chapman et al.[4] have shown that reflection spectra of asteroids can provide clues to their composition. Dollfus[5] and Hapke[6] have used albedo, polarization data, and color indexes (Gehrels, 1970) for this purpose, and have made comparisons with terrestrial, lunar, and meteoritic samples. This is a most promising development. The five known classes of chondrites can be grouped into compositional sequences, on the basis of oxidation state, iron content, Mg/Si ratio, etc. Presumably these trends reflect conditions in the solar nebula that varied in some systematic way with distance, time, height above median plane, etc. (Anders, 1971). It will be most interesting to see whether these sequences can also be recognized among the asteroids, and whether they are functions primarily of a, i, or radius R. The pyroxene band at 0.9 μm, which is the most distinctive feature in the reflection spectra, will depend both on oxidation state (which determines Fe^{2+}/Fe_{total}, and hence the Fe^{2+} content of the pyroxene) and Mg/Si ratio, which determines the pyroxene/olivine ratio.

The degree of fragmentation of an asteroid family (Anders, 1965) can also provide a useful clue. Iron meteorites with a narrow spread of cooling rates apparently come from near the center of their parent body, which must therefore be highly fragmented. Among the chondrites, the proportion of highly recrystallized ones (petrologic type 6) is a clue to degree of fragmentation. For example, only 27 percent of the H-chondrites are type 6, compared to 68 percent of the L-chondrites. Either the L-chondrite parent body was larger and generally hotter, or it was more highly fragmented. (The latter interpretation is more in line with the 520 million yr outgassing event for the L-chondrites; Anders[7].)

---

[4]See p. 51.
[5]See p. 95.
[6]See p. 67.
[7]See p. 431.

APPROPRIATE TARGETS FOR AN ASTEROID MISSION

I have argued in my companion paper[8] that only high-velocity asteroids, about 10 percent of the total, are potential sources of meteorites. Little or no material reaches us from the remaining 90 percent, including the entire outer half.

If we are successful in matching each meteorite class to its parent body, we will certainly know quite a bit about the high-velocity objects in the inner half of the belt. There will not be much point in sending spacecraft to this relatively well-known part of the asteroid belt.

At this point it is well to consider the nature of the Eros group. There can be no question that Eros and Amor are some of the most accessible asteroids, but they seem to be transient objects. All five have short lifetimes against planetary capture. According to Öpik's (1963) calculations, the lifetimes (in aeons) are as follows:

433 Eros	1.84
1221 Amor	5.31
1620 Geographos	0.15
1627 Ivar	4.02
1685 Toro	0.18

These are probably overestimates, being based on the initial orbit only. Monte Carlo calculations, which consider the change in collision probability after each orbital change in planetary encounters, sometimes give lifetimes up to an order of magnitude shorter for similar objects. In any case, the lifetimes for *orbital change* are much shorter than those for *planetary collision.* Thus it is unlikely that these objects formed where they are now found.

We can try to estimate the origin of the three Mars-crossing objects, making use of the fact that their velocity relative to Mars remains approximately invariant in successive encounters. (The velocity is not strictly invariant because the orbit of Mars has nonzero e and i; this causes a slight acceleration of the asteroid at each encounter.) Figure 4 compares U_M, the velocity relative to a circular orbit at 1.524 AU, for the Mars-crossing asteroids.

Eros may have been derived from family 31 after some acceleration by Mars, or from family 5. Amor and Ivar may be members of the Hungaria group at 1.9 AU; but this group itself is probably derived from one of the families in the asteroid belt proper: 5, 29, or even 30. Thus there is not much point in obtaining samples of these stray objects because their original location in the asteroid belt is almost as uncertain as that of meteorites.

If missions with sample return capability are ever sent into the asteroid belt, they should seek to complement the knowledge gained from meteorites. As I

---

[8]See p. 429.

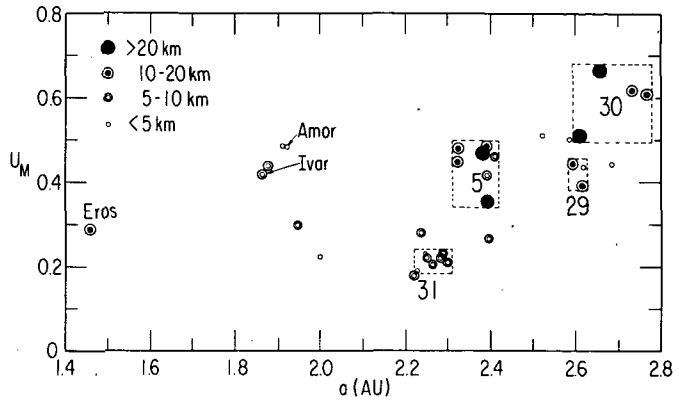

Figure 4.—Mars-crossing asteroids. Eros has nearly the same encounter velocity with Mars U_M as families 31 or 5, and may be a stray member of one of them. Amor and Ivar appear to be related to the Hungaria group at 1.9 AU, which in turn may be derived from families 5, 29, or even 30.

argued in my companion paper,[9] perhaps as much as 10 percent of the asteroid belt (mainly the high-velocity objects in the inner half) may contribute meteorites to the Earth. The remaining $\geqslant 90$ percent is out of communication with us. If the optimists are right, we may soon gain a good understanding of the "communicating" 10 percent of the belt. Combining this knowledge with telescopic observations, we can then extrapolate at least the gross trends of the "noncommunicating" 90 percent. Some crucial questions will undoubtedly remain when all ground-based studies have been pushed to the limit, and at that stage, perhaps 10 yr from now, further progress will require space missions. We do not know what sort of target will have highest scientific interest at that time: a Trojan, a Hilda group asteroid, a few nearly spherical asteroids (small or large), in the near or far parts of the belt, a few highly irregular objects, a Hirayama family, etc. Any choice we make now is likely to seem trivial or uninformative a decade hence.

If the pessimists are right, even the "communicating" 10 percent of the asteroid belt will be *terra incognita* to us by the time ground-based work has reached its limits. In that case, a methodical exploration of the asteroid belt may well be justified. Whatever the GNP at that time, it seems certain that the number of missions will be orders of magnitude smaller than the number of asteroids. Targets therefore will have to be selected with very great care. In any event, because proximity is not a critical mission constraint (Bender and Bourke[10]), asteroids in the main belt would seem more worthwhile than stray objects such as Eros.

---

[9]See p. 429.
[10]See p. 503.

ACKNOWLEDGMENTS

The Monte Carlo results in figures 2 and 3 are unpublished data by P. J. Mellick. This work was supported in part by AEC Contract AT(11-1)-382 and NASA Grant NGL 14-001-010.

REFERENCES

Alfvén, H., and Arrhenius, G. 1970, Mission to an Asteroid. Science **167**, 139-141.

Anders, E. 1965, Fragmentation History of Asteroids. Icarus **4**, 399-408.

Anders, E. 1971, Meteorites and the Early Solar System. Ann. Rev. Astron. Astrophys. **9**, 1-34.

Arnold, J. R. 1965, The Origin of Meteorites as Small Bodies. II. The Model. Astrophys. J. **141**, 1536-1547.

Bhandari, N. 1969, On Orbital Velocities of Some Stone Meteorites. Paper presented at the Cosmic Ray Conf. (Delhi).

Gehrels, T. 1970, Photometry of Asteroids. Surfaces and Interiors of Planets and Satellites (ed., A. Dollfus), p. 319. Academic Press, Inc. New York.

Levin, B. Yu., and Simonenko, A. N. 1969, Meteorite Radiants and Orbits. Meteorite Research (ed., P. M. Millman), ch. 46, pp. 552-558. D. Reidel. Dordrecht.

Lowrey, B. E. 1970, Orbital Evolution of Lost City Meteorite. GSFC preprint X-644-70-444.

McCord, T. B., Adams, J. B., and Johnson, T. V. 1970, Asteroid Vesta: Spectral Reflectivity and Compositional Implications. Science **168**, 1445-1447.

Millman, P. M. 1969, Astronomical Information on Meteorite Orbits. Meteorite Research (ed., P. M. Millman), ch. 45, pp. 541-551. D. Reidel. Dordrecht.

Öpik, E. J. 1963, Survival of Comet Nuclei and the Asteroids. Advances in Astronomy and Astrophysics 2 (ed., Z. Kopal), pp. 219-262. Academic Press, Inc. New York.

Wänke, H. 1966, Der Mond als Mutterkörper der Bronzit-Chondrite. Z. Naturforsch. A **21**, 93-110.

Wetherill, G. W. 1968, Dynamical Studies of Asteroidal and Cometary Orbits and Their Relation to the Origin of Meteorites. Origin and Distribution of the Elements (ed., L. H. Ahrens), pp. 423-443. Pergamon Press. Oxford.

Wetherill, G. W. 1969, Relationships Between Orbits and Sources of Chondritic Meteorites. Meteorite Research (ed., P. M. Millman), ch. 48, pp. 573-589. D. Reidel. Dordrecht.

DISCUSSION

KUIPER: As a ground-based observer most of my life, I would naturally sympathize with the point of view of Anders. I think all of us who are working in the laboratory or as astronomers feel that we can do 10 times better or we would not be in the business in the first place. We see many possibilities ahead. I think at the same time it is not right for us to say that the rest must wait until we have made progress. I am all for an accelerated ground-based program for 5 yr, but let us not stop the space missions if they can be ready before that.

KIANG: Past attempts at determining the size and shape have had little success, and this is not due to any lack of effort. Here we seem to have an objective that will always evade us however hard we may try from the ground but that can easily be attained by an asteroid mission. Another objective of this nature is the number density of small bodies in the asteroidal belt. At present this is based on brute extrapolation.

DUBIN: I agree with Anders regarding the importance of the ground-based studies of meteorites relative to the understanding of the asteroids, but it appears that the ground-based work cannot resolve the problem in the sense indicated from the Prairie

Network results shown by McCrosky[11] earlier. McCrosky showed that most of the bright meteors were of type A and C and of low density. The chondrite, Lost City, was one case in a sample of between 100 and 1000 events. In addition, Anders showed that a significant fraction of the mass of the meteoroid, in fact the interesting outer crust, is always ablated during atmospheric entry. I question, accordingly, how these limitations of the sample of meteorites can give a satisfactory model of the early solar nebula and the asteroids.

ALFVÉN: Anders feels that so much information about asteroids could be obtained from the study of meteorites that this, for the time being, ought to substitute for actual exploration in space.

To investigate the evolutionary history of the solar system, it is necessary to pool information from a number of sciences including chemistry, geology, meteoritics, celestial mechanics, and plasma physics. Specialists in any one of these fields may make important contributions but hardly without collaboration with scientists in other fields. This seems not to be generally understood. There have been numerous attempts from astrophysicists to clarify the evolutionary history of the solar system without taking notice of the results of the chemists. Similarly, some competent chemists still tend to draw their conclusions from chemical considerations alone, neglecting the laws of physics. It is obviously unreasonable to write one evolutionary history for physicists and another, completely different, for chemists.

The most important task of the cosmic sciences today is to draw borderlines between speculation and science in its real sense. It is obvious that one of the borders is set by the reach of spacecraft. For example, before the first soft landing on the Moon there were, understandably in view of lacking evidence, many speculations about the chemical composition and physical structure of the lunar surface. We know now that all this had very limited scientific value except as a stimulus toward the actual revealing experiment. For asteroids, a similar situation prevails today, only the uncertainties are wider yet.

During this symposium there has been much discussion about the origin of meteorites. There has been rather extensive support for the view that there is an association between meteorites, comets, and Mars-crossing asteroids, although the arguments for this view are still speculative. Anders, however, believes that the meteorites also come from the main belt asteroids and that certain groups of meteorites should be associated with certain asteroid families. His hypothesis is not demonstrably supported by the laws of celestial mechanics.

UREY: It is my expectation that Eros would have a composition very similar to some meteorite with only minor differences in composition and mineralogy. Also, I suspect that it is a fragment from some violent collision because of its elongated shape. Because of this origin and its very low gravitational field, I believe that it will have no "soil" on its surface and therefore no scooping of soil or drilling of a core can be made. I strongly suspect that a mission to Eros will be very disappointing to experimenters, the scientific community, NASA, Congress, and the public. I would be delighted to support a mission to Ceres. It may be a fragment of some larger body or it may be a primary object. It may have free rocks and some layer of soil on its surface. Possibly it is a little sister of my lunar-sized bodies or it may be a daughter of them. I would be most interested in seeing a mission to Ceres or the other larger asteroids.

WHIPPLE: I do feel that interest by astronomers in the solar system, particularly in asteroids and smaller bodies, has been negative over the years. Thus I certainly am delighted to see this broad interest of so many coming here to discuss this. It looks to me that it is a healthy attitude toward these problems but I feel this should be supported at a higher level than ever.

However, I have a point about landing on an asteroid. It seems to me that we would like to find a broken-up body so that its surface would give us a historical record,

---

[11] See p. 395.

analogous to geology on the walls of the Grand Canyon. I am sure that the formation processes of asteroids must lead to such historical layers. Perhaps Ceres is not a good choice because its early formations will probably be covered over. On the other hand, I suspect it would be hard to choose an asteroid that would not lead to exciting and unexpected results.

GREENSTADT: Anders' argument against an early asteroid mission and Anders' and Urey's skepticism regarding the value of an Eros mission obtain part of their force from an implicit assumption that such a mission would be created at great expense solely for its own objectives. However, this is not the case. If solar electric and nuclear electric propulsion are to be developed in an orderly way because they are useful for future solar system missions in general, then a proper question is whether Eros, or another Mars-crossing asteroid, would be a suitable target for an early launch with electric-propulsion technology. The choice may be not whether an Eros rendezvous is the best of all asteroid mission objectives, but whether it is best among alternatives for application of early electric-propulsion launches.

Page intentionally left blank

EXPLORATION IN THE SOLAR SYSTEM WITH ELECTRIC SPACECRAFT

ERNST STUHLINGER
NASA George C. Marshall Space Flight Center

The landings of instrumented probes and astronauts on the Moon and the short glimpses at Venus and Mars that distinguished the spaceflight program of the last decade yielded such an impressive wealth of new knowledge that the President, in his programmatic speech of 1970, mentioned the continuing exploration of the solar system as one of the national goals during the decade of the seventies.

This exploration will be accomplished with unmanned spacecraft, except for the remaining three Apollo flights in 1971 and 1972 and Skylab in 1973. Planetary exploration will include photographic coverage of the surfaces of the celestial bodies; closeup pictures of specific surface features; magnetic and gravitational measurements; observations of atmospheres, ionospheres, and radiation belts; analysis of surface material in situ; and, as far as possible, the return of surface samples for careful chemical and mineralogical analyses and for age determinations.

In addition to the Moon and the nine planets, two other groups in the solar family recently have aroused great interest among astronomers and cosmologists: asteroids and comets. Asteroids, unlike heavier celestial bodies, have not been subjected to heavy bombardment by meteoroids since the time of their formation about 4.5 billion yr ago. They are expected to consist of undisturbed and unmodified primordial planetary matter not to be found at any other place in the solar system. Comets are of particular interest because they are covered, in all likelihood, by a thick layer of frozen material, such as water, ammonia, methane, cyanogen, perhaps even formaldehyde and other more complex compounds, which the nucleus of the comet accumulates while slowly moving through its apogee far away from the Sun, in many cases even beyond the orbit of Pluto. As the comet moves through its perigee, the Sun gradually melts and removes the frozen cover. A probe cruising through the cometary tail would be able to sample and analyze the interplanetary matter that a comet collects in space and displays in the proximity of the Sun.

Missions to planets, asteroids, and comets, as outlined in this exploration program, have several features in common. Each mission will last between 1 and several yr; each spacecraft must possess a considerable capability to

maneuver and to change its flight velocity during the entire duration of the mission; the payload capability should be large; and the amount of available electric power for the transmission of data should be high. Some of these features of planetary missions are listed in table I, in comparison with less demanding missions to other targets. It is obvious that the requirements of planetary missions exceed those of other missions by a considerable margin. The question is well justified, therefore, whether a propulsion system other than the conventional chemical rocket motor may be appropriate for the long and demanding transfer from the vicinity of Earth to a planet, an asteroid, or a comet. The answer to this question should be an emphatic yes. Electric rocket motors, more specifically ion motors, seem to be ideally suited for space missions that extend over time periods of 1 or more yr. In fact, the electric propulsion system, when used on planetary missions, offers a high incremental velocity, an almost unlimited reignition capability, a large payload fraction, a long operating lifetime, and a sizable electric power source available for data transmission after the target has been reached. Electric-propulsion systems have been under study and development for many years, and they are now ready for applications.

An electric-propulsion system requires a source of electric power on board the spacecraft. Two prime sources of electric energy are appropriate for electric spacecraft propulsion, solar electric power supplies, and nuclear electric power plants. Solar electric power supplies have been used in space with great success for over 12 yr. They have an operable lifetime of years, and their present conversion efficiency of about 12 percent is entirely satisfactory for flight missions as envisioned during this decade. Solar electric power holds great promise for electrically propelled spacecraft that orbit around or land on Mercury, Venus, or Mars; meet with a comet; or descend to the surface of an asteroid. Even sample-return missions to all these targets will be possible. The decrease of solar energy flux with increasing solar distance makes solar electric power sources less capable near the outer planets. Highly elliptic orbiters around Jupiter, and flybys near the more distant planets, would still show considerable payload gains if an electric stage were used on the spacecraft; however, in view of the large amount of electric power needed to transmit observational data from these remote targets, nuclear electric power sources will be preferable on missions to the outer planets. Also, nuclear electric power

TABLE I.–*Classes of Rocket Flight Missions*

Mission	Timespan	Flight distance, km	Total velocity increment, $km\text{-}s^{-1}$
Ballistic	Minutes	10^3	5
Orbital	Hours	10^4	10
Lunar	Days	10^6	25
Planetary	Years	10^9	50

will enable a spacecraft to achieve a circular orbit even around the remotest planet. At present, nuclear electric power sources for planetary flight in the kilowatt range are not yet available. The first power plants of that kind may be ready for use toward the end of this decade.

Several different kinds of electric propulsion systems have been under study, among them the resistojet, the arc jet, the ion engine, and the plasma engine. For planetary missions, the ion engine is the best choice; the following description will concentrate on this type of electric propulsion. However, the basic relations to be described apply to all systems that need an electric power source.

In an ion rocket, the exhaust beam consists of ions; they are accelerated within the thrustor by an electrostatic field. Before entering the accelerating field, the propellant atoms must be ionized. The exhaust velocity of the ions v is a function of their specific charge ϵ/μ and the potential difference across the accelerating field U:

$$v = \sqrt{\frac{2\epsilon U}{\mu}}$$

The beam of ions represents a current I according to

$$I = \frac{\dot{M}\epsilon}{\mu}$$

where $\dot{M}$ is the propellant consumption. The product

$$UI = W$$

represents the power contained in the beam. The thrust force F exercised by this ion beam upon the thrustor is expressed by the relations

$$F = \dot{M}v = \frac{2W}{v} = W\sqrt{\frac{2\mu}{U\epsilon}} \tag{1}$$

An electric rocket has three main components: payload, propellant, and power source. The mass of the thrustor, which is small compared to the mass of the power source, is usually included in the mass of the power source to simplify computations. The power source is characterized by its "specific mass" α, measured in kilograms per watt. The lower the specific mass, the more attractive the power source. On the basis of existing technologies, a solar electric space power source can be built with a specific mass on the order of 0.03 to 0.02 kg/W. An improvement to 0.015 or even 0.01 kg/W may be expected toward the end of the decade.

The performance of a chemical rocket under no-drag and no-gravity conditions is expressed by the well-known Tsiolkovskiy equation (explained in fig. 1(*a*)):

$$\frac{M_L}{M_0} = e^{-u/v} \tag{2}$$

It says in essence that the payload capability M_L/M_0 or the terminal velocity u of a rocket increases continuously with increasing exhaust velocity[1] v as shown in figure 2(*a*). The corresponding equation for electric rockets is shown in figure 1(*b*). This equation contains the variables α (specific mass, measured in kilograms per watt) and T (total propulsion time). For chemical rockets, $\alpha = 0$;

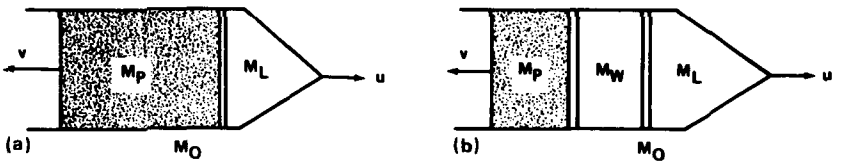

Figure 1.–Equations for two rocket systems. (*a*) Chemical (endogenous). (b) Electric (exogenous).

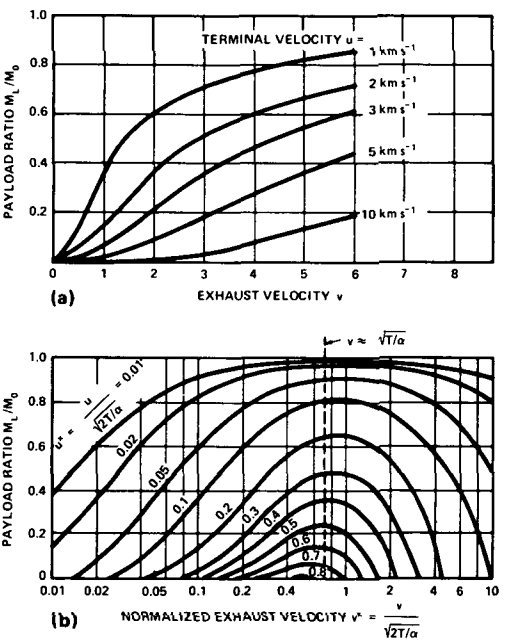

Figure 2.–Payload ratio as a function of exhaust velocity and terminal velocity. (*a*) Chemical or endogenous systems. (*b*) Electric or exogenous systems.

[1]Rocket engineers frequently use the term "specific impulse" I_{sp} instead of exhaust velocity v. Generally $I_{sp} = v/g_0$; g_0 = Earth's gravitational acceleration.

in this case, the equation for electric rockets reduces to equation (2). Figure 2(*b*) indicates that an electric rocket, for a given terminal velocity u, a given specific mass α, and a given total propulsion time T, has an optimum exhaust velocity v at which its payload ratio M_L/M_0 is a maximum. The designer will choose this optimum exhaust velocity to obtain a maximum payload ratio. The physical reason for the existence of an optimum exhaust velocity is obvious. At higher exhaust velocities, the increase in power supply mass would reduce the payload, and at lower velocities, the necessary increase in propellant mass again would reduce the payload. The following approximations can be obtained from the electric rocket equation and other well-known relations:

$$v_{\text{opt}} \approx \sqrt{\frac{T}{\alpha}} \tag{3}$$

$$a_{\max} = \frac{F}{T} \approx \sqrt{\frac{1}{\alpha T}} \tag{4}$$

where $a_{\max}$ is the maximum acceleration obtainable with negligible payload. The simple relations expressed by equations (1) to (4) permit a quick assessment of the design requirements and performance capabilities of an electric propulsion system. However, for careful optimization studies and trajectory computations, an analytical method (Irving and Blum, 1959) has found wide application. Combining equations (1) and (4), we obtain

$$a_t = \frac{F_t}{M_t} = \frac{\dot{M}_t v_t}{M_t}$$

$$W = \frac{\dot{M}_t v_t^2}{2}$$

hence

$$-\frac{dM}{M_t^2} = \frac{a_t^2}{2W}\, dt$$

and

$$\frac{1}{M_T} - \frac{1}{M_0} = \frac{1}{2W}\int_T a_t^2 \, dt$$

The terminal mass M_T consists of power source and payload. Obviously, a maximum payload will be obtained when the integral on the right-hand side is a minimum. It is the task of the project planner to find that trajectory which,

under the constraints of starting point, target point, total traveltime, total initial mass, total available power, and specific mass of the power source, makes the integral a minimum. This problem can be solved with the methods of variational calculus. In fact, computer programs exist already for numerous planetary trajectories and their optimization, and specific missions (for example, a rendezvous with asteroid Eros in 1975 or 1977) can be programed and computed easily. The computation results in optimum figures for the exhaust velocity, the program for thrusting and coasting periods, the guidance program, the actual payload capability, etc.

It is obvious from equations (1) and (4) that the thrust acceleration of an electrically propelled spacecraft will always be low, on the order of $10^{-4}\, g_0$. However, the thrust force on planetary missions will always act over a long period of time, on the order of months or even years. For this reason, the total impulse generated by an electric-propulsion system is of considerable magnitude. In fact, an ion thrustor powered with 16 kW of electric power and operating for 350 days generates the same total impulse as the hydrogen-oxygen rocket engine RL 10 used on the second stage of the Saturn I rocket (six engines) and on the Centaur rocket stage (two engines). (See table II.)

Before the propellant particles can be subjected to the accelerating force of an electric field, they must be ionized. Three different ionization methods have been developed to a high degree of efficiency and reliability: the electron bombardment method (Kaufman engine), developed at the NASA Lewis Research Center; the radiofrequency ion source (Loeb engine), developed at the University of Giessen in West Germany; and the contact ionization method, developed mainly at Electro-Optical Systems Corp. and at Hughes Research Laboratory. All three systems fulfill the requirements of an electric propulsion system, and all have undergone long-time laboratory testing. Furthest advanced in development, testing, and flight applications is the Kaufman engine in which ionization of the vaporized propellant is accomplished by electron bombardment; it is shown in figures 3 and 4.

The first application of an electric propulsion system to a space probe, as far as publicly known, occurred in 1964 on the Soviet spacecraft Zond 2. Numerous electric thrustors for attitude and station control were used on U.S. satellites, as shown in table III. An ion thrustor for prime propulsion was applied on the U.S.S.R. space probe Yantar in 1969. Two American test vehicles for ion thrustors, SERT 1 and 2, were launched in 1964 and 1970. Although not completely successful, they definitely proved the proper functioning of ion propulsion systems under space conditions, and they established full confidence in this method of rocket propulsion. The SERT 2 test vehicle with two 1 kW ion engines is shown in figure 5. Design lifetime of SERT 2 was 1 yr. Project cost, including the Atlas/Agena carrier vehicle, amounted to approximately 12 million dollars.

Experience shows that a thrustor designed for about 2.5 to 3 kW power consumption represents an optimum thrustor size. Thrustors of this type can

TABLE II.–*Comparison of Chemical and Electric Rockets With Equal Propulsion Capabilities*

Rocket engine	Thrust, N	Specific impulse, s	Time of propulsion	Mass of engine and power source, kg	Mass of propellant, kg	Total impulse,[a] N-s
Chemical, $H_2 + O_2$, RL 10 (Centaur)	70 000	445	7 min	140	7000	3×10^7
Electric, 16 kW	1	3000	350 days	350	800	3×10^7

[a]Total impulse = thrust × time.

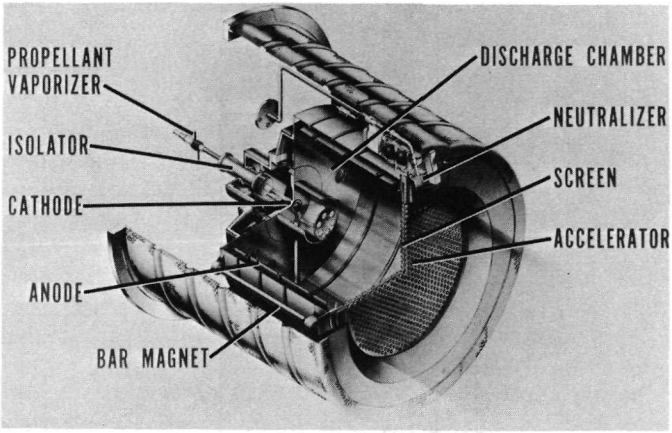

Figure 3.–Cut-away drawing of ion engine (electron bombardment or Kaufman type).

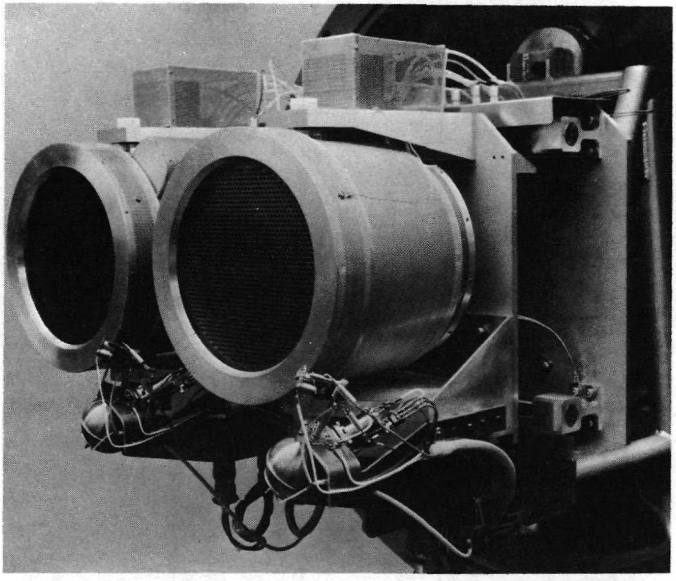

Figure 4.–Cluster of two ion engines (electron bombardment or Kaufman type).

be clustered easily for higher power and thrust levels. A propulsion system with three thrustors, consuming 8 kW of power, would be an adequate system for "easy" planetary missions. More demanding missions could be carried out with vehicles consisting of two or three modules of the 8 kW type. An artist's conception of an electrically propelled spacecraft is depicted in figure 6.

TABLE III.—*Flights Having Electric Thrustors for Spacecraft Control*

Vehicle	Date of launch	Functions of thrustors	Type	Propellant
Zond 2 (U.S.S.R.)	1964	Attitude control	Plasmajet	?
Sert 1	July 1964	Spin	Ion bombardment	Hg
Vela 5	July 1965	Velocity correction	Resistojet	N_2
Vela 6	July 1965	Velocity correction	Resistojet	N_2
Vela 7	April 1967	Velocity and spin	Resistojet	N_2
Vela 8	April 1967	Velocity and spin	Resistojet	N_2
ATS 1	December 1966	Stationkeeping	Resistojet	NH_3
ATS 2	April 1967	Stationkeeping	Resistojet	NH_3
ATS 3	November 1967	Stationkeeping	Resistojet	NH_3
ATS 4	August 1968	Stationkeeping	Ion (contact)	Cs
ATS 5	August 1969	Stationkeeping	Ion (contact)	Cs
YANTAR (U.S.S.R.)	January 1969	Prime propulsion	Ion (bombardment)	N_2, Ar
SERT 2	February 1970	Prime propulsion	Ion (bombardment)	Hg
Various vehicles of the Department of Defense	Classified	Stationkeeping and maneuvers	Ion (contact)	Cs
			Ion (bombardment)	Hg
			Resistojet	NH_3
			Colloid	Glycerol

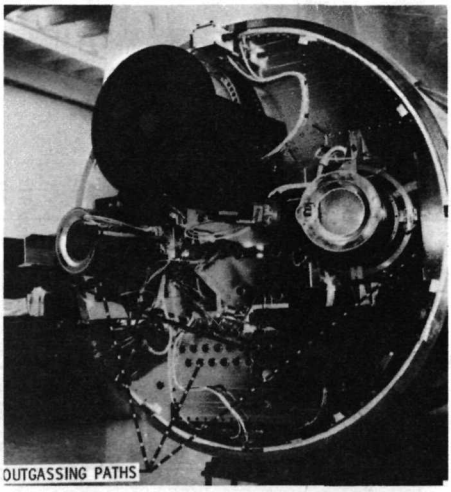

Figure 5.–Rear view of SERT 2 with two electric thrustors.

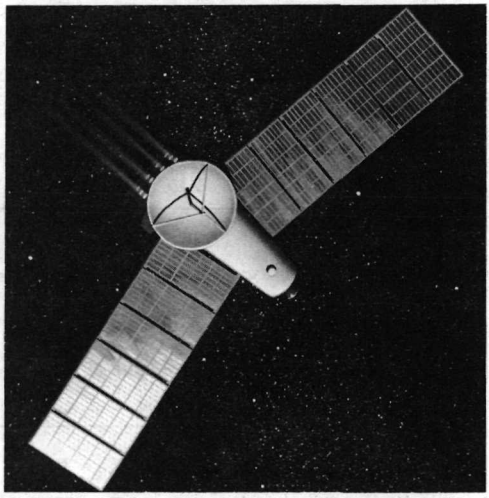

Figure 6.–Solar electric spacecraft on flight to Mars.

Table IV lists a number of desirable flight missions throughout the solar system that could be accomplished with electrically propelled vehicles. The first part contains missions powered with solar electric power; three different vehicle sizes and power levels are envisioned. The second part, containing more demanding missions to the outer planets, is based on a future nuclear electric power source of about 150 kW.

TABLE IV.–*Potential Missions for Electrically Propelled Spacecraft*

Power source	Departure	Arrival	Destination	Electric power, kW
Solar electric	1974	1975	Asteroid flyby (Eros)	8
	1976	1977	Asteroid landing (Eros)	8
	1976	1976	Venus orbiter	16
	1976	1978	Comet (Kopf)	24
	1977	1978	Execliptic	8
	1977	1978	Solar probe (0.1 AU)	16
	1977	1979	Jupiter flyby (or highly elliptic orbiter)	24
	1977	1980	Saturn flyby	24
	1978	1978	Mercury orbiter	16
	1978	1978	Mars orbiter	24
	1978	1979	Asteroid landing	24
	1978	1980	Comet (Encke)	24
	1979	1980	Mars landing	24
	1979	1982	Uranus flyby	24
Nuclear electric	1980	1982	Jupiter orbiter	150
	1980	1982	Comet (d'Arrest)	150
	1981	1984	Saturn orbiter	150
	1981	1985	Neptune orbiter	150
	1982	1986	Comet (Halley)	150
	1982	1986	Uranus orbiter	150
	1982	1987	Pluto orbiter	150

NOTE.–All launch vehicles would be of the Titan class except Eros flyby, which would use the Atlas/Centaur; see p. xxv.

The total masses of the spacecraft listed in table IV, at the beginning of their planetary trajectories, vary between about 500 and 6000 kg. Most of them could be launched also with a space shuttle instead of a Titan. In this case, a chemical kick stage must be provided to accelerate the spacecraft from the shuttle orbit into the planetary transfer trajectory.

The list of potential projects on table IV starts with an asteroid flyby. Asteroid Eros has a fairly eccentric trajectory; every 2 yr it approaches the Sun with a perigee of only 1.3 or 1.2 AU. In 1977, the Earth-Eros distance will be less than one-third the shortest Earth-Mars distance.

The proposed asteroid flyby mission in 1975 would represent a relatively easy mission with modest velocity requirements and with a guidance system that would have to guide the spacecraft only to a distance of about 100 km from the asteroid for photography, temperature measurements, and some other unsophisticated observations. Most of the instruments for this flyby mission would be available from previous projects, such as Surveyor, Mariner, and Lunar Orbiter. The spacecraft could be launched with an Atlas/Centaur. Although this flight would not yet provide all the desired information on Eros, it would obtain important data on size, shape, mass, rotation, surface features,

and other properties of the asteroid that must be known for a successful follow-on project, the landing and data-return mission to Eros. Equally important would be another objective met by this simple flyby mission, a full-scale test flight of the complete electric propulsion system. From the standpoint of the spacecraft engineer, such a test flight would be very desirable before a spacecraft as complex and expensive as an asteroid landing and sample-return vehicle is committed for flight. Evidently, a project of this kind would not only be a highly valuable preparatory step for an asteroid lander mission but also a most important achievement with respect to the evolution of electric spacecraft for planetary exploration. Although data from the flyby mission would become available not more than a year before the launching of the lander mission, these data would be valuable for instrument settings and other details of the lander mission and as a confirmation of design data chosen for the lander. If the flyby should reveal severe deviations of the asteroid features from anticipated properties, the launching of the lander would have to be postponed.

None of the projects listed in table IV has attained the status of an approved project; all of them have only been the subjects of very preliminary studies. However, the list of potential projects may indicate the great promise that electric propulsion holds for a broad program of planetary exploration that could begin in the midseventies and would provide a rich harvest of knowledge of our entire solar system.

REFERENCE

Irving, I. H., and Blum, E. K. 1959, Comparative Performance of Ballistic and Low Thrust Vehicles for Flight to Mars. Vistas Astronaut. **2**, 191.

DISCUSSION

WETHERILL: I think it would be a mistake to overemphasize differences in the merits of cometary and asteroidal missions. There are considerable savings in a program of missions using similar spacecraft; the cost per launch is much less for multiple missions than for single missions. These savings could be realized by development of a multipurpose solar electric spacecraft suitable for both asteroid and comet missions. From the point of view of scientific priorities, I think as much emphasis should therefore be placed on the sum of the value of these two types of missions as on the difference in their value.

I understand that the NASA Office of Advanced Research and Technology (OART) is requesting funds for a solar electric interplanetary mission in the budget currently before Congress, and I wonder what plans exist for obtaining scientific advice in planning these missions.

SOBERMAN: In the past, mission definition has taken place with little input from the scientific community. At the time of the "Announcement of Flight Opportunity," the proposing scientists are faced with a vehicle for which at least a preliminary design exists. This "preliminary design" in practice is difficult, if not impossible, to modify. Even in the case of the Grand Tour missions, the so-called scientific definition phase must contend with the constraints of the TOPS vehicle.

I propose that NASA set up a definition team of scientists to work with the mission planners at the earliest stages so that the result would be system-optimized to perform the science.

DWORNIK: At NASA Headquarters, the Office of Space Science and Applications (OSSA) in fact does conduct an early mission definition phase that involves the scientific community. Scientists were invited to participate in the early planning phase of the Viking and the Mariner-Venus '73 and Mariner-Mercury '73 missions in order that spacecraft and mission constraints would not freeze out certain types of experiments. Specifically, the Mariner 1973 program actually altered early spacecraft and mission constraints to accommodate experiments.

BARBER: In the final recommendations, OSSA requires sufficient information for mission selection. Also at NASA Headquarters, OART is trying to provide some of this information for evaluation by OSSA. The initial thrust of our studies is to decide the technology feasibility of such small-body missions. We at OART are now at the point where we have a fairly systematic approach to the technology problem. The remainder of the work is to evaluate the scientific impact of the solar electric trajectory and spacecraft. The question as to what should be the science is not being considered at this time because the investigation is primarily technology oriented. When the actual mission is chosen, one would expect to turn to the scientist. At that time, the primary responsibility will transfer from OART to OSSA.

Page intentionally left blank

ASTEROID RENDEZVOUS MISSIONS

D. F. BENDER AND R. D. BOURKE
Jet Propulsion Laboratory

The earliest flights to concentrate solely on the nature of particular asteroids will probably be of the simple flyby or rendezvous type. That is, data will be obtained by close investigation of these bodies without actually coming in contact with their surface. The technology of flyby missions to bodies at planetary distances is well established; there have been five successful Mariners to date and more flights are scheduled. Unfortunately, ballistic flyby missions suffer from the fact that the spacecraft is near the body of interest for a short period of time (relative velocities at asteroid encounters are 5 to 12 km/s). This problem is acute because spatial resolution of the onboard instruments must be very high, and typical flyby velocities will preclude detailed observations.

These problems lead to consideration of *rendezvous* missions wherein the spacecraft is placed into the same heliocentric orbit as the asteroid and therefore remains close to it over a long period of time. This will allow long-term observations of the body over a range of aspects, distances, and phase angles. Probably most of the surface would be available for observation by this technique.

There are two principal means of achieving rendezvous and these are classified as "ballistic" (or "impulsive" or "high thrust") and "low thrust." In the first method, the spacecraft is given substantial velocity changes at various points in its flightpath and travels ballistically in between them. These velocity changes occur upon leaving Earth, upon arriving at the asteroid, and possibly at one point in between. They are imparted by a conventional rocket engine and occur over a very short time compared with the total flight, hence the term "impulsive." The other method is to continuously thrust the vehicle over most of its flight with a high-specific-impulse, low-acceleration engine. The current concept for doing this uses solar electric propulsion wherein solar power is converted to electricity that drives electron-bombardment mercury-ion thrustors.[1] This requires very large lightweight solar arrays. These engines operate for nearly the whole flight and are directed in such a way as to continuously and optimally change the orbit of the spacecraft until it coincides with the orbit of the asteroid. One concept for a solar electrically powered spacecraft suitable for an asteroid rendezvous is shown in figure 1. The technology of

[1]See p. 491.

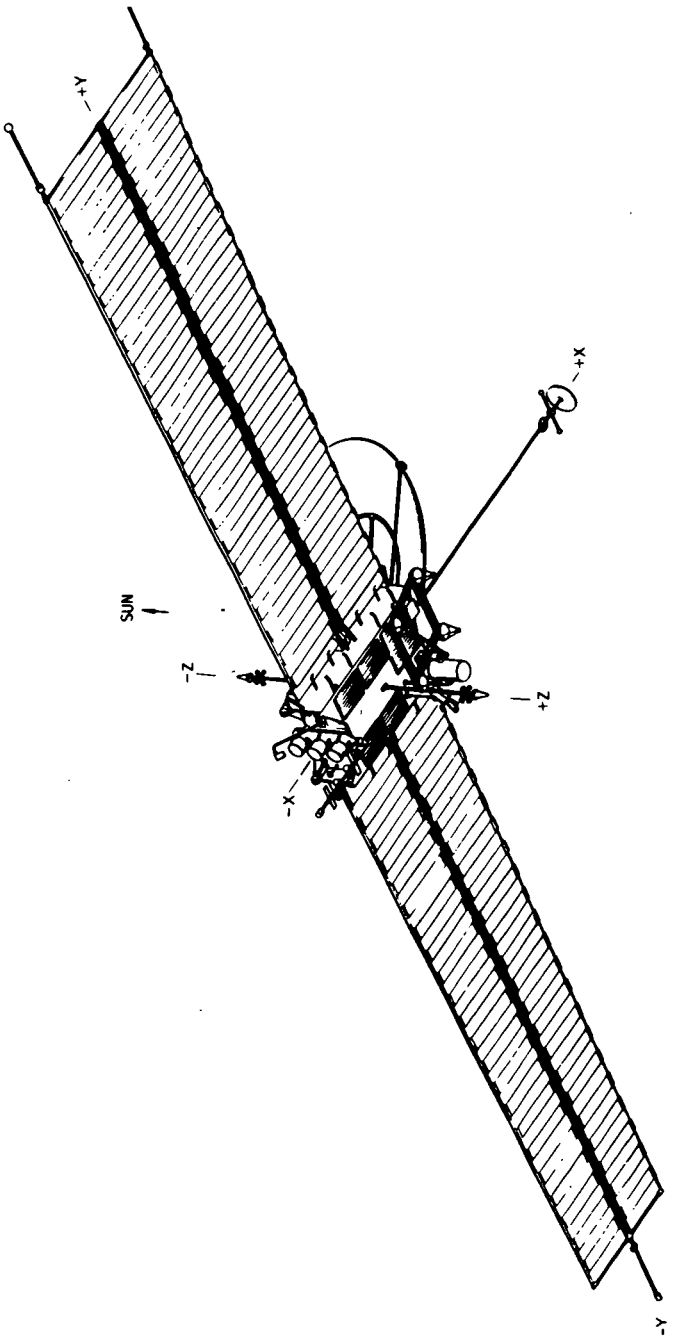

Figure 1.–Typical solar electric spacecraft. Gross power level = 6.4 kW; spacecraft gross mass = 580 kg.

these vehicles is reviewed by Bartz and Horsewood (1969). This review includes an extensive bibliography.

The remainder of this paper deals with the rendezvous by means of a low-thrust, solar electrically propelled vehicle because (1) this approach is generally better from a payload and flight-time basis compared to the high-thrust method and (2) it has a large degree of flexibility and can be applied to a variety of missions. It should be emphasized that here we are concentrating on rendezvous missions only, which are necessary precursors to the more complex landing or sample-return missions. The remainder of the paper deals with our results to date.

ASTEROID SELECTION

In choosing an asteroid for a mission target, one would first assume that size would be the major criterion and pick the largest one because it would present the largest surface for study. Thus a mission to Ceres would be studied at the outset as well as missions to the other asteroids if they are significantly less demanding in terms of energy and/or flight time. Such other possible targets may traverse the main asteroid belt near Ceres but have smaller inclinations, or else they may have smaller orbits passing inside that of Mars. In addition to Ceres,, we have considered here missions to three bright asteroids with inclinations successively smaller than Ceres and to one with a significantly smaller orbit than Ceres as illustrated by the orbital elements of table I. Pallas and Juno were not considered because of their high inclinations of 34°.8 and 13°.0, respectively.

To estimate flight times for transfers to be accomplished in less than one revolution about the Sun, we indicate the value of the trip time T_H for a Hohmann transfer from Earth to a circular orbit at the radius of the semimajor axis. This serves as a guide because the Hohmann transfer, which uses a heliocentric central angle of 180°, is an optimal impulsive transfer between two circular orbits. It generally occurs, however, that optimal low-thrust rendezvous trajectories utilize central angles considerably greater than 180° so that flight times can be expected to be 20 to 50 percent greater than T_H.

TABLE I.–*Orbital Properties of Selected Asteroids*

Asteroid no.	Name	i	a, AU	e	T_H, days	Synodic period, yr
1	Ceres	10°.6	2.77	0.076	473	1.28
4	Vesta	7.1	2.36	.089	398	1.40
10	Hygiea	3.8	3.15	.100	546	1.22
20	Massalia	.7	2.41	.143	407	1.37
433	Eros	10.8	1.46	.223	249	2.29

T_H = time for Hohmann transfer from r = 1 AU to $r = a$.

Fortunately, for solar electric propulsion, the choice of flight time is not particularly critical for determining mission feasibility.

RESULTS

Launch Date Selection

Ranges of possible launch dates to be used as initial estimates of detailed searches may be found using a simple procedure that is described below. We first replace the orbits of Earth and the target asteroid by circular coplanar orbits, and we choose the time of flight and central angle to be traversed. The procedure is illustrated in figure 2, which shows launch date possibilities for Vesta from 1975 to 1977. We plot the mean anomaly of Vesta M_2 versus the mean anomaly of Earth M_1 as it actually occurs for the launch years we wish to consider. That is

$$M_2 = \frac{n_2}{n_1} M_1 + \text{const} \tag{1}$$

Using the time of flight t_f and the central angle $\Delta\theta$ to be traversed on the transfer orbit, we plot the mean anomaly on the target orbit M_2 at the time of departure versus the mean anomaly on Earth orbit M_1 at the time of departure. The relationship to be plotted is obtained by expressing the longitude of the arrival point in terms of the motion of the spacecraft along the transfer orbit and the motion of the target. Thus we obtain

$$M_1 + \lambda_{p_1} + \Delta\theta = M_2 + \lambda_{p_2} + n_2 t_f \tag{2}$$

or

$$M_2 = M_1 + \lambda_{p_1} - \lambda_{p_2} + \Delta\theta - n_2 t_f \tag{3}$$

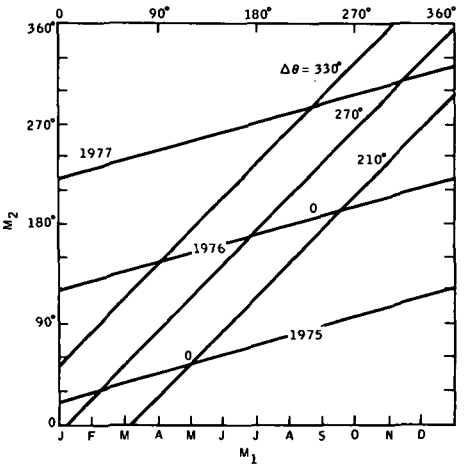

Figure 2.–Vesta launch possibilities (1975-77), 500 day flights.

where λ_p is the longitude of perihelion and n is the mean orbital rate. Intersections of lines for equations (1) and (3) indicate values of M_1 for which launches meeting the requirements chosen for t_f and $\Delta\theta$ selected are possible. The corresponding calendar date can be read from the abscissa.

We may choose a different value for $\Delta\theta$ and plot another curve of M_2 versus M_1 thus obtaining a range of launch dates for the chosen range of central angles. Having found a reasonable range of launch dates, we make a search over that range by means of a computer program that determines payloads and accurate trajectory characteristics for the particular type of mission under consideration. The optimum launch dates found for the solar electric-propulsion missions are indicated by an O.

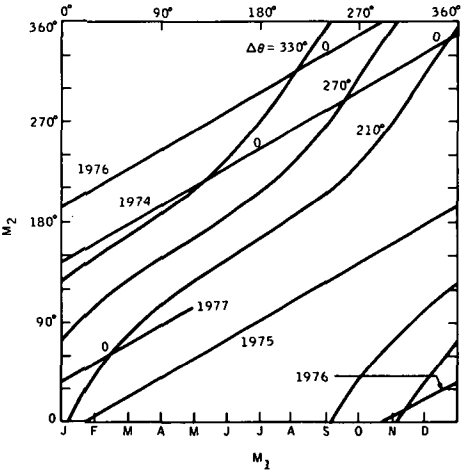

Figure 3.–Eros launch possibilities (1974-77), 360 day flights.

Equations (2) and (3) can be modified to be more representative of the true situation by including the effect of the eccentricities of the two orbits. True anomaly intervals are used to obtain the longitude at arrival and thus M_2 versus M_1. The relation is now a curve that oscillates about the straight line and must be computed for each case of $\Delta\theta$ and t_f desired. Such a graph is shown for Eros for 1974 to 1977 in figure 3.

Mission Data

For each asteroid chosen, the low-thrust program CHEBYTOP (Han, Johnson, and Itzen, 1969) was used in a launch-day scan mode to locate the departure data that resulted in greatest payload for a given flight time. The launch vehicle chosen was the Titan IIID/Centaur, except for Eros in which the Atlas/Centaur was used. The remaining spacecraft and launch parameters

required as input for Ceres, Vesta, Massalia, and Hygiea rendezvous are as follows:

(1) Hyperbolic departure velocity at Earth, v_{hl} = 5 km/s
(2) Total mass injected (at v_{hl} = 5 km/s), 3450 kg
(3) Thrustor specific impulse, I_{sp} = 3500 s (exhaust velocity c = 34.3 km/s)
(4) Tankage factor, 6 percent (propellant and tank mass = 1.06 X mass of propellant needed)
(5) Engine efficiency, 0.667
(6) Propulsion system specific mass, 30 kg/kW

The power level at 1 AU P_0 is calculated by the program, but the payload results quoted have been scaled to correspond to a power level of 16 kW.

The optimum hyperbolic escape velocity depends on the size of the target orbit, and for Eros it is very close to 2 km/s. With a Titan IIID/Centaur launch vehicle, payloads for Eros missions would be more than 2000 kg, which is considered to be more than necessary for preliminary missions. For this reason, the smaller Atlas/Centaur launch vehicle, which results in a total injected mass of 1000 kg at v_{hl} = 2 km/s, was used. Otherwise the values listed pertain also to Eros missions.

Mission data results are presented in table II. Here flight time, payload, and encounter geometry are shown for at least two launch dates for each asteroid in the period from 1974 to 1977. It is interesting to note that inclination does

TABLE II.–*Solar Electric Asteroid Rendezvous Missions (Launch Vehicle Titan IIID/Centaur)*

Asteroid	Estimated window	Launch date	Flight time, days	Payload, kg	Encounter conditions		
					Solar distance, AU	Earth-Sun-asteroid angle	Earth asteroid distance, AU
Ceres	7/75-9/75	7/20/75	600	588	2.58	11°	1.61
	10/76-12/76	11/21/76	600	643	2.92	6	1.91
Vesta	2/75-5/75	4/22/75	560	795	2.55	30	1.76
	6/76-9/76	8/11/76	560	476	2.18	68	2.03
Hygiea	7/75-9/75	9/4/75	650	204	2.94	80	2.94
	10/76-12/76	11/6/76	650	450	2.89	50	2.37
Massalia	2/74-4/74	2/6/74	500	358	2.70	40	2.04
	5/75-7/75	5/15/75	500	553	2.10	69	1.98
Eros	4/74-2/75	6/18/74	360	[a]580	1.47	36	.88
		12/7/74	360	[a]534	1.78	129	2.52
	8/76-2/77	2/14/77	360	[b]485	1.55	140	2.40

[a]Atlas/Centaur launch vehicle (fully optimized trajectory data) ($P_0 \leq 10$ kW).
[b]Atlas/Centaur launch vehicle (P_0 = 10 kW).

not have a significant effect on payload over the range selected. Rather the payloads fluctuate a great deal because of the varying relationships between relative orbit nodes and perihelion from one launch opportunity to the next. It is clear that missions to any of these five asteroids (and of course many others) are possible with solar electrically propelled spacecraft launched by a Titan IIID/Centaur or an Atlas/Centaur and that a substantial scientific payload can be delivered.

Eros Trajectory

To determine requirements on the design of an asteroid rendezvous spacecraft, some details of a flight to Eros have been generated. The selected launch date[2] is in December 1974 and the launch vehicle postulated is the Atlas/Centaur. The spacecraft is equipped with the solar panels developing 10 kW at 1 AU and, except for a 10 day coast period in the middle of the flight, the engines thrust continuously for the 360 day trip to Eros.

This combination of launch vehicle, power, and flight time allow a net spacecraft mass at the target in excess of 500 kg. This includes 50 to 100 kg of science instruments. A breakdown of the spacecraft mass at launch is given in table III.

Figure 4 shows the relative positions of Earth, the spacecraft, and Eros projected into the ecliptic for various dates along the trajectory. After May 1975, the spacecraft and Eros are in the same position to the scale of this drawing, but a good deal of their separation is normal to the ecliptic and hence does not show in this projection.

The most vital part of the flight from the standpoint of scientific return begins when the spacecraft approaches the asteroid. In this phase there are a number of problem areas, two of which are discussed below.

To begin with, the position of the asteroid is not sufficiently well known for spacecraft navigation purposes. We expect an a priori error on the order of a few thousand kilometers. Because this is much larger than the intended closest approach distance to Eros (which is on the order of the dimensions of Eros

TABLE III.—*Spacecraft Mass Budget*

Component	Mass, kg
Power and propulsion system (10 kW)	300
Mercury propellant	150
Net spacecraft (including scientific payload)	500
Gross spacecraft mass at launch	950

[2]There are no firm NASA plans to launch an Eros mission at this date; it is used for example purposes only.

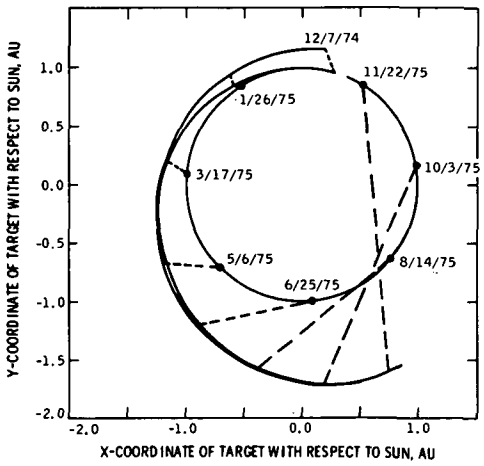

Figure 4.–Eros rendezvous ecliptic plane projection. Thrust is fixed at 90°, P_0 = 10 kW, I_{sp} = 3500, and t_f = 360 days. Launch date is December 7, 1974. The launch vehicle is the Atlas/Centaur.

itself), the error must be corrected. Before a flight, the ephemeris of the target would be improved to the largest extent possible by ground-based observations.[3] Further improvement can be made by correcting the ephemeris of the target by using optical observations taken from the spacecraft while in flight. This procedure was tested on Mariners 6 and 7 and it is scheduled to be operationally demonstrated on the Mariner-Mars 1971 orbiter arriving late this year. It is a vitally necessary component of the Outer Planet Grand Tour Flight.

Using typical optical system performance, it should be possible to begin resolving Eros when the spacecraft is 200 000 km away although it may be visible as a bright object well before this. The position of the asteroid against the star background, when combined with Earth-based radio-tracking data from the spacecraft, provides sufficient information to determine the spacecraft's position relative to the asteroid. The information can then be used to reprogram the thrust history for the remainder of the flight, thereby correcting any errors.

Another problem that arises is due to the fact that the thrust beam must be directed nearly toward the asteroid near the end of the flight. This can be seen from figure 5, which shows the asteroid-spacecraft-thrust beam angle as a function of date throughout the mission. Note that the angle goes to zero as the spacecraft approaches the asteroid. (This phenomenon is characteristic of any rendezvous trajectory because the spacecraft must slow down with respect to the target on the approach.) Thus observations from the spacecraft during

[3]See p. 639.

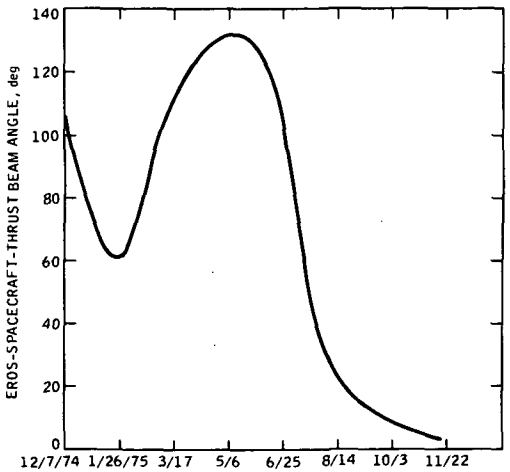

Figure 5.–Eros rendezvous approach conditions.

this phase would have to be made through the exhaust. Two possible solutions to this problem are (1) to momentarily cease thrusting on the approach and reorient the spacecraft to allow observations or (2) to initially rendezvous with a point some distance from the asteroid, take the appropriate observations, then slowly close in on it. These and other methods are currently under study.

ACKNOWLEDGMENTS

The authors are indebted to many members of the staff of the Jet Propulsion Laboratory for their contributions to the work on which this article is based. In particular, we would like to thank J. M. Driver, C. G. Sauer, and Dr. C. L. Yen for their assistance in generating the mission analysis data. This paper presents the results of one phase of research carried out at the Jet Propulsion Laboratory, California Institute of Technology, under contract NAS 7-100, sponsored by NASA.

REFERENCES

Bartz, D. R., and Horsewood, J. L. 1969, Characteristics, Capabilities and Costs of Solar Electric Spacecraft for Planetary Missions. J. Spacecr. Rockets 6(12), 1379-1390.

Han, D. W., Johnson, F. I., and Itzen, B. F. 1969, Chebychev Trajectory Optimization Program. D2-121308-1 Final Rept. (NAS2-5185), The Boeing Co.

Page intentionally left blank

SAMPLE-RETURN MISSIONS TO THE ASTEROID EROS

ALFRED C. MASCY
NASA Ames Research Center
and
JOHN NIEHOFF
IIT Research Institute

MISSION SELECTION

Of the many asteroids that are cataloged, selection of a target planetoid was narrowed to the Mars-crossing asteroids. The main belt and Trojan asteroids are much farther away and require longer voyage times and propulsive energy to accomplish sample returns. Within the Mars-crossing group, those asteroids were surveyed that have orbits inclined less than 15°, perihelia within 0.2 AU of Earth's orbit (and therefore require less propulsive energy), and diameters greater than 1 km (to assist terminal observation and rendezvous). Eros was chosen as representative of this class.

The mission consists of the following phases: (1) Earth departure; (2) trans-Eros trajectory; (3) Eros approach, rendezvous, site selection, topographical coverage, and docking; (4) surface operations including sample acquisition; (5) Eros departure; (6) trans-Earth trajectory; (7) Earth approach, capsule separation, and orbit capture maneuver; and (8) in-orbit quarantine until deboost command or orbit retrieval.

CANDIDATE EXPERIMENTS

A number of scientific instruments were considered in formulating a baseline Eros rendezvous/sample-return mission. These candidate instruments are listed in table I along with related science measurables, the mission phases during which they would operate, and an indication of what their mass and power requirements are expected to be. The instruments are divided into two categories: (1) those instruments *essential* for sample return and (2) those *desirable* for a viable rendezvous and landing science mission. Because not all instruments would operate simultaneously, the total power requirement is somewhat less than the accumulated one. By far the most important phases of the mission for instrument operation are stationkeeping and landing. Because the total science payload is only 90 kg, it was assumed that all instruments presented in table I would be included in the science payload of the baseline

TABLE I.—*Candidate Experiments for Eros Rendezvous/Sample-Return Missions*

Generic instrument description	Science measurables	Mission phase of operation						Mass, kg	Power, W
		Outbound transfer	Rendez-vous	Station-keeping	Landing	Surface activity	Return transfer		
Essential instrument package:									
Television	Asteroid shape; surface topography and appearance		X	X		X		18	25
Radar altimeter	Mass determination			X	X			12	10
Scoop/digger	Surface sample collection					X		9	5
Drill (3 m penetration)	Core sample collection					X		14	[a]300
Subtotal								53	40
Additional desirable instruments:									
Micrometeorite detectors	Velocity and momentum of particles	X		X		X	X	5	1
Thermal gradient detector	Thermal balance					X		5	11
Photometer/ polarimeter	Surface albedo; atmospheric halo			X		X		4	4
Active seismometer	Internal structure					X		7	2
IR radiometer	Surface temperature			X				2	5
Magnetometer	Remnant magnetic field	X		X		X	X	2	3
Surface material analyzer	Surface composition					X		12	15
Subtotal								37	26
Total								90	66

[a]Battery operated.

mission. These instruments are only suggested as typical of what a rendezvous/sample-return payload might be and are not a specifically recommended set of experiments. A description of another payload complement is found in the Meissinger and Greenstadt paper.[1] A mass of 150 kg, including the 90 kg of science and support equipment, is assigned to the trans-Eros and asteroid surface operations. This mass is jettisoned upon departure from Eros.

RENDEZVOUS OPERATIONS

It is assumed that a number of stationkeeping maneuvers would be required following rendezvous with Eros before landing (or docking) on the asteroid. These maneuvers would achieve the necessary reconnaissance needed for landing site selection (preferably on one of the poles) and most importantly provide ample time for the remote sensing measurements indicated in table I at various locations around the asteroid.

The recommended sequence of maneuvers is illustrated in figure 1. They start at point 1, which is 1000 km from the asteroid in the solar direction. This position seems most compatible with rendezvous because the asteroid should be well lighted in a dark sky for optical tracking during final rendezvous. The sequence of maneuvers allows the spacecraft to approach the asteroid to within 250 km from three directions: Sun side, terminator, and dark side. The first two approaches should permit an accurate determination of the polar direction[2] (for landing) and provide good surface appearance data under limiting illumination conditions. The third approach would permit a search

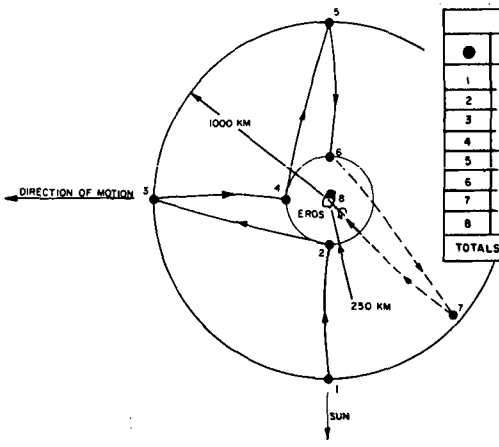

STATION-KEEPING SEQUENCE

●	OBJECTIVE	ΔV, M/S	TIME, DAYS
1		0.89	
2	OBSERVATION	2.52	10
3	TRANSLATION	3.19	5
4	OBSERVATION	2.53	10
5	TRANSLATION	3.23	5
6	OBSERVATION	2.32	10
7	TRANSLATION	3.85	5
8	DOCKING	1.16	10
TOTALS		19.69	55

Figure 1.–Stationkeeping profile for 1977 Eros sample-return mission. Dashed line indicates out-of-plane motion.

[1]See p. 543.

[2]*Editorial note:* By 1975 we should know the orientation of the rotation axis to within a few degrees; see p. 133.

from the dark side for a dust cloud or atmospheric halo around Eros, using photometers. The final approach is recommended along the rotation axis to landing. The entire sequence would take about 55 days as shown in the figure. Remote teleoperator landing of a spacecraft is described by Meissinger and Greenstadt;[3] however, because of the large communication distance, response times are on the order of a half hour.

The stationkeeping and landing operations were regarded as essentially the same for both the ballistic and low-thrust flight modes. The weight breakdowns for the baseline mission assume that the entire spacecraft (less outbound propulsion) is docked with the asteroid during sample collection and surface experimentation. A budget of 75 m/s has been allowed for all stationkeeping, docking, and separation maneuvers at Eros. A conservative estimate of 350 kg is assigned to the landing mechanism and maneuver/docking propulsion inert mass. This mass is jettisoned upon departure from Eros.

PROPULSIVE ENERGY REQUIREMENTS

The analysis of round-trip interplanetary space missions generally requires the survey of compatible outbound and return trajectories. Whereas one-way orbiter or flyby missions may utilize near-optimum outbound trajectories, round-trip missions compromise the performance on both outbound and return legs so that the overall mission energy requirements are minimized. An expedient method of examining large quantities of round-trip trajectory

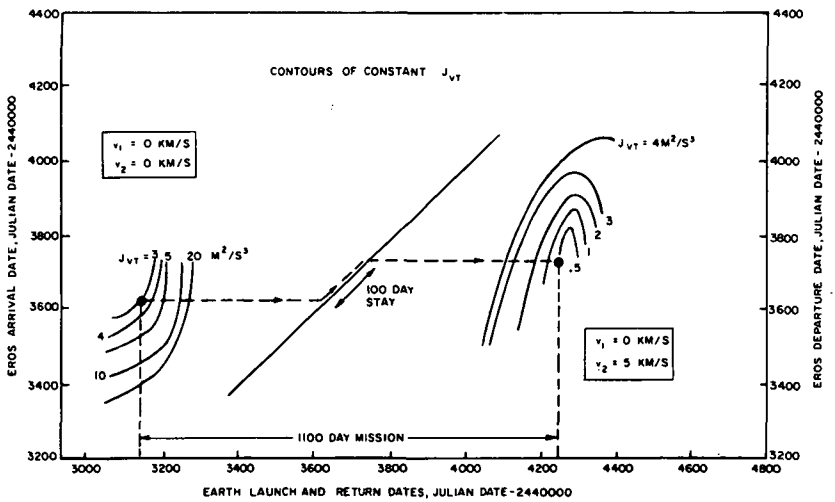

Figure 2.–Solar electric contour map for 1977 Eros sample-return mission. v_1 is the hyperbolic excess velocity at Earth departure, v_2 is the hyperbolic excess velocity at Eros arrival, and J_{VT} is a measure of electric-propulsion energy requirements.

[3]See p. 552.

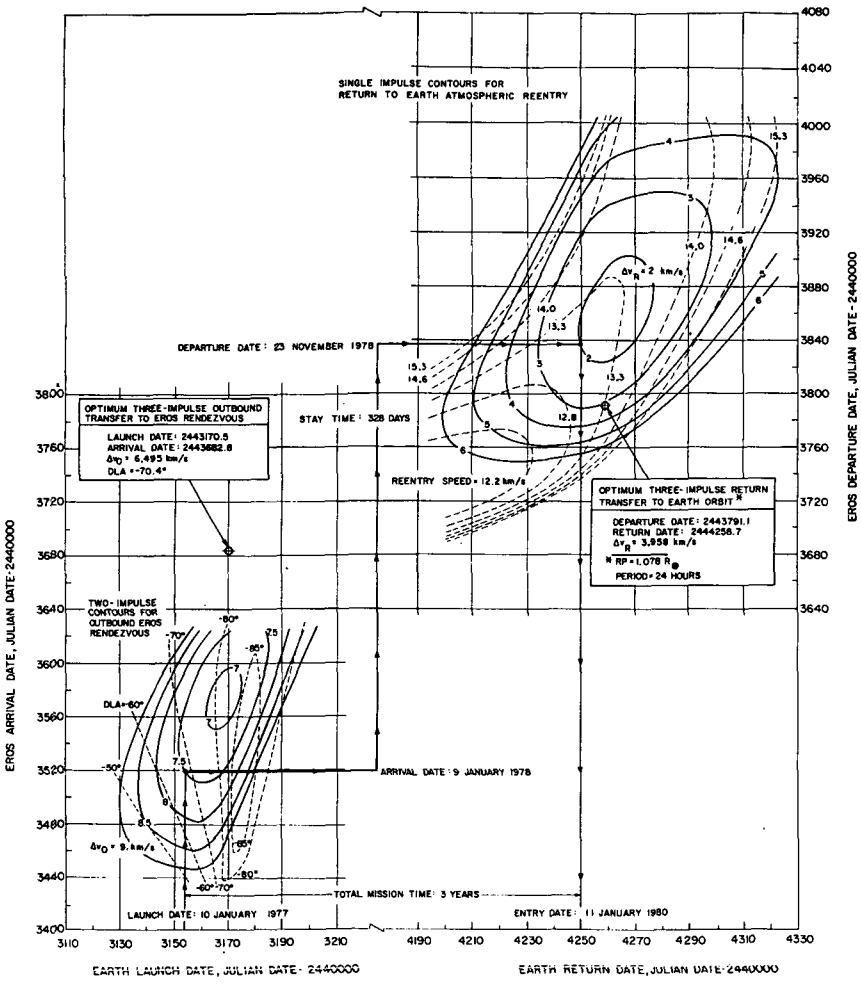

Figure 3.–Ballistic impulse contour map for 1977 Eros sample-return mission.

characteristics is shown in figures 2 and 3 for the 1977 opportunity to Eros as accomplished by an electric-propulsion flight mode and a chemical-propulsion flight mode, respectively.

ELECTRIC-PROPULSION FLIGHT MODE

A measure of the propulsive energy requirements for electrical rocket systems that employ finite-thrust trajectories is given by the time-integrated effect of the continually applied low acceleration. In figure 2, this energy measure has the symbol J with units of square meter per cubic second. The higher the J, the more difficult the mission. Mascy, Dugan, and Pitts (1968)

have shown that the systematic mapping of this energy parameter provides a convenient technique for determining the best launch and arrival dates and the effect of varying trip times and stay times. For both figures 2 and 3, the launch and return dates at Earth are given along the abscissa and the arrival and departure dates at Eros are given along the ordinate. An example of an 1100 day mission is shown in figure 2 departing from Earth on Julian date 2443150, arriving at Eros 2443625, staying 100 days, departing from Eros 2443725, and returning to Earth on 2444250. In a similar manner, one can fashion missions of varying outbound or return-leg trip times, launch dates, stay times, etc.

The electric-propulsion system assumed in this report utilizes solar photovoltaic cells to convert the Sun's energy into electrical energy for acceleration of ionized mercury propellant. A power level of 10 kW and a thrustor specific impulse of 3000 s are used in the analysis. Similar to the systems and technology described in the TRW, Inc., report, the overall electric-propulsion module has a mass of 300 kg. An additional mass of approximately 400 kg has been assigned to the interplanetary bus, which comprises the engineering subsystems such as communications and data handling, central computer and mission sequencer, thermal and attitude control, and support structures. The launch vehicle used to inject the solar electrically propelled interplanetary vehicle onto a trans-Eros trajectory is the Titan IIID/Burner II.

CHEMICAL-PROPULSION FLIGHT MODE

In figure 3 is presented the contours of impulsive velocity increment, which is a measure of the propulsive energy requirements for chemical rocket systems that employ ballistic trajectories. This energy measure has the symbol Δv with the units kilometers per second. The higher the Δv, the more difficult the mission. The outbound transfer contours in the lower left give the total impulse for two maneuvers: (1) impulsive escape from a 185 km (100 n. mi.) parking orbit at Earth and (2) impulsive rendezvous at Eros. In the background, dotted contours of declination of the launch asymptote (DLA) are given. Notice that the region of minimum total outbound impulse, $\Delta v_O < 7.5$ km/s, lies over absolute values of DLA that are greater than $-70°$. This implies a serious problem for launches from the Eastern Test Range because range safety constraints require that DLA $< 36°$. Return transfer contours of impulsive departure velocity at Eros are presented in the upper right of figure 3. Dotted curves of Earth reentry speed of the return-sample capsule are shown in the background. The region of minimum departure impulse, $\Delta v_R < 2$ km/s, lies over Earth reentry speeds of less than 13.7 km/s (45 000 ft/s), which should not pose a reentry technology problem. A sample mission that requires a total trip time of 3 yr is laid out with the arrowed line. The stay time at Eros would be almost 1 yr, 328 days. To use outbound and return transfers that are reasonably close to minimum required energies, it can

be observed from the figure that one is forced to accept a total trip time on the order of 3 yr.

In addition to the direct two-impulse transfers discussed thus far for ballistic systems, optimum three-impulse trajectories were also investigated for the following reasons: (1) a potential for lower total impulse, due to the 11° inclination of Eros' orbit to the ecliptic; (2) the possibility of improving the launch problem due to large DLA values; and (3) the inclusion of Earth capture-orbit recovery, rather than direct reentry, as a more cautious mission profile in view of back-contamination uncertainty. Optimum three-impulse outbound and return (to Earth orbit) transfer points are included in figure 3. The total outbound impulse Δv_O is indeed less than required by the minimum two-impulse transfer, but a DLA of −70°.4 does not solve the launch problem. The three-impulse return transfer to Earth orbit requires a Δv_R of less than 4 km/s, which, although difficult, is not impossible to achieve with chemical propulsion.

Table II summarizes the transfer characteristics for the two most promising ballistic mission profiles for the launch opportunities of 1974, 1977, and 1979. Both profiles utilize three-impulse outbound transfers to Eros rendezvous. The first profile uses a minimum single-impulse return trajectory to Earth reentry, whereas the second profile requires a three-impulse return transfer to Earth orbit. Note that, for the multi-impulse return, the arrival impulse provides a 12 hr Earth orbit that is more practical for subsequent recovery than the 24 hr orbit suggested in figure 3. Only the 12 hr recovery orbit is considered in the remainder of this paper. The results presented in table II are quite variant. The best (lowest total impulse) outbound transfer occurs in 1977. The best launch conditions occur in 1974 when DLA = −49°.1. The best return transfers occur in 1979. In 1974, the best single-impulse return trajectory to Earth reentry is worse than the three-impulse transfer ending in Earth orbit. The stay times are variable, ranging from 88 to 378 days depending upon the opportunity and return transfers selected. The one parameter that does not vary much is the total trip time, which is always very nearly 3 yr. This was observed earlier and apparently is quite stable regardless of launch opportunity or mission profile.

The launch vehicle used to inject the ballistic chemically propelled interplanetary vehicle into a trans-Eros trajectory is the Titan IIID(7)/Centaur. For the ballistic flight mode, all major impulsive velocity increments, including a 200 m/s guidance requirement, are provided by a space-storable chemical-propulsion system that has an assumed specific impulse of 385 s. An interplanetary bus has been assumed for the chemical flight mode that has a mass of 250 kg and comprises the engineering subsystems.

Upon return to Earth, both the electric- and chemical-propulsion flight modes assume a small solid rocket engine to provide the required velocity increment to place the return capsule (containing the sample) into orbit. Characteristics of the final orbit are: 500 km periapsis altitude, 40 000 km apoapsis altitude, and 12 hr period.

TABLE II.—*Ballistic Transfer Characteristics for Eros Sample-Return Missions*

Parameter	1974			1977			1979		
	3-impulse outbound	1-impulse return	3-impulse return	3-impulse outbound	1-impulse return	3-impulse return	3-impulse outbound	1-impulse return	3-impulse return
Stay time, days	–	309.5	310.6	–	190.2	88.3	–	349.9	378.4
Launch date, Julian date 2440000	2435.2	3094.0	3095.1	3170.5	3843.0	3771.1	3905.0	4688.0	4716.5
Launch impulse,[a] km/s	4.677	6.213	2.394	4.655	1.710	1.105	4.295	0.999	1.166
Launch DLA, deg	-49.1	–	–	-70.4	–	–	-81.3	–	–
Midcourse date, Julian date 2440000	2678.1	–	3298.3	3417.2	–	4029.9	4082.7	–	–
Midcourse impulse, km/s	0.299	–	1.079	1.030	–	0.987	0.984	–	–
Arrival date, Julian date 2440000	2784.5	3352.8	3532.6	3682.8	4260.2	4259.2	4338.1	4993.8	4991.7
Arrival impulse,[b] km/s	1.763	–	1.759	0.810	–	2.120	2.290	–	2.402
Reentry speed, km/s (ft/s)	–	14.143 (46 370)	–	–	13.348 (43 760)	–	–	13.203 (43 320)	–
Total impulse, km/s	6.738	6.213	4.231	6.495	1.710	4.212	7.569	0.999	3.568
Transfer time, days	349.3	258.8	437.5	512.3	417.2	488.1	433.1	305.8	275.2
Total trip time, days	–	917.6	1097.4	–	1089.7	1088.7	–	1088.8	1086.7

[a]Launch impulse at Earth from 185 km (100 n. mi.) circular parking orbit.

[b]Arrival impulse at Earth (when applicable) for capture into 12 hr orbit, $R_p = 1.078R_\oplus$, $e = 0.7419$. R_p is the radius of periapsis and $R_\oplus$ is the radius of Earth (6375 km).

MISSION RESULTS

Effect of Trip Time

With the assumptions made earlier, round-trip missions of various overall times were investigated for an Earth launch opportunity occurring during 1977. The sensitivity to trip time of capsule mass returned to Earth orbit is shown in figure 4 for the solar electric flight mode. There is a strong effect of overall time on the Eros round-trip mission with the maximum returned mass of 260 kg obtained for a time of 1100 days or approximately 3 yr. Capsule mass decreases very rapidly for trip times much shorter or longer than the optimum. The same characteristic has been found for the chemical flight mode.

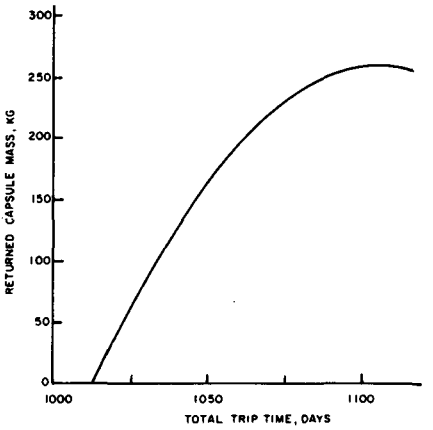

Figure 4.–Trip-time effect on returned capsule mass. Solar electric flight mode; Titan IIID/Burner II; 1977 launch opportunity; stay time = 50 days; Earth return orbit = 500 X 40 000 km.

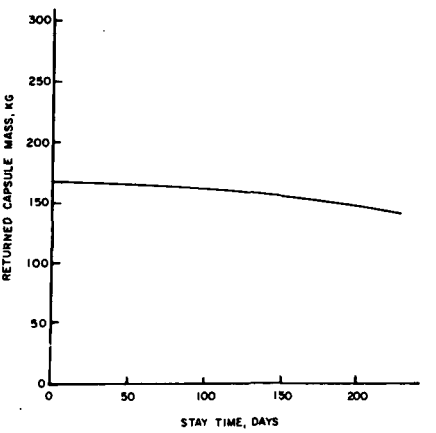

Figure 5.–Stay-time effect on returned capsule mass. Solar electric flight mode; Titan IIID/Burner II; 1977 launch opportunity; trip time = 1050 days; Earth return orbit = 500 X 40 000 km.

Effect of Stay Time

Stay time is defined as the total time spent in the vicinity of Eros. It includes the rendezvous and stationkeeping maneuvers, topographical survey, surface operations, and departure maneuvers. An investigation of the effect of stay time on returned mass is shown in figure 5 for the solar electric flight mode. Over a range of stay times, there does not appear to be any significant effect on the capsule mass. This allows the freedom to perform whatever operations in the vicinity of Eros are desired. Additionally, it was found that the optimum total trip time remains relatively constant at 3 yr as stay time is varied. That is, trip time is not appreciably shortened or lengthened as stay time is varied.

Effect of Launch Year Opportunity

In addition to the 1977 launch opportunity discussed thus far, other launch years were surveyed. Opportunities for round-trip missions to Eros occur about 2 yr apart, and their effect on returned mass is shown in figure 6. The open bars relate to the return capsule mass in Earth orbit and the shaded bars are merely an estimate of the soil sample size contained within the capsule. A scaling law used on a recent Mars sample-return study (Friedlander, 1970) relates the sample mass m_s to the return capsule mass m_c by the relationship

$$m_s = 0.44\,(m_c - 29.5)$$

In figure 6(*a*) is shown the ballistic flight mode. For the years surveyed, the launch opportunity in 1977 results in the maximum sample returned. Similarly, for the solar electric flight mode shown in figure 6(*b*), the year 1977 is the most favorable opportunity for a sample return from Eros. Preceding and succeeding years have decreasing return mass. A preliminary estimate of the synodic cycle is 16 yr, at which time (1993) a most favorable opportunity should occur again.

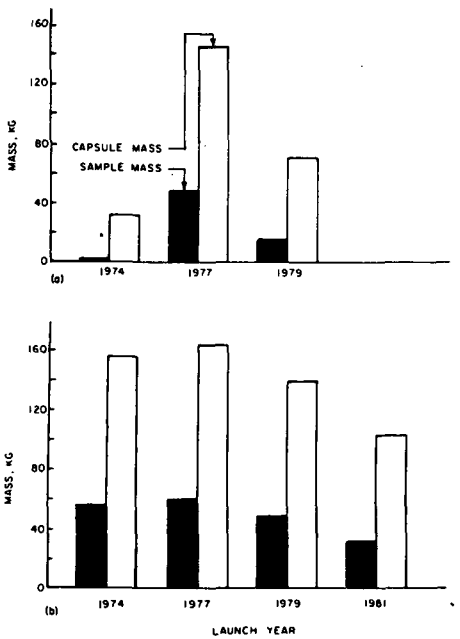

Figure 6.–Launch opportunity effect on returned mass. (*a*) Ballistic flight mode; Titan IIID(7)/Centaur/385; total trip time = 3 yr; stay time is variable (88 to 378 days); Earth return orbit = 500 X 40 000 km. (*b*) Solar electric flight mode; Titan IIID/Burner II; total trip time = 3 yr; stay time = 50 days.

1977 TRAJECTORY GEOMETRY

Ecliptic projections of the outbound and return trajectories for the 1977 Eros round-trip mission are shown in figure 7(*a*) for the solar electric flight mode and in figure 7(*b*) for the ballistic flight mode. Both outbound and inbound trajectories for both modes have approximately 300° of travel angle. Launch dates from Earth are in early 1977. Arrival dates at Eros are at about mid-June 1978 at which time Earth is 2.2 AU from Eros, almost directly behind the Sun. After a stay time at Eros, departure takes place in latter September with Earth still about 2.2 AU away and very close to the sunline. Return dates back at Earth are approximately mid-January 1980, 3 yr after launch. In table III is given a flight plan that details the events, dates, and

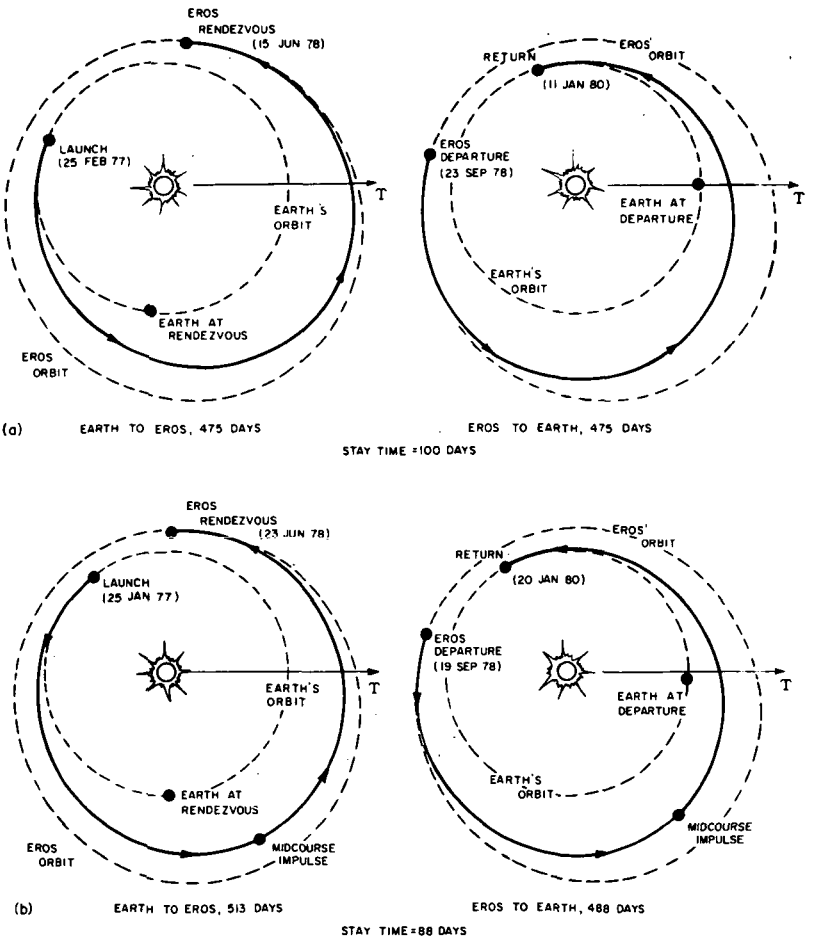

Figure 7.—Transfer profiles for a 3 yr Eros sample-return mission. ϒ indicates the vernal equinox. (*a*) Solar electric; stay time = 100 days. (*b*) Ballistic; stay time = 88 days.

TABLE III.–*Flight Plans for 1977 Eros Sample-Return Missions*

Event	Parameter[a]	Ballistic flight				Solar electric flight			
		Dates	Mass, kg	Time, days	Pertinent parameters[b]	Dates	Mass, kg	Time, days	Pertinent parameters[c]
Launch	Date	1/25/77				2/25/77			
	Required gross mass		3240				1760		
	Candidate launch vehicle				TIIID(7)/C				TIIID/BII
	C_3, km^2/s^2; DLA, deg				33.5; −70				12.3; −45
	LV payload capability, kg				3700				1800
Earth-departure	Date	1/26/77				2/26/77			
	Injected mass		3085				1675		
	Outbound transfer time			513				475	
Eros rendezvous	Date	6/23/78				6/15/78			
	Mass		1595				1415		
	Science payload, kg				90				90
	Stationkeeping maneuvers				7				7
	Stationkeeping time, days				60				70
Docking	Date	8/20/70				8/25/78			
	Mass		1565				1390		
Separation	Date	9/17/78				9/21/78			
	Mass		1435				1265		
	Stay time			88				100	
Eros departure	Date	9/19/78				9/23/78			
	Mass		1030				910		
	Return transfer time			488				475	
Earth approach	Date	1/19/80				1/10/80			
	Separated payload mass		210				140		
Earth-orbit capture	Date	1/20/80				1/11/80			
	Capsule mass		90				90		
	Orbit perigee altitude, km (n. mi.)				500 (270)				500 (270)
	Orbit period, hr				12				12
Synopsis	Return sample mass		25				25		
	Total trip time			1089				1050	

[a]LV = launch vehicle.
[b]T = Titan; C = Centaur.
[c]T = Titan; B = Burner.

masses for the 1977 Eros sample-return mission. A fixed sample size of 25 kg was assumed for each flight mode. Provisions were made in the launch vehicle capabilities to provide for a nominal DLA less than 36°.

SOLAR INTERFERENCE POTENTIAL

It is observed from the solar electric and ballistic transfer profile graphs (figs. 7(*a*) and 7(*b*), respectively) that Earth is nearly opposite Eros, on the opposite side of the Sun, during rendezvous, stationkeeping, and docking with the asteroid. The question of whether the Sun will interfere with the necessary spacecraft/Earth communications link during these critical maneuvers was investigated. Current Deep-Space Network (DSN) communications capability requires that the Earth/spacecraft line of sight be at least 2° off the Earth/Sun line (Douglas Aircraft Corp., 1965). In figure 8, the Earth/Eros line-of-sight trajectory during the 1978 Eros encounter is shown projected in a plane normal to the Earth/Sun line, positioned at the Sun. Dots are placed along this trajectory at 15 day intervals. The point of maximum solar interference (3° separation between Eros and the Sun as seen from Earth) occurs on Julian date 2443710 (July 20, 1978). The arrival and departure points for the ballistic and solar electric baseline mission profiles are also shown on the trajectory. In both cases, these points bracket the maximum solar interference date. Fortunately, this interference (3°) appears acceptable for reliable DSN communications. Further study of this problem is needed using more recent elements of Eros' orbit to accurately determine its line-of-sight trajectory. If further communication degradation were to result, it would be necessary to shift the entire stay time by 50 to 100 days. This, of course, would have an effect on the energy requirements and payload capability of the sample-return mission.

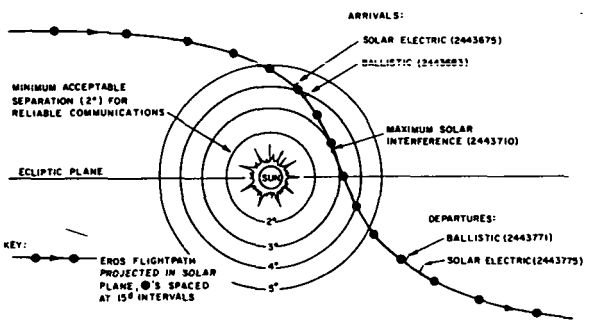

Figure 8.–Solar interference potential during 1978 Eros rendezvous.

CONCLUDING REMARKS

On the basis of the largest amount of sample material returned to Earth orbit, the 1977 launch opportunity appears to be the most favorable during a

synodic cycle of approximately 16 yr. Mission times are invariant and are approximately 3 yr in length. Lengthy stay times do not decrease significantly the amount of sample returned. A sample size of 25 kg may be returned in this mission by either a Titan IIID/Burner II with a 10 kW solar electrically propelled vehicle or a Titan IIID(7)/Centaur/385 chemically propelled vehicle. Severe range safety problems exist (DLA = $-70°$) for the ballistic flight mode. This launch problem is diminished through the use of the solar-powered flight mode. Communications between Eros and Earth during the 1978 rendezvous may be somewhat impaired because of solar interference.

Although this paper has considered round-trip sample-return missions to the asteroid Eros, many of the mission characteristics and results are applicable to other asteroids in the Mars-crossing group, such as Geographos, Apollo, Toro, and Amor. It was noted that launch opportunities to Eros occur in 1977, 1979, etc. Preliminary investigations indicate that launch opportunities to Geographos occur during the alternate years; i.e., 1976, 1978, etc. Missions to this asteroid also require 3 yr to complete a sample return.

REFERENCES

Friedlander, Alan L. 1970, Solar Electric Propulsion Capabilities for Mars Surface Sample Return Missions. Internal Document, Illinois Inst. Technol. Res. Inst. Chicago.

Mascy, Alfred C., Dugan, Duane W., and Pitts, Samuel W. 1968, Applications of Combined Electric, High-Thrust Propulsion Systems. J. Spacecr. Rockets 5(7), 785-791.

Douglas Aircraft Corp. 1965, Study of Conjunction Class Manned Mars Trips–Part II. NASA CR 64119.

TRW, Inc. Study of a Common Solar-Electric Propulsion System for High-Energy Unmanned Missions. Contract NAS2-6040 for NASA Advanced Concepts and Missions Div., Moffett Field, Calif.

MULTIPLE ASTEROID FLYBY MISSIONS

DAVID R. BROOKS AND WILLIAM F. HAMPSHIRE II
NASA Langley Research Center

The use of spacecraft for studying the physical properties of the asteroid belt can be approached in several ways. Certainly the simplest approach is to send a spacecraft into the asteroid belt and measure the effects of the environment encountered; this has the advantage of not requiring a vehicle to be targeted to any particular destination. With such an approach, properties may be obtained for those classes of objects that are populous enough to provide a significant number of encounters within the measurement range of the spacecraft. Unfortunately, the large asteroids do not constitute such a class of objects; the probability of an undirected spacecraft passing within measurement range of an asteroid having a diameter of 1 or more km is negligible.

For studying the properties of the large asteroids as a class, as opposed to studying one particular asteroid, it is clear that a way must be found to sample the population of large asteroids by studying more than one, preferably with the same equipment on the same mission. This task requires the assumptions that the position of likely targets can be predetermined with sufficient accuracy and that the spacecraft has onboard guidance and propulsion for maneuvering to preselected positions in space and time. It is assumed that the permanently numbered asteroids (presently 1748 in *Ephemeris,* 1971) is the group of objects from which minor planet targets will be chosen, because the assignment of a permanent number to an asteroid usually denotes a reasonably well-known ephemeris based on numerical integration of osculating orbital elements.

It is the purpose of this paper to define various types of multiple asteroid flyby missions involving the 1748 numbered asteroids, to determine the magnitude of impulsive Δv demands for performing typical missions, and to relate these requirements to spacecraft capabilities planned or envisioned for other applications. A particular goal of the study is to identify possible multiple flyby missions whose in-flight propulsive requirements are attainable with reasonably sized chemical systems, rather than being so large as to make advanced propulsion schemes necessary or highly desirable for effective spacecraft performance. The idea of searching for close asteroid encounters that can be obtained with small Δv maneuvers is not new. Bender (1967) has

conducted a similar study in a search for cis-Martian asteroid encounter opportunities; and the desirability of multiple flyby missions has been mentioned recently by several authors involved in solar electric mission analysis (Archer, 1970; Brooks, 1970; Wrobel and Driver, 1969).

RANDOM ENCOUNTERS WITH LARGE ASTEROIDS

It was stated in the introduction that the probability of a spacecraft encountering large asteroids by chance was negligible. Deferring for a moment the definition of "encounter," this statement can be justified easily. Actual count of the 1748 numbered asteroids shows that at any given time an average of about 431 are contained in a washer-shaped volume having an inside radius of 1.8 AU, an outside radius of 3.7 AU, and a thickness of 0.2 AU, centered about the ecliptic plane. If these asteroids are assumed to be uniformly distributed in the volume, $\pi(3.7^2 - 1.8^2)0.2$ AU^3, and to have, on the average, velocities equal to the circular velocity, the number of encounters to be expected by a spacecraft in this volume for a time $t_2 - t_1$ is

$$N = \frac{431}{6.56} \pi R_E^2 \int_{t_1}^{t_2} \left| \mathbf{v}_{SC} - \mathbf{v}_C \right| dt \qquad (1)$$

where $\mathbf{v}_{SC}$ and $\mathbf{v}_C$ are the spacecraft and circular velocity vectors and πR_E^2 is the constant cross-sectional area of a spherically symmetric encounter volume of radius R_E about the spacecraft.

The question of what R_E must be to result in a useful encounter cannot and need not be answered exactly. Bender (1967) assumed that the closest distance of approach should be less than 2×10^4 km for telescopic observation. For asteroid mass determinations based on perturbations of a spacecraft's velocity, passage distances are required that range from 10^3 km for smaller numbered asteroids to as much as 10^6 km for Ceres (Meissinger, 1971, personal communication). For the purposes of obtaining a number from equation (1), assume that the largest radius at which useful data can be obtained is $R_E = 10^{-4}$ AU (1.5×10^4 km). For this radius, a spacecraft in a 1 by 3 AU orbit in the ecliptic will encounter an average of only 6×10^{-6} asteroids per orbit.

Accounting for all those asteroids that could be observed from Earth and cataloged along with the present 1748 numbered asteroids will improve, of course, the chances of a random encounter. However, even if the total number of large asteroids is as high as 10^5, the sample trajectory given above will still yield only 3×10^{-4} encounters per orbit—an increase of about 50 times above the previous result. An encounter radius as large as 0.1 AU, on the other hand, should result in about six encounters with the numbered asteroids per orbit for the same trajectory.

The pertinent conclusion to be drawn from the foregoing discussion is that a spacecraft must be maneuvered to result in close encounters with the numbered asteroids because the radius of the sphere in which encounters are likely to take place (0.1 AU) is large compared to the distance required for a measurement (10^{-4} AU). It is a good approximation to assume that a spacecraft must be guided to hit the target asteroid.

MISSION ANALYSIS

Multiple asteroid flyby missions that involve maneuvering a spacecraft away from a nominal trajectory with onboard propulsion may be categorized as follows:

(1) Opportunities resulting from randomly generated trajectories that combine flybys of several asteroids, none of which are preselected, into one mission requiring a small total Δv for maneuvering
(2) Multiple flyby missions that are required to include particular asteroids of known scientific interest; for example, Ceres
(3) Missions to major planets that include favorable opportunities for maneuvering close to one or more asteroids

Additional categories might involve circularizing the spacecraft orbit in the asteroid belt or rendezvous with a major asteroid. Such maneuvers require large values of Δv compared to those resulting from the present study of multiple flybys, hence they belong to a different type of mission that involves much larger spacecraft and an advanced propulsion system such as solar electric-ion engine propulsion.

The basic logic for examining multiple flyby missions is contained in a computer program that compares cartesian position coordinates of a spacecraft with the positions, at the same time, of the 1748 numbered asteroids. The asteroid positions are obtained by using the osculating elements in the 1971 *Ephemeris* volume as Kepler elements and by advancing the listed mean anomalies along unperturbed ellipses to the desired time. The positions so generated are considered to be exact for the purposes of this study. The spacecraft trajectory may be a Keplerian ellipse in the ecliptic, generated internally by the computer program, or an externally generated trajectory, as in the case of missions involving major planets. As the positions of spacecraft and asteroids are computed, their relative separations are compared against a preselected search radius, and all asteroids passing within the search radius are counted as possible targets for that particular mission. For a search radius of 0.1 AU, a sizable number of encounters can be expected on the average—about six, according to equation (1), for a trajectory to 3 AU.

To determine impulsive Δv requirements for multiple flyby missions, various asteroid flyby sequences are examined after possible targets are identified. First, the spacecraft is retargeted at Earth launch to intercept one of the asteroids. Then, an algorithm that solves Lambert's problem is utilized to

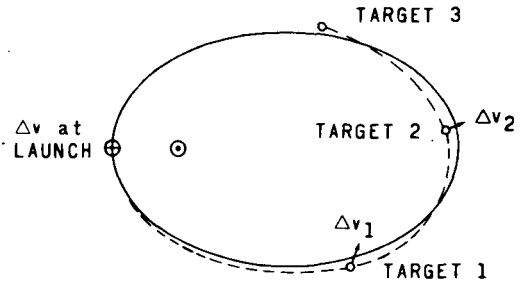

Figure 1.–Typical trajectory for a multiple asteroid flyby mission.

determine the impulsive Δv required for the spacecraft to encounter the second target at the time of closest approach to the second target. This process is then repeated as necessary to complete the desired sequence. The asteroids are assumed to be massless points that are intercepted exactly by the spacecraft. Figure 1 illustrates how the Δv maneuvers are performed for a three-asteroid sequence. The Δv required at Earth for the spacecraft to intercept the first target is assumed to be provided by the launch vehicle and is not charged against the capability of the spacecraft.

RESULTS

Random Search Trajectories

For spacecraft trajectories that are not constrained to intercept a major planet or some particular asteroid, a Keplerian ellipse in the ecliptic can be specified by the launch date and aphelion; the perihelion is assumed to be at the launch point. Table I shows a listing of asteroid encounters resulting from 11 such trajectories, launched between Julian dates 2444500 (late 1980) and 2445000 (early 1982) at 50 day intervals to an aphelion of 3 AU. The search radius is 0.1 AU. The number of encounters ranges from 8 to 15, and the average number is 10 per mission, as compared to the 6 per mission predicted by equation (1). The agreement between these two numbers is acceptable, considering the simplifying assumptions made in deriving equation (1) and the fact that the listings in table I are not sufficient to constitute a statistically significant sample.

Additional details concerning the seven closest encounters during the trajectory launched on Julian date 2444800 (mid-1981) are given in table II; this launch date yielded the largest number of different targets of the 11 launch dates shown in table I. The encounters take place over a time of 659 days, representing a range in spacecraft true anomaly of 115°. Certainly, it will not be possible, in general, to maneuver to all asteroids passing within 0.1 AU of a spacecraft. For example, consecutive flybys of all the asteroids listed in table II would require an impulsive Δv of 41.6 km/s, computed as indicated in

TABLE I.—*Numbered Asteroids Passing Within 0.1 AU of a Spacecraft in a 1 by 3 AU Orbit Launched on the Julian Date Shown*

Julian date, 244*XXXX*										
4500	4550	4600	4650	4700	4750	4800	4850	4900	4950	5000
548	255	797	1720	985	290	1515	1665	1019	1446	1601
1382	1130	770	1082	878	377	149	449	841	1729	1153
1153	1389	1300	1350	1727	1576	725	939	355	1448	248
1635	90	462	846	1704	1443	1110	1069	228	1293	557
834	1199	1383	732	1379	898	76	1462	787	1635	90
308	180	424	91	62	447	1674	243	1029	701	888
1053	647	1362	1382	1289	1645	1068	178	518	832	1085
1739	1064	1705	969	513	1357	870	317	996	1745	1337
	1270		810	632	62	1593	1225	1147	1562	497
				1741	1278	1740				518
				644	1056	479				
				220	1292	561				
						30				
						1720				
						822				

the previous section. When encounters with the spacecraft occur in relatively rapid succession (for example, 1515 → 149 and 1740 → 561 in table II), it will generally be required to make a choice between two targets. There are, however, several opportunities for flying close to three asteroids for a total impulsive Δv of less than 1 km/s; such missions are listed in table III. It is always assumed that the spacecraft is launched from Earth to intercept the first target in a multiple flyby sequence. All seven of the asteroids in table II are

TABLE II.—*Data for the Seven Closest Asteroid Encounters With a Spacecraft Launched on Julian Date 2444800 Into a 1 by 3 AU Orbit*

Asteroid no.	Julian date, 244*XXXX*	Radius, AU	True anomaly[a]	Minimum separation, 10^6 km	Relative velocity, km/s
1515	4971	1.97	118°	5.3	11.4
149	4980	2.02	121	5.4	11.1
1674	5134	2.72	154	6.7	8.3
870	5422	2.91	194	7.6	5.1
1740	5508	2.69	207	7.1	9.2
561	5528	2.63	211	4.0	10.5
1720	5630	2.16	233	2.8	12.3

[a]Of the spacecraft.

TABLE III.–*Impulsive Δv Requirements for Three-Asteroid Encounters Involving the Close Approaches Listed in Table II*

Encounter sequence[a]	Impulsive Δv, km/s
1515→1674→561	0.93
1515→870→1720	.79
1515→561→1720	.81
1515→1674→1740	.69
1515→1674→1720	.88
149→870→561	.93
149→870→1720	.58
1674→561→1720	.89

[a]Only those sequences for which the impulsive Δv is less than 1 km/s are listed.

included in one or more of the triple flybys listed in table III. A four-asteroid mission, 1515 → 1674 → 561 → 1720, is possible with a total impulsive Δv of only 0.8 km/s.

Trajectories to a Preselected Asteroid

For missions that are constrained to include a close flyby of a particular asteroid, a Keplerian ellipse in the ecliptic is still used for the spacecraft trajectory; but the launch date and aphelion are adjusted to include an encounter with the desired asteroid when it passes through the ecliptic. Data for generating trajectories to Ceres and Vesta are readily available in the NASA *Planetary Flight Handbook* (Lockheed Missiles & Space Co., 1966). As an example for this study, the trajectory resulting from a late 1975 launch to

TABLE IV.–*Data for the Five Closest Asteroid Encounters With a Spacecraft Constrained to Pass Near 1 Ceres During a 1975 Launch Opportunity*

Asteroid no.	Julian date, 244*XXXX*	Radius, AU	True anomaly[a]	Minimum separation, 10^6 km	Relative velocity, km/s
632	2956	2.37	131°	4.5	14.0
1435	2985	2.53	137	6.5	5.9
946	3260	2.30	174	5.7	4.6
947	3313	3.32	180	2.8	4.0
1	3568	2.83	212	5.3	9.8

[a]Of the spacecraft.

Ceres[1] was examined for other close asteroid approach opportunities. Data for the five closest approaches are summarized in table IV. They take place over a period of 612 days and a spacecraft true anomaly range of 81°. For the trajectory studied here, 1 Ceres was encountered last, but this would not be generally true. Of the several theoretically possible multiple asteroid missions for this trajectory, two triple flybys can be performed with an impulsive Δv of less than 1 km/s: 632 → 946 → 1 with Δv = 0.73 km/s and 632 → 947 → 1 with Δv = 0.24 km/s.

Asteroid Encounters on Trajectories to Jupiter

The possibility of passing close to an asteroid enroute to a major planet provides extra motivation for performing the planetary mission if the required maneuvering can be assumed to have no significant effect on the primary mission goal. As an example of such a mission, a 1975 trajectory to Jupiter has been examined for close approaches to asteroids, and those passing within 0.1 AU are tabulated in table V. Of course, because of the relatively short time spent in the asteroid belt on this trajectory, there are not as many close approach opportunities as for the previous two mission types. Nevertheless, the encounter sequence 666 → 396 → Jupiter can be performed with an impulsive Δv of only 0.52 km/s. It should be noted that the flyby velocities for this type of trajectory are necessarily higher than for trajectories having an aphelion in the asteroid belt.

TABLE V.–*Asteroid Encounters on a Trajectory to Jupiter Launched During a 1975 Opportunity*

Asteroid no.	Julian date, 244*XXXX*	Radius, AU	Minimum separation, 10^6 km	Relative velocity, km/s
1636	2734	1.97	12.9	16.7
666	2736	1.99	9.7	16.2
27	2751	2.12	8.6	18.0
396	2875	3.06	7.1	10.2

DISCUSSION OF RESULTS

It is clear that the Δv results presented above should be taken only as representative of what can be expected for multiple asteroid flyby missions. Most important, computing asteroid positions from Kepler's equations does

[1]Ceres has an aphelion of 2.9776 AU, a perihelion of 2.5574 AU, and an orbital inclination of 10°.6.

not make the best use of available data. However, a computer search for possible targets based on integrated orbits for all the asteroids would require excessive computation time. Once possible targets have been identified for a particular mission, the asteroid positions during encounters need to be recomputed from integrated orbits that take planetary perturbations into account. This will improve the position data to some extent, but it is certain that the actual Δv needed for a particular mission will require significant adjustments once attitude control is included and midcourse correction requirements are analyzed, based on spacecraft and asteroid ephemeris uncertainties.

The particular multiple flyby missions selected to serve as examples of various mission types are, like the Δv values, only representative of what can be expected. It is likely that better mission opportunities could be found if an extensive parametric survey of asteroid belt trajectories were undertaken. However, even the small number of trajectories presented in this study demonstrate that there is an abundant supply of multiple asteroid flyby missions that can be performed for less than 1 km/s, and it should be possible to keep within a Δv of 1 km/s for many missions even after guidance and attitude control requirements are satisfied. Thus, the results of this study indicate that the stated goal of identifying multiple asteroid flyby missions suitable for reasonably sized chemical systems can be achieved.

The quantitative meaning of "reasonably sized" can be made clear by relating the Δv requirements resulting from this study to representative requirements and capabilities of currently funded projects. It has been possible to find multiple asteroid missions involving flybys of two or three asteroids with impulsive Δv values between 0.1 and 1 km/s. (Flybys of more than three asteroids can be expected to require more Δv.) In table VI, the Δv range between 0.1 and 1 km/s is compared with Pioneer F and G and Viking spacecraft capabilities and also with the requirements for some representative interplanetary maneuvers, particularly those in the asteroid belt. It is of interest to note that the Δv for a loose Jupiter orbit (1.2 by 120 Jupiter radii) is about 0.7 km/s for v_∞ of 7 km/s, and this value lies within the range of multiple flyby requirements. The Pioneer F and G spacecraft have a Δv capability of about 0.2 km/s, of which only 0.1 km/s is available for maneuvering, but the possibility of uprating a Pioneer spacecraft for the Jupiter orbiter mission is being seriously studied by NASA Ames Research Center (Howard F. Matthews, 1971, personal communication). Such a spacecraft could just as well be used for the missions studied here. The Viking orbiter spacecraft also has ample propulsive capability for multiple flyby missions; about 1.5 km/s is required for Mars orbit insertion and subsequent orbit adjustments. Plane changes, circularizing, and rendezvous maneuvers in the asteroid belt require progressively more Δv, and some examples are given in table VI.

The mission analysis in this study has considered only the impulsive Δv values that can be delivered to a good approximation by chemical rockets; the

TABLE VI.—*Comparison of Multiple Flybys With Other Missions*

Mission	Impulsive Δv, km/s
Multiple flybys	0.1 to 1.0
Pioneers F and G[a]	0.1
Jupiter orbit[b]	0.7
Viking orbiter	1.5
Plane change at 3 AU:[c]	
5°	1.1
10°	2.1
Circularize:	
2 AU	3.8
4 AU	5.5
Ceres rendezvous	8.0 to 10.0
Solar electric propulsion (SEP), per 100 days[d]	0.3 to 0.5

[a]Does not include attitude control and midcourse guidance capability. Pioneers F and G may be uprated for use as Jupiter orbiters.

[b]1.2 by 120 Jupiter radii, v_∞ = 7 km/s.

[c]From a 1 by 3 AU ellipse.

[d]At 3 AU.

performance of low-thrust systems, like solar electric-ion engine systems, are also of great interest. With SEP, the propulsive performance is limited not by the properties of the propellant (ionized mercury), as is the case with a chemical rocket, but by the available power and time. The initial acceleration of payload-optimized SEP spacecraft at 1 AU is generally between 0.3 and 0.5×10^{-6} km/s^2 (Brooks, 1970). At 3 AU, the available solar power is decreased by a factor of 9 and, at a constant radius of 3 AU, the velocity of an SEP spacecraft may be increased proportionally with time in the amount of 0.3 to 0.5 km/s for every 100 days of thrusting time. Therefore, multiple flyby missions for SEP spacecraft have to be chosen carefully to allow sufficient time intervals between one target and the next.

For this study, no attempt has been made to select asteroids on any basis other than their availability as low-energy targets. Clearly, such a determination should be made, and the foregoing results demonstrate that there are enough approximately equivalent mission opportunities to allow a selective approach in mission analysis. Apart from ranking asteroids in order of scientific interest, which is an important task in itself, the criteria that could be applied to an asteroid for the purpose of easing demands on a multiple flyby spacecraft are (1) low identification number, (2) low orbital inclination, and (3) asteroid near aphelion at encounter. The first criterion assumes that low number is associated with high mass and large size, thereby making mass determination

and optical observation easier. The remaining two criteria serve to minimize the relative flyby velocity, thus making tracking easier during the encounter. The encounter duration, based on a minimum relative flyby velocity of about 5 km/s and an encounter radius of 10^{-4} AU, will be no greater than about 1.7 hr.

CONCLUSIONS

It has been shown that the probability of passing close enough to a large asteroid to allow performance of useful measurements is negligible. However, if a spacecraft is assumed to have some onboard propulsion for maneuvering close to an asteroid, many multiple asteroid flyby missions can be identified that require a total impulsive Δv of less than 1 km/s, and therefore lie within the capability of available chemical-propulsion systems. These include triple asteroid flybys that may involve a major asteroid such as Ceres and double asteroid flybys followed by a flyby of Jupiter. Compared with other useful maneuvers in the asteroid belt, multiple flybys require less impulsive Δv, and some of the triple flyby sequences require less impulsive Δv than a loose elliptical orbit around Jupiter. Spacecraft having suitable propulsive capability include the Viking orbiter and possibly the Pioneer spacecraft (which can be uprated for a Jupiter orbiter mission).

It is expected that the impulsive Δv results for particular missions will be affected significantly by midcourse and guidance requirements once these are analyzed; but the large number of apparently attractive missions indicates that it will still be possible to find missions that can be performed for less than 1 km/s. The large number of possible missions also indicates that asteroid targets can be selected on the basis of size and orbital properties to ease the problems of observation during the encounter.

REFERENCES

Archer, J. L. 1970, Mission Modes to the Outer Solar System. AIAA Paper 70-58 presented at AIAA 8th Aerosp. Sci. Meeting (New York), Jan. 19-21.

Bender, D. F. 1967, Asteroid Encounters on Mars Missions. AAS Space Flight Mechanics Specialist Symp. (ed., M. L. Anthony), pp. 423-432. AAS Sci. Technol. Ser., vol. 11.

Brooks, D. R. 1970, Solar-Electric Missions to Specific Targets in the Asteroid Belt. AIAA Paper 70-1120 presented at AIAA 8th Elec. Propulsion Conf. (Stanford), Aug. 31-Sept. 2.

Lockheed Missiles & Space Co. 1966, Planetary Flight Handbook, Part 5–Trajectories to Jupiter, Ceres, and Vesta. Space Flight Handbooks, vol. III. NASA SP-35.

Wrobel, J. R., and Driver, J. M. 1969, Current Status of Solar Electric-Propelled Asteroid Probe Studies. AIAA Paper 69-1105 presented at AIAA 6th Ann. Meeting Tech. Display (Anaheim, Calif.), Oct. 20-24.

DISCUSSION

GEHRELS: If asteroid encounters are possible on trajectories to Jupiter, why have such missions not been included on Pioneers F and G, which were originally identified as asteroid/Jupiter missions?

BROOKS: It was apparently concluded that the study of possible hazards to spacecraft penetrating the asteroid belt was of higher priority than studies of asteroids per se. Also, the close encounters I described require maneuvering capability beyond the existing Pioneer F and G design. A capability of 0.5 to 0.6 km/s is possible without major redesign of the spacecraft. A capability of 0.9 km/s may be possible with the same type of propulsion system (hydrazine), but a major redesign of the spacecraft may be necessary. Such a capability would be required for a Jupiter orbiter, as I pointed out in the paper.

FORWARD: Is it possible to send multiple flyby missions into "clumps" of asteroids or to match the orbits of, for example, the Trojan asteroids?

BROOKS: Matching orbits requires much more propulsive capability than flyby missions, and therefore such a maneuver was not considered in this paper. Flying into a group of asteroids would still mean, in general, that only one member of the group could be approached closely. This is because maneuvering from one point to another point close in time, but not on the unperturbed trajectory, requires a large velocity change.

Page intentionally left blank

MANNED MISSION TO AN ASTEROID

HARVEY HALL
NASA, Office of Manned Space Flight

If manned missions to the planets are to be considered at some time in the future, as has long been imagined, it appears to be reasonable to explore the feasibility of carrying out a manned mission to an asteroid as an intermediate step between lunar and planetary missions. If study shows that it is possible to conduct such a mission with Apollo-type hardware, and if the answer to the first question is yes, then an asteroid flight should probably be considered while Apollo-type facilities are still in existence. Once these facilities have been dismantled, it may be many years, perhaps a generation, before a new era in space exploration would make such a manned flight possible.

With these thoughts in mind, an analysis was undertaken to determine whether an asteroid mission is practicable. An overriding consideration is the reliability of the life-support system. Life-support systems for Skylab—the final manned mission now being planned after Apollo—are being designed for missions of 56 days. Most planetary round-trip missions that have been studied would take much longer than this to complete; namely, of the same order as the planet period, or a year or so. It would presently be impracticable to design life-support systems for such long missions, approximately 10 times as long as the Skylab mission. Consequently, to be considered as a possibility, an asteroid mission based on the use of Apollo-type hardware would have to be found that could be completed within a couple of months.

To explore this question, it is necessary to know how the difficulty of such a mission would compare with a mission to Mars. The comparison is in terms of the total Δv and the total mission time required. For purposes of comparison, a rough approximation of Δv needed for two types of missions is given in table I.

The total mission Δv provides a sensitive indicator of mission difficulty or cost because once the types of rocket fuel, engines, etc., have been selected,

TABLE I.—*Comparison of Missions*

Mission	Total Δv, km/s	Mission time
Moon (Apollo)	20	1 week
Mars	40	1 yr

the mass ratio, or ratio of gross takeoff weight to gross weight less fuel, depends exponentially on Δv. To double Δv, for example, may increase total takeoff weight by a factor of 7 or more. The total cost may easily increase at even a higher rate, depending on the amount of new technology needed.

Total mission time is also a sensitive index of mission cost in the present state of the art. The reason for this is that the cost of extending the operating time of the life-support and other essential subsystems needed, while maintaining the same level of mission reliability, may be greater than the cost of the original subsystems, even many times greater. For this reason, an asteroid mission that could be completed in 2 or 3 months, with perhaps 2/3 the Δv requirements of a Mars mission, might have much to recommend it as an intermediate U.S. mission.

In this paper, an approximate method has been derived for studying the cases that would be worth considering. Generally these are limited to asteroids with the following orbital features:

(1) Perihelion in or near the ecliptic plane
(2) Perihelion within ~0.1 AU of Earth's orbit
(3) Aphelion less than approximately 1.5 or 2 AU
(4) Angle between orbital plane and ecliptic plane less than 10° to 12°
(5) Launch window available at desired time

There are probably many asteroids that meet the first four conditions. Some of them (e.g., Eros) have a launch window within the next 5 to 10 yr. But better choices may be available at a later time because not all of the ephemerides are accurately known, and further work done in cataloging and classifying them might reveal a number of interesting new possibilities.

The results of the study show that

(1) Mission times of the order of 3 months or less are feasible.
(2) Asteroid missions needing a total Δv of 24 to 30 km/s, or perhaps somewhat less, exist.
(3) The built-in requirements that exist for all missions create a basic minimum Δv that cannot be reduced much below 18 to 21 km/s unless a "freak" asteroid that comes very close to Earth can be found.

The more or less irreducible requirements include

(1) Earth escape: 10 km/s
(2) First retro (or speedup) from Earth: 0.9 to 0.6 km/s
(3) Correction for radial velocity gained (or lost) during transit: 1.5 to 2 km/s
(4) Speedup (or slowdown) to asteroid velocity prior to rendezvous and docking: 2 to 10 km/s
(5) Plane change (if any): 0 to 4.5 km/s

(6) Orbital transfer from asteroid to Earth (equal radial and transverse transit times): 3 km/s
(7) Final plane change (if any): 0 to 4.5 km/s

Only the root mean square is needed of items (3) through (7). However, there is a practical minimum for Δv as noted above, and a minimum of perhaps 6 to 8 weeks transit time for even the most accessible asteroid.

Eros, for which the next launch window will be in 1975, is not a favorable case from the viewpoint of total Δv. The total Δv needed in 1975 would be comparable with the amount needed for a Mars mission. This tends to rule out Eros although the total mission could be completed in the favorable time of about 90 days, compared with over a year for Mars.

To establish a lower limit on Δv and mission time, a hypothetical asteroid was studied having the following orbital characteristics:

$$r_P = 0.99 r_E$$
$$r_A = 1.4 r_E$$
$$\phi = 0$$

where r_P is the perihelion distance, r_A is the aphelion distance, r_E is the Sun-Earth distance, and ϕ is the angle between the orbital plane and the ecliptic. Such an asteroid may not exist. Many small asteroids having favorable orbital characteristics have been observed over the years, only to be lost again before their orbits could be established.

The requirements are still of the order of magnitude of 20 to 24 km/s. The results for this hypothetical asteroid show that mission times as short as 6 or 7 weeks are feasible.

Page intentionally left blank

DESIGN AND SCIENCE INSTRUMENTATION OF AN UNMANNED VEHICLE FOR SAMPLE RETURN FROM THE ASTEROID EROS

H. F. MEISSINGER AND E. W. GREENSTADT
TRW, Inc.

Unmanned missions to the asteroids have been proposed and investigated as part of the overall plan of exploration of the solar system. A principal incentive for landing on an asteroid and retrieving a surface sample for return to Earth is the expectation that detailed laboratory analysis of the sample material's chemical composition, crystal structure, surface texture, magnetic characteristics, radioactive state, and age can provide essential clues, not available by other means, to the origin of asteroids and possibly the history and formative processes of the solar system (Alfvén and Arrhenius, 1970*a,b;* Bratenahl;[1] Friedlander and Vickers, 1964; IIT Research Institute, 1964; Öhman, 1963). The results may indicate, for example, to what extent accretion or fragmentation processes have been involved in the formation of asteroids.

Asteroids of the Apollo family, such as Icarus, Geographos, and Eros, periodically approach very close to Earth. Except for the Moon, they are in fact Earth's closest neighbors in space. Eros, in particular, is reasonably accessible to Earth for a landing and sample-return mission with launch opportunities recurring about every other year, at a much smaller propulsion energy than would be required for comparable missions to other planetary bodies, owing to the proximity of its orbit and its almost negligible gravity. A mission to Eros would be desirable also as a precursor to a more complex and costly Mars sample-return mission.

The use of solar electric propulsion as the means of primary propulsion during the outbound and return phases permits the use of a smaller booster than would be required for a ballistic mission with equivalent payload capability and thus can achieve a significant cost saving. The use of electric propulsion also alleviates launch date constraints, provides flexibility in mission profile selection and guidance, and facilitates execution of the final approach and descent phases under remote control from Earth. It permits extended hover phases in close proximity of the asteroid during which television (TV) images can be transmitted to Earth and necessary corrective commands

[1]See p. 561.

returned to the landing vehicle, with round-trip communication delays of 35 to 40 min. A fully autonomous vehicle that would perform the final approach and landing at Eros without assistance by ground control would be more complex, more costly, and less reliable.

This paper discusses the scientific objectives to be achieved by an Eros landing and sample-return mission, the instrument payload to be carried, and the mission profile and critical mission phases to be executed. The conceptual design of a solar electric-propulsion spacecraft bus, or stage, capable of returning to Earth a capsule with 100 kg of Eros surface sample material will be described. The round-trip mission time is about 1000 days. The results of this investigation indicate the feasibility of this mission based on available electric-propulsion technology plus existing spacecraft design concepts and flight hardware. Such a bus could be developed in time to meet the 1977 launch opportunity. Similar opportunities occur approximately every other year.

MISSION OBJECTIVES AND SCIENTIFIC INSTRUMENTATION

It is believed that detailed examination of matter from an asteroid will provide information valuable to an understanding of the processes of planetary formation and of solar system hetegony (Alfvén and Arrhenius, 1970*b*). No foreseeable development of onsite techniques can hope to achieve the detail or depth of analysis that is possible with full laboratory equipment, as experience with lunar samples from Apollo has readily demonstrated. The central aim of an asteroid sample-return mission, therefore, will be to acquire asteroidal material to permit such an examination by laboratory analysis. It does not follow, however, that ambient or onsite measurements will have no place on an asteroid return-sample payload. Such measurements will contribute significantly to interpretation of laboratory results. Hence, instrumental surveillance of the target asteroid will be an important phase of the mission before, during, and after touchdown and perhaps after takeoff as well.

Surveillance will serve two functions, both of which encompass extensive local measurements. These functions are (1) selection of an optimal landing spot and (2) characterization of the physical context in which the asteroid is found and from which the samples are taken. These functions are naturally interrelated.

Several factors may enter the selection of an exact landing point. One major consideration involves the relative motion of the spacecraft with respect to the terrain at touchdown, which dictates landing near a pole of the asteroid's axis of rotation. Another consideration will be the angle of solar illumination. These are described in a later section. In addition, unpredictable properties of the asteroid may contribute to site selection. Among them would be local topography, which might determine that one area would be more level or more varied in composition than another or that samples would be obtained with more facility there than elsewhere, and local magnetic signature, which might

suggest that samples from one spot would be more revealing of the early planetary environment than those taken from another.

The physical significance of laboratory analyses of returned samples could be seriously compromised without reasonably complete specification of the immediate and general present environment from which the samples come. It will be important to know how representative of the body composition and of the site materials the returned samples will be. For example, the cumulative effect of solar-wind impact on some surface materials may be influenced by a strong local magnetic field. Therefore, instruments measuring directly the local field, its gradient, and the resulting solar-wind deflection would be very important as part of the scientific instrument package. Complete field, particle, and optical characterization of the solar wind around the asteroid, of the asteroid as a whole, and of the landing site will therefore be essential for successful completion of the mission objectives.

To summarize, the overall mission purpose of collecting samples of asteroidal material from which comprehensive inferences on solar system formation can be obtained with minimal ambiguity will be served by three interrelated mission objectives:

(1) Examination of the asteroid's geometrical configuration and of its environment, including its interaction with the solar wind, if any
(2) Acquisition of samples of asteroidal material from the surface for return to Earth
(3) Observation and characterization of the site from which samples are taken and documentation of the relationship of the samples to the site and of the site to the asteroid

The scientific objectives described above will be served by groups of instruments that provide the following functions:

(1) Measurement of the ambient solar wind, the distant electromagnetic properties of the body, and the interaction, if any, of the body with the solar wind
(2) Observation of the asteroid's size, configuration, surface features, rotation, and optical properties
(3) Detection of gaseous ionized envelope or plasma sheath
(4) Examination of the surface and subsurface characteristics at the landing site
(5) Observation of surface features at the landing site
(6) Observation of ambient conditions at the site
(7) Acquisition of sample material

The instruments needed to perform the tasks included in the above functional categories are given in the following list. Asterisks denote items that might be assigned a lower priority than the others because their data would be unessential to success of the mission, being partially redundant in relation to

what laboratory analysis would discover or being partially deducible from other sources.

(1) Ambient background and interaction measurements:
  (*a*) Plasma probe
  (*b*) dc magnetometer and gradiometer
  (*c*) ac magnetometer
  (*d*) Plasma wave detector
  (*e*) Dust (micrometeoroid) detector
  (*f*) Cosmic-ray telescope*
  (*g*) Gravity gradiometer
(2) Asteroid observation:
  (*a*) Imaging telescope (TV)
  (*b*) IR, UV, and visible spectrophotometers
  (*c*) Photopolarimeter
(3) Gas envelope detection:
  (*a*) Low-energy plasma analyzer
  (*b*) Ion mass spectrometer*
(4) Surface examination:
  (*a*) Surface scraper
  (*b*) Seismic detector, possibly with "thumper"
  (*c*) α-Scattering analyzer*
(5) Surface observation: Imaging telescope (TV), as in function (2)
(6) On-site ambient environment detection: same as function (1)
(7) Sample acquisition:
  (*a*) Loose matter collector
  (*b*) Core borer

The scientific value of the mission would be enhanced if certain instruments were left on the surface together with the communication system required for telemetering their data to Earth. The weight of the devices left behind would be taken up, in part, by the collected samples. Detached instruments would include those for functions (1) and (5) plus the low-energy plasma analyzer (function (3)) and the seismic detector (function (4)). However, extended autonomous operation of a telemetry system and its power source on the asteroid with communication distance to Earth in excess of 2 AU involves technical problems not considered within the scope of this paper.

MISSION PROFILE

Trajectories, performance characteristics, and payload capabilities for one-way and round-trip missions to Eros have been investigated by Friedlander, Mascy, Niehoff, and others (Friedlander and Vickers, 1964; IIT Research Institute, 1964; Mascy and Niehoff[2]) for both ballistic and low-thrust

[2]See p. 513.

propelled vehicles. Figure 1 shows representative outbound and inbound trajectories of a 1050 day round-trip mission with a 50 day stopover at Eros for the 1977 launch opportunity, based on data obtained by Mascy.[3] The mission uses solar electric propulsion both ways, with thrust characteristics and thrust pointing angles optimized to return a maximum amount of asteroid sample material to Earth. The vehicle is launched by a Titan IIID/Burner II booster and uses 10 kW of initial propulsive power at Earth departure. Low thrust is applied continuously during the outbound phase such that the vehicle arrives at Eros with zero relative velocity v_∞ and can land on the asteroid with almost no additional propulsive effort. Similarly, low thrust is applied continuously during the return trip to reduce the approach velocity on returning to Earth and the required Earth capture maneuver. We assume that the sample-return capsule carried by the interplanetary bus vehicle will be inserted into an eccentric Earth parking orbit for subsequent retrieval by orbital shuttle or by a deorbit maneuver, atmospheric entry, and parachute landing. This mission profile is shown schematically in figure 2 and is used as a basis for defining the vehicle design features and operational characteristics to be discussed below.

We note in figure 1 that the outbound trajectory departing from Earth on February 25, 1977, swings in a wide arc to an aphelion distance of 1.67 AU to achieve the desired velocity matching with the target at the encounter date of July 10, 1978, near perihelion. A gradual plane change necessary to attain the 10°.8 orbital inclination of Eros is included in the outbound propulsion phase.

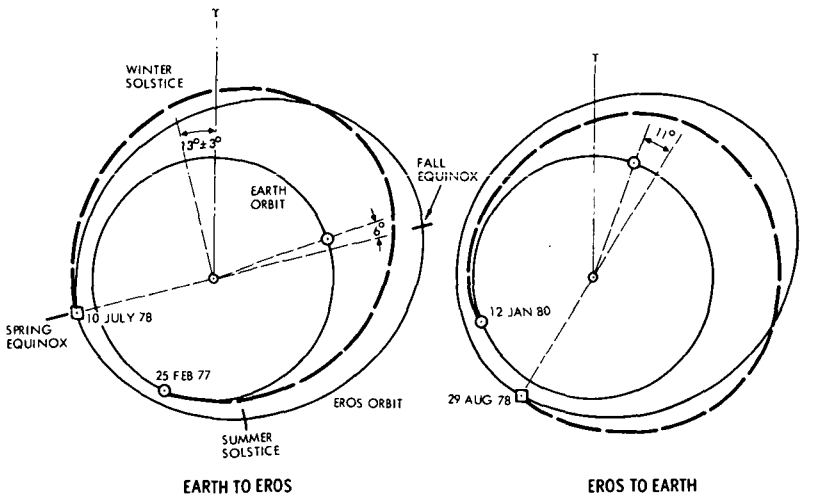

Figure 1.—Eros round-trip trajectory.

[3]Specific data used in this article are based on work by Mascy and Niehoff and are essentially in agreement with data published in their paper in this volume on p. 513.

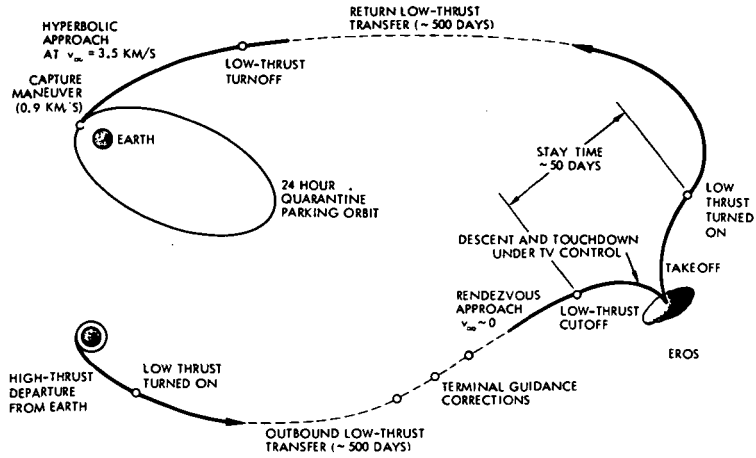

Figure 2.–Eros round-trip mission profile (schematic).

The return trip departing Eros on August 29, 1978, and arriving at Earth on January 12, 1980, has similar characteristics. Mission opportunities with comparable characteristics occur about every 2 yr. 1977, 1979, and 1981 are favorable mission years (Mascy and Niehoff[4]).

A characteristic feature of this class of mission profiles is the large communication range to Earth (2.1 AU) and the fact that Earth and Eros are in almost exact opposition at encounter. These conditions do not change much during the 50 day stopover because Earth and Eros move nearly at the same rate. In the reference trajectory, the arrival at Eros occurs a short time after syzygy. Communication blackout must be avoided during this critical part of the mission. The Earth-Sun separation angle subtended at Eros is initially 3°. This gives a margin of only 1° from the blackout zone, 2° on both sides of the solar disk, which is assumed under conditions of average solar activity. Actually, because during the late 1970's solar activity will be increasing toward a maximum level, a larger margin than 1° would be desirable. The separation angle increases to 5°.5 during the 50 day stopover. Therefore, a 20-day delay in arrival will increase the margin by 1°. This can be achieved with only a minor change in payload performance owing to the flexibility of low-thrust missions, as shown by Mascy.[5] A delay in arrival date is also desirable to improve seasonal conditions at the preferred polar site as discussed below.

ADVANTAGES OF USING ELECTRIC PROPULSION

Several major performance advantages accrue in this mission from the use of electric propulsion. The first, and by far the most important one, is the large

[4]See p. 522.
[5]See p. 525.

reduction of propellant mass due to the high specific impulse at which electric thrustors operate compared to chemical rockets. Typically, the difference in specific impulse is one order of magnitude. To carry a specified amount of payload mass on a trip requiring a major propulsive maneuver away from Earth, as in a rendezvous mission, a spacecraft using electric propulsion is launched with an initial mass two to three times smaller than a corresponding chemically propelled spacecraft. This permits the use of a smaller, less costly booster. Conversely, given the same booster size, the electrically propelled vehicle carries a much larger payload than the chemically propelled one.

Second, out-of-plane maneuvers for a change of orbit inclination or nodal points can be accomplished at a modest extra propellant cost along with the primary in-plane maneuver necessary to achieve the desired aphelion, perihelion, or matching of the target velocity. Changes in mission profile, launch windows, and trip times involve smaller weight penalties than in ballistic missions, essentially as a result of the flexibility in three-dimensional orbit geometry.

Third, the extended thrust phase permits a continuous correction of guidance errors at practically no extra propellant expenditure, simply through deflection of the thrust vector from its nominal orientation. In a rendezvous mission with a target of poorly defined ephemeris such as a small asteroid, low-thrust terminal corrections can be made after the target is acquired by an onboard optical sensor.

Finally, the prolonged low-velocity approach to the target permits extended visual observation and reconnaissance via TV link, the selection of an appropriate landing zone by ground control, and final corrections for obstacle avoidance. The ability to hover for an extended period over the landing site at an altitude where the small electric thrust is sufficient to balance the small local gravity is particularly desirable in view of the very time-consuming round-trip signal transmission process (35 to 40 min). In this context, the ability to transmit video images at high bit rates, using the excess solar electric power not needed for thrust purposes at this time, is a major asset in landing on an entirely unknown target body.

LANDING SITE SELECTION

Eros is an elongated body with dimensions estimated to be 35 by 16 by 7 km; it rotates around the axis of its shortest dimension at a rate of one revolution per 5.27 hr. By landing at or near one of the poles as illustrated in figure 3, appreciable relative terrain motions in circumferential and radial direction are avoided. Other major advantages in selecting a polar landing site are these:

(1) The local gravity is greater than at the tips of the elongated body and centrifugal effects are minimized, hence the tendency to bounce off after landing is reduced (Staley, 1970).

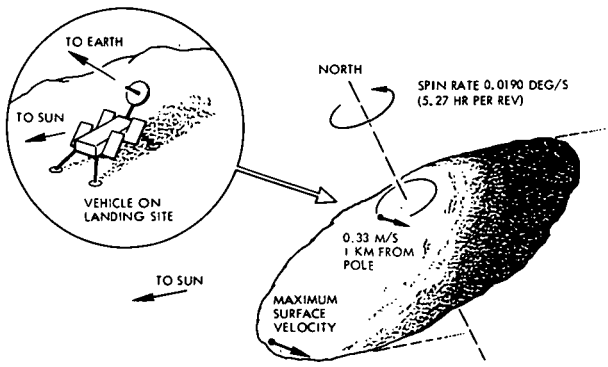

Figure 3.–Landing site selection on rotating small asteroid; assumed dimensions: 35 by 16 by 7 km. The body has the following estimated surface motion characteristics: maximum horizontal velocity = 5.8 m/s, maximum radial velocity = 1.6 m/s, maximum radial excursion = 9.5 km. The effective accelerations (cm/s^2) at the tip of the cigar-shaped body are the following (Staley, 1970): gravity, 0.264; centripetal, 0.192; downward, 0.072.

(2) For the same reason, sample material to be picked up at the landing site includes meteoroids that cannot collect at points of lower effective gravity.
(3) Day/night cycles are avoided by landing in a Sun-illuminated polar area. This simplifies power generation and minimizes thermal design problems.
(4) Uninterrupted communication with Earth is facilitated, as will be discussed below.
(5) The polar area provides greater visual contrast of surface features and smaller contrast fluctuation during the daily revolution than other areas, particularly at the time of arrival. This assists landing point selection and obstacle avoidance.

Present best estimates of the polar axis orientation of Eros are given by Vesely[6] as 13° ± 3° in longitude and 28° ± 1° in latitude relative to the ecliptic. (Earlier estimates gave the same mean values but included uncertainties of about ±25°). This information enables us to select in advance the polar region best suited for landing, given the reference trajectory shown previously in figure 1. The trajectory plot indicates the position of equinoxes and solstices of Eros derived from the estimated mean polar axis orientation. We note that the nominal arrival date of July 10, 1978, practically coincides with the estimated time of the asteroid's vernal equinox. This timing is quite unfavorable for a polar landing because of the uncertain illumination of the landing site, marginal availability of solar electric power, and marginal Earth

[6]See p. 133.

visibility for downlink telemetry. However, with time elapsing after equinox landing, conditions in the north polar region become favorable as the terminator recedes and the shadow-free area around the pole spreads out. Therefore, the vicinity of the north pole is clearly the preferred landing area.

A 20 day delay in arrival, previously suggested for improvement of the Earth-Sun separation angle, would allow the subsolar point to move about 18° north of the equator. This assures adequate illumination of the polar region, with 18° elevation of the Sun, and adequate downlink capability with 21° elevation of Earth above the horizon. At a 2 to 3 km distance from the pole these conditions are still approximately valid because of the very pronounced flattening of the figure of Eros. This is illustrated in figure 4 by contours of the shadow-free area around the pole at three dates past equinox, with the subpolar point 10°, 20°, and 30° north of the equator.

The uncertainty in the actual pole orientation of Eros requires a conservative landing date selection with a postequinox time margin of at least 2 to 3 weeks. There is even the possibility of postponing the landing maneuver for several weeks if necessary after arrival, and using the time interval for exploration of ambient conditions and remote observation of surface features. Electric propulsion provides easy and inexpensive maneuverability during this exploration phase. A particularly valuable task would be to monitor physical properties of the asteroid from a stationary position and to detect periodic variations with the changing relative orientation of the rotating asteroid body. This can be accomplished most effectively by hovering at a station close to the asteroid's equatorial plane. Comprehensive imaging of a large portion of the asteroid's body can thus be obtained. Certain quantities, e.g., magnetic field strength, solar-wind direction, or gravity gradient, might display repetitive

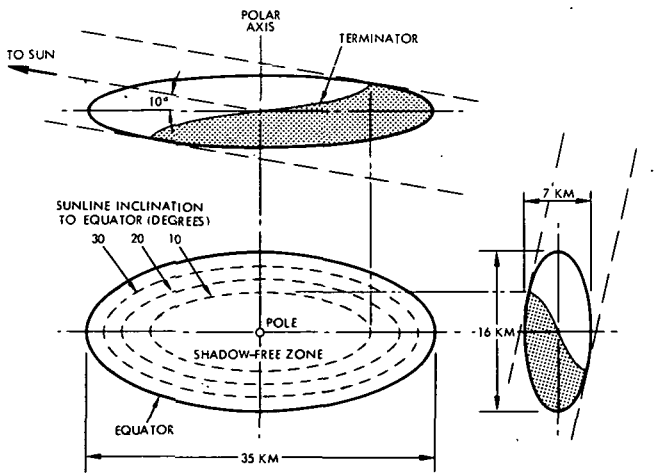

Figure 4.–Lighting geometry on ellipsoidal asteroid with assumed dimensions of Eros.

signal patterns containing harmonics of the asteroid's rotational frequency. These would indicate the presence and approximate locations of magnetic and gravitational inhomogeneities.

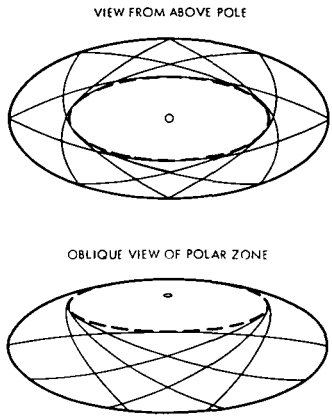

Figure 5.–Delineation of polar region by successive terminators.

Visual identification of the pole prior to selecting the site is a reasonably simple task using the polar illumination characteristics explained above. The spacecraft is targeted to arrive at a position from where it can observe the north polar region. An extended hover period lasting from one to several revolutions of the asteroid, with low thrust used for position control, is sufficient to obtain a sequence of TV images that permit reconstruction of the shadow-free envelope. The envelope is formed by successive terminator lines as illustrated in figure 5. The pole can be readily determined as the centroid of the shadow-free zone. Irregularities of the terrain can also be detected conveniently by this technique. Landmarks at the pole identified by contrasting features serve as a guide for the subsequent descent and landing phase.

FLIGHT SEQUENCE

Major events of the flight sequence were previously illustrated in figure 2. The vehicle is launched from the Eastern Test Range on a near-easterly azimuth and injected into an escape trajectory at a hyperbolic excess velocity of 3 km/s. After booster separation, the solar array paddles are deployed and the vehicle assumes cruise attitude with the Sun and a selected reference star providing three-axis orientation. The electric thrustors operate continuously during the 500 day transfer phase to Eros to provide the necessary velocity increment for a zero-velocity rendezvous. The thrust is oriented in forward direction approximately at right angles to the sunline with an out-of-plane component added to attain Eros' orbit inclination of 10°.8.

Guidance corrections are carried out by thrust angle adjustments on command from the Deep Space Instrumentation Facility (DSIF) ground station, which supports the mission by intermittent tracking and orbit determination. Typical guidance accuracies of 1000 to 3000 km relative to Earth coordinates are achievable; however, the uncertainty of the asteroid ephemeris, estimated to be at least 5000 km, necessitates the use of onboard terminal guidance sensors. An optical technique will be used that determines the orientation of the target line of sight relative to selected reference stars. Repeated fixes taken during the final 50 to 100 days before encounter permit updating the relative trajectory and performing terminal guidance corrections. A terminal guidance accuracy of 100 to 200 km can thus be achieved.

The transfer trajectory is aimed at a point located about 50 nominal asteroid radii (400 km) above the north polar region. The terminal approach and descent phase includes several extended hover intervals to permit observation by scientific instruments and reconnaissance by ground control via TV link. The descent sequence is illustrated in figure 6. As previously discussed, the initial approach might also include a hover period of several days for observation near the equator (not shown in the diagram).

The first hover phase at 400 km altitude is used to determine the pole position of the rotating asteroid from a sequence of TV frames. The vehicle then descends to a second hover position about 25 km above the pole, from which a higher resolution image of the pole region can be obtained. A preferred landing area can be selected at this time.

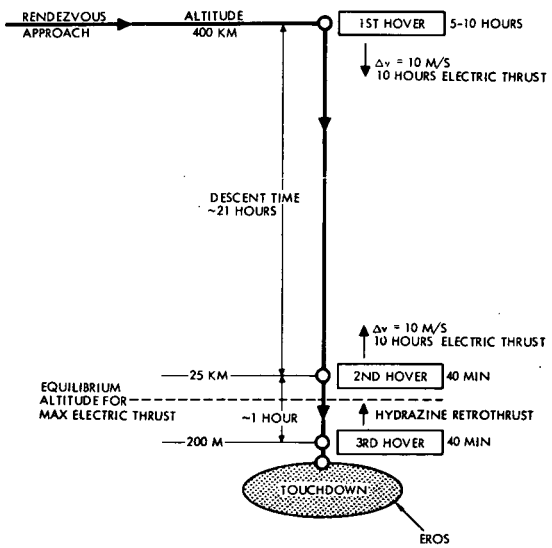

Figure 6.–Terminal approach and descent phases. Total descent time is 28 to 33 hr. A hover period of several days near the equator could also be included during the approach (as discussed in text).

Electric thrust is sufficient to hold the vehicle in stationary position against the small local gravity during hover phases 1 and 2. A set of small hydrazine rockets provides acceleration and deceleration on descent from hover position 2 to position 3.

At hover position 3, located 200 m above the terrain, a final check of the landing site is made to take corrective action for obstacle avoidance, if necessary. This 40 min hover phase requires use of the hydrazine rockets in an intermittent thrust mode. The final descent to touchdown ends in a free fall from about 50 m altitude, resulting in an impact velocity of about 0.7 m/s based on an assumed gravity acceleration of 0.5 cm/s^2.

Autonomous control of the descent phase velocity profile from an altitude of about 10 km is achieved by means of a radar altimeter and a three-beam Doppler radar system that operates in a manner similar to the Apollo lunar module landing radar. The threshold velocity detectable by this system is 1.5 m/s. The descent is in nearly vertical direction, which simplifies the onboard computation of velocity and attitude corrections. In addition to the radar system, the vehicle uses a vertical attitude gyro as a redundant attitude control reference.

The solar array is designed for retraction by the rollup storage mechanism. After completion of the final electric thrust operation, about 2 hr prior to landing, the solar array is retracted for protection against dynamic loads at impact but with a sufficient portion of array paddles protruding to provide about 200 W to operate housekeeping systems and the landing radar.

The liftoff and return flight sequence will not be discussed in detail. In principle, this sequence is a reversal of the outbound transfer but with the approach guidance to Earth made simpler by the absence of target ephemeris uncertainty and by the availability of a DSIF station on the ground.

VEHICLE CONFIGURATION AND DESIGN CHARACTERISTICS

Conceptual configurations of the solar electric spacecraft during cruise and after landing are shown in figure 7. The vehicle consists of a center structure that houses the electric-propulsion module, engineering subsystems, scientific instruments, sample collection tools, and the sample-return capsule. Attached to the center body are two pairs of lightweight solar array paddles that are deployed from storage drums in window-shade fashion by means of extendable tubular booms. The flexible landing gear consists of four legs having footpads lined with crushable material for absorbing impact energy as in the Surveyor spacecraft. Spring-released anchoring devices, not shown in the sketch, are used to secure the vehicle's position after touchdown under the extremely small surface gravity of Eros. This configuration is derived from an earlier solar electric spacecraft design study (TRW, Inc., 1970).

The electric-propulsion module, mounted opposite the payload bay, is shown in greater detail in figure 8. It consists of electric power conditioning units (PCU's), an array of electron-bombardment mercury ion thrustors

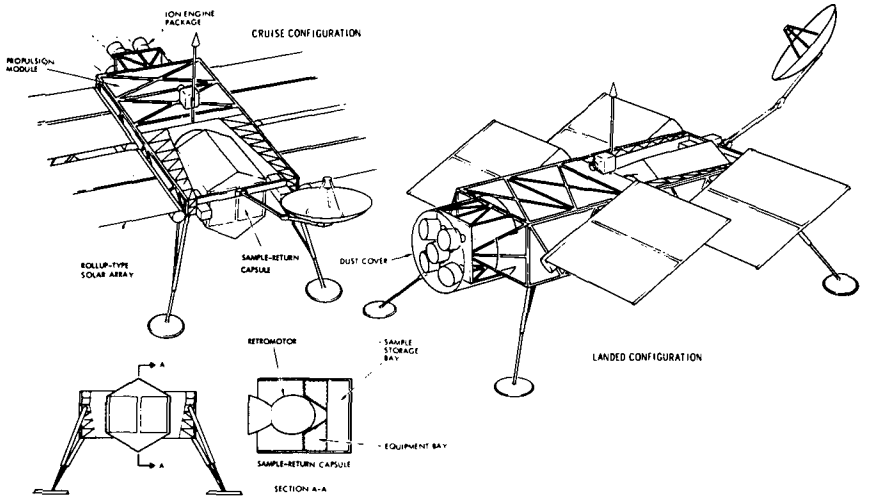

Figure 7.–Solar electric bus vehicle in cruise and landed configurations.

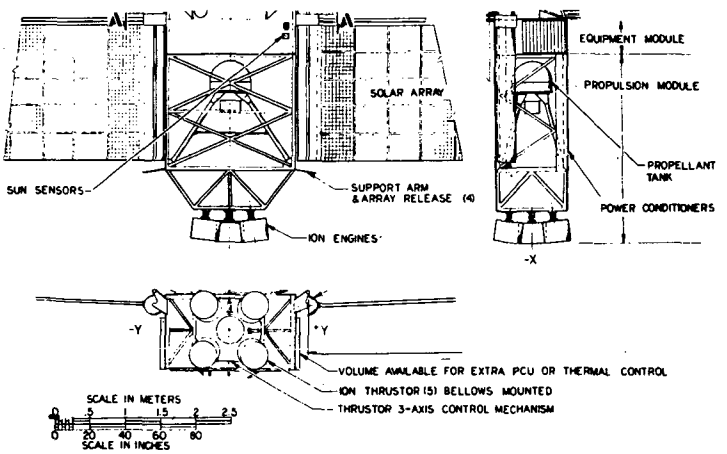

Figure 8.–Electric-propulsion module.

mounted on a flexible support fixture for thrust vector control, a propellant tank, and a feed system. The high density of the mercury propellant permits storage of a 750 kg propellant load in a 0.5 m diameter compact spherical tank located near the vehicle's center of mass. This minimizes the change of mass distribution and its effect on attitude control during cruise and landing. Five ion thrustors are provided, only two of which are normally in use during the outbound and inbound transfer phases. The three remaining thrustors serve as standby units to assure a high system reliability in a mission that requires a

total thrust time of 1000 days. The delicate thrustor system uses a shroud for protection against dust stirred up during touchdown and surface operations. Dust covers must also be provided for the apertures of optical and other sensors.

The rollout solar array with each paddle measuring 2 by 14 m when fully extended provides 12 kW of initial power at 1 AU, 10 kW of which is used to operate the electric-propulsion system. The remaining power is used for housekeeping and telemetry and includes a 10 percent margin against contingencies such as solar array performance degradation due to solar flares. Prior to landing, the paddles are retracted for protection against the landing impact and flying dust. Subsequently, small paddle segments are extended to generate power of about 400 W for surface operations, housekeeping, and high-data-rate telemetry of TV pictures. After takeoff from Eros, the array is again fully extended for the return cruise.

As shown in the design illustration, the four solar paddles can be rotated around their deployment booms to improve array illumination primarily during the approach, descent, and hover phases, and after landing. During the transfer phase, small changes in solar array orientation relative to the center body are useful but not required, permitting an additional degree of freedom for optimum thrust vector pointing. During the landed phase, array reorientation may be required to accommodate changes in Sun elevation. By splitting the array into four narrow paddles instead of two, field-of-view obscuration of the optical sensors and the high-gain antenna due to paddle reorientation can be avoided.

These deployment and orientation sequences are compatible with design specifications of the rollout array shown in the design illustrated. A full-scale 2.5 kW engineering model of this array design has been developed for NASA by General Electric and has successfully completed extensive electrical, thermal, and mechanical tests in the laboratory.

A set of four differentially throttlable hydrazine thrustors, each with a maximum thrust level of 4 N (1 lb), are centrally mounted on the underside of the center body. They provide thrust required during the descent and ascent phase and support the vehicle during the extended final hover phase prior to touchdown. With an assumed small surface gravity of 0.5 cm/s^2, the total hydrazine propellant consumption for a 40 min hover period is 16 kg for a vehicle of 1400 kg gross mass. The total maneuver sequence performed by the hydrazine thrustors requires about 40 kg of propellant, equivalent to 60 m/s of Δv expenditure.

A variety of optical sensors are required to control vehicle operations on approach to the asteroid, during the final descent phase, during landed operations, and during ascent. The use of a TV system is required both for the vehicle control operations and the scientific observations that follow:

(1) Approach guidance
(2) Reconnaissance and landing site selection

(3) Obstacle avoidance by command control from Earth
(4) Remote manipulation on the surface under TV monitoring
(5) Surface panoramic view and detail feature observation

These operations will require wide-angle and narrow-angle, high-resolution TV image systems. Three or more separate TV systems mounted on two-axis gimbal platforms with different and overlapping fields of view are envisioned. For landing site inspection and selection an image system with at least 0.0014° resolution will be required comparable to the planetary image system of the TOPS spacecraft.

The attitude reference sensors include fixed, fine and coarse, Sun sensors, and a one-axis gimbaled star sensor that uses an electronic image scanning principle similar to the Mariner star tracker. This device permits use of alternate reference stars that come into view at different times in the mission and can be tracked without interference by the long solar array paddles and other deployed appendages (Meissinger and Benson, 1970). An additional optical sensor is required for locking the high-resolution TV camera on the asteroid during the approach and hover phases when successive TV frames of the polar area must be taken for determining the location of the pole and selecting a landing site.

The communication system operates on S-band and uses design principles developed for and successfully used on Pioneer spacecraft. The 2.4 m diameter parabolic high-gain antenna dish is mounted on a hinged deployment arm that permits Earth pointing in all directions relative to the vehicle body without obstruction by other deployed appendages, using a two-axis rotation joint. The same deployed configuration is used during cruise and landed operations. In addition to the high-gain antenna, a pair of omniantennas is provided, one on each side of the center body, to maintain an uplink command capability in all vehicle attitudes.

A 100 W solid-state transmitter composed of four parallel 25 W channels provides incremental power options desirable for flexible use of the telemetry system. Low telemetry power and bit rates are used at times when power is needed primarily for propulsion purposes. High bit rates are available for telemetry of TV images during critical mission phases. Table I lists representative bit rates and communication intervals per TV frame at 2.1 AU communication range for 25 and 100 W of transmitter power with ground coverage by 25.9 and 64.0 m DSIF antennas. The effect of TV image data compression by a 2:1 ratio is also shown. The unprocessed TV image is assumed to contain 2.5×10^6 bits. Bit rates of 4096 bps are available for telemetry to the 25.9 m ground station and 65 536 bps to the 64.0 m ground station using 100 W of transmitter power. This corresponds to telemetry intervals of 610 and 38 s per TV frame without data compression and to 305 and 19 s with data compression, respectively. The lower time intervals are quite small compared to the 17.5 min one-way transmission time delay from Eros. A principal advantage of the electric spacecraft is the ability to meet high data

TABLE I.–*Eros-to-Earth Communication Data Rates*

Downlink option		Data rate, bps	Single TV frame transmission time, s	
Transmitter power, W	DSIF antenna, m		Unprocessed data	With 2:1 data compression
25	25.9	1 024	2440	1220
100	25.9	4 096	610	305
25	64.0	16 384	152	76
100	64.0	65 536	38	19

Average communication range during stopover: 2.1 AU; S-band telemetry; 2.4 m spacecraft antenna; TV frame contains 2.5×10^6 bits (unprocessed).

rate requirements without demanding coverage by the 64.0 m DSIF station, owing to the large unused power capacity available for telemetry during critical mission events.

The following list is a summary of system characteristics based on performance data from Mascy and Niehoff:[7]

(1) Launch vehicle: Titan IIID/Burner II
(2) Launch date: February 25, 1977
(3) Arrival at Eros: July 10, 1978
(4) Return to Earth: January 12, 1980
(5) Round-trip time: 1050 days
(6) Stay time: 50 days
(7) Propulsion power at 1 AU: 10 kW
(8) Mercury ion thrustors: five (two plus three spares)
(9) Specific impulse I_{sp}: 3000 s
(10) Peak power to thrustor: 4.6 kW
(11) Maximum thrust force per thrustor: 0.214 N (48 mlb)

Mass estimates of the electric bus vehicle and the sample-return capsule, also based on the performance data of Mascy and Niehoff, are given in table II. By holding the return sample mass to 100 kg, a 10 kW bus vehicle launched by Titan IIID/Burner II has adequate performance margin. A much larger sample mass of 200 to 300 kg can be returned by using a higher powered bus vehicle (15 kW), which would require the more costly Titan IIID/Centaur booster.

We conclude this discussion with a chart (fig. 9) showing the current status of critical subsystems that are required to develop the electric bus vehicle for this mission. In all categories except the solar array, a first generation subsystem with adequate performance to achieve the mission has been flight proven and would be ready for application to the system. Technology

[7]See p. 524.

TABLE II.–*Mass Estimates*

System	Mass, kg
Vehicle:	
Earth departure	1760
Eros arrival	1415
Earth approach	1000
Sample-return capsule in Earth orbit	380
Sample material	100
System breakdown:	
Bus vehicle plus capsule at Earth departure:	
Solar electric propulsion	300
Low-thrust propellant	520
Hydrazine propellant	40
Structure and subsystems	420
Science instruments	200
Return capsule (includes retropropellant, no sample)	280
Total	1760
Capsule (including sample):	
Structure and mechanisms	60
Subsystems and sample storage	120
Retropropellant	100
Sample material	100
Total:	
Before retro	380
After retro	280

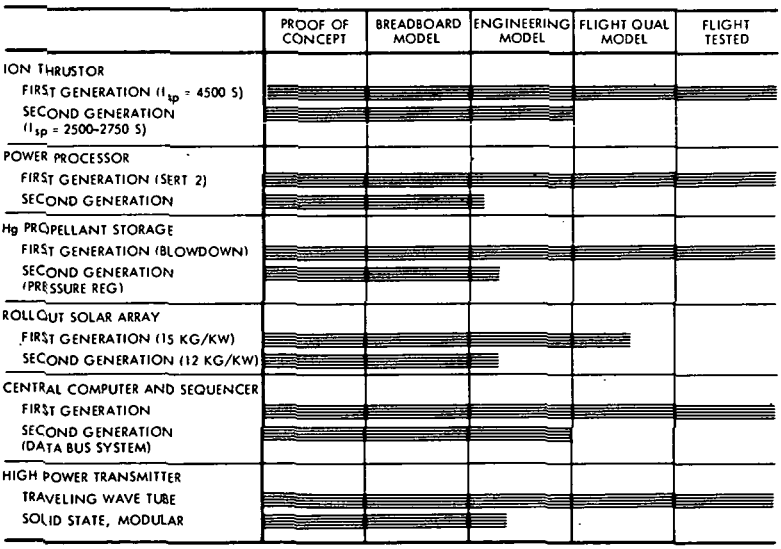

Figure 9.–Technology status of critical subsystems as of January 1971.

improvements obtainable from second generation subsystems will add performance gains that are, however, not critical to mission accomplishment. As seen in the chart, the improved subsystems are well along in their development toward flight application.

CONCLUSION

Preliminary analysis and conceptual design study of a solar electric bus vehicle for an Eros sample-return mission show that no major obstacle exists today in terms of technical feasibility, design approach, and operational concepts to early adoption of a program aimed at exploring nearby asteroids such as Eros and returning soil samples. Solar electric propulsion provides basic advantages in payload capacity, mission flexibility, and operational convenience needed to make such a mission more cost effective, more reliable, and more exciting from a scientific exploration standpoint. However, more detailed study of vehicle design, mission implementation, mission timing, performance tradeoffs, and cost factors are required to further substantiate these predictions. It appears that even with an early start of such a program it would not be realistic to expect to meet a launch date prior to the 1977 opportunity. Subsequent launch opportunities for Eros sample-return missions occur about every 2 yr. These opportunities as well as missions to other nearby asteroids require further study.

REFERENCES

Alfvén, H., and Arrhenius, G. 1970*a*, Structure and Evolutionary History of the Solar System. I. Astrophys. Space Sci. 8(3), 338-421. Structure and Evolutionary History of the Solar System. II. Astrophys. Space Sci. 9(1), 3-33.

Alfvén, H., and Arrhenius, G. 1970*b*, Mission to an Asteroid. Science **167**, 139-141.

Friedlander, A. L., and Vickers, R. S. 1964, A Survey of Missions to the Asteroids. IIT Res. Inst. Rept. M-3.

IIT Research Institute. 1964, Digest Report–Missions to the Asteroids.

Meissinger, H. F., and Benson, R. A. 1970, Design Characteristics of Solar Electric Spacecraft for Multiple Interplanetary Missions. AIAA paper 70-645 presented at AIAA 6th Propulsion Joint Specialist Conference (San Diego), June 15-19.

Öhman, Y. 1963, The Asteroids as Possible Research Objects for Future ESRO Missions. Copers LPSC 89. European Preparatory Commission for Space Research; Landing Programmes Subcommittee.

Staley, D. O. 1970, Man on an Asteroid. J. Geophys. Res. 75(28), 5571-5573.

TRW, Inc. 1970, Study of a Solar Electric Multi-Mission Spacecraft. Final Summary Tech. Rept. (revised). TRW document 09451-6001-R0-03.

POTENTIALS OF ASTEROID SPACE MISSIONS

A. BRATENAHL
Jet Propulsion Laboratory

There is an important relation between the development of solar electric spacecraft and the possible inclusion within the space program of new missions devoted primarily to asteroid investigations. The notion that space missions to asteroids have a high potential to return critically needed data will be illustrated in some detail.

One might wonder why there is so much material on solar electric spacecraft at an asteroid colloquium. For 2 yr, independent teams have been working on feasibility studies and preliminary plans for solar electric spacecraft. For the studies to be realistic, it is necessary to consider the missions on which these hypothetical spacecraft might be flown, and this is discussed, for example, in the previous papers in this session. In addition to missions, the scientific objectives must also be considered to bring into evidence the varieties of data to be acquired and thereby define the science instrument payload in some detail.

All this activity has produced several kinds of results. We now have an understanding of technique and possible science return for several kinds of asteroid missions. The space science planners find a growing awareness that the asteroid exploration may provide a rich storehouse of clues as to the origin of the solar system. There is now a real possibility that some of these missions will become a reality.

The present studies represent the final stage in the 10 yr technological development of solar electric spacecraft. (See Stuhlinger, in this volume.[1]) The next step, if this 10 yr history, representing a sizable investment in technology, is to continue, is to put this technical knowledge into practice. If this happens, and if at the same time interest within what might be called the asteroid sector of the scientific community is sufficiently high, solar electric spacecraft will be built and asteroid missions will be among those on which they will be flown.

In spite of the vast amount of facts known, it is not hard to find critically important knowledge gaps, weaknesses, and ambiguities that seriously hinder theoretical progress. The following is a partial list of knowledge gaps and

---

[1]See p. 489.

insecure facts that could be cleared up by a multiple asteroid flyby mission, such as that discussed by Brooks and Hampshire:[2]

(1) Asteroid size, shape, albedo, distribution of surface reflectance, phase function for angles up to 90°, surface composition by reflectance spectroscopy (McCord, Adams, and Johnson, 1970; Chapman, Johnson, and McCord[3]) for selected bodies down to absolute magnitude 14.5, surface temperature (in support of the work of Allen[4]), and mass of larger asteroids (Anderson[5])
(2) The existence and nature of the small-body population, down to micrometeoroids, including orbital characteristics, cumulative space density including possible fine structures such as jetstreams (many papers on this latter subject are presented in this colloquium), the population index, and possibly the particle mass density and composition
(3) Facts relating to the space distribution of the particles giving rise to the zodiacal light

I should note that Pioneers F and G, bound for Jupiter in 1972 and 1973, will be the first spacecraft to gather data in the asteroid belt.

I should like now to go into more detail regarding how the objectives previously mentioned might be achieved, illustrating this particularly with the use of television. I have made no attempt to optimize television equipment; I am merely examining what the planned Mariner Venus-Mercury television system could accomplish on an asteroid mission. Figure 1 is a composite of two graphs. The inner rectangle has been adapted from a portion of figure 6 in the report of the Palomar-Leiden survey of faint minor planets (van Houten et al., 1970). In the plot of the log of the number per half-magnitude interval against absolute magnitude of the asteroids in the distance group 2.6 to 3.0 AU, the circles are the Palomar-Leiden results and the x's are the older McDonald survey results. Note particularly the break in the curve from about 11 to a little over 12 in magnitude. The outer rectangle is miss distance b versus diameter d, both in kilometers. The abscissa of the two graphs are matched, assuming an asteroid albedo of 0.16. The symbol appearing in the lower center is not the letter L, but is an indicator of how far the inner graph would move to the right and the diagonal lines would move upward if the albedo were 0.10, a more favorable situation. The diagonals represent lines of constant angular disk size corresponding to asteroid diameters and miss distance. The camera and optics chosen for this discussion have a field of view of 1°.1 by 1°.4, and the format is a frame with 700 by 832 pixel, or image, elements. A reasonable accuracy requires 10 pixel elements. In the number pairs on the diagonal lines, the first

[2]See p. 527.
[3]See p. 51.
[4]See p. 41.
[5]See p. 577.

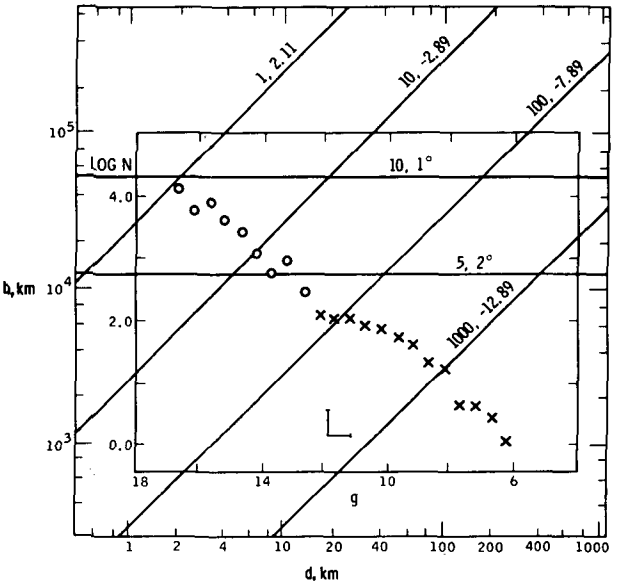

Figure 1.–Relations governing applicability of television to asteroid flyby missions.

is the number of pixel elements across the diameter, and the second is the apparent magnitude as seen by the camera. Thus, the practical limit of 10 pixel elements corresponds to an apparent magnitude of −2.89. The horizontal lines concern the passage of the asteroid past the spacecraft: The first number in the number pair is the velocity in kilometers per second and the second number is the angular rate in degrees per minute. The television camera and other equipment can be mounted on a scan platform that is controlled by a star tracker. The practical upper limit for the scan rate of the platform and cameras for accurate pointing lies somewhere between these two lines.

A study of figure 1 shows that it is possible to make adequate disk measurements of asteroids lying on both sides of the interesting break in the distribution curve. Judging by the magnitudes in this range of usefulness, it seems entirely possible to obtain reflectance spectra of the type that Chapman and McCord get for asteroids in this range. The same is true of other optical measurements, including infrared radiometry and zodiacal light photopolarimetry. The small-particle sensors are discussed by Kinard and O'Neal[6] and Soberman, Neste, and Petty[7] for Pioneers F and G. On an asteroid mission, these may be considerably enlarged. There are also other types of small-particle sensors such as the one described by Berg and Richardson (1969), which is an impact detector to determine velocity, energy, and direction. There are

[6]See p. 607.
[7]See p. 617.

promising instruments, in the breadboard stage of development, to determine composition by time-of-flight mass spectroscopy (Grün, 1970; Roy and Becker, 1970).

The small-particle population can provide diagnostic evidence for phenomena currently going on in the asteroid belt, as well as data on hazards to spacecraft. To facilitate this discussion, figure 2 represents a model synthesized by Kessler (1970, and in this volume[8]). It is assumed here that the small particles and subvisual asteroid population can be represented by a power-law spectrum in mass in which N is the cumulative space density per cubic meter and the exponent is 0.84. The curve at the high-mass end represents the contribution of visual asteroids and the low-mass cutoff is at 10^{-9} g. Also shown is Kessler's model of the cometary meteoroid population. The horizontal bars represent the range of practical applicability of various instruments and techniques.

The power-law exponent can provide clues to the collisional and possibly accretive processes currently taking place (Dohnanyi, 1969, and in this volume;[9] Hellyer, 1970; Piotrowski, 1953). The small-particle cutoff yields information on the interaction of particles to radiation, presumably the Poynting-Robertson effect. It is evident that the sensors have a capability of determining both the small-particle cutoff and the power-law exponent, if a particle population of this nature exists. Moreover, data may be obtained regarding jetstreams, the subject appearing in several titles in this colloquium.

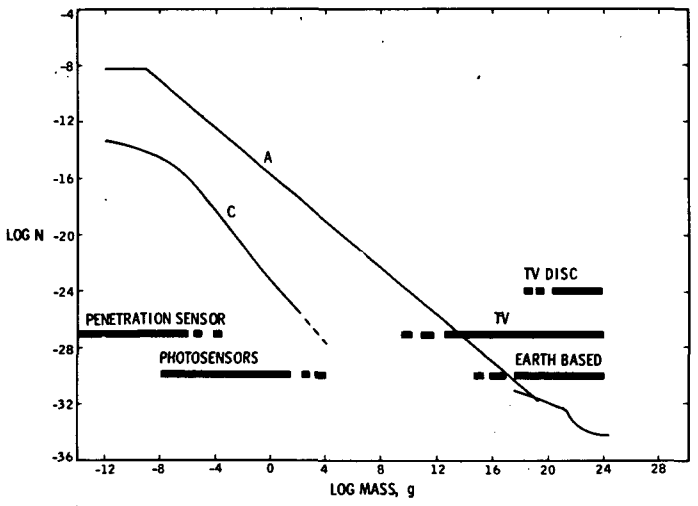

Figure 2.–Kessler model. Cumulative space density in ecliptic plane at 2.5 AU. Curve A, asteroid population; curve C, cometary population.

[8]See p. 595.
[9]See p. 263.

Of course, cometary meteor streams are well known, and these are also accessible to the sensors.

The curves in figure 2 apply to points in space in the ecliptic plane at the solar distance of 2.5 AU. To obtain similar curves at other points, the Kessler model provides radial and latitude functions by which the curves are simply multiplied. This, of course, assumes that the curves are functionally separable from each other and from possible mass dependence. Kessler's radial curves are particularly interesting in their own right (fig. 3). The asteroid curve *A* is obtained by computer calculation, employing the orbital elements of all numbered asteroids, with correction for observational selection, and represents the sum of the contributions of each asteroid to the local space density. The effect of Jupiter is to concentrate the perihelia close to Jupiter's perihelion. The location of perihelia and aphelia of Earth, Mars, and Eros are shown. Off scale to the right would be Jupiter at 4.95 and 5.25 AU. The effect of the planets in depressing the local space density is noticeable. (See also Williams.[10]) The cometary curve, of course, is not so well known; but to the extent it can be believed, it represents a young population with moderate to large eccentricities, whereas the asteroid curve represents an old population with small eccentricities (Marsden, 1970).

From the point of view of mission analysis, Eros is a prime target for rendezvous, landing, or even sample-return missions (Bender and Bourke;[11] Mascy and Niehoff;[12] Meissinger and Greenstadt[13]) because of its orbital

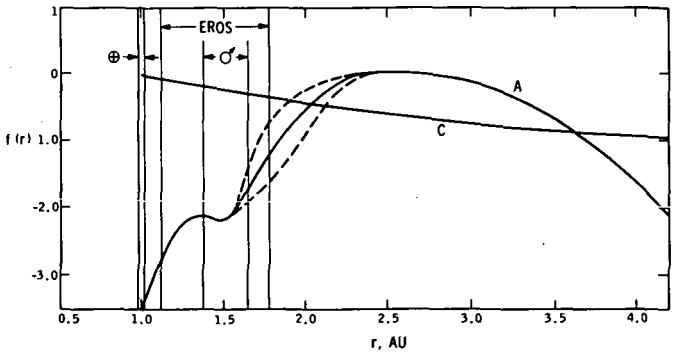

Figure 3.—Kessler model. Asteroid and cometary radial functions. Also shown are regions swept out by Earth, Mars, and Eros. $f(r)$ is the log of the ratio of the asteroid spatial density at distance r to the spatial density at the center of the asteroid belt. Broken lines show the asymmetry of distribution in heliocentric longitude: upper and lower curves correspond to longitudes of Jupiter's perihelion and aphelion, respectively.

[10]See p. 177.
[11]See p. 503.
[12]See p. 513.
[13]See p. 543.

characteristics and low gravity. There is great scientific interest in Eros. Does its shape imply that it is a fragment of a larger parent body? Is it solid iron (Anders, 1964)? Is it a potential source of stony meteorites, in the sense that eventually it will be scattered by Mars into Earth-crossing orbit (Wetherill and Williams, 1968)? Is it, despite its shape, a defunct cometary nucleus with possibly an associated non-Earth-crossing meteoroid stream (Marsden, 1970)? Is it, as Alfvén and Arrhenius suggest (1970*a,b*, and in this volume[14]), a very ancient body and a possible source of primordial grains and gently treated meteoroidal material?

ACKNOWLEDGMENT

This report presents results of one phase of research carried out at the Jet Propulsion Laboratory, California Institute of Technology, under Contract no. NAS7-100.

REFERENCES

Alfvén, H., and Arrhenius, G. 1970*a*, Mission to an Asteroid. Science **167**, 139-141.

Alfvén, H., and Arrhenius, G. 1970*b*, Structure and Evolutionary History of the Solar System, I. Astrophys. Space Sci. **8**, 338-421.

Anders, E. 1964, Origin, Age and Composition of Meteorites. Space Sci. Rev. **3**, 583.

Berg, O. E., and Richardson, F. F. 1969, The Pioneer 8 Cosmic Dust Experiment. Rev. Sci. Instr. **40**, 1333-1337.

Dohnanyi, J. S. 1969, Collisional Model of Asteroids and Their Debris. J. Geophys. Res. **74**(10), 2531-2554.

Grün, E. 1970, Massenspectrometrische Analyse von Ionen beim Aufschlag schneller Staubteilchen. Ph. D. Thesis. Univ. of Heidelberg.

Hellyer, B. 1970, The Fragmentation of the Asteroids. Mon. Notic. Royal Astron. Soc. **148**, 383-390.

Houten, C. J. van, Houten-Groeneveld, I. van, Herget, P., and Gehrels, T. 1970, Palomar-Leiden Survey of Faint Minor Planets. Astron. Astrophys. Suppl. **2**, 339-448.

Kessler, D. J. 1970, Meteoroid Environment Model–1970 (Interplanetary and Planetary). NASA SP-8038.

McCord, T. B., Adams, J. B., and Johnson, T. V. 1970, Asteroid Vesta: Spectral Reflectivity and Compositional Implications. Science **168**, 1445-1447.

Marsden, B. G. 1970, On the Relationship Between Comets and Minor Planets. Astron. J. **75**, 206-217.

Piotrowski, J. 1953, The Collision of Asteroids. Acta Astron. **5**, 115-136.

Roy, N. L., and Becker, D. G. 1970, Design, Fabrication and Test of the Breadboard Unit of the Cosmic Dust Analyzer Experiments. Final rept. NASA contract NAS 9-9309, TRW rept. 10735-6001-RO-00.

Wetherill, G. W., and Williams, J. G. 1968, Evaluation of the Apollo Asteroids as Sources of Stone Meteorites. J. Geophys. Res. **73**, 635-648.

[14]See p. 473.

POSSIBLE MAGNETIC INTERACTION OF ASTEROIDS WITH THE SOLAR WIND

EUGENE W. GREENSTADT
TRW, Inc.

Investigation of extraterrestrial objects is habitually accompanied by the observation of extraterrestrial magnetic fields, which often have significant effects on the solar wind in the vicinity of the objects. Should we be surprised to find this experience repeated at an asteroid?

A recent study considered the conditions that would have to be satisfied by the surface magnetic field of a small planetary body at asteroidal distances so that the field would be an obstacle capable of stopping the solar wind or deflecting it sufficiently to generate a detectable magnetic interaction (Greenstadt, 1971). Meteoritic and lunar data indicate that magnetic field levels associated with material found in, or retrieved from, the extraterrestrial environment are compatible with levels demanded by the limiting conditions for the existence of identifiable magnetospheres around the largest asteroids. The conditions for asteroidal magnetospheres in the region $1 \leqslant r \leqslant 3.5$ AU, as applied to hypothetical spherical bodies of dipole magnetic signature, are summarized below and related to measurements of meteorite magnetizations, fields detected on the lunar surface, and magnetizations of lunar samples.

CONDITIONS FOR MAGNETOSPHERIC TYPE OF INTERACTION

The magnetic field of a small planetary body must fulfill three scaling conditions to maintain a recognizable magnetic cavity from which the solar wind is excluded. First, the magnitude B_s of the stopping field transverse to the solar-wind flow at the upwind interface, or subsolar magnetopause, must be large enough to balance the bulk flow pressure; otherwise, there can be no magnetospheric barrier as we know it. Second, the field must extend at least the order of its own proton gyroradius across the solar-wind flow direction (Shkarofsky, 1965); otherwise, the plasma will be deviated rather than halted; edge-effect instabilities will predominate; the barrier, if any, will be ephemeral; and the field and plasma will intermingle, generating electromagnetic noise in various plasma wavemodes (Bernstein, Ogawa, and Sellen, 1968; Sellen and Bernstein, 1964). Finally, the field must extend upwind from the body a sufficient distance, on the order of the geometric mean of proton and electron

gyroradii, to reverse the solar-wind particles before they intersect the body's surface (Dungey, 1958, p. 143); otherwise, only the body itself will properly constitute a barrier. Figure 1 illustrates these three conditions conceptually.

The conditions just enumerated yield expressions (Greenstadt, 1971) for the stopping field,

$$B_s \cong 9.39 v_{sw} r^{-1} n_1{}^{1/2} \times 10^{-2}\ \gamma$$

the proton radius,

$$p \cong 111 r n_1{}^{-1/2}\ \text{km}$$

and the stopping distance,

$$L \cong 2.595 r n_1{}^{-1/2}\ \text{km}$$

where v_{sw} is the solar-wind velocity in kilometers per second, r is the solar distance in astronomical units, and n_1 is the solar-wind proton number density at $r = 1$ AU, per cubic centimeter. These quantities are plotted in figure 2 for a quiet solar wind with $v_{sw} = 320$ km/s, $n_1 = 5\ \text{cm}^{-3}$. The number distribution of asteroids versus solar distance r is superimposed (Alfvén and Arrhenius, 1970), and the radii and the orbital semimajor axes of several selected asteroids are indicated in the figure. Note that except for Eros, their sizes are comparable to, or larger than, the "quiet" proton gyroradius p.

If a dipolar field is assumed for an asteroid so oriented that the solar-wind velocity v_{sw} is in the plane of the dipole's equator, i.e., the magnetic axis is normal to the solar-wind flow, then the equatorial surface field B_a must exceed the following values to permit the establishment of a magnetosphere:

For the proper minimal upwind stopping distance,

$$B_0 = 9.39 \frac{v_{sw}}{r} n_1{}^{1/2} \left(1 + 2.595 \frac{r}{R n_1{}^{1/2}}\right)^3 10^{-2}\ \gamma \qquad (1)$$

and for an upwind standoff distance and, therefore, a lateral dimension greater than $2p$,

$$B_0 = 10.3 \frac{v_{sw} r^2}{n_1} \frac{1}{R^3} 10^5\ \gamma \qquad (2)$$

where R is the radius of a postulated spherical asteroid, in kilometers. Steps in derivation of expressions (1) and (2) are given by Greenstadt (1971).

Figures 1 and 2 illustrate that for large asteroids, the criterion of adequate lateral dimension is satisfied by the diameter of the body itself, so that the criterion of stopping distance, equation (1), is the important one B_0 must

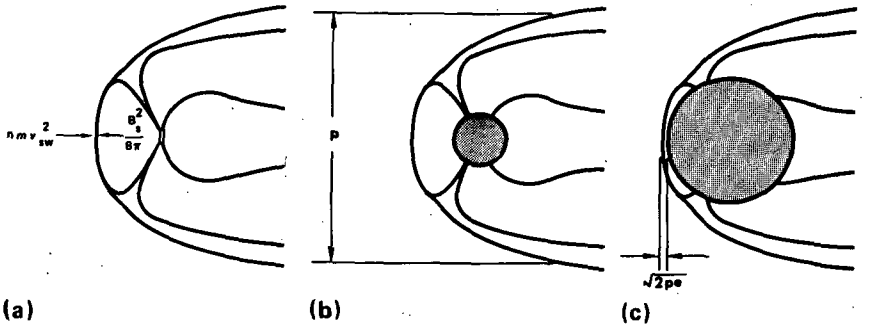

Figure 1.–Conceptual view of conditions governing minimal asteroid magnetospheres caused by dipole field, as seen in noon-midnight meridian plane. (*a*) A solar-wind pressure of density nm grams per cubic centimeter and at velocity v_{SW} from the left of the diagram is balanced by energy of stopping field B_S. (n is the proton number density and m is the proton mass.) (*b*) Proton gyroradius p is at least commensurate with magnetospheric diameter. (*c*) Balance takes place far enough, at stopping distance approximating geometric mean of proton and electron gyroradii p and e (in field B_S), to keep particles from hitting surface.

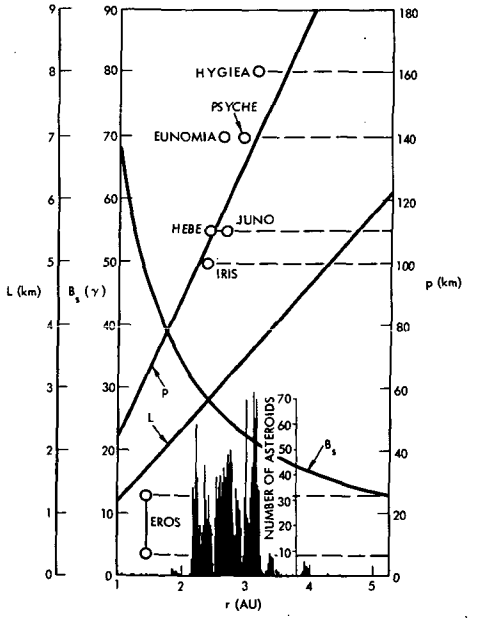

Figure 2.–Dependence of stopping field B_S, stopping distance L, and proton gyroradius p in field B_S on heliocentric distance r for quiet solar wind. Asteroid number distribution at bottom; dimensions and orbital semimajor axes of selected asteroids shown above on p, r scales, respectively. Dimensions of elongated Eros are from Roach and Stoddard (1938).

satisfy to guarantee a magnetopause standing away from the surface. For smaller asteroids, the field of equation (2) must provide the minimal transverse dimension, the diameter of the body being too small; the condition for minimal stopping distance is then automatically satisfied, because $L \ll p$ always.

APPLICATION TO ASTEROIDS UNDER QUIET SOLAR-WIND CONDITIONS

Figure 3 shows the dependence of minimal surface field B_0 on asteroid radius R for the quiet conditions defined above at selected heliocentric distances. The distinct behavior of the two sets of curves reflects the distinction between criteria of stopping distance and lateral dimension for magnetosphere maintenance. The shaded area representing acceptable combinations of R and $B_a \geqslant B_0$ is bounded by curves corresponding to the range of most common asteroid aphelia, $2 \leqslant r \leqslant 3.5$ AU. Values of R corresponding to

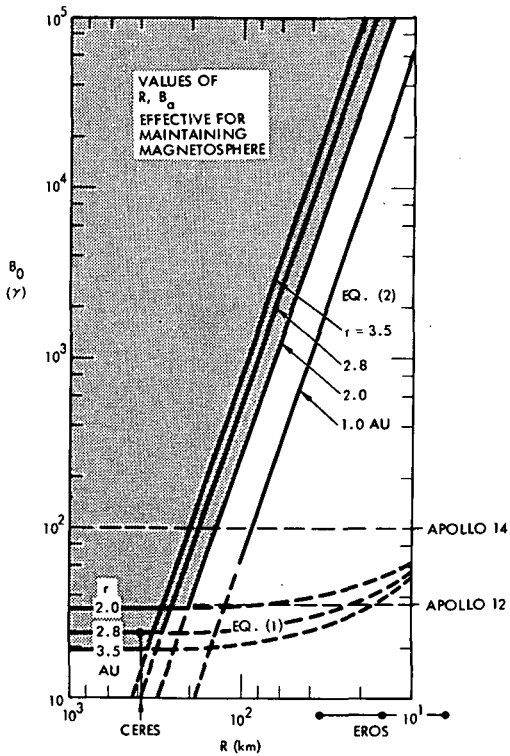

Figure 3.–Dependence of minimal equatorial dipole surface field B_0 on assumed asteroidal radius R (curves), defining values of R and surface field B_a (shaded) capable of maintaining magnetosphere. Local fields measured by Apollos 12 and 14 indicated at right; radii of Ceres and Eros at bottom. R increases to the left.

Ceres and to Eros, a proposed destination for an asteroid mission, are indicated at the bottom of the figure. The range of dimensions of ellipsoidal Eros was obtained from Roach and Stoddard (1938). The lines designated Apollo 12 and Apollo 14 will be discussed in a later paragraph.

The scale of minimal fields B_0 covered in figure 3 is well within the range found for naturally occurring objects on Earth and in the solar system. Minimal surface fields as low as a few tens of gammas are sufficient to form an identifiable magnetic cavity around the largest asteroids. Fields on the same order as Earth's, $B_0 = 50\,000\gamma$, on the other hand, would be necessary for bodies of radii a few tens of kilometers to maintain magnetospheres against the pressure of the undisturbed solar wind at normal asteroid distances. The requirement on Eros' field is somewhat more lenient because of its smaller semimajor axis, but depends on which dimension is chosen to represent it in this application. In any case, minimal surface fields above 1000γ to $10\,000\gamma$ do not seem so unlikely that asteroids of radius 20 to 30 km or less should be excluded from consideration as magnetically potent objects on the basis of B_0 alone. Larger bodies are perhaps more easily envisioned as likely to display the small surface fields required of them, however.

RELATIONSHIP TO EVIDENCE OF EXTRATERRESTRIAL MAGNETIZATIONS

Equivalent Magnetization

In the preceding paragraphs, specification of fields was limited to "surface" values. Induced fields involving plasma sheaths or conducting materials are, of course, potential sources of B_a. For this discussion, however, the source of B_a will be attributed to hypothetical asteroidal magnetization to relate B_a directly to lunar and meteoritic measurements. In this context, minimal equivalent uniform magnetizations for spherical asteroids having radii corresponding to the B_0 curves for $r = 2.8$ AU in figure 3 run between 6×10^{-5} and 2.5×10^{-1} emu/cm^3. At an assumed density of 3 g/cm^3, magnetizations might also be expressed as 2×10^{-5} to 8.34×10^{-2} emu/g. Because many asteroids are apparently not spherical, these figures can only serve as order of magnitude approximations.

If the conditions on B_0 are thought of in terms of equivalent magnetization, what are the prospects that these conditions will be met by any asteroid? The evidence on which to base an answer to this question is sparse, being limited to a few data on meteoritic and lunar materials.

Meteorite Magnetizations

Magnetic characterizations of meteoritic material have led to the inference that the samples examined had been naturally magnetized in fields of extraterrestrial origin. Remanences of several samples of about 5×10^{-5} to 4×10^{-3} emu/cm^3 were attributed by Lovering (1959) to cooling in the

presence of a magnetic field. Stacey et al. (1961) investigated the thermomagnetic properties of chondritic meteorites and concluded that measured magnetizations resulted from cooling in extraterrestrial fields of 0.15 to 0.9 Oe. Additional results of a similar nature were reported by Stacey and Lovering (1959). The source of meteorite magnetizations was credited by the authors to cooling in the crust or mantle of a primary meteorite body with a fluid core generating an appreciable field much like Earth's. Insofar as the results cited apply to material that may be representative of objects in the asteroid belt, the presence there of small planetary bodies with magnetizations comparable to those required for minimal magnetospheres is not ruled out and would be consistent with the meteorite data.

Apollo Measurements

Direct measurements of local, steady magnetic fields have been made on the lunar surface with magnetometers carried by Apollos 12 and 14. Preliminary results from Apollo 14 indicate that a field of 100γ was detected, but data were insufficient for determining the extent or character of the source (Palmer Dyal, personal communication). Apollo 12's ALSEP magnetometer, self-contained and more elaborate than Apollo 14's, gave steady readings in the neighborhood of 36γ, together with gradient measurements that have been analyzed in some detail. The steady field was attributed to a source of moment between 1.4×10^{14} and 1×10^{23} γ-cm^3 located from 0.2 to 200 km from the apparatus (Dyal, Parkin, and Sonett, 1970).

The horizontal lines in figure 3 are entered at the appropriate field levels for the Apollo 12 and 14 results. The Apollo 12 measurement is shown as a line running from R = 200 km to small values of R beyond the edge of the graph. The Apollo 14 measurement is drawn as a dashed line across the graph because no dimensional inferences are available. The Apollo 12 field value is 50 percent larger and the Apollo 14 value four times larger than the B_0 that would be needed to give Ceres a distinct magnetosphere. The Apollo 14 field is, in fact, about double the stopping field at the subsolar point of Earth's magnetopause. The Apollo 14 field, in contrast, is a factor of 30 smaller than the B_0 necessary for Eros to balance the solar wind magnetically, even if its size were taken as large as 35 km. Neither result provides a combination of R and B_a unambiguously inside the shaded region. On the other hand, neither result is confined to combinations of R and B_a so far from the minimal curves of the shading boundary as to make later discovery of admissible combinations highly improbable, at least for asteroids of dimensions above 100 km. Eros would not be a candidate for magnetic opposition to the solar wind, based on these figures.

Lunar samples returned to Earth by Apollo 11 have been tested in the laboratory for their magnetic properties. A variety of results was described by numerous authors in the Moon issue of *Science* (Abelson, 1970). Of

importance to this discussion was the measurement of a remanent magnetization of one breccia sample of 2.8×10^{-3} emu/g (Strangway, Larson, and Pearce, 1970), attributable to ancient cooling in the presence of a field comparable to that of Earth and substantially within the range of equivalent minimal magnetizations imposed by the curves of figure 3.

The origin of the onsite fields on the Moon and of returned sample magnetizations in lunar samples is unsettled. Interpreted at face value, the levels of field and magnetization recorded so far are on the order of those that could support the establishment of well-defined magnetic envelopes around the larger asteroids of radii greater than about 100 km.

SOLAR-WIND INTERACTION

Magnetospheric Interaction

A full-scale asteroidal magnetosphere will interact with the solar wind in a familiar way and should be detectable by conventional spacecraft magnetometers, although a close flyby will be necessary (Greenstadt, 1971). The interaction would include generation of a plasma shock ahead of the body and a magnetic tail downstream. The latter might be the most reliable indication of the existence of an asteroidal magnetic field, for a mission of limited target capability, because it would extend considerably behind the asteroid and be detectable much further from the body than would the magnetosphere proper. Transient components of Explorer 35's magnetometer measurements in the lunar wake have been attributed to the effect of asteroid-sized deposits of fossil magnetism on the Moon's surface (Binsack et al., 1970). The distance at which Explorer 35 detected these fluctuations behind the assumed lunar anomalies is equivalent to 5 to 10 Ceres radii and 20 to 40 radii of a 100 km asteroid.

Magnetospheric interaction would not be confined to simple exclusion of the solar wind from a magnetic cavity, but would include the generation of plasma waves and electromagnetic noise that would also be detectable far from the body.

Submagnetospheric Interaction

Fields less than those required for maintaining magnetospheres might still perturb the solar wind sufficiently to create measurable wave signals, as discussed by Greenstadt (1971). This type of "submagnetospheric" interaction seems the most probable, because the uniform magnetization of entire asteroids, especially the larger ones, that would be necessary to satisfy the stated conditions on B_0 would be an unjustified assumption. The convenient assumptions of dipolar fields and axes normal to the solar wind are also unlikely. Especially interesting prospects would be the presence of a severely tilted or displaced dipole or a field of multipole origin in a body of nonuniform magnetization, or perhaps inhomogeneous conductivity. A hovering rendezvous

spacecraft might record a complex magnetic signature as the asteroid rotated in the solar wind nearby. A magnetometer might thus serve as an important advance guide to favorable locations on the asteroid for collection of the most scientifically useful samples. Correlation of magnetic signature with optical appearance and other physical characteristics of the asteroid might yield definitive inferences on how it was formed. The question of how various combinations of asteroid features, including detectable magnetic fields and noise wakes, or even miniature magnetospheres, might relate to asteroidal formation is a suitable subject for further study. There seems to be no reason at present to believe that measurements made by a sensitive magnetometer borne to the neighborhood of an asteroid will prove less valuable than the many measurements made by similar instruments carried by spacecraft to numerous other destinations in the solar system.

CONCLUSION

The fields demanded by theory in order that the larger asteroids support a magnetic interaction with the solar wind are compatible with fields found associated with extraterrestrial objects. Steady fields detected by Apollo magnetometers on the lunar surface are comparable to equatorial fields with which the largest asteroids could support small magnetospheres. Magnetizations found in meteorites and in material from the lunar surface could, if duplicated in the bodies of the few asteroids of radius greater than 100 km, maintain magnetic cavities, or, more probably, multilobed magnetic cavities around these small planets. It would be worthwhile to conduct a theoretical investigation in advance of an asteroidal mission to determine the extent to which magnetic measurements at an asteroid might serve to distinguish among models of asteroidal origin.

REFERENCES

Abelson, P. H., ed. 1970, Magnetic and Electrical Properties. Science **167**(3918), 691-711.

Alfvén, H., and Arrhenius, G. 1970, Structure and Evolutionary History of the Solar System, I. Astrophys. Space Sci. **8**, 338.

Bernstein, W., Ogawa, H. S., and Sellen, J. M., Jr. 1968, Streaming Plasma Transport and Cutoff in Transverse Magnetic Fields. Phys. Rev. Lett. **20**, 903.

Binsack, J. H., Mihalov, J. D., Sonett, C. P., and Moutsoulas, M. D. 1970, Possible Lunar Surface Fossil Magnetism (abstract). EOS, Trans. Amer. Geophys. Union **51**, 774.

Dungey, J. W. 1958, Cosmic Electrodynamics. Cambridge Univ. Press. London.

Dyal, P., Parkin, C. W., and Sonett, C. P. 1970, Apollo 12 Magnetometer: Measurements of a Steady Magnetic Field on the Surface of the Moon. Science **169**, 762.

Greenstadt, E. W. 1971, Magnetic Interaction of Asteroids With the Solar Wind. Icarus **14**, 374.

Lovering, J. F. 1959, The Magnetic Field in a Primary Meteorite Body. Amer. J. Sci. **257**, 271.

Roach, F. E., and Stoddard, L. G. 1938, A Photoelectric Light-Curve of Eros. Astrophys. J. **88**, 305-312.

Sellen, J. M., Jr., and Bernstein, W. 1964, Interaction of Collisionless Plasma Streams With Transverse Magnetic Fields. Phys. Fluids 7, 977.

Shkarofsky, I. P. 1965, Laboratory Simulation of Disturbances Produced by Bodies Moving Through a Plasma and of the Solar Wind Magnetosphere Interaction. Astronaut. Acta 11, 169.

Stacey, F. D., and Lovering, J. F. 1959, Natural Magnetic Moments of Two Chondritic Meteorites. Nature 183, 529.

Stacey, F. D., Lovering, J. F., and Parry, L. G. 1961, Thermomagnetic Properties, Natural Magnetic Moments, and Magnetic Anisotropies of Some Chondritic Meteorites. J. Geophys. Res. 66, 1523.

Strangway, D. W., Larson, E. E., and Pearce, G. W. 1970, Magnetic Properties of Lunar Samples. Science 167(3918), 691-693.

Page intentionally left blank

FEASIBILITY OF DETERMINING THE MASS OF AN ASTEROID FROM A SPACECRAFT FLYBY

JOHN D. ANDERSON
Jet Propulsion Laboratory

APPROXIMATION TO DOPPLER OBSERVABLE

The orbit of a spacecraft with respect to an asteroid can be approximated to zero order by a hyperbola of zero bending angle (fig. 1). In an orbital system of coordinates (x_ω, y_ω), the zero-order orbit is given by

$$x_\omega = r' \cos f = b \tag{1}$$

$$y_\omega = r' \sin f = v(t - T) \tag{2}$$

where r' is the distance between the asteroid and the spacecraft, f is the true anomaly, b is the impact parameter or miss distance, v is the constant

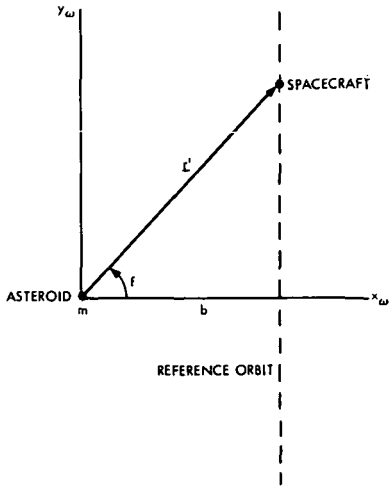

Figure 1.–Geometry of the flyby reference orbit in an orbit-plane coordinate system. The actual orbit is developed to the first order in the mass m as a perturbation from this reference orbit.

hyperbolic velocity, t is the time of observation, and T is the time of closest approach. After this zero-order solution is substituted into the two-body equations of motion, an approximation to the actual orbit can be obtained. The approximate equations of motion are given by

$$\ddot{x}_\omega = -\frac{Gmb}{r'^3} \tag{3}$$

$$\ddot{y}_\omega = -\frac{Gmv(t-T)}{r'^3} \tag{4}$$

where

$$r'^2 = b^2 + v^2(t-T)^2 \tag{5}$$

and the results of integration of equations (3) and (4) to the first order in Gm are

$$\dot{x}_\omega = -\frac{Gm}{bv}\sin f \tag{6}$$

$$\dot{y}_\omega = v + \frac{Gm}{bv}\cos f \tag{7}$$

where the constants of integration have been chosen such that v is the hyperbolic velocity at infinity. It is not necessary to carry the integration further because the mass m of the asteroid will be determined from Doppler data. Of course, the expressions for $\dot{x}_\omega$ and $\dot{y}_\omega$ can also be obtained from the hyperbolic orbital equations by establishing approximations for large eccentricities, but the perturbational derivation presented here is slightly easier and more straightforward.

For purposes of determining the mass of an asteroid from the velocity history given by equations (6) and (7), it is sufficient to consider the geocentric range rate $\dot{\Delta}'$ to the spacecraft. If the orientation of the spacecraft orbit is referred to the plane of the sky (fig. 2), then the range rate is given by

$$\dot{\Delta}' = \dot{\Delta} - (\dot{x}_\omega \sin\omega + \dot{y}_\omega \cos\omega)\sin i + O\left(\frac{r'}{\Delta}\right) \tag{8}$$

(where O means "on the order of magnitude of") and from equations (6) and (7),

$$\dot{\Delta}' = \dot{\Delta} - v\cos\omega\sin i - \frac{Gm}{bv}\cos(f+\omega)\sin i + O\left(\frac{r'}{\Delta}\right) \tag{9}$$

Note that the range rate is independent of the location of the node of the spacecraft's orbit on the plane of the sky, but it does depend on the argument of the perifocus and the inclination.

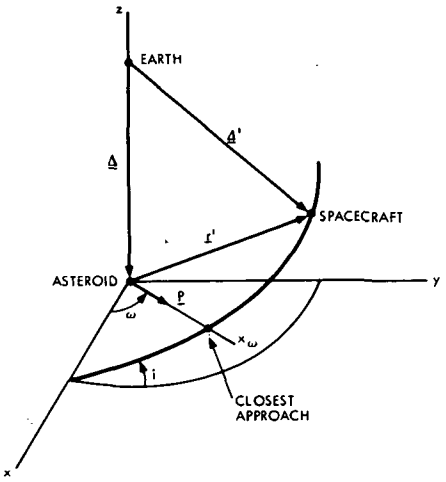

Figure 2.–Geometry of spacecraft encounter with an asteroid in a plane of the sky coordinate system.

However, in a determination of the mass, it is impossible to separate the function sin i from Gm. Therefore, it is convenient to define a quantity, $Gm \sin i$, that can be determined from the range-rate curve. Also, because the zero-order range rate contains no information about the mass of the asteroid, the only term of interest in equation (9) is the one containing Gm. A Doppler observable z that carries all the information on the mass can be defined by

$$z = -\frac{\zeta}{bv} \cos(f + \omega) \tag{10}$$

where

$$\zeta = Gm \sin i \tag{11}$$

COVARIANCE ANALYSIS

There are a number of unknown parameters in the expression for z, but the ones of particular interest to the flyby data are ζ, b, and T. The velocity v and the argument of the perifocus ω can be determined from the ephemerides of the spacecraft and asteroid outside the flyby region, although a reasonably accurate velocity ephemeris for the asteroid is needed for this purpose and also for a determination of the inclination i, a quantity required for the separation of Gm from the mass function ζ.

The sensitivity of z to the three parameters ζ, b, and T can be obtained by partial differentiation, where the true anomaly f is related to b and T by the relation

$$\tan f = \frac{v}{b}(t - T) \tag{12}$$

The differentiation yields the following three expressions:

$$\frac{\partial z}{\partial \zeta} = -\frac{1}{bv}\cos(f+\omega) \tag{13}$$

$$\frac{\partial z}{\partial b} = \frac{\zeta}{b^2 v}(\cos^3 f\cos\omega - 2\sin f\sin\omega + \sin^3 f\sin\omega) \tag{14}$$

$$\frac{\partial z}{\partial T} = -\frac{\zeta}{b^2}\cos^2 f\sin(f+\omega) \tag{15}$$

To construct a covariance matrix on the three parameters, it is necessary to form the products and cross products of the three partial derivatives and then to integrate over f from $-\pi/2$ to $\pi/2$, the limits of the zero-order reference orbit. The integration can be performed either with respect to time t or the true anomaly f. For the former, an integration with respect to t implies a sampling of the Doppler data at equal intervals of time. With f as the independent variable, the sampling is assumed to occur at equal intervals of the true anomaly. This is probably closer to the actual situation in which it would be expected that the sampling of data would be most frequent around the time of closest approach. Besides, an integration with respect to time results in the same functional form for the standard error on ζ, but the numerical coefficient is smaller than for the integration in the true anomaly. Thus, a sampling at equal intervals of f yields a more conservative estimate of the expected accuracy in ζ than does a sampling at equal intervals of t. In view of all the simplifying assumptions of this analysis, a conservative estimate is preferable.

The integrals of interest are

$$\int_{-\pi/2}^{\pi/2}\left(\frac{\partial z}{\partial \zeta}\right)^2 df = \frac{\pi}{2b^2v^2} \tag{16}$$

$$\int_{-\pi/2}^{\pi/2}\left(\frac{\partial z}{\partial b}\right)^2 df = \frac{\zeta^2\pi}{4b^4v^2}\left(\frac{9}{4} - \cos 2\omega\right) \tag{17}$$

$$\int_{-\pi/2}^{\pi/2}\left(\frac{\partial z}{\partial T}\right)^2 df = \frac{\zeta^2\pi}{8b^4}\left(\frac{3}{2} - \cos 2\omega\right) \tag{18}$$

$$\int_{-\pi/2}^{\pi/2}\frac{\partial z}{\partial \zeta}\frac{\partial z}{\partial b}\,df = -\frac{\zeta\pi}{8b^3v^2}(4 - \cos 2\omega) \tag{19}$$

$$\int_{-\pi/2}^{\pi/2} \frac{\partial z}{\partial \zeta} \frac{\partial z}{\partial T} df = \frac{\zeta \pi}{8b^3 \nu} \sin 2\omega \tag{20}$$

$$\int_{-\pi/2}^{\pi/2} \frac{\partial z}{\partial b} \frac{\partial z}{\partial T} df = -\frac{\zeta^2 \pi}{16b^4 \nu} \sin 2\omega \tag{21}$$

From equations (20) and (21), it is apparent that at $\omega = 0°$ and $\omega = 90°$ the correlation of T with ζ and b is zero. Therefore, it is reasonable to neglect the correlation with T in all cases, and to compute the two-dimensional covariance matrix on ζ and b. The inverse covariance matrix **J** is defined by

$$\mathbf{J} = \frac{1}{h_f \sigma_z^2} \int_{-\pi/2}^{\pi/2} \begin{pmatrix} \left(\frac{\partial z}{\partial \zeta}\right)^2 & \frac{\partial z}{\partial \zeta} \frac{\partial z}{\partial b} \\ \frac{\partial z}{\partial \zeta} \frac{\partial z}{\partial b} & \left(\frac{\partial z}{\partial b}\right)^2 \end{pmatrix} df \tag{22}$$

where h_f is the sample interval in the true anomaly and σ_z is the standard error on the Doppler measurements represented by z. At the time of closest approach, the sample interval h_f in the true anomaly is related to the sample interval h in time by

$$h_f = \frac{\nu}{b} h \tag{23}$$

The inverse covariance matrix in terms of h can be obtained by substituting equations (16), (17), and (19) into equation (22).

$$\mathbf{J} = \frac{\pi}{2b\nu^3 h \sigma_z^2} \begin{pmatrix} 1 & -\frac{\zeta}{b}(1 - \tfrac{1}{4}\cos 2\omega) \\ -\frac{\zeta}{b}(1 - \tfrac{1}{4}\cos 2\omega) & \frac{\zeta^2}{2b^2}\left(\frac{9}{4} - \cos 2\omega\right) \end{pmatrix} \tag{24}$$

The inverse can be obtained easily, and the standard deviation on ζ is simply the upper left element of the resulting matrix.

$$\sigma_\zeta^2 = \frac{4b\nu^3}{\pi} \left(\frac{9 - 4\cos 2\omega}{2 - \cos^2 2\omega}\right) h \sigma_z^2 \tag{25}$$

From this expression for the error in the mass function, it can be seen that a better determination of the mass is obtained by viewing the flyby along the orbit path ($\omega = 0°$) rather than across it ($\omega = 90°$). However, the ratio of the

two standard errors for $\omega = 90°$ and $\omega = 0°$ is only $\sqrt{2.6}$, and the sensitivity to ω is not particularly great. At $\omega = 30°$, the expression for $\sigma_\zeta{}^2$ is a minimum, and the resulting value of $\sigma_\zeta{}^2$ is about the best that can be expected from the flyby data. This minimum value of $\sigma_\zeta{}^2$ is

$$\sigma_\zeta{}^2 = \frac{16bv^3}{\pi} h\sigma_z{}^2 \tag{26}$$

NUMERICAL RESULTS

The percentage error in the mass m of the asteroid is related to the error in ζ by

$$\frac{\sigma_m}{m} = \frac{\sigma_\zeta}{\zeta} = \frac{\sigma_\zeta}{Gm \sin i} \tag{27}$$

and from equation (26)

$$\left(\frac{\sigma_m}{m}\right)^2 = \frac{16bv^3}{G^2m^2\pi} h\sigma_z{}^2 \csc^2 i \tag{28}$$

The mass m can be replaced by the radius R of the asteroid by means of the relation

$$m = \frac{4}{3} \pi\rho R^3 \tag{29}$$

where ρ is the mean density. The substitution for m can be made in equation (28) and the expression can be rearranged to yield the closest approach distance b as a function of the percentage error in the mass.

$$b = \frac{\pi^3(G\rho)^2}{9h\sigma_z{}^2} \frac{R^6}{v^3} \left(\frac{\sigma_m}{m}\right)^2 \sin^2 i \tag{30}$$

As an estimate of the accuracy in the Doppler data, we will assume that $\sigma_z = 0.5$ mm/s and that $h = 60$ s. This assumption is consistent with the present capability of the NASA/JPL Deep Space Net. In addition, a mean density of 3.33 g/cm^3 will be assumed in the evaluation of equation (30). In units of kilometers and seconds, equation (30) then reduces to

$$b = 1.132 \times 10^{-2} \frac{R^6}{v^3} \left(\frac{\sigma_m}{m}\right)^2 \sin^2 i \tag{31}$$

or

$$\log b = -1.946 + 6 \log R - 3 \log v + 2 \log \frac{\sigma_m}{m} + 2 \log (\sin i) \tag{32}$$

A plot of log b as a function of log R is shown in figure 3 for a range of values of v and for a 1 percent determination of the mass. The region of inaccessibility to a flyby ($b \leqslant R$) is below the dashed line on this plot. The inclination angle is assumed equal to its optimum value of 90°.

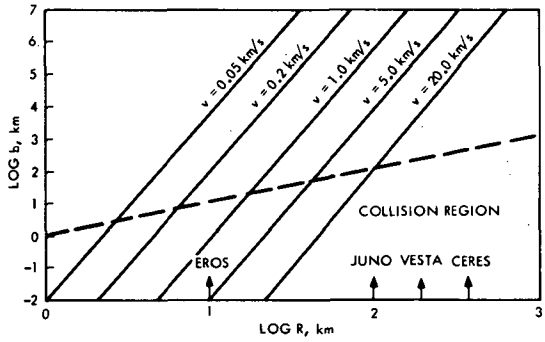

Figure 3.–Miss distance b required to determine the mass of an asteroid of radius R to an accuracy of ±1 percent. Curves are shown for various flyby velocities v. A density of 3.33 g/cm^3 is assumed in converting from mass to radius. The Doppler data are assumed accurate to 0.5 mm/s at a sample rate of one per minute.

Flyby velocities for asteroid missions should be on the order of 5 km/s. At this speed it should be possible to obtain a 1 percent determination of the masses of the larger asteroids. Ceres would require a flyby distance of 23×10^6 km, Pallas would require 1.7×10^6 km, and Vesta, 0.4×10^6 km. The closest approach to Juno, on the other hand, would have to be on the order of 9100 km for a 1 percent determination of its mass.

For a smaller asteroid such as Eros, any determination of its mass is practically out of the question for a flyby mission. However, for rendezvous missions with approach speeds less than 1 km/s, a 10 percent determination of the mass of an asteroid like Eros appears feasible for closest approach distances on the order of a few hundred kilometers. Of course, information on the mass could be destroyed by the performance of terminal maneuvers during the rendezvous.

ACKNOWLEDGMENTS

The author wishes to thank D. L. Cain and J. Lorell of the Jet Propulsion Laboratory for many helpful discussions on the contents of this paper. This paper presents the results of one phase of research carried out at JPL, California Institute of Technology, under NASA Contract no. NAS 7-100.

Page intentionally left blank

ASTEROID MASS DISTRIBUTION MEASUREMENT WITH GRAVITY GRADIOMETERS

ROBERT L. FORWARD
Hughes Research Laboratories

A determination of the internal structure and composition of the asteroids will give us important information concerning the origin of the solar system and the formation of the planets. We can obtain this information by measuring the total mass and the internal mass distribution through the use of spacecraft missions to flyby or to rendezvous, orbit, and land on the asteroids. The Doppler tracking technique used for mass measurement on planetary probes is suitable only for a flyby mission of the larger asteroids (> 20 km) because the gravity force field of the smaller asteroids is not strong enough to appreciably affect the trajectory of the probe during a flyby. If a rendezvous mission is used and the spacecraft is placed in orbit about an asteroid, the mass can be determined from the orbital period, but the effect on the spacecraft orbit due to the mass anomalies under the surface will not be easily seen unless the anomaly is very large because again the gravity force field decreases rapidly with decrease in anomaly size. The magnitude of the gradient of the gravity force field is independent of the asteroid or anomaly size, however, and a gravity gradient sensing technique for sensing of the gravity field of the asteroid will perform equally well on all except the very smallest (< 1 km) asteroids. Thus, if we desire to obtain mass measurements of the smaller asteroids during a flyby or to obtain detailed mass anomaly maps of the asteroids from an orbital survey prior to landing, it would be desirable to include a gravity gradiometer as part of the spacecraft instrument package.

GRAVITY GRADIOMETER INSTRUMENTATION

The various gravity gradient instruments that could be used to measure the gravity gradient field of an asteroid from a spacecraft all work on the principle of measuring the differential tensions, compressions, or torques induced in the sensor by the gradient of the gravity force field (the tidal effect) of the asteroid. There are many techniques and configurations possible (a fairly complete bibliography is available in (Bell, Forward, and Williams, 1970), but the instruments presently under serious consideration for spacecraft missions are those that measure the gravity gradient torque. These torque gradiometers

use the same physical principle for their operation as the gravity gradient stabilized satellites. The gravity gradient satellites we are familiar with have an elongated dumbbell shape and are very large and massive in an attempt to obtain engineeringly significant torque levels out of the gravity gradient field. The gradiometers are smaller so that they can be enclosed for protection from nongravitational forces, and therefore must have high sensitivity. The typical signal levels encountered by these instruments range from 10^{-9} to 3×10^{-6} s^{-2} (1 to 3000 Eötvös units (EU)) and the present designs have a noise level of 10^{-9} s^{-2} at 10 s integration time (Bell, Forward, and Williams, 1970).

One type of torque gradiometer is a single dumbbell in a cylindrical or spherical case that is floated at neutral buoyancy using the techniques developed for high-precision floated gyros (Trageser, 1970). Highly sensitive torque pickoffs and electromagnetic servodrivers are used to keep the float balanced and to read out the gravity gradient torques. (See fig. 1.)

A second technique, based on free-fall modifications of the old Eötvös torsion balance gradiometer, would use one or more dumbbells connected by fine quartz torsion fibers with capacitive pickoffs and electrostatic feedback. The gravity gradient signal would be that of the relative torque between the two sensing arms. (See fig. 2.)

A third variation also uses two opposed dumbbells, but they are connected by a stiff torsion spring that forms a resonant mechanical structure. (See fig. 3.) The entire device is then rotated at 60 to 1800 rpm so that the gravity gradient field is "chopped" by the rotating arms (Bell, Forward, Williams, 1970; Forward, Pilcher, and Norwood, 1967). The resonant frequency of the sensor structure is chosen at twice the rotation frequency, and the gravity gradient field induces vibrations into the rotating sensor structure at its

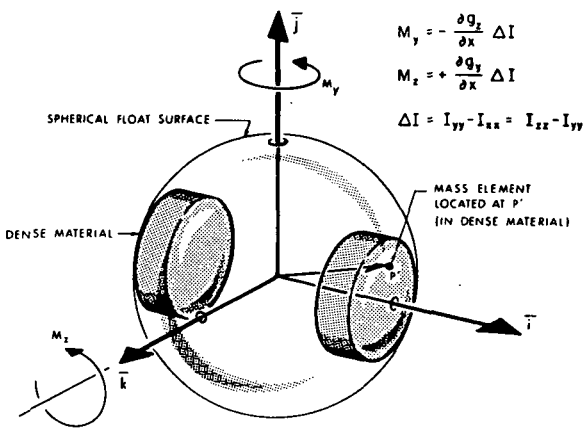

Figure 1.–Schematic of spherical floated torque gradiometer (from MIT Charles Stark Draper Laboratory, Cambridge, Mass.).

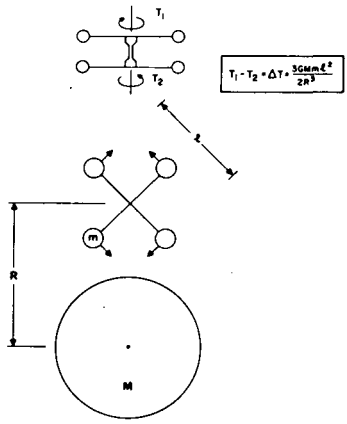

Figure 2.–Differential gravity gradient torques on a two-dumbbell torque gradiometer sensor structure. (The rotation axis of the rotating version of this type of gradiometer structure would be out of the page.)

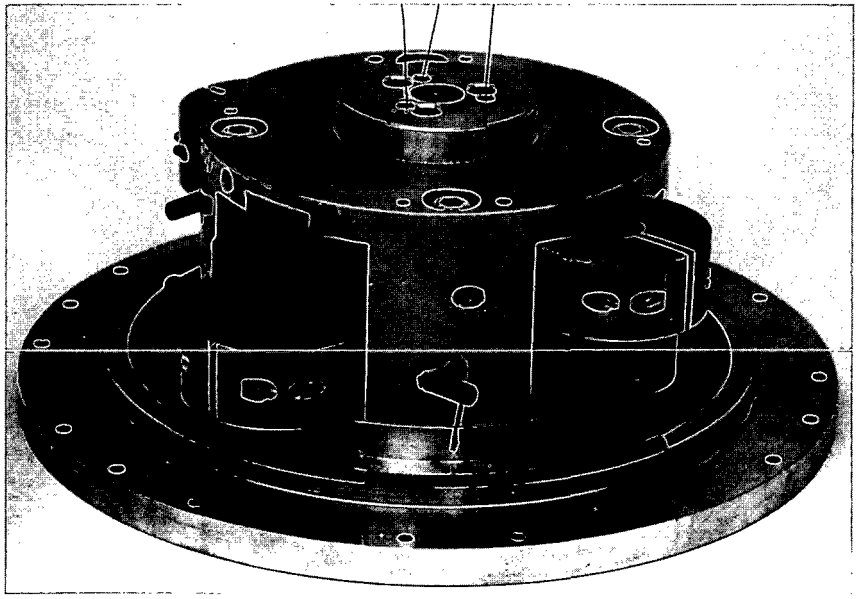

Figure 3.–Rotating gravity gradiometer.

resonant frequency. Piezoelectric transducers on the torsion spring convert the resonant mechanical vibrations into ac voltages whose amplitude and phase give the strength and direction of the gravity gradient field. If the rotating gradiometer is installed in a spin-stabilized spacecraft and the sensor resonance

is tuned to twice the spacecraft rotation frequency, the spacecraft then provides the rotation needed for the sensor operation. This mode of operation has the advantage that because the spacecraft is rotating along with the sensor, its gravity field is fixed with respect to the sensor arms and the sensor does not see the spacecraft gravity field, only the asteroid field.

The various possible versions of the gravity gradiometer are just leaving the laboratory and are far from being tested flight hardware, but we can expect that by the time the asteroid missions begin, the instrumentation will be available. However, the gradiometer instrumentation adds significantly to the cost, weight, and power budgets of the spacecraft, whereas Doppler tracking is practically free. Therefore, the gravity gradiometer instrumentation should only be included on those missions for which the Doppler tracking data are not adequate for determination of the mass or mass distribution. In the following sections we will try to give some general guidelines that show when one technique is preferred over the other. This hopefully will help those who are planning the missions to obtain the maximum scientific return from each flight.

MASS MEASUREMENT DURING A FLYBY

In figure 4 we have plotted the flyby altitude at which we can expect to obtain a 1 percent measurement of the mass of asteroids of various radii using both the Doppler velocity tracking technique and the gravity gradient sensing technique. We assumed that the accuracy limit was set by the present sensitivity of the two systems, 10^{-9} s^{-2} (1 EU) at 10 s for the gradiometer system and 0.5 mm/s at 60 s for the Doppler tracking system. The purpose of

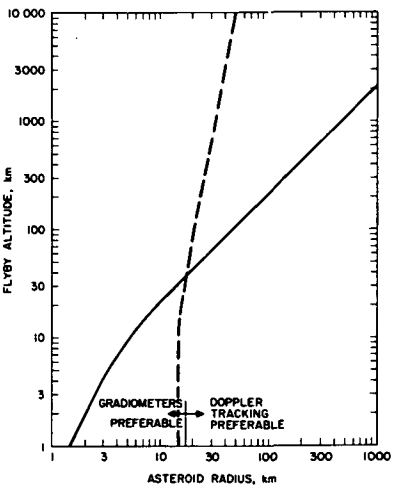

Figure 4.–Flyby altitude for 1 percent mass measurement (flyby velocity = 1 km/s) using Doppler tracking (broken curve) and gravity gradiometer techniques (solid curve).

this graph is not to say that one technique is better than another, but to bring out the general features of the advantages and disadvantages of the two complementary techniques. This graph is for a flyby velocity of 1 km/s. Other curves with flyby velocities from 0.1 to 10 km/s show the same general result. As we can see, the Doppler tracking technique is preferable for the larger asteroids, but becomes quite insensitive for the smaller asteroids, even for very close flybys. This general conclusion that the Doppler tracking technique is not suitable for flyby missions to the smaller asteroids is discussed in greater detail in the paper by John D. Anderson in these proceedings.[1] (The Doppler tracking curve in fig. 4 is taken from fig. 3 in his paper.) The gravity gradiometer technique will give results for all asteroids above 1 km, but its measurement range for the larger asteroids is poorer than the Doppler tracking technique. Future increases in the accuracy of either system will not change these general conclusions significantly because of the rapid falloff of both curves. A change in sensitivity of an order of magnitude will only shift the curves a factor of 2 in asteroid radius or in flyby altitude.

ASTEROID RENDEZVOUS MISSIONS

When we investigate techniques for mass measurement and mass anomaly measurement that are applicable to a rendezvous mission to an asteroid, we find four techniques that can be considered: orbital velocity tracking, orbital period measurement, gravity gradient measurement, and acceleration measurement (after landing). All of these techniques can give accurate measurement of the mass of the larger asteroids, although the orbital velocity and the accelerometer techniques become less accurate for the smaller asteroids.

The orbital velocity of a spacecraft about an asteroid

$$v = (GM/R)^{1/2}$$

ranges from 300 m/s for Ceres to 9 mm/s for a 10 m radius asteroid. The velocity about the larger asteroids is high enough that present Doppler velocity tracking techniques are more than adequate for an accurate mass measurement. For the smaller asteroids, however, it is better to measure the time for one orbital period rather than the orbital velocity directly. The orbital period for a close orbit is independent of the mass of the asteroid and is a function of the average asteroid density

$$T = (3\pi/G\rho)^{1/2}$$

The period ranges from about 3 hr for an iceball to 1 hr for a very dense asteroid.

---

[1]See p. 577.

If the rendezvous vehicle lands on the asteroid, then we can use gravimeters or the spacecraft navigation accelerometers to measure the gravity force to obtain an estimate of the mass. The acceleration field

$$a = GM/R^2$$

ranges from 0.03 g for Ceres to 10^{-6} g for a 10 m radius asteroid. Although quite small, these acceleration levels can be measured to high accuracy by any number of available accelerometers and gravimeters. Both the accelerometer technique and the orbital period technique, however, are limited to obtaining an estimate of the total mass or average density of the asteroid. If we are interested in obtaining data on the internal density distribution of the asteroid, the use of the Doppler velocity tracking and the gravity gradiometer techniques from orbit are most suitable.

The horizontal gravity gradient of an asteroid is

$$\Gamma = \frac{GM}{R^3} = \frac{4}{3}\pi G\rho$$

If the gradiometer is in a close orbit about the asteroid so that the distance from the center of the asteroid is nearly equal to the radius, then the gravity gradient is only a function of the average asteroid density, and varies from 6×10^{-7} s^{-2} (600 EU) for an iceball to 5×10^{-6} s^{-2} (5000 EU) for a very dense asteroid.

The data that can be obtained on the internal mass distribution of an asteroid from Doppler tracking and gravity gradiometer measurements using an orbiting vehicle are compared in the following figures. Figure 5 shows a schematic of the hypothetical asteroid that was used in the computer simulations. The asteroid is 100 km in radius and has an average density of 3.5 g/cm^3. Embedded in this asteroid are spherical mass anomaly regions with radii of 1, 3, 10, and 30 km and a density difference of 0.5 g/cm^3. If the orbiting

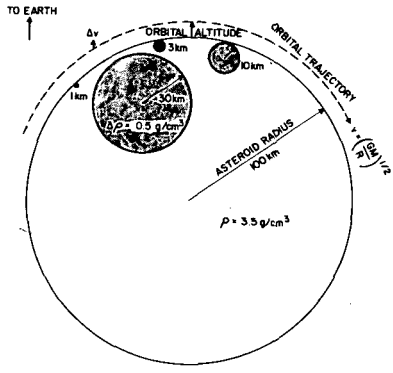

Figure 5.–Asteroid model used in computer simulations.

vehicle is 1 km above the surface, then the output of the Doppler tracking system and the gravity gradiometer system during the passage over the anomalies is as shown in figure 6. At this altitude we can see that the gradiometer system gives significantly improved resolution and signal level for the smaller anomalies. If the altitude is raised to 3 km (to possibly avoid collision with the surface features), then we obtain the comparative plots shown in figure 7. The advantage of the gradiometer data is now not so

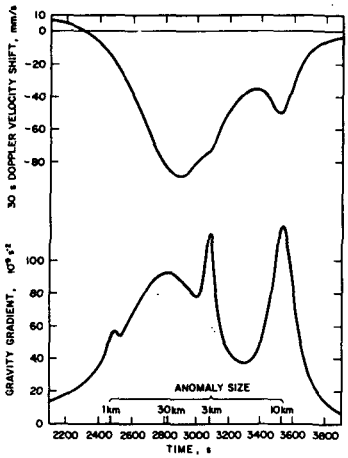

Figure 6.–Gravity gradient and Doppler tracking signal variations from an orbit 1 km above a 100 km radius asteroid.

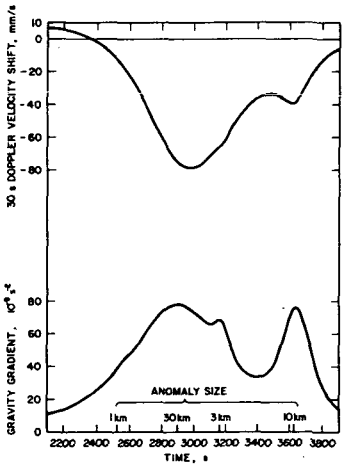

Figure 7.–Gravity gradient and Doppler tracking signal variations from an orbit 3 km above a 100 km radius asteroid.

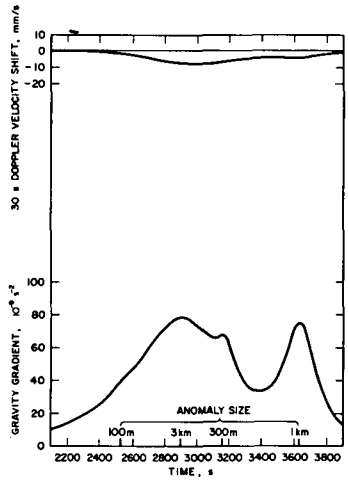

Figure 8.—Gravity gradient and Doppler tracking signal variations from an orbit 300 m above a 10 km radius asteroid.

significant, and the advantages of the slight improvement in data must be weighed against the costs. The significant advantage of the gradiometer technique is shown in figure 8 where we have assumed a decrease in scale of the simulation by a factor of 10. Instead of a spacecraft in an orbit 3 km above a 100 km asteroid with 1 to 30 km sized anomalies, we have simulated a spacecraft in an orbit 300 m above a 10 km asteroid with 100 to 3000 m sized anomalies. The orbital period has not changed, because the asteroid density is assumed to be the same, so the time required for the measurement is the same. The gravity gradient signal has the same magnitude and resolution for the 10 km asteroid as it had for the 100 km asteroid, but the Doppler velocity signal has decreased by an order of magnitude and the accuracy of this technique for mass anomaly measurement has decreased in the same proportion.

SUMMARY

As a general rule, our studies show that the average density of an asteroid can best be obtained by Doppler tracking techniques if the mission is a flyby mission to one of the larger asteroids. If the mission involves a flyby of a smaller asteroid, or a rendezvous and orbit of any asteroid, the addition of a gravity gradiometer to the spacecraft instrument package will give a significant improvement in the quality of the gravity data and should be seriously considered for such missions.

REFERENCES

Bell, C. C., Forward, R. L., and Williams, H. P. 1970, Simulated Terrain Mapping With the Rotating Gravity Gradiometer. Proc. Invitational Symp. Dyn. Gravimetry (Fort Worth), Mar. 16-17, pp. 45-60.

Forward, R. L., Pilcher, L. S., and Norwood, Virginia T. 1967, Asteroid Belt Investigation Using Small, Spin-Stabilized Fly-By Probes. Proc. AAS Symp. Planet. Geol. Geophys. (Boston), May 25-27, pp. 327-347.

Trageser, M. B. 1970, A Gradiometer System for Gravity Anomaly Surveying. Proc. Invitational Symp. Dyn. Gravimetry (Fort Worth), Mar. 16-17, pp. 1-43.

DISCUSSION

HARRIS: With a gravity gradiometer is there an ambiguity in the density distribution?

FORWARD: There is always a mathematical ambiguity in the details of the internal density distribution of an object obtained from external gravity data alone. The ambiguity will have to be resolved with additional data obtained from magnetic, acoustic, or borehole surveys along with reasonable assumptions for the types of materials (rock, iron, ice, etc.)

Page intentionally left blank

ESTIMATE OF PARTICLE DENSITIES AND COLLISION DANGER FOR SPACECRAFT MOVING THROUGH THE ASTEROID BELT*

DONALD J. KESSLER
NASA Manned Spacecraft Center

The present lack of exact information about the distributions of asteroids and asteroidal meteoroids causes the largest uncertainty in the description of the interplanetary meteoroid environment between the orbits of Mars and Jupiter. Observed asteroids are inferred to have diameters from a few kilometers to a few hundred kilometers. The presence of these larger bodies suggests the presence of smaller, unobservable bodies. When asteroids collide, fragments are produced that eventually collide with other fragments. Because of this continuous collision process, much smaller asteroids most probably exist. Such asteroidal meteoroids, if present in sufficient number, could pose considerable danger to spacecraft.

ASTEROID MASS DISTRIBUTION

Various methods have been used to predict the number of smaller bodies in the asteroid belt. These methods include estimates of the mass distribution that are inferred from lunar and Martian crater distributions (Baldwin, 1964; Hartmann, 1965, 1968; Marcus, 1966, 1968), meteorite finds (Brown, 1960; Hawkins, 1964), and theoretical and experimental studies of rock crushing laws (Dohnanyi, 1969; Hawkins, 1960; Piotrowski, 1953). The number of smaller asteroids can also be estimated by the trend set by the larger asteroids. Most analyses indicate that the number of asteroids of mass m and larger (the cumulative mass distribution) varies as $m^{-\alpha}$, where α is a constant. In extrapolating from the distributions for larger asteroids, a greater value for α indicates a larger number of smaller asteroids.

Several difficulties arise from inferring asteroid influx rates from lunar and Martian crater counts:

(1) The ages of the impacted surfaces are unknown.
(2) Controversy still exists about whether the craters were formed by asteroids, comet nuclei, secondary ejecta, or volcanism.

*The full text of this paper appears in NASA SP-8038, Oct. 1970.

(3) The surface features of craters are eroded (by smaller meteoroids on the Moon or by atmospheric wind on Mars), which causes the smaller craters to disappear more rapidly than the larger craters.

(4) A surface can become saturated so that larger craters will obliterate a significant number of smaller craters. When this occurs, the number of impacting particles cannot be determined, and the original distribution is difficult to determine. Saturation appears to have taken place on the surface of Mars and in the lunar highlands (Marcus, 1966, 1968).

If meteorites are assumed to be of asteroidal origin, problems still exist in relating a meteorite mass to its original mass, because of ablation and fragmentation. Hawkins (1964) deduced the mass distribution of stony and iron meteorites and predicted their cumulative mass distribution in space to vary as m^{-1} and $m^{-0.7}$, respectively. Brown (1960), on the other hand, found both stony and iron meteorites to vary as $m^{-0.77}$.

Several investigators have attempted to predict the number of smaller asteroids by theoretical and experimental studies of the effects of collisions between rocks. Piotrowski (1953) found that under certain restrictive conditions, erosion and breakup of asteroids would lead to a cumulative mass distribution that varies as $m^{-2/3}$. Hawkins (1960), however, pointed out that as terrestrial rocks are crushed, the value of α increases and approaches -1. Dohnanyi (1969) used experimental results of hypervelocity impacts to determine a rock crushing law for the asteroids and their debris. He found that a steady-state solution exists if the cumulative mass distribution varies as $m^{-0.84}$. Dohnanyi also pointed out that his results are consistent with the observed asteroids of Kuiper et al. (1958).

Kessler (1969) used the individual orbits and absolute magnitudes of asteroids given in the 1967 *Ephemeris* volume to obtain the spatial density (number density) of asteroids as a function of absolute magnitude at various positions in space (every 0.1 AU between 1.0 and 4.5 AU, and every 45° of heliocentric longitude). The results for 1.5, 2.0, and 2.5 AU are shown in figures 1, 2, and 3, respectively. The upper line in each figure partially corrects for selection effects. Except for a flattening of the curve, which occurs around absolute magnitude 11 (particularly noticeable in fig. 2), the mass distributions given by Kessler (1969) are consistent with Dohnanyi's results. An upper limit to the spatial density of asteroids is given by Kessler (1968) by the requirement that the intensity of the counterglow is not exceeded by the total light reflected by the asteroids.

The cumulative asteroid spatial density S at 2.5 AU (Kessler, 1969) is shown in figure 4, along with the various models that have been discussed. Spherical particles with a mass density of 3.5 g/cm^3 and a geometric albedo of 0.1 were used. For a spatial density greater than 10^{-15} or 10^{-16} particles/m^3, the probability of encounter must be considered for large spacecraft (i.e., a

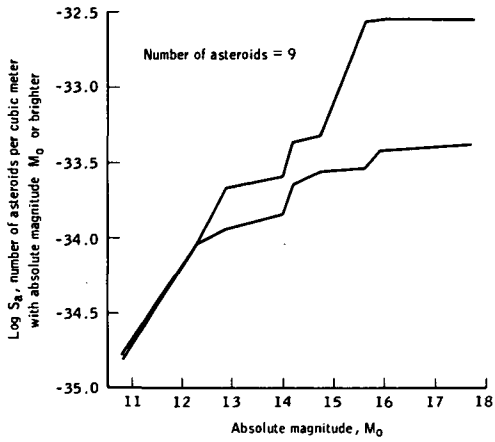

Figure 1.–Average asteroid spatial density in the ecliptic plane at 1.5 AU.

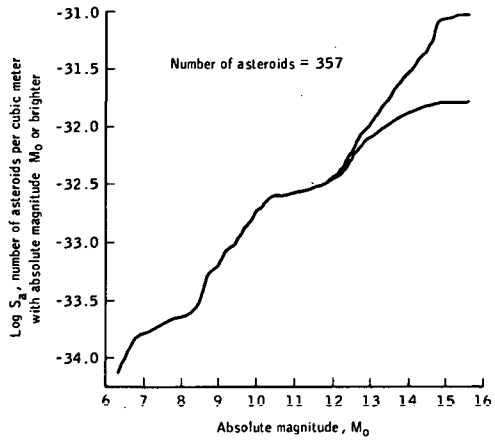

Figure 2.–Average asteroid spatial density in the ecliptic plane at 2.0 AU.

spacecraft with 500 m^2 of surface area exposed to the environment for 1 yr). Therefore, if the asteroid spatial density varies as m^{-1} (as suggested by Hawkins, 1960, and shown in fig. 4), such a spacecraft would require protection against impacts by masses as large as 10^3 g. However, this mass distribution exceeds the upper limit given by Kessler (1968) for masses less than 10^4 g. If the asteroid mass distribution varies as $m^{-2/3}$ (Piotrowski, 1953), the spacecraft would have to be protected against asteroidal meteoroids of only 10^{-5} g (compared with cometary meteoroids of 10^{-3} or 10^{-2} g).

The asteroid mass distribution suggested by Dohnanyi (1969) ($S \sim m^{-0.84}$) gives an intermediate result that is consistent with the upper limit for asteroid

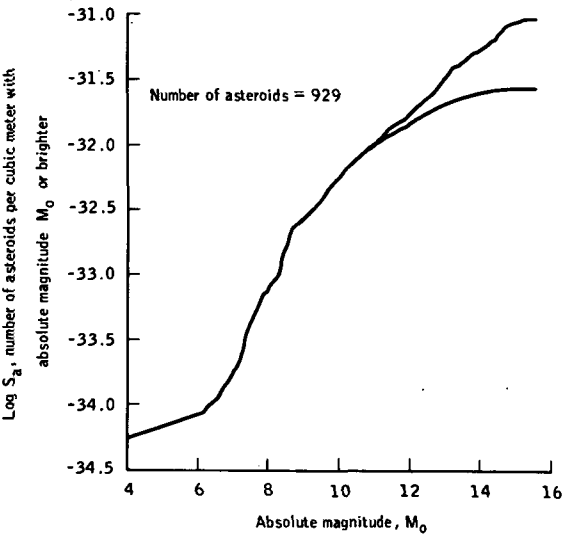

Figure 3.—Average asteroid spatial density in the ecliptic plane at 2.5 AU.

masses greater than 10^{-9}. When Dohnanyi's mass distribution is extrapolated from the larger asteroids of Kessler (1969) at $R = 1.0$ AU, the resulting flux comes within a few percent of the flux found by Whipple (1967) from the Apollo asteroids, and the flux of meteoroids estimated from meteorite finds by Hawkins (1964) and Brown (1960). Such a mass law also gives results consistent with Öpik's prediction (Whipple, 1967) that the ratio of the number of Mars-crossing to Earth-crossing asteroids (of the same size) should be 300.

Thus, this asteroid mass distribution will be adopted, and the assumption will be made that the mass distribution is independent of the distance from the Sun. The spatial density of asteroids with an absolute magnitude M_0 less than 10 can then be expressed as

$$\log S_a = 0.504M_0 + C_R \tag{1}$$

where S_a is the number of asteroids per cubic meter of absolute magnitude M_0 and brighter, and C_R is a constant for each distance R from the Sun.

The irregularity in the size distribution between asteroids with absolute magnitudes of 10 and 12 suggests that for $M_0 > 12$, S_a in equation (1) should be reduced by a factor of 7.6, or

$$\log S_a = 0.504M_0 + C_R - 0.88 \tag{2}$$

The value of C_R is then evaluated for each distance from the Sun by fitting equation (1) or (2) to the larger asteroids given by Kessler (1969); selection

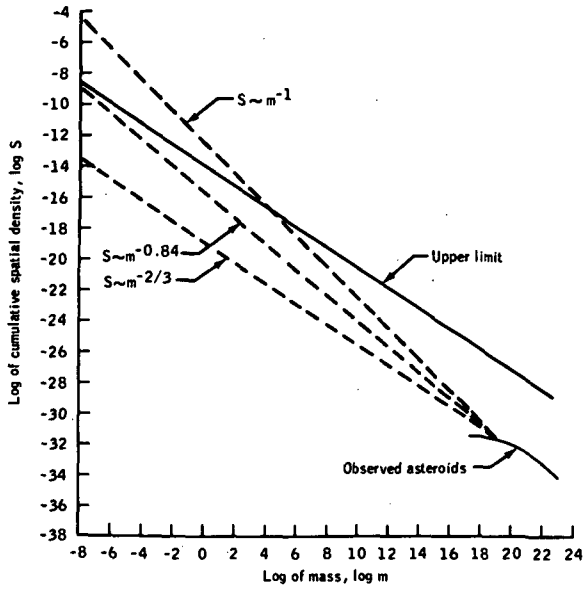

Figure 4.–Various asteroid mass-distribution models at 2.5 AU.

effects are minimal at the larger sizes. At $R = 2.5$ AU, $C_{2.5} = -37.18$. If a radial distribution is defined such that

$$f(R) = C_R - C_{2.5} \tag{3}$$

the spatial density in the ecliptic plane for the smaller asteroids becomes

$$\log S_a = 0.504M_0 - 38.06 + f(R) \tag{4}$$

where $M_0 > 12$. The function $f(R)$ was evaluated from equation (3) and is given in figure 5.

If the adopted values for asteroid mass density (3.5 g/cm^3) and geometric albedo (0.1) are used,

$$\log S_a = 0.84 \log m - 15.79 + f(R) \tag{5}$$

where $10^{-9} \leqslant m \leqslant 10^{19}$, and S_a is the number of asteroids per cubic meter near the ecliptic plane of mass m (in grams) or larger at distance R in astronomical units from the Sun. Equation (5) is limited to masses larger than 10^{-9} g for two reasons: (1) If the mass distribution is extrapolated to masses smaller than 10^{-9}, the upper limit given by Kessler (1968) would be exceeded; and (2) solar radiation pressure and the Poynting-Robertson effect would

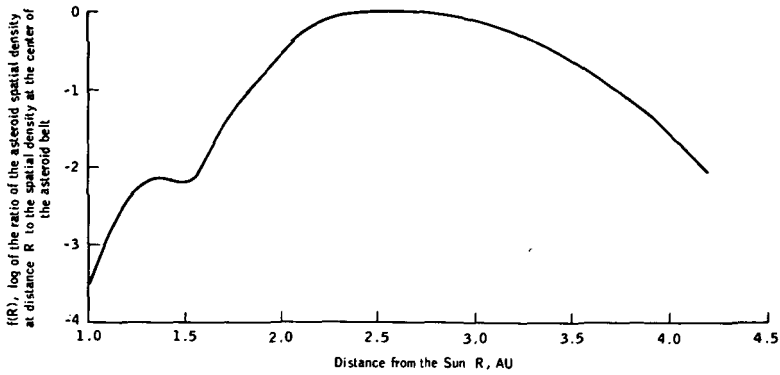

Figure 5.—Asteroid radial distribution.

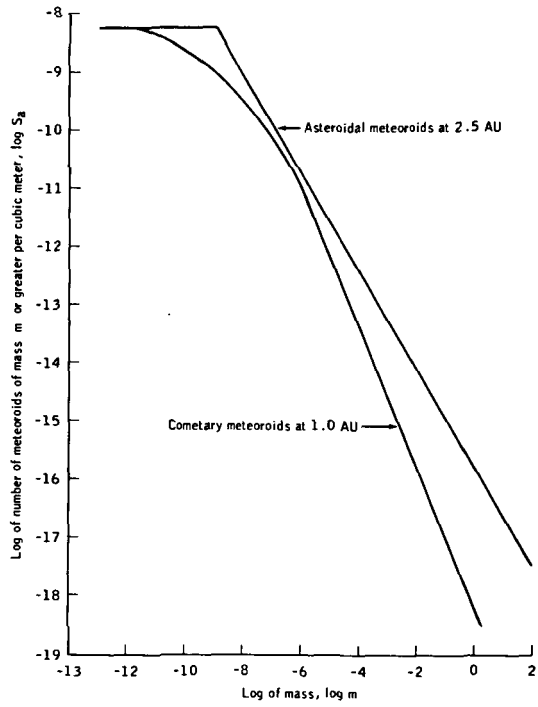

Figure 6.—Asteroid mass distribution compared to the cometary mass distribution near Earth.

probably cause the mass distribution between 10^{-12} and 10^{-6} g to change in a manner similar to the change in cometary meteoroids in the same mass range. Such a change can be approximated by limiting the distribution to asteroids of 10^{-9} g or larger. Use of a curved function similar to the function for cometary

meteoroids would imply more knowledge of the asteroid mass distribution than is available. Equation (5) is compared with cometary meteoroids at 1 AU in figure 6.

LATITUDE AND LONGITUDE DEPENDENCE

The asteroid spatial density is a function of both heliocentric latitude and longitude. At a latitude of 16° from the ecliptic plane, the number of asteroids is reduced by about an order of magnitude from that given by equation (5). Between 1.5 and 2.4 AU, the spatial density is longitudinally dependent and reaches a maximum dependency at R=1.8 AU. At R=1.8 AU, the spatial density increases or decreases by one-half an order of magnitude in the direction of Jupiter's longitude of perihelion or the opposite direction, respectively. A complete discussion is contained in NASA SP-8038 (1970).

RELATIVE VELOCITY

The asteroids given in the 1967 *Ephemeris* volume were used to compute the average velocity of asteroids relative to a spacecraft. The asteroid data were corrected for observational selection effects (Kuiper et al., 1958), and weighted according to the probability of collision (Wetherill, 1967) with the spacecraft, and the velocity of each asteroid relative to the spacecraft was computed. Velocity distributions are obtained at distance R from the Sun for a spacecraft whose velocity vector makes an angle θ with a circular orbit in the same plane. The speed of the spacecraft is σ, in units of the speed necessary to maintain a circular orbit of radius R around the Sun. The average asteroid velocity $\bar{v}_a$ is then found from each distribution. The velocity parameter $\bar{U}_a$ is introduced and is less dependent on distance from the Sun than is $\bar{v}_a$. The values of $\bar{U}_a$ shown in figure 7 were computed for R = 2.5 AU, but can be used with fair accuracy for all distances by applying the relationship

$$\bar{v}_a = \bar{U}_a R^{-1/2} \tag{6}$$

where R is in astronomical units, $\bar{v}_a$ is in meters per second, and $\bar{U}_a$ is given in figure 7. A more detailed discussion, which introduces a slight R dependence of $\bar{U}_a$, is contained in NASA SP-8038 (1970).

FLUX AND NUMBER OF IMPACTS

Flux on a randomly tumbling surface is related to spatial density and relative velocity by

$$F_a = \tfrac{1}{4} S_a v_a \tag{7}$$

where F_a is the number of asteroid impacts per square meter per second. The total number of impacts on a spacecraft is given by

$$N_a = \int F_a A \, dt \tag{8}$$

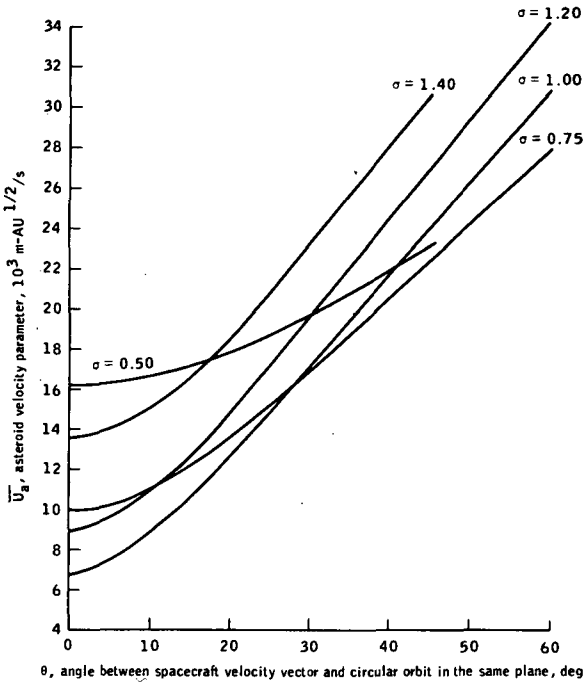

Figure 7.—Average relative velocity of asteroid particles at R = 2.5 AU where σ is the ratio of the heliocentric spacecraft speed to the speed of a spacecraft in a circular orbit at the same distance from the Sun.

where A is the surface area of the spacecraft in square meters, t is the time of spacecraft exposure to the environment, and the limits of integration are the beginning and end times of the mission.

UNCERTAINTIES

The model that describes the asteroid size distribution is anchored at the large-mass end by the observed asteroids and is assumed to vary as $m^{-\alpha}$. The assumption of the $m^{-\alpha}$ dependence and the uncertainty in the value of α probably constitute the largest uncertainties in the asteroidal-meteoroid-environment model. An upper limit for the number of smaller asteroids is established by not allowing the number to be so great as to produce more reflected sunlight than is observed in the counterglow (Kessler, 1968). The value of α that was chosen for the model was not arbitrary, but (as was pointed out previously) was a value that agreed with the steady-state mass distribution based on collisions within the asteroid belt. The choice of a value for α is also consistent with a limitation in particle mass to 10^{-9} g and larger, again based on counterglow observations. A larger value for α than that selected for the

model would lead to a particle cutoff at larger masses, to remain consistent with counterglow observations. Because no method exists for establishing the proper cutoff, the upper limit of the flux of particles with greater than a given mass is just the value that would not produce reflections exceeding that of the counterglow. The ratio of this upper limit to the model used (eq. (5)) is $26m^{0.17}$ ($m \geqslant 10^{-9}$ g). Thus, if the asteroid mass is limited to particles of 10^{-9} g or larger, the flux predicted from the model is essentially at the upper limit, whereas if the asteroid mass is limited to particles 1 g or larger, the limit of uncertainty permits the actual flux to be higher than the flux predicted by the model by a factor of 26.

Additional uncertainty is introduced through the geometric albedo used in relating a particle distribution to the counterglow. Theoretically, geometric albedo may range from zero to infinity; however, the extremes of this range are never observed. A geometric albedo of 0.1 is used for estimating the mass of the visual asteroids in the asteroid-environment model. If the true albedo, however, is as low as 0.05, the ratio of the upper limit of the asteroid flux predicted by the model becomes $52m^{0.17}$.

The lower limit of the meteoroid population in the asteroid belt is set by the cometary environment. If the cometary meteoroid size distribution shown in figure 6 is assumed to vary as R^{-3} (which is an extreme case), the ratio of the asteroid-model environment to the cometary environment in the heart of the asteroid belt is $4.7 \times 10^3\ m^{0.37}$ ($m \geqslant 10^{-6}$). This expression implies that the meteoroid flux in the asteroid belt could range from a factor of almost 30 lower than predicted by the asteroid model at $m = 10^{-6}$ g to a factor of nearly 5000 lower for $m = 1$ g.

IMPACTS ON A SPACECRAFT

If a typical trajectory through the asteroid belt (e.g., a mission to Jupiter) is integrated by using equations (8), (7), (6), and (5) and figures 5 and 7, the total number of asteroid impacts per square meter of spacecraft surface area is given by

$$\log \frac{N_a}{A} = -5.0 - 0.84 \log m \tag{9}$$

The average asteroid velocity relative to the spacecraft would be approximately 15 km/s.

As can be seen from equation (9), the probability is small that a spacecraft with a random trajectory through the asteroid belt will collide with any of the large observed asteroids. In fact, only one asteroid of 10^{19} g or larger could be expected to pass within 10^7 km of the spacecraft.

The real danger to spacecraft is from the much smaller asteroidal meteoroids. Equation (9) predicts an average of one asteroidal meteoroid impact of 10^{-6} g or larger for every square meter of spacecraft surface area.

The upper limit for asteroidal particles of this size is about five impacts per square meter. Near the Earth, the flux of cometary meteoroids of 10^{-6} g or larger is about three impacts per square meter per year (NASA SP-8013, 1969), with an average velocity relative to the spacecraft of 20 km/s. Thus, for meteoroids in this size range, the asteroid belt is not likely to be more hazardous than the meteoroid environment near Earth.

However, assume that it is desired to insure that a spacecraft having 100 m^2 of surface area has at least a 0.99 probability of not being penetrated by a meteoroid. The spacecraft must then be designed to withstand (from eq. (9)) an impact by a particle of $10^{-1.2}$ g with a relative velocity of 15 km/s. (This compares with a cometary particle mass of $10^{-2.4}$ g for a similar spacecraft near Earth for 1 yr.) If the spacecraft were designed to withstand an impact from a $10^{-1.2}$ g meteoroid (which could add hundreds of kilograms to the spacecraft weight), and the upper limit to the asteroid flux were encountered, then the probability of no penetration would be reduced to 0.72. To design a spacecraft using the upper limit would require protection against a 10 g asteroidal meteoroid, which would severely increase the weight of the spacecraft.

REFERENCES

Baldwin, Ralph B. 1964, Lunar Crater Counts. Astron. J. 69(5), 377-392.

Brown, Harrison. 1960, The Density and Mass Distribution of Meteoritic Bodies in the Neighborhood of the Earth's Orbit. J. Geophys. Res. 65(6), 1679-1683.

Dohnanyi, J. S. 1969, Collisional Model of Asteroids and Their Debris. J. Geophys. Res. 74(10), 2531-2554.

Hartmann, William K. 1965, Secular Changes in Meteoritic Flux Through the History of the Solar System. Icarus 4(2), 207-213.

Hartmann, William K. 1968, Lunar Crater Counts–VI: The Young Craters Tycho, Aristarchus, and Copernicus. Communications of the Lunar and Planetary Lab., vol. 7, no. 119, pp. 145-156. Univ. of Arizona Press. Tucson.

Hawkins, Gerald S. 1960, Asteroidal Fragments. Astron. J. 65(5), 318-322.

Hawkins, G. S. 1964, Interplanetary Debris Near the Earth. Ann. Rev. Astron. Astrophys. 2, 149-164.

Kessler, Donald J. 1968, Upper Limit on the Spatial Density of Asteroidal Debris. AIAA J. 6(12), 2450.

Kessler, D. J. 1969, Spatial Density of the Known Asteroids in the Ecliptic Plane. NASA TM X-58026.

Kuiper, G. P., Fujita, Y., Gehrels, T., Groeneveld, I., Kent, J., Van Biesbroeck, G., and Houten, C. J. van. 1958, Survey of Asteroids. Astrophys. J. Suppl. Ser. 32, vol. III, pp. 289-335.

Marcus, A. H. 1966, A Stochastic Model for the Formation and Survival of Lunar Craters. Icarus 5, 165-200.

Marcus, A. H. 1968, Number Density of Martian Craters. Bellcomm Rept. TR-68-710-1.

NASA SP-8013. 1969, Meteoroid Environment Model–1969 (Near Earth to Lunar Surface).

NASA SP-8038. 1970, Meteoroid Environment Model–1970 (Interplanetary and Planetary).

Piotrowski, S. 1953, Collisions of Asteroids. Acta Astron. 5, (Oct.), 115-138.

Wetherill, G. W. 1967, Collisions in the Asteroid Belt. J. Geophys. Res. 72(9), 2429-2444.

Whipple, Fred L. 1967, On Maintaining the Meteoritic Complex. Smithson. Astrophys. Observ. Special Rept. 239. (Also available in NASA SP-150, 1967, pp. 409-426.)

DISCUSSION

ALFVÉN: Have you made any estimates on how much danger a space mission to a comet might have, considering the fact that comets are associated with meteor streams?

KESSLER: No.

Page intentionally left blank

DESCRIPTION OF PIONEER F AND G ASTEROID BELT PENETRATION EXPERIMENT

WILLIAM H. KINARD AND ROBERT L. O'NEAL
NASA Langley Research Center

A NASA Langley Research Center meteoroid detection experiment will be performed on both the Pioneer F and G missions. The objective of this experiment is to obtain data that will indicate the population of meteoroids in the 10^{-9} to 10^{-8} g mass range in interplanetary space and, in particular, the region of the asteroid belt, and establish a first indication of the meteoroid penetration hazard to spacecraft in the asteroid belt. Specifically, the experiment will detect meteoroid penetrations of stainless steel targets 25 and 50 μm (1 and 2 mils) thick as the Pioneer spacecraft travel in interplanetary space through the asteroid belt to Jupiter and beyond.

The large asteroids that are visible from Earth are, of course, much too sparse to present a hazard to spacecraft. The spacecraft designer is concerned about the population of the more numerous smaller mass particles in the asteroid belt. The environmental model (NASA SP-8038, 1970),[1] which is generally used in spacecraft design, for the distribution of these smaller mass asteroidal particles is presented in figure 1. In this model, the concentration of asteroidal meteoroids as a function of mass is based on an extrapolation of the data of number and mass for visible asteroids, with the number of smaller asteroids being limited to the estimated number that will reflect no more sunlight than is observed in the counterglow. The variation of the number of asteroidal meteoroids of all masses as a function of radial distance from the Sun, space longitude, etc., is assumed to vary as the asteroids are observed to vary.

The possibility of large errors existing in this model is recognized. The model represents an extrapolation of some 20 to 30 orders of magnitude from the asteroid data, which have intrinsic uncertainties resulting from the unknown albedo, density, and shape. There are also uncertainties in the limits placed on the model by the observed intensity of the counterglow. If a pessimistic view of all of these uncertainties is taken in spacecraft design considerations, the meteoroid shielding requirements would inflict severe weight penalties. It is therefore important to better define the population of

[1]See also p. 595.

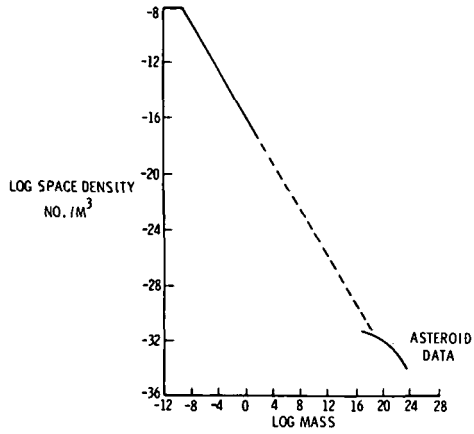

Figure 1.–Interplanetary meteoroid environment at 2.5 AU.

the smaller asteroidal particles, and flight experiments are necessary to generate the required environment definition.

APPROACH

The asteroid belt penetration experiment objectives, as previously stated, will be accomplished by measuring the time, and thus the frequency, of meteoroid penetrations in stainless steel targets during interplanetary flight. The pressurized cell type of detector is being used to detect penetrations. In principle, the detector consists of a cavity that is gas pressurized and is equipped with a pressure monitoring device. If and when a meteoroid penetrates the test material, the gas in the cavity will leak out and the loss in pressure will be detected. The number of cells that have been punctured will be determined at each interrogation of the spacecraft.

Impact tests have shown that cell penetrations can be expected from impacts of meteoroids of approximately 10^{-9} g mass or larger. These tests indicate that each 25 μm (1 mil) cell penetration could be interpreted as an impact of approximately a 10^{-9} g mass meteoroid or larger and each 50 μm cell penetration could be interpreted as an impact of 10^{-8} g mass meteoroid or larger. Additional impact tests are being conducted to better define the requirements for detector penetration.

The pressure cells to be flown on the Pioneer F spacecraft will all have 25 μm (1 mil) thick target material. The decision on the target thickness for the pressure cells on the Pioneer G spacecraft will be dependent on the data from Pioneer F. If the expected number of 25 μm penetrations is detected on the Pioneer F mission, then 50 μm thick test material will be flown on Pioneer G. If the 25 μm penetrations detected by Pioneer F are fewer than expected, and if additional data are needed to form a reasonable 25 μm data sample, then the Pioneer G spacecraft will also fly 25 μm target material.

SYSTEM DESCRIPTION

Some details of the systems comprising the penetration experiment are discussed in the following paragraphs. The weight of the experiment hardware is approximately 13.3 N (3 lbf) and the power required by the experiment is 1 W.

Pressurized Cell Penetration Detector

The experiment has 0.47 m^2 (5 ft^2) of detector area composed of 216 individual pressurized cells. The 0.47 m^2 is made up of 12 panels, each with approximate overall dimensions of 20 by 30 cm (8 by 12 in.) and composed of 18 individual pressurized cells. Figure 2 is a photograph of one detector panel.

The panels are made of 21-6-9 stainless steel. Each of the panels is made by resistance welding a 25 μm (1 mil) thick and a 50 μm thick sheet of stainless steel together in an "air mattress" configuration to form the individual cells. The cells will be pressurized with a nitrogen and argon gas mixture. The mixture will be 75 percent argon and 25 percent nitrogen. Each cell will be pressurized to a pressure of 115 kN/m^2 (16.7 psia).

The pressure switch that is used to indicate the loss of pressure in each cell is a cold-cathode device. The switch, as can be seen in figure 2, consists of two electrodes in a pressure cavity that is connected by a copper tube to the pressure cell. Approximately 525 V is impressed continuously across the two

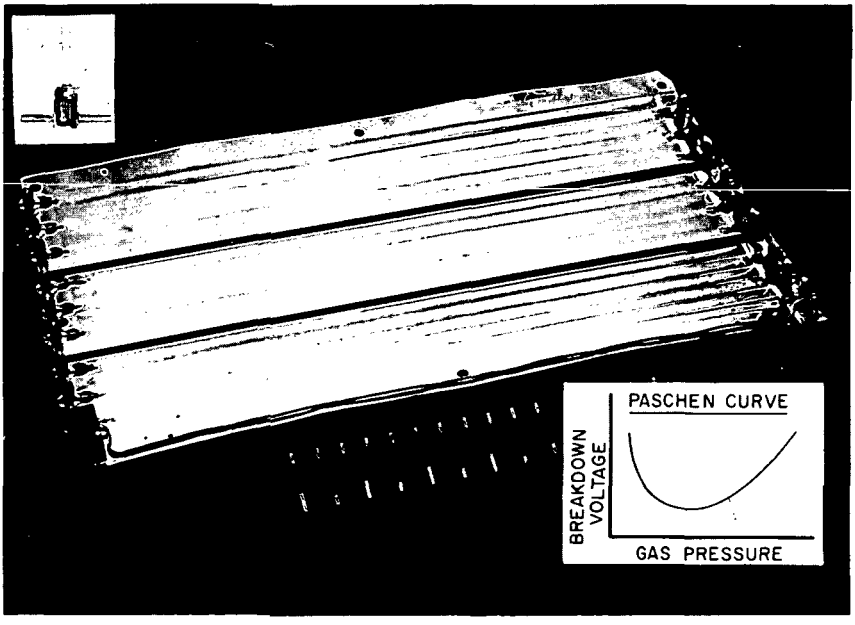

Figure 2.–Pioneer F and G penetration detector.

electrodes, which are insulated from each other and from the panel. In the event of a cell puncture, the device will act as a glow tube because of ionization of the internal gas and it will conduct an electric current during a limited pressure range as the cell leaks down. The device will start conducting when the pressure in the cell drops below about 14 kN/m^2 (2 psia) and it will stop conducting when the pressure drops below about 0.14 kN/m^2. The tips of the two electrodes in the pressure cavity are electroplated with a small amount of ^{63}Ni to enhance ionization of the gas.

Electronics

A functional block diagram of the experiment electronics is shown in figure 3. The experiment is divided into two essentially independent parts for maximum experiment reliability. One electronic system is used for half of the penetration detectors and another electronic system is used for the other half. A common dc/dc power converter takes power from the spacecraft power system and supplies power for the pressure switches, for each of the two signal conditioning circuits, and for each of the two recycling event counters. The pulse resulting from the discharge of any pressure switch will be shaped and stored by a counter. With a discharge, an event counter will advance one count and will be locked out so it cannot advance again for a period of 86 min. This is to insure that any multiple pulsing on the initiation of a switch discharge will not be interpreted by the system as multiple penetrations. The probability of another legitimate impact and switch discharge during this lockout period is small.

Each of the event counters has a capacity of 32 counts before recycling. The time of a sensor puncture will be assumed to be the time at which an

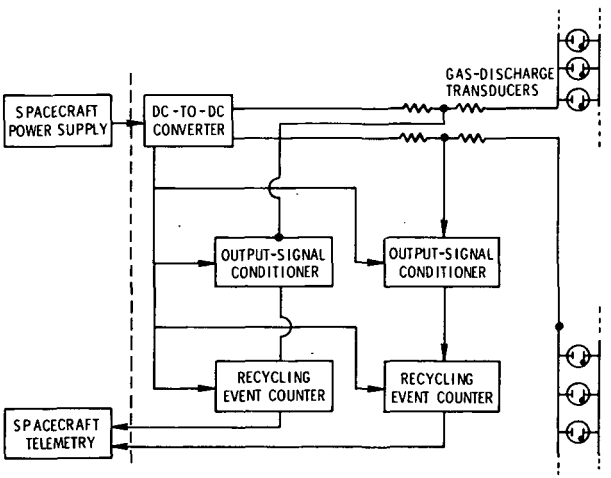

Figure 3.–Instrumentation schematic.

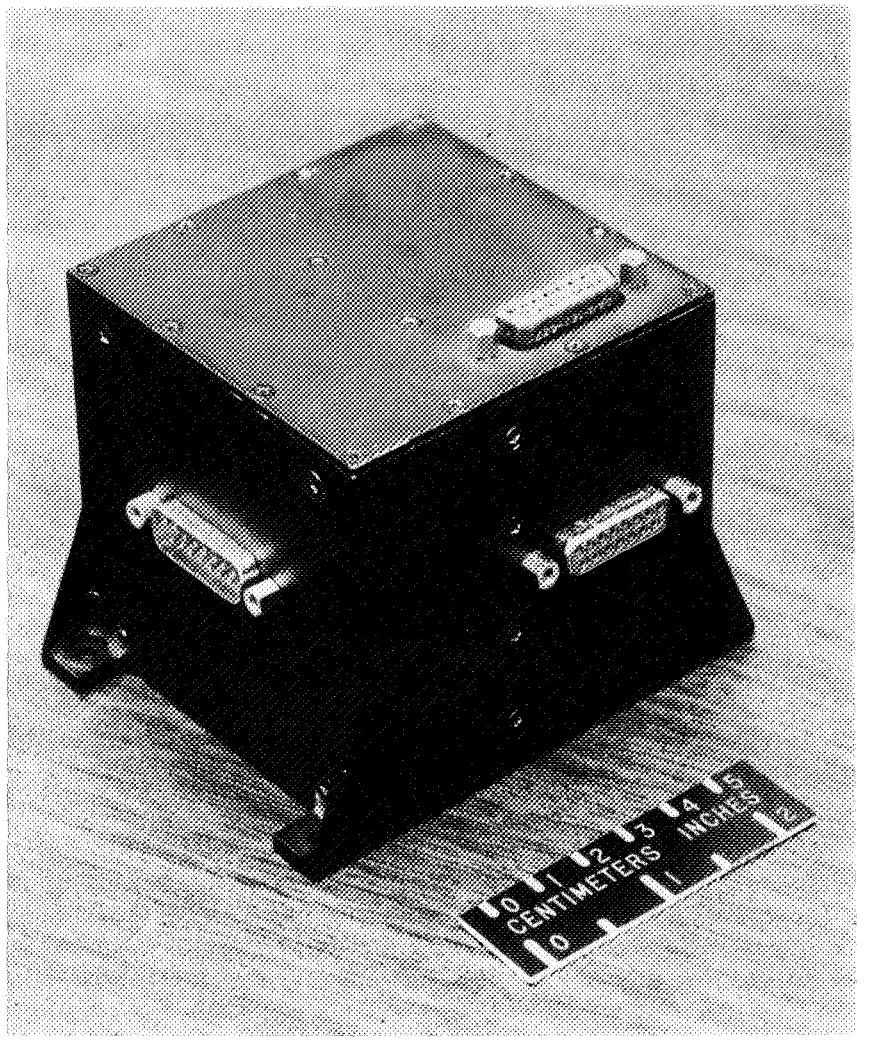

Figure 4.–Electronic module.

interrogation shows an increase in a counter reading. Two 6 bit words accommodate the output from the two counters.

Figure 4 is a photograph of the packaged electronic subsystem.

SPACECRAFT MOUNTING

An artist's sketch of the Pioneer F and G spacecraft is shown in figure 5. The 12 penetration detector panels will be mounted on the back side of the spacecraft high-gain antenna dish as is shown in the inserted sketch. A wiring

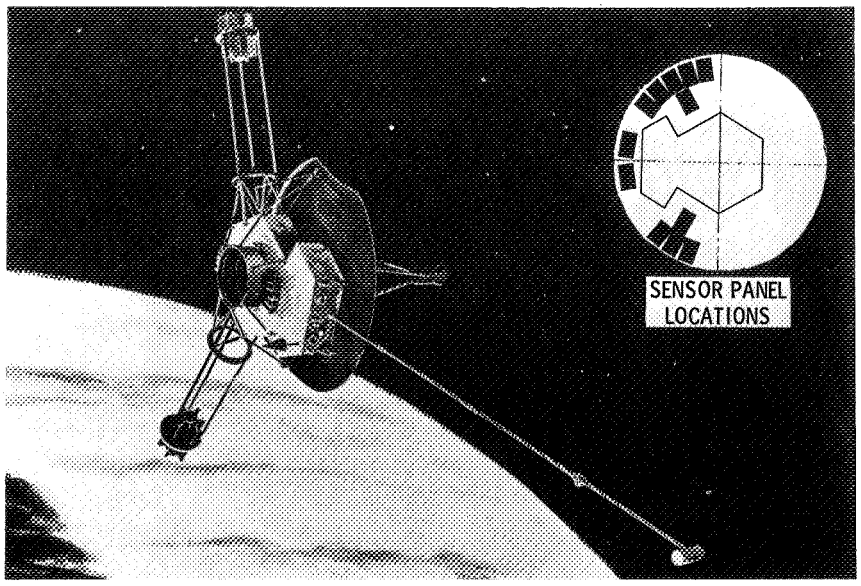

Figure 5.–Pioneer F and G spacecraft. Sensor panels are located on the back of the antenna dish.

harness will connect the panels to the experiment electronics, which will be located inside the spacecraft scientific instrument compartment.

TRAJECTORY AND ORIENTATION

The trajectory for the Pioneer F and G missions to Jupiter is shown in figure 6. The spacecraft, flying near the plane of the ecliptic, will enter the region of the asteroid belt approximately 150 days after launch, and they will remain in the belt for approximately 200 days. The launch of Pioneer G is planned to take place approximately 390 days after the launch of Pioneer F or essentially just after Pioneer F traverses the asteroid belt. The spacecraft are scheduled to reach Jupiter approximately 600 days after launch.

The spacecraft will spin about an axis through the center of the high-gain antenna dish. With the exception of the first few hours of the mission, the spin axis will essentially be oriented such that it intersects the Earth throughout the mission. This spacecraft orientation places the detector panels in a reasonably good viewing position to intercept asteroidal particles.

It is assumed that the asteroidal particles are in near-circular orbits and thus the relative impact velocity vector between the particles and the spacecraft will remain near the spin axis. As is illustrated in figure 7, the relative velocity vector will be only 28° off the spin axis at 1.6 AU, and it will diminish to only 8.5° off the spin axis at 2.5 AU. As the spacecraft leaves the asteroid belt at

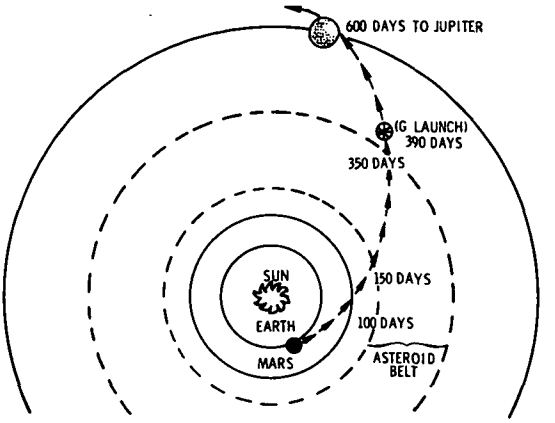

Figure 6.–Trajectory profile.

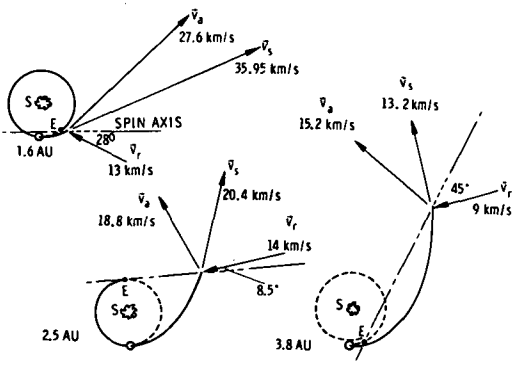

Figure 7.–Spacecraft orientation. v_a = velocity of asteroidal particles; v_s = velocity of spacecraft; v_r = relative impact velocity

about 3.8 AU, the relative velocity vector will increase to about 45° off the spin axis.

It is assumed that the cometary particles in interplanetary space are near omnidirectional and thus that the detector panel orientation is not critical for their detection.

ESTIMATE OF PENETRATIONS

Table I presents the number of detected penetration events that are indicated by Kessler's model of the interplanetary meteoroid environment (ref. 1). As already discussed, this model, and thus the predicted events, can be grossly in error and one would be presumptuous to place much confidence in such predictions.

TABLE I.–*Estimate of Penetration History*

Position, AU	Penetrations of 25 μm (1 mil) target				Penetrations of 50 μm (2 mil) target			
	Asteroidal	Cometary	Total	Cumulative	Asteroidal	Cometary	Total	Cumulative total
1.00 to 1.33	0	13	13	13	0	5	5	5
1.33 to 1.66	1	10	11	24	0	4	4	9
1.66 to 2.00	7	6	13	37	2	3	5	14
2.00 to 2.33	32	6	38	75	11	3	14	28
2.33 to 2.66	37	4	41	116	15	2	17	45
2.66 to 3.00	35	2	37	153	7	2	9	54
3.00 to 3.33	8	1	9	164	7	2	9	63
3.33 to 3.66	2	1	3	167	3	2	5	68
3.66 to 4.00	0	0	0	167	0	1	1	69
4.00 to 4.33	0	1	1	168	0	1	1	70
4.33 to 4.66	0	2	2	170	0	1	1	71
4.66 to 5.00	0	1	1	171	0	1	1	72

CONCLUDING REMARKS

The pressure cell type of penetration detector was chosen for the Pioneer F and G missions for a number of reasons. It is an extremely simple detector, the data from it are easy to interpret, and it is essentially unaffected by the environments encountered, other than, of course, the meteoroid environment.

Successful flight experiments on Explorers 13, 16, and 23, and all Lunar Orbiter spacecraft have proven the pressure cell penetration detector to be the most reliable meteoroid detector yet used in space. The actual penetration measurements are valuable to spacecraft technology. There remains, of course, an uncertainty in the interpretation of the penetration events in terms of the mass of the impacting meteoroid. However, there does exist a background of many years in penetration research and, based on this background, it is felt that the uncertainty in the interpretation of penetration data in terms of the mass of the impacting meteoroid is a minimum uncertainty.

REFERENCE

NASA SP-8038. 1970, Meteoroid Environment Model–1970 (Interplanetary and Planetary).

[*Editorial note: The Pioneer Mission to Jupiter is described in NASA SP-268.*]

Page intentionally left blank

ASTEROID DETECTION FROM PIONEERS F AND G?

ROBERT K. SOBERMAN
General Electric Space Sciences Laboratory and Drexel University

and

SHERMAN L. NESTE AND ALAN F. PETTY
General Electric Space Sciences Laboratory

INSTRUMENT DESCRIPTION

The Pioneer asteroid/meteoroid detector (Sisyphus[1] or A/MD) is an optical instrument designed primarily to make measurements of small interplanetary particles that pass within about 1 km of the spacecraft. Because it is an optical system, it can also detect larger bodies at greater distances. We can approximate the amount of light incident upon the instrument resulting from an assumed spherical object by

$$I = \frac{I_0 r \pi a^2}{2s^2 \pi R^2} = \frac{I_0 r}{2s^2}\left(\frac{a}{R}\right)^2 \tag{1}$$

where I_0 is the solar irradiance at 1 AU, r is the reflectivity of the object (equal to 3/2 the "geometric albedo"), a is the radius of the object, s is the distance from the Sun in astronomical units, and R is the range from the object to the detector. A Sun-object-instrument angle of approximately 45° is assumed. For a single detector, one would have no way of distinguishing objects with the same a/R ratio. The Sisyphus concept provides a means of determining the range and, hence, the size of the object.

Consider three optically alined telescopes equipped with photomultipliers as defining three parallel cones in space. If the telescopes are identical, then the edges of the fields of view remain at a fixed distance from each other regardless of range. Any luminous object that crosses through the intersecting fields of view is then detected by each of the photomultipliers. From the entrance and exit times in each field of view, one can completely calculate the trajectory of the object in space, provided only that one has sufficiently good optics and a sufficiently long baseline between telescopes.

[1] Refers to man's never-ending confrontation with the environment; i.e., space rocks.

For the mathematics of the system, we define three cones as shown in figure 1; their half angles are θ. Lines joining their apexes form an arbitrary triangle in the plane perpendicular to their axes. For purposes of convention, the vector from the base of the ith cone to the particle's entrance into that cone is designated $\boldsymbol{\rho}_i$ and the vector to the particle's exit is $\boldsymbol{\sigma}_i$. Times of entrance and exit at the ith cone are designated τ_{ij} where j is 1 for an entrance point or 2 for an exit point. v is an arbitrary velocity vector and l_{ij} is the distance between the ith and jth cone.

Using this convention, five independent vector equations result:

$$\left.\begin{aligned}
\sigma_1 &= \rho_1 + (\tau_{12} - \tau_{11})\mathbf{v} \\
\rho_2 &= \rho_1 + (\tau_{21} - \tau_{11})\mathbf{v} - l_{12} \\
\sigma_2 &= \rho_1 + (\tau_{22} - \tau_{11})\mathbf{v} - l_{12} \\
\rho_3 &= \rho_1 + (\tau_{31} - \tau_{11})\mathbf{v} - l_{13} \\
\sigma_3 &= \rho_1 + (\tau_{32} - \tau_{11})\mathbf{v} - l_{13}
\end{aligned}\right\} \qquad (2)$$

By breaking these into components, we have 15 equations in 15 unknowns; therefore, a solution exists. Because the derivation is long and tedious, it is omitted here. The solution has been programed for computer use.

The above vector equations remain unchanged if the cone axes are misalined (i.e., not parallel). However, the 15 component equations are more complex

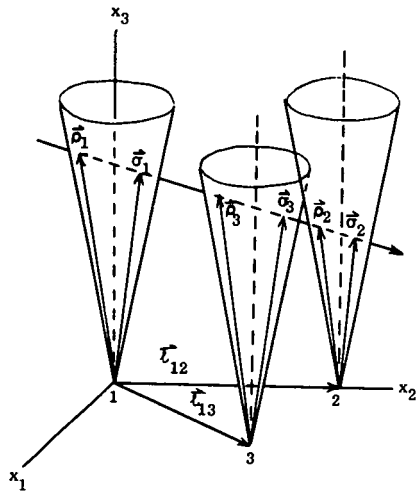

Figure 1.– Sisyphus geometry (for convention only).

because they involve two additional angles for each cone necessary to specify its orientation. This misalined case has been reduced from the 15 original equations to 3 equations in 3 unknowns. Because of their complexity, further reduction appears impractical. Numerical solutions are obtained by computer iteration.

Thus, independent of the amplitude of the signals detected by the individual optical systems, one can establish the three velocity components and the range of the body. Using this calculated range, the measured light intensity at the detector, and the known solar intensity, one can solve equation (1) for the product of the reflectivity and the cross-sectional area, and thus determine the mean radius of the body to an uncertainty of the square root of the reflectivity. Further, from the real time at which the event took place; the known position, velocity, and orientation of the vehicle from which the measurement was made; and the three velocity components of the body, the complete orbit of the body in the solar system can be determined.

The A/MD, as designed for the Pioneer F and G missions, uses four 20 cm Cassegrainian telescopes, each coupled to a photomultiplier tube (S20 photocathode) as sensor. The four optics are arranged in a square array 22 cm on a side. The use of four telescopes yields an inherent redundancy because any three sensors yield all of the required data. If a particle exceeds the threshold in all four fields of view, one obtains four sets of solutions to equation set (2). An artist's sketch of the A/MD instrument on the Pioneer spacecraft is shown in figure 2. The instrument hardware (excluding spacecraft mounting panel) has a mass of 2.4 kg and an average power requirement of 2.0 W.

The A/MD is a background-limited detector. The noise inherent in such a detector is given by

$$i_n = \sqrt{2\, i_b q f} \tag{3}$$

where i_b is the total background current, q is the unit electrical charge, and f is the bandwidth of the circuitry

Because the Pioneer is a rotating spacecraft, the sky background viewed by the telescopes is continuously varying. The threshold in each telescope is designed to "follow" the background and high-frequency noise. Because the telescopes remain approximately alined, the background and, consequently, the thresholds of all four telescopes should remain approximately equal. The background is averaged through a comparatively long time constant circuit that has the effect of introducing a delay in the background response. The relative threshold for each telescope at any instant t is designed to be self-setting at a value of

$$T_{\text{rel}} = K_1 i_n(t) + K_2 i_b(t) - i_b(t - \Delta t) \tag{4}$$

The operating modes of the instrument with the values for K_1, K_2, and the time constant Δt for background averaging are given in table I. A computer

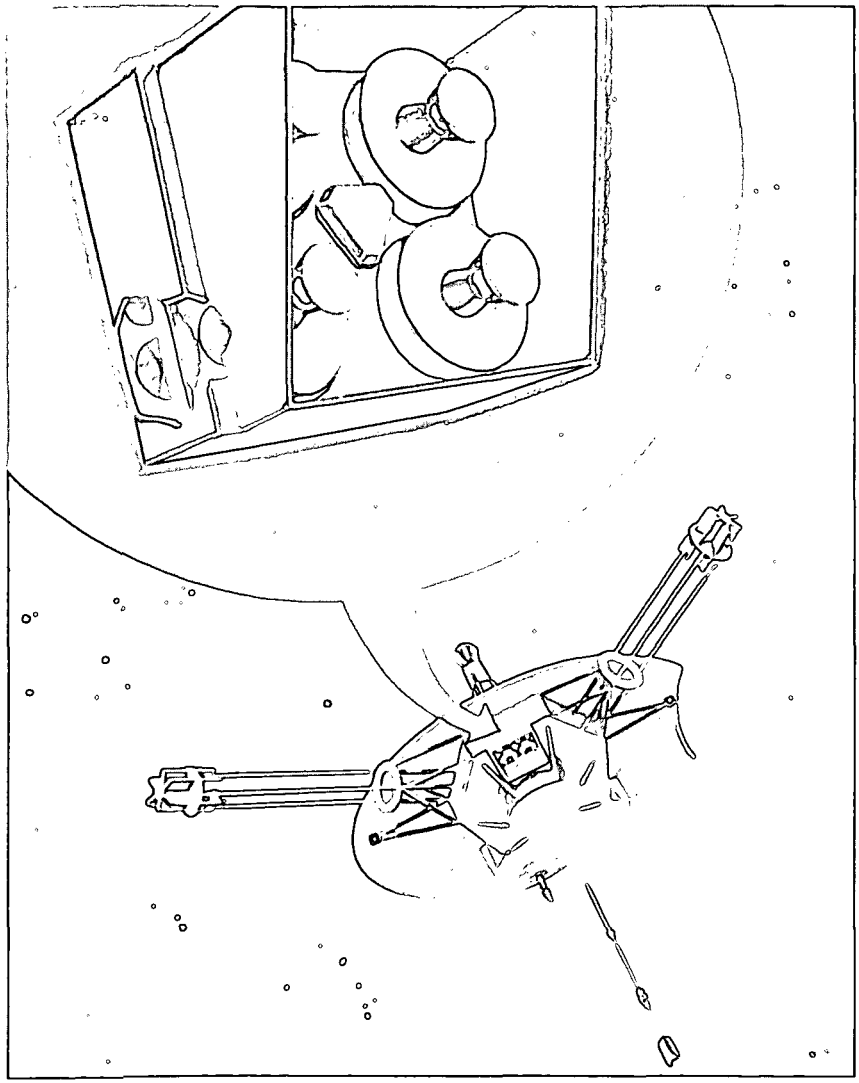

Figure 2.–Artist's sketch of Pioneer F and G A/MD.

program that calculates the change in the relative threshold over a complete spacecraft rotation as a function of the orientation of the spacecraft spin axis has been written (Soberman and Neste, 1971). The program has a sky brightness map (Roach and Megill, 1961) built in. A typical output for the wideband instrument mode is shown in figure 3.

Because the instrument is "triggered" by noise when the intensity exceeds the threshold value, a technique for reducing the number of false events must

TABLE I.–*Modes of Pioneer F and G Sisyphus Instrument*

Operating mode	Bandwidth *f*, kHz	K_1	K_2	Time constant, s
Wideband	500	2.0	1.1	0.047
Mediumband	160	2.0	1.1	.047
Narrowband	13	2.0	1.1	.047
High threshold	([a])	2.0	1.2	.047
Calibration	13	2.0	1.1 to 1.2	.5

[a]For all three bandwidths.

be employed. This is accomplished by a simple threefold coincidence requirement that must be fulfilled before an event is considered legitimate and is recorded. This means that the transit time of a particle through the overlap region of three of the four fields of view must be greater than or equal to a predetermined minimum (3.2 μs). This criterion limits the number of recorded false events to approximately one per month for the wideband mode.

In addition, the thresholds are designed to have hysteresis to reduce the probability of rejecting a legitimate signal. For example, if a target is passing through the field of view and noise or fluctuations in target intensity cause the level to drop below the threshold before coincidence is confirmed, the signal would be regarded as an error and rejected. However, if the threshold is reduced to a lower level after being exceeded, the probability of dropouts due

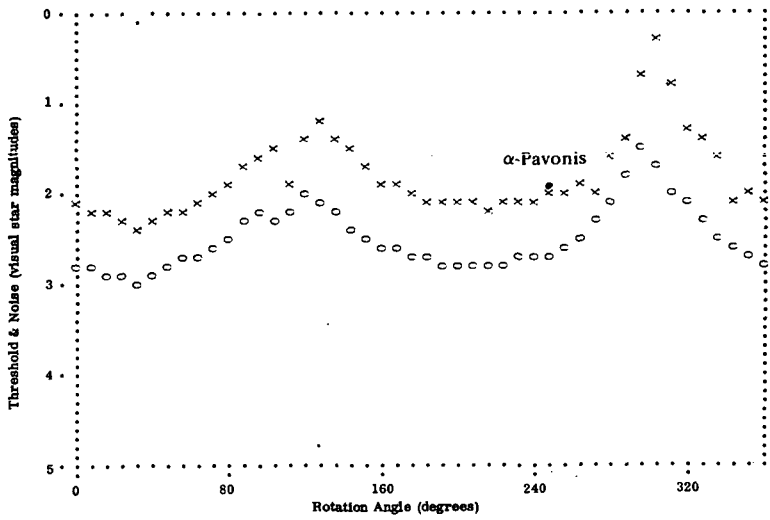

Figure 3.–Computer-generated cyclic threshold variation for Pioneer F and G A/MD in the wideband mode. Galactic longitude = 333°; galactic latitude = 0°; bandwidth = 500 kHz. x indicates threshold; o indicates noise.

to noise is reduced. The rate at which the threshold is reduced and the level to which it is reduced do not affect noise rejection nor prevent a legitimate end of signal determination.

Because the threshold follows the background, a distant large asteroid moving with low relative angular velocity will, in several time constants of the averaging circuit, be considered as part of the background. When this happens, a false termination of the signal will occur. Another problem relating to the measurement of relatively slow-moving asteroids is the star exclusion circuit of the A/MD. To limit the amount of data telemetered, any "event" that recurs on successive vehicle rotations is ignored after the first measurement. Thus, if such a relatively slow-moving asteroid is detected, it can only be measured once in a given region of the sky. Operation in the "star exclusion disabled" mode, which would allow multiple measurements of the passage of slow-moving asteroids through the complete field of view, is incompatible with the present Pioneer A/MD telemetry assignment. Modifications of that assignment were considered too costly in view of the low probability of such measurements. (See below.)

ASTEROID BELT MODELS

Current models of the particle number density within the asteroid belt are usually expressed by a relationship of the form

$$N(a) = Ca^{-\alpha} \tag{5}$$

where a is the particle radius and C and α are constants. The major uncertainty, and point of controversy, between the various models lies in determining the value of α. Arguments for the various values of α are usually based on theoretical studies regarding the collision and subsequent fragmentation of particles within the belts. On the basis of such a grinding mechanism, Piotrowski (1953) argues that particles near $a = 1$ cm should follow an $\alpha = 3$ law. However, Anders (1965) does not believe that the fragmentation history of the asteroids has progressed as far as does Piotrowski and favors a value of α more nearly equal to 2.

A more recent model of the asteroid distribution is that published by Dohnanyi (1969) in which he considers the evolution of a system of particles undergoing inelastic collisions and fragmentation.[2] He derives a theoretical density function for asteroids given by

$$f(m)\,dm = 2.48 \times 10^{-19}\, m^{-1.837}\, dm \tag{6}$$

where m is the particle mass. After performing the integration and expressing the number density in the form of equation (5), we obtain

$$N(a) \approx 9.7 \times 10^{-23}\, a^{-2.5} \tag{7}$$

[2]See p. 263.

where a is the particle radius in meters. Following Dohnanyi, a particle density of 3.5×10^3 kg/m^3 was assumed in the conversion from mass to radius.

Figure 4 presents some recent data on the cumulative asteroid distribution. The histograms are for the McDonald survey (Kuiper et al., 1958) and the more recent Palomar-Leiden survey (PLS) (van Houten et al., 1970). Distributions are shown for power-law exponents of -3 (Piotrowski), -2.5 (Dohnanyi), -2 (Anders), and the literal interpretation of the PLS of -1.75. Implicit in

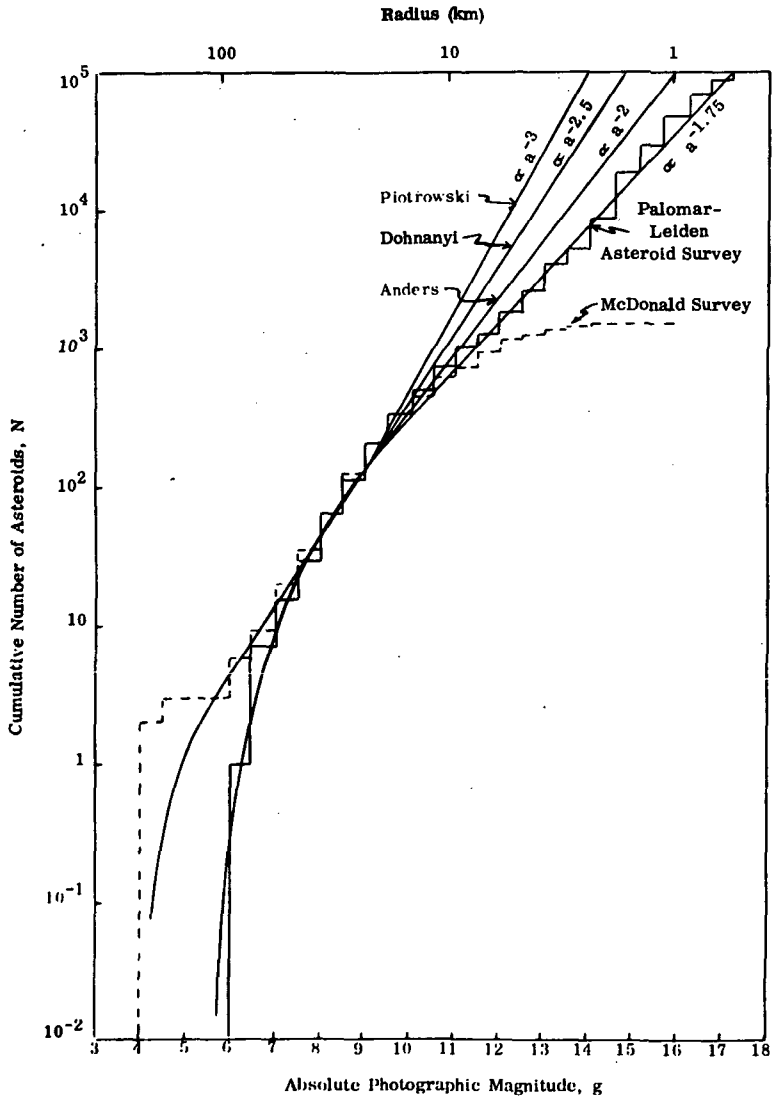

Figure 4.–Cumulative asteroid distribution.

accepting any of the three steeper values is the assumption of a systematic selection process in the surveys. How far any of these extrapolations can be extended is problematical. For a portion of the present analysis it is necessary to extrapolate beyond the point of any reasonable confidence. However, until the Pioneer spacecraft have actually penetrated the asteroid belts, these extrapolations form the only source from which anticipated data rates can be inferred.

If we assume an average asteroid velocity of 15 km/s relative to the Pioneer spacecraft, a cumulative asteroidal flux can be calculated for each of the

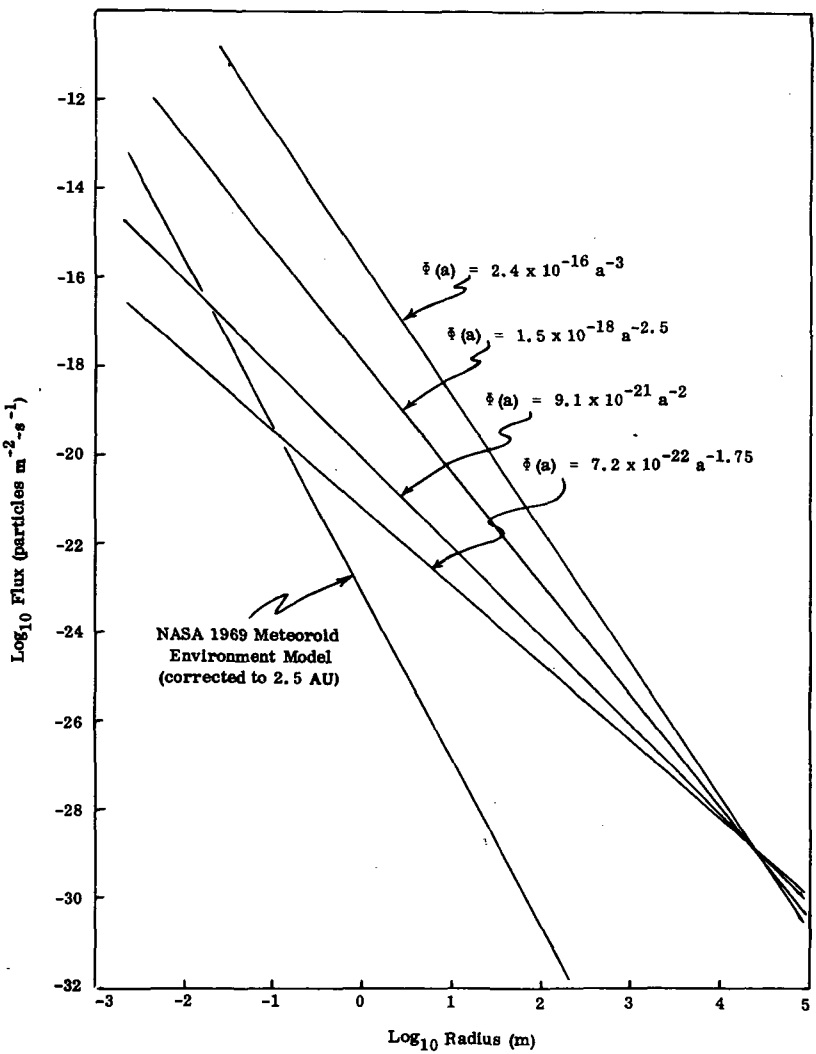

Figure 5.–Asteroid and cometary meteoroid flux models at 2.5 AU.

distribution models. These are presented in figure 5 for the four models, together with a flux model for the meteoroid environment at 2.5 AU. The meteoroid environment was taken from NASA SP-8013 (1969), corrected for the Earth's focusing effect and reduced by an inverse-square dependence on the heliocentric distance.

Estimates of particle reflectivity are also open to speculation. For the present purposes, three values have been chosen. As pointed out above, the reflectivity used is equal to 3/2 the geometric albedo. The three values used are a reasonable lower limit of 0.07, a meteoroid value of 0.20, and the mean for the asteroids Ceres, Pallas, Juno, and Vesta (Gehrels, 1970), which is 0.3. This last was converted from a geometric albedo of 0.2 (the value used by Dohnanyi, 1969).

ASTEROID EVENT RATES

The anticipated A/MD event rates during the Pioneer transit of the asteroid belts can be determined for the various power-law models and particle reflectivities as shown below.

The area surrounding the field of view of the A/MD can be approximated as a truncated cone:

$$A \approx \pi\theta(R^2 - R_{\min}{}^2) \tag{8}$$

and

$$dA \approx 2\pi\theta R\, dR \tag{9}$$

for small θ (the half angle of the telescopes). In the wideband mode, it was shown in figure 3 that the mean sensitivity of the A/MD instrument is approximately 1.75 visual stellar magnitudes. This can be translated through equation (1) in terms of a range to radius relationship applicable at a heliocentric distance of 2.5 AU:

$$R/a = 1.5 \times 10^5\, r^{1/2} \qquad s = 2.5 \tag{10}$$

Substituting this into equation (8), the effective detector area as a function of particle radius can then be expressed as

$$dA(a) = 1.4 \times 10^{11}\, \theta r a\, da \tag{11}$$

The asteroid number density can be written as

$$N(a) = 8.7 \times 10^{-34} \left(\frac{a}{a_0}\right)^{-\alpha} \tag{12}$$

and converted to a particle flux per unit area with the assumption of an average particle velocity v:

$$\Phi(a) = 8.7 \times 10^{-34} \left(\frac{a}{a_0}\right)^{-\alpha} v \tag{13}$$

The event rate E is then determined from the integral

$$E = \int_A \int_\Phi d\Phi dA = \int_A \Phi \, dA \tag{14}$$

$$= 1.2 \times 10^{-22} \theta r v a_0{}^{\alpha} \int_{a_{\min}}^{a_0} a^{1-\alpha} \, da \tag{15}$$

For $\alpha \neq 2$,

$$E = 1.2 \times 10^{-22} \frac{\theta r v}{2 - \alpha} \left(a_0{}^2 - a_0{}^{\alpha} a_{\min}^{2-\alpha}\right) \tag{16}$$

and for $\alpha = 2$,

$$E = 1.2 \times 10^{-22} \theta r v a_0{}^2 \ln \frac{a_0}{a_{\min}} \tag{17}$$

Using the values

$$\theta = 4.0^\circ$$

$$v = 1.5 \times 10^4 \text{ m-s}^{-1}$$

$$a_0 = 2.6 \times 10^4 \text{ m}$$

$$a_{\min} = 10^{-4} \text{ m}$$

for $\alpha \neq 2$,

$$E = 1.3 \times 10^{-19} [6.8 \times 10^8 - 10^{4\alpha - 8} (2.6 \times 10^4)^{\alpha}] \frac{r}{2 - \alpha} \tag{18}$$

and for $\alpha = 2$,

$$E = 1.7 \times 10^{-9} r \tag{19}$$

From this, we can obtain an event rate for each set of assumptions.

Because the A/MD is oriented at an angle of 45° from the spacecraft (S/C) spin axis, its field of view will describe a 49° right cone in space of wall width approximately 8°. (See fig. 6.) Any particle that takes more than approximately 12 s (the vehicle rotation period) to pass through the 8° instrument field of view must be seen by the system (i.e., it cannot escape from the

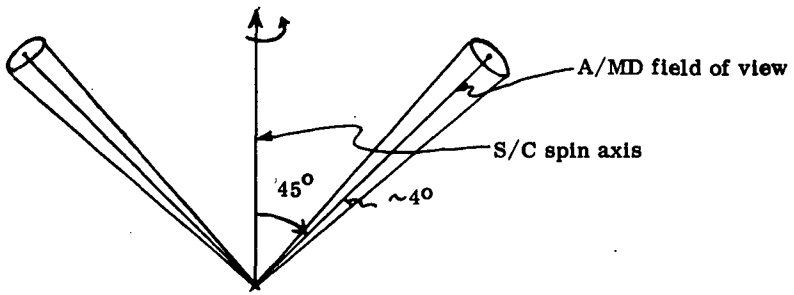

Figure 6.–Effective viewing field for large asteroids (angular velocity < 0.68 deg/s).

45° + 4° cone described during the vehicle rotation without being detected). Thus, for large bodies moving at low relative angular velocity, the effective field of view becomes 98°. As an example, for a minimum asteroid size (radius) of 10 m and a reflectivity of 0.2, the effective detection range is 650 km in the wide bandwidth mode. Event rates can thus be calculated for large asteroids using the effective cone area measured in square meters.

$$A = \pi R^2 \sin 49°$$

$$= 5.3 \times 10^{10} a^2 r \qquad s = 2.5 \tag{20}$$

This yields event rates of

$$E = 9.2 \times 10^{-23} \frac{rv}{2 - \alpha} \left(a_0^{\,2} - a_0^{\,\alpha} a_{\min}^{\,2-\alpha} \right) \qquad \alpha \neq 2 \tag{21}$$

$$= 9.2 \times 10^{-23} r v a_0^{\,2} \ln \frac{a_0}{a_{\min}} \qquad \alpha = 2 \tag{22}$$

where $a_{\min}$ is now equal to 10 m. The computations have been carried out for the combinations of α and r to yield the event rates shown in tables II and III.

From tables II and III and from the nature of the A/MD, it is apparent that for power-law distributions steeper than those with $\alpha = 2$, the event rate would be dominated by small particles. Although larger bodies would tend to predominate for power-law distributions with $\alpha = 2$ or less, it is unlikely that the A/MD would detect any asteroid events. In point of fact, if α is much less than 2.5, it is possible that passage of the Pioneer spacecraft through the asteroid belt would not even be noted. In figure 7, we have plotted the anticipated cometary meteoroid event rate as a function of heliocentric distance. The values from table II are shown in the asteroid region. Included also is a maximum value based upon a zodiacal light interpretation (Kessler,

TABLE II.–*Asteroidal Events Per Day, Wideband Mode*

r	α			
	1.75	2.0	2.5	3.0
0.07	2.1×10^{-6}	1.0×10^{-5}	1.7×10^{-2}	140
0.2	6.0×10^{-6}	2.9×10^{-5}	4.8×10^{-2}	400
0.3	9.0×10^{-6}	4.4×10^{-5}	7.3×10^{-2}	600

Angular velocity > 0.685 deg/s.

TABLE III.–*Large Asteroid* (a > *10 m*) *Events Per Day, Wideband Mode*

r	α			
	1.75	2.0	2.5	3.0
0.07 ...	2.3×10^{-6}	4.5×10^{-5}	7.1×10^{-4}	1.5×10^{-2}
0.2	6.5×10^{-6}	1.3×10^{-4}	2.0×10^{-3}	4.2×10^{-2}
0.3	9.7×10^{-6}	1.9×10^{-4}	3.0×10^{-3}	6.3×10^{-2}

Angular velocity <0.685 deg/s.

1968). From this figure, one can see how the cometary flux might predominate during asteroidal passage. For small particles, the velocity determinations of the A/MD should, however, enable us to distinguish cometary from asteroidal material if both are noted.

Assuming a uniform distribution in the asteroid belt, the probability of the A/MD detecting a single large asteroid ($a \geqslant 10$ m) during the entire passage can be calculated from table III. The results are presented in table IV. Although the extrapolation is more reasonable in this limited size region, it is obvious from table IV that the distribution slope still dictates the probability of detecting a large asteroid.

The apparent magnitudes of 1735 asteroids that the Pioneer F spacecraft might encounter have been computed (NASA PT-204, 1970). For the vehicle trajectory ephemerides, which were used in that study, the brightest apparent magnitude anticipated is approximately 6.5. As shown above, the mean threshold for the wideband of the A/MD is about 1.75. Consequently, it is unlikely that any of the asteroids considered would be detected. However, as stated in the study, the results are "subject to a very large uncertainty."

One way of increasing the probability of large-body detection would be to narrow the bandwidth of the A/MD. In the narrowband mode, the mean threshold would be approximately 2.75 visual stellar magnitudes. (See fig. 8.) In this mode, linear velocity determination for small particles would be extremely poor at best. However, for large-body detection beyond the effective triangulation range of the Pioneer A/MD version, those consequences are

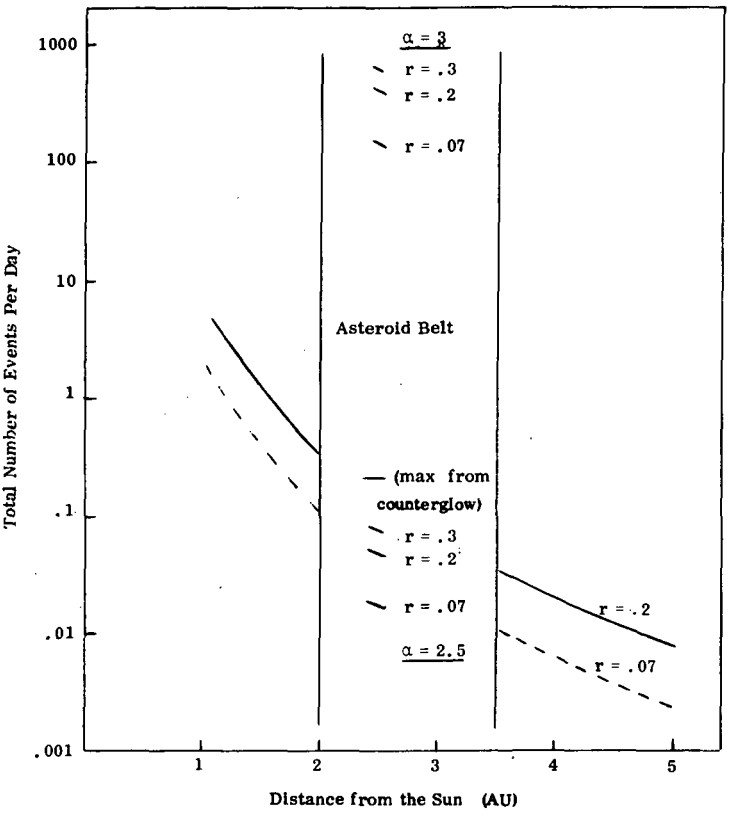

Figure 7.–Anticipated cometary meteoroid event rate for Pioneer F and G A/MD as a function of heliocentric distance with inferred asteroidal event rates.

TABLE IV.–*Probability of Detecting a Large Asteroid (a > 10 m) During a Mission, Wideband Mode*

r	α			
	1.75	2.0	2.5	3.0
0.07 ...	0.03	0.7	10	89
0.2	.10	1.9	26	~100
0.3	.15	2.8	33	~100

Values are in percent.

immaterial. Should there prove to be a lack of particles within the wideband threshold capability, the option of switching to narrowband would be exercised. This option may also be exercised if representative data have already been obtained for the small particles. The result of switching to the

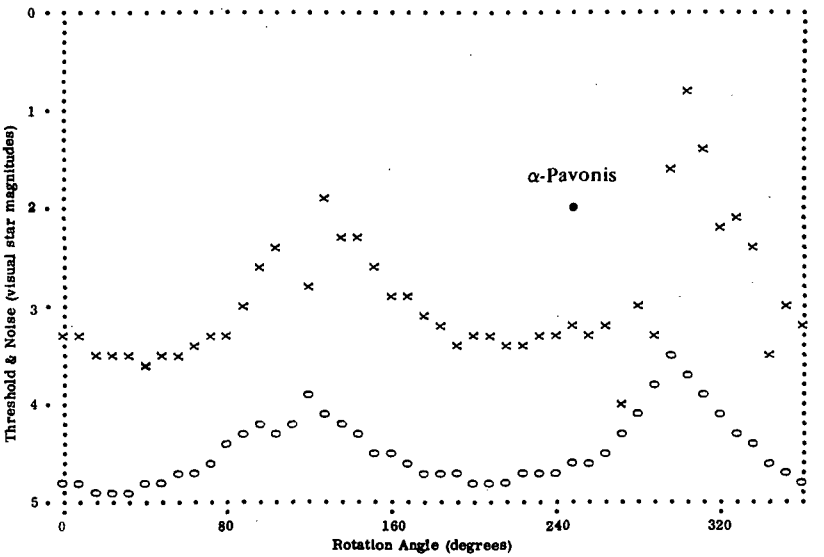

Figure 8.–Computer-generated cyclic threshold variation for Pioneer F and G A/MD in the narrowband mode. Galactic longitude = 333°, galactic latitude = 0°, bandwidth = 13 kHz. x indicates threshold, o indicates noise.

TABLE V.–*Probability of Detecting a Large Asteroid (a > 10 m) During a Mission, Narrowband Mode*

r	α			
	1.75	2.0	2.5	3.0
0.07 . . .	0.09	1.7	24	~100
0.2	.24	4.9	53	~100
0.3	.37	6.9	67	~100

Values are in percent.

narrowband mode in terms of the probability of seeing a single large asteroid is shown in table V.

ACKNOWLEDGMENTS

This effort was partially supported by NASA under contract NAS2-5609. The authors are indebted to Marie Wise for her assistance, patience, and forbearance.

REFERENCES

Anders, E. 1965, Fragmentation History of Asteroids. Icarus 4, 399.

Dohnanyi, J. S. 1969, Collisional Model of Asteroids and Their Debris. J. Geophys. Res. 74(10), 2531.

Gehrels, T. 1970, Photometry of Asteroids. Surfaces and Interiors of Planets and Satellites (ed., A. Dollfus), p. 317. Academic Press, Inc. New York.

Houten, C. J. van, Houten-Groeneveld, I. van, Herget, P., and Gehrels, T. 1970, Palomar-Leiden Survey of Faint Minor Planets. Astron. Astrophys. Suppl. Ser. 2, 339.

Kessler, D. J. 1968, Upper Limit on the Spatial Density of Asteroidal Debris. AIAA J. 6(12), 2450.

Kuiper, G. P., Fujita, Y., Gehrels, T., Groeneveld, I., Kent, J., Van Biesbroeck, G., and Houten, C. J. van. 1958, Survey of Asteroids. Astrophys. J. Suppl. Ser. 3, 289.

NASA PT-204. 1970, Pioneer F Asteroid Analysis. NASA Ames Research Center.

NASA SP-8013. 1969, *Meteoroid Environment Model–1969* (Near Earth to Lunar Surface).

Piotrowski, S. 1953, The Collisions of Asteroids. Acta Astron. 5, 135.

Roach, F. E., and Megill, L. R. 1961, Integrated Starlight Over the Sky. Astrophys. J. 133, 228.

Soberman, R. K., and Neste, S. L. 1971, Sisyphus Threshold Program (THRESH1). General Electric PIR 2R90-34.

DISCUSSION

GREYBER: It seems to me that a telescope using a computer-controlled imaging system, such as an image-orthicon tube, would be preferable for optical detection of asteroids from a spacecraft traversing the asteroid belt to the method chosen by Soberman, especially on a stabilized, nonspinning spacecraft. Stirling Colgate has developed such technology for the rapid detection of supernovas in external galaxies. In principle for asteroid detection one would write a computer program that would "ignore" the background of stars and search for objects moving rapidly across the field of view; i.e., planets, comets, and asteroids.

[*Editorial note: The Pioneer Mission to Jupiter is described in NASA SP-268.*]

Page intentionally left blank

OBSERVATIONS IN THE ASTEROID BELT WITH THE IMAGING PHOTOPOLARIMETER OF PIONEERS F AND G

C. E. KENKNIGHT
University of Arizona

GENERAL DESCRIPTION

Astronomical measurements of the brightness, color, and polarization of light from solar system bodies at phases not visible from Earth are planned for Pioneers F and G. An imaging photopolarimeter (IPP) in the scientific payloads will make these measurements and produce line-scan color images of Jupiter. The IPP collects light with a 2.5 cm aperture telescope that is able to turn in the plane containing the spin axis. Data are taken in scans around the spin axis along a cone whose apex angle is periodically changed by stepping the telescope. The light is analyzed for polarization, divided into blue and red components, and detected by four photomultipliers having electron channel multipliers. Appendix A gives a summary of instrument characteristics.

SCIENTIFIC EXPERIMENTS

Modes of operation of the IPP include (1) standby, (2) zodiacal light, (3) polarimetry, and (4) imaging. Standby is not a data mode but power is applied to the instrument except for the detectors. Imaging is designed for the bright surface of Jupiter at encounter so that the instantaneous field of view (0°.0297) and dwell time per field of view (1 ms) are too small to be of interest in the asteroid belt. Both polarimetry and zodiacal light modes allow detection of objects brighter than 5 mag. (See app. B.) The polarimetry mode is more suited to stellar objects provided their sky position is known, whereas the zodiacal light mode is designed to measure the distribution of sky glow periodically between launch and Jupiter encounter. The sky accessible to the instrument is from 29° from the earthward spin axis (limited by the communication antenna) to 170° from that axis.

Observations in the zodiacal light mode will yield brightness and polarization maps of the sky. Subtraction of the maps made at different radial distances from the Sun will permit separation of the zodiacal light component from unresolved stars, galactic scattered light, etc. After separation, the radial distribution of zodiacal light scatterers can be inferred. Strips of the zodiacal

light map are slightly overlapped because the field of view is 2°.3, the largest possible within the overall design, whereas the cone angle is stepped by 1°.8. Each scan contains 64 sectors of 5°.6 in the plane perpendicular to the spacecraft spin axis. The telemetry gives 1024 intensity levels for a measurement. The measurement cycle at each cone angle requires 20 rolls: 8 for data, 2 for calibration with the aperture closed or with a radioisotope-activated phosphor light source in view, and 10 for data readout. At a nominal 5 rpm spin rate, an entire map requires about 5 hr of observations. The operation is automatic after selection of the mode and of the detector sensitivity. Stepping can be inhibited or reversed by command to concentrate observations on a particular portion of the sky. Online data analysis will include displays of the data for a strip, which can be checked against prepared scans from star charts. Extensive observations to search for asteroidal object encounters will be avoided unless experience with other experiments suggests that our instrument is not apt to be damaged by small-particle impacts. In standby the IPP will point toward the antenna.

The field of view and the telescope step angle is 0°.5 in the polarimetry mode. The detectors are sampled every 0°.5 in this mode so the data fill the allowed memory in 70° of roll angle. These data are read out in the remainder of a roll. Observations may begin from a roll angle at which a brightness threshold is exceeded or from commandable roll angles. The latter is more suited to the asteroid belt observations. The measurement cycle requires four rolls: (1) calibration lamp and dark current if sensitivity is low, or dark current if sensitivity is high; (2) clear aperture; (3) depolarizer; and (4) half-wave retarder plate to rotate linear polarization by 45°. Stepping proceeds automatically unless inhibited, and it may be reversed. A sector of roll angle 70° long could be assembled into a map comparable to a zodiacal light map. The polarimetry map could be acquired at 4/3 the zodiacal light mapping rate in cone angle but a search of the whole sky would be prohibitive in the polarimetry mode.

The probability of observing a numbered asteroid without highly accurate aiming is extremely small. Using the relation $B = B(1, 0) + 5 \log rd + F(\alpha)$ and the estimates $B(1, 0) = 10$ mag for the absolute magnitude of an asteroid with 20 km radius, $r = 3$ AU, and $F(90°) = 2.7$ mag as for the Moon (Harris, 1961), we may determine the miss distance $d \cong 1.0 \times 10^{-2}$ AU giving an observed magnitude $B = 5$. A computer search for numbered asteroids near the Pioneer F trajectories was performed at NASA Ames Research Center (1970). The miss distances were 0.03 AU or greater, but usually larger than 0.1 AU. The 20 asteroids reported usually have orbits that could not be reached without a change-of-plane maneuver by the spacecraft. One exception is 554 Peraga, whose inclination and node might permit a near passage. Its absolute magnitude $B(1, 0) = 9.4$ and it is the largest of the 20 asteroids. Aiming for this asteroid to within 0.01 AU would make it detectable, but would add a significant constraint to the Jupiter transfer orbit.

APPENDIX A–SUMMARY OF PROPERTIES OF IPP

Modes of operation:

1–Standby
2–Zodiacal light
3–Polarimetry
4–Imaging (for details see Gehrels, Suomi, and Krauss, 1972)

Telescope: Maksutov type with 2.5 cm aperture and 8.6 cm focal length

Instantaneous field of view:

Mode 2: 2°.3 square
Mode 3: 0°.5 square
Mode 4: 0°.03 square

Spectral bandpass:

Blue: 390 to 500 nm
Red: 595 to 720 nm

Polarization analyzer:

Mode 2: symmetrical Wollaston prism
Mode 3: symmetrical Wollaston prism and achromatic half-wave retardation plate

Calibration:

Mode 2: radioisotope-activated phosphor light source
Mode 3: solar diffuser, tungsten filament lamp and Lyot depolarizer

Detectors: Two dual-channel Bendix Channeltrons

Look angle step:

Mode 2: 1°.8 every 20 rolls
Mode 3: 0°.5 usually every four rolls
Mode 4: 0°.03 every roll
(Step direction or "no step" commandable)

Look angle range: 10° to 170° from earthward spin axis (the antenna is seen from 10° to 29°)

Sampling angle:

Mode 2: complete roll at 512 bps or higher telemetry rate
Mode 3: 70° of roll at 1024 bps or higher telemetry rate
Mode 4: 14° (29° at low sampling rate) at 1024 bps or higher telemetry rate
(Start of sampling in modes 3 and 4: one of 64 commandable angles or automatic at an increase in light in excess of a threshold)

Analog/digital conversion:

Mode 2: four channels, 10 bits each, after each integration period of 1/64th of roll
Mode 3: four channels, 10 bits each, after each 16 ms integration
Mode 4: two channels, 6 bits each, alternate channels every 0.5 ms (1 ms at low sampling rate)
(Five temperatures, 10 bits each)

Telemetry:

Mode 2: 50 bits status, 50 bits temperatures, 2560 (maximum) bits detector data every other roll

Mode 3: 50 bits status, 50 bits temperatures, 6044 (maximum) bits detector data every roll

Mode 4: 50 bits status, 6094 (maximum) bits detector data every roll

(Data buffered by spacecraft data storage unit and sent in telemetry format D1 or D2)

(One analog word (standby status) in subcommutated science data)

Commands: 3, mode initiate; 4, telescope step control; 4, data sampling control; and 2, gain control

Size: 18 by 19 by 47 cm

Mass: 4.2 kg

Power: 3.5 W

APPENDIX B–CALCULATION OF THE SENSITIVITY OF THE IPP IN THE POLARIMETRY MODE

The signal current at the cathode is $I = sSEhA$ where s is the response at the effective wavelength relative to the peak response (0.88 in B, 0.39 in R); S is the peak cathode response of the cathode (S-20 extended, about 45 mA/W); E is the optical efficiency including reflectivities, obscuration, and a factor of 0.5 for polarization state (0.18 in B, 0.23 in R); h is the object intensity in watts per square centimeter passed by the filter; and A is the mirror area (5.0 cm^2).

If H is the solar flux at each filter (about 200 W/m^2), then

$$\log h/H = 0.4(M - m)$$

where M is the solar magnitude and m is the object magnitude. Consider $m = 5$ and $M = -26.9$. Then $h = 3.4 \times 10^{-15}$ W/cm^2 and $I_R \cong I_B = 1.2 \times 10^{-16}$ A.

Shot noise is a lower estimate of the system noise

$$I_n = (2KqI\,\Delta f_n)^{1/2}$$

where $K = 1.4$ is a noise factor given by the supplier, q is the electron charge 1.6×10^{-19} C, and Δf_n is an effective noise bandwidth $(4t_s)^{-1}$ for a system time constant t_s and a single time constant noise filter. For the signal to rise to 0.999 of its steady-state value in this mode, $t_s = t_i/6.9$, where t_i is the time for the spacecraft to turn one field of view,

$$t_i = \frac{0.46 \text{ deg}}{28 \text{ deg/s}} = 16 \text{ ms}$$

Therefore $\Delta f_n = 108$ Hz and $I_n = 0.62 \times 10^{-16}$ A. By comparison the dark current is about 0.05×10^{-16} A in the blue tubes, and somewhat larger in the red tubes.

Evidently the signal to noise ratio for a 5 mag object and one detector is $I/I_n = 2$. Because the signal is divided between two pixels on the average, the recognition of a signal is somewhat poorer than this signal to noise ratio would indicate. But the use of four detectors during four rolls at a particular cone angle in this mode brings the signal to noise ratio to 8. Thus a 5 mag object is barely recognizable.

ACKNOWLEDGMENTS

The University of Arizona (T. Gehrels) has overall responsibility for the program, Dudley Observatory (J. L. Weinberg) has responsibility for observations and analysis of the zodiacal light, and Santa Barbara Research Center is responsible for fabrication and testing of the instrumentation. We thank C. F. Hall and his staff at the Pioneer Project Office, NASA Ames Research Center, for their effective cooperation.

REFERENCES

Gehrels, T., Suomi, V. E., and Krauss, R. J. 1972, On the Capabilities of the Spin-Scan Imaging Technique. Space Research XII (ed., A. C. Strickland). Akad. Verlag. Berlin.

Harris, D. 1961, Photometry and Colorimetry of Planets and Satellites. Planets and Satellites (eds., G. Kuiper and B. Middlehurst), pp. 272-342. Univ. of Chicago Press. Chicago.

NASA Ames Research Center. 1970, Pioneer F Asteroid Analysis. Pioneer Program Document PT-204.

[*Editorial note: The Pioneer Mission to Jupiter is described in NASA SP-268.*]

Page intentionally left blank

PRECISION OF EPHEMERIDES FOR SPACE MISSIONS

B. G. MARSDEN
Smithsonian Astrophysical Observatory

One of the most extensive programs of systematic observations of minor planets currently being conducted is that at the Crimean Astrophysical Observatory. The observed positions, together with the residuals from the predictions in the annual *Ephemeris* volumes, have been listed in the Minor Planet Circulars for several years now; and inspection of the residuals yields information about the accuracy of minor planet ephemerides as a whole.

The observations are made using a 40 cm *f*/4 double astrograph, the limiting magnitude being about 18. Between June 1968 and October 1969, corresponding to one synodic period of an average minor planet, about 40 percent of all the numbered objects were observed. These observations may be regarded as reasonably representative of all the planets. Observations were made of 60 of the objects with numbers in the 100's and only 29 of those in the 1100's, but in general the distribution was surprisingly uniform.

Figure 1 shows, on a logarithmic scale, the distribution of the residuals in right ascension for the 694 planets involved. We have not considered the

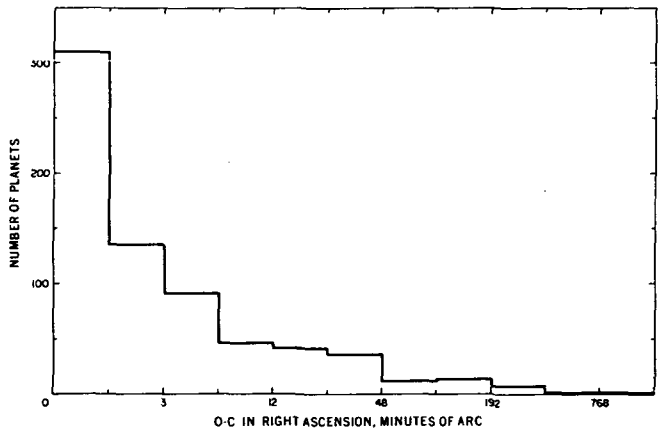

Figure 1.–Distribution of the $O - C$ residuals in right ascension for 694 minor planets observed between June 1968 and October 1969 at the Crimean Astrophysical Observatory.

residuals in declination, but they are generally not as important. It may be seen that 64 percent of the planets had residuals of less than 3′; and, again, there was little difference between high and low numbered objects. For astrometric purposes this limit may be regarded as very satisfactory. If one wishes to send a space probe to a minor planet, however, it certainly is not satisfactory. At a typical opposition distance of 1.8 AU from Earth, 3′ corresponds to 2.3×10^6 km. Furthermore, 16 percent of the minor planets had residuals exceeding 12′, and 1.6 percent (11 objects in all) were found 3° or more from their predicted positions. Four of these 11 objects, having numbers in the 1200 to 1500 range, had been observed relatively poorly in the past, and the new Crimean observations have been highly valuable for redetermining their orbits. This was not true of the lower numbered objects; but, again, for three of these (two of which were brighter than 14 mag), the current *Ephemeris* volume contains new orbits. It should be pointed out perhaps that some of the large residuals are due to misidentifications, although this effect should not greatly distort the general features of the distribution.

In general, however, thanks to the Cincinnati Observatory, the Institute of Theoretical Astronomy in Leningrad, the Latvian State University Observatory, and the modern computers available to these institutions, the immense task of keeping track of the minor planets is well under control. In the 1971 volume, there are only four minor planets for which the ephemerides have been calculated without consideration of perturbations, and two of these have not been identified with certainty since their discovery oppositions. For the majority of minor planets (those calculated in Leningrad) perturbations by Jupiter and Saturn are applied; although for about 30 percent of them, allowance is made for perturbations by all the planets from Venus to Neptune.

This is, of course, the point: If perturbations by all the major planets are consistently applied, and if new differential corrections are performed every 10 yr or so, it should be possible to supply, for 90 to 95 percent of the numbered planets, ephemerides that are in error by no more than a few seconds of arc. For astrometric purposes, it would obviously be pointless to make the necessary effort, although observers making photometric and polarimetric measurements would find it highly convenient if the planets that concern them could be relied upon to be within, say, 1′ of their predicted positions. Perhaps the time has come to draw up a comprehensive selected list, comprising 200 or 300 objects, even very faint ones, of potential astrophysical interest and for which reliable ephemerides would be guaranteed.

For space mission purposes, one is interested only in a handful of very selective objects. The observed positions would be reduced to the FK4 system, the orbit corrections performed as rigorously as possible, and perturbations by all the major planets taken into account. Perhaps the positions and masses of these perturbing planets will have to be improved. It is rather ironic that so many attempts have been made in recent years to use observations of minor planets for determining the mass of Jupiter because the average of these new determinations is practically identical with the IAU adopted value. On the

other hand, there are at least five minor planets—433 Eros, 887 Alinda, 944 Hidalgo, 1221 Amor, and 1566 Icarus—for which recent orbit calculations have easily revealed severe inadequacies in the adopted masses of Earth or Saturn. Many of the bright, well-observed minor planets have geocentric distances in the range 0.9 to 1.2 AU at favorable oppositions. Very great care in the orbital computations on 4 Vesta and 8 Flora, for example, could produce predictions a few years ahead that are good to 1″. This corresponds to an uncertainty of 700 to 900 km in the plane of the orbit. The real difficulty is that we have no direct information about the range, although it might be reasonable to multiply these uncertainties by a factor between, say, 2 and 5.

On the other hand, a more convenient and interesting objective for a space probe may be one of the minor planets that approach Earth very closely. Two obvious choices are Icarus and Eros. Although the best predictions for the former were in error by 20″ at the time of recovery in 1968, this corresponds to a distance, in the orbit plane, of only 1100 km. The extensive series of observations obtained that year should improve matters in the future (although to my knowledge no observations have been made since 1968, and not for the lack of suitable occasions); and, furthermore, the radar experiments established the range very exactly. Eros has a much longer observational history; and its larger size, lower orbital eccentricity, and larger perihelion distance make it a more attractive target. Neither of these objects has an aphelion distance of more than 2.0 AU, however; and they can hardly be regarded as representative minor planets. It is also questionable whether what may be our only chance of subjecting a minor planet to close inspection from space should be spent on a chunk of iron, which is what Eros is quite widely thought to be.

We suggest, therefore, that 887 Alinda be put forward as another candidate. Though far from a typical minor planet, its aphelion distance is almost 4 AU, and it spends most of its time in and around the main belt. That it is one of the half dozen or so minor planets most likely to be defunct cometary nuclei could allow us to settle the very important question of interrelation of minor planets and comets. Alinda's libration about the 3:1 mean motion resonance with Jupiter implies that it is approximately in a 1:4 mean motion resonance with Earth, and it has been observed only on its close approaches to Earth. Following its discovery in 1918, it was observed faithfully every 4 yr until 1942; it was not observed again until late 1957, when two positions were measured on a single night. Two yr ago, in preparation for the favorable 1969-70 opposition, we made a redetermination of the orbit. Although recognizing the great weight we were placing on the isolated pair of observations in 1957, we concluded that it was necessary to use the mass of Earth consistent with the radar determinations of the astronomical unit, rather than the IAU value. The maximum residual of this orbit in 1969-70 was about 3″, even though Alinda came within 0.23 AU of Earth; and as a result of a solution that incorporated the new observations, these residuals were reduced by a maximum of 2″.6. For no orbital element did the correction exceed three times the mean error of its determination. A change of 2″.6 at 0.23 AU

corresponds to 430 km, whereas the formal spatial difference between the two orbit solutions was 540 km.

In view of the paucity of observations since 1942, this result may seem very encouraging; but it should be pointed out that the orbit has been exclusively conditioned to observations covering an arc of about 7 months centered on perihelion. We have no information about the error in the remainder of the orbit; however, because any space probe would presumably intercept Alinda near perihelion, this is of little consequence. As for the more severe difficulty of establishing the range, it is worth considering the possibility of bouncing a radar beam off Alinda on its next return. At the end of 1973 it will approach to within 0.14 AU, or 3.5 times the least distance of Icarus in 1968. Although cataloged as 1.5 mag brighter (absolutely) than Icarus, the recent observations suggest that 3 mag, or a factor of 16, may be more correct. Alinda could thus be expected to have a radius of 3 km, and the strength of the radar echo will be $3.5^4/16$, nine times weaker than that for Icarus. Success, coupled with concentrated astrometric and physical observations in 1973-74, and possibly even astrometric observations at other oppositions,[1] could then lead the way to a prediction in error by not more than a few tens of kilometers and a space probe launched to Alinda in 1977.

[1]Very faint images of Alinda were photographed by E. Roemer in May and June 1971 with the Steward Observatory's 229 cm reflector on Kitt Peak. This tiny minor planet was then more than 3.6 AU from the Sun.

DISCOVERY AND OBSERVATION OF CLOSE-APPROACH ASTEROIDS

ELIZABETH ROEMER
University of Arizona

Close-approach asteroids, members of the so-called Apollo and Amor groups, are of considerable current interest as potential targets for probes and also in connection with the question of identification of the parent bodies of the meteorites. The possibility that some of these asteroids may be surviving comet nuclei has been suggested earlier. (See, e.g., Öpik, 1963.) Relatively few objects of this type are known; all are small bodies found accidentally in the course of work not always related to investigations of minor planets. The known Apollo and Amor asteroids, and notes as to their present observational status, are listed in table I. (See also table II of Marsden.[1]) Except when they are relatively close to Earth (many can approach within 0.10 AU), these objects are faint and often in very awkward positions as well, low in the evening or morning sky at twilight. When they are close, the rate of apparent motion is very great—Icarus was 12 mag and moving 1 deg/hr at its closest approach (to 0.04 AU) in June 1968. Thus even a favorable and accurately predicted apparition presents a share of observational difficulties. Sometimes years go by without a reasonable opportunity for observation—definitely a problem in determination of reliable orbits. Only when these small asteroids are relatively close to Earth, with fast apparent motion, are they bright enough for investigation of physical characteristics. Under such circumstances, if the prediction of position is within a few minutes of arc, the fast motion may be an asset in the sense that it quickly attracts the eye and aids in identification ("bird-in-the-bush effect").

It obviously would be extremely interesting to know more of the population statistics of this class of objects and to extend the list of individual members for which any sort of physical information is available. Proposals have been made for search programs to these ends. The practical execution of a useful search entails massive work, however, and is fraught with problems, some of very recent origin.[2]

The critical considerations in planning a search are (1) where and how to observe so as to maximize the chances of photographing an interesting object

[1]See p. 419.
[2]See p. 649.

TABLE I.—*Current Observational Status of Apollo and Amor Objects* ($q \leqslant 1.15$ *AU*)[a]

Object	Discoverer, observatory	Status	Date observed	Next search opportunity
1953 EA	A. Wilson, Palomar	Recoverable?	Mar. 9 to June 17, 1953	1973
887 Alinda	Wolf, Heidelberg	Secure	–	–
1948 EA	Wirtanen, Lick	Recoverable?	Mar. 5 to Sept. 28, 1948	Oct. 1971 to Dec. 1972
1960 UA	Giclas, Lowell	Recoverable	Oct. 22, 1960, to Feb. 6, 1961	1977
1936 CA Adonis	Delporte, Uccle	Recoverable?	Feb. 12 to Apr. 11, 1936	1977
1580 Betulia	Johnson, Johannesburg	Secure	–	–
1968 AA	Cesco and Samuel, Observatorio Austral Yale-Columbia	Secure	Jan. 1 to Feb. 9, 1968; June 1, 1970, to Jan. 24, 1971	–
1221 Amor	Delporte, Uccle	Secure	–	–
1937 UB Hermes	Reinmuth, Heidelberg	Lost	Oct. 25-29, 1937	–
1627 Ivar	Hertzsprung, Johannesburg, and Hoffmeister, Boyden	Secure	–	–
1950 DA	Wirtanen, Lick	Lost?	Feb. 23 to Mar. 12, 1950	1974
1971 FA	Gehrels, Palomar	Secure?	Mar. 24 to May 26, 1971	Oct. 1971 to Mar. 1972
1932 HA Apollo	Reinmuth, Heidelberg	Recoverable?	Apr. 27 to May 15, 1932	Oct. to Dec. 1971
1950 LA	Wilson and Wallenquist, Palomar	Lost?	June 19 to Sept. 16, 1950	–
1566 Icarus	Baade, Palomar	Secure	–	–
1685 Toro	Wirtanen, Lick	Secure	–	–
1959 LM	Hoffmeister, Boyden	Lost	June 5-11, 1959	–
433 Eros	Witt, Berlin	Secure	–	–
1620 Geographos	Wilson and Minkowski, Palomar	Secure	–	–
1947 XC	Giclas, Lowell	Lost	Dec. 12, 14, 1947	–

[a]The order in which objects are listed is that of decreasing aphelion distance, making this table directly comparable with table II of Marsden, p. 419, in which orbital elements q, Q, e, i, and P and the absolute magnitude $B(1, 0)$ may be found. The object 1947 XC, of which the orbital elements are very uncertain, has been added. B. G. Marsden has very kindly supplied information regarding future search opportunities in advance of publication.

and (2) how to manage examination of the plates to maximize the chance of the object being promptly recognized. Whether or not objects are found, one would like at least to be able to specify what volume of space was searched, its location with respect to Earth and Sun, and the brightness (size) limit to which discovery should have been complete. Because trailing of images decreases the brightness limit of detection, some interpretable decision needs to be made as to how to compensate for apparent motion of possible objects in any particular field.

Very fast, wide-field optical systems are now available that make rapid coverage of vast areas of the sky entirely feasible. Even rapid, unknown rates of apparent motion (which depend on the character of the heliocentric orbit, but more critically on the geocentric distance) are a less serious problem than they were formerly with slower optical systems. But when and how should the second plate be taken for best detection of a moving object?

The most critical difficulty comes in examination of the photographic records. Blink examination of rich star fields can take days and even weeks per field, without necessarily reaching to the plate limit. Objects displaced by considerable amounts between exposures can still be missed unless the motion during a single exposure is enough to attract attention. Examination should be carried out at the same rate at which observational material is obtained if there is to be feedback into the observational program to secure continuing observations of any interesting objects that might be found. Without possibility of following up on discoveries, much of the value of the search effort is lost.

In fact, no more sophisticated examination than a reasonably careful survey of the plate with a hand magnifier was involved in discovery of some of the known objects of the Apollo class. Others were evident on the most cursory naked-eye inspection. The critical point is that whatever information is to be obtained from the plates must be abstracted promptly (i.e., the day after observation), and further observations must be obtained immediately (within a night or two, depending on the rate of motion and on the equipment available for followup).

Full details of the discovery of Icarus and of the struggle to keep it under observation during the first critical weeks have been published by Richardson (1965). Similar sagas can be related regarding the difficult and critical first weeks of observation of most of those objects of table I for which reasonably reliable orbits have eventually been determined. In each success story, and in some failures, someone gave close support with computations of orbits and ephemerides, and someone was in a position to continue with observations and measurements of position as the new objects faded beyond the reach of the instruments with which they were discovered. Names that recur repeatedly are L. E. Cunningham, H. M. Jeffers, Seth B. Nicholson, Paul Herget, and in recent years B. G. Marsden.[3] It is this immediate effort, and not so much the care that

[3]And E. Roemer [editor's footnote].

goes into calculation of the definitive orbit, months or years after the discovery, that really determines whether the new object can be reobserved at future apparitions.

Even though Apollo and Adonis have usually been considered lost, very considerable effort was expended in keeping Apollo under observation for nearly 3 weeks in 1932 and Adonis for 2 months in 1936. The situation with Hermes in 1937 was so extreme that every observation save one (14 in all, obtained at four observatories) was made quite accidentally with small patrol cameras. At its closest approach to Earth, to about 0.005 AU on October 30, 1937, Hermes was 8 mag and moving 5 deg/hr. Many attempts were made to obtain observations, but, because of the very rapid motion, only one was successful. A number of plates are known to cover the proper fields, but Hermes was traveling too fast to leave a trace. In 9 days it had traveled completely across the sky—comparison with the problems of meteor photography may not be entirely out of order. The orbit, from a 4 day arc, was determined essentially by the geocentric parallax, to which the Johannesburg observations were critically important, as, indeed, they have been for many other, more ordinary asteroids.

In relation to current proposals to conduct a planned search for close-approach asteroids, it may be worthwhile to mention the survey conducted under the direction of C. W. Tombaugh (1961; Tombaugh et al., 1959) from December 1953 to October 1958 for small natural satellites of Earth. Tombaugh's project was, in fact, inspired by his experiences, together with H. L. Giclas, at the Lowell Observatory in 1943 in the attempt to recover the lost asteroid Adonis during a close approach to Earth.

In the course of the satellite search, Tombaugh and his coworkers took and examined more than 15 000 photographs. Various cameras, including a 22 cm *f*/1.6 Schmidt, were employed to search systematically, with appropriate telescope driving rates, for Earth satellites in near-circular orbits ranging through periods from 2 to 24 hr and to limits of 12 to 14 mag. Several promising, but faint, objects were found. Vigorous efforts to reobserve them, however, failed in every case. Although it was felt that most of these objects, originally recognized from weak images near the plate limit, probably were spurious, the possibility remains that some were objects in highly eccentric geocentric orbits, or small asteroids passing close by Earth in heliocentric orbit. In either case it would have been extremely difficult to know in what position to search, and for what rate of motion to compensate. It would be very discouraging indeed to conduct a comparable search at the present time, with the abundance of space "junk" to identify and discount.

It would seem that the most productive avenues open at the present time toward discovery and observation of close-approach asteroids are likely to lie in two directions: (1) encouragement of observers who take wide-field plates for various astronomical purposes to look for and report potentially interesting objects to a center at which both observing and computing resources are

available for immediate, but probably somewhat selective, followup and (2) devotion of adequate efforts toward reobservation of those known Apollo and Amor objects, unseen since their discovery apparitions, for which a reasonable search prediction can be made.

Wide-field plates taken with fast cameras show so many asteroid trails that some basis for selection must be applied by even the most enthusiastic asteroid hunter. It has been said that for an asteroid to attract the attention of a Palomar Schmidt observer, the trail "must be an inch long, or must be directed the wrong way" (Struve, 1952; the quotation is apparently attributed to Jesse Greenstein). Any object found far from the ecliptic must either have a high inclination or be relatively close to Earth. If there are other asteroids in the field, distinctly different motion will identify potentially interesting objects. The typical minor planet near opposition has a daily motion, in the retrograde direction, in the range from 5′ to 15′. Near quadrature the motion will be of comparable magnitude, but in the direct sense. At discovery 1960 UA was between 11 and 12 mag and had a direct motion of about 2 deg/day, exemplifying the fact that an object close to Earth may have large direct motion even at opposition.

On occasion it may be necessary to infer the direction of motion from characteristics of the trail on a single plate. This was, in fact, the situation at the discovery of Icarus. The usual rule is, in the absence of complicating effects such as variable transparency because of clouds or changing altitude, that the *beginning* of the trail is denser than the end (Miller, 1965). In estimating the magnitude, necessary for the guidance of other observers, correction should be applied for any appreciable trailing.

Marsden (1969) has recently redetermined the orbits of several of the known Apollo and Amor asteroids and provided search ephemerides for several for which he considers recovery efforts reasonable. Included are Apollo and Adonis, as well as 1948 EA and 1953 EA. Even though bands as long as 75° across the sky may need to be searched, every encouragement should be given to the effort, at the appropriate times, to reobserve these objects. It seems clear that search efforts in these cases would have a much better chance of contributing useful information than would a comparable amount of time spent in a general effort to discover new objects.

While observing with the 122 cm Schmidt on Palomar Mountain late in March in a survey of the western equilateral point for faint Trojans, Tom Gehrels discovered several asteroids that, by their motion, seemed sufficiently interesting to warrant further observation. One of these, of about 16 mag, and with opposition motion of about 40 arcmin/day in the retrograde direction, has turned out to be a new Apollo asteroid (Gehrels, Roemer, and Marsden, 1971). This motion is some two to three times that of a typical asteroid, but by no means sufficiently extreme to make the asteroid an immediate Apollo suspect. The object was, in fact, at a distance of about 0.9 AU from Earth at the time of discovery. The high orbital inclination (22°) and present

orientation of the line of nodes preclude approaches to Earth closer than about 0.3 AU, the first Apollo asteroid to which a comparable statement presently applies. The new Apollo, designated 1971 FA, was kept under observation through May 26. There is an extended favorable opportunity for observation in late 1971, and it seems that this new close-approach asteroid will be put in secure status with little additional effort.

REFERENCES

Gehrels, T., Roemer, E., and Marsden, B. G. 1971, Minor Planets and Related Objects. VII. Asteroid 1971 FA. Astron. J. 75, in press.

Marsden, B. G. 1969, Minor Planet Circ. nos. 3014-3018. Cincinnati. (Some of this work has been refined and extended more recently.)

Miller, W. C. 1965, Photographic Discrimination Between the Beginning and End of a Trail Produced by a Moving Object. Publ. Astron. Soc. Pac. 77, 391-392.

Öpik, E. J. 1963, The Stray Bodies in the Solar System. Part 1. Survival of Cometary Nuclei and the Asteroids. Advances in Astronomy and Astrophysics (ed., Z. Kopal), vol. 2, pp. 219-262. Academic Press, Inc. New York and London.

Richardson, R. S. 1965, The Discovery of Icarus. Sci. Amer. 212(4), 106-115.

Struve, O. 1952, The Minor Planets. Sky and Telescope 11, 163-166.

Tombaugh, C. W. 1961, The Trans-Neptunian Planet Search. Planets and Satellites. The Solar System (eds., G. P. Kuiper and B. M. Middlehurst), vol. III, ch. 2. Univ. of Chicago Press. Chicago.

Tombaugh, C. W., Robinson, J. C., Smith, B. A., and Murrell, A. S. 1959, The Search for Small Natural Earth Satellites. Final Technical Report, N. Mex. State Univ.

MANMADE OBJECTS—A SOURCE OF CONFUSION TO ASTEROID HUNTERS?

KAARE AKSNES
Jet Propulsion Laboratory
California Institute of Technology

On October 7, 8, and 9, 1970, Charles Kowal, in search of fast-moving asteroids, exposed three photographic plates of an area of the sky near the ecliptic with the 122 cm Schmidt reflector of the Hale Observatories. Several weeks later Eleanor Helin of the California Institute of Technology examined the plates under a blink microscope and discovered a fast-moving object of about 15 mag. During the 15 min exposures the object had left a slightly bumpy trail indicating light variations with a period of a few minutes.

Four positions of the object were reported to the author, who derived the heliocentric orbit defined in table I. From table II it is seen that the residuals of that orbit are not very satisfactory. Note that the third and the fourth position represent the end points of the same trail. There is a clear indication that after October 9, the predicted heliocentric positions would soon diverge from the actual positions. This circumstance, and the fact that the orbit is so similar to that of Earth, suggested that the object could actually be moving in an Earth-centered orbit. The orbital elements listed in the second column of table I were derived by means of a computer program for heliocentric orbits simply by introducing Earth's mass in place of the mass of the Sun, whose geocentric coordinates were replaced by zeros.

Interestingly enough, as seen from table I, most of the elements of the geocentric orbit fall between those of the strongly perturbed Earth satellite Explorer 33 (IMP 4) at two different epochs. Unfortunately, a complete and accurate set of orbital elements could not be obtained for this and most other satellites orbiting Earth at great distances. The elements shown in the table are taken from two issues of NASA Goddard Space Flight Center's *Satellite Situation Report* (1969, 1970). The rather different eccentricities may preclude that the object in question is Explorer 33, but there are many other candidates, including payloads and spent rockets.

The two sets of residuals listed in table II favor the geocentric orbit rather strongly. Not included in this table is a highly uncertain December 3, 1970, observation that agreed with the predicted geocentric position to within a degree, however. A fictitious fifth observation has been added to illustrate that

TABLE I.–*Orbital Elements*

Orbital elements	Heliocentric orbit[a]	Geocentric orbit[a]	Explorer 33 (IMP 4)[b]	
Epoch, ephemeris time	Oct. 8, 1970	Oct. 8, 1970	July 15, 1969	Nov. 30, 1970
T, ET	Dec. 6.8113, 1970	Oct. 13.1275, 1970		
ω (1950.0), deg	238.656	314.861		
Ω (1950.0), deg	196.888	226.071		
i (1950.0), deg	0.108	4.403	56.7	23.4
q	0.977 00 AU	60 934 km	267 000 km	197 000 km
e	0.052 38	0.859 74	0.523	0.444
a	1.031 00 AU	434 444 km	560 000 km	354 000 km
n, deg/day	0.941 50	10.914 54	7.34	14.47
P	1.0469 yr	32.9835 days	49.08 days	24.88 days

[a]Orbit referred to ecliptic.
[b]Orbit referred to celestial equator.

TABLE II.–*Residuals*

U.T. (1970)	α (1950)	δ (1950)	Heliocentric orbit		Geocentric orbit	
			Δα cos δ	Δδ	Δα cos δ	Δδ
Oct. 7.35088	$01^h\ 22^m\ 12^s.40$	10° 17′ 03″.0	−2″.6	−1″.0	−0″.3	0″.0
Oct. 8.36112	01 36 49.40	11 24 09.0	4.3	1.2	.5	−.1
Oct. 9.45256	01 56 10.00	12 51 35.0	4.9	.9	−2.0	.2
Oct. 9.46298	01 56 14.90	12 52 10.0	−4.0	−1.3	1.8	−.1
Oct. 10.00000[a]	02 11 25.80	14 06 18.0	990	360	0	0

[a]Fictitious observation satisfying geocentric orbit exactly.

after October 9 the heliocentric motion falls very rapidly behind the geocentric motion. This is even more obvious from figure 1 where the object's geocentric angular velocity *df/dt* has been plotted against time. It seems that if the last observation had occurred a little later, the possibility of a heliocentric orbit could probably have been ruled out entirely, whereas if it occurred a little sooner it might not have been possible to distinguish the two types of orbits at all. For comparison, the apparent angular velocities of the asteroid Hermes, when it was closest to Earth in 1937, and of a fast-moving object recently observed by Lynds (Federer and Ashbrook, 1971; Marsden, 1971) are indicated in the figure. Apart from the Earth crossers, a typical asteroid would appear to move across the sky at a rate of a fraction of a degree per day.

It is, of course, important to establish as early as possible whether an observed fast-moving object is an asteroid or a manmade object of some type.

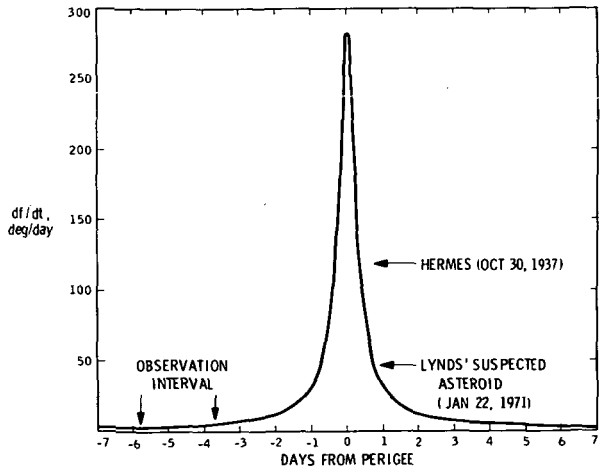

Figure 1.–Angular velocity versus time in geocentric orbit. a = 434 000 km, e = 0.860, and n = 10.915 deg/day.

We have just seen that the apparent motion of the object is not a reliable criterion for making such a distinction. What about the orientation of the orbital plane? Unfortunately, the artificial objects that get far enough away from Earth to be of interest here move in direct orbits close to the ecliptic, as do most of the asteroids. The best clue as to the true nature of a fast-moving object is probably to be found in its physical appearance. Unless a space probe is stabilized, it is likely to tumble with a consequent light variation having a period of perhaps a few minutes, as was the case with Helin's object. An asteroid would have to be very small to tumble that fast, the shortest period of light variation on record being $2^h\ 16^m.4$ for Icarus (Gehrels et al., 1970).

If the distance of the object can somehow be estimated (e.g., from its observed angular velocity), its size can be calculated on the basis of its apparent magnitude and an assumed albedo. Thus, when Helin's object was observed at about 15 mag, it was about 450 000 km from Earth, according to both orbits derived for it. On the assumption of full-phase illumination and an albedo of 0.07, typical for asteroids, a diameter of roughly 12 m (40 ft) results. This number can be reduced to one more appropriate for a space probe by adopting a much higher and presumably more realistic albedo. For the sake of argument, let us assume that Lynds' object has the same size. The reported magnitude of 10.5 to 11 then puts the object at a distance of about 60 000 km from Earth, which is close to the pericentric distance derived for Helin's object. It is therefore, perhaps, more likely that Lynds was observing an Earth satellite rather than an asteroid.

The main purpose of the above discussion has been to draw attention to the probably increasing problem of distinguishing fast-moving asteroids from manmade objects, and to establish the reality of the problem through an actual example. Unfortunately, a satisfactory solution to this problem has not been found.

ACKNOWLEDGMENT

This paper presents the results of one phase of research carried out at the Jet Propulsion Laboratory, California Institute of Technology, under NASA contract NAS 7-100.

REFERENCES

Federer, Charles A., Jr., and Ashbrook, Joseph, eds. 1971, Fast-Moving Asteroid. Sky and Telescope 41(3), 153.

Gehrels, T., Roemer, E., Taylor, R. C., and Zellner, B. H. 1970, Asteroid (1566) Icarus. Astron J. 75, 186-195.

Marsden, B. G. 1971, Fast-Moving Asteroid? IAU Circ. 2303.

NASA Goddard Space Flight Center. 1969, Satellite Situation Report 9(13).

NASA Goddard Space Flight Center. 1970, Satellite Situation Report 10(13).

FUTURE WORK

TOM GEHRELS
The University of Arizona

In the past decade the question has been raised, at IAU meetings, as to whether more asteroids should be discovered, and the answer now is: "Yes, indeed, do discover as many comets and asteroids as possible." Marsden[1] gives strong encouragement to search for "lost" comets and asteroids. The more ephemerides known the better physical and statistical studies we can make. We have completion of the asteroids now to about 14 mag. With existing patrol instruments of about 25 cm opening, for instance at Indiana and in South Africa, the limiting magnitude for an extended program is about 16.

Another survey such as the Yerkes-McDonald survey but to somewhat fainter limit than before (~16th mag) would be valuable to reach completion, and to provide a uniform set of observations for improved statistical studies. The principal problem at present for such a survey lies not in the availability of funds or telescopes, but in the lack of dedicated personnel such as Van Biesbroeck and the van Houtens to execute the enormous task of blinking, identification, etc.

Any photographic surveying of the sky would increase the chance of discovering additional asteroids that cross the orbit of Mars. Special searches for Mars-orbit crossers could be made perhaps with long exposures on baked IIIa-J emulsion at the Palomar Big Schmidt. All photographic observers should be aware of the importance of reporting trails within 24 hr to an observer who will follow the object. Even if the trail is only two or three times the usual length, it may belong to an Apollo (this was the case for 1971 FA);[2] because people until now have noticed only long trails, there are many Mars crossers still to be discovered. It is not clear, however, how to distinguish, from a single night's observation, the real asteroids from space hardware. (See Aksnes.[3])

Two weeks after the colloquium, I used the Palomar Big Schmidt to take plates for Trojans in the following lagrangian point of Jupiter, and the plates were, as before, sent to the van Houtens for blinking, reduction, and analysis (van Houten et al., 1970). The statistics of the Trojans in the *Ephemeris* are peculiar: The following point has only about half the number of objects as are present in the preceding point. If this is a real effect, we should then find only

[1]See p. 413. [2]See p. 647. [3]See p. 649.

350 Trojans this time compared to 700 in the preceding point; this will be a challenging problem for theoretical work.

Tombaugh (1961) has reported on the completion of asteroids outside the orbit of Jupiter.[4] Kowal[5] and others have searched in vain for Trojans of Saturn; Rabe does not give us too much likelihood of stability in the lagrangian points L_4 and L_5 of Saturn because of perturbations by Jupiter. The plates taken in March 1971 for the Trojan survey in the following lagrangian point happened to cover also L_4 of the Neptune-Sun system; we blinked these, with 1 day interval, and found no Trojan of Neptune; the limit of this reconnaissance is estimated to be $B(a, 0) \sim 20.0$. Further search for Trojans of Neptune might be considered, with longer exposures on baked IIIa-J and/or a larger telescope. Objects of asteroidal size farther out than ~30 AU are not detectable. (See Tombaugh, 1961.)

As interested users of the astrometric work and of that in celestial mechanics we gain the impression that the computation of the orbits is well controlled. The Institute of Theoretical Astronomy in Leningrad and the Minor Planet Center at Cincinnati, assisted by many other people and observatories, can very well keep up with the needs now that high-speed electronic computers are available. All users and interested parties will join me in strongly endorsing these programs, the development of new techniques and additional high-precision studies of orbital characteristics, as well as the production of ephemerides. We presently lack extended ephemerides in the yearly book, but these will be published again in the near future.

The naming of minor planets by the discoverer should be controlled to follow tighter rules than are presently applied. Perhaps Asteroid Commission 20 of the IAU would look into this. Rules might be followed similar to those for naming regions on Mars and on the Moon. Members of the IAU might wish to consider action on the proposal I made in Brighton, in 1970, to form a new IAU commission for physical studies of minor planets.

Additional determinations of asteroid diameters should be made with micrometer, disk meter, and other techniques. The infrared method pioneered by Allen[6] and Matson[7] is promising, especially for making comparisons. For absolute determination and calibration we need more asteroids that have had their diameters determined by direct means, and this remark applies also to the indirect method from the polarization-phase relation as Veverka and others have tried on Icarus.[8] Even with the conventional micrometer it may be possible to observe more asteroids, when at perihelion, with an apparent diameter larger than 0".3.[9] Dollfus[10] has discussed various techniques and their possibilities for diameter measurements.

It is exceedingly important to get more sizes and masses so as to obtain the densities of the minor planets, and I am referring to the beautiful new work of

---

[4]See p. xvii.
[5]See p. 185.
[6]See p. 41.
[7]See p. 45.
[8]See p. 91.
[9]See p. 30.
[10]See p. 25.

Hertz and Schubart.[11] Whereas on past occasions the density 3 g/cm^3 has been used hypothetically for asteroids, from a comparison with the Moon or meteorites, the time has now come to *determine* the density and from that infer the applicability of comparison with the Moon and meteorites.

This is not to say that the surface of the Moon and studies of meteorites are not important to the understanding of asteroids. But the fundamental data should come first, and we should have no patience with supporting observational conclusions because they fit preconceived notions.

I make a plea to obtain good magnitudes of asteroids and cometary nuclei together with photographic observations of position. As for the comets and their secular brightness decrease, again see Marsden.[12] There is a continued need for good magnitudes of asteroids because even in the 1971 *Ephemeris* volume about 50 are completely unreliable; they could be off by one or two magnitudes. The combination of magnitudes from various sources needs to be redone as there is some indication in the Palomar-Leiden survey that the most recent combination of asteroid magnitudes may have included very poor observations and that therefore the precision could be improved by actually eliminating the poorer, older observations. Photographic photometry must, of course, be done carefully to avoid inherent problems that are absent in photoelectric work (Gehrels, 1970).

Detailed spectrophotometry of asteroids is a new field; Chapman et al.[13] give two pages of suggestions for future work such as the possible extension to longer wavelengths and the addition of more laboratory comparisons of rocks and meteorites. This type of work needs close calibration with solar-type stars.

Van Houten[14] has mentioned that the phase function of Trojans may be flatter, and the one of faint asteroids steeper, than that of the brighter asteroids and this should be checked with precise photoelectric observations. He suggested also that a lightcurve of Thule should be obtained and that more color observations should be made of family members and field asteroids. The latter suggestion ties in, of course, with the wish of Chapman et al. to do more spectrophotometric work on various asteroids, families, and groups. The reddening with phase of asteroids is not very well known; Icarus has an exceptional value of $U - V$, and a bluing with increasing phase angle.

There is much work to be done on lightcurves of minor planets for the determination of their rotation rate, their shapes, and the orientation of their rotational axes.[15] These are all possible with careful work on sets of lightcurves and, from laboratory comparison studies, it is perhaps possible to get an indication of the rigidity of the body. But even getting good statistics on the occurrence of nearly spherical asteroids that may be original accretions is important and relatively easy; simple lightcurve surveying of asteroids that are available at the time the observer has equipment ready and photometric sky overhead still is urgently needed. Sets of lightcurves are terribly demanding on

[11] See p. 33.
[12] See p. 413.
[13] See p. 63.
[14] See p. 184.
[15] See p. 147.

preparation, telescope time, and weather. The lightcurve work should be done for objects fainter than about 16 mag as these may be collision fragments, in contrast to the brighter ones.[16] Electronic image intensification may have to be applied for the work on faint asteroids; offset appears too complicated for moving objects.

Further suggestions for future work in photometric studies are made in sec. X of Gehrels (1970). Matson[17] indicated future work in infrared photometry; there still are observational discrepancies. The sense of rotation of an asteroid can be determined with observations on only two separate nights, before and after opposition,[18] and this would be a vast improvement in the amount of telescope time needed to determine the sense of rotation by photometric astrometry.[19] On the other hand, Allen[20] has suggested that the infrared and visual lightcurve work be done simultaneously, and from this work there would be additional information on the much-discussed question concerning how much of the light variation is caused by the change in projected area of the asteroid, and how much by nonuniform reflectivity over the surface.

The statistics on the orientation of rotation axes are just coming in. Burns' paper[21] is stimulating, but the theoretical problem needs a better observational basis, and never again from application of the amplitude-aspect plot.[22] On the other hand, the problem is straightforward, given enough time with the Asteroid Telescope, enough computer time, and enough high-school teachers to operate both.

The telescope referred to is a 1.8 m Cassegrain reflector being built north of Tucson on Mt. Lemmon at 2800 m altitude. The characteristics are a yoke mounting that allows access with full aperture to about +77° declination, and with some obscuration to +90°; access to the horizon; disk drives; fast slewing (~100 deg/min); one-man operation, without night assistant; and computer control (Nova 1200) of the dome and other telescope functions. The name "Asteroid Telescope" indicates that its schedule can be preempted whenever necessary for the work on asteroids and comets, including that in support of space missions.

I would not be the one to minimize polarization work. The apparition of Icarus in 1968 has shown that much can be learned from the combination of polarimetry, photometry, and radar work when the range of phase angles is sufficiently large, as is the case with closely approaching asteroids. Radar yielded an indication of the roughness of Icarus in 1968, but only because there was a set of lightcurves obtained at the same time. Few people have access to the large radio telescopes and we wish to leave with them a request to observe nearby objects whenever possible. There are close approaches soon of Toro and Eros, and future tasks for radar observations, perhaps even of Ceres,

---

[16]See p. xx.
[17]See p. 45.
[18]See p. 49.
[19]See p. 128.
[20]See p. 43.
[21]See p. 257.
[22]See p. 139.

have been mentioned by Goldstein.[23] Marsden[24] makes a request for an observation of Alinda in 1973 and he alerts us to make physical observations during the perihelion passage of Hidalgo in 1976-77.

Surface texture may also be studied from photometry and polarimetry, including laboratory measurements. Much work is left to be done in the laboratory on samples from various parts of the Moon, and in laboratory studies of scattering properties of clumps of grains.[25] An improved understanding seems to be needed of the domains of applicability of the Fresnel law and Mie theory for dusty surfaces. For the comparison of meteorites and asteroids, Anders[26] gives an explicit enumeration of future work. I have the impression that the greatest advance in zodiacal light measurements will be made by using spacecraft.[27]

As for the theoretical work on minor planets, I see three principal approaches: (1) the studies of origin and evolution; (2) the detailed studies of accretion and fragmentation mechanisms; and (3) the study of interrelations of particles, meteorites, comets, and asteroids. All three approaches are needed to consider specific problems such as that of the extraordinary shape and smoothness of Geographos, shown in the frontispiece. The fragmentation theory proposed by Brecher[28] may explain the shape, rather than the "must be iron" reaction to that picture that I have heard so often. For iron composition, there are too many asteroids with large light variation; e.g., Geographos, Eros, Daedalus, and several in the asteroid belt. Are the surfaces of small asteroids sandblasted clean—clean to penetration of infrared radiation—or is there a regolith with clumps of dust or even a thick layer of dust? Photopolarimetric observations, at the telescope and in the laboratory, can provide basic inputs, but a range of theoretical studies is needed, including that of collision probabilities. The interpretation of the number-size distribution bears on this problem in addition to the broader problems of accretion versus fragmentation and asteroid evolution. Although Anders concludes that asteroids with $B(1,0) < 11$ are original condensations, Dohnanyi concludes they may be collisional fragments.

Experimenters should search for new techniques and theoreticians should search for new approaches. The approach of Trulsen, Baxter, Lindblad, and Danielsson is a new one and the study of Alfvén's jetstreams presents great promise. Further work on the statistics of jetstreams and other suggestions are made at the end of the paper by Trulsen[29] and also in various discussions. The theory of resonance and commensurability still seems to be incomplete.

We have exchanged during this colloquium a large amount of information, some of which was very new to some of us. It was good to meet and to compile all this material in a book. Now, armed with additional information, we should continue to work on the main questions: Do the meteorites originate from the

---

[23]See p. 170.
[24]See pp. 416 and 642.
[25]See pp. 67, 90, and 95.
[26]See p. 479.
[27]See pp. 377 and 363.
[28]See p. 305.
[29]See p. 327.

comets, from Apollo asteroids, or from common asteroids? What kind of cores do comets have? Is the collision theory of the origin of asteroid families the appropriate one? To what extent are the jetstreams caused by selection effects?

As for space missions, we trust that this colloquium stimulated the planning of how to get to the asteroids, financially as well as technically. The wish of scientists to be involved in the early stages of mission planning, before the spacecraft is defined, came out clearly in the discussions.[30] Hills[31] has given some basic reasons for asteroid missions. Suggestions for actual experiments have been made[32] but systematic and thorough planning is needed. The idea of missions to the asteroids is relatively new to the scientific community, and this explains why there is a shortage, in this book, of ideas on what to do when we get there, other than to determine the chemical composition, an idea so obvious that it was not even discussed. Forward's paper[33] on the gravity measurements was a surprise to most of us because we believed that Anderson[34] was the only one exploring this field.

Even flyby missions, without encounter or sample return, will be valuable because of the resolution possible on the surface and because of the large range of phase angles. The possibility of a multiple mission[35] appears attractive. Ground-based observations of spacecraft, not only for asteroid missions, and of their perturbed trajectories will continue to be used in the determination of fundamental astronomical constants and of planetary masses.[36]

Ground-based observations in astrometry of candidates for flyby and encounter, such as Eros, need to be encouraged and supported; the scarcity of manpower is a principal hurdle. This work needs to be done now, as well as in the future, to obtain the coverage required for precision. A list of potential targets should be established as soon as possible;[37] the suggestion of Marsden[38] to consider Alinda should not go unnoticed even though it was not made as a part of the Great Debate.

The debate between Alfvén[39] and Anders[40] was of great interest; their debates are continued, or prestaged, by the other papers of Anders[41] and Arrhenius and Alfvén.[42] It is clear that a lot of work on the clarification of the solar system can be done on cosmic material that comes to us as meteorites. It is clear that a landing on one asteroid is not the end of our investigations, both ground-based and in space, because great differences between various asteroids are apparent (e.g., Icarus is rough and nearly spherical, Alinda smooth and spherical, Daedalus rough and elongated, and Geographos smooth and elongated). The consensus of those present was to increase ground-based efforts, and to consider the Debate in target selection, but there was a keen interest in space investigation of asteroids. The prospect of a space mission to

---

[30] See p. 500.
[31] See p. 225.
[32] See p. 561.
[33] See p. 585.
[34] See p. 577.
[35] See p. 527.
[36] See pp. 13 and 577.
[37] See p. 639.
[38] See p. 641.
[39] See p. 473.
[40] See p. 479.
[41] See p. 429.
[42] See p. 213.

an asteroid will generally stimulate ground-based studies; this effect was seen strongly in the revival of respectability and activity in the early 1960's in planetary exploration when promoted by the Soviet and U.S. space programs.

REFERENCES

Gehrels, T. 1970, Photometry of Asteroids. Surfaces and Interiors of Planets and Satellites (ed., A. Dollfus), ch. 6. Academic Press, Inc. London and New York.

Houten, C. J. van, Houten-Groeneveld, I. van, and Gehrels, T. 1970, The Density of Trojans Near the Preceding Lagrangian Point. Astron. J. **75**, 659-662.

Tombaugh, C. W. 1961, The Trans-Neptunian Planet Search. Planets and Satellites (eds., G. P. Kuiper and B. M. Middlehurst). Univ. of Chicago Press. Chicago.

Page intentionally left blank

GLOSSARY[1]

a	semimajor axis of the orbit
aeon	10^9 yr
AGK2	*Zweiter Katalog der Astronomischen Gesellschaft*
α	phase angle, which is the angle at the asteroid between the radius vectors to Earth and to the Sun; right ascension
AU	astronomical unit, a of Earth
$B(a, 0)$	the mean opposition magnitude as defined by

$$B(a, 0) = B(1, 0) + 5 \log a(a - 1)$$

β	ecliptic latitude
C_3	injection energy into Earth-escape hyperbola, km^2/s^2
δ	declination
e	eccentricity of the orbit
e'	proper eccentricity
Ephemeris	*Ephemerides of Minor Planets,* published yearly by the Russian Academy of Sciences, Institute of Theoretical Astronomy, Leningrad, U.S.S.R.
FK4	*Fourth Fundamental Catalogue,* Berliner Astronomisches Jahrbuch
g	absolute magnitude;[2] $g \simeq B(1, 0) - 0.10$
G	universal constant of gravitation
i	inclination of the orbit
i'	proper inclination
I	intensity
IAU	International Astronomical Union
L	angular momentum
λ	ecliptic longitude; wavelength
m	mass
mag	astronomical magnitude $\propto -2.5 \log_{10} I$
MDS	McDonald Survey of Asteroids
MPC	*Minor Planet Circulars,* published by the Minor Planet Center, Cincinnati, Ohio
μm	1 μm = 1·micrometer = 1 micron
N	number
obliquity	the angle between the rotational axis and the perpendicular to the orbital plane
$O - C$	observed value minus computed value
ω	angular velocity
Ω	nodal longitude

[1]The symbols of this glossary are commonly used, unless defined differently by individual authors.

[2]For the newer, more explicit, definition of absolute magnitude, see under *UBV* below.

P	period of rotation about the body axis, or orbital period; polarization
PLS	Palomar-Leiden Survey of Faint Asteroids
r	the distance from the Sun
R	radius of the object
ρ	density
q	perihelion distance
Q	aphelion distance
t	time or epoch
T	temperature
U	Jacobian encounter velocity, defined by E. Öpik in Irish Astron. 8, 191, 1968.
UBV	the photometric system described by H. L. Johnson in ch. 11 of *Basic Astronomical Data,* K. Aa. Strand, ed., University of Chicago Press, 1963. Photographically, as well as photoelectrically, the magnitude B can be observed. It is related to the absolute magnitude, $B(1, 0)$, at unit distances and zero phase by $$B = B(1, 0) + 5 \log r\Delta + F(\alpha)$$ where Δ is the distance from Earth and $F(\alpha)$ is the phase function.
v	linear velocity
V	volume

LIST OF PARTICIPANTS

Aksnes, Kaare; JPL
Alfvén, Hannes; UCSD and Royal Inst. Tech, Stockholm
Allen, David; Hale Observ.
Anders, Edward; Chicago
Anderson, John; JPL
Arnold, Jim; UCSD
Arrhenius, Gustaf; UCSD
Bandermann, Lothar; Hawaii
Bandurski, Eric; Arizona
Barber, Thomas; NASA Hdq.
Battle, Bill; Arizona
Baxter, David; UCSD
Bender, David; JPL
Binder, Alan; IIT Res. Inst.
Bourke, Roger; JPL
Bratenahl, Alex; JPL
Brecher, Aviva; UCSD
Brooks, David; NASA, LRC
Brunk, William; NASA Hdq.
Bruwer, J.; Johannesburg
Burns, Joseph; Cornell
Chapman, Clark; MIT
Coffeen, David; Arizona
Cook, Allan; Smithsonian
Coyne, George; Arizona
Cristescu, Cornelia; Bucharest
Crossley, Dennis; UCSD
Cunningham, Leland; UC Berkeley
Danielsson, Lars; UCSD
Debehogne, Henri; Brussels
Delsemme, Armand; Toledo
Dohnanyi, Julius; Bellcomm
Dollfus, Audouin; Meudon
Doose, Lyn; Arizona
Dubin, Maurice; NASA Hdq.
Dunlap, Larry; Arizona
Dwornik, Steve; NASA Hdq.
Edmondson, Frank; Indiana
Edmondson, Margaret; Indiana
Fink, Uwe; Arizona
Forward, Robert; Hughes Res. Lab.
Fountain, John; Arizona
Friichtenicht, J.; TRW
Gardner, Jack; JPL
Gault, Donald; NASA, ARC
Gehrels, Tom; Arizona
Giclas, Henry; Lowell Observ.
Gill, Jocelyn; NASA Hdq.
Giuli, Tom; NASA, MSC
Goldstein, Richard; JPL
Greenstadt, Eugene; TRW
Greyber, Howard; Martin-Marietta
Hall, Charles; NASA, ARC
Hall, Harvey; NASA Hdq.
Hämeen-Anttila, Antero; Oulu
Hämeen-Anttila, Jyrki; Arizona
Hanner, Martha; Dudley Observ.
Hapke, Bruce; Pittsburgh
Harris, Dan; Arizona
Hartmann, Bill; IIT Res. Inst.
Helin, Eleanor; CIT
Herget, Paul; Cincinnati
Herman, Dan; NASA Hdq.
Herrick, Sam; UCLA
Hills, Jack; Michigan
van Houten, Kees; Leiden
Howes, Morris; Arizona
Ip, Wing-Huen; UCSD
Jeffries, Anthony; Arizona
Johnson, David; NASA, ARC
Johnson, Torrence; MIT
Kaula, William; UCLA
KenKnight, Charles; Arizona
Kerridge, John; NASA, ARC
Kessler, Don; NASA, MSC
Kiang, Tao; Dunsink
Kinard, William; NASA, LRC

Klepczynski, Bill; Naval Observ.
Kowal, Charles; CIT
Kraemer, Bob; NASA Hdq.
Kuiper, Gerard; Arizona
Lacis, Anthony; Iowa
Larson, Steve; Arizona
Lindblad, Bertil; Lund
Love, Lynne; UCSD
McCrosky, Richard; Smithsonian
Marsden, Brian; Smithsonian
Mascy, Alfred; NASA Hdq.
Matson, Dennis; CIT
Matthews, Mildred; Arizona
Meissinger, Hans; TRW
Milet, Bernard; Nice
Miner, Ellis; JPL
Modzeleski, Vincent; Arizona
Mohammed, M. J.; Arizona
Mulholland, Derral; CIT
Muncaster, George; Arizona
Nagy, Bart; Arizona
Nagy, Lois; Arizona
Niehoff, John; IIT Res. Inst.
O'Handley, Douglas; JPL
Pierce, David; El Camino Col.
Pilcher, Fred; Illinois Col.
Rabe, Eugene; Cincinnati
Randić, Leo; Arizona
Roberts, David; IIT Res. Inst.
Roberts, Phil; JPL
Robey, Donald; North American
Roemer, Elizabeth; Arizona
Roosen, Rob; NASA, GSFC
Sather, Bob; Arizona
Schubart, Joachim; Heidelberg
Sekanina, Zdenek; Smithsonian
Serkowski, Krzysztof; Arizona
Sill, Godfrey; Arizona
Singer, Fred; Interior Dept.
Soberman, Bob; G.E. Space Sci. Lab.
Sonett, Chuck; NASA, ARC
Staley, Dean; Arizona
Strom, Bob; Arizona
Stuhlinger, Ernst; NASA, MSFC
Suess, Hans; UCSD
Taylor, Ron; Arizona
Thomas, Bob; Arizona
Tomasko, Martin; Princeton
Toms, Ron; NASA Hdq.
Trulsen, Jan; Tromsø
Urey, Harold; UCSD
Van Biesbroeck, George; Arizona
Vesely, Carl; Arizona
Veverka, Joe; Cornell
Wamsteker, Willem; Arizona
Weinberg, Jerry; Dudley Observ.
Wetherill, George; UCLA
Whipple, Fred; Smithsonian
Williams, Jim; JPL
Wilson, Micheline; Arizona
Wolstencroft, Ramon; Hawaii
Wood, Chuck; Arizona
Young, Maria; Arizona
Zellner, Ben; Arizona

INDEX

☆ U. S. GOVERNMENT PRINTING OFFICE : 1972 O - 458-796

Physical Studies of Minor Planets

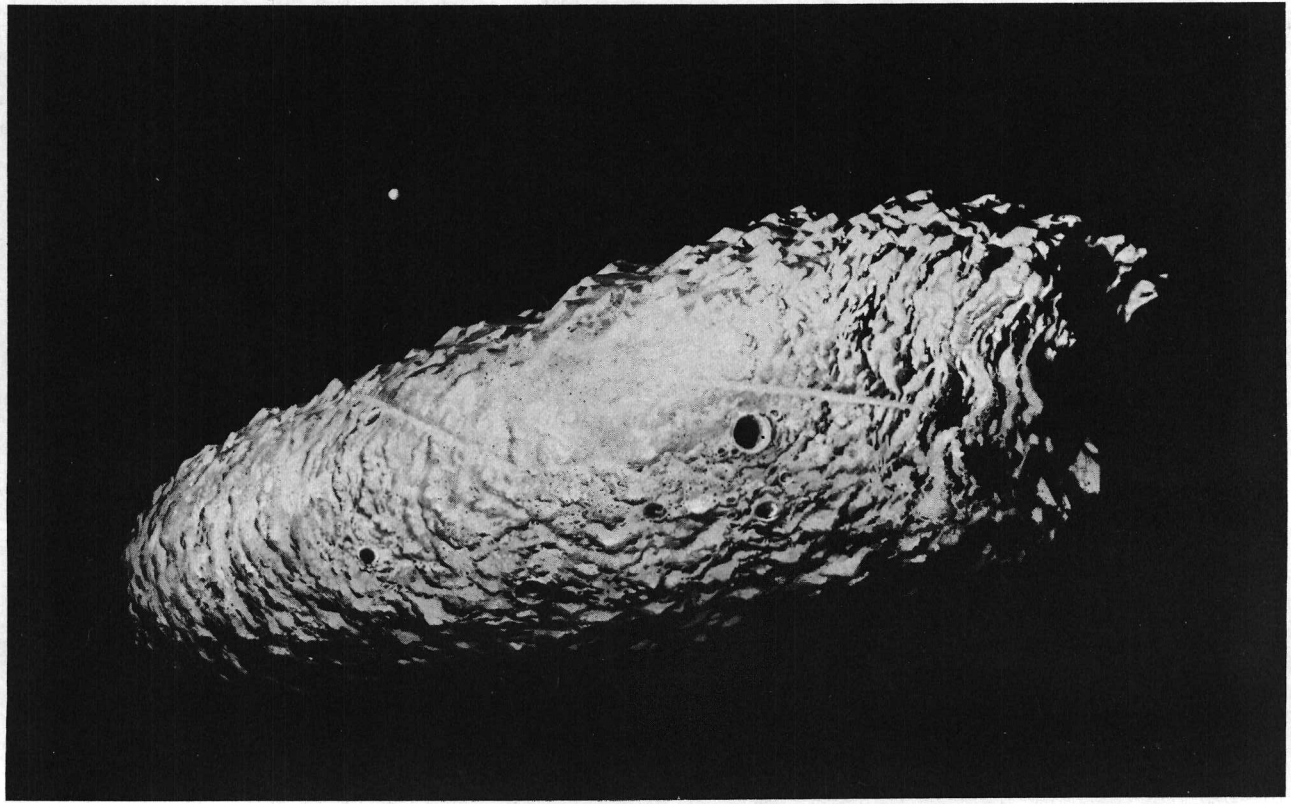

Geographos, from a painting by Davis Meltzer (COURTESY NATIONAL GEOGRAPHIC SOCIETY)

NASA SCIENTIFIC AND TECHNICAL PUBLICATIONS

TECHNICAL REPORTS: Scientific and technical information considered important, complete, and a lasting contribution to existing knowledge.

TECHNICAL NOTES: Information less broad in scope but nevertheless of importance as a contribution to existing knowledge.

TECHNICAL MEMORANDUMS: Information receiving limited distribution because of preliminary data, security classification, or other reasons.

CONTRACTOR REPORTS: Scientific and technical information generated under a NASA contract or grant and considered an important contribution to existing knowledge.

TECHNICAL TRANSLATIONS: Information published in a foreign language considered to merit NASA distribution in English.

SPECIAL PUBLICATIONS: Information derived from or of value to NASA activities. Publications include conference proceedings, monographs, data compilations, handbooks, sourcebooks, and special bibliographies.

TECHNOLOGY UTILIZATION PUBLICATIONS: Information on technology used by NASA that may be of particular interest in commercial and other non-aerospace applications. Publications include Tech Briefs, Technology Utilization Reports and Notes, and Technology Surveys.

Details on the availability of these publications may be obtained from:

SCIENTIFIC AND TECHNICAL INFORMATION OFFICE
NATIONAL AERONAUTICS AND SPACE ADMINISTRATION
Washington, D.C. 20546